

**Faunal, sedimentological and
geochemical indicators of dysoxia in
Cretaceous marine sediments**

Ellen Louise Weavers

University of Greenwich

A thesis submitted in partial fulfilment
of the requirements for the degree of
DOCTOR OF PHILOSOPHY

Submitted April 2010

ACKNOWLEDGEMENTS

Completing this PhD would not have been possible without the support and encouragement of my friends and advisors. I would like to thank my supervisors Dr David Wray and Professor Andy Gale for giving me the opportunity to study a subject so close to my geological heart. Many thanks are also due to Atiya Raza and Florence Lowry for their expertise, friendship and patience. I am truly grateful to Peter Gunning, Aurora Antemir, Genaro Rebolledo-Mendez and Alberto Sanchez-Medina for the loyal friendship, language lessons and continuous entertainment they have provided. Peter in particular has shown extraordinary patience in teaching me so much about making diagrams, fixing computers and killing pot plants.

The generosity of the Cambridge University Department of Earth Sciences and Corpus Christi College, Cambridge, has literally been critical in allowing me to complete this project. I am particularly grateful to Jan Leaver and the Corpus Christi Porters for making my stay so pleasant. Thanks are also due to Mike Boyd and David Barnett whose friendship kept me sane through an intense summer.

I have been blessed with many other amazing friends and particular thanks are due to Bethany Audley, Laura Jude, Silvia Miotti, Jin Chin, Catherine Burgess, Hannah Torrance, Becca Reed, Katie Richardson, Juliet Biggs, Stuart Pegg, Becky Walker, Paula Rees and Nick Lang. I cannot think of enough words to express how grateful I am to have the friendship and support of Amelia Richter and her husband Simon in my life. And despite the ocean between us, Elizabeth Sowers has also played a major role in getting me through the last few years and I continue to miss her muchly. The good humour of the past and present pupils of the King's School Rochester has been vital in keeping me smiling and I hope that I have managed to teach them something.

None of this would be possible without the love and support of my family. My wonderful grandparents have provided boundless enthusiasm and encouragement, despite the fact that I once threw my vest at Nana. My parents are truly the best people I know and have invested a lot of their time and energy in perfecting a feigned interest in mud. They have literally come to the rescue countless times and I do not know how I will ever repay them. I would like to dedicate this work to them but promise that this does not mean that they have to read it.

ABSTRACT

Cretaceous marine sediments worldwide are characterised by the occurrence of ‘Oceanic Anoxic Events’ during which organic matter was extensively deposited in ‘black shale’ facies. Although diverse criteria for the recognition of low oxygen levels have been described previously they have not been fully calibrated. This project compares palaeo-oxygenation related features of lower Cretaceous rocks from the shallow sea muds of the Gault Clay (south east England) and Niveau Pacquier and Briestroffer sequences (south east France), and the Tarfaya Basin upwelling-zone Amma Fatma sediments (Morocco). The palaeo-oxygenation indicators investigated include:

- sedimentological proxies, including ichnology, sedimentology, taphonomy and pyrite framboid size distribution;
- faunal proxies including macrofaunal properties, and biofacies models;
- geochemical proxies, including trace-element abundances [Mo, V, Ni, Mn], element ratios and parameters [U/Th, authigenic U (U_a), V/Cr, Ni/Co, Ni/V, (Cu+Mo)/Zn, V/Sc and V/(V+Ni)] and Fe-S-C systematics [Total Organic Carbon (TOC), Total Sulphur/TOC ratio, Degree of Pyritisation and the Indicator of Anoxia].

The presence of lamination is found to be a key sedimentological indicator of restricted bottom water oxygenation conditions. New descriptive categories of pyrite morphology are proposed as the use of numerical categories of pyrite framboid diameters is found to have variable success for palaeo-oxygenation determination. Interpretation of faunal proxies can be limited by poor preservation, but taphonomy-related indicators are found to correlate well with proposed palaeo-oxygenation conditions. Molybdenum is found to be the most reliable of the trace-metal enrichment proxies studied and altered numerical boundaries are proposed for U_a , U/Th, V/Cr and Ni/Co. Of the Fe-S-C systematics indicators, Total Organic Carbon and the Indicator of Anoxia are found to provide the greatest definition between palaeo-oxygenation data sets. Combinations of trace metal and Fe-S-C indicators such as [Molybdenum Enrichment Factor x Indicator of Anoxia], and plots of U_a against TOC are proposed to provide the strongest palaeo-oxygenation proxies and distinguish between oxic/dysoxic, anoxic and euxinic conditions.

CONTENTS

	Pages
<u>1. INTRODUCTION</u>	1
<u>1.1 Introduction to low oxygen events</u>	
1.1.1 Terminology	2
1.1.2 Cretaceous Oceanic Anoxic Events	4
<u>1.1.2.1 High-Productivity Models</u>	7
<u>1.1.2.2 Preservation Models</u>	8
<u>1.2 Introduction to the sites</u>	
1.2.1 Niveau Pacquier	11
1.2.2 Briestroffer	14
1.2.3 Folkestone Gault Clay	16
1.2.4 Amma Fatma	18
<u>1.4 Introduction to the proxies and the project structure</u>	20
<u>2. SEDIMENTOLOGICAL FEATURES</u>	
<u>2.1 Introduction</u>	
2.1.1 Sedimentology	22
2.1.2 Ichnology	
<u>2.1.2.1 Background</u>	26
<u>2.1.2.2 Bioturbation Indices</u>	28
<u>2.1.2.3 The presence of particular ‘species’</u>	31
<u>2.1.2.4 Ichnofacies and Ichnocoenoses</u>	32
<u>2.1.2.5 Taxonomic Assessment of Trace Assemblage features</u>	33
<u>2.1.2.6 Patterns of Tiering</u>	35
2.1.3 Pyrite Framboids	38
<u>2.2 Methodology</u>	
2.2.1 Sedimentology	42
2.2.2 Ichnology	43
2.2.3 Pyrite Framboids	43
<u>2.3 Discussion of Results</u>	

2.3.1 Niveau Pacquier samples	
<u>2.3.1.1 Sedimentology</u>	44
<u>2.3.1.2 Ichnology</u>	46
<u>2.3.1.3 Pyrite Framboids</u>	47
2.3.2 Briestroffer samples	
<u>2.3.2.1 Sedimentology</u>	53
<u>2.3.2.2 Ichnology</u>	54
<u>2.3.2.3 Pyrite Framboids</u>	55
2.3.3 Folkestone Gault Clay samples	
<u>2.3.3.1 Sedimentology</u>	59
<u>2.3.3.2 Ichnology</u>	60
<u>2.3.3.3 Pyrite Framboids</u>	64
2.3.4 Amma Fatma samples	
<u>2.3.4.1 Sedimentology</u>	67
<u>2.3.4.2 Ichnology</u>	70
<u>2.3.4.3 Pyrite Framboids</u>	70
<u>2.4 Conclusions</u>	73
<u>3. PALAEOLOGY</u>	
<u>3.1 Introduction</u>	77
3.1.1 Macrofossils	
<u>3.1.1.1 Variations in benthic abundance and diversity</u>	78
<u>3.1.1.2 Variations in the size of benthos</u>	80
<u>3.1.1.3 Variations in burrow depth</u>	81
<u>3.1.1.4 Changes in the predominant modes of life</u>	81
<u>3.1.1.5 Variations in the proportion of shelly taxa</u>	83
<u>3.1.1.6 The presence of particular ‘tolerant’ species</u>	83
<u>3.1.1.7 Taphonomy</u>	85
3.1.2 Models of Macrofaunal and Sedimentological response to low oxygen conditions	
<u>3.1.2.1 The Rhoads-Morse-Byers Model</u>	89
<u>3.1.2.2 Morris’ Categories</u>	92
<u>3.1.2.3 Oxygen-Restricted Biofacies</u>	93

<u>3.1.2.4 Wignall's 'Shelf Model'</u>	95
<u>3.1.2.5 Arthur and Sageman's Infaunal and Epifaunal Biofacies Levels</u>	97
<u>3.1.2.6 Summary</u>	100
<u>3.2 Methodology</u>	102
<u>3.3 Discussion of Results</u>	
3.3.1 The Niveau Pacquier sequence, Vocontian Basin	103
<u>3.3.1.1 Analysis of Fossil Assemblages</u>	103
<u>3.3.1.2 Application of Biofacies Models</u>	105
3.3.2 The Briestroffer sequence, Vocontian Basin	108
<u>3.3.2.1 Analysis of Fossil Assemblages</u>	108
<u>3.3.2.2 Application of Biofacies Models</u>	109
3.3.3 The Folkestone Gault Clay	111
<u>3.3.3.1 Analysis of Fossil Assemblages</u>	111
<u>3.3.3.2 Application of Biofacies Models</u>	115
3.3.4 Amma Fatma	116
<u>3.3.4.1 Analysis of Fossil Assemblages</u>	116
<u>3.3.4.2 Application of Biofacies Models</u>	118
<u>3.4 Conclusions</u>	120
<u>4. TRACE METAL PALAEO-OXYGENATION PROXIES</u>	
<u>4.1 Introduction</u>	
4.1.1 Introduction to Trace Metal Palaeo-Oxygenation Proxies	123
4.1.2 Correcting for Detrital Sources	125
4.1.3 Explanation of Trace Metal Enrichments	
<u>4.1.3.1 Molybdenum</u>	127
<u>4.1.3.2 Vanadium</u>	128
<u>4.1.3.3 Nickel</u>	129
<u>4.1.3.4 Manganese</u>	129
4.1.4 Explanation of Trace Metal Ratios	
<u>4.1.4.1 Uranium based ratios</u>	130
<u>4.1.4.2 V/Cr</u>	132

<u>4.1.4.3 V/Sc</u>	132
<u>4.1.4.4 Ni/Co</u>	133
<u>4.1.4.5 Ni/V</u>	133
<u>4.1.4.6 V/(V+Ni)</u>	133
<u>4.1.4.7 (Cu+Mo)/Zn</u>	134
<u>4.1.4.8 Cerium anomaly</u>	134
<u>4.2 Methodology</u>	135
<u>4.3 Discussion of Results</u>	
4.3.1 Niveau Pacquier	
<u>4.3.1.1 Trace Metal Enrichments</u>	138
<u>4.3.1.2 Trace Metal Ratios</u>	145
4.3.2 Briestroffer Layers	
<u>4.3.2.1 Trace Metal Enrichments</u>	154
<u>4.3.2.2 Trace Metal Ratios</u>	161
4.3.3 Folkestone	
<u>4.3.3.1 Trace Metal Enrichments</u>	167
<u>4.3.3.2 Trace Metal Ratios</u>	172
4.3.4 Amma Fatma	
<u>4.3.4.1 Trace Metal Enrichments</u>	175
<u>4.3.4.2 Trace Metal Ratios</u>	179
<u>4.4 Conclusions</u>	
4.4.1 Trace Metal Enrichments	182
4.4.2 Trace Metal Ratios	182
<u>5. Fe-S-C SYSTEMATICS</u>	
<u>5.1 Introduction</u>	
5.1.1 Introduction to Pyrite Formation	184
5.1.2 Introduction to the Proxies and the Related Terminology	
<u>5.1.2.1 Carbon, sulphur and the S/C ratio</u>	186
<u>5.1.2.2 Iron pools</u>	190
<u>5.1.2.3 Ternary plots of Fe, S and C</u>	191
<u>5.1.2.4 Degree of Pyritisation</u>	192
<u>5.1.2.5 Indicator of Anoxia</u>	199

5.2 Methods of Analysis

5.2.1 Carbon

5.2.1.1 Organic Carbon (TOC) and Inorganic Carbon (C_{In}) 202

5.2.1.2 Total Carbon (TC) 202

5.2.2 Sulphur

5.2.2.1 Pyrite Sulphur (S_{Py}) 203

5.2.2.2 Total Sulphur (TS) 205

5.2.3 Iron

5.2.3.1 Pyrite Iron (Fe_{Py}) 206

5.2.3.2 Dithionite Extractable Iron (FeD) 206

5.2.3.3 Hot HCl extractable Iron (FeH) 207

5.2.3.4 Total Iron (FeT) 207

5.3 Discussion of Results

5.3.1 Carbon, Sulphur and the S/C ratio

5.3.1.1 Total Sulphur 208

5.3.1.2 Total Organic Carbon and Inorganic Carbon 208

5.3.1.3 The S/C ratio 214

5.3.2 Iron pools 217

5.3.3 Ternary plots of Fe, S and C 221

5.3.4 The Degree of Pyritisation

5.3.4.1 The Degree of pyritisation 225

5.3.4.2 Combination of the Degree of Pyritisation with the
S/C ratio 225

5.3.4.3 Comparison of DOP calculation methods 235

5.3.5 The Indicator of Anoxia 236

5.4 Conclusions 236

6. DISCUSSION

6.1 Sedimentology 239

6.2 Palaeontology 245

6.3 Trace Metal Geochemistry 249

6.4 Fe-S-C Systematics 261

6.5 Conclusions 267

<u>6.6 Further Work</u>	268
<u>7. REFERENCES</u>	270
<u>APPENDIX A: SEDIMENTARY PROXIES DATA</u>	299
<u>APPENDIX B: PALAEOLOGICAL DATA</u>	301
<u>APPENDIX C: TRACE ELEMENT PROXIES DATA</u>	308
<u>APPENDIX D: Fe-S-C PROXIES DATA</u>	327

FIGURES LIST

Figure Caption	Page
<i>Figure 1.1: Location map of the Niveau Pacquier (NP) (Latitude 44° 24' 13.0"N, Longitude 5° 31' 32.2"E) and Briestroffer (BL) (Latitude 44° 24' 11.9"N, Longitude 5° 31' 34.7"E) sample sites near Rosans, south east France.</i>	11
<i>Figure 1.2: Key to the stratigraphic logs.</i>	12
<i>Figure 1.3: Stratigraphic log of the sequence laid down in the Vocontian Basin between the Upper Aptian and the Upper Albian (after Bornemann et al., 2005). The labelled sections represent the Niveau Pacquier OAE1b sequence (labelled NP Section) and the Briestroffer OAE1d sequence (labelled BL section)</i>	13
<i>Figure 1.4: Stratigraphic log of the studied Niveau Pacquier section</i>	14
<i>Figure 1.5: Stratigraphic log showing the Briestroffer sequence according to Gale et al. (1996), which contains seven black shale horizons, and the section studied which encompasses the lower four of these black shale horizons.</i>	15
<i>Figure 1.6: Location map of the Gault Clay exposure (labelled FEW site) (Latitude 51° 5' 1.0"N, Longitude 1° 11' 56.0"E) at Copt Point, Folkestone, south east England.</i>	16
<i>Figure 1.7: Stratigraphic logs of the Folkestone Gault Clay exposure, with beds assigned by Owen (1971), and the section studied, which is centred around the base of Bed VII.</i>	17
<i>Figure 1.8: Location map of the Amma Fatma sequence (AF site) (Latitude 28° 11' 53.5"N, Longitude 11° 46' 32.2"W) in the Tarfaya Basin, Morocco.</i>	18
<i>Figure 1.9: Stratigraphic log of the investigated Amma Fatma sequence.</i>	19
<i>Figure 2.1: Classification of sedimentary rocks according to the Udden-Wentworth scale, with later additions by Krumbein (1934).</i>	22
<i>Figure 2.2: Classification of fine-grained sedimentary rocks (according to Pettijohn, 1975).</i>	23
<i>Figure 2.3: Inter-relationship of the behavioural modes assigned by Seilacher (1953) (after Pemberton et al. 1992).</i>	26
<i>Figure 2.4: The Bioturbation Index (Reineck, 1963) from Taylor and Golding (1993).</i>	28
<i>Figure 2.5: Schematic diagrams of ichnofabric indices with descriptions (from Droser and Bottjer, 1986).</i>	29
<i>Figure 2.6: Bedding plane bioturbation indices, taking into account variations in size, shape and distribution (from Miller and Smail, 1997).</i>	30
<i>Figure 2.7: A general model of oxygen- dependant trace fossil associations, adapted from Ekdale and Mason (1988).</i>	34
<i>Figure 2.8: Inter-relationship between environmental factors and some ichnofaunal aspects for deep-sea sediments, assuming that only one factor is varied at a time (adapted from Wetzel, 1991).</i>	35
<i>Figure 2.9: Schematic block diagram illustrating burrow size, bioturbation depth and tiering structure across a hypothetical seafloor oxygenation</i>	36

<i>gradient and expected trace-fossil cross cutting relationships in strata deposited at various sites along the gradient.</i>	
<i>Figure 2.10: Schematic diagrams representing trace fossil associations and cross-cutting relationships expected in sediment deposited under stable conditions of oxygenation (A), gradually decreasing oxygen availability (B), gradually increasing oxygen availability (C), rapidly decreasing oxygen availability (D) and rapidly increasing oxygen availability (E) (after Savdra and Bottjer, 1986).</i>	37
<i>Figure 2.11: The formation of pyrite framboids syngenetically at a redox boundary within the water column and diagenetically, at a redox boundary within the sediment.</i>	40
<i>Figure 2.12: Scanning Electron Microscope images, of sediment from 1.15m in the Folkestone Gault Clay sequence, showing 1. Pyrite framboids; 2. A close up of microcrysts within a framboid which hasn't been overgrown; 3. Framboids with single euhedral crystals.</i>	41
<i>Figure 2.13: Stratigraphic log of the studied Niveau Pacquier sequence. The pale grey represents the grey clays of the Marnes Bleues Formation and the black represents the Niveau Pacquier black shales.</i>	44
<i>Figure 2.14: Backscatter scanning electron microscope image of a polished slab of Niveau Pacquier black shale (from 1.2 m above the base of the black shale horizon). The dull grey forms represent carbonate micro- and nanofossils whereas the bright specks represent pyrite framboids. The scale bar represents ~200µm.</i>	45
<i>Figure 2.15: The mean and range of pyrite framboid diameters for the Niveau Pacquier sample range. The dark shading corresponds to the Black Shale samples whereas the light diamond data points represent the Grey Clay samples.</i>	47
<i>Figure 2.16: The two-tailed Student's t-test results for the Niveau Pacquier framboid diameter data sets. The test shows that the grey clay and black shale data sets are distinguishable as the P value is below 0.05.</i>	47
<i>Figure 2.17: A cumulative bar chart to represent the percentage proportion of framboids within each size range for the Niveau Pacquier samples (based on the numerical boundaries implied by Wilkin et al., 1997). Along the top, the black sections represent the Black Shale samples whereas the pale grey sections represent the Grey Clay samples.</i>	48
<i>Figure 2.18: Comparison of the Standard Deviation and Mean of framboid diameters for the Niveau Pacquier samples.</i>	50
<i>Figure 2.19: Plot of the calculated skewness of framboid diameter data for the Niveau Pacquier samples. Along the top, the black sections represent the Black Shale samples whereas the pale grey sections represent the Grey Clay samples.</i>	51
<i>Figure 2.20: Backscatter scanning electron microscope images of pyrite overgrowth of framboids (a, c) and a framboid cluster (b) in Niveau Pacquier Grey Clay samples.</i>	52
<i>Figure 2.21: Stratigraphic log of the studied Briestroffer section, including four of the Briestroffer black shale bands.</i>	53
<i>Figure 2.22: The Mean and Range of pyrite framboid diameters for the Briestroffer sample range. The dark triangular data points represent the Black Shale samples whereas the light diamond data points represent the Grey Clay samples.</i>	55

<i>Figure 2.23: The two-tailed Student's t-test results for the Briestroffer sequence framboid diameter data sets. The test shows that the grey clay and black shale data sets are distinguishable as the P value is below 0.05.</i>	55
<i>Figure 2.24: A cumulative bar chart to represent the percentage proportion of framboids within each size range for the Briestroffer samples (based on the numerical boundaries implied by Wilkin et al., 1997). Along the top, the black sections represent the Black Shale samples whereas the pale grey sections represent the Grey Clay samples.</i>	56
<i>Figure 2.25: Comparison of the Standard Deviation and Mean of framboid diameter for the Briestroffer samples.</i>	57
<i>Figure 2.26: Plot of the calculated skewness of framboid diameter data for the Briestroffer samples. The shaded points represent the black shale samples whereas the unshaded data points represent the grey clay samples.</i>	57
<i>Figure 2.27: Backscatter scanning electron microscope pictures illustrating the general spread of framboids, which show up as white specks, in a Black Shale (a) and Grey Clay sample (b). Scale bar represents ~200 μm.</i>	58
<i>Figure 2.28: Stratigraphic log of the Folkestone Gault Clay section.</i>	59
<i>Figure 2.29: Photograph and sketch showing second tier <i>Thalassinoides</i> infilled with shell debris, and pyritised burrows (coloured pale blue) thought to represent fourth tier forms. The background is mottled with Chondrites. The sample was collected from -0.1 m.</i>	62
<i>Figure 2.30: Photograph and sketch of a pyritised burrow showing a possible lining (darker blue) and reaction halo (pale yellow). The sample was collected from -0.4 m.</i>	62
<i>Figure 2.31: Triagonal junction of pyritised traces (pale blue) with a reaction halo (pale yellow). The sample was collected from -0.4 m.</i>	63
<i>Figure 2.32: Photograph and sketch showing the same pyritised burrow forms (pale blue) and smaller pyritised burrows (purple). The sample was collected from -0.3 m.</i>	63
<i>Figure 2.33: Pale Chondrites in a darker sediment matrix. The sample was collected from -0.7 m.</i>	63
<i>Figure 2.34: The Mean and Range of pyrite framboid diameters for the Folkestone Gault Clay sample range.</i>	64
<i>Figure 2.35: A cumulative bar chart to represent the percentage proportion of framboids within each size range for the Folkestone Gault Clay samples (based on the numerical boundaries implied by Wilkin et al., 1997).</i>	65
<i>Figure 2.36: Comparison of the standard deviation and mean of framboid diameters for the Folkestone Gault Clay samples.</i>	66
<i>Figure 2.37: Plot of the calculated skewness of framboid diameter data for the Folkestone Gault Clay samples.</i>	66
<i>Figure 2.38: Backscatter SEM images of framboid clusters, euhedral crystals and large framboids from 1.1 m (a), and 1.2 m (b, c and d) above the base of Bed VII in the Folkestone Gault Clay. The scale bars represent 20 μm (a, b and c) and 5 μm (d).</i>	67
<i>Figure 2.39: Stratigraphic log of the Amma Fatma section.</i>	68
<i>Figure 2.40: Backscatter SEM images of sediment fabric from the laminated marls and massive limestone. The scale bar represents 200 μm.</i>	69
<i>Figure 2.41: The Mean and Range of pyrite framboid diameters for the Amma Fatma sample range. The dark bands represent the laminated dark</i>	70

<i>shale samples whereas the pale bands represent the more carbonate-rich material.</i>	
<i>Figure 2.42: The two-tailed Student's t-test results for the Briestroffer sequence framboid diameter data sets. The test shows that the paler sediment and the dark marl data sets are distinguishable as the P value is below 0.05.</i>	70
<i>Figure 2.43: A cumulative bar chart to represent the percentage proportion of framboids within each size range for the Amma Fatma samples (based on the numerical boundaries implied by Wilkin et al., 1997). Along the top, the dark sections represent the laminated dark shale samples whereas the pale sections represent the more carbonate-rich samples.</i>	71
<i>Figure 2.44: Comparison of the Standard Deviation and Mean of framboid diameters for the Amma Fatma samples.</i>	72
<i>Figure 2.45: Plot of the calculated skewness of framboid diameter data for the Amma Fatma samples.</i>	73
<i>Figure 3.1: The ternary diagram of bivalve life modes which Morris (1979) proposed could be used to distinguish palaeo-oxygenation regimes.</i>	82
<i>Figure 3.2: Table linking taphofacies with water oxygenation, sediment geochemistry and sedimentation rates. Adapted from Brett and Baird (1986).</i>	87
<i>Figure 3.3: Three-dimensional block diagram showing the relationship between authigenic mineral formation and current energy, sedimentation rate and level of substrate oxygenation. Substrate oxygenation variation is based on a stratified ocean model where oxygenation varies with depth. Adapted from Speyer and Brett (1988).</i>	88
<i>Figure 3.4: Summary diagram representing a variety of proposed oxygen-related biofacies models (adapted from included references).</i>	90
<i>Figure 3.5: Summary diagram to show the proposed ranges of palaeo-oxygenation conditions for the Niveau Pacquier black shale according to a range of macrofaunal models.</i>	106
<i>Figure 3.6: Summary diagram to show the proposed ranges of palaeo-oxygenation conditions for the Marnes Bleues grey clay within the Niveau Pacquier sequence according to a range of macrofaunal models.</i>	106
<i>Figure 3.7: Summary diagram to show the proposed ranges of palaeo-oxygenation conditions for the Briestroffer black shales according to a range of macrofaunal models.</i>	109
<i>Figure 3.8: Summary diagram to show the proposed ranges of palaeo-oxygenation conditions for the Marnes Bleues grey clay within the Briestroffer sequence according to a range of macrofaunal models.</i>	109
<i>Figure 3.9: Macrofossil species richness, total abundance of macrofossils, Shannon Index (H) and Equitability (E) throughout the Folkestone Gault Clay sequence. The ORB ranges on the species richness graph refer to the ranges proposed in the Oxygen-Restricted Biofacies scheme (Wignall and Hallam, 1991).</i>	112
<i>Figure 3.10: Ternary diagram of bivalve life modes from the Folkestone Gault Clay (based on Morris, 1979).</i>	113
<i>Figure 3.11: Summary diagram to show the proposed ranges of palaeo-oxygenation conditions for the Folkestone Gault Clay according to a range of macrofaunal models.</i>	115

<i>Figure 3.12: Ternary diagram of bivalve life modes from the 'lucina bed' of the Amma Fatma sequence (based on Morris, 1979).</i>	117
<i>Figure 3.13: Summary diagram to show the proposed ranges of palaeo-oxygenation conditions for the Amma Fatma dark marls according to a range of macrofaunal models.</i>	119
<i>Figure 3.14: Summary diagram to show the proposed ranges of palaeo-oxygenation conditions for the Amma Fatma 'lucina bed' according to a range of macrofaunal models.</i>	119
<i>Figure 4.1: Element/Al ratio for Mo, V, Ni and Mn for the Niveau Pacquier sequence. The pale purple points represent the grey clay samples whereas the shaded dark purple triangular points are from the black shale data set.</i>	139
<i>Figure 4.2: Enrichment factors for Mo, V, Ni and Mn for the Niveau Pacquier sequence. The pale purple points represent the grey clay samples whereas the shaded dark purple triangular points are from the black shale data set.</i>	140
<i>Figure 4.3: Trace metal excess values for Mo, V, Ni and Mn for the Niveau Pacquier sequence. The pale purple points represent the grey clay samples whereas the shaded dark purple triangular points are from the black shale data set.</i>	141
<i>Figure 4.4: Major elements (Al_2O_3 wt% and SiO_2 wt%) and element ratios (Si/Al and Ti/Al) for the Niveau Pacquier sequence. The pale purple points represent the grey clay samples whereas the shaded dark purple triangular points are from the black shale data set.</i>	143
<i>Figure 4.5: Major elements (as $CaCO_3$ wt% and P_2O_5 wt%) and element ratios (K/Al) for the Niveau Pacquier sequence. The pale purple points represent the grey clay samples whereas the shaded dark purple triangular points are from the black shale data set.</i>	144
<i>Figure 4.6: The two-tailed Student's t-test data for Niveau Pacquier elemental enrichment factors. The test shows that for molybdenum and vanadium, the two sample sets are clearly distinguishable as the P values are below the 0.05% confidence level. However, the P values for nickel and manganese are well above this confidence level, showing that the black shale and grey clay samples do not show up as separate groups within these sets of data.</i>	146
<i>Figure 4.7: Plots of the mean and range of the Mo, V, Ni and Mn data for the grey shale sample set and the black shale sample set of the Niveau Pacquier sequence.</i>	146
<i>Figure 4.8: Plots of the ratios highlighted by Jones and Manning (1994), including their tentative boundaries for the oxic-dysoxic transition and the dysoxic-anoxic transition, applied to the Niveau Pacquier sequence. The pale purple points represent the grey clay samples whereas the shaded dark purple triangular points are from the black shale data set.</i>	147
<i>Figure 4.9: The two-tailed Student's t-test data for Niveau Pacquier element ratios suggested by Jones and Manning (1994). The test shows that for all ratios, the grey mud and black shale samples are statistically separate data sets as all P values fall well under the 0.05% confidence limit.</i>	148
<i>Figure 4.10a: Plots of the mean and range of the Ua and U/Th data for the grey shale sample set and the black shale sample set of the Niveau Pacquier sequence.</i>	148

<i>Figure 4.10b: Plots of the mean and range of the V/Cr and Ni/Co data for the grey shale sample set and the black shale sample set of the Niveau Pacquier sequence.</i>	149
<i>Figure 4.11: Summary of the Niveau Pacquier environments of deposition suggested by the elemental ratios, based on the tentative boundaries set by Jones and Manning (1994).</i>	151
<i>Figure 4.12: Plots of the other ratios including tentative boundaries for V/Sc (Kimura and Watanabe, 2001) and V/(V+Ni) (Schovsbo, 2001) for the Niveau Pacquier sequence.</i>	152
<i>Figure 4.13: The two-tailed Student's t-test data for Niveau Pacquier other element ratios test shows that for all ratios apart from (Cu+Mo)/Zn, the two data sets are statistically separate data sets as all P values fall under the 0.05% confidence limit.</i>	153
<i>Figure 4.14: Plots of the mean and range of the other elemental ratios for the grey shale and the black shale sample sets of the Niveau Pacquier sequence.</i>	153
<i>Figure 4.15: Enrichment factors of Mo, V, Ni and Mn. The pale blue data points represent samples from the grey clay sequence, whereas the shaded dark blue points represent samples from the black shale layers in the Briestroffer sequence.</i>	155
<i>Figure 4.16: Major elements (Al₂O₃ wt% and SiO₂ wt%) and element ratios (Si/Al and Ti/Al) for the Briestroffer section. The pale blue data points represent samples from the grey clay sequence, whereas the shaded dark blue points represent samples from the black shale layers in the Briestroffer sequence.</i>	156
<i>Figure 4.17: Major elements (as CaCO₃ wt% and P₂O₅ wt%) and element ratios (K/Al) for the Briestroffer section. The pale blue data points represent samples from the grey clay sequence, whereas the shaded dark blue points represent samples from the black shale layers in the Briestroffer sequence.</i>	157
<i>Figure 4.18: Plot of SiO₂ against Al₂O₃ for the Niveau Pacquier (NP), Briestroffer (BL) and Amma Fatma (AF) data sets.</i>	159
<i>Figure 4.19: The two-tailed Student's t-test data for the Briestroffer elemental enrichment factors. The test shows that all of the elements pass the t-test with a P value below the confidence limit of 0.05%.</i>	159
<i>Figure 4.20: Plots of the mean and range of the Mo, V, Ni and Mn data for the grey clay sample (GC) set and the black shale (BS) sample set of the Briestroffer sequence.</i>	160
<i>Figure 4.21: The two-tailed Student's t-test data for the Briestroffer element ratios favoured by Jones and Manning (1994). The test shows that for all ratios, the grey mud and black shale samples are statistically separate data sets with the Ua data being the most convincing.</i>	161
<i>Figure 4.22: Plots of the mean and range of the Ua, U/Th, V/Cr and Ni/Co data for the grey shale sample set and the black shale sample set of the Briestroffer sequence.</i>	162
<i>Figure 4.23: Plots of the ratios highlighted by Jones and Manning (1994), including their tentative boundaries for the oxic-dysoxic transition and the dysoxic-anoxic transition, for the Briestroffer sequence. The pale blue data points represent samples from the grey clay sequence, whereas the shaded dark blue points represent samples from the black shale layers in the Briestroffer sequence.</i>	163

<i>Figure 4.24: Summary of the Briestroffer environments of deposition suggested by the elemental ratios, based on the tentative boundaries set by Jones and Manning (1994).</i>	164
<i>Figure 4.25: Plots of the other ratios including tentative boundaries for V/Sc (Kimura and Watanabe, 2001) and V/(V+Ni) (Schovsbo, 2001) for the Briestroffer sequence.</i>	165
<i>Figure 4.26: The two-tailed Student's t-test data for the other Briestroffer element ratios. The test shows that only the (Cu+Mo)/Zn and V/Sc ratios provide differentiation between the two data sets.</i>	166
<i>Figure 4.27 (a): Mean and range plots the Ni/V, (Cu+Mo)/Zn and V/(V+Ni) element ratio data sets from the Briestroffer sequence.</i>	166
<i>Figure 4.27 (b): Mean and range plots for the cerium anomaly and V/Sc elemental ratio data sets from the Briestroffer sequence.</i>	167
<i>Figure 4.28: Enrichment factor data for Mo, V, Ni and Mn from the Folkestone Gault Clay.</i>	169
<i>Figure 4.29: Plot of molybdenum against Al₂O₃ for the Niveau Pacquier (NP), Briestroffer (BL), Folkestone Gault Clay (FEW), and Amma Fatma (AF) data sets, and 'average shale' (Wedepohl, 1971).</i>	170
<i>Figure 4.30: Major elements (as Al₂O₃ wt%, CaCO₃ wt% and P₂O₅ wt%) and element ratios (Ti/Al, K/Al) for the Folkestone Gault Clay section. The pale blue data points represent samples from the grey clay sequence, whereas the shaded dark blue points represent samples from the black shale layers in the Briestroffer sequence.</i>	171
<i>Figure 4.31: Elemental ratio data for the Folkestone Gault Clay, using oxic-dysoxic and dysoxic-anoxic boundaries tentatively suggested by Jones and Manning (1994).</i>	172
<i>Figure 4.32: Summary of the Folkestone Gault Clay environment of deposition suggested by the elemental ratios, based on the tentative boundaries set by Jones and Manning (1994).</i>	173
<i>Figure 4.33: Plots of the Ni/V, (Cu+Mo)/Zn, V/(V+Ni) and the Cerium anomaly for the Folkestone Gault Clay sequence.</i>	174
<i>Figure 4.34: Enrichment factors for Mo, V, Ni and Mn from the Amma Fatma sequence.</i>	175
<i>Figure 4.35: Major elements (Al₂O₃ wt% and SiO₂ wt%) and element ratios (Si/Al and Ti/Al) for the Amma Fatma section.</i>	177
<i>Figure 4.36: Major elements (as CaCO₃ wt% and P₂O₅ wt%) and element ratios (K/Al) for the Amma Fatma section.</i>	178
<i>Figure 4.37: Elemental ratio data for the Amma Fatma sequence, using oxic-dysoxic and dysoxic-anoxic boundaries tentatively suggested by Jones and Manning (1994).</i>	180
<i>Figure 4.38: Elemental ratio data for the Amma Fatma sequence using the tentative boundary proposed by Kimura and Watanabe (2001) for the V/(V+Ni) ratio.</i>	181
<i>Figure 4.39: Summary of the Amma Fatma environment of deposition suggested by the elemental ratios, based on the tentative boundaries set by Jones and Manning (1994).</i>	182

<i>Figure 5.1: Idealised S/C plots of normal marine environments and euxinic environments, and a more realistic S/C plot for euxinic environments (adapted from Raiswell and Berner, 1985).</i>	188
<i>Figure 5.2: Theoretical interpretations of Fe-S-C ternary diagrams (adapted from Arthur and Sageman, 1994).</i>	192
<i>Figure 5.3: Diagrammatic explanations of the two possible causes of a positive S/C slope in euxinic conditions (from Raiswell and Berner, 1985).</i>	196
<i>Figure 5.4: Proposed S/C, DOP vs. Corg and FeT vs. Corg plots for the two possible scenarios that could lead to a positive S/C slope in euxinic conditions – (a) organic carbon limited pyrite formation; and (b) reactive iron limited pyrite formation (adapted from Raiswell and Berner, 1985).</i>	197- 198
<i>Figure 5.5: Labeled photograph of the reaction apparatus used by the University of Leeds in the determination of Chromium Reducible Sulphur.</i>	205
<i>Figure 5.6: Total sulphur, Total Organic Carbon (TOC), inorganic carbon and calcium carbonate contents (in wt%) for the Niveau Pacquier samples. The proposed division of 2 wt% TOC is represented by the red line.</i>	209
<i>Figure 5.7: Total sulphur, Total Organic Carbon (TOC), inorganic carbon and calcium carbonate contents (in wt%) for the Briestroffer samples. The proposed division of 2 wt% TOC is represented by the red line.</i>	210
<i>Figure 5.8: Total sulphur, Total Organic Carbon (TOC), inorganic carbon and calcium carbonate contents (in wt%) for the Folkestone Gault Clay samples. The proposed division of 2 wt% TOC is represented by the red line.</i>	211
<i>Figure 5.9: Total sulphur, Total Organic Carbon (TOC), inorganic carbon and calcium carbonate contents (in wt%) for the Amma Fatma samples. The proposed division of 2 wt% TOC is represented by the red line.</i>	212
<i>Figure 5.10: Plot of Total Organic Carbon against Inorganic Carbon (wt % CaCO₃) for the Niveau Pacquier Grey Clay and Black Shale samples, the Briestroffer Grey Clay and Black Shale samples, the Folkestone Gault Clay samples and the Amma Fatma samples.</i>	214
<i>Figure 5.11: A plot of sulphur vs. organic carbon of the Niveau Pacquier sample sets.</i>	215
<i>Figure 5.12: A plot of sulphur vs. organic carbon of the Briestroffer sample sets.</i>	215
<i>Figure 5.13: A plot of sulphur vs. organic carbon of the Folkestone Gault samples.</i>	216
<i>Figure 5.14: A plot of sulphur vs. organic carbon of the Amma Fatma samples.</i>	216
<i>Figure 5.15: A cumulative bar chart of the Niveau Pacquier samples, showing the relative proportions of Pyrite Iron (Fe_{P_y}), Non-pyritic Highly Reactive Iron (FeD), Poorly Reactive Iron (FeH-FeD) and Unreactive Iron (FeT-FeH-Fe_{P_y}).</i>	218
<i>Figure 5.16: A cumulative bar chart of the Briestroffer samples, showing the relative proportions of Pyrite Iron (Fe_{P_y}), Non-pyritic Highly Reactive Iron (FeD), Poorly Reactive Iron (FeH-FeD) and Unreactive Iron (FeT-FeH-Fe_{P_y}).</i>	218
<i>Figure 5.17: A cumulative bar chart of the Folkestone Gault Clay samples, showing the relative proportions of Pyrite Iron (Fe_{P_y}), Non-pyritic Highly Reactive Iron (FeD), Poorly Reactive Iron (FeH-FeD) and Unreactive Iron</i>	219

<i>(FeT-FeH-Fe_{PV}).</i>	
<i>Figure 5.18: A cumulative bar chart of the Amma Fatma samples, showing the relative proportions of Pyrite Iron (Fe_{PV}), Non-pyritic Highly Reactive Iron (FeD), Poorly Reactive Iron (FeH-FeD) and Unreactive Iron (FeT-FeH-Fe_{PV}).</i>	219
<i>Figure 5.19: Plot of Pyrite Iron against Total Iron for the Niveau Pacquier Grey Clay and Black Shale samples, the Briestroffer Grey Clay and Black Shale samples, the Folkestone Gault Clay samples and the Amma Fatma samples.</i>	220
<i>Figure 5.20: Ternary Fe-S-C plots of the: (a) Niveau Pacquier Grey Clay samples; and (b) Niveau Pacquier Black Shale samples. The blue line represents the 'ideal' regression line of data from normal marine settings whereas the red line represents full pyritisation of iron within an euxinic setting (after Arthur and Sageman, 1994).</i>	222
<i>Figure 5.21: Ternary Fe-S-C plots of the: (a) Briestroffer Grey Clay samples; and (b) Briestroffer Black Shale samples. The blue line represents the 'ideal' regression line of data from normal marine settings whereas the red line represents full pyritisation of iron within an euxinic setting (after Arthur and Sageman, 1994).</i>	223
<i>Figure 5.22: Ternary Fe-S-C plots of the Folkestone Gault Clay samples. The blue line represents the 'ideal' regression line of data from normal marine settings whereas the red line represents full pyritisation of iron within an euxinic setting (after Arthur and Sageman, 1994).</i>	224
<i>Figure 5.23: Ternary Fe-S-C plots of the Amma Fatma samples. The blue line represents the 'ideal' regression line of data from normal marine settings whereas the red line represents full pyritisation of iron within an euxinic setting (after Arthur and Sageman, 1994).</i>	224
<i>Figure 5.24: The Degree of Pyritisation, Indicator of Anoxia (IA) and Total Iron data for the Niveau Pacquier samples (Black Shale samples are identified as the darker shaded data points compared to the lighter Grey Clay data points).</i>	226
<i>Figure 5.25: The Degree of Pyritisation (DOP), Indicator of Anoxia (IA) and Total Iron data for the Briestroffer samples (Black Shale samples are identified as the darker shaded data points compared to the lighter Grey Clay data points).</i>	227
<i>Figure 5.26: The Degree of Pyritisation (DOP), Indicator of Anoxia (IA) and Total Iron data for the Folkestone Gault Clay samples. The red line marks the Normal Marine – Restricted boundary (Raiswell et al., 1988), and the dashed purple line marks the lower limit that Raiswell et al. (1988) suggested defines 90% of Inhospitable Bottom Water samples.</i>	228
<i>Figure 5.27: The Degree of Pyritisation (DOP), Indicator of Anoxia (IA) and Total Iron data for the Amma Fatma samples. The red line marks the Normal Marine – Restricted boundary (Raiswell et al., 1988), and the dashed purple line marks the lower limit that Raiswell et al. (1988) suggested defines 90% of Inhospitable Bottom Water samples.</i>	229
<i>Figure 5.28: DOP against TOC, and FeT against TOC plots for the Niveau Pacquier samples.</i>	231
<i>Figure 5.29: DOP against TOC, and FeT against TOC plots for the Briestroffer samples.</i>	232

<i>Figure 5.30: DOP against TOC, and FeT against TOC plots for the Folkestone Gault Clay samples.</i>	233
<i>Figure 5.31: DOP against TOC, and FeT against TOC plots for the Amma Fatma samples.</i>	234
<i>Figure 6.1: Proposed position of the redox boundary (red line) under the range of different palaeo-oxygenation regimes (adapted from Arthur and Sageman, 1994).</i>	243
<i>Figure 6.2: Proposed categories of pyrite morphology with examples (pale yellow represent pyrite and the scale bar represents 20 μm in each diagram).</i>	244
<i>Figure 6.3: Table combining the water oxygenation and sediment geochemistry categories from the taphonomy scheme of Brett and Baird (1986) (Figure 3.2) with the proposed descriptive categories of pyrite morphology (Figure 6.2).</i>	247
<i>Figure 6.4: Summary plot of molybdenum enrichment factor data for the Niveau Pacquier, Briestroffer, Folkestone Gault Clay and Amma Fatma sediments. The red line represents the enrichment factor of 'normal shale' (Wedepohl, 1971).</i>	251
<i>Figure 6.5: Summary plot of vanadium enrichment factor data for the Niveau Pacquier, Briestroffer, Folkestone Gault Clay and Amma Fatma sediments. The red line represents the enrichment factor of 'normal shale' (Wedepohl, 1971).</i>	253
<i>Figure 6.6: Summary plot of nickel enrichment factor data for the Niveau Pacquier, Briestroffer, Folkestone Gault Clay and Amma Fatma sediments. The red line represents the enrichment factor of 'normal shale' (Wedepohl, 1971).</i>	254
<i>Figure 6.7: Summary diagram of palaeo-oxygenation conditions of the four study sites according to the trace-metal ratio numerical boundaries proposed by Jones and Manning (1994).</i>	256
<i>Figure 6.8: Numerical boundaries proposed by Jones and Manning (1994) to define palaeo-oxygenation conditions.</i>	257
<i>Figure 6.9: Numerical boundaries proposed to define palaeo-oxygenation conditions based on the data from this study.</i>	257
<i>Figure 6.10: V/Sc summary plot for Niveau Pacquier, Breistroffer and Amma Fatma samples. The red line represents the upper limits of 'normal marine' conditions according to Kimura and Watanabe (2001).</i>	259
<i>Figure 6.11: Plot of authigenic uranium (Ua) against TOC for each data set (Niveau Pacquier (NP), Amma Fatma (AF), Briestroffer (BL) and Folkestone Gault Clay (FEW)). A numerical boundary at a Ua value of 1, and another at a TOC value of 2 wt% allows division of the data into three zones which may represent different palaeo-oxygenation regimes.</i>	262
<i>Figure 6.12: Summary plot of Indicator of Anoxia data for the Niveau Pacquier, Briestroffer, Folkestone Gault Clay and Amma Fatma sediments.</i>	265
<i>Figure 6.13: Plots of the molybdenum Enrichment Factor multiplied by the Indicator of Anoxia ([Mo EF x IA]) for the (a) Niveau Pacquier; (b) Briestroffer; (c) Folkestone Gault Clay; and (d) Amma Fatma samples. In (a) and (b) the darker triangular colour data points represent the black shale samples and the lighter colour circular data points represent the grey clay samples.</i>	266

1. INTRODUCTION

“The phenomenon of severe oxygen depletion in continental shelf waters is of great significance to both geologists and marine biologists.”

(Tyson and Pearson, 1991, p.1)

While small-scale seasonal anoxia is observed during the summer on modern continental shelves (Tyson and Pearson, 1991), there is evidence that larger scale Oceanic Anoxic Events have occurred in the past, giving rise to supra-regional deposition of organic-rich sediments (Schlanger and Jenkyns, 1976). The study of low-oxygen events such as these generate interest from a variety of sources. A large proportion of the world’s petroleum is associated with ancient marine organic-rich sediments whose sedimentological, geochemical and faunal characteristics suggest that oceanic bottom waters were oxygen-depleted or oxygen-free during the time of deposition (Tyson and Pearson, 1991). In addition to this, Oceanic Anoxic Events are believed to coincide with extremes of climate (Reichelt, 2005) and ocean stagnation plays a major part in many of the models used to explain the occurrence of low-oxygen conditions (Koutsoukos *et al.*, 1991). This has particular connotations for forward outcome modelling of global warming and rapid climate change scenarios.

In modern low-oxygen settings it is possible to compare sediment properties directly with the dissolved oxygen contents of the overlying waters. As this is not possible for ancient deposits, a number of sedimentological, geochemical and faunal proxies have been proposed to give an indication of the oxygenation conditions at the time of deposition. Interpretation of these proxies is key to understanding the extent of oxygen reduction and the nature of these low oxygen events. While some work has been done to compare and contrast the results of different proxies (e.g. Jones and Manning, 1994), there is still considerable debate about the applicability and reliability of these techniques. This project compares the results of a variety of palaeo-oxygenation proxies run on samples from four different Cretaceous marine sequences which are thought to have been laid down under a range of different oxygenation regimes. The following sections introduce the project in more detail:

- **Section 1.1** outlines the terminology used to describe low-oxygen facies and introduces some of the main theories proposed to explain the formation of Oceanic Anoxic Events;
- **Section 1.2** introduces the four Cretaceous marine sequences investigated in this project;
- **Section 1.3** introduces the range of proxies investigated and outlines the project structure.

1.1 Introduction to low-oxygen events

1.1.1 Terminology

Two distinct schemes are used to describe oxygen-poor environments. Marine biologists and geochemists use the ‘-oxic’ scheme defined by precise measured oxygen values or implied oxygen values in ancient settings (Wignall, 1994). In contrast, the ‘-aerobic’ palaeoecological terminology proposed by Rhoads and Morse (1971) is based on ‘biofacies’ data for modern environments in which oxygen could be measured but the boundaries are defined by characteristic faunal and sedimentological changes.

The Biofacies Scheme is based on the effects of oxygenation levels on metazoan organisms, and Rhoads and Morse (1971) identified three categories of oxygenation conditions for which they proposed critical ranges of dissolved oxygen. These categories were recognised using faunal diversity, general degree of calcification, size, and trophic groupings of macrofauna and the occurrence of bioturbation:

- >1 ml/l dissolved oxygen – **Aerobic** conditions in which oxygen plays no role in limiting metazoan life and there is evidence of organisms, environments and/or processes that require, or are characterised by, the availability of free molecular oxygen.
- 1.0-0.1 ml/l dissolved oxygen – **Dysaerobic** conditions in which oxygen limitation plays a role in limiting metazoan life.
- <0.1 ml/l dissolved oxygen – **Azoic** – (the term Azoic has since widely been replaced with the term **Anaerobic**) in which the dissolved oxygen levels are thought to be too low to support metazoan life and there is evidence of organisms, environments and/or processes characterised by the absence of free molecular oxygen.

Rhoads and Morse (1971) suggested that the boundary between **dysaerobic** and **anaerobic** was transitional over the 0.1-0.3 ml/l range, but the data for their model came from environments very different and more stable than the shelf environments seen in ancient anoxic settings. This initial model has undergone several changes and the critical oxygen level for the suppression of obvious bioturbation, and therefore the boundary between **dysaerobic** and **anaerobic** conditions, is now suggested to correlate with 0.2 ml/l dissolved oxygen (e.g. Thompson *et al.*, 1985). Further additions to the model include dividing **dysaerobic** conditions into **upper** and **lower** factions (e.g. Rhoads *et al.*, 1991). Evidence such as the presence of non-fossilising polychaetes in traditionally '**anaerobic**' settings has led several authors to suggest a re-definition of the boundary as the term **anaerobic** was initially taken to mean no life conditions present (Tyson and Pearson, 1991) (see **Section 3.1.2**). Further additions to this scheme include the introduction of the term **exaerobic** to describe environments with dissolved oxygen contents of 0.1-0.2 ml/l which exist near to the dysaerobic/anaerobic boundary and are characterised by deposition of laminated strata and anomalous occurrences of shelly faunas (Savdra and Bottjer, 1987). Strictly these biofacies descriptions relate to the oxygen conditions at the sediment/water interface (Wignall, 1994).

The geochemical scheme was initially described by Breck (1974) who described three oxygen regimes defined by geochemical criteria:

- **oxic** – where oxygen is freely available;
- **suboxic** – a transitional regime characterised by drastic pH change and the appearance of NO₂ from nitrate reduction which is suggested to occur below 0.2 ml/l;
- **anoxic** – which is characterised by the absence of oxygen and the presence of sulphate reduction.

Strictly this form of environmental scheme should only be used to describe oxygen conditions at defined positions within the water column, for example dysoxic bottom waters (Wignall, 1994). Berner (1981) made adjustments to this scheme, in particular removing the term **suboxic**, which he felt had been falsely taken as equivalent to dysaerobic conditions, and instead labelling the categories as **oxic**, **post-oxic non-sulphidic anoxia** and **sulphidic anoxia**. Berner (1981) also used the terms **euxinic**

to describe **sulphidic anoxic** waters, allowing the term '**anoxic**' to refer solely to non-sulphidic conditions. He also suggested the use of the term **semi-euxinic** for environments where the water column regularly fluctuates between **dysaerobic** and **euxinic** conditions.

Attempts to correlate the two main schemes of criteria in defining levels of oxygen has led to the use of the term **dysoxic** to indicate that range of oxygen values associated with **dysaerobic biofacies**, for example Levin (2003) summarised a form of combining the geochemical and biofacies-based schemes:

- Anoxic conditions imply no dissolved oxygen
- Microxic implies up to 0.1ml/l dissolved oxygen (Bernhard and Sen Gupta, 1999)
- Dysoxic/dysaerobic are effectively interchangeable terms to imply 0.1-1.0ml/l dissolved oxygen

Levin (2003) also used the term **hypoxia** to imply physiologically stressful low-oxygen conditions, although he did point out that the actual dissolved oxygen level required for hypoxia is different for different species.

1.1.2 Cretaceous Oceanic Anoxic Events

The mid-Cretaceous appears to have had an extreme "greenhouse climate" (Barron and Washington, 1985) with a palaeoclimate that was affected by the major plate movements of the time and enhanced basaltic magmatism with the production of new oceanic crust and the extensive formation of continental flood basalts (Reichert, 2005). During this time, vast shelf areas were flooded (Hay *et al.*, 1999) with the Aptian representing one transgressive phase, with a mid-Aptian break related to a brief sea-level fall, and the Albian being characterised by three major flooding events, at or near the substage boundaries (Reichert, 2005). These extreme oceanic and climatic conditions may have coincided during the mid-Cretaceous to initiate the formation of black shale strata. Schlanger and Jenkyns (1976) suggested that these widespread and broadly synchronous organic carbon-rich deposits formed as the result of what they called Oceanic Anoxic Events (OAEs). They suggested that these events were caused by an expanded Oxygen-Minimum Zone (OMZ) within the water column due to the effects of transgressive sea-level pulses and reduced bottom-water oxygenation. Schlanger and Jenkyns (1976) identified two Cretaceous OAEs – the

longer and more complex Barremian-Albian OAE (OAE 1) and the shorter Cenomanian-Turonian OAE (OAE 2). Further work led to the division of OAE 1 into four separate low-oxygen events that are separated by times of dominantly oxic conditions:

- OAE 1a in the Early Aptian (e.g. Schlanger & Jenkyns, 1976; Bralower *et al.*, 1994);
- OAE 1b in the Early Albian (e.g. Br  h  ret, 1986; Herrle *et al.*, 2003);
- OAE 1c and 1d in the Late Albian (e.g. Erbacher *et al.*, 1996).

Despite the use of the term ‘Oceanic’ within the event description, Schlanger and Jenkyns (1976) were keen to point out that Oceanic Anoxic Events did not represent global anoxia. Further to this, Whatley *et al.* (2003) did not believe that Ocean Anoxic Events represent true anoxia. Instead they suggested that they represent sections of either time, space, or a combination of both, in which a substantial reduction in the level of dissolved oxygen in an ocean (or part of it) occurred.

The nature of these OAEs and the origin of the associated organic-rich sediments is still hotly debated. Tyson (1987) listed five factors that he considered to be important controls of organic matter preservation:

- **Sediment texture and grain size** – Tyson (1987) suggested that low porosity and permeability enhances organic matter preservation as it reduces the infiltration of oxygen-carrying waters and so reduces the likelihood of oxidation of organic matter after burial.
- **Water depth** – Tyson (1987) pointed out that greater transit times through the water column means greater exposure to oxygen-rich waters and therefore more organic matter oxidation. He suggested that transit time is a function of the degree of wind-mixing of the water column (basin size, climate, palaeogeography), particle size, salinity, and water depth, and that generally it is lower in shallower water, and therefore preservation is increased. However, this does not explain the regular occurrence of deep-water black shales.
- **Sedimentation rate** – M  ller and Suess (1979) proposed that high sedimentation rates enhance organic matter preservation by removing organic material from the near-surface zone of intense bacterial activity and oxidation. However, Tyson (1987) noted that many ancient black shales appear to have

exceedingly slow accumulation rates but suggests that this is hard to quantify in ancient sediments.

- **Primary production and rate of organic matter supply to the sediment** – Tyson (1987) noted that primary productivity is controlled by the supply of nutrients and that high nutrient levels causing high productivity leads to an increased flow of organic matter to the sea floor. He suggested that a large supply of organic matter to the sea floor induces ‘organic overloading’ where all available oxidants are overwhelmed, leading to benthic anoxia and the survival of a significant proportion of organic matter in the sediments below. Morford and Emerson (1999) studied the effects of ocean productivity on atmospheric carbon dioxide levels and agreed that a stronger biological pump in the ocean leads to the depletion of oxygen in the bottom waters by increased organic matter degradation.
- **Bottom-water oxygenation** – Tyson (1987) found that the only common theme in all models of black shale production is low oxygen or truly anoxic bottom waters, although the debate centers on whether this is a cause or a consequence of the processes involved in the formation of black shales.

A variety of models have been proposed to explain the formation of organic-rich shales and the discussion of these differing models tends to focus on the interplay between productivity and water-column stratification leading to reduced bottom-water oxygenation. Koutsoukos *et al.* (1991) summarised several models that have been suggested for the origin of OAE 1 and 2 and found that the proposed triggers for reduction of oxygenation fell within these categories:

- restricted palaeogeographic settings;
- sluggish or non-existent circulation;
- increased continental run-off linked to salinity stratification within the water column;
- local upwelling conditions and expansion of existing oxygen-minimum zones;
- high phytoplankton productivity;
- intense and widespread deep-sea volcanic activity;
- development of a mid-water oxygen-minimum layer.

It is possible that a combination of some or all of these processes on a regional or larger scale may initiate, or simply act to prolong the imprint of these low-oxygen events in the sediment record (Koutsoukos *et al.*, 1991).

In essence, the debate is focussed on two general types of models which encompass many of the factors identified by Koutsoukos *et al.* (1991) – (a) high productivity models and (b) preservation models (Wignall and Newton, 2001).

1.1.2.1 High-Productivity Models

High-productivity models suggest that nutrient-stimulated high primary productivity increases the flux of organic matter to the sea floor which means that more oxygen is used up from the water column in the decay of this material (Wignall and Newton, 2001). In these models the dysoxia or anoxia is thought to be a consequence, not a cause, of the elevated organic carbon flux (Pederson and Calvert, 1990), and events such as plankton blooms have been invoked as the cause of specific high-productivity black shales (e.g. Leckie, 1990). In support of this model, Wignall (1994) suggested that there are common reports of a high abundance of lipid-rich material in black shales which he believed suggests a planktonic origin for the organic matter. Tyson (1987) concluded that primary productivity is controlled by the supply of nutrients and the highest supplies are found in zones of upwelling along the western margins of continents and in shelf seas with high runoff from the adjacent land. This could explain the fact that although black shales are typically associated with deep-water basinal locations, thin examples often occur in more marginal locations, particularly within transgressive sedimentary records (Wignall and Newton, 2001). Erbacher *et al.* (1996) proposed two different modes of OAE development involving increased organic carbon fluxes to the sea floor from differing sources, related to particular phases in transgressive and regressive sequences:

- Erbacher *et al.* (1996) coined the phrase ‘productivity-OAEs’ (p-OAEs) for anoxic events during transgressive sequences at times of maximum flooding/sea-level highstands (OAE 1b and 1d, OAE2). They suggested that the reduction in oxygenation was caused by leaching of nutrients from coastal low lands which led to increased fertilization and increased productivity in adjacent ocean basins. They suggested that this leads to the expansion of the Oxygen-Minimum Zone (OMZ) ocean-wide and high productivity anoxia

develops in the pelagic environment causing increased preservation of organic matter. The OMZ is caused by the decay of organic material from plankton directly below the oceanic thermocline and in normal conditions exhibits a 25-50% reduction in dissolved oxygen (Tyson and Pearson, 1991). Tyson and Pearson (1991) suggested that this level of reduced oxygenation is not great enough to have a pronounced biological or geochemical effect, but that dysoxic or suboxic conditions can be reached in areas where upwelling leads to high productivity along the ocean margins. In summary, Erbacher *et al.* (1996) suggested that anoxic events are triggered by leaching of nutrients from weathering during flooding, which increases the production of marine organic material and the resultant flux of organics to the sea floor.

- Erbacher *et al.* (1996) used the phrase ‘detrital-OAEs’ (d-OAE) to describe anoxic events that occur during regressive periods at a time of maximum sea-level fall (OAE 1c). They suggested that in this case, a high input of organic matter from detrital sources and high sedimentation rates leads to increased preservation of black shale organic matter. In this model the increase in the flux of organic matter to the sea floor induces anoxia, but the detrital origin of the organic material means that no increase in productivity occurs.

1.1.2.2 Preservation Models

Preservation models suggest that dysoxia/anoxia is the cause of enhanced organic matter preservation under conditions that are not necessarily highly productive (Demaison and Moore, 1980). In these models, advective supply of dissolved oxygen to bottom waters is usually considered to be inhibited by the presence of a strong density interface such as a thermocline or pycnocline within the water column which limits mixing (Wignall and Newton, 2001). In the Black Sea the presence of anoxic bottom waters beneath a halocline, which has developed due to salinity contrasts, led to it initially being proposed as the model for the deposition of many ancient black shales (Wignall, 1994). However, Hallam (1980) pointed out that while the Black Sea provides an excellent example of a barred ‘euxinic’ basin model, this does not fit the environment of the majority of ancient ‘black shales’ which were evidently marine. Also in the majority of examples where density interfaces have been inferred to explain ancient black shale deposits, they are suggested to be in the form of a thermocline rather than a halocline (Wignall and Newton, 2001). Rhoads and Morse

(1971) believed that the epicontinental sea basins which formed much of the Palaeozoic strata were oxygen-stratified and it is suggested that the oxic-dysoxic-anoxic partitioning was relatively stable because of restricted vertical circulation which in itself was a function of palaeogeography and palaeoclimate (Speyer and Brett, 1988). In contrast to this idea, Wilson and Norris (2001) used stable-isotope records from foraminifera to show that the thermal structure of surface waters in the western tropical Atlantic Ocean underwent pronounced variability about 100 Ma which they suggested culminated in a collapse of upper-ocean stratification during OAE-1d. Wilson and Norris (2001) suggested that their results are inconsistent both with explanations for OAEs based on ocean stagnation, and with the traditional view that past warm periods were more stable than today's climate.

A potential flaw in preservation models is the relationship between ocean circulation and surface productivity. While ocean mixing acts to destroy vertical gradients in oxygen and other chemical species, it also returns nutrients to the surface that fuel the biological activity and organic-matter decomposition required to sustain gradients (Hotinski *et al.*, 2001). Seasonal stratification is observed in modern shelf environments during the summer where the reduced wind-driven turbulence allows a strong thermocline to develop (Tyson and Pearson, 1991). Tyson and Pearson (1991) suggested that Milankovitch-scale climate variations may be responsible for allowing the formation of more established thermocline development in shallow waters during 'favourable' periods and that this may hold the key to the initiation of black shale deposition. However, they also noted that modern-day summer stratification does lead to a reduction of the vertical mixing of nutrients and so reduces productivity which theoretically would minimize black shale deposition as the organic carbon flux to the sea floor would be reduced. Similar questions have been raised about the end Permian anoxic event. While this is commonly believed to have been caused by ocean stagnation, Hotinski *et al.* (2001) pointed out that complete stagnation would lead to decreasing upwelling supplies of nutrients to the photic zone which should cause decreased productivity. Hotinski *et al.* (2001) modeled the biogeochemical system and showed that a low equator-to-pole temperature gradient could have led to weak ocean circulation and widespread anoxia. However they suggested that at least half of this oxygenation effect is due to decreased oxygen solubility in the warmer polar waters where water sinks to form bottom water. Hotinski *et al.* (2001) claimed

that their model results were consistent with Herbert and Sarmiento's (1991) box model of the Cretaceous and that the reduced gradient scenario leads to widespread anoxia but relatively high rates of ventilation and reduced productivity would have kept deep-ocean environments at the oxic/anoxic boundary rather than fully anoxic.

Some authors have proposed that the mechanism for black shale formation involves a compromise between these two models. Adelson *et al.* (2001) suggested that a balance occurs between these two ideas and that low-oxygen conditions arise when respiration of organic matter within the water column approaches or exceeds ventilation in deep waters. They concluded that nutrient fluxes externally control the extent of sinking organic matter and therefore control deep-water respiration. In contrast, they stated that advective and diffusive processes control deep-water ventilation which controls the oxygen levels within the water. They suggested that either an increase in nutrients or reduction in ventilation, due to weather and climate or external changes in adjacent basins, can lead to reduced oxygen levels. Morford and Emerson (1999) agreed that a combination of the organic carbon 'rain rate' and bottom-water oxygen concentration strongly affects the extent of oxygen penetration in pore waters beneath the sediment surface. They suggested that changes in either the rain rate of organic matter or the deep-ocean oxygen concentration result in a change of redox state in the surface sediments which could further emphasise the effects of either model in the preservation of organic matter.

It is possible that different mechanisms are responsible for different low oxygen events. While stating that most OAEs are thought to be caused by high productivity, Erbacher *et al.* (2001) suggested that stable-isotope data from OAE 1b point to increased thermohaline stratification as the probable cause of ocean anoxia. They suggested that OAE 1b is associated with an increase in surface-water temperatures and runoff that led to decreased bottom-water formation and elevated carbon burial in the restricted basins of the western Tethys and North Atlantic. In contrast, Nederbragt *et al.* (2001) studied micro- and nanofossil data from a section across the Albian OAE 1d at the Albian-Cenomanian boundary and suggest that improved preservation of organic matter due to a decrease in oxygen content in a shallow oxygen-minimum zone is a more likely cause for the Albian-Cenomanian boundary anoxic event than an increase in productivity. Turgeon and Creaser (2008) concluded

that while either increased primary productivity or enhanced preservation scenarios can explain the preservation of high levels of organic matter in black shales, the current debate is focussed on the nature of the trigger mechanism which they proposed, for OAE 2, is related to large-scale magmatic activity.

1.2 Introduction to the sites

1.2.1 Niveau Pacquier

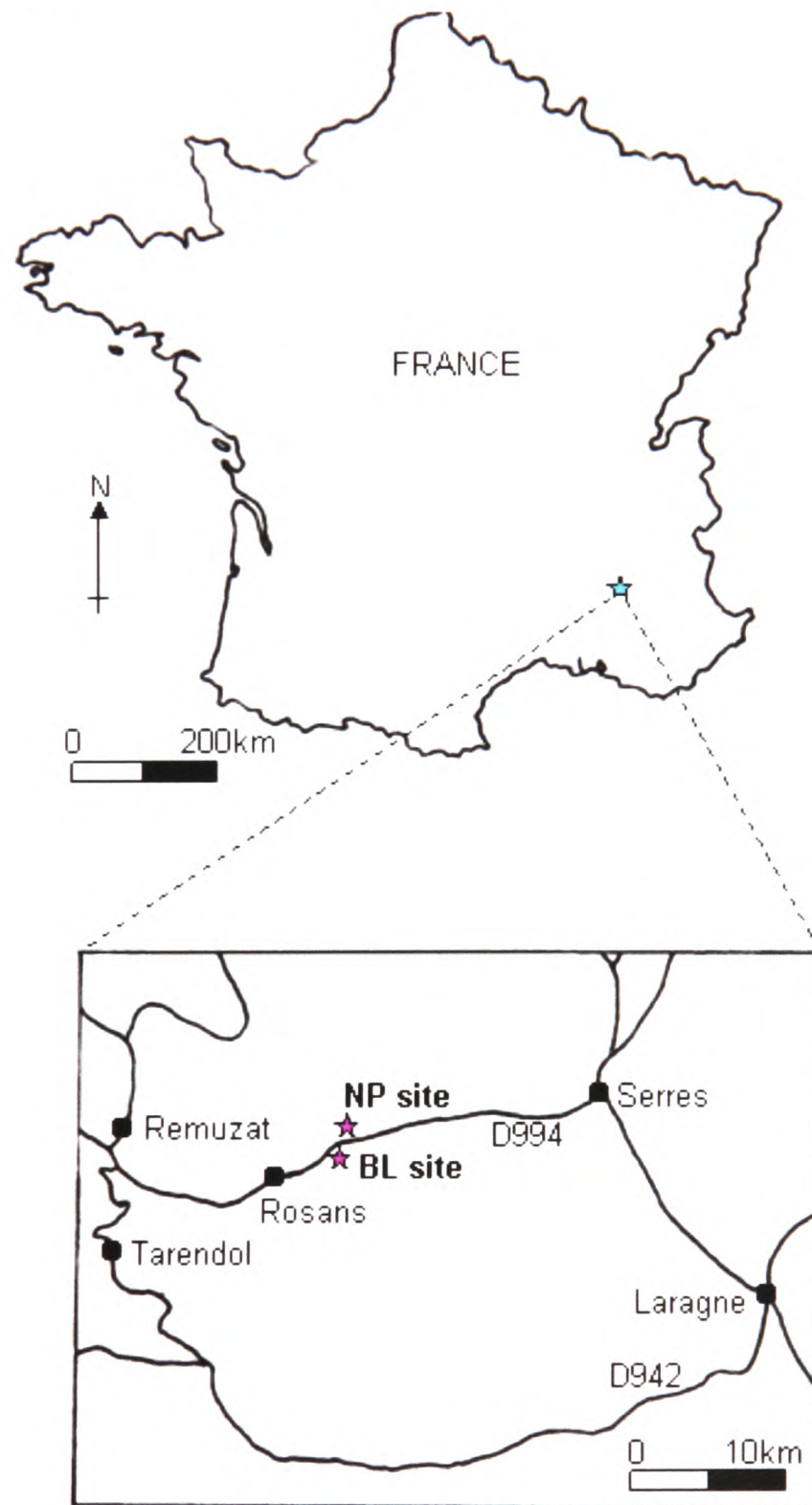


Figure 1.1: Location map of the Niveau Pacquier (NP) (Latitude 44° 24' 13.0"N, Longitude 5° 31' 32.2"E) and Briestroffer (BL) (Latitude 44° 24' 11.9"N, Longitude 5° 31' 34.7"E) sample sites near Rosans, south east France.

The Niveau Pacquier Formation of the Vocontian Basin, south east France (see *Figure 1.1*), is thought to represent part of the super-regional deposition of black shales associated with the Late Aptian-Early Albian Oceanic Anoxic Event 1b (OAE1b) (Br  h  ret, 1986). Similar horizons have been found in several Ocean Drilling Program and Deep Sea Drilling Project sites in the Atlantic ocean (e.g. Br  h  ret, 1997; Erbacher *et al.*, 2001; Herrle *et al.*, 2003).

Sedimentological and geochemical samples were collected for this study by the author from an exposure of the Niveau Pacquier Formation at Col de Palluel in the Vocontian Basin, South East France (see *Figure 1.2 and 1.3*). The section is found on the north side of the D994 road at a sharp bend 5 km from Rosans (see *Figure 1.1*). Samples were collected from a section starting in the Marnes Bleues Formation 1 m below the base of the main black shale horizon, and finishing in the Marnes Bleues 1.75 m above this point (see *Figure 1.4*). The palaeontological samples used in this study were collected from this site by Professor Andy Gale, and stored at the Oxford University Museum of Natural History.

The base of the first black shale horizon has been proposed as the Global Boundary Point for the Aptian-Albian boundary and coincides with the first appearance of the ammonite *Leymeriella tardefurcata* (Kennedy *et al.*, 2000).

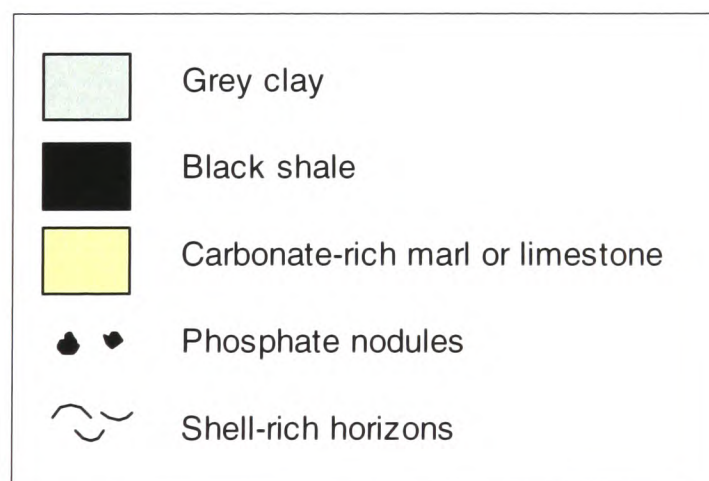
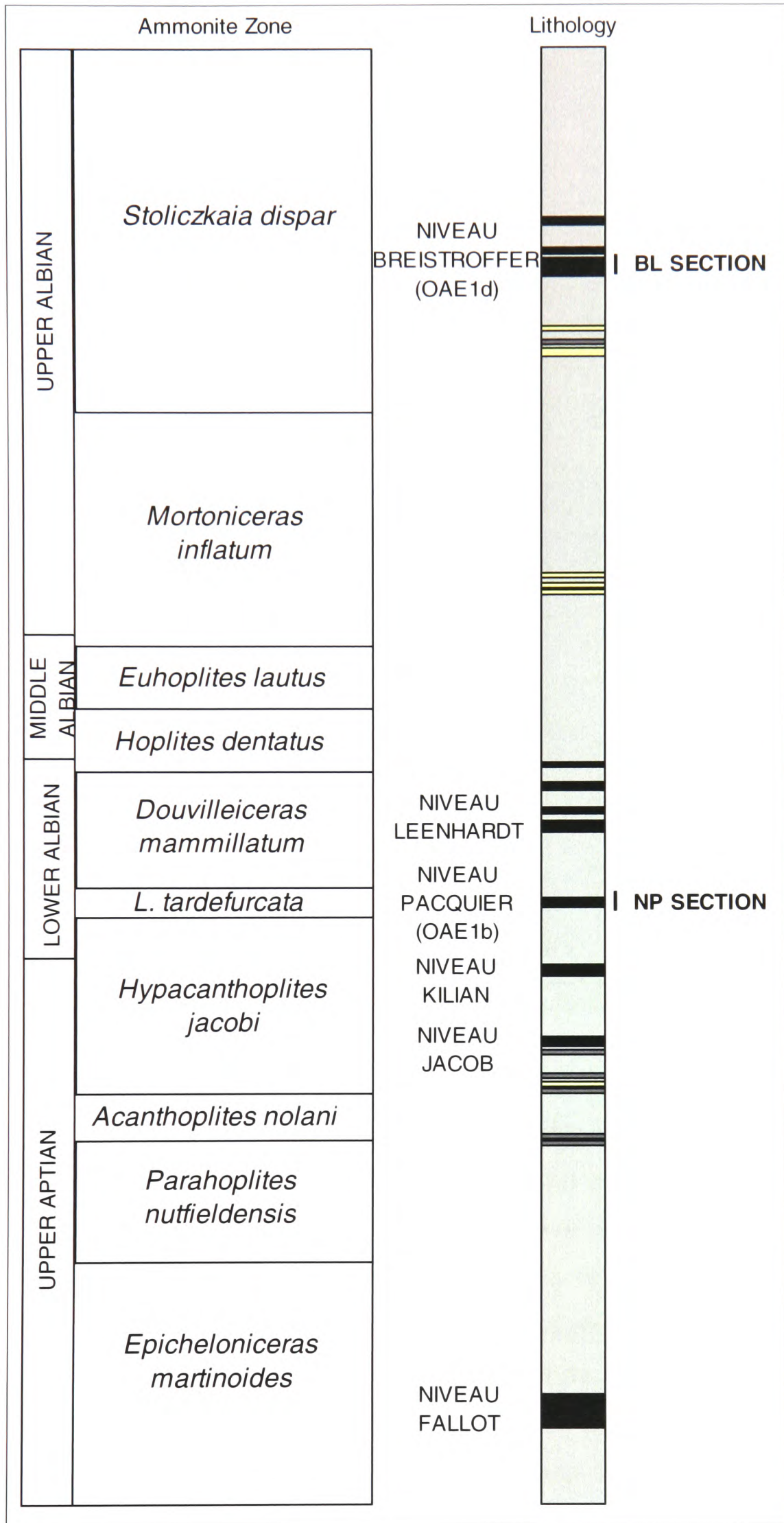


Figure 1.2: Key to the stratigraphic logs.

*Figure 1.3: Stratigraphic log of the sequence laid down in the Vocontian Basin between the Upper Aptian and the Upper Albian (after Bornemann *et al.*, 2005). The labelled sections represent the Niveau Pacquier OAE1b sequence (labelled NP Section) and the Briestoffer OAE1d sequence (labelled BL section) (on next page).*



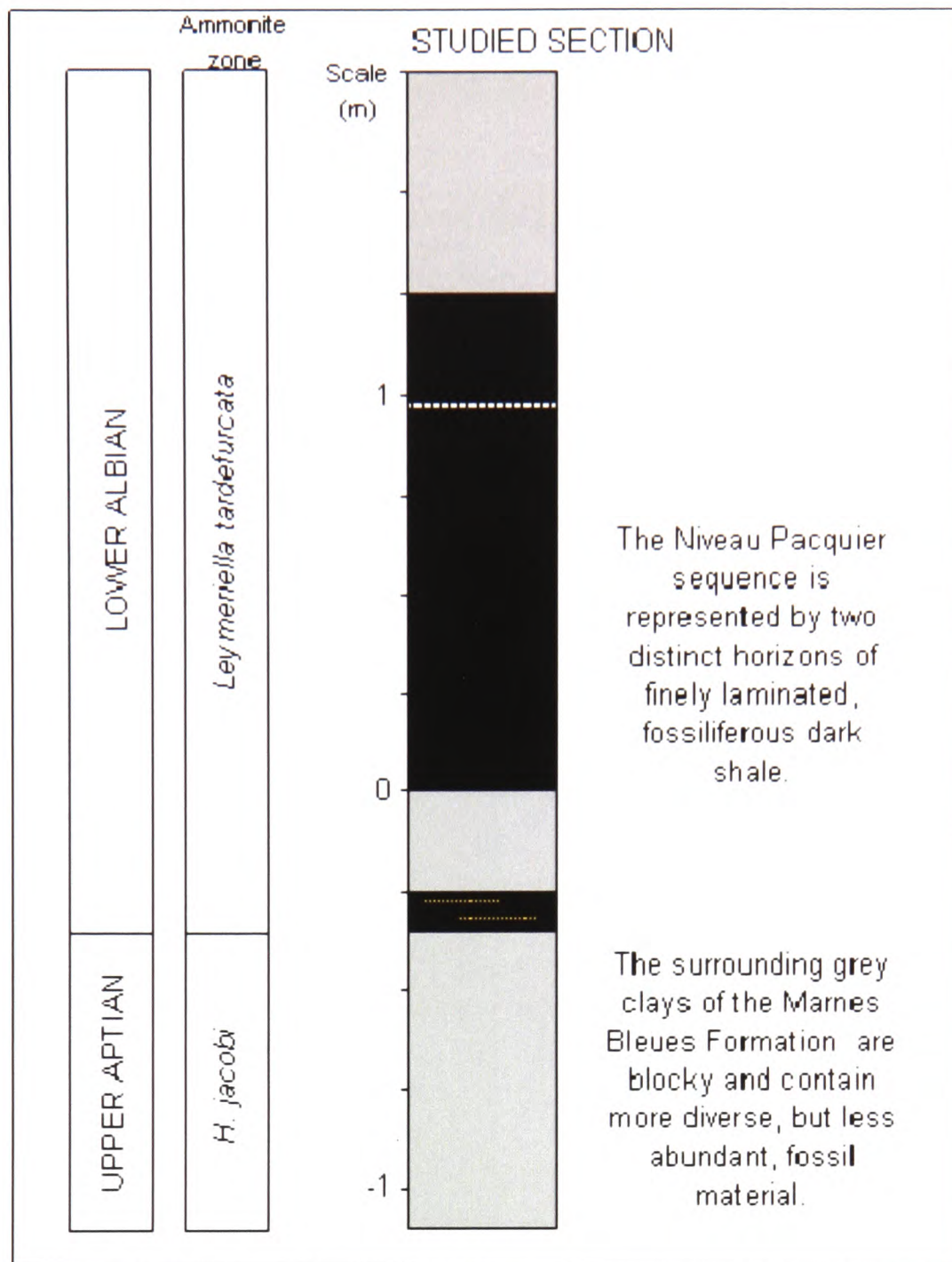


Figure 1.4: Stratigraphic log of the studied Niveau Pacquier section

1.2.2 Briestroffer

The Late Albian OAE 1d has been studied in strata from the Vocontian Basin in south east France (Br  chet, 1988; Giraud *et al.*, 2003) and the Mazagan and Blake Nose Plateau in the Atlantic Ocean (Nederbragt *et al.* 2001; Wilson and Norris 2001). Wilson and Norris (2001) provided an overview of the supra-regional occurrence of the OAE 1d black shales. Sedimentological and geochemical samples were collected for this study by the author from an exposure of the sequence of black shales referred to as Niveau Briestroffer (Br  chet, 1988) at Col de Palluel in the Vocontian Basin, south east France (see *Figure 1.3*). The section is found on the south side of the D994 road, on the northern slope of Mount Risou, at a sharp bend 5 km from Rosans (see *Figure 1.1*). Gale *et al.* (1996) use the term ‘Niveau Briestroffer’ to describe a bundle of five black shale units within 10 m of the section at Col de Palluel (see

Figure 1.5). The palaeontological samples used in this study were collected from this site by Professor Andy Gale, and stored at the Oxford University Museum of Natural History.

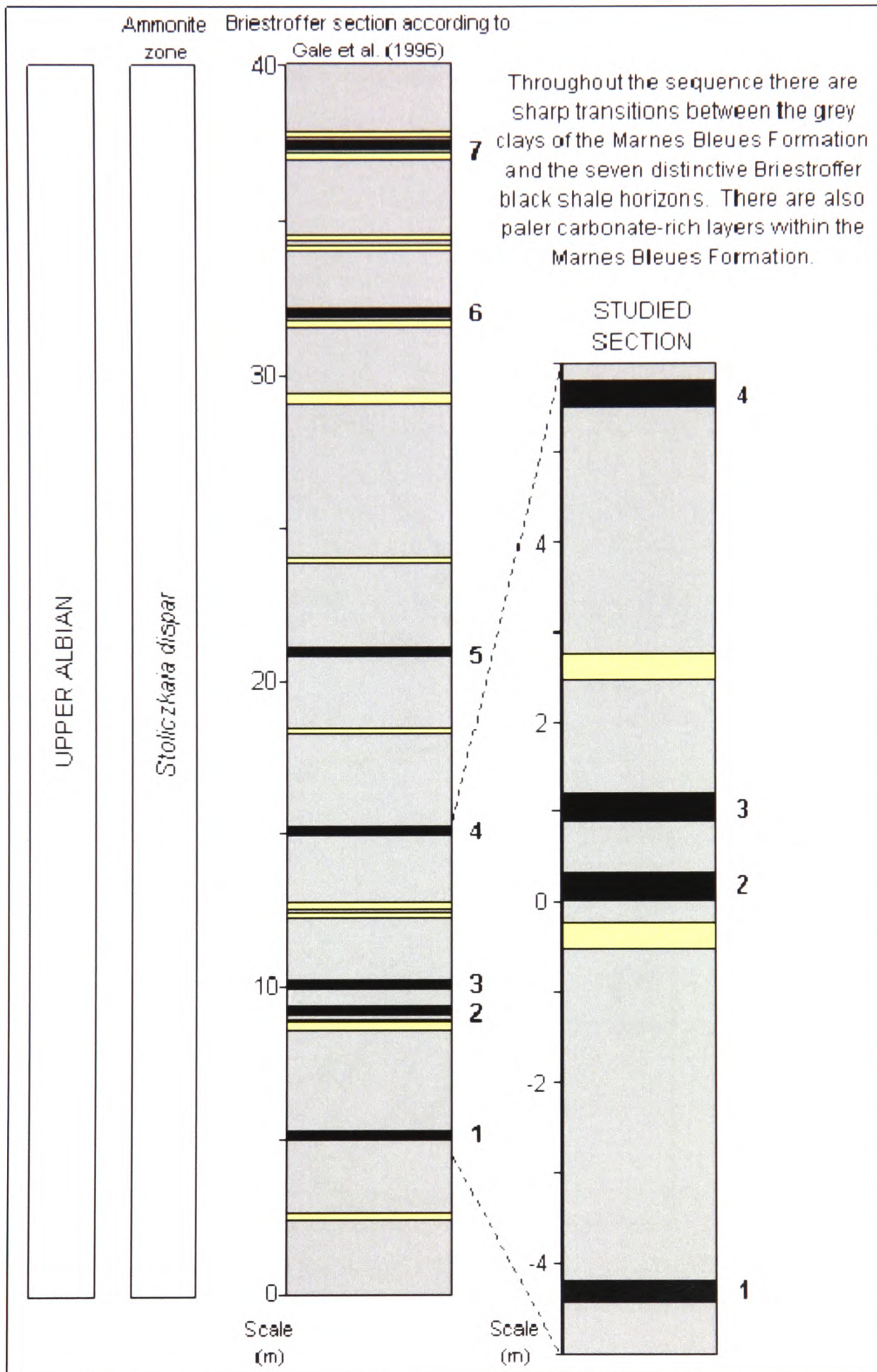


Figure 1.5: Stratigraphic log showing the Briestroffer sequence according to Gale et al. (1996), which contains seven black shale horizons, and the section studied which encompasses the lower four of these black shale horizons.

In contrast, Br  chet (1997) described the Niveau Briestroffer strata as seven black shale bundles within a 40 m section labelled BR1 to BR7. Gale *et al.*'s (1996) shale units comprise BR2 and BR3 of Breheret's scheme. For sampling purposes the base of Gale *et al.*'s (1996) second black shale horizon was taken as the reference point and samples were collected to 5 m below and 6 m above this point, encompassing four black shale horizons (see *Figure 1.5*).

1.2.3 Folkestone Gault Clay

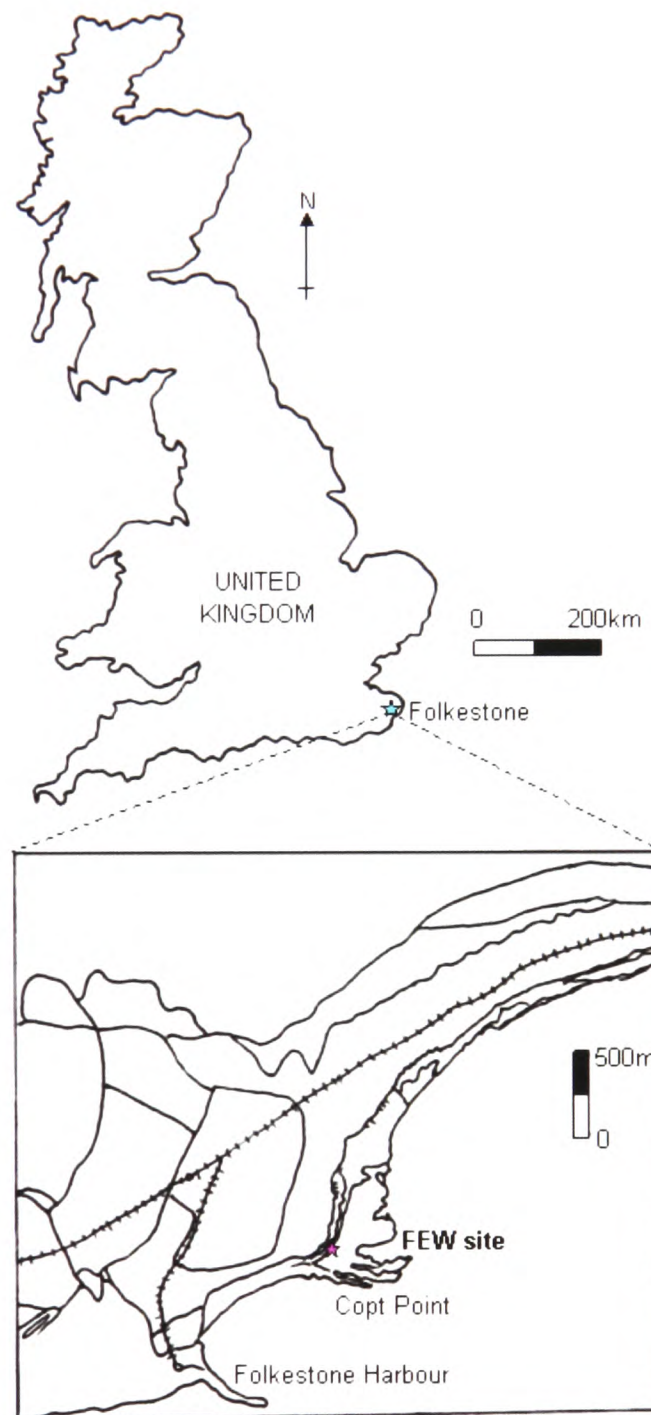


Figure 1.6: Location map of the Gault Clay exposure (labelled FEW site) (Latitude 51° 5' 1.0"N, Longitude 1° 11' 56.0"E) at Copt Point, Folkestone, south east England.

The late Albian Gault Clay sequence in Folkestone consists of grey bioturbated marine clays containing several horizons rich in phosphatic nodules (see *Figure 1.7*). All sampling of the Gault Clay section was carried out by the author.

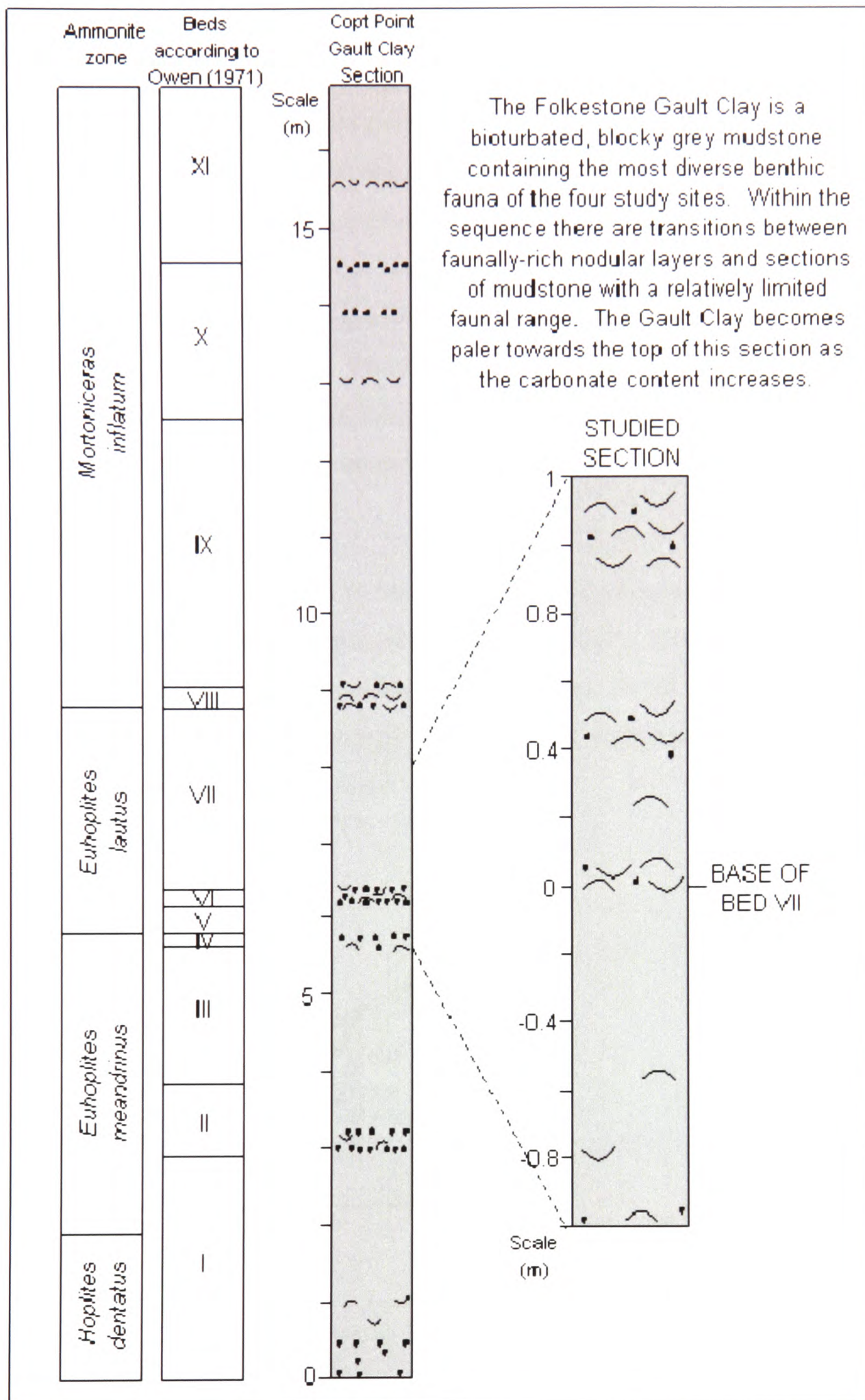


Figure 1.7: Stratigraphic logs of the Folkestone Gault Clay exposure, with beds assigned by Owen (1971), and the section studied, which is centred around the base of Bed VII.

The relatively diverse benthos observed throughout the sequence is indicative of a more oxygenated depositional environment than the other studied sites and so provides a good basis for comparison of the results of various palaeo-oxygenation proxies. The Gault Clay overlies the Lower Greensand in the Weald sequence and was deposited during a transgressive episode that resulted from regional subsidence and eustatic sea-level rise. The examined section forms a cliff exposure of the Gault Clay at Copt Point in Folkestone, 400 m along the beach from the eastern end of the promenade (see *Figure 1.6*). The Gault Clay was sub-divided into thirteen 'beds' by Owen (1971) and the samples for this study were collected through a section from 1 m below the base of Bed VII up to 1.15 m above this point (see *Figure 1.7*).

1.2.4 Amma Fatma

The Amma Fatma sequence is found within the Tarfaya basin which lies along the Atlantic coast in south west Morocco (see *Figure 1.8*). The sampled section is a low cliff exposure located 65 km south west of Tantan, on the west side of the Oued El Amra where it meets the coastal lowland. The samples used in this study were collected by Professor Andy Gale.

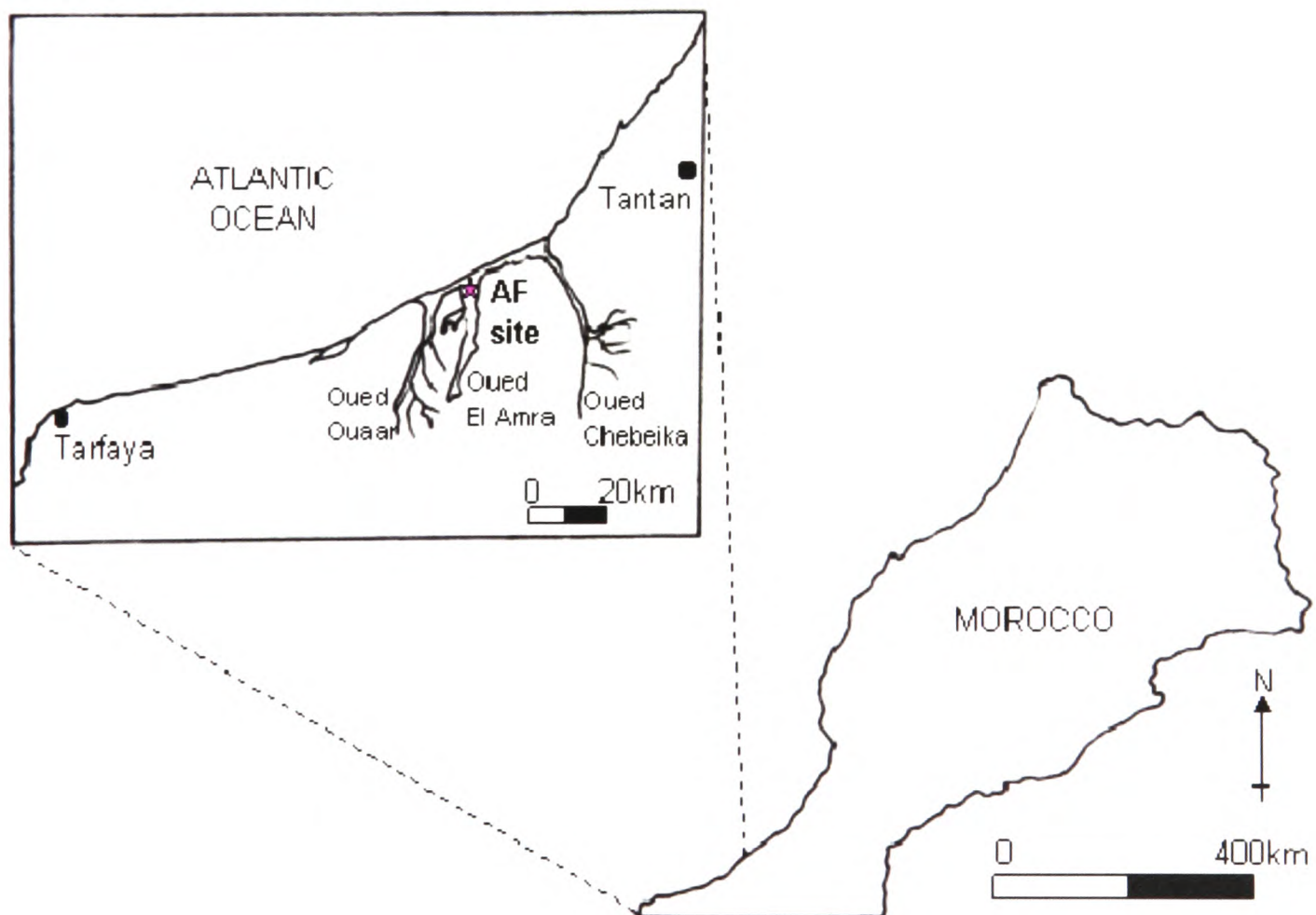


Figure 1.8: Location map of the Amma Fatma sequence (AF site) (Latitude 28° 11' 53.5"N, Longitude 11° 46' 32.2"W) in the Tarfaya Basin, Morocco.

The sedimentary evolution of the basin has been driven by subsidence since the Triassic which has been closely linked to the opening of the Atlantic Ocean (El Albani *et al.* 2001). While the Lower Cretaceous sediments are mainly deltaic (Kolonic *et al.*, 2002), the Upper Cretaceous deposits are characterised by dark laminated marls and lighter, often nodular limestones (Luning *et al.*, 2004) which are thought to have resulted from repeated and widespread flooding from a series of major transgressive cycles (Kolonic *et al.*, 2002). The resultant sediments are rich in biogenic carbonate and organic matter and are thought to have been laid down in a nutrient-rich environment where an open-shelf upwelling system had developed (Kuhnt *et al.*, 2001).

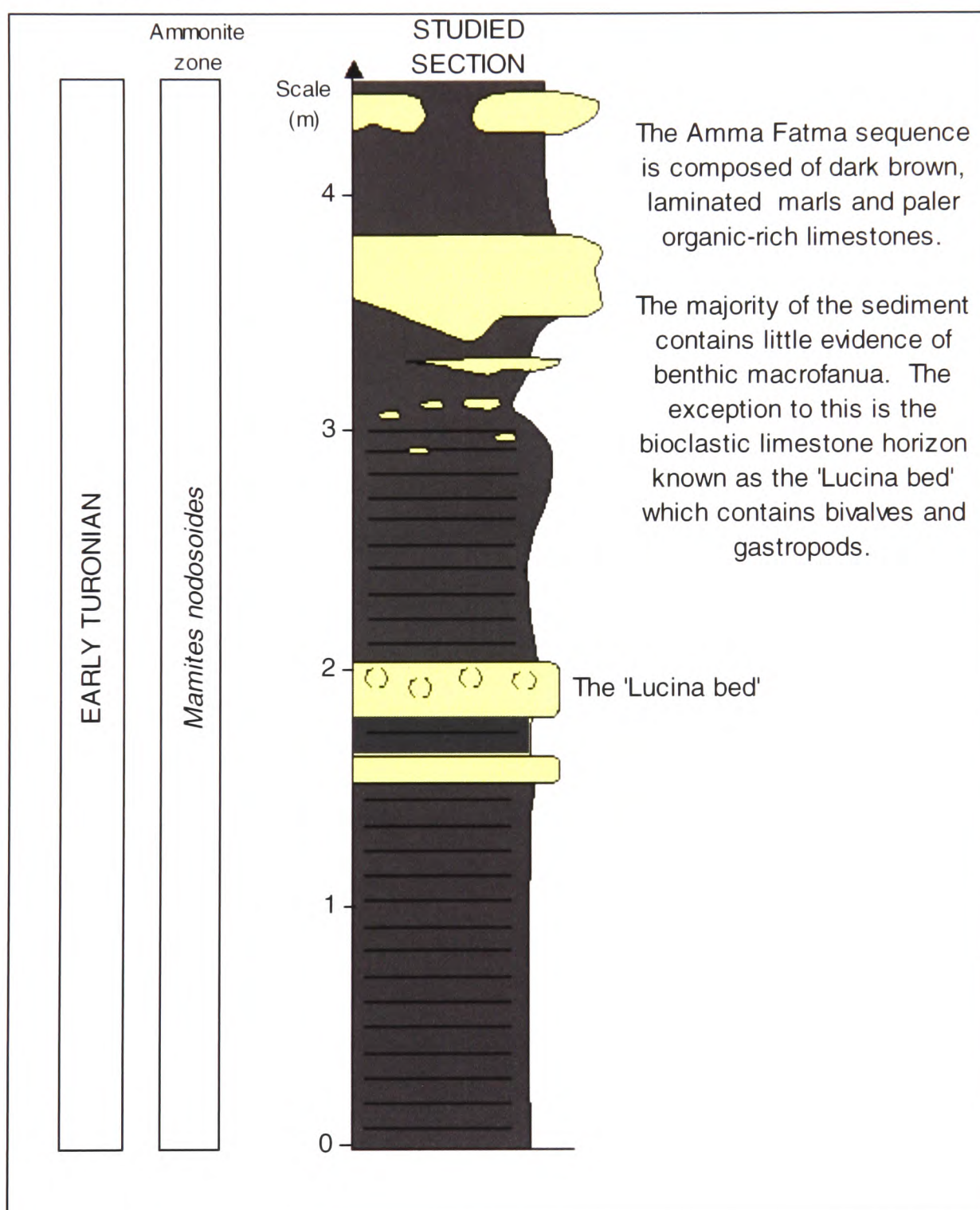


Figure 1.9: Stratigraphic log of the investigated Amma Fatma sequence.

The Tarfaya Basin sediments of Later Cenomanian to Early Turonian age are associated with OAE 2 and the dark marls of the Amma Fatma sequence have been dated to the Early Turonian (El Albani *et al.*, 2001). The investigated sequence corresponds with 0.5 to 5.5 m on the complete sequence log recorded by El Albani *et al.* (2001, page 877) and includes the bioclastic limestone horizon referred to informally as the 'Lucina bed' (see *Figure 1.9*).

1.4 Introduction to the proxies and the project structure

Within this project, four broad categories of palaeo-oxygenation proxies are investigated and the background, methodology and results for each category are described in four separate chapters (see references within):

- **Chapter 2 - SEDIMENTOLOGICAL FEATURES**

Low-oxygen events were initially recognised due to the distinctive nature of the organic-rich sediments that they form and it is suggested that characteristics such as sediment colour, the presence of laminations and fissility can be used to indicate palaeo-oxygenation. In addition to this, the nature, size and tiering structure of trace fossils is also believed to be indicative of palaeo-oxygenation conditions. The third category of sedimentological proxies focuses on the form and distribution of pyrite within the sediment, in particular on the size distribution of pyrite framboids.

- **Chapter 3 – PALAEONTOLOGY**

Low oxygen conditions are believed to have a strong biological impact and the investigated macrofaunal proxies are based on interpreting evidence of this. These include measures such as benthic abundance, the size of the specimens, predominant modes of life and the dominance of particular indicator species. Several authors have combined proxies of this nature with sedimentological information to create a variety of biofacies models. It has also been suggested that various aspects of the taphonomy of an assemblage can be used to interpret palaeo-oxygenation conditions.

- **Chapter 4 - TRACE METAL PALAEO-OXYGENATION PROXIES**

When organic-rich sediments are compared to values for 'average shale' they are often found to be enriched in certain trace elements such as molybdenum, nickel and vanadium, while demonstrating depletion in other elements such as

manganese. It is thought that these patterns are related to the redox behaviour of these elements and so several proxies have been suggested linking the relative enrichment of such elements with palaeo-oxygenation. Because of difficulties associated with normalising trace metal levels and determining the proportion of detrital and authigenic inputs, a number of trace metal ratios have also been suggested including authigenic uranium ($U_a = U_{\text{total}} - \text{Th}/3$), U/Th, V/Cr, V/Sc, V/Ni, Ni/Co, V/(V+Ni), (Cu+Mo)/Zn and the Cerium Anomaly. These tend to compare elements which are thought to be affected by redox conditions to elements which are believed to be entirely detrital in origin.

- **Chapter 5 - Fe-S-C SYSTEMATICS**

There is a strong link between the abundance of organic matter and sulphate reduction, and the subsequent formation of iron sulphides. It is therefore believed that iron, carbon and sulphur systematics are strongly linked to each other and to redox conditions. This has led to the proposal of a number of proxies thought to reflect the influence of palaeo-oxygenation including Total Sulphur, Sulphur/Carbon ratios, Total Organic Carbon, the comparison of varyingly reactive iron pools, the Degree of Pyritisation and the Indicator of Anoxia.

In the final chapter (**Chapter 6 – DISCUSSION**) the results for the full range of proxies are discussed and compared allowing comments to be made on the reliability and applicability of the investigated proxies. Potential new indicators of palaeo-oxygenation are proposed and compared against the results for the existing proxies.

CHAPTER 2: SEDIMENTOLOGICAL FEATURES

2.1 Introduction

2.1.1 Sedimentology

Low oxygen events have typically been recognised in ancient deposits by the sedimentary characteristics and the high organic contents of sediments associated with deposition under anoxic conditions. This has led to the general classification of 'Black Shale'. However Raiswell *et al.* (1987) pointed out that organic-rich sediments can be formed under a range of normal marine to euxinic environments. Hallam (1980) suggested that 'Black Shale' had become a general term that was applied to a range of argillaceous rocks that did not strictly fit this classification. Sediments are classified by the grade scale that was introduced by Udden (1914), modified by Wentworth (1922) and converted into logarithmic form (the ϕ scale) by Krumbein (1934) (see *Figure 2.1*).

ϕ scale	Size range	Aggregate name (Wentworth Class)
< -8	> 256 mm	Boulder
-6 to -8	64-256 mm	Cobble
-5 to -6	32-64 mm	Very coarse gravel
-4 to -5	16-32 mm	Coarse gravel
-3 to -4	8-16 mm	Medium gravel
-2 to -3	4-8 mm	Fine gravel
-1 to -2	2-4 mm	Very fine gravel
0 to -1	1-2 mm	Very coarse sand
1 to 0	½-1 mm	Coarse sand
2 to 1	¼-½ mm	Medium sand
3 to 2	125-250 μ m	Fine sand
4 to 3	62.5-125 μ m	Very fine sand
8 to 4	3.90625-62.5 μ m	Silt
> 8	< 3.90625 μ m	Clay
>10	< 1 μ m	Colloid

Figure 2.1: Classification of sedimentary rocks according to the Udden-Wentworth scale, with later additions by Krumbein (1934).

The names assigned to fine-grained sedimentary rocks also takes into account the degree of consolidation (see *Figure 2.2*)

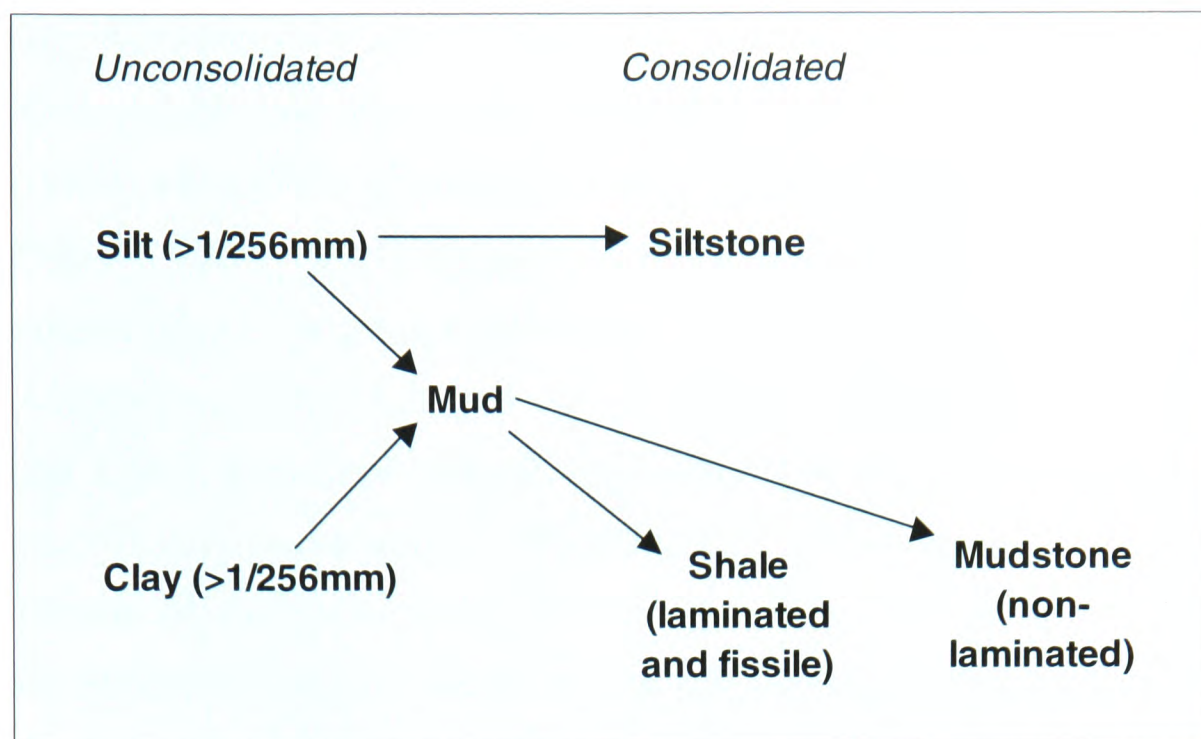


Figure 2.2: Classification of fine-grained sedimentary rocks (according to Pettijohn, 1975).

Picard (1971) stated that fine-grained sedimentary rocks constitute approximately half of the geological column, but of these, it is black shales in particular that have been associated with periods of low oxygenation in the geological record. Tyson (1987) defined black shales as dark coloured, fine-grained mudrocks having sedimentological, palaeoecological and geochemical characteristics associated with deposition under oxygen-deficient or oxygen-free bottom waters. Hallam (1980) suggested that black shales are sediments in which the content of the organic matter rarely exceeds a few percent. He clarified the point that when the organic matter content is considerably higher the rock may yield petroleum upon distillation and therefore would be described as an oil shale, rather than a black shale. While some authors associate black shales with the terms ‘organic-rich shale and bituminous shale’ (Stow 1987), Wignall and Hallam (1992) suggested that this is misleading as some low-oxygen deposits are not high in organic matter. However the faunal content of dysoxic and anoxic sediments is characteristically reduced relative to other types of deposits (Hallam, 1980) (see **Chapter 3**). In terms of composition, Hallam (1980) stated that the dominant inorganic constituents of low-oxygen sediments are phyllosilicate clay minerals, occasionally with some detrital quartz sand or silt. He suggested that the calcite content is normally restricted to concretions, but that laminate bituminous limestones are by no means rare. Pyrite tends to be a key component in low-oxygen sediments, and exists in a variety of forms including disseminated cubic crystals or framboids. Wilkin *et al.* (1996) proposed that the

morphology and size of the pyrite forms present could in itself provide a proxy for bottom-water oxygenation conditions (see **Section 2.1.3**).

Spears (1980) identified the three features common to the majority of black shales:

- **Colour** - Spears (1980) suggested that the colour of black shales is due to the organic matter contained within them, but he also pointed out that it depends on the type and distribution as well as the actual amount present. This means that a black shale could conceivably contain less organic matter than a grey shale in some circumstances. While Hallam (1980) suggested that pyrite may actually be more responsible for the characteristic dark colouration of black shales than the organic matter, Arthur and Sageman (1994) suggested that if this were the case then the colour would fade substantially on weathering. However, while they accepted that colour is a dominant definer of low-oxygen sediments, Arthur and Sageman (1994) warned that the term black shale can be misleading. They suggested that sediments which contain a few percent organic matter are commonly green in colour, or brown if partially oxidised, and that sediments with greater than 25% calcium carbonate are normally much lighter in colour. Sediment colour can also be influenced by thermal maturity as organic matter darkens during maturing processes (Philip, 2005). Spears (1980) suggested that colour charts should be comprised in order to make comparison between sites possible.
- **Lamination** - Spears (1980) defined a lamina as a stratum less than 1cm in thickness. Hallam (1980) went as far as to say that laminae of organic matter arranged parallel to the bedding is the most characteristic lithological feature of black shales as it is believed that laminae are normally totally or partially destroyed by bioturbation in oxic conditions (Spears, 1980). Wignall (1994) suggested that laminations could be a strong indicator of suboxic or anoxic conditions because even within dysoxic settings, all sedimentary features can be destroyed by bioturbation. Wignall *et al.* (2005) suggested that the laminae may result from the formation of a planar fabric of aligned clay/mica minerals (e.g. O'Brien and Slatt, 1990). They supported the idea that the development of fine silt laminae undisrupted by burrowing is evidence for the development of severely oxygen-poor bottom waters. However, they also suggested that laminae are not always present in sediments deposited under low oxygen

conditions, and that the absence of them may reflect a rapid depositional rate of the fine-grained material that did not permit platy particle alignment. Wignall (1994) recognised that some black shales which are not laminated display signs of compaction which is indicative of relatively continuous sedimentation, compared to the periodic accumulation of sediment that would cause laminations. Arthur and Sageman (1994) pointed out that while at least 10% lamination is a defining feature of most black shale horizons, there are also a variety of organic carbon-rich non-laminated mudstones and clays, that can contain relatively large amounts of calcium carbonate or silica. They also found that alternating light and dark laminations are relatively common in black shales from the Cretaceous to recent, and that black shales often show event beds and horizons that suggest that erosion has occurred, such as calcium-carbonate-rich lenses representing winnowed biogenic debris.

Fissility - Spears (1980) defined fissility as the property of splitting or separating along approximately parallel surfaces in the plane of bedding. A number of schemes have been devised to describe the fissility of a sediment, including that of McKee and Wier (1953) which was based on the frequency of the splitting:

- Papery – less than 2 mm
- Shaly or platy – 2 mm to 1 cm
- Flaggy – 1 cm to 5 cm
- Slabby – 5 cm to 30 cm
- Blocky – 30 cm to 100 cm
- Massive – greater than 100 cm

White (1961) suggested that as fissility does not appear to increase with depth of burial, it must be related to a depositional feature. Some authors (including Spears, 1980; Hallam 1980, O'Brien and Slatt, 1990) believed that the weathering of laminae is responsible for the pronounced fissility of black shales, which are often referred to as 'paper shales'. However, Wignall (1994) has observed fissility in the absence of lamination in black shales and instead suggested that the papery fissility is the result of weathering of the compacted fabric of parallel aligned organic matter and clay particles common to the majority of black shales.

2.1.2 Ichnology

“Biogenic sedimentary structures are autochthonous indicators of environmental conditions” (Wetzel, 1991, p. 47)

2.1.2.1 Background

A trace fossil, or ichnofossil, is any indirect evidence of ancient life. Technically, this refers to biogenic structures which are features caused by an organism while it was still living and these structures can therefore be classified on the basis of behavioural associations (Seilacher, 1953). Different behavioural modes were assigned categories by Seilacher (1953) based on basic biological functions such as feeding, dwelling and locomotion (see *Figure 2.3*). Where multiple or overlapping types of behaviour can be interpreted from one trace Seilacher (1953) suggested that the classification should generally be applied to the predominant motive of the organism.

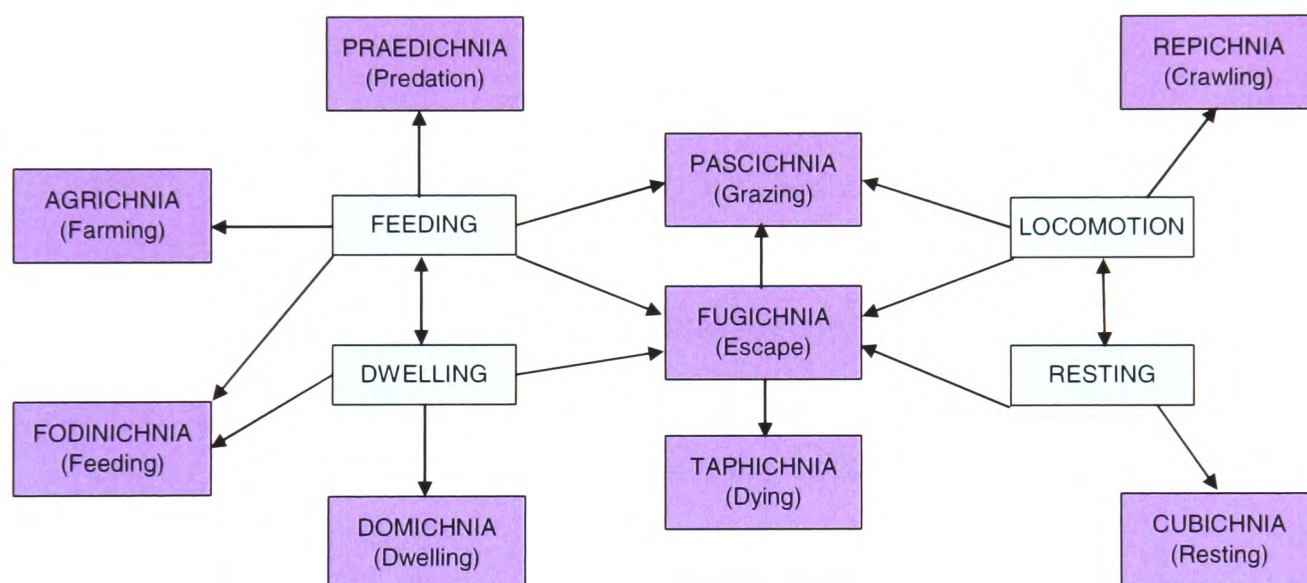


Figure 2.3: Inter-relationship of the behavioural modes assigned by Seilacher (1953) (after Pemberton et al. 1992).

Löwemark *et al.* (2004) suggested that the abundance, diversity and behaviour of benthic burrowing organisms are controlled by the following abiotic factors:

- Substrate properties;
- Nutrient availability;
- Temperature;
- Salinity;
- Bottom and pore-water oxygenation;
- Current activity;
- Sedimentation rate.

However, some studies of deep-sea macrobenthos communities have found no general correlation between community patterns and sediment parameters (e.g. Levin *et al.*, 2000). Instead, Löwemark *et al.* (2004) suggested that large-scale variations in hydrography, food flux and bottom-water oxygenation were responsible for the variations observed.

If the effect of these factors can be interpreted and differentiated, ichnofossils can therefore be used to interpret palaeo-oxygenation conditions. Reineck (1963) was the first author to propose a **Bioturbation Index** in order to semi-quantitatively identify the extent of bioturbation of different sediments. Wetzel (1991) identified four more interpretive techniques, incorporating information about environmental signals:

- The identification of typical “**index**” **trace fossils** is used as an indicator for specific environmental conditions. For example, Bromley and Ekdale (1984) suggested that the presence of the trace fossil *Chondrites* is to some extent linked to the presence of poorly oxygenated bottom waters.
- The grouping of trace fossils into certain **ichnofacies** (Seilacher 1958, 1964, 1967). Ichnofacies are facies models based on recurring **ichnocoenoses**, which in turn means “an ecologically pure assemblage of trace fossils, i.e. deriving from the work of a single endobenthic community” (Bromley, 1996). Frey *et al.* (1990) suggested that the presence of a particular ichnofacies is mainly determined by the environmental factors and so can be used to interpret conditions.
- The **taxonomic analysis of trace-fossil assemblages**. Interpretation of particular assemblages, including potential mode of life of the original animals, diversity and burrow diameter, can provide an understanding of fauna-environment relationships (examples are given in Curran, 1985; Frey and Bromley, 1985).
- Analysis of the **vertical zonation of trace fossils** within the sea floor, which is defined by cross-cutting relationships of the burrows (for examples, see Reineck *et al.*, 1967; Ekdale and Bromley, 1984; Savrda and Bottjer, 1986). The different burrowing depths of infaunal organisms within the sea floor depend on environmental conditions and hence have ecological significance. Reineck *et al.* (1967) introduced the term “Gefügestockwert” (“tier of

sedimentary structures”) to describe this vertical structure of fossil communities, and this became known as simply ‘tiering’ (Ausich and Bottjer, 1982).

These approaches are believed to allow trace-fossil assemblages to be used to imply bottom-water conditions at the time of sediment deposition.

2.1.2.2 Bioturbation Indices

In a general sense, the degree of bioturbation is believed to be directly linked to the oxygenation level at the sediment/water interface - Leszczynski *et al.* (1996) suggested that fine-grained sediments displaying no evidence of bioturbation are associated with anoxic conditions, and that bioturbated sediments are indicative of oxic conditions. However, they were quick to point out that many different factors influence the type and amount of bioturbation and that this complicates models of oxygen-related variations. Many workers have attempted to allocate semiquantitative categories to describe the amount of biogenic disturbance of sediment in a given stratigraphic sequence (e.g. Reineck, 1963; Droser and Bottjer, 1986).

GRADE	BIOTURBATION	CLASSIFICATION
0	0%	No bioturbation
1	1-4%	Sparse bioturbation, bedding distinct, few discrete traces and/or escape structures
2	5-30%	Low bioturbation, bedding distinct, low trace density, escape structures often common
3	31-60%	Moderate bioturbation, bedding boundaries sharp, traces discrete, overlap rare
4	61-90%	High bioturbation, bedding boundaries indistinct, high trace density with overlap common
5	91-99%	Intense bioturbation, bedding completely disturbed (just visible), limited reworking, later burrows discrete
6	100%	Complete bioturbation, sediment reworking due to repeated overprinting

Figure 2.4: The Bioturbation Index (Reineck, 1963) from Taylor and Golding (1993).

In Reineck's (1963) original scheme, categories are assigned between two extremes: 0% bioturbation (no evidence of biogenic mixing of sediments) and 100% bioturbation (complete biogenic mixing of sediments). The categories between these end members describe relative ranges of 'biogenic disturbance', and each category was assigned a number between zero and six (see *Figure 2.4*). The descriptions of each category are designed to allow field identification of each grade, but these categories, and similar schemes that rely on descriptions, can be argued to be entirely qualitative. Droser and Bottjer (1986) provided schematic diagrams of their ichnofabric indices in order to allow more visual comparisons (see *Figure 2.5*).

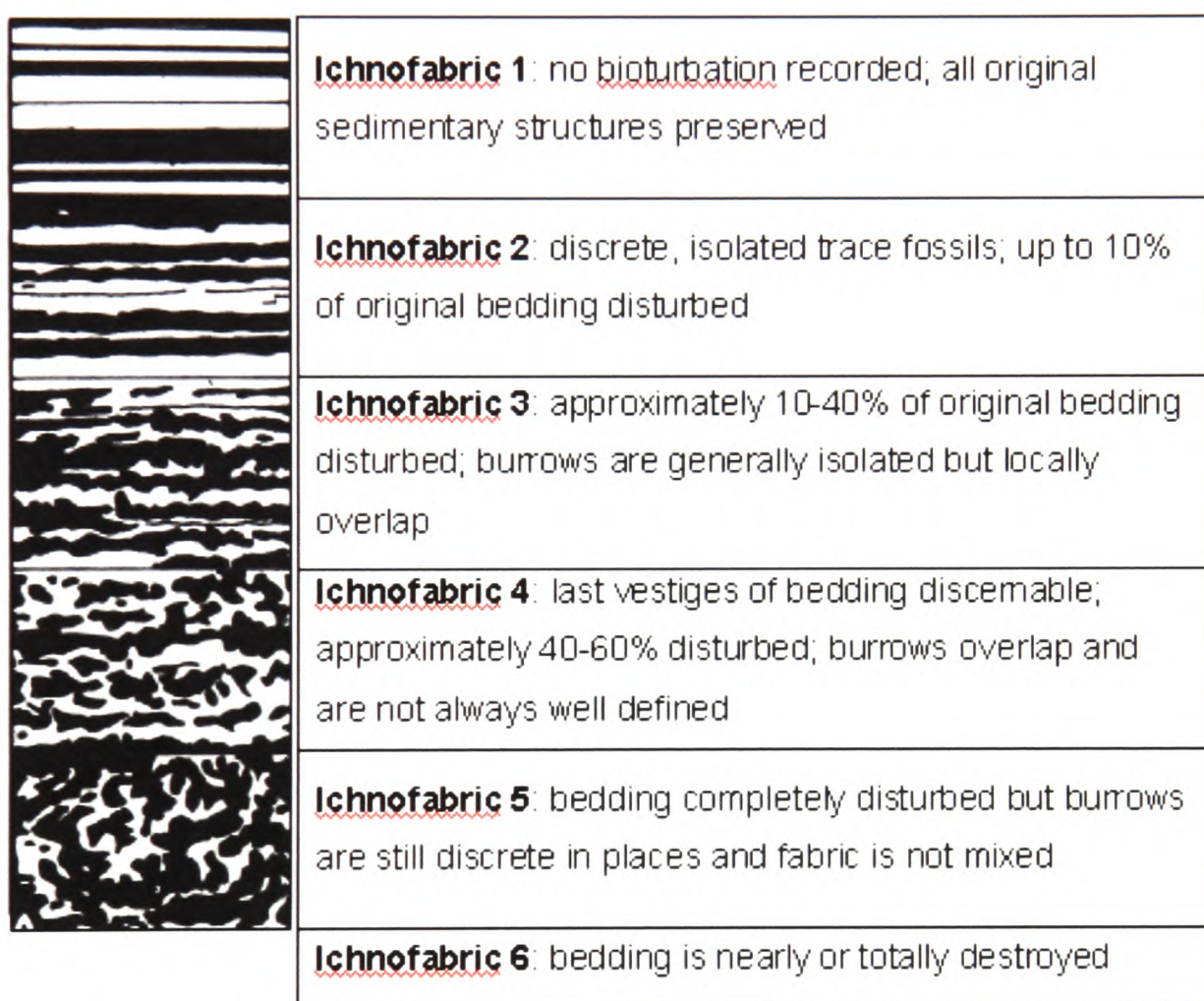


Figure 2.5: Schematic diagrams of ichnofabric indices with descriptions (from Droser and Bottjer, 1986).

Miller and Smail (1997) took this a step further, providing a range of diagrams designed to enable clear classification unskewed by variations in size, shape and distribution of trace fossils (see *Figure 2.6*). While most schemes have been designed to recognise the degree of bioturbation on vertical sections, the scheme by Miller and Smail (1997) was primarily designed to interpret bedding plane surfaces.

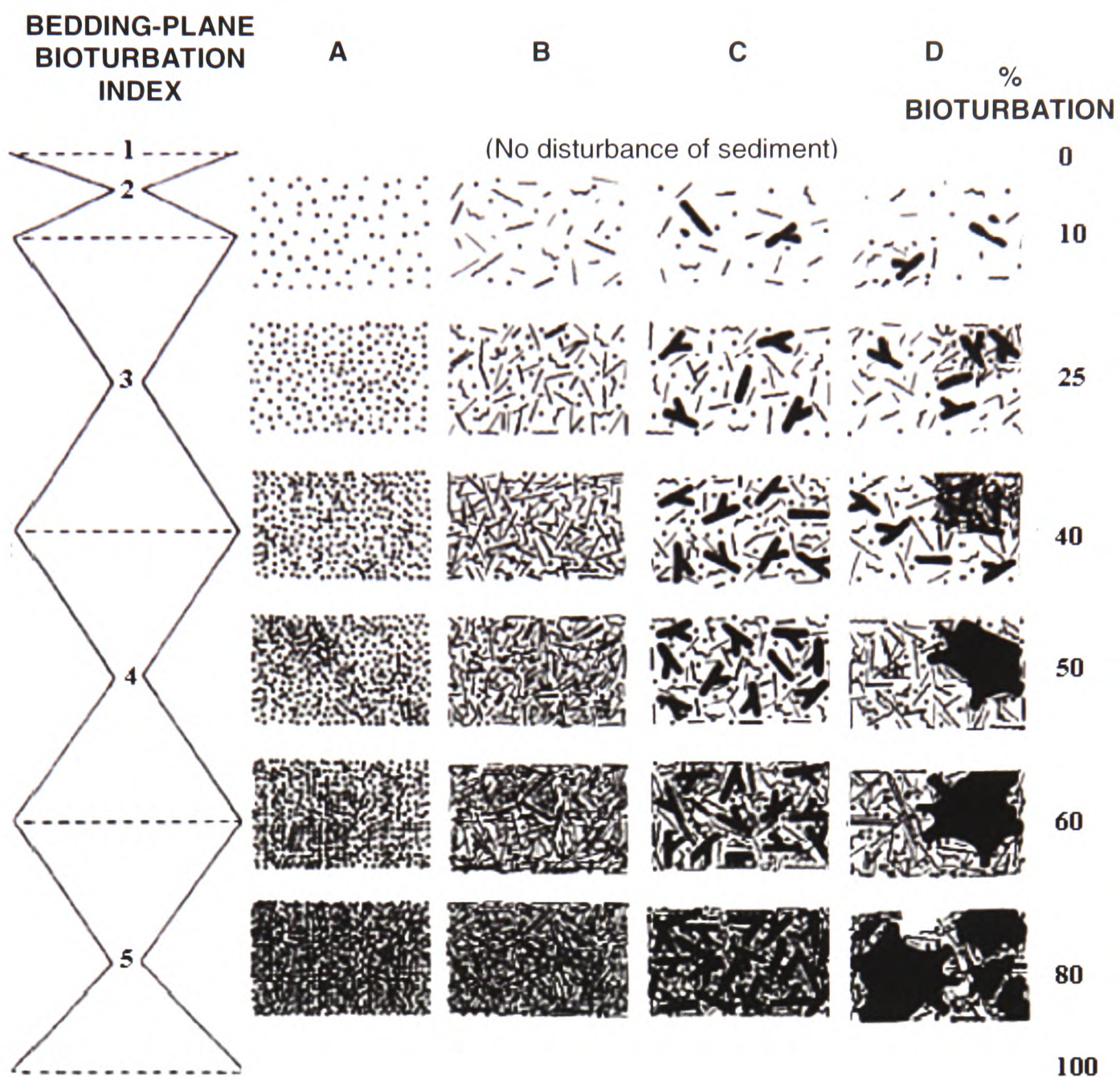


Figure 2.6: Bedding plane bioturbation indices, taking into account variations in size, shape and distribution (from Miller and Smail, 1997). A: Same size and shape, and an even distribution of trace fossils; B: Same size but different shape, and an even distribution; C: Different size and shape, and an even distribution; D: Different size and shape, and an uneven distribution of trace fossils.

Miller and Smail (1997) also proposed the use of image analysis where trace fossils are manually coloured in on digital photographs and software is then used to calculate the percentage area of the coloured sections. Marenco and Bottjer (2006) suggested a possibly quicker variation on this idea using a quadrat format and using the software to calculate the percentage of squares within the quadrat that show any sign of biological disturbance.

While these methods do provide a numerical comparison between sites, the extent of bioturbation is proportional to the sedimentation rate and the burrowing rate, the latter of which is a function of oxygen availability and food supply. Because these other factors could influence the extent of bioturbation, some authors have suggested comparing the results with diversity and type of trace fossil which may provide an independent indicator of oxygen levels.

2.1.2.3 The presence of particular 'species'

Some authors have suggested that the dominance of particular trace forms may indicate low-oxygen conditions. Bromley and Ekdale (1984) suggested that an assemblage dominated by *Chondrites* represents anoxic conditions. In support of this, Baas *et al.* (1998) found massive occurrences of *Chondrites* in the modern environment beneath Heinrich layers in the North Atlantic. Heinrich events represent reduced or halted thermohaline circulation events, which normally result in low oxygen levels in bottom waters. Ekdale and Mason (1988) also suggested that *Teichichnus* may represent the work of opportunistic deposit feeders able to live in dysoxic conditions and Leszczynski *et al.* (1996) agreed that the increased organic matter in the sediment due to low oxygen conditions would favour *Teichichnus* production. Savdra and Bottjer (1986) suggested that the dominance of one form such as *Chondrites* could represent the rapid response of opportunistic animals dominating an unexploited niche created by environmental changes. They suggested that the animals responsible would have a broad environmental tolerance and that *Chondrites* represents a pioneering form dominating during oxygenation after an oxygen-depleted event.

However, Leszczynski *et al.* (1996) suggested that the dominance of forms thought to be tolerant to low oxygen conditions may just represent preservation of only the deepest burrowing forms in a tier system. They identify *Thalassinoides*, *Planolites*, *Teichichnus*, and *Chondrites* as lower tier ichnospecies and suggested that as oxygen levels decrease, the benthic boundary layer shortens and an upward shifting of tiers would occur. They suggested that this tier migration and overwriting could explain the dominance of deep burrowing forms in upper levels.

2.1.2.4 Ichnofacies and Ichnocoenoses

Savdra and Bottjer (1989) introduced the concept of Oxygen-Related Ichnocoenoses based on the proposed oxygen tolerance of trace fossil forms outlined by Bromley and Ekdale (1984). Bromley and Ekdale (1984) suggested that tiering hierarchies were based on oxygen tolerance, with more animals more adapted to low oxygen conditions being able to occupy lower tiers within the sediment. From this study, Savdra and Bottjer (1989) suggested that *Chondrites* was the formed by the most tolerant species, followed by *Zoophycos*, *Thalassinoides* and then *Planolites*. They suggested that the presence of certain group of these and related forms could be used to imply bottom water conditions. Löwemark *et al.* (2004) identified six dominant types of trace fossils in Late Quaternary sediments of the southwestern Iberian margin and from these forms, they determined eight distinct ichnocoenoses:

- indistinct bioturbation;
- *Planolites*-dominated;
- *Thalassinoides*-dominated;
- *Chondrites*-dominated;
- *Planolites* and *Thalassinoides*-dominated;
- pyritized microburrows such as *Trichichnus* and ‘*Mycellia*’-dominated;
- *Chondrites*, *Trichichnus*, and ‘*Mycellia*’-dominated;
- *Zoophycos*-dominated.

Löwemark *et al.* (2004) suggested that the primary controls on the occurrence of these ichnocoenoses were bottom-water oxygen conditions and organic carbon contents. Ekdale and Mason (1988) also recognised a range of ichnofacies that should be expected from rising oxygen levels, based on the mode of burrow formation (see **Section 2.1.2.5**). Savdra and Bottjer (1989) did warn, however, that it is important to distinguish between traces that were formed when the sediment:water interface was at different relative heights, and that full analysis of cross-cutting relationships is required. Löwemark *et al.* (2004) agreed that variations in ichnocoenosis that are caused by fluctuations of environmental conditions on the seafloor are recorded in the stratigraphic column at a certain depth below the surface corresponding to the penetration depths of the organisms. They referred to this as a stratigraphic offset, and suggested that the magnitude of this offset is controlled by substrate properties as well as environmental factors. They suggested that an increase

in bottom-water oxygen content from dysoxic to oxic conditions might cause a reworking of dysoxic structures and therefore will shift the boundary between dysoxic and oxic traces downwards, far below the actual level of changing conditions. Under the opposite conditions they suggested that decreasing oxygen level will result in a smaller offset as this would cause a condensation of the tiers.

2.1.2.5 Taxonomic Assessment of Trace Assemblage Features

Bottom-water oxygen levels have been proposed to have an effect on several parameters of trace-fossil assemblages:

- **Burrow diameter:** Löwemark *et al.* (2004) suggested that bottom-water oxygenation affects burrow type, abundance and diameter. In general, lower oxygen levels are believed to result in smaller burrow sizes and this can therefore be used as an indicator for such conditions (Savrdrá and Bottjer, 1989).
- **Species diversity:** In modern environments Smith *et al.* (2000) found that species diversity correlated with trace-fossil diversity, so the less diverse burrows associated with low oxygenation levels directly indicate a decrease in macrofossil diversity. This is complicated by the fact that low-oxygen tolerant species may thrive with the increased organic matter content, giving increased population densities of dysoxic benthic organisms (Levin *et al.*, 2000) and this may explain the massive occurrences of forms such as *Chondrites*.
- **Mode of formation of burrows:** Ekdale and Mason (1988) suggested that Phanerozoic trace fossils change their behavioural character at distinct oxygenation levels. They suggested that, in response to increasing oxygenation, the preserved trace-fossil assemblages should change from one dominated by subsurface deposit feeding structures (fodinichnia) through one dominated by grazing traces (pascichnia) to one dominated by dwelling structures (domichnia) (see *Figure 2.7*). However, Wheatcroft (1989) suggested that the opposite trend occurs, stating that the succession of trace-fossil associations under increasing oxygenation should change from a dominance of domichnia to one of fodinichnia. Wheatcroft (1989) suggested that during low oxygen conditions, the first colonists would be small, tube

building, surface-deposit feeders of suspension feeders, but while Ekdale and Mason (1988) recognised that this may apply to some organisms, they stated that domichnia are rare in dysoxic sediments with laminations and high Total Organic Carbon. This, however, is not supported the work of Leszczynski *et al.* (1996) who found only domichnial burrow structures in a laminated pelagic limestone, which they suggested represented the work of pioneers in a dysoxic sea floor.

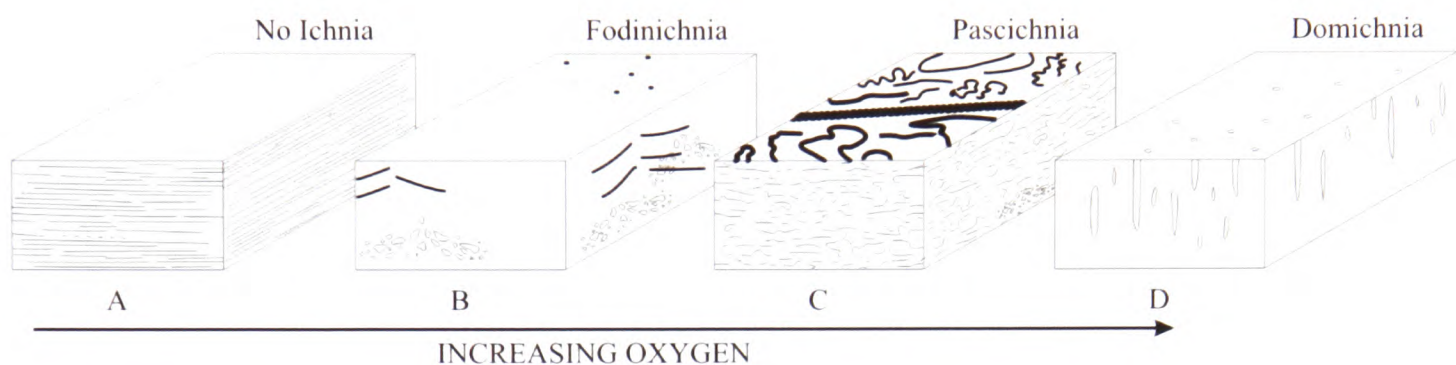


Figure 2.7: A general model of oxygen- dependant trace fossil associations, adapted from Ekdale and Mason (1988).

- **Mode of life:** Rhoads and Boyer (1982) noted that colonisation by suspension feeders only is a common event on present-day poorly oxygenated bottoms. This could mean that recognition of trace assemblages formed predominantly by suspension feeding animals could be an indicator of low-oxygen conditions. However, Rhoads and Boyer (1982) pointed out that in fossil examples, the traces of pioneer bottom colonization by suspension feeders is usually obliterated by the subsequent activity of deposit feeders.

Wetzel (1991) pointed out that there are unfortunately a variety of factors that influence trace assemblage parameters (see Figure 2.8) and so interpretation of purely oxygen-related variations can be difficult.

Ichnofaunal aspect		Burrow diameter	Penetration depth	Type of feeding burrow			Degree of bioturbation	Tiering	Ichnofauna
Environmental Factor	Trend			Ratio of open tubes to simple tunnels	Ratio U- to J-tubes	Burrows dug with digging appendages			
Oxygenation	Decrease	Decrease	Decrease	Decrease	Increase		Decrease	Decrease	Changes
Benthic food content	Increase	Increase possible	Increase	Increase possible	Increase possible			Increase	Increase
Sedimentation rate	Increase	Changes possible	Increase	Increase			Threshold	Increase	Changes
Grain size	Increase		Threshold	Decrease	Decrease	Increase	Threshold		Changes
Coarse event sediments	Increase		Threshold			Threshold	Threshold	Threshold	Changes
Suspension content	Increase			Increase possible		Changes possible	Unknown	Unknown	Changes

Figure 2.8: Inter-relationship between environmental factors and some ichnofaunal aspects for deep-sea sediments, assuming that only one factor is varied at a time (adapted from Wetzel, 1991). He noted that many of the features that decrease with decreasing oxygen do so only below a specific threshold (1-2 ml O₂/l). Where threshold is entered, this infers that above a certain level, results will differ from below that level.

2.1.2.6 Patterns of Tiering

The most complex ichnological analysis involves the interpretation of burrow tiering within the sediment. Within marine sediments, animals occupy burrows at varying depths, creating a set of overlapping tiers relating to the sediment surface at that time (Reineck *et al.*, 1967). Modern normal marine sediment contains a mixed layer 3-10 cm thick, and then a transition layer which extends down to 20-35 cm below the surface (Ekdale and Bromley, 1984). The shallowest tiers, which are rapidly developed are generally occupied by active infaunal sediment eaters, and domichial burrows, whereas the deeper tiers develop more slowly and are created by more elaborate systems, often created by animals that are tolerant to low-oxygen conditions (Ekdale and Bromley, 1984). Under low-oxygen conditions, it is generally accepted that the vertical extent of the tiering decreases (see Figure 2.9) but this basic assumption is complicated by other factors:

- An increased sedimentation rate causes an increase in the mixed layer, and tiering depth can increase (Tyson, 1995) but in turn, rapid sedimentation leads to a succession dominated by only shallow tiers.
- In fully oxygenated conditions, restricted food availability can cause a reduced vertical extent of the tiers and loss of the deepest tiers (Wetzel, 1991).

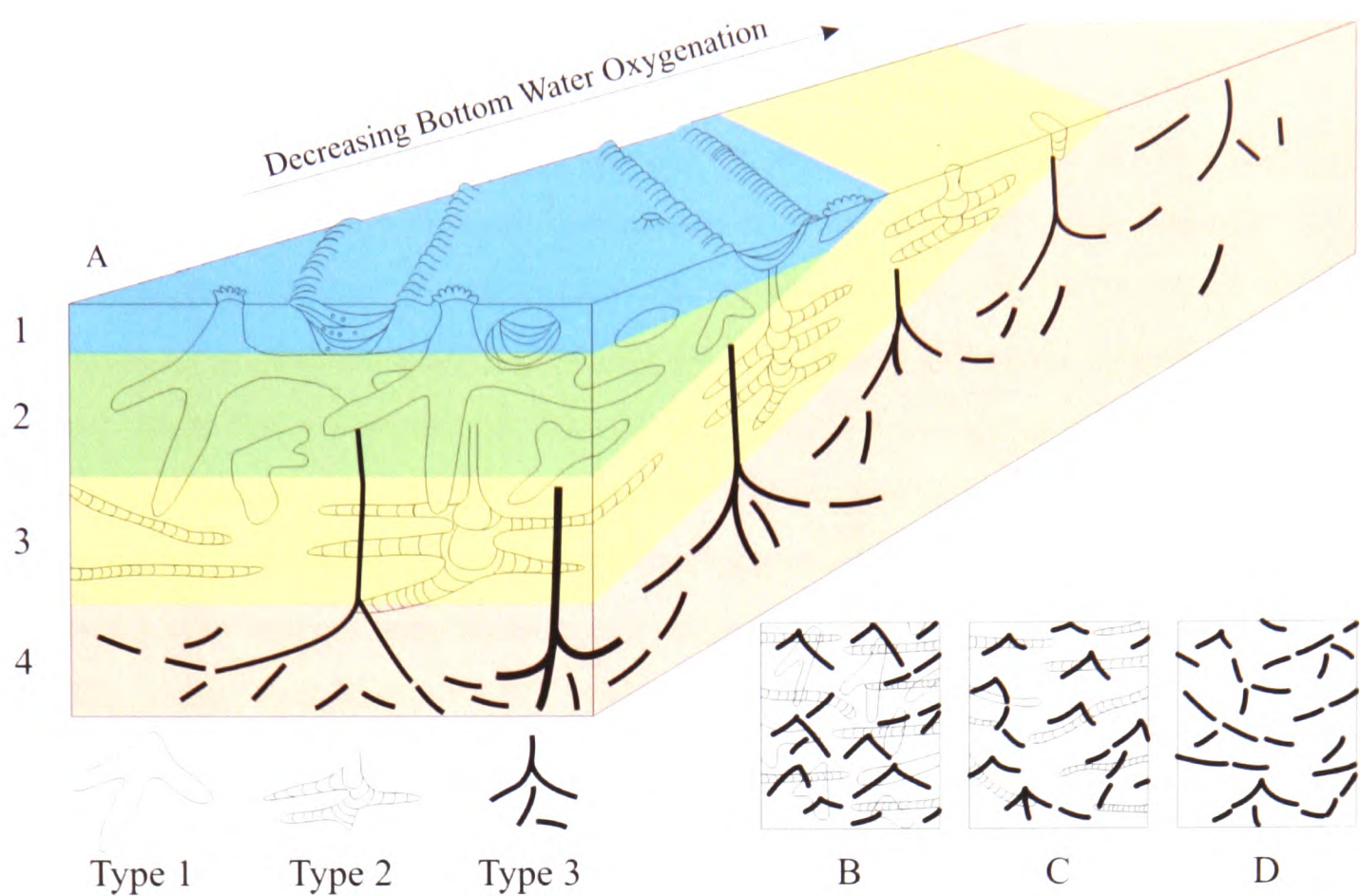


Figure 2.9: Schematic block diagram illustrating burrow size, bioturbation depth and tiering structure across a hypothetical seafloor oxygenation gradient and expected trace-fossil cross-cutting relationships in strata deposited at various sites along the gradient. Tier level 1 represents the mixed surface layer of the sediment column and represents an interval of complete bio-homogenization. Tier levels 2, 3 and 4 represent tier levels occupied by organisms that normally penetrate and live below the surface layer (from Savdra and Bottjer, 1989).

Leszczynski *et al.* (1996) suggested that the only way to recognise whether limited tiers are due to low oxygen is to examine the type of burrow making up these shallow tiers – if low-oxygen conditions persist they would expect to see the forms normally making up the deepest tiers dominating the shallow tiers. They suggested that the trace fossils referred to *Thalassinoides*, *Planolites*, *Teichichnus*, and *Chondrites* are representative of deepest tier forms. In normal marine sediments, the *Planolites* tier is situated at 10–20 cm below surface (Löwemark *et al.*, 2004) and in deep-marine sediments, *Thalassinoides* burrows generally occupy a tier at 10–30 cm, depending on sedimentation rate (Wetzel, 1991). Assemblages dominated by these forms are thought to represent preservation of only the deepest forms, suggesting that the vertical extent of tier development has decreased (Leszczynski *et al.*, 1996). Löwemark *et al.* (2004) suggested that lower oxygen conditions will suppress

suspension feeders as well as larger endobenthos, leading to decreased tiering depth, and bioturbation dominated by small traces such as *Chondrites*.

Tier analysis is further complicated by the continual superposition of the whole tier set on each level, as continuous sedimentation raises the level of the surface. The overwhelming number of individuals of the macrofauna are concentrated to the uppermost cm of the sediment (Flach *et al.*, 2002) and this means that the observed ‘fossil’ trace fauna does not necessarily correspond to the composition of the living fauna. Löwemark *et al.* (2004) suggested that the upper tiers of the bioturbation are more or less destroyed by later, deep-reaching bioturbation when the former near-surface layers become deep layers due to the accumulation of new sediment. Because of this, Savdra and Bottjer (1986) proposed a scheme to identify oxygenation events by the pattern of superposition of tier structures (see *Figure 2.10*).

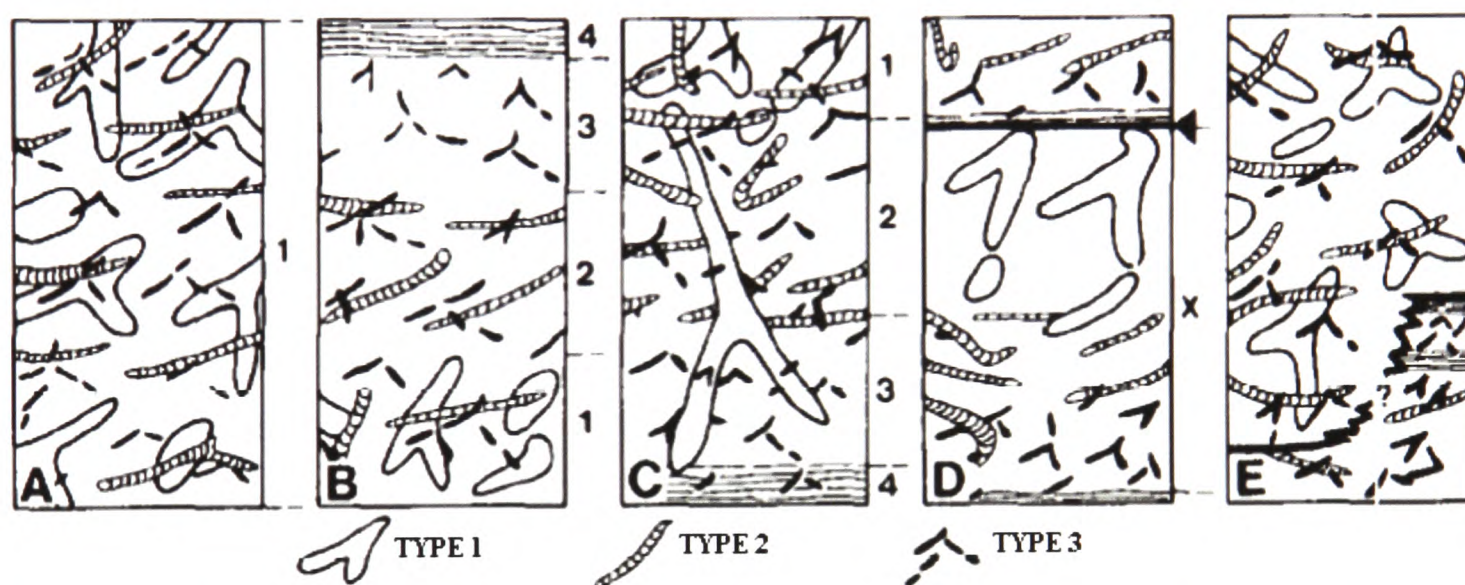


Figure 2.10: Schematic diagrams representing trace fossil associations and cross-cutting relationships expected in sediment deposited under stable conditions of oxygenation (A), gradually decreasing oxygen availability (B), gradually increasing oxygen availability (C), rapidly decreasing oxygen availability (D) and rapidly increasing oxygen availability (E), (after Savdra and Bottjer, 1986).

There are several problems associated with using ichnology to identify oxygenation conditions. Firstly, different types of trace fossils have widely different preservation potential – Bromley and Uchman (1999) highlighted this with the example of *Ophiomorpha* which is easy to recognise due to its special lining structure, whereas the closely related *Thalassinoides* is notoriously difficult as it lacks a lining. There are also a number of other factors that effect the type of traces formed. Löwemark *et*

al. (2004) suggested that the presence of a coarse sediment inhibits the formation of small traces such as *Chondrites* and pyritized microburrows. However, they suggested that larger traces, in particular *Planolites*, benefit from coarser sediments. Löwemark *et al.* (2004) believed that the oxygen level determines the overall type of bioturbation whereas the substrate variations may modulate smaller fluctuations within the ichnocoenosis. They also suggested that food supply may account for variations in the type of traces within a similar level oxygenation environment.

2.1.3 Pyrite Framboids

“Framboids are densely-packed, raspberry-like, spherical aggregates of equigranular, micron-sized crystals or microcrysts. They range from a few microns to several tens of microns in diameter” (Wignall and Newton, 1998, p. 537).

A range of theories have been proposed for the formation of framboids including:

- purely biogenic origins, for example pyrite fossilization of bacterial colonies (see Love 1957);
- indirect biogenic models, for example replacement of organic spherical globules or gaseous vacuoles (see Kalliokoski and Cathles, 1969; Rickard, 1970);
- inorganic models based on laboratory synthesis (see Sweeney and Kaplan, 1973; Graham and Ohmoto, 1994).

Pyrite framboids have been produced via a variety of experimental methods (for examples, see Berner, 1969; Farrand, 1970; Sunagawa *et al.*, 1971; Sweeney and Kaplan, 1973; Kribek, 1975; Graham and Ohmoto, 1994; Wilkin and Barnes, 1996). The results of these experiments discount a range of the proposed theories for framboid formation, including those based directly on biological activity, and those relating to spherical substrates as precursors to the formation.

Wilkin and Barnes (1997) presented a model based on work by Taylor (1982) on the formation of magnesioferrite framboidal forms in siliceous, volcan-exhalative sediments. Taylor (1982) suggested that primary aggregates of this ferromagnetic mineral formed because of magnetic attraction and consequent aggregation. He suggested that pyrite framboids could also form via magnetic aggregation through a magnetic iron monosulphide precursor. In 1996, Wilkin and Barnes noted in

experiments, that when greigite formed and rapidly converted to pyrite, framboids were produced. In 1997, Wilkin and Barnes took this one step further and proposed a model of formation based on the ferromagnetic properties of this pyrite precursor:

1. Initial nucleation and growth of an iron monosulphide;
2. Reaction of the initial monosulphide to greigite;
3. Aggregation of greigite microcrystals due to ferrimagnetic attraction;
4. Replacement of greigite by pyrite.

In support of this theory, Wilkin and Barnes (1997) noted that the literature provides examples of framboidal morphology in other magnetic minerals, including magnetite, magnesioferrite and greigite. They also suggested that the recorded occurrences in non-magnetic minerals such as limonite, hematite and chalcocite represent oxidised or replaced pyrite framboids. This model firmly links framboid formation to the redox boundary between oxic and anoxic waters, as greigite formation requires weakly reducing conditions (Wilkin and Barnes, 1997). However, in 2000, Butler and Rickard synthesised framboidal pyrite directly from iron monosulphides, without a greigite intermediary phase. It is possible that framboids form in a variety of ways, but as the reaction between ferrous iron and hydrogen sulphide to form pyrite requires the presence of partially oxidised sulphur species (Canfield and Thamdrup, 1994; Wilkin and Barnes, 1997) most authors concur that growth occurs at, or very close to, the redox boundary (Wignall and Newton, 1998).

Working on this assumption, Raiswell and Berner (1985) suggested two distinct modes of framboid formation, depending on the location of the redox interface in relation to the sediment-water boundary:

- Under dysoxic or oxic water columns, this key redox interface is located at or beneath the sediment-water interface (Wilkin *et al.*, 1996). In these conditions pyrite framboids would form '**diagenetically**' within the porewaters of the sediment.
- In euxinic water columns the redox interface occurs within the water column (Wilkin *et al.*, 1996) and pyrite framboids form '**syngenetically**' at this point in the water column.

Raiswell and Berner (1985) suggested that these framboid 'populations' could be distinguished by the general size and variability of the framboids, and could therefore be used as an indicator of palaeo-oxygenation levels.

After investigating the Crystal Size Distribution Theory introduced by Randolph and Larson (1988), Wilkin *et al.* (1996) suggested that framboid size is generally determined by residence time near the anoxic-oxic boundary. They suggested that framboids growth times are shorter when the boundary is within the water column, as when the framboids reach a certain size their ‘hydrodynamic instability’ causes them to fall away and settle on the sediment surface (see *Figure 2.11*). Under these conditions, the resultant framboids will be relatively small and have a restricted size range.

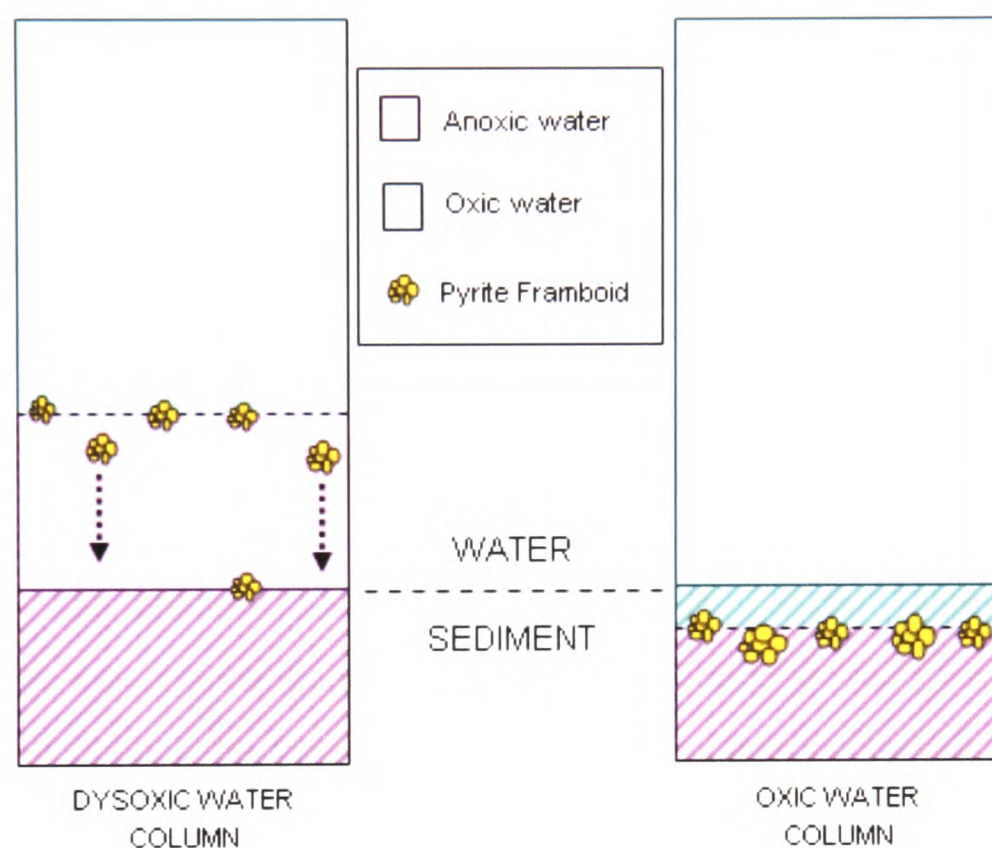


Figure 2.11: The formation of pyrite framboids syngenetically at a redox boundary within the water column and diagenetically, at a redox boundary within the sediment.

In contrast, they suggested that when framboids form within the sediment, growth times can be much longer and so larger, and more varied framboids are found. Suits and Wilkin (1998) suggested that an overall lower proportion of pyrite nucleation sites within the sediment may also contribute the larger and more variable size of diagenetic framboids. They also noted that diagenetic pyrite can be identified by textural features such as filling and overgrowth, and that euhedral crystals were more commonly associated with these diagenetic assemblages (see *Figure 2.12*). Wilkin and Barnes (1997) found that while framboids are indicative of fast reaction rates, euhedral crystals result from slower reaction rates. Therefore the association of

euhedral pyrite crystals with diagenetic framboids supports the idea of longer residence time near the redox boundary.



1. Scale bar represents 20 μm 2. Scale bar represents 5 μm 3. Scale bar represents 20 μm

Figure 2.12: Scanning Electron Microscope images, of sediment from 1.15m in the Folkestone Gault Clay sequence, showing 1. Pyrite framboids; 2. A close up of microcrystals within a framboid which hasn't been overgrown; 3. Framboids with single euhedral crystals.

The idea of syngenetic framboid formation is supported by the discovery of framboids suspended in anoxic water columns, for example in the Black Sea (Ross and Degens, 1974). But while Lyons (1997) found that in the Black Sea nearly all pyrite forms within the water column, Roychoudery *et al.* (2003) suggested that this is possibly not a 'typical' example of a euxinic basin as pyritisation occurs under iron-limited conditions, and the iron is completely used up in the water column. In fact, Wilkin and Barnes (1997) found that in the euxinic sediments of the Pettaquamscutt estuary (Rhode Island, USA) at least 30% of pyrite forms within the sediment. This raises some questions about the general applicability of this technique and Suits and Wilkin (1998) pointed out that the ratio of pyrite formed syngenetically to that formed diagenetically should be considered when interpreting the Fe-S-C relationships and stable isotope ratios of pyrite in ancient shales.

Studies of trends down the length of cores have shown that framboid size distribution is relatively fixed very early in diagenesis, and the correlation between size distributions in modern and ancient sediments suggests that framboid size is maintained during advanced diagenesis and lithification (Wilkin *et al.*, 1996). With this in mind, Wignall and Newton (1998) proposed a set of criteria to distinguish palaeo-oxygenation levels in the Jurassic Kimmeridge Clay. They distinguished:

- Euxinic conditions (H_2S bearing, O_2 -free bottom waters) as having tiny framboids (<5 μm) with a narrow size range;
- Lower dysaerobic conditions as having a similar distribution but with the addition of rare large diameter framboids;

- Upper dysaerobic conditions as showing a dramatic increase in framboid size and loss of framboids of $<3\ \mu\text{m}$.

However, this classification scheme refers directly to the Kimmeridge Clay and so care must be taken in applying these numerical boundaries directly to other localities. This is highlighted by a study of Holocene Black Sea sediments by Wilkin *et al.* (1997) which recorded a marked difference from the Kimmeridge Clay results:

- Under euxinic conditions, 95% of the framboids were $<7\ \mu\text{m}$ in diameter.
- Under oxic or dysoxic water columns, over 95% of the framboids were $< 25\ \mu\text{m}$ in diameter, 40% of framboids are between $7\ \mu\text{m}$ and $25\ \mu\text{m}$, and framboids up to $50\ \mu\text{m}$ in diameter are present.

Lash and Blood (2004) suggested that increased density may be responsible for the larger framboids observed within some euxinic settings, as this would increase the hydrodynamic stability of the framboids, allowing them longer growth times at the redox interface. Muramoto *et al.* (1991) found that syngenetic framboids in the Black Sea were commonly associated with biogenic particles, which supports reports that an algal film forms at the redox interface, again allowing longer residency times at this interface.

While there have been questions raised about the direct applicability of numerical limits, it appears that differences in framboid populations are recognisable in ancient marine sediments. The technique may be especially valuable in the analysis of weathered samples where oxidation can destroy the original geochemical character but leave the framboids pseudomorphed by iron oxide weathering products (Luning *et al.*, 2003). However, while Wilkin *et al.* (1996) suggested that framboid size distribution is preserved over geological time, Wilkin *et al.* (1997) stated that this technique should only be applied as a palaeo-redox indicator where secondary growth is limited.

2.2 Methodology

2.2.1 Sedimentology

The colour and fissility of sediment material was recorded by the author during field observations and laboratory examinations of samples. Cut and polished sections were examined in order to study sediment fabrics and further samples were set into resin and polished for examination under the Scanning Electron Microscope (SEM).

2.2.2 Ichnology

The degree of bioturbation was assessed by the author in the field using a variety of bioturbation indices (see *Figures 2.4 – 2.6*). Observations about the trace fossil forms and their interaction were made in the field locations and slabs were collected for identification of individual trace-fossil taxa.

2.2.3 Pyrite Framboids

There have been several approaches to measuring framboid diameter. Wignall *et al.* (1996) concentrated the pyrite fraction by centrifuging sediment in bromoform, and then examined the heavy fraction under SEM. Ohfuji and Akai, (2002) picked framboidal pyrite and greigite grains for SEM from residues after washing sediment through a 200 mesh sieve. Wilkin *et al.* (1997) prepared polished thin sections by impregnating sediment cores with a low-viscosity epoxy. After the epoxy cured the core sections were cut, ground and polished with diamond pastes. They measured framboid size distributions using photographs from an optical microscope using a calibrated scale prepared from a photograph of an engraved micrometer. Several authors, for example Wignall *et al.* (2005), measured framboid diameters directly from backscatter SEM images of polished blocks. This appears to be the most convenient methodology for examining mudstones, but it is thought that this tends to underestimate the true diameter. However, calculations by Wilkin *et al.* (1996) showed that this underestimation does not exceed 10% and so data measured using this method has an acceptable error range.

Sediment samples were set in resin and polished by Storecore UK, before being coated with carbon and examined by the author under a JEOL Scanning Electron Microscope. Pictures were taken of framboids and the diameter was measured using the scaling on the associated software programme. The diameter of 50 framboids was measured from each sample, as further data collection from the same sample produced variations less than 0.1 % from the mean recorded from measuring 50 framboids. Traditionally the data is represented in box and whisker plots, but Wilkin *et al.* (1996) suggested using the ratio of standard deviation to mean. This ratio appears to be relatively constant in framboid size distributions from euxinic sediments (0.34+/-0.02), whereas the ratio is quite variable (0.55+/-0.15) in non-euxinic sediments. They also suggest examining the skewness of the data, and recording the occurrence of other pyrite morphologies present in the sediment.

2.3 Results

2.3.1 The Niveau Pacquier Sequence, Col de Palluel, Vocontian Basin, S.E. France

2.3.1.1 Sedimentology

The Niveau Pacquier sequence comprises two finely laminated 'paper like' dark shale horizons within the blocky dark clays of the Marnes Bleues Formation (see *Figure 2.13*).

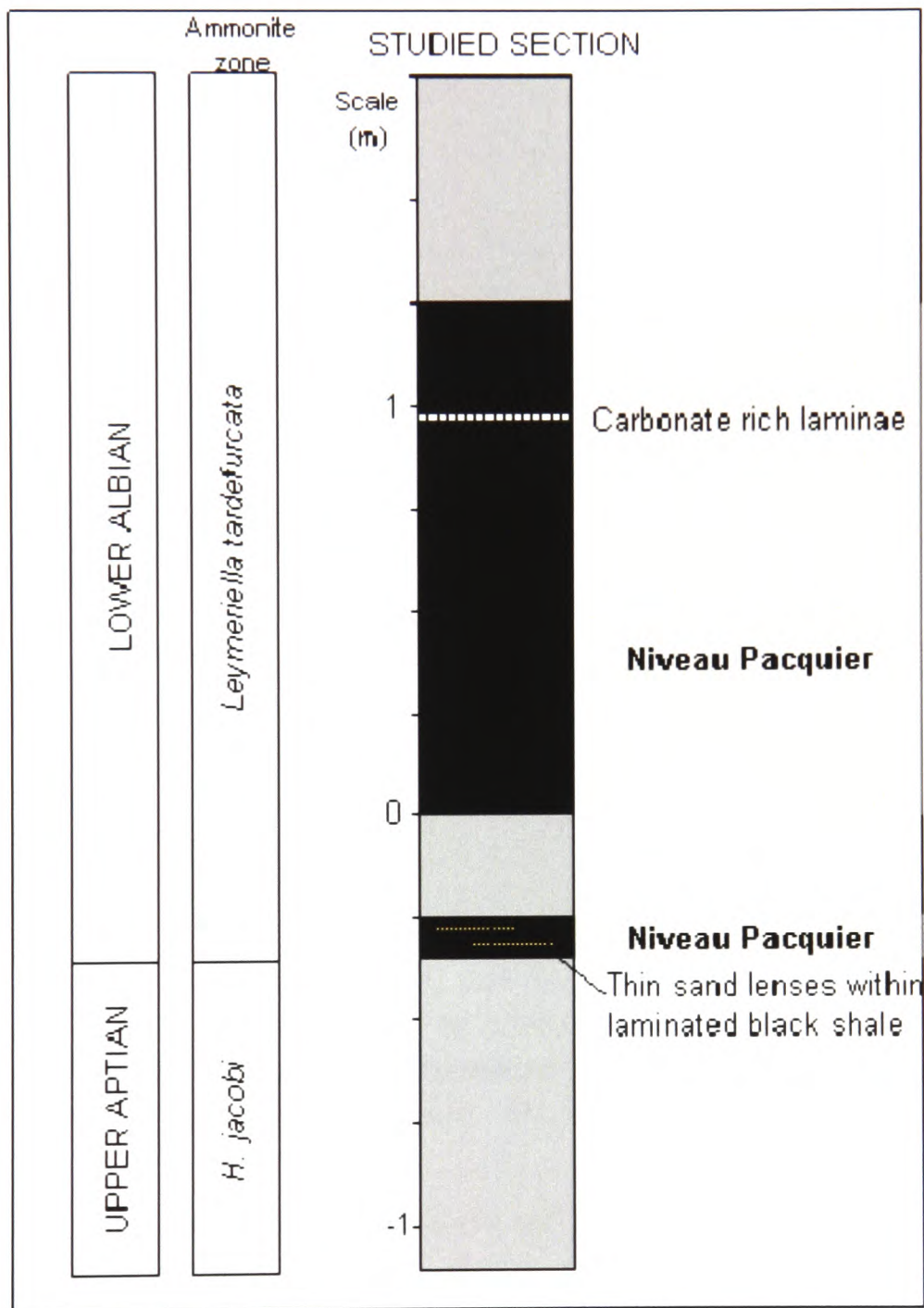


Figure 2.13: Stratigraphic log of the studied Niveau Pacquier sequence. The pale grey represents the grey clays of the Marnes Bleues Formation and the black represents the Niveau Pacquier black shales.

The Niveau Pacquier sequence contains many slickensides and gypsum bands - the presence of gypsum is often associated with the weathering of iron sulphide. The black shale is relatively fossiliferous with a mainly ammonite fauna, some of which are fragmented, and which are preserved mainly as impressions or pyrite film. The

Marnes Bleues sequence contains much less fossil material although the diversity of fauna is greater (see **Chapter 3**). Within the Marnes Bleues Formation, the fossil material tends to still be carbonate based, whereas macrofossil carbonate preservation is only observed towards the very top of the Niveau Pacquier Formation. Carbonate microfossils however, such as planktic foraminifera, appear to be relatively well preserved throughout the Niveau Pacquier Formation as well as in the Marnes Bleues (see *Figure 2.14*).

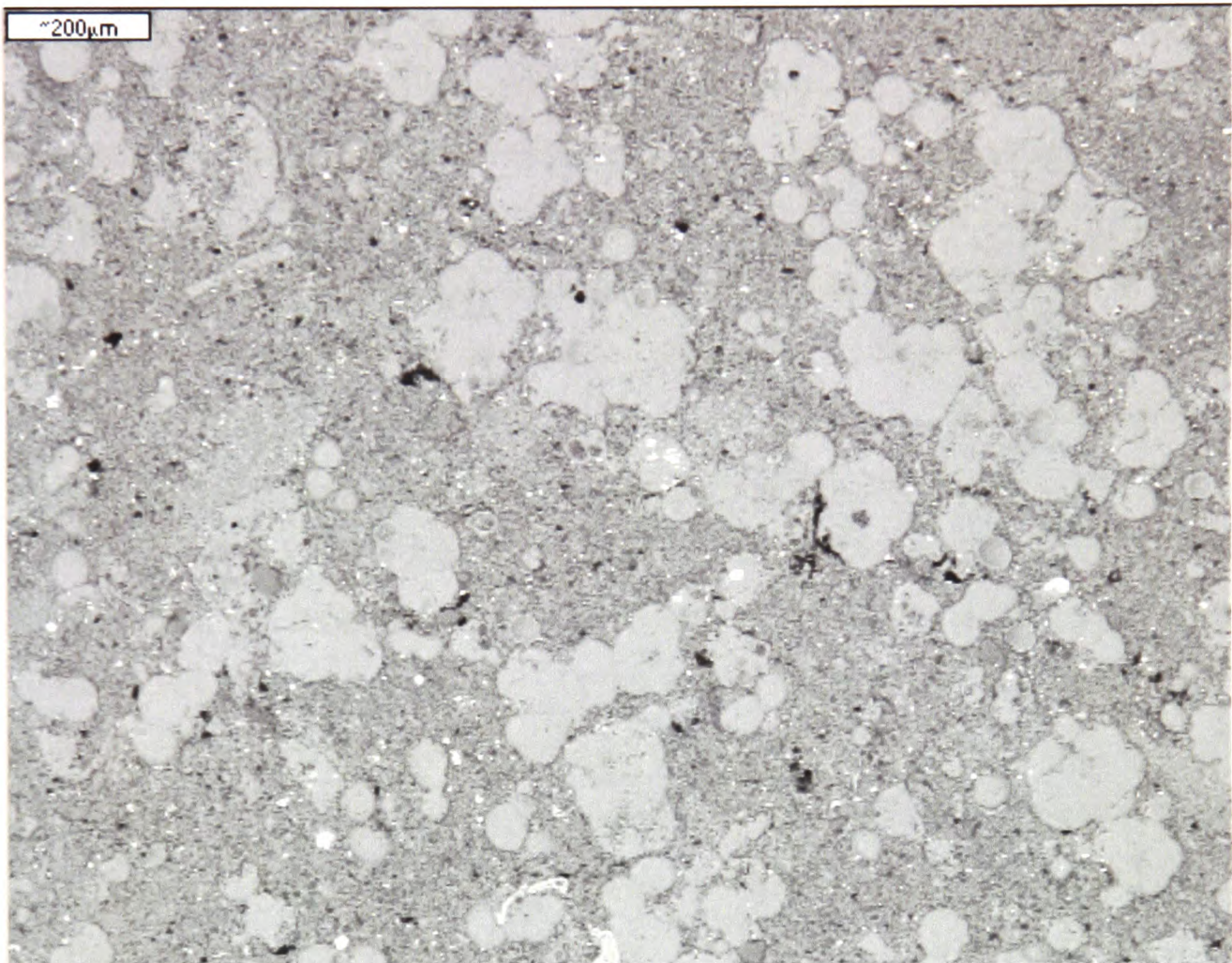


Figure 2.14: Backscatter scanning electron microscope image of a polished slab of Niveau Pacquier black shale (from 1.2 m above the base of the black shale horizon). The dull grey forms represent carbonate micro- and nanofossils whereas the bright specks represent pyrite framboids. The scale bar represents ~200 μ m.

The first black shale layer is ~7 cm thick and the transitions between this and the Marnes Bleues Formation is very sharp. Within this sequence there are very thin (~3 mm) sandstone lenses exhibiting cross bedding. The lenses of sand appear to have a rippled interface with the laminated material and possibly represent the distal end of a turbidite. Above this black shale layer there is ~29 cm of Marnes Bleues clay followed by a sharp transition, marked by sudden lamination and an increase in the abundance of preserved ammonites, into the main black shale horizon. The termination of the black shale layer is equally as sharp, with a clear transition into

unlaminated Marnes Bleues clays, followed by a thin 1 cm band of black shale material about 7 cm above the termination of the main sequence.

- **Colour** – The Marnes Bleues Formation is a dark grey mudstone. However, the Niveau Pacquier Formation is dark grey to black, indicating a higher organic carbon content (see *Figure 5.6*) associated with deposition under lower oxygen conditions. There are pale horizons within the sequence, associated with nanofossil material, and one thin nanno-limestone horizon.
- **Lamination** – While the Niveau Pacquier black shales are highly laminated, the Marnes Bleues Formation comprises massive clays. There is little physical evidence of bioturbation within the Marnes Bleues clays in the field section or the slabs held in the collection at the Oxford University Museum of Natural History. However, limited sedimentological information is retained through the sequence apart from the suggestion of bedding on a large scale, which could be indicative of almost complete homogenisation by bioturbation. The fine laminations suggest that the Niveau Pacquier formation was laid down under anoxic conditions, where bioturbation was suppressed. However, the lack of evidence of bioturbation or laminations in the Marnes Bleues material does not rule out the possibility that this was also laid down under relatively oxygen-restricted conditions.
- **Fissility** - The Niveau Pacquier black shales show the ‘papery’ fissility common to many low-oxygen deposits. On the other hand, the Marnes Bleues formation weathers in a ‘blocky’ way.

2.3.1.2 Ichnology

The Niveau Pacquier black shale horizons contain fine laminations, with little evidence of bioturbation. This would correspond to Bioturbation Index value of 0 according to Reineck (1963), an Ichnofabric index of 1 according to Droser and Bottjer (1986), or 0% bioturbation according to Miller and Smail (1997). In terms of oxygenation, this is believed to correspond with anoxia. The grey clay samples again show little evidence of bioturbation but there is also limited evidence of sedimentary structures. It is difficult therefore to classify the sediment as it could represent almost no bioturbation (0 or 1 on Reineck’s (1963) Index, 1 or 2 on Droser and Bottjer’s (1986) scale, or between 0 and 10% using Miller and Smail’s (1997) approximations) or full homogenisation of the sediment. The values given here represent just some of

the schemes proposed to semi-quantify the degree of bioturbation, and the differing values highlights the problem with using the different scales. The use of estimated percentage cover would seem to be the most directly comparable method, avoiding the confusion of different numbering systems for the descriptive schemes. The lack of trace-fossil evidence means that further environmental interpretation is not possible.

2.3.1.3 Pyrite Framboids

The variation in mean and range of the framboid distributions for each sample do seem to vary in the expected manner between the grey clay and black shale samples (see *Figure 2.15* and *Appendix A, Table A.1*).

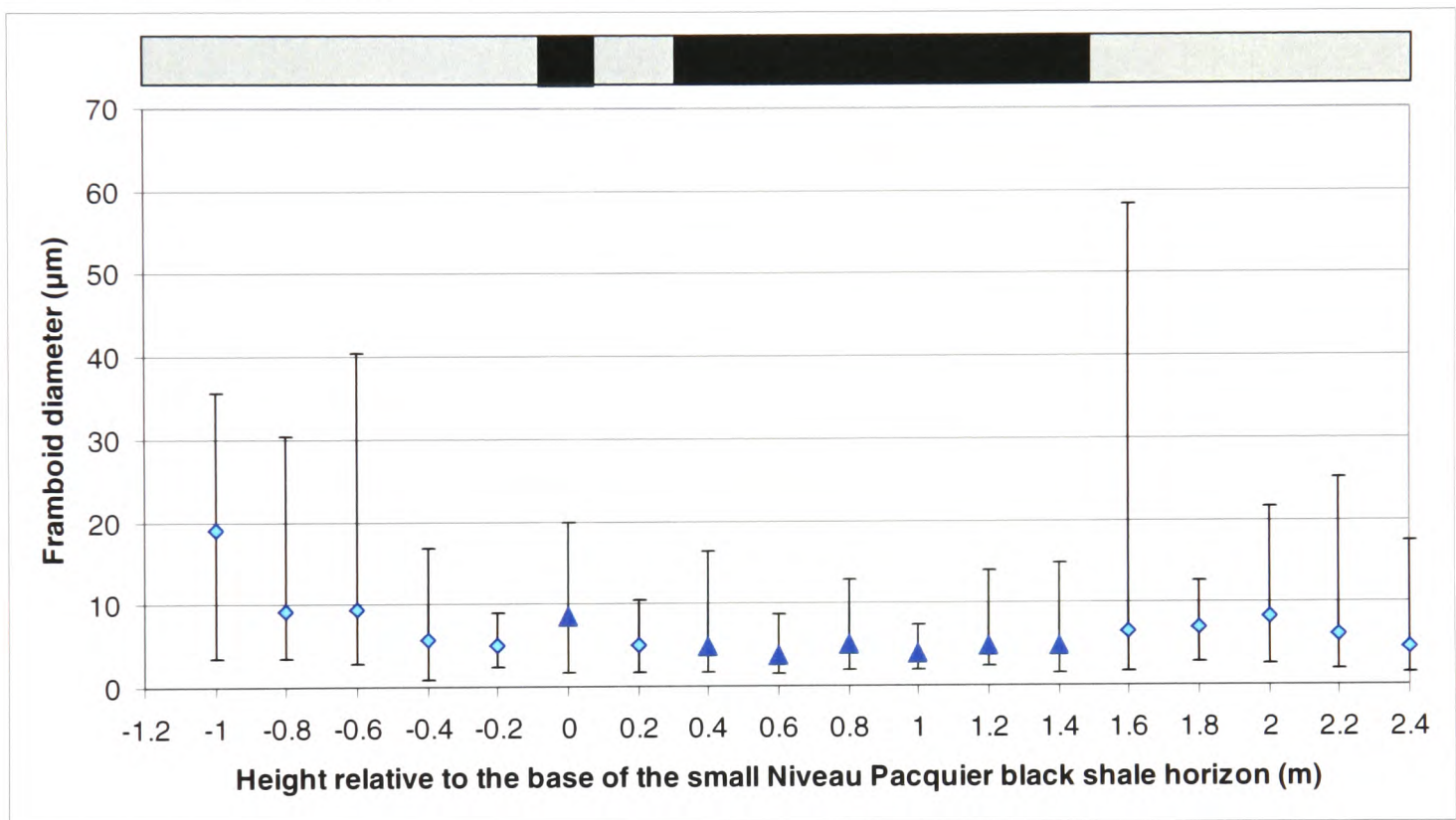


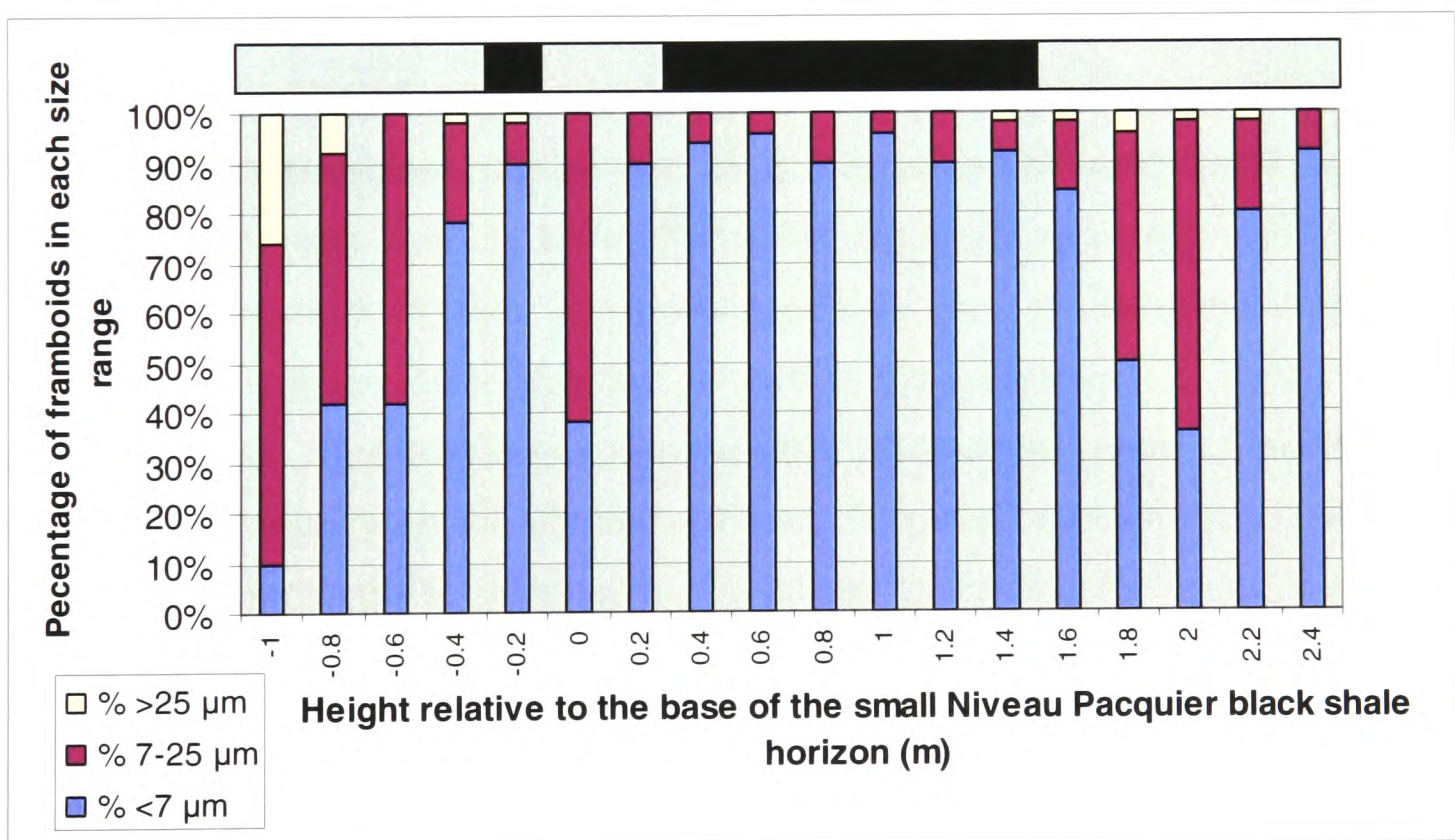
Figure 2.15: The mean and range of pyrite framboid diameters for the Niveau Pacquier sample range. The dark shading corresponds to the Black Shale samples whereas the light diamond data points represent the Grey Clay samples.

In general, the black shale samples do show a restricted range in the size of framboids, which would support the idea of framboid formation within the water column. The results from the two-tailed Student's t-test show that the black shale and grey clay data sets are statistically distinct (see *Figure 2.16*).

Grey Clay		Black Shale		P value
Mean	Variance	Mean	Variance	
7.8	38.5	5.1	8.3	2.5×10^{-17}

Figure 2.16: The two-tailed Student's t-test results for the Niveau Pacquier framboid diameter data sets. The test shows that the grey clay and black shale data sets are distinguishable as the P value is below 0.05.

Using a cumulative graph of the numerical boundaries proposed by Wilkin *et al.* (1997), all Black Shale samples plot with 90% or more frambooids falling below $<7 \mu\text{m}$ in diameter (see *Figure 2.17*). This fits best with that suggestion of Wilkin *et al.* (1997) that, in the Black Sea, samples with 95% or more frambooids within this range represent sediments laid down under anoxic conditions. Variations in frambooid sizes have been well recorded between different sites, for example between the Kimmeridge Clay (Wignall and Newton, 1998) and the Black Sea (Wilkin *et al.*, 1997), and therefore it seems possible that while two black shale samples do plot within Wilkin *et al.*'s (1997) range, a cut off of 90% may well represent this same boundary for the Niveau Pacquier samples. However, it should be noted that two grey clay samples also plot with 90% or more frambooids $<7 \mu\text{m}$. While the sample from 2.4 m is firmly within the Marnes Bleues grey clays, the sample from 0.2 m is just below the main black shale horizon. It could be suggested that this sample corresponds to transitional palaeo-oxygenation conditions or represents a black shale sample that underwent later re-oxidation. However, the trace-element and trace-element ratio data for this sample give no indication of low-oxygen conditions during formation (see *Figures 4.3 and 4.8*).



*Figure 2.17: A cumulative bar chart to represent the percentage proportion of frambooids within each size range for the Niveau Pacquier samples (based on the numerical boundaries implied by Wilkin *et al.*, 1997). Along the top, the black sections represent the Black Shale samples whereas the pale grey sections represent the Grey Clay samples.*

Wignall and Newton's (1998) environmental descriptions do not seem to fit the data as well. The black shale samples more closely represent Wignall and Newton's (1998) description of Lower Dysaerobic conditions where the size range is similar to that proposed for euxinic settings (all framboids <5 µm in size) but occasional larger framboids are present. All of the main black shale sequence samples show a mean framboid diameter of less than 5 µm, whereas the majority of grey clay samples have a mean value higher than this and this cut-off could possibly represent the boundaries of Lower Dysaerobic facies. Many of the grey clay samples include much larger maximum framboid diameters, and several of them have no framboids <3 µm in diameter. This more closely fits Wignall and Newton's (1998) description of Upper Dysaerobic conditions.

Both Wilkin *et al.*'s (1997) and Wignall and Hallam's (1992) framboids size ranges for euxinic conditions are similar and the slight variation may simply be due to differences between the sites investigated. Both descriptions include a greater limitation in framboids sizes than demonstrated by the black shale samples which suggests that conditions at the time of deposition of the Niveau Pacquier sequence were not truly euxinic. However, Wilkin *et al.*'s (1997) model groups dysoxic and oxic conditions together, suggesting that only true euxinic conditions could affect framboids size distributions. On the other hand, Wignall and Newton's (1998) model distinguishes between euxinic, lower dysaerobic and upper dysaerobic conditions. However, descriptions of lower dysaerobic conditions show the redox boundary as being at the sediment:water interface or within the sediment (e.g. Arthur and Sageman, 1994). This does not explain the relatively restricted range of framboids suggested for lower dysaerobic settings as theoretically only framboids formed within the water column should be restricted in size as their increasing mass causes them to fall away from the redox boundary.

The ratio of syngenetic to diagenetic framboids formed should aid in the distinction between lower dysaerobic and anoxic, or true euxinic conditions. If the models of framboids formation are correct then the syngenetic:diagenetic ratio should be strongly affected by the proximity of the redox boundary to the sediment:water interface. If the redox boundary within the water column is very close to the sediment surface then larger framboids should start to appear. In contrast, as soon as

the redox boundary is predominantly at the surface or within the sediment then larger diagenetic framboids should become dominant. In essence the scenario where the redox boundary is close to the sediment:water interface, where fluctuations may allow the formation of some larger diagenetic forms, matches Wignall and Newton's (1998) proposed range for lower dysaerobic conditions. However the point at which the redox boundary meets the sediment surface is theoretically the boundary between anaerobic and dysoxic conditions. This would suggest that Wignall and Newton's (1998) lower dysaerobic conditions actually represent the anaerobic:lower dysaerobic transition zone and this may be the setting for the deposition of the Niveau Pacquier sequence.

Wilkin *et al.* (1996) proposed using a plot of Standard Deviation against Mean for framboid distributions, and suggested that euxinic conditions would be represented by a narrow range of 0.34 ± 0.02 . This does not seem to provide a reliable distinction between the two data sets, as both the black shale and grey clay samples plot with a regression line within the proposed limits for non-euxinic deposition (see *Figure 2.18*) and the grey clay data set demonstrates poor correlation with an R^2 value of 0.47.

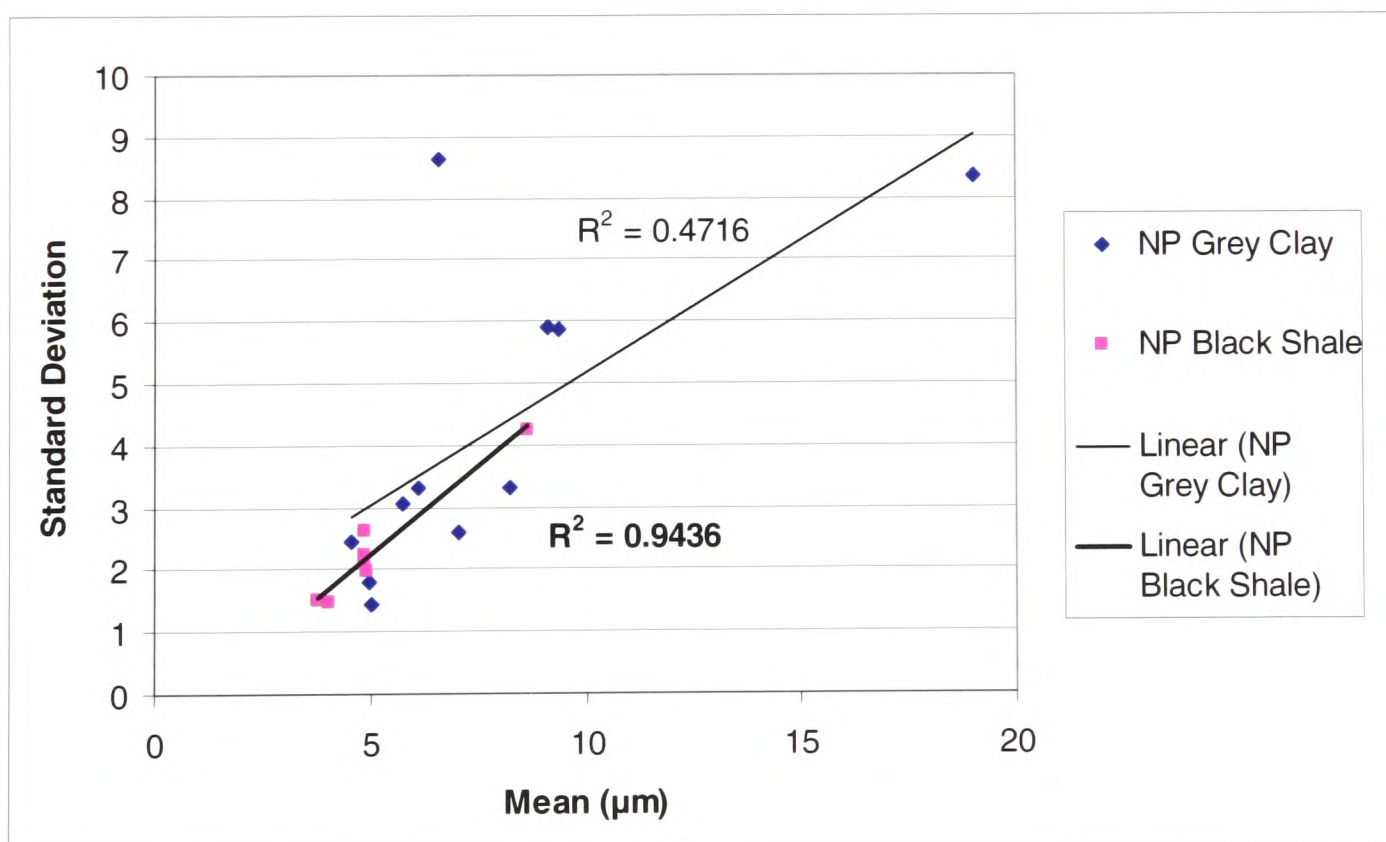


Figure 2.18: Comparison of the Standard Deviation and Mean of framboid diameters for the Niveau Pacquier samples.

If the proposed ranges are correct, this suggests that while the black shale samples may have been laid down under low-oxygen bottom-waters, the conditions were not so extreme that free hydrogen sulphide was present. Wilkin *et al.* (1996) also suggested that a calculation of skewness should separate sample sets such as these, but a plot of the calculated skew (see *Figure 2.19*) does not seem to show any correlation with the sample sets.

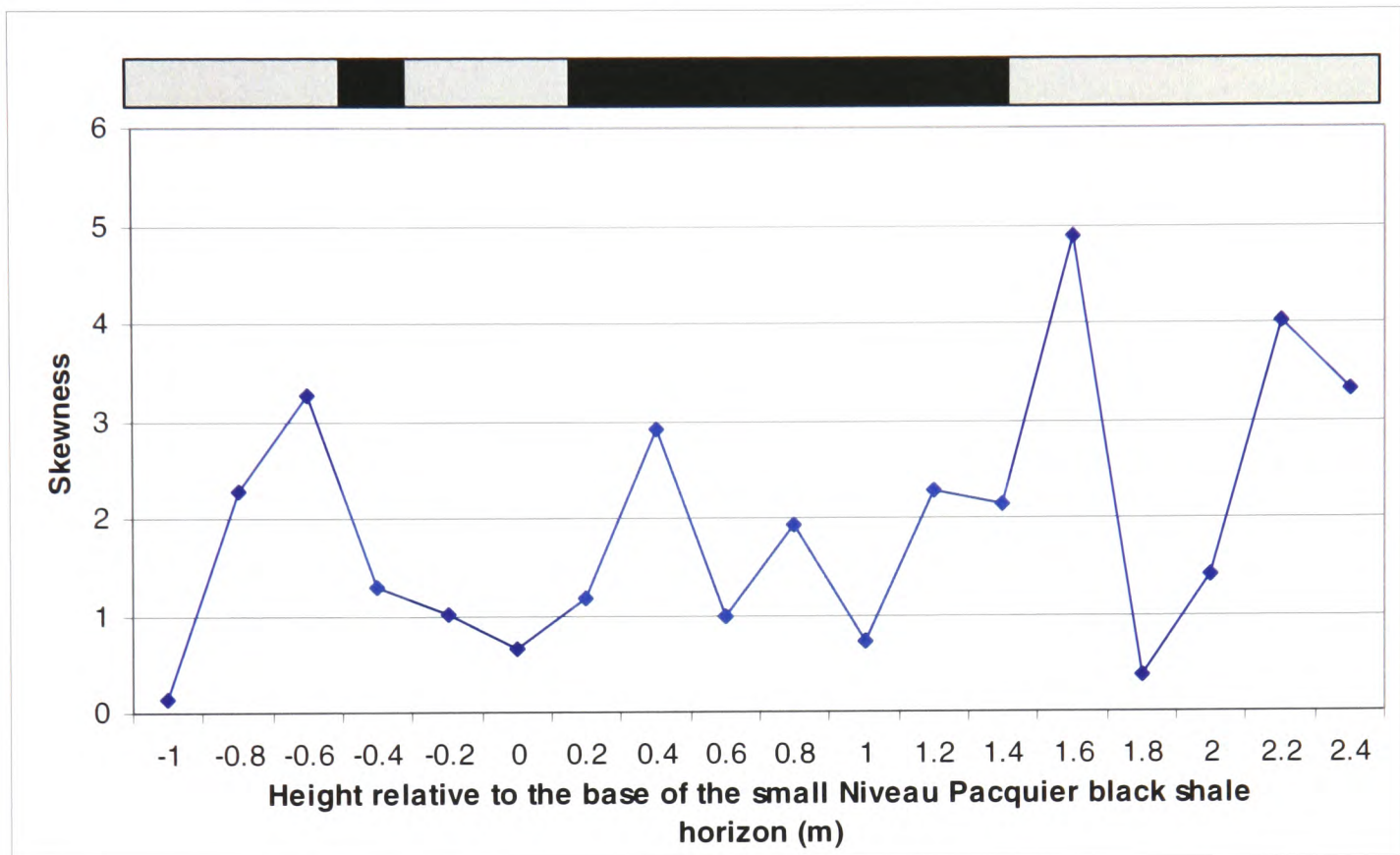


Figure 2.19: Plot of the calculated skewness of framboid diameter data for the Niveau Pacquier samples. Along the top, the black sections represent the Black Shale samples whereas the pale grey sections represent the Grey Clay samples.

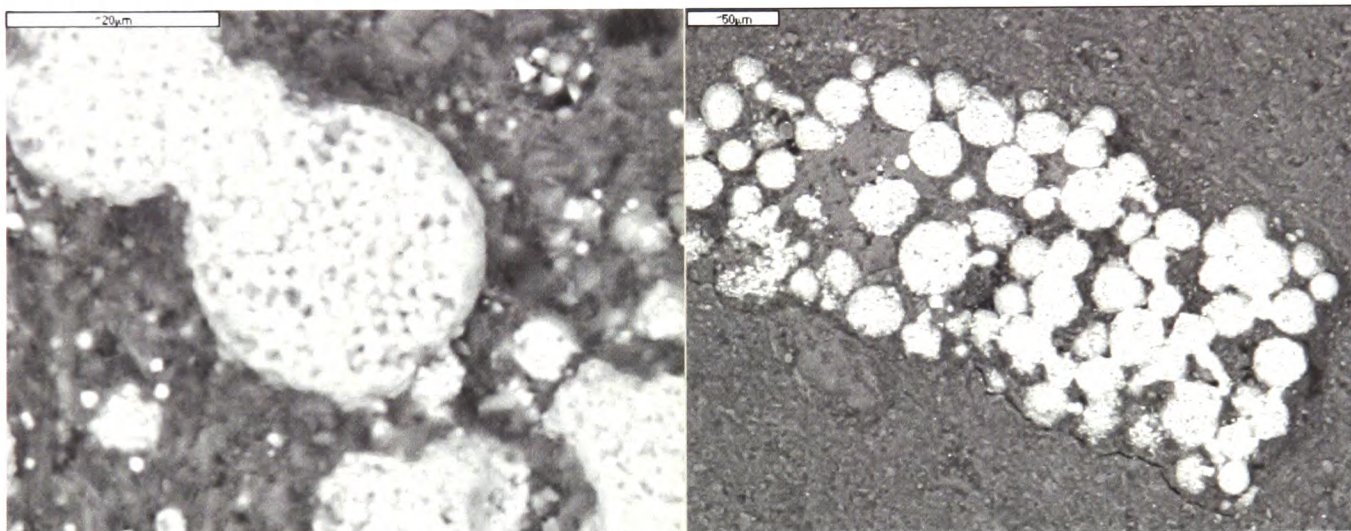
While there is debate about the interpretation of numerical categories in the models proposed, there does seem to be a big distinction between the black shale and grey clay samples in terms of pyrite morphology and distribution. The following proposed categories below seem to neatly divide the two sample sets, with the black shales all falling within the following category:

- **Category 1:** A random covering of small framboids where groups of framboids and euhedral crystals are rare and only occasionally framboids are associated with shell material.

This distribution of pyrite correlates with the idea that framboids formed at a redox boundary which was within the water column. In contrast, the grey clay samples tend to fall into two categories.

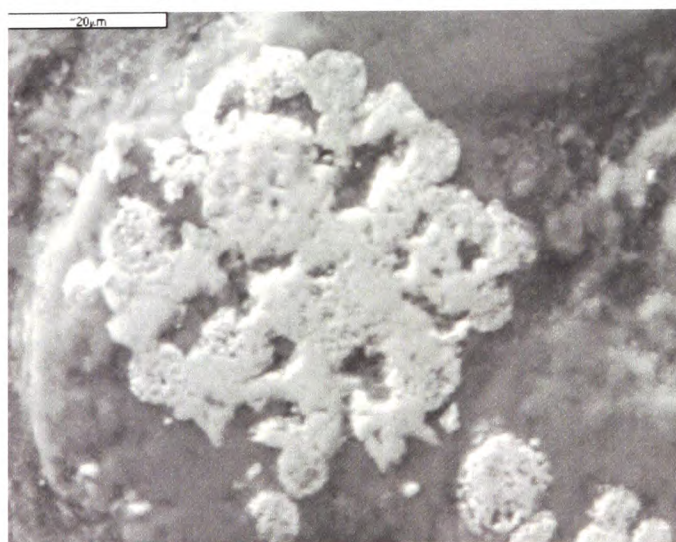
- **Category 2a:** Some samples contain relatively common large framboids often made of comparatively large crystals, clusters of framboids and common euhedral crystals which are occasionally larger than individual framboids.
- **Category 2b:** Other samples contain only rare framboids, usually associated with cavities within shell material.

The distribution of pyrite within the first type of samples suggests that pyrite formation occurred within relatively organic-rich sediments. Wilkin and Barnes (1997) suggested that the presence of large euhedral crystals indicates that pyrite formation occurred slowly within the sediment, under a relatively oxic water column. The presence of a relatively oxic water column would suggest that the organic content of the sediment would be relatively low and this may restrict pyrite formation. The large clusters of framboids may form associated with concentrations of organic matter such as within a burrow system (see *Figure 2.20b*). Also, pyrite overgrowth was observed in some of these samples, which also suggests that pyrite formation occurred within the sediment (see *Figure 2.20a and c*).



(a) Sample from 0.2 m, scale bar $\sim 20 \mu\text{m}$

(b) Sample from 1.0 m, scale bar $\sim 50 \mu\text{m}$



(c) Sample from 2.0 m, scale bar $\sim 20 \mu\text{m}$

Figure 2.20: Backscatter scanning electron microscope images of pyrite overgrowth of framboids (a, c) and a framboid cluster (b) in Niveau Pacquier Grey Clay samples.

The distribution of pyrite within the second type of samples may represent sediments which formed under a more oxic water column, or formed under fluctuating redox conditions, or just contained lower organic matter. This would have restricted the amount of pyrite that could form which would explain the rare occurrence of framboids. The association of framboids with apparent cavities within shell material may represent pyrite formation within reducing microenvironments created due to breakdown of localised concentrations of organic matter.

2.3.2 The Briestroffer Sequence, Col de Palluel, Vocontian Basin, S. France

2.3.2.1 Sedimentology

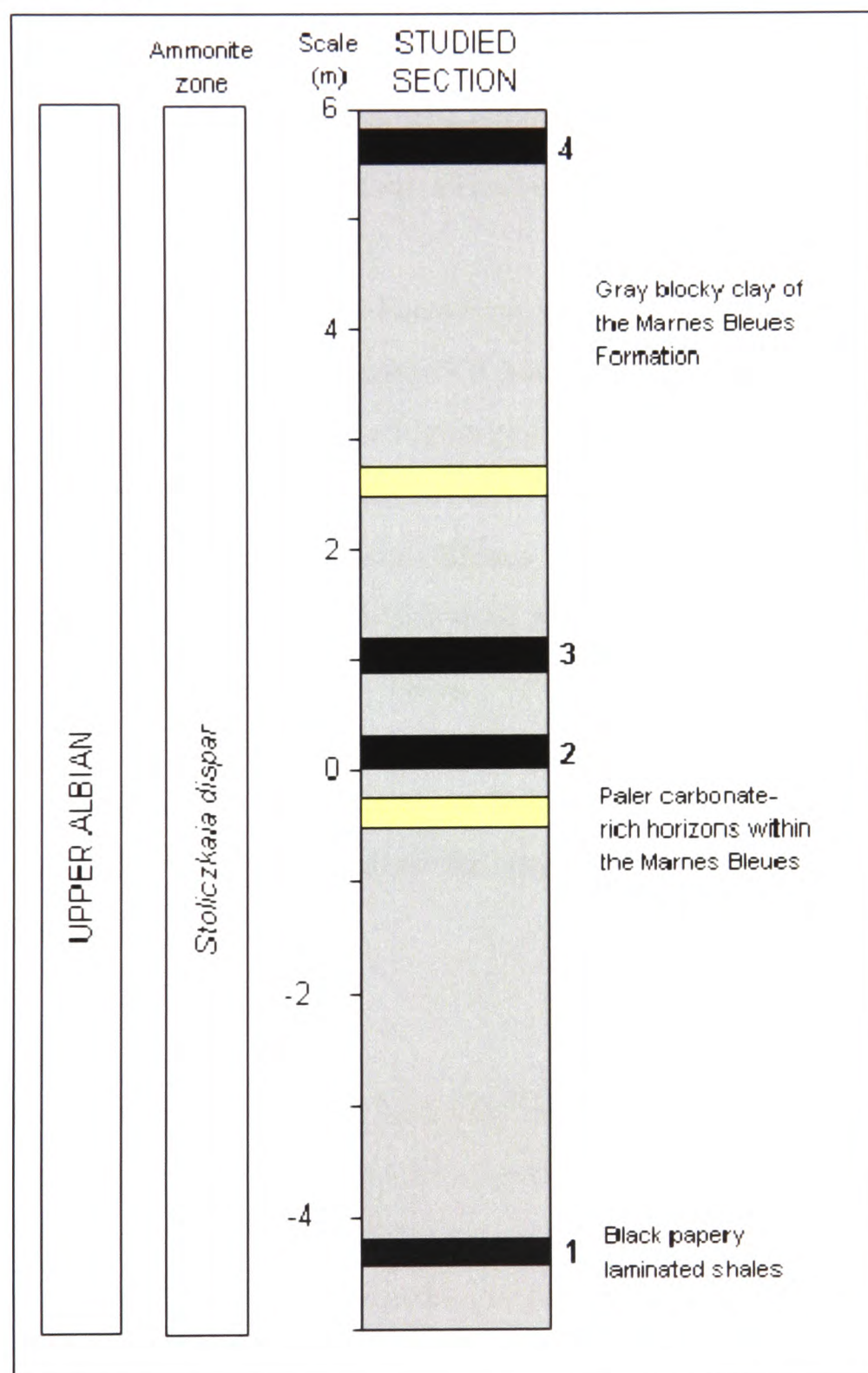


Figure 2.21: Stratigraphic log of the studied Briestroffer section, including four of the Briestroffer black shale bands.

The Breistroffer sequence is comprised of 4 Breistroffer layers of black paper shales within massive scale bedding of the Marnes Bleues (see *Figure 2.21*). The transition between the grey clays and the paper shales is abrupt and each Briestroffer layer is between 20-25 cm thick. Within the Marnes Bleues formation there are paler, carbonate-rich bands between the black shale events and these alternating extremes of depositional environments are thought to represent the effect of varying climate under the effect of Milankovitch cycles (Br  h  ret, 1994). The nature of these alternating sediments suggests that OAE 1d was a fluctuating, drawn-out event in contrast to the more confined black shales of the Niveau Pacquier sequence (OAE 1b). These Breistroffer layers show good preservation of a range of fossil material, namely pyrite films of ammonites and belemnites. The fossil content is lower in the Marnes Bleues formation, with some localised areas containing bivalves (see **Chapter 3**). The section studied includes the lower four Briestroffer layers of Gale *et al.*'s (1996) Briestroffer sequence (see *Figure 1.5*).

- **Colour** – The Marnes Bleues Formation is a dark grey mudstone with lighter bands representing the carbonate-rich horizons. The Briestroffer Layers are dark grey to black, indicating a higher organic carbon content (see *Figure 5.7*) associated with deposition under lower oxygen conditions.
- **Laminations** – While the Marnes Bleues Formation is massive, only showing bedding on a large scale, the black shale horizons show fine lamination. This suggests deposition under highly restricted oxygen conditions where bioturbation was strictly limited.
- **Fissility** - While the Marnes Bleues Formation weathers in a 'blocky' way, the Briestroffer black shales show the 'papery' fissility common to many low oxygen deposits.

2.3.2.2 Ichnology

Again, the Briestroffer black shale horizons contain fine laminations, with little evidence of bioturbation. This would correspond to Bioturbation Index value of 0 according to Reineck (1963), an Ichnofabric index of 1 according to Droser and Bottjer (1986), or 0% bioturbation according to Miller and Smail (1997). In terms of oxygenation, this is believed to correspond with anoxia. The grey clay samples show little evidence of bioturbation but there is also limited evidence of sedimentary

structures. It is difficult to therefore to classify the sediment as this could represent almost no bioturbation (0 or 1 on Reineck's (1963) Index, 1 or 2 on Droser and Bottjer's (1986) scale, or between 0 and 10% using Miller and Smail's (1997) approximations) or full homogenisation of the sediment. The lack of trace fossil evidence means that further environmental interpretation is not possible.

2.3.2.3 Pyrite Framboids

In contrast to the Niveau Pacquier sequence, there seems to be less differentiation in pyrite framboid diameters between the Briestroffer black shale and grey clay sample sets (see *Figure 2.22* and *Appendix A, Table A.2*). The results from the two-tailed Student's t-test show that the black shale and grey clay data sets are statistically distinct (see *Figure 2.23*), although the separation is not as reliable as it is for the Niveau Pacquier data sets.

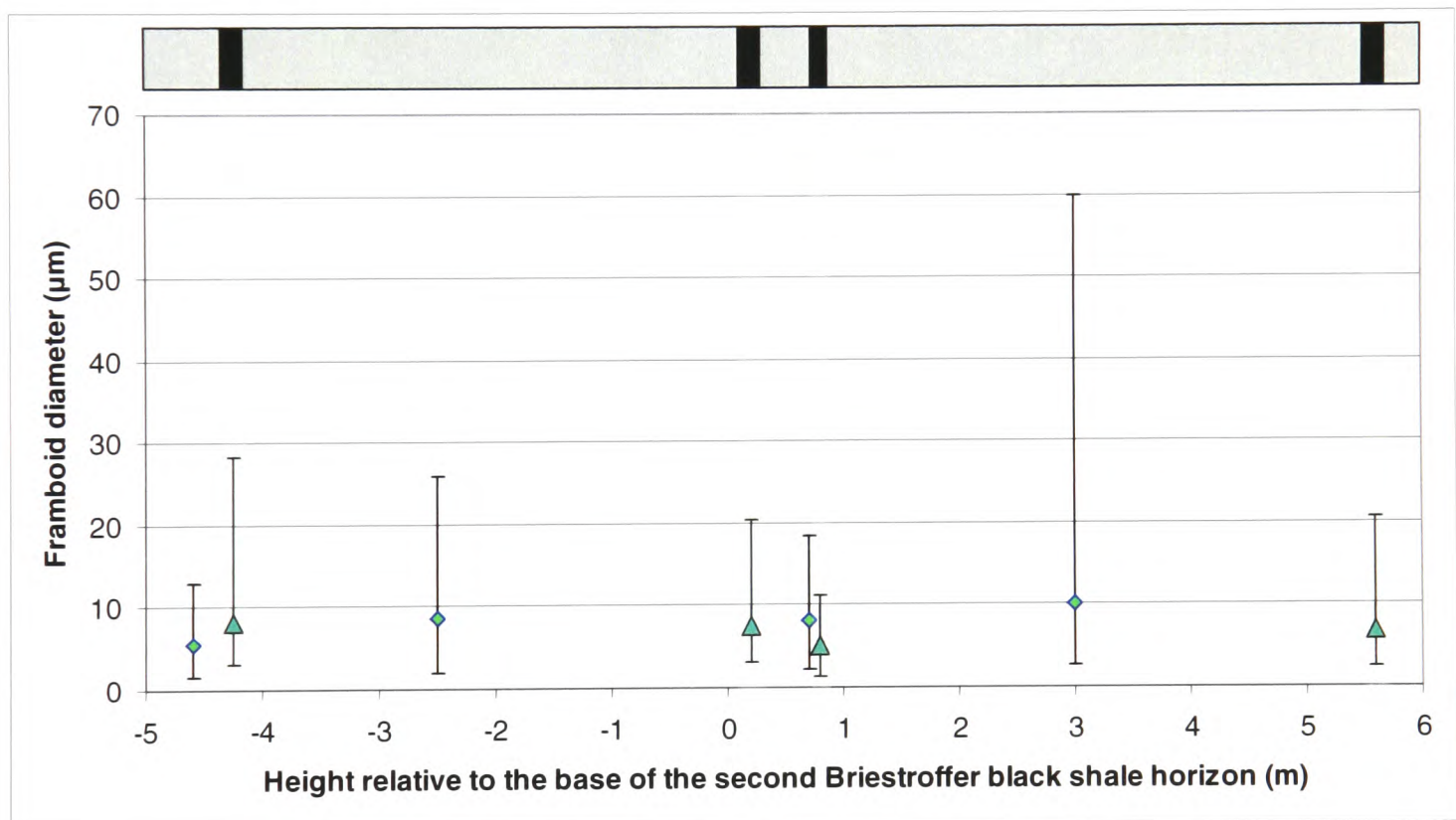


Figure 2.22: The Mean and Range of pyrite framboid diameters for the Briestroffer sample range. The dark triangular data points represent the Black Shale samples whereas the light diamond data points represent the Grey Clay samples.

Grey Clay		Black Shale		P value
Mean	Variance	Mean	Variance	
8.1	28.6	6.8	14.2	0.0073

Figure 2.23: The two-tailed Student's t-test results for the Briestroffer sequence framboid diameter data sets. The test shows that the grey clay and black shale data sets are distinguishable as the P value is below 0.05.

The cumulative graph of framboid size (see *Figure 2.24*) does show that, generally, the grey clay samples from the Marnes Bleues do contain proportionally less

framboids $<7 \mu\text{m}$ in diameter. However, none of the Briestroffer black shale samples contain 90% $<7 \mu\text{m}$ as seen in the Niveau Pacquier samples, let alone the 95% proposed by Wilken *et al.* (1997) to represent anoxic conditions.

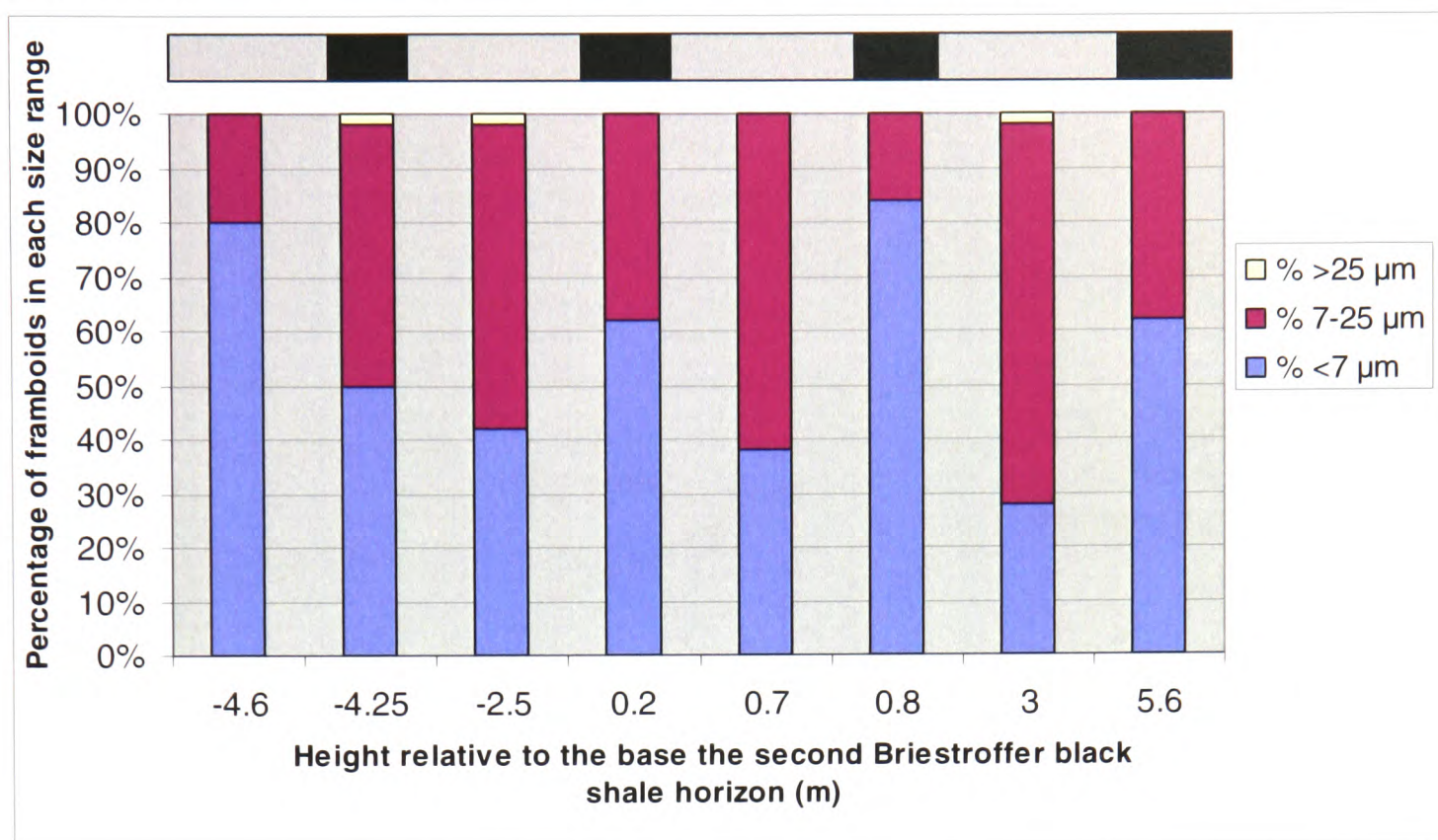


Figure 2.24: A cumulative bar chart to represent the percentage proportion of framboids within each size range for the Briestroffer samples (based on the numerical boundaries implied by Wilkin *et al.*, 1997). Along the top, the black sections represent the Black Shale samples whereas the pale grey sections represent the Grey Clay samples.

Only two samples contain no framboids $<3 \mu\text{m}$ in diameter, which would fit with Wignall and Newton's (1998) description of Upper Dysaerobic settings. However, the two samples represent black shale sediments and so should theoretically represent lower oxygenation settings than the Marnes Bleues samples. The Marnes Bleues samples, along with the remainder of the black shale samples, fit Wignall and Newton's (1998) description of Lower Dysaerobic settings. None of the samples have mean framboid diameter of $<5 \mu\text{m}$, which was the boundary suggested to differentiate the Niveau Pacquier samples. All of this indicates that either the Briestroffer sequence never reached the same extent of oxygenation depletion as the Niveau Pacquier sequence, or that the duration of low-oxygen events was low or fluctuation occurred, allowing framboid formation within the sediment even during the Briestroffer events.

The linear correlation of the Standard Deviation against the Mean plots within the 'non-euxinic' range proposed by Wilken *et al.* (1996) for the Black Shale samples

(see Figure 2.25). Unfortunately the small sample size makes the data unreliable, as demonstrated by the lack of a statistically valid linear correlation for the Grey Clay samples. The skewness plot (see Figure 2.26) proposed by Wilken *et al.* (1996) again seems to show little correlation with sediment type, and could not be used to differentiate the sample sets.

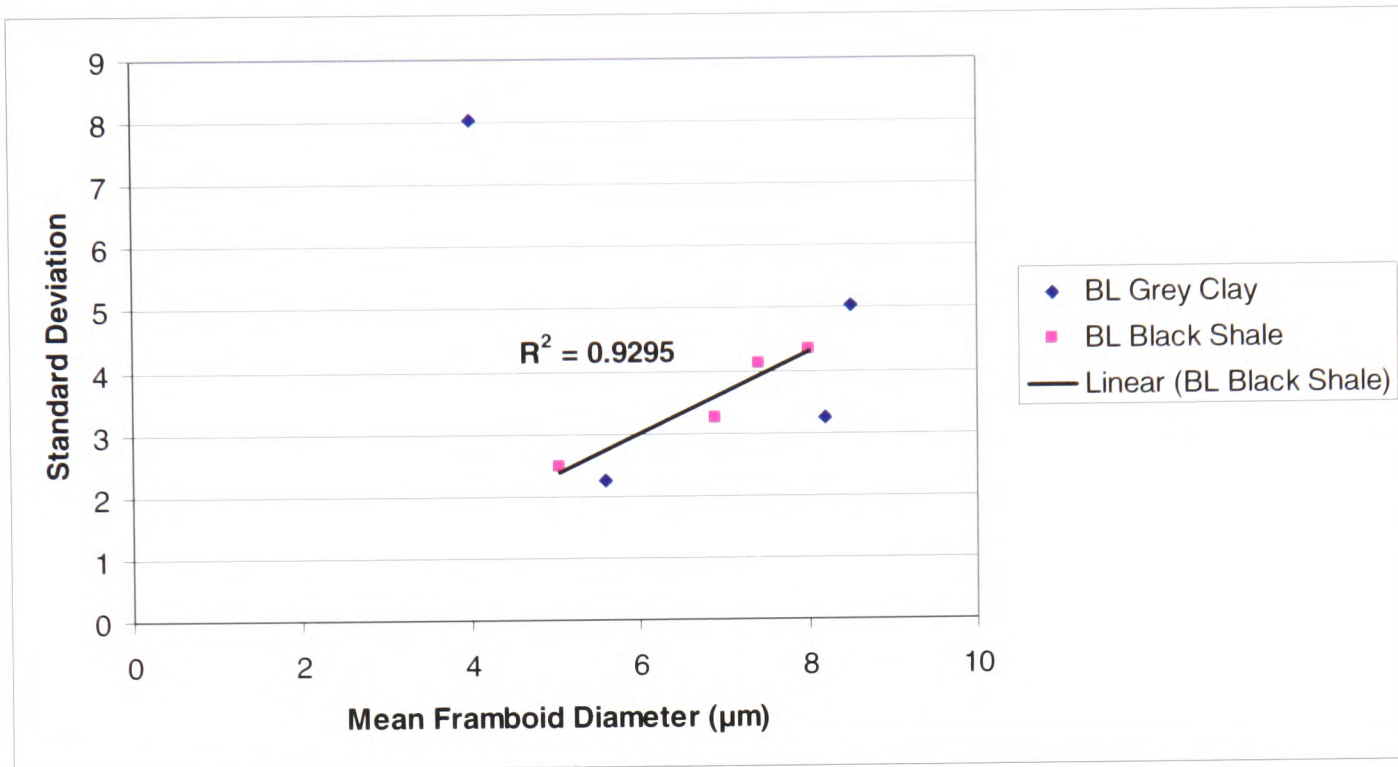


Figure 2.25: Comparison of the Standard Deviation and Mean of frambooid diameter for the Briestroffer samples.

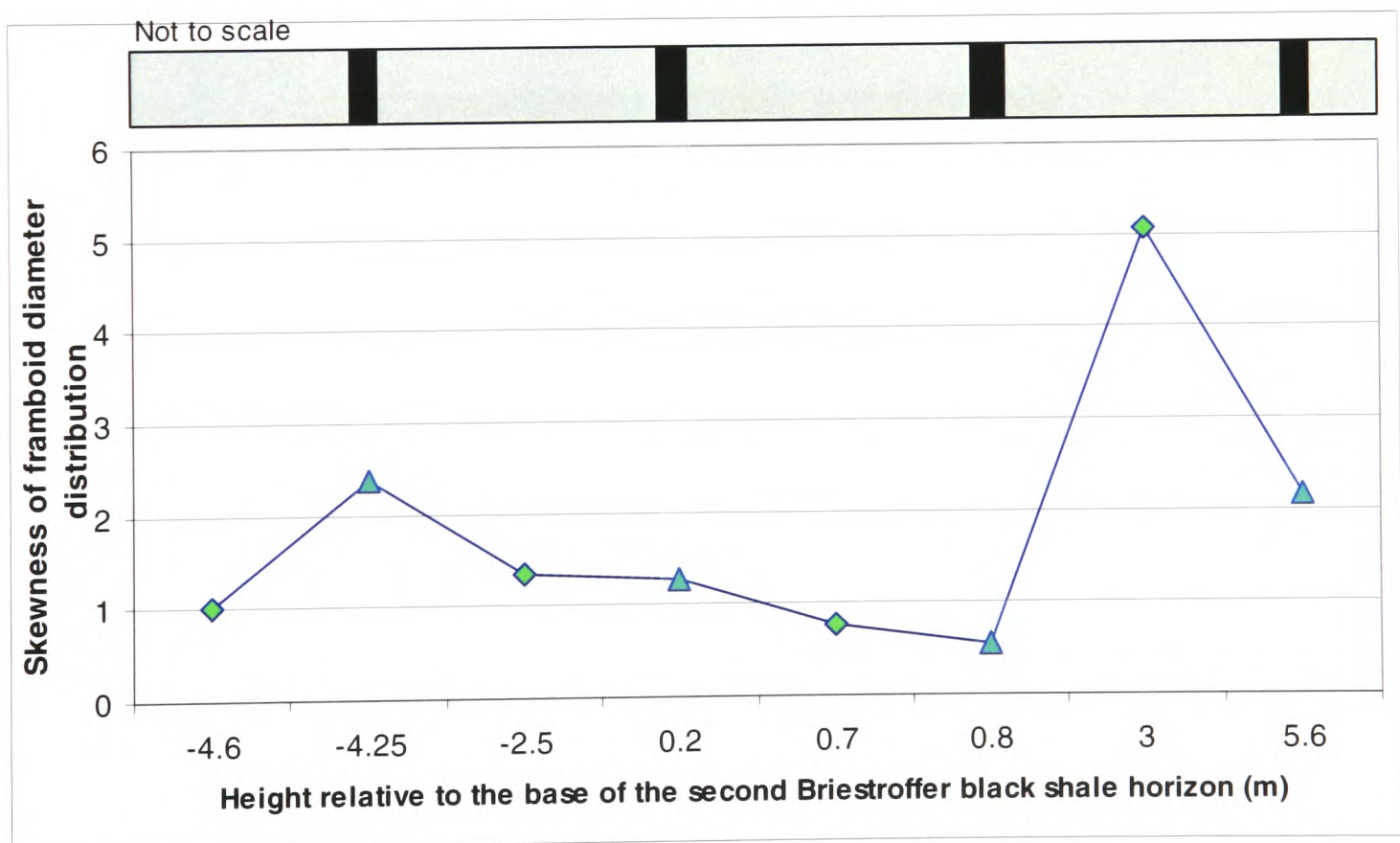
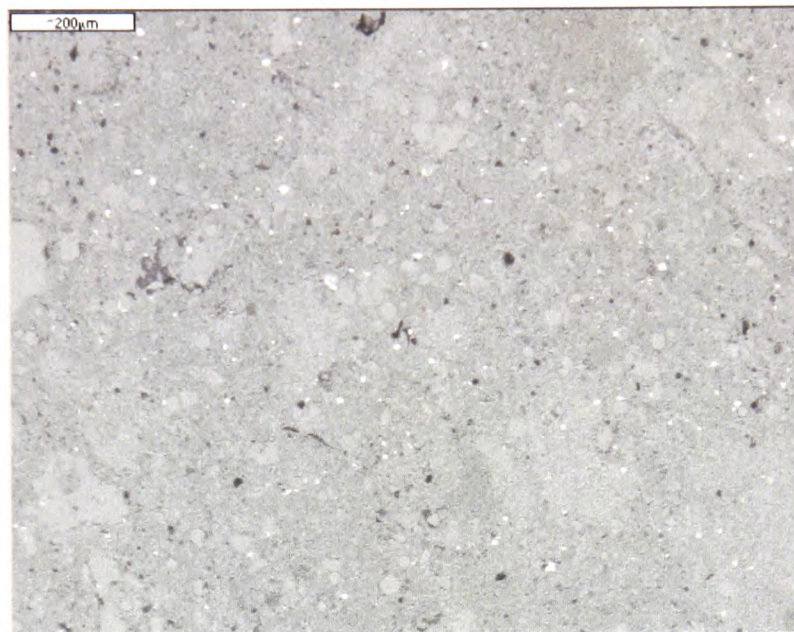
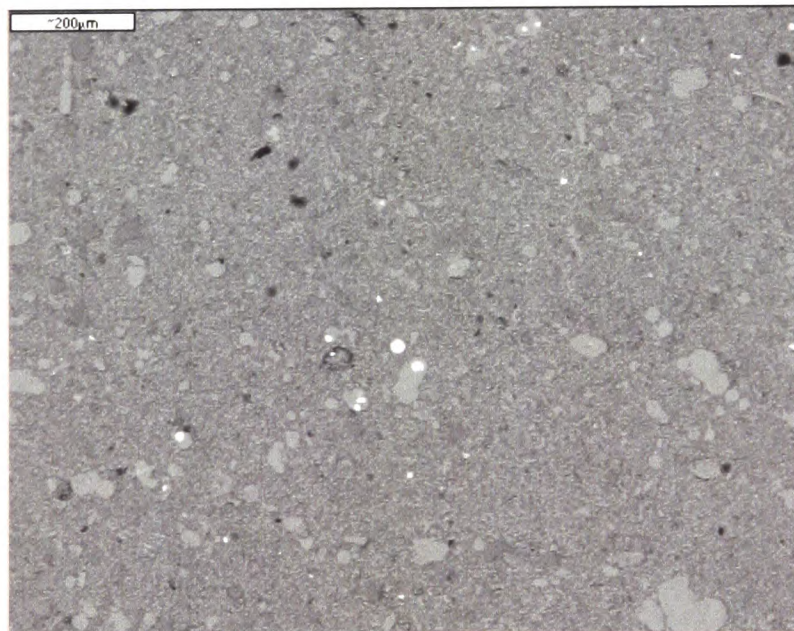


Figure 2.26: Plot of the calculated skewness of frambooid diameter data for the Briestroffer samples. The shaded points represent the black shale samples whereas the unshaded data points represent the grey clay samples.

Although the numerical data concerning framboid diameter is not as convincing as that for the Niveau Pacquier sequence, in general, the form and distribution of pyrite within the samples seem to follow the same trend. The black shale samples tend to show the same random spread of small framboids with limited evidence of euhedral crystals or framboid clusters (see *Figure 2.27a*), thereby falling into **Category 1**. Again, matching the two different types of grey clay samples from the Niveau Pacquier, half of the grey clay samples contain large framboids, large clusters of framboids and common euhedral crystals (see *Figure 2.27b*) (**Category 2a**).



(a) Sample from 5.6 m (Black Shale) showing common small framboids.



(b) Sample from -2.5 m (Grey Clay) showing rarer, larger framboids

Figure 2.27: Backscatter scanning electron microscope pictures illustrating the general spread of framboids, which show up as white specks, in a Black Shale (a) and Grey Clay sample (b). Scale bar represents ~200 μm .

The other half of the samples seem to meet the description of **Category 2b**, with very rare framboids mainly concentrated in what appears to be cavities in shell material, with occasional large euhedral crystals also contained within these spaces. The one exception is the sample from -2.45 m below the base of the second Briestroffer layer which should represent black shale material, but which contains a number of small euhedral crystals and large framboids. While the numerical aspect of the framboids data from the Briestroffer sequence does not clearly distinguish differing oxygen regimes for the two sets of samples, the proposed descriptive categories do clearly differentiate between the grey clay and black shale samples

2.3.3 The Folkestone Gault Clay

2.3.3.1 Sedimentology

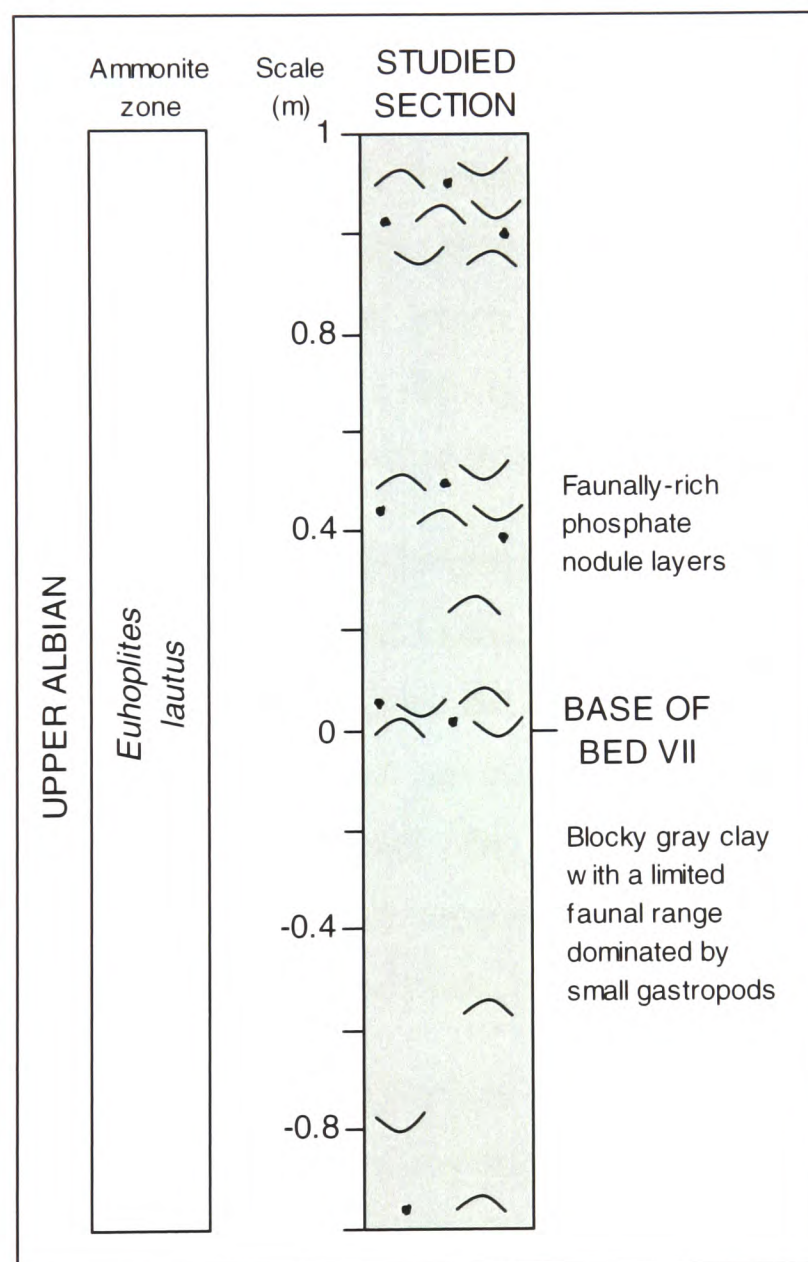


Figure 2.28: Stratigraphic log of the Folkestone Gault Clay section.

The Folkestone Gault Clay is a fossiliferous, blocky, grey mudstone. Transitions were observed between nodular, faunally rich layers, and layers with limited faunal range composed mainly of small gastropods (see *Figure 2.28*). There were also transitions between light and dark *Chondrites*. (see *Figure 2.33*). In terms of taphonomy, fossils are preserved as original material, pyrite and phosphate infills.

- **Colour** – the Folkestone Gault Clay is light grey, suggesting relatively oxygenated depositional conditions. The colour becomes lighter towards the top of the sequence due to the increase in carbonate content (see *Figure 4.30*).
- **Lamination** – the clay sequence is highly bioturbated and no laminations are visible. ‘Beds’ are assigned by occurrence of nodule bands or highly fossiliferous horizons (see *Figure 2.28*).
- **Fissility** – the clay breaks in a blocky fashion.

2.3.3.2 Ichnology

In terms of the Bioturbation Indices, the Folkestone Gault Clay appears to represent roughly 60% bioturbation. This corresponds with a Bioturbation Index value of 4 according to Reineck’s (1963) scheme, which is described as “High bioturbation, bedding boundaries indistinct, high trace density with overlap common.” Along with large, obvious traces, the sediment is mottled throughout with *Chondrites*.

Chondrites and *Thalassinoides* are both identifiable within the sequence, along with smaller pyritised burrows. Bromley and Ekdale (1984) identified *Chondrites* as the trace of a relatively oxygen-tolerant animal, but it is only assemblages dominated by this form alone that are thought to represent anoxic conditions. However, Leszczynski *et al.* (1996) recognised the combination of *Chondrites* and *Thalassinoides* as lower tier forms and suggest that an assemblage dominated by these represents formation under relatively low, possibly dysoxic, oxygen conditions.

In terms of burrow dimensions, *Thalassinoides* is generally represented by pyritised burrows up to 3 mm wide. There are many fragments of smaller pyritised burrows preserved (1-2 mm wide) which Leszczynski *et al.* (1996) referred to as *Trichichnus* and ‘*Mycellia*’. *Chondrites*, which is represented by a mottling on the exposed surfaces (see *Figure 2.33*) is generally 1-2 mm wide. The trace assemblage represents quite a high diversity of forms, which clearly indicates that oxygen was not severely restricted in bottom waters. In terms of mode of formation of burrows, Frey

(1970) suggested that *Trichichnus* is the semi-permanent burrow of a deposit feeder, and Osgood (1970) suggested that *Chondrites* represents the feeding system of another unknown infaunal deposit feeder. Bromley (1996) described *Thalassinoides* as a fodinichia trace. Ekdale and Mason (1988) suggested that assemblages dominated by feeding tracks represents a relatively low-oxygen regime, and that as oxygen increases, the assemblage will become dominated by pascichnia (grazing trails). However, Wheatcroft (1989) suggested that the opposite trend occurs, and there is still debate about this. In terms of modes of life of the species responsible for the traces, the assemblage represents mainly deposit feeders. This, however, does not give much information about palaeo-oxygenation, as Rhoads and Boyer (1982) suggested that deposit feeders' traces are likely to have obliterated any previous traces anyway.

The tier structure of the trace fossil assemblage appears to have four divisions:

- First tier – shallow level full reworking of sediment material.
- Second tier – forms such as *Thalassinoides*, represented by a collection of shell material. The burrow boundaries have been almost obliterated but the outlines are preserved by this infill of shell debris (see *Figure 2.29*).
- Third tier – the tier is dominated by *Chondrites* which is highlighted by a pale sediment infill (see *Figure 2.33*). The *Chondrites* effectively overwrites much of the second tier. There are also smaller pyritized burrows throughout the sequence (1-2 mm wide) which are probably associated with third tier (see *Figure 2.32*).
- Fourth tier – is comprised of long vertical pyritized burrows that appear to link complex trigonal junction horizontal burrow systems to the surface. The burrows sometimes have a reaction halo which suggests the burrows were rich in organics and that oxic water was supplied to the burrow by surface connection (see *Figures 2.30 and 2.31*). *Chondrites* is observed in the halo but never cutting across the actual burrow which supports the idea of these being a lower tier. If these burrows represented a higher tier, then they would have been preferentially reworked during the formation of *Chondrites*, as this tends to concentrate in areas of high organic content. However, the burrows are relatively large (~3 mm wide and up to 30 cm long) which goes against the suggestion that burrow diameter decreases as you move down the tier

system. There appears to be a concentration of these vertical burrows leading from around +0.4 m from the base of Bed VII but there is no evidence of sequence condensation. This may suggest that this horizon represented more oxic bottom waters which allowed these large burrows to be formed deep into the sediment, with the oxic waters being supplied by the vertical columns.



Figure 2.29: Photograph and sketch showing second tier *Thalassinoides* infilled with shell debris, and pyritised burrows (coloured pale blue) thought to represent fourth tier forms. The background is mottled with *Chondrites*. The sample was collected from -0.1 m.



Figure 2.30: Photograph and sketch of a pyritised burrow showing a possible lining (darker blue) and reaction halo (pale yellow). The sample was collected from -0.4 m.

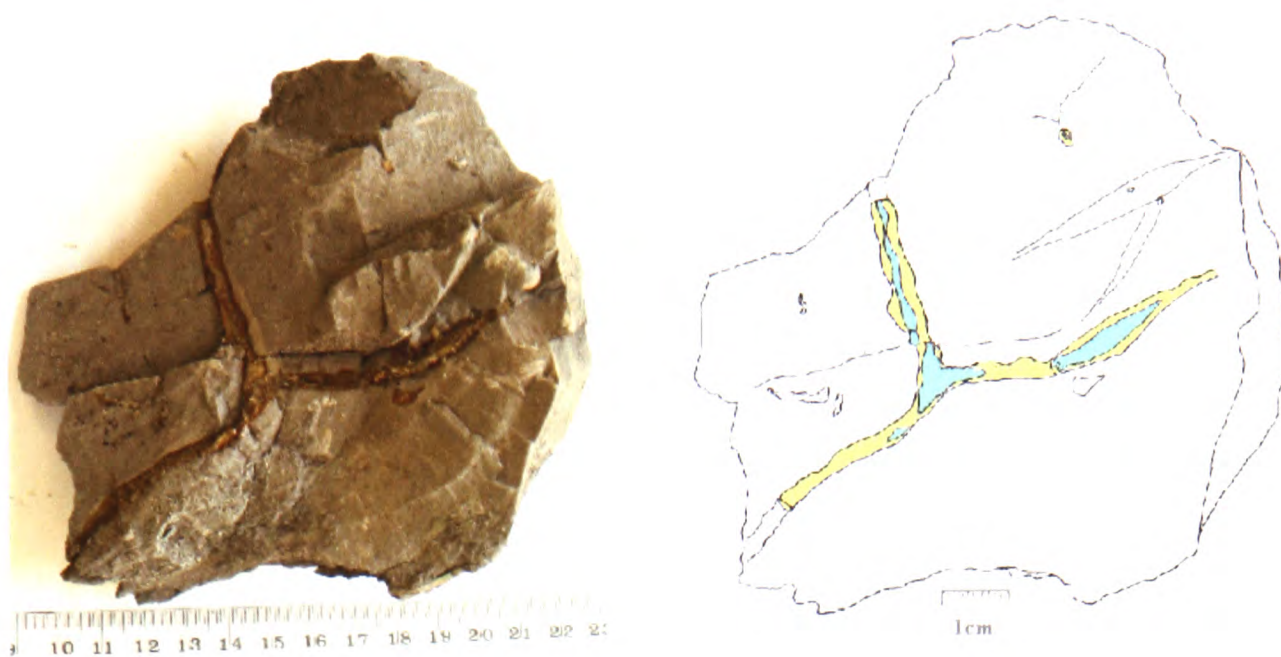


Figure 2.31: Triagonal junction of pyritised traces (pale blue) with a reaction halo (pale yellow). The sample was collected from -0.4 m.

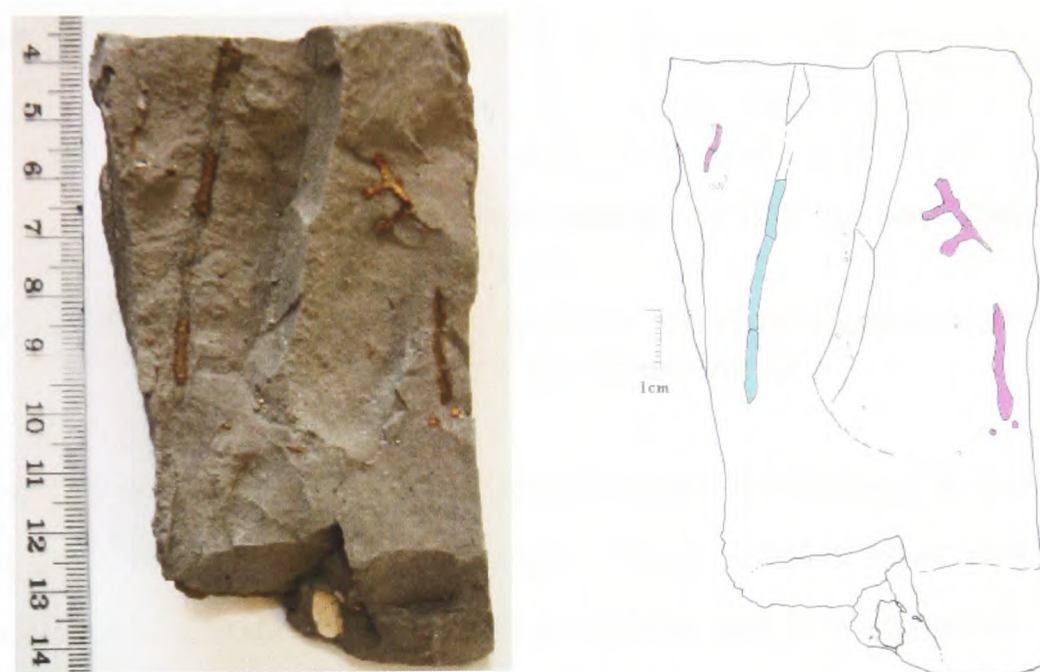


Figure 2.32: Photograph and sketch showing the same pyritised burrow forms (pale blue) and smaller pyritised burrows (purple). The sample was collected from -0.3 m.



Figure 2.33: Pale Chondrites in a darker sediment matrix. The sample was collected from -0.7 m.

2.3.3.3 Pyrite Framboids

The pyrite framboid size distribution of the Folkestone Gault Clay samples vary considerably throughout the sequence (see *Figure 2.34* and *Appendix A, Table A.3*).

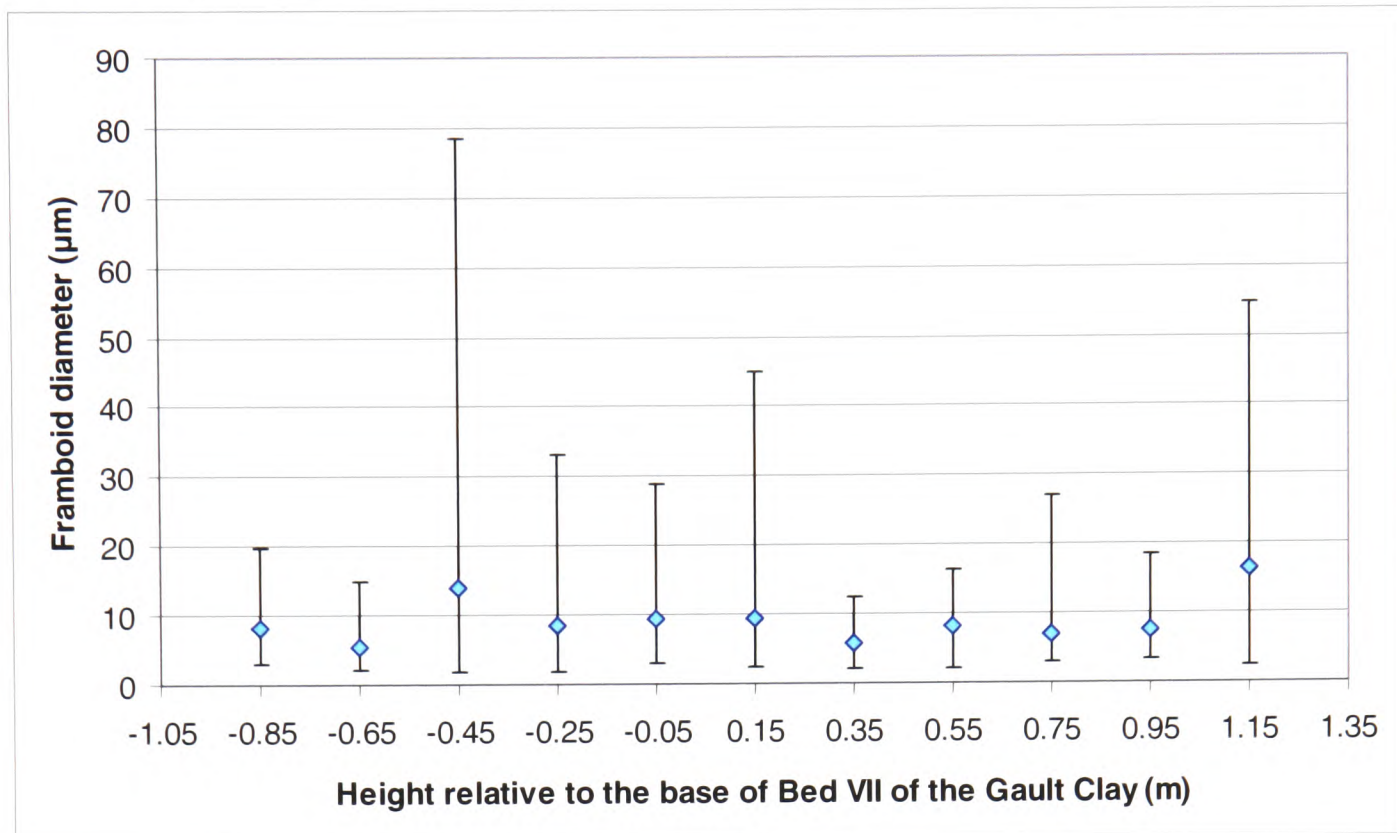


Figure 2.34: The Mean and Range of pyrite framboid diameters for the Folkestone Gault Clay sample range.

The majority of samples have a maximum framboids diameter between 10 µm and 35 µm but three samples exceed this range. These samples from -0.45 m, 0.15 m and 1.15 m all coincide with horizons rich in nodular and fossil material. The presence of much larger framboids in these samples, in particular the sample from 1.15 m of which 25% of the framboids are >25 µm in diameter, may be indicative of more oxygenated conditions during the formation of these layers. This provides some evidence to suggest that there were subtle variations in oxygenation during the deposition of the Gault Clay, although not all of the fossiliferous layers have such large framboids. The distribution would seem to correlate with deposition under relatively oxic conditions as the relatively large size range of framboids observed within most sample could not have been formed at the oxic-anoxic interface within the water column and so are likely to have formed at this boundary within the sediment, under a relatively oxic water column.

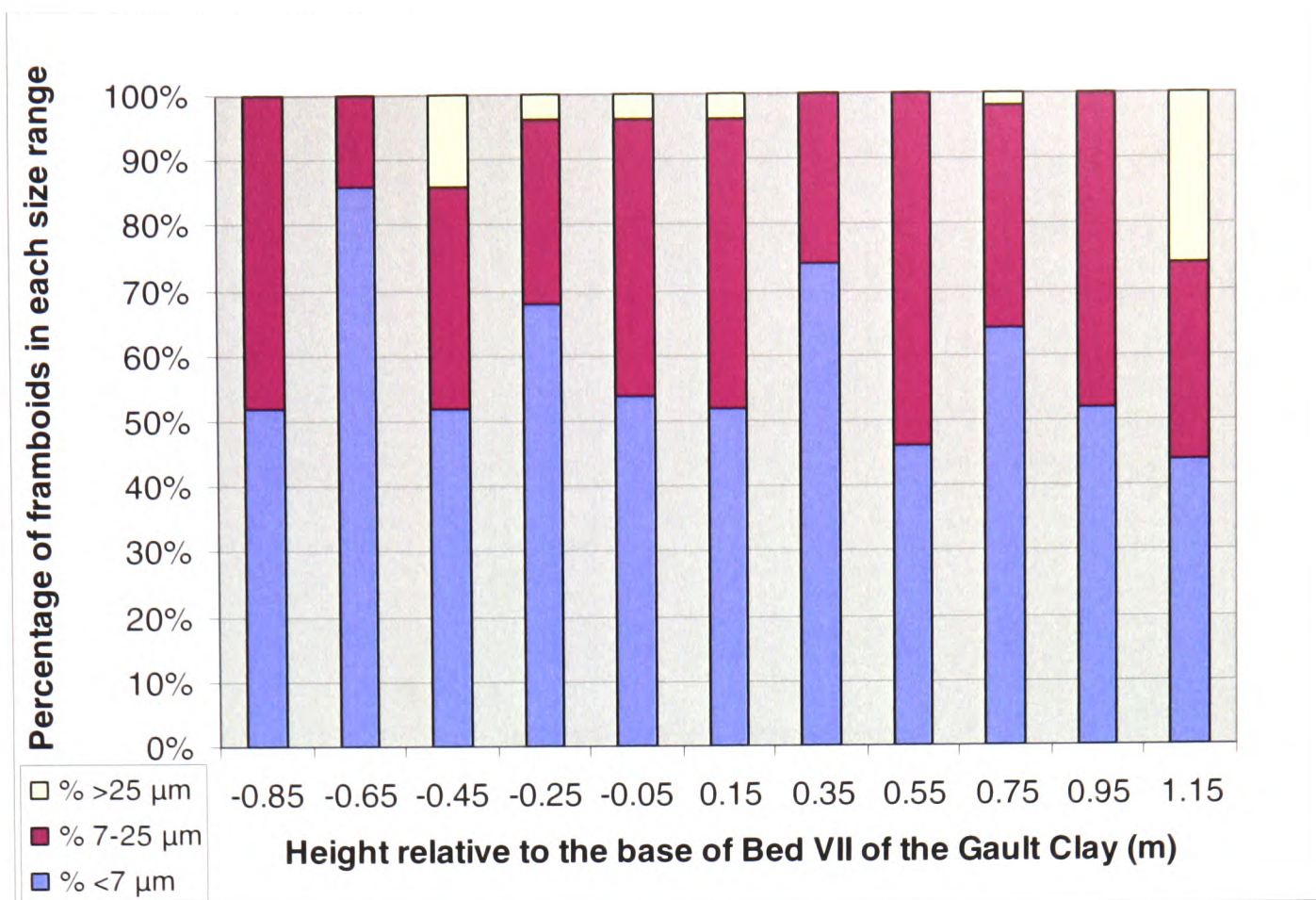


Figure 2.35: A cumulative bar chart to represent the percentage proportion of framboids within each size range for the Folkestone Gault Clay samples (based on the numerical boundaries implied by Wilkin *et al.*, 1997).

The cumulative bar chart of size ranges (see Figure 2.35) shows that the distributions fit relatively well with Wilken *et al.*'s (1997) description of oxic and dysoxic conditions having 40% of framboids within the range 7-25 μm, as this size range makes up between 15% and 55% of the distribution in each sample. The samples clearly do not cross the proposed boundary for euxinic conditions (95% or more framboids <7 μm) as 85% is the highest proportion of this size range in any sample. However, nearly half of the samples contain framboids with diameters <3 μm and Wignall and Newton (1998) suggested that loss of framboids below this limit marked the transition from lower dysaerobic to upper dysaerobic conditions.

A plot of standard deviation against mean (see Figure 2.36) does not seem to represent the conditions, as the Folkestone Gault Clay samples plot well outside the limits suggested for either normal marine or euxinic conditions. Also, the calculation of skewness (see Figure 2.37) seems to show little correlation with the proposed conditions of formation.

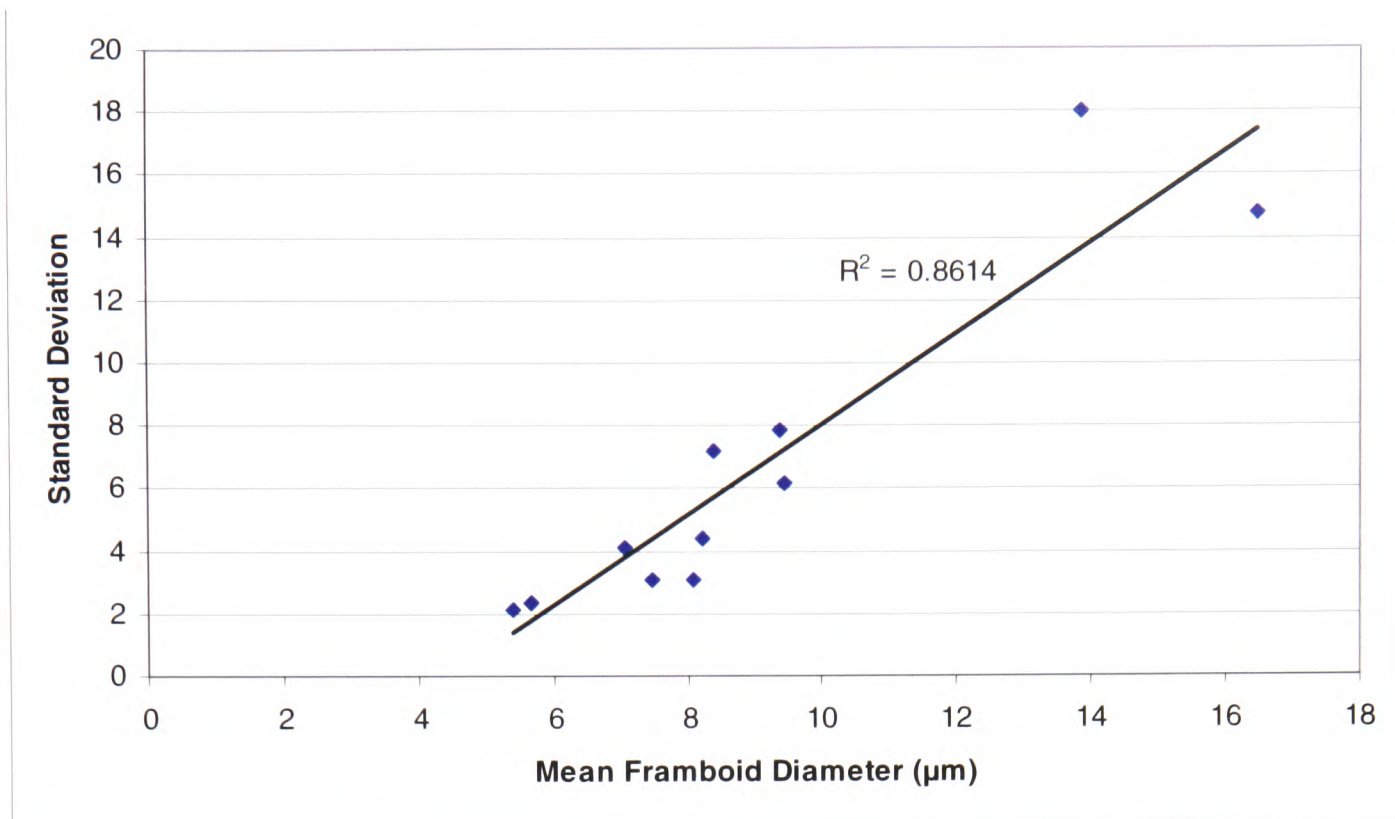


Figure 2.36: Comparison of the standard deviation and mean of framboid diameters for the Folkestone Gault Clay samples.

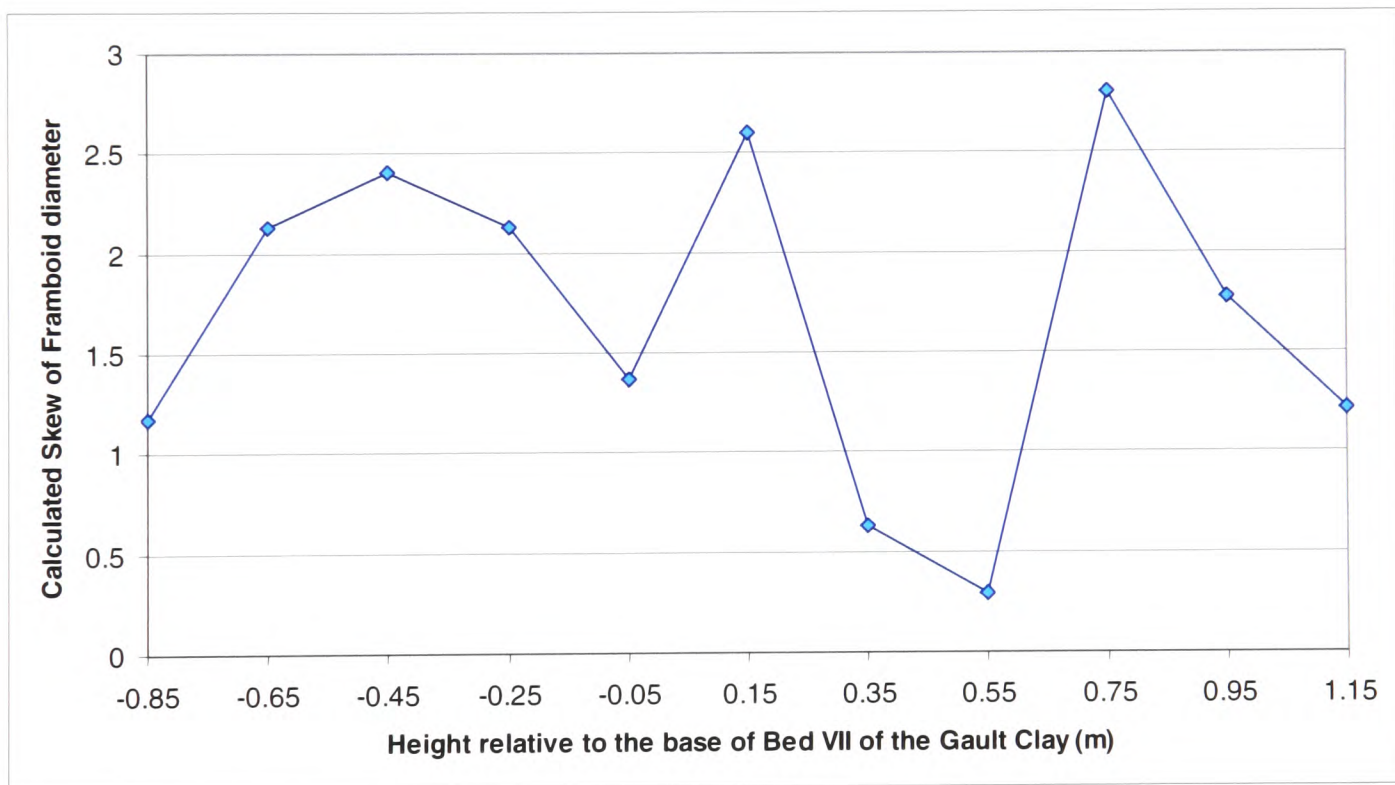


Figure 2.37: Plot of the calculated skewness of framboid diameter data for the Folkestone Gault Clay samples.

All samples easily fit the description for the **Category 2a** of the proposed pyrite morphology and distribution scheme which again suggests a relatively oxygenated depositional environment. There are relatively large framboids, framboid clusters, and euhedral crystals within each sample (see Figure 2.38), including the sample from -0.65 m which has a narrow size range including 85% <7 μm . There is,

however, no evidence of rare framboids limited to shell cavities – the Folkestone Gault Clay should represent the most oxic of depositional environments out of the four sites and so this would suggest that more oxic water column conditions are not responsible for the occurrence of these limited framboid distributions.

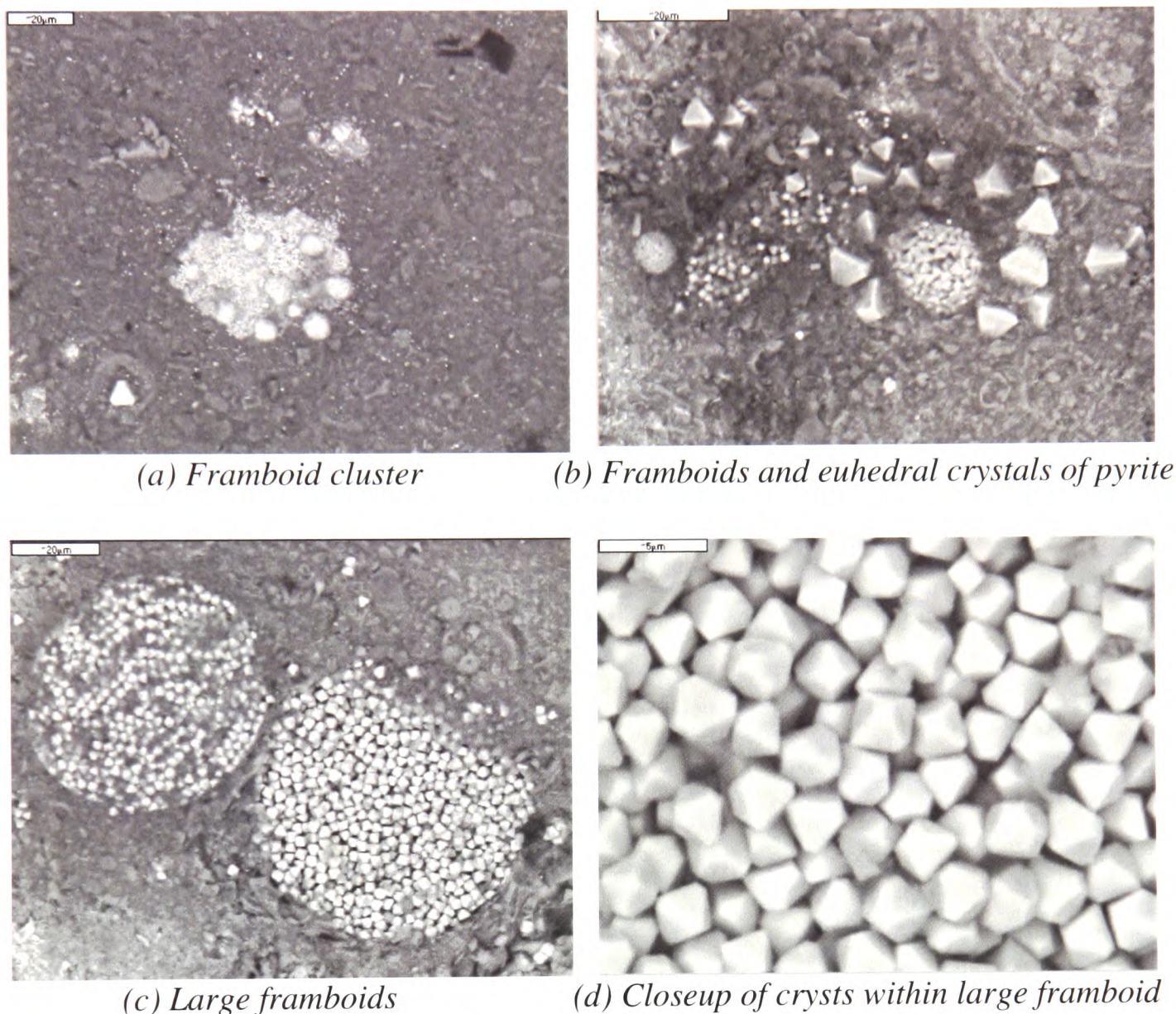


Figure 2.38: Backscatter SEM images of framboid clusters, euhedral crystals and large framboids from 1.1 m (a), and 1.2 m (b, c and d) above the base of Bed VII in the Folkestone Gault Clay. The scale bars represent 20 μm (a, b and c) and 5 μm (d).

2.3.4 The Amma Fatma Sediments

2.3.4.1 Sedimentology

The Amma Fatma sequence is composed of organic-rich marls and limestones (see *Figure 2.39*). The sediments contain carbonate concretions, which preserve original sedimentary structures.

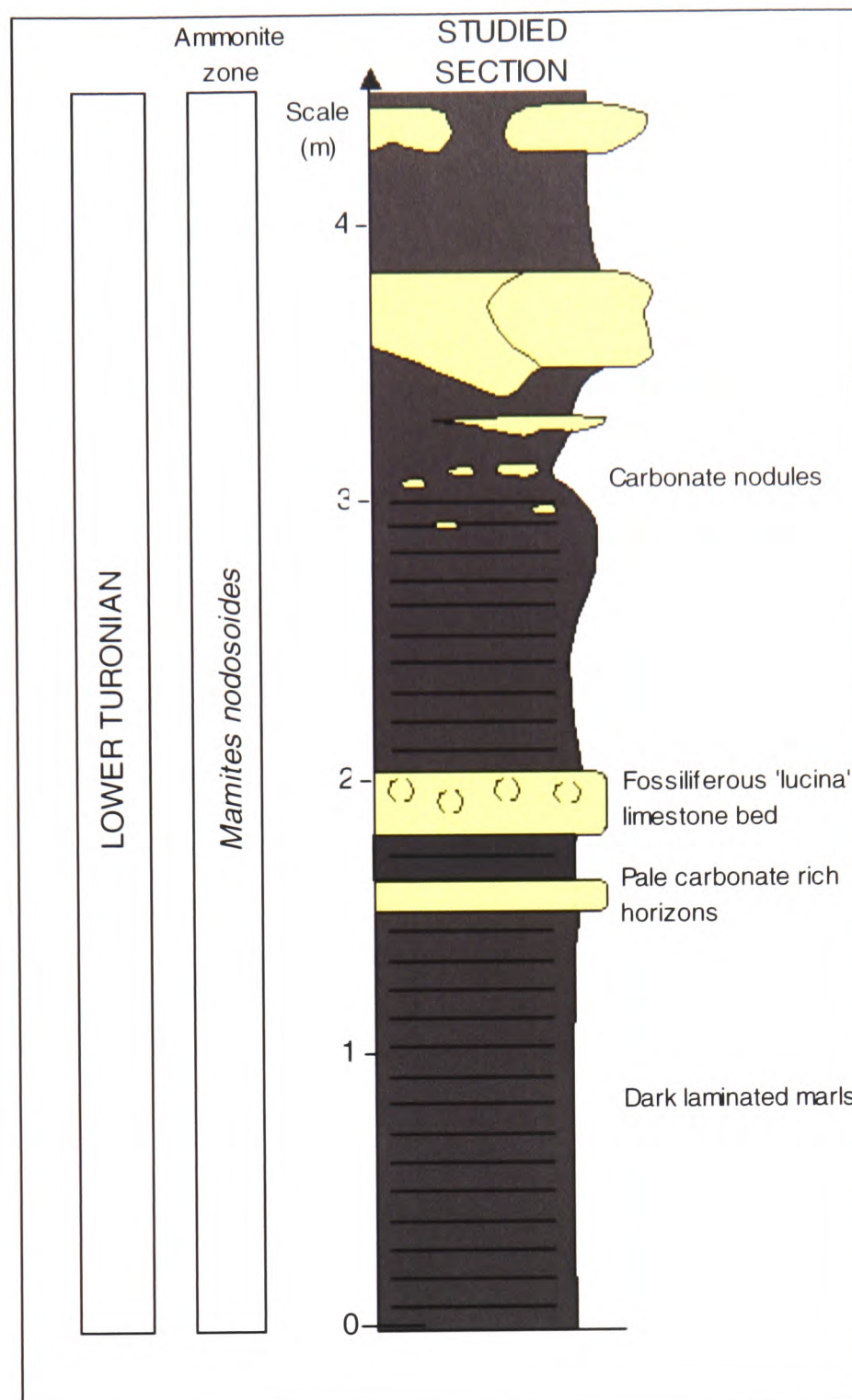
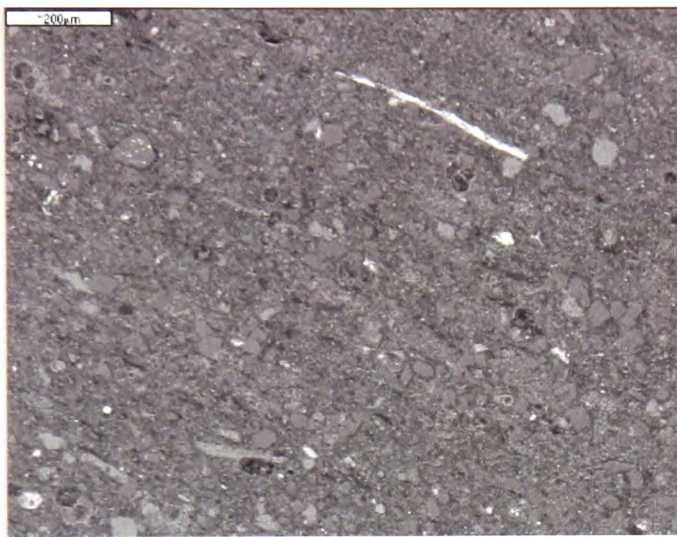


Figure 2.39: Stratigraphic log of the Amma Fatma section.

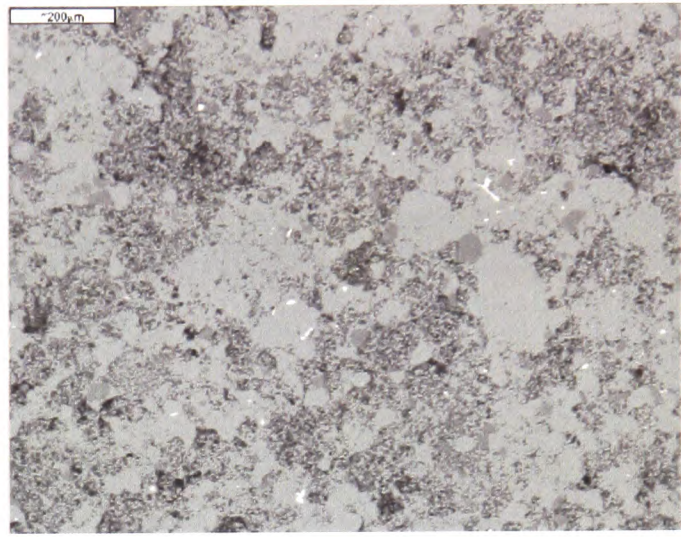
- **Colour** – The dark marls within the sequence are represented by dark grey-brown sediments between 0-1.5 m, 1.6-1.8 m, 2.1-3.5 m and 3.7 m upwards. The much paler brown, carbonate-rich samples represent organic-rich limestones. The samples match the description of Arthur and Sageman (1994) who suggested that carbonate-rich sediments with high organic carbon contents are normally represented by a range of brown colours when weathered. In addition, the Amma Fatma sediments only exhibit a moderate thermal maturity (Nzoussi-Mbassani *et al.*, 2003) which may also explain their paler colour in comparison to the Vocontian Basin black shales. The

lighter horizons represent higher carbonate contents and probably lower organics, suggesting a higher level of oxygen availability during deposition.

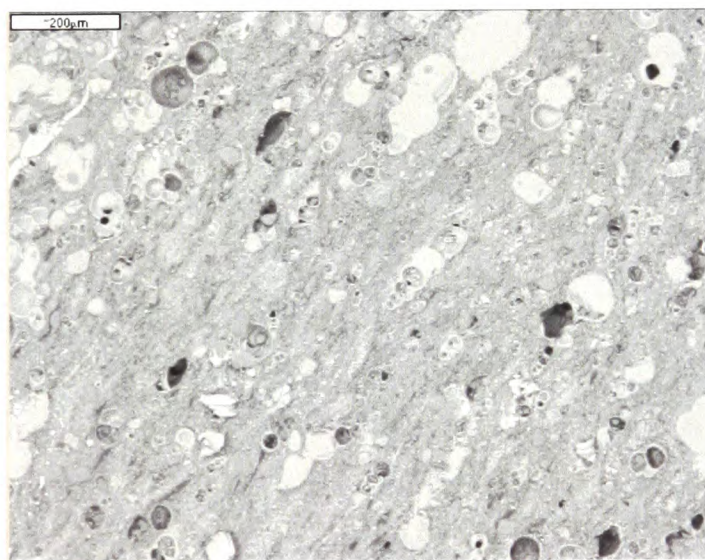
- **Laminations** - The dark marls are finely laminated and the orientation of the sediment fabric is visible under the SEM (see *Figure 2.40*), with more organic-rich dark horizons between paler carbonate-rich laminae. The carbonate-rich layers are more massive and show little evidence of sedimentary structures (see *Figure 2.40*) and this again suggests deposition under slightly higher oxygen availability.



Sample from 0.7 m – laminated marl



Sample from 1.95 m – massive limestone



Sample from 2.6 m – laminated marl

Figure 2.40: Backscatter SEM images of sediment fabric from the laminated marls and massive limestone. The scale bar represents 200 μm.

- **Fissility** – Despite the fine laminations in the dark marls, the sediment is not highly fissile. This would seem to support Wignall's (1994) suggestion that laminae are not necessarily responsible for papery fissility and that not all laminated sediments weather to display this. The more carbonate-rich sediments are blocky.

2.3.4.2 Ichnology

The samples available of the Amma Fatma sequence were too small to allow proper interpretation of trace-fossil assemblages, and the material available shows no clear evidence of bioturbation.

2.3.4.3 Pyrite Framboids

The pyrite framboid distribution within the Amma Fatma sequence does not necessarily match preconceptions concerning sediment type and colour associated with low-oxygen deposition. Nearly all of the samples, including the marls and most of the carbonate-rich horizons, demonstrate a relatively low average framboid diameter of below 8 μm (see *Figure 2.41* and *Appendix A, Table A.4*).

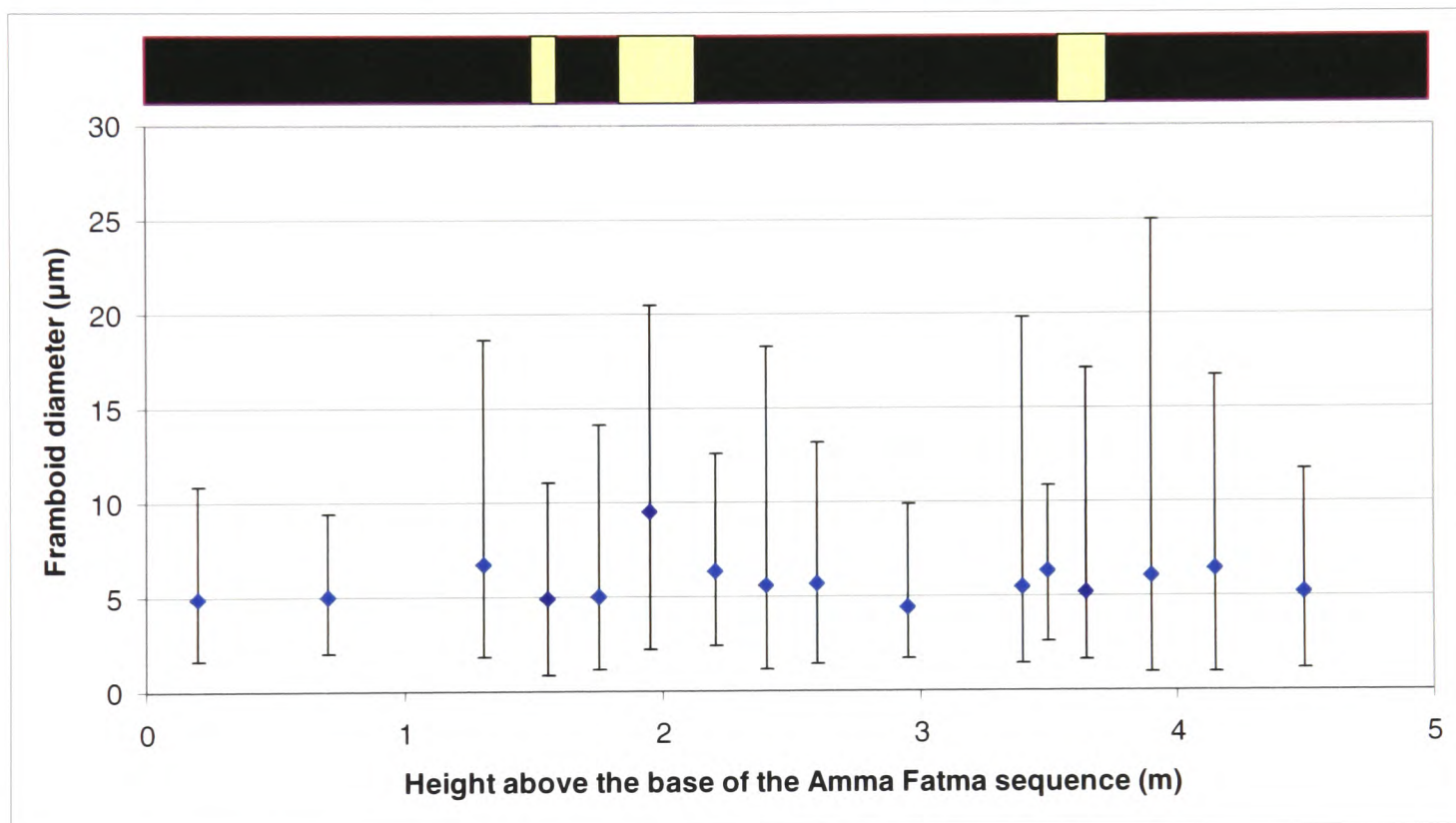


Figure 2.41: The Mean and Range of pyrite framboid diameters for the Amma Fatma sample range. The dark bands represent the laminated dark shale samples whereas the pale bands represent the more carbonate-rich material.

Despite the visual similarity of the data, the results from the two-tailed Student's t-test show that the dark marls and the pale carbonate-rich sediment do narrowly qualify as statistically distinct data sets (see *Figure 2.42*).

Pale Limestone		Dark Marl		P value
Mean	Variance	Mean	Variance	
6.6	17.2	5.6	9.2	0.011

Figure 2.42: The two-tailed Student's t-test results for the Briestoffer sequence framboid diameter data sets. The test shows that the paler sediment and the dark marl data sets are distinguishable as the P value is below 0.05.

Several dark marl samples have average framboid diameters below 5 μm although the upper limits of the range extend beyond this boundary proposed by Wignall and Newton (1988) to represent euxinic deposition. This matches Wignall and Newton's (1998) proposed description of Lower Dysaerobic sediments. The same is true for the first carbonate-rich horizon which is represented by the sample from 1.55 m above the base of the sequence. The second carbonate-rich horizon, however has the highest average framboid diameter of the entire sequence. In contrast, the greatest range of framboid diameters is demonstrated by a dark marl sample from 3.9 m above the base of the sequence. It is, however, worth noting that compared to the three other sites investigated, the framboid diameter size range is relatively restricted within the Amma Fatma sequence, implying that this site represents one of the lower oxygenation regimes of the four sites.

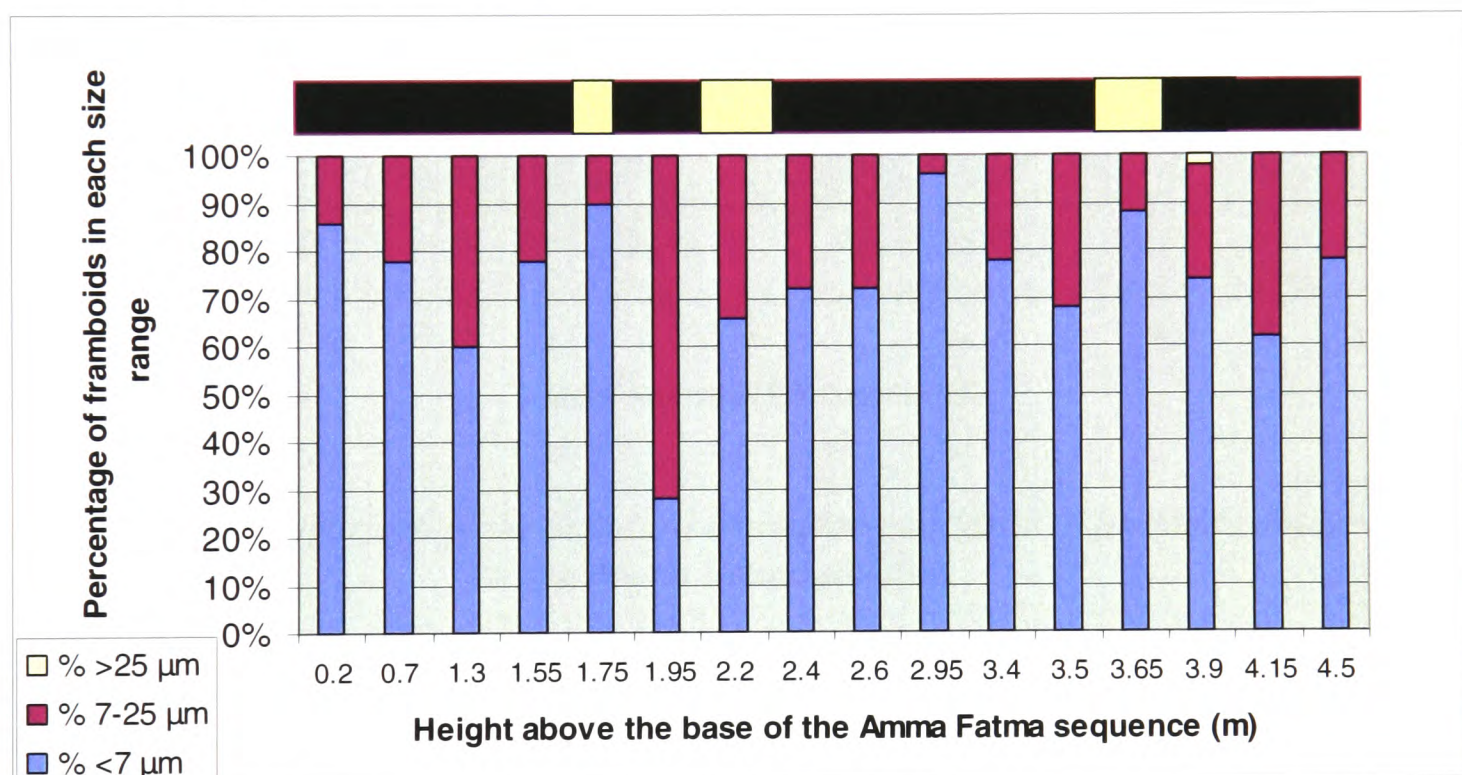


Figure 2.43: A cumulative bar chart to represent the percentage proportion of framboids within each size range for the Amma Fatma samples (based on the numerical boundaries implied by Wilkin et al., 1997). Along the top, the dark sections represent the laminated dark shale samples whereas the pale sections represent the more carbonate-rich samples.

The cumulative bar chart of framboid diameter also demonstrated the relatively restricted range of framboid diameters for most of the dark marls (see Figure 2.43). However, only two of the dark marls have greater than 90% of framboids with a diameter <7 μm and there is considerable variation between each sequence. Again, the second carbonate-rich horizon appears to represent the most oxic setting and this is corroborated by the highly fossiliferous nature of the horizon. The remaining carbonate-rich horizons, however, have similar framboid diameter distributions to the

dark marls, suggesting deposition occurred under relatively restricted oxygenation conditions.

The data plot with a line of regression associated with non-euxinic deposition on a plot of standard deviation against mean, according to the numerical limits proposed by Wilkin *et al.* (1996) (see *Figure 2.44*). Again, the calculation of skewness (see *Figure 2.45*) seems to show little correlation with the proposed conditions of formation.

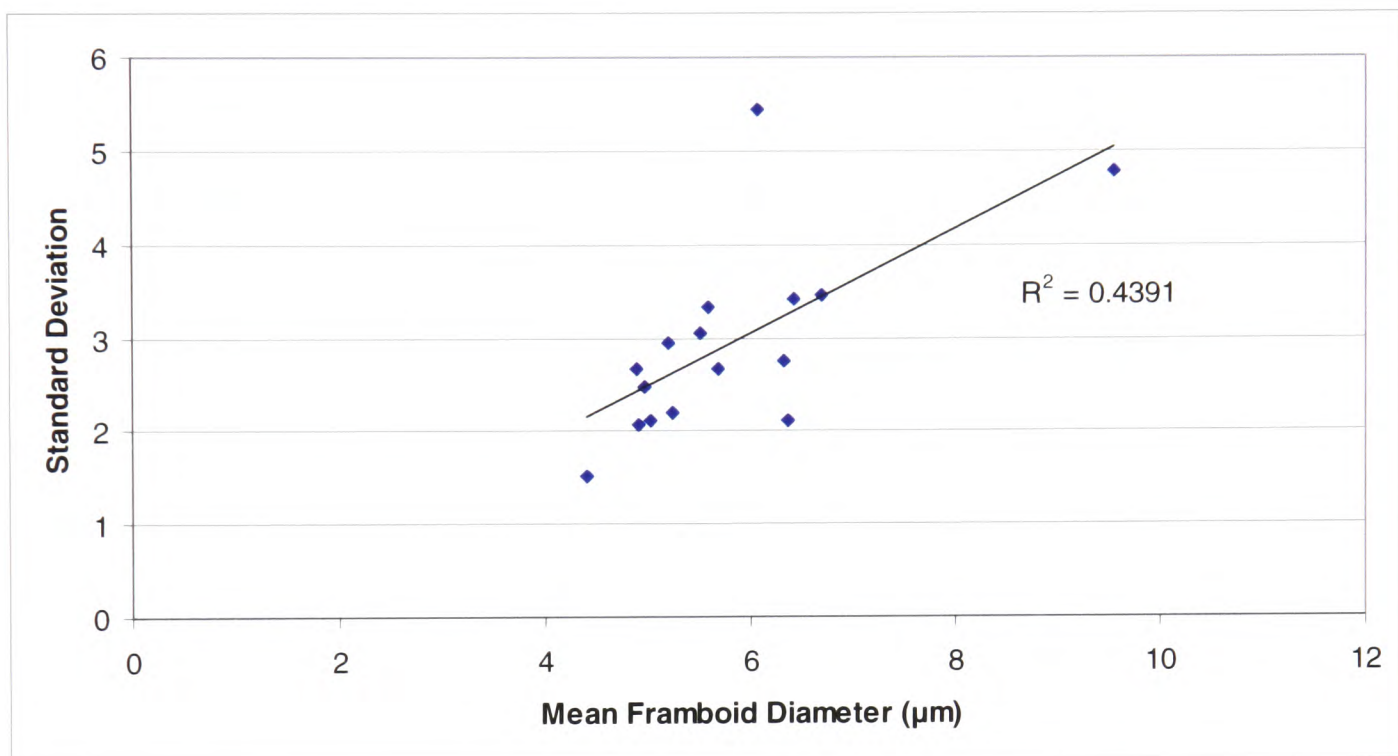


Figure 2.44: Comparison of the Standard Deviation and Mean of framboid diameters for the Amma Fatma samples.

Applying the same descriptive categories of pyrite distribution to the Amma Fatma sequences seems to clearly distinguish the sedimentary horizons. In general, the dark marls fit the description proposed for lower oxygenation regimes, with small scattered framboids and very rare isolated euhedral crystals. The only real exception is the sample from 2.6 m which is very fossiliferous and contains lots of crystals, suggesting a more oxygenated regime which is not identified by the framboid diameter data. The upper sequence of dark marls, however, have increasingly rare framboids through the sequence and clusters start to appear right at the top of the marls. In contrast to the marls, the very carbonate-rich layers tend to fit a category implying higher oxygenation levels, with rarer framboids and occasional large crystals. The 1.95 m carbonate layer has particularly rare framboids and this correlates with framboid diameter data suggested more oxic depositional conditions.

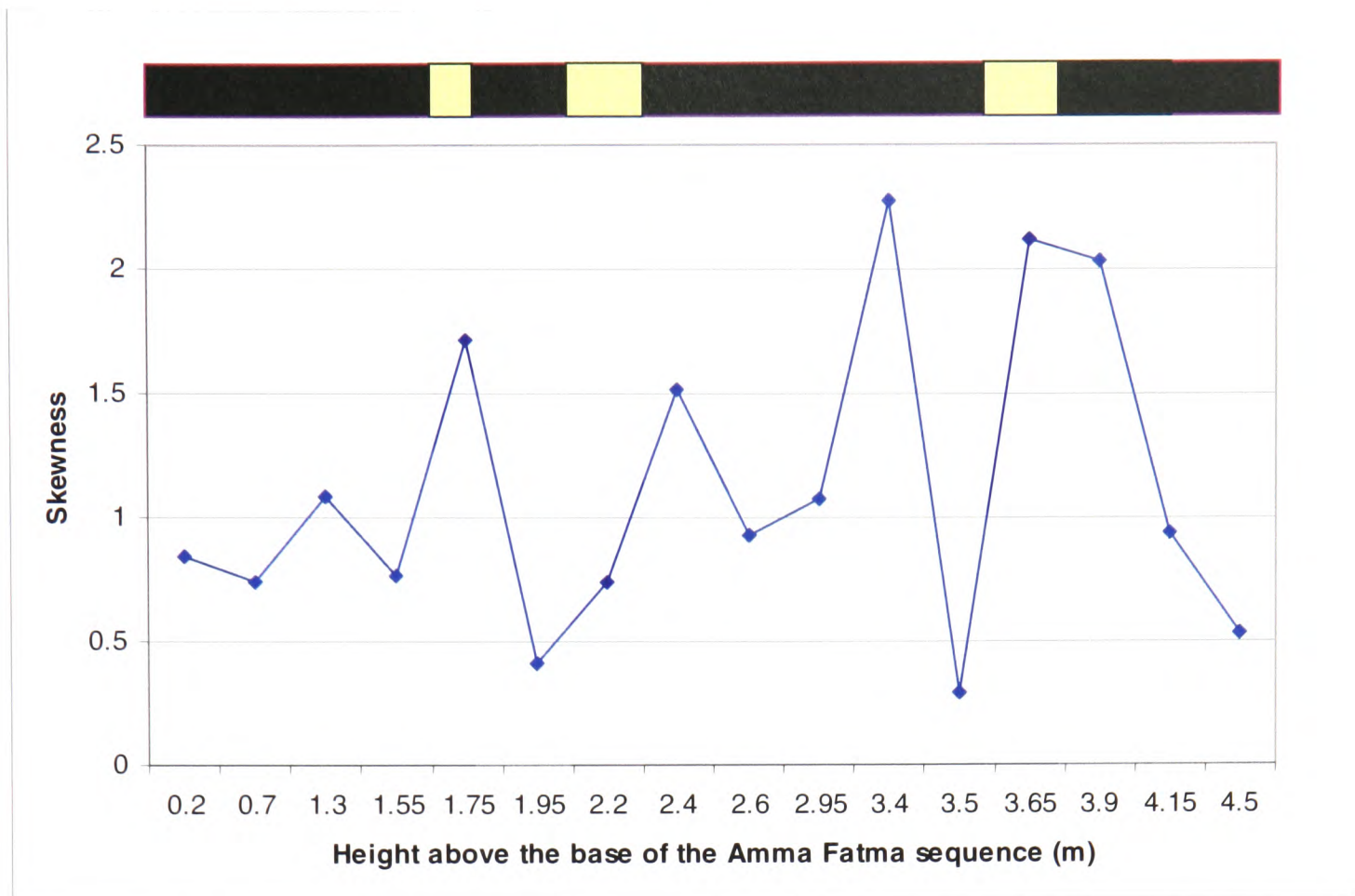


Figure 2.45: Plot of the calculated skewness of framboid diameter data for the Amma Fatma samples.

2.4 Conclusions

- The Black Shale horizons of Niveau Pacquier and Briestroffer samples are both dark, well-laminated, papery and lacking in evidence of bioturbation. This would seem to suggest deposition under anoxic conditions. This is supported by the Niveau Pacquier pyrite framboid data, where over 90% of framboids are $<7 \mu\text{m}$ in diameter.
- The grey clay samples of the Niveau Pacquier and Briestroffer sequences are also relatively dark, but blocky, and show little evidence of sedimentary structures, including trace fossils. This would suggest deposition under more oxic conditions than the Black Shales. This proposal of a higher level of oxygenation compared to the Black Shale samples is again supported by the increased range in pyrite framboid diameters observed in the majority of samples.
- The Folkestone Gault Clay samples are paler than those from the other sites, blocky and almost fully bioturbated. The trace fossils present, however, would seem to suggest slightly dysoxic conditions, rather than fully oxic bottom-waters. The pyrite framboid data plots the Folkestone Gault Clay

samples within a similar range to the oxic/dysoxic range proposed by Wilkin *et al.* (1997).

- The Amma Fatma sediments range from pale to dark brown, suggesting a range in the proportions of carbonate and organic carbon present, and accordingly the level of oxygen availability at the time of deposition. The darker sediments which show evidence of lamination, and little bioturbation were probably laid down under anoxic, if not euxinic bottom-water conditions. While the framboid diameter data does not greatly separate the darker marls and paler carbonate-rich material, descriptive categories do suggest a slight variation in oxygenation regimes.
- Sedimentology appears to be a clear indicator of lower oxygen conditions but it is important to recognise the effect of carbonate composition on the colour – not all low-oxygen horizons are represented by black shales. The presence of laminations seems to be a reliable indicator of low oxygen, and this is related to the absence of bioturbation. The presence of papery fissility, on the other hand, is not as reliable an indicator of low-oxygen conditions, as the Amma Fatma sequence was blocky throughout.
- In terms of ichnological approaches, the use of Bioturbation Indices possibly has the greatest application in terms of recognising and categorising low-oxygen events. While comparisons of trace-fossil assemblages and their parameters are very useful in analysing variations within a sequence, comparison between sites is limited by the other factors which affect the type and form of trace fossils present.
- Pyrite framboids appear to identify broad trends and the boundaries proposed by Wilkin *et al.* (1997) to identify euxinic and oxic/dysoxic conditions do seem to loosely apply to the data. While Wilkin *et al.* (1997) proposed 95% or more framboids with a diameter $<7\ \mu\text{m}$ as a boundary to identify anoxic deposition, the Niveau Pacquier data suggest that imposing a boundary at 90% $<7\ \mu\text{m}$ may be useful for separating Lower Dysaerobic sediments from more oxygenation settings. Wignall and Newton (1998) suggested that euxinic deposition is represented by a limited range of framboid diameters all under $5\ \mu\text{m}$. The Niveau Pacquier data suggest that this boundary may also be applied to recognise Lower Dysaerobic facies, if the mean framboid diameter is below

this value. However, these boundaries are not particularly reliable as some Niveau Pacquier grey clays also fit these descriptions and the boundaries do not translate particularly well to the other sites. Although the boundaries proposed do not clearly differentiate the different sediments, the Student's t-test results did show statistical distinction between the data sets within the Niveau Pacquier, Briestroffer and Amma Fatma sequences. The use of Standard Deviation vs. Mean plots does not seem to reliably differentiate the oxygenation variations within the sample sets and the calculation of skewness shows little correlation with sedimentary characteristics.

The use of descriptive categories seems to provide a more reliable distinction between the sediment types, with Anoxic or Lower Dysaerobic sediments being categorised by:

- **Category 1 – Redox boundary within the water column:** A random covering of small framboids where groups of framboids and euhedral crystals are rare and only occasionally framboids are associated with shell material. This correlates with the concept of framboids forming at a redox boundary which was within the water column.

In contrast, the Upper Dysaerobic or Oxic samples tend to fall into two descriptive categories:

- **Category 2a – Redox boundary within the sediment:** In the first category of samples, large framboids are relatively common and are often composed of comparatively large crystals. Clusters of framboids and euhedral crystals are common, with the latter occasionally larger than individual framboids. Overgrowth of framboids is also common. This category may correlate with pyrite formation that occurred slowly within relatively organic-poor sediment, under a relatively oxic water column. The large clusters of framboids may form associated with concentrations of organic matter such as within a burrow system.
- **Category 2b – Redox boundary within the sediment:** In the second category of samples, framboids are rare and are usually associated with cavities within shell material. This distribution of pyrite may correlate with sediments which formed under a more oxic water column, or formed under fluctuating redox conditions, or just

contained less organic matter. Restricted availability of organic matter may have limited pyrite formation which would explain the rare occurrence of framboids. The association of framboids with apparent cavities within shell material may represent pyrite formation within reducing microenvironments created due to breakdown of localised concentrations of organic matter.

CHAPTER 3: PALAEOONTOLOGY

3.1 Introduction

Many of the original interpretations of black shales assumed that organic-rich deposits formed under anoxic waters, and therefore authors believed that no benthos could survive these conditions (Wignall, 1994). Many suggested that the macrofossil material found in such deposits must have been pseudoplanktic or pseudopelagic and must have dropped into the sediments on death (e.g. Seilacher and Westphal, 1971). However, it soon became clear that organic-rich sediments can also form under oxygen-poor conditions as well as under true anoxic water columns (Wignall, 1994). Jacobs and Lindenberg (1998) pointed out that generally in the sedimentary record only long periods of low oxygen are easily recognisable due to the reduced bioturbation. However, they suggested that this gives a misleading impression of the biological impact of low-oxygen conditions, as it is not just complete or long periods of anoxia that cause biological effects. Wignall (1994) suggested that a number of factors control the level of oxygen needed to actually eliminate all benthos:

- Temperature – the solubility of oxygen decreases with increasing temperature so fauna that exists in warmer settings should be better adapted to low-oxygen conditions. However, Wignall (1994) noted that the opposite trend had been observed in arctic settings.
- Salinity – organisms appear to be less able to deal with decreasing oxygen levels in lower salinity conditions.
- The presence of free hydrogen sulphide in the water column – hydrogen sulphide is toxic to many marine species.
- The rate of declining oxygen levels – Wignall (1994) proposed that if oxygen levels drop slowly, species are more able to adapt and develop a level of tolerance.

However, Bosence and Allison (1995) pointed out that all palaeoenvironmental analysis relies on the principle of taxonomic uniformitarianism and it is important to bear in mind that the ecology and tolerance of organisms may have evolved through time.

Rhoads and Morse (1971) were the first to identify dysaerobic environments, which they defined as having dissolved oxygen concentrations between 0.1 and 1.0 ml/l. They summarised the work of many authors and identified a number of characteristics of benthic assemblages that seemed to be affected by decreasing oxygen levels:

- benthic diversity (see **Section 3.1.1.1**)
- species size (see **Section 3.1.1.2**)
- depth of burrowing (see **Section 3.1.1.3**)
- benthic life modes (see **Section 3.1.1.4**)
- presence or absence of shelly faunas (see **Section 3.1.1.5**)

Other indicators of palaeo-oxygenation conditions that have been used by a range of authors, include the presence of particular species that are thought to be relatively tolerant of low-oxygen conditions (e.g. Wignall, 1994) (see **Section 3.1.1.6**) and variations in taphonomy within sequences (e.g. Speyer and Brett, 1988) (see **Section 3.1.1.7**).

Rhoads and Morse (1971) were the first to combine these trends into a model of benthic environments under differing oxygen conditions, which they applied to explain the Cambrian explosion in terms of rising oxygen levels. Since this initial work several authors have suggested modifications to the model, and a range of other models have been proposed which authors suggest allow identification of low-oxygen conditions (e.g. Byers, 1977; Morris, 1979; Wignall and Hallam, 1991; Wignall, 1994; Arthur and Sageman, 1994) (see **Section 3.1.2**).

3.1.1 Macrofossils

3.1.1.1 Variations in benthic abundance and diversity

Hallam (1980) suggested that one of the most notable features of black shales is that the faunal content is characteristically restricted and the rocks may often appear rather barren of fossils in comparison to other types of deposits. He suggested that burrowing infaunal forms are almost invariably absent and that if an assemblage of epifauna is present it will be of the high-density, low-diversity type indicative of high stress environments. He also pointed out that while benthic diversity will be low, black shale sequences may be highly fossiliferous due to relatively abundant nektonic

forms which can be in an excellent state of preservation. Jacobs and Lindenberg (1998) agreed that low-oxygen conditions have a stronger effect on diversity than on the abundance of fossil material. However, while the general trend of decreasing diversity with lowering oxygen levels is agreed upon, the pattern of this decrease is debated. Where Rhoads and Morse (1971) described a relatively rapid drop in benthic species richness across the aerobic:dysaerobic boundary, Savdra *et al.* (1984) found a more gradual decline across this boundary.

In contrast to this trend, Wignall (1994) pointed out that a diverse dysaerobic fauna is observed within the Californian Oxygen-Minimum Zone but he suggested that this is possibly due to the stability of the environment, where low-oxygen conditions have persisted for decades. He suggested that variable low-oxygen environments are characterised by a very different benthic fauna in which episodes of extreme colonisation are represented by abundant but species-poor assemblages throughout the sequence. Arthur and Sageman (1994) pointed out that there are constant references in the black shale literature to small thin-shelled taxa which are normally benthonic as well as shell horizons containing abundant specimens of a single or few species, and they agreed that these horizons probably represented brief episodes of opportunistic colonisation.

Several measures of diversity and abundance have been used in order to quantify this trend. Wignall (1994) suggested that while the use of absolute abundance, rather than percentage abundance, is useful in determining how 'fossiliferous' sample are, it is not low abundances that identify low-oxygen environments, but rather poor species richness. Unfortunately, the number of species, or species richness, is strongly sample size dependant (Sanders, 1986) and Arthur and Sageman (1994) found that species richness and abundance did not indicate the severity of oxygen depletion suggested by other faunal indicators they investigated. However, Sageman and Bina (1997) suggested that oxygenated environments can be recognised by this sample size dependence, as the high diversity allows the occurrence of rare species which means that species richness increases with sample size. On the other hand, they suggested that low-oxygen environments are dominated by one or a few opportunistic species and that the lack of rare species means that the species richness should not increase with sample size.

Another approach, the Shannon Index (**H**), is believed to demonstrate 'dominance' which is calculated as:

$$H = - \sum_{i=1}^S p_i \ln p_i$$

H	Shannon's diversity index
S	Total number of species in the community (richness)
p_i	Proportion of S made up of the <i>i</i> th species

Shannon's equitability (**E_H**) can be calculated by dividing **H** by **H_{max}**, where **H_{max}** is equal to **lnS**. Equitability assumes a value between 0 and 1:

$$E_H = H / H_{max} = H / \ln S$$

A high value of **H** is thought to indicate high species richness and a value of **E_H** = 1 represents a completely even distribution, which is commonly associated with more oxic environments. The Shannon Index has the advantage that it is not as affected by sample size except when samples are very small (Wignall, 1994). Sageman and Bina (1997) proposed the use of plots of **H** against **S**, **E_H** against **S**, and **H** against **E_H**, in order to fully interpret the assemblage properties. However, Jacobs and Lindenberg (1998) pointed out that care needs to be taken in analysing faunal trends as increased preservation in low-oxygen environments may create a bias in the data.

3.1.1.2 Variations in the size of benthos

Hallam (1980) suggested that in sediments representing low-oxygen conditions, the individual fossils are often smaller in size than representatives of the same species in other types of deposits. He proposed that this was probably the result of a higher proportion of juvenile mortality than the dwarfing of adult forms. However, Wignall (1994) pointed out that for organisms that respire across their surface, smaller size will be beneficial in low-oxygen environments as it provides a greater surface area to volume ratio. He did suggest, however, that for species with more developed breathing apparatus such as the gill structure of bivalves, adult forms would be more tolerant to low-oxygen conditions than juveniles. He noted that there is often a

bivalve population observed with no juveniles and that this gives a distinctive size distribution curve (Zeuthen, 1953).

3.1.1.3 Variations in burrow depth

Under oxic water columns, burrowing organisms can burrow down into anoxic sediment by mucus lining their burrow walls and irrigating the burrows with oxic water from the sediment surface (Wetzel, 1991). Wignall (1994) suggested that under normal oxic waters there is a sharp boundary between reduced and oxygenated sediment which he refers to as the Redox Potential Discontinuity. He suggested that the depth of this discontinuity is controlled by the depth of bioturbation and irrigation. However, when oxygen availability decreases at the sediment surface, he suggested that it becomes harder to irrigate burrows and so burrows tend to become shallower. Wignall (1994) pointed out that there is evidence in previous work (for example Stachowitz, 1991) that suggests that if oxygen levels decrease, the Redox Potential Discontinuity rises and infaunal organisms are eventually driven out onto the surface. (also see **Section 2.1.2**)

3.1.1.4 Changes in the predominant modes of life

Rhoads and Morse (1971) suggested that in upper dysaerobic conditions, deposit feeders dominated, but that in lower dysaerobic conditions only tiny nematodes remain actively burrowing within the sediment. To some extent, the work of Morris (1979) supported this proposal. He proposed that ternary diagrams of bivalve life modes could be used to determine between oxygenation regimes (see *Figure 3.1*) as he suggested that:

- Normal shales are dominated by infaunal suspension feeders;
- Restricted shales are dominated by deposit feeders (this environmental division is thought to correspond to the upper dysaerobic classification of Rhoads and Morse, 1971);
- Bituminous shales are dominated by epifaunal suspension feeders (this environmental division is thought to correspond to the lower dysaerobic classification of Rhoads and Morse, 1971).

However, Wignall (1994) suggested that there were errors made in the analysis – he suggested that some of the Kimmeridge Clay bivalves were assigned incorrect life modes, and the Oxford Clay samples were missing some species and included

gastropods. Wignall (1994) went as far as to suggest that bivalve trophic group dominance has a minimal relationship with oxygen tolerance. He believed that the majority of the fauna observed in low-oxygen sediments is due to opportunistic colonisation during brief oxygenation events and so bears little relationship to the actual low-oxygen setting. He suggested that suspension feeders may be prevalent in bituminous shales purely because they are better adapted to being opportunistic colonisers.

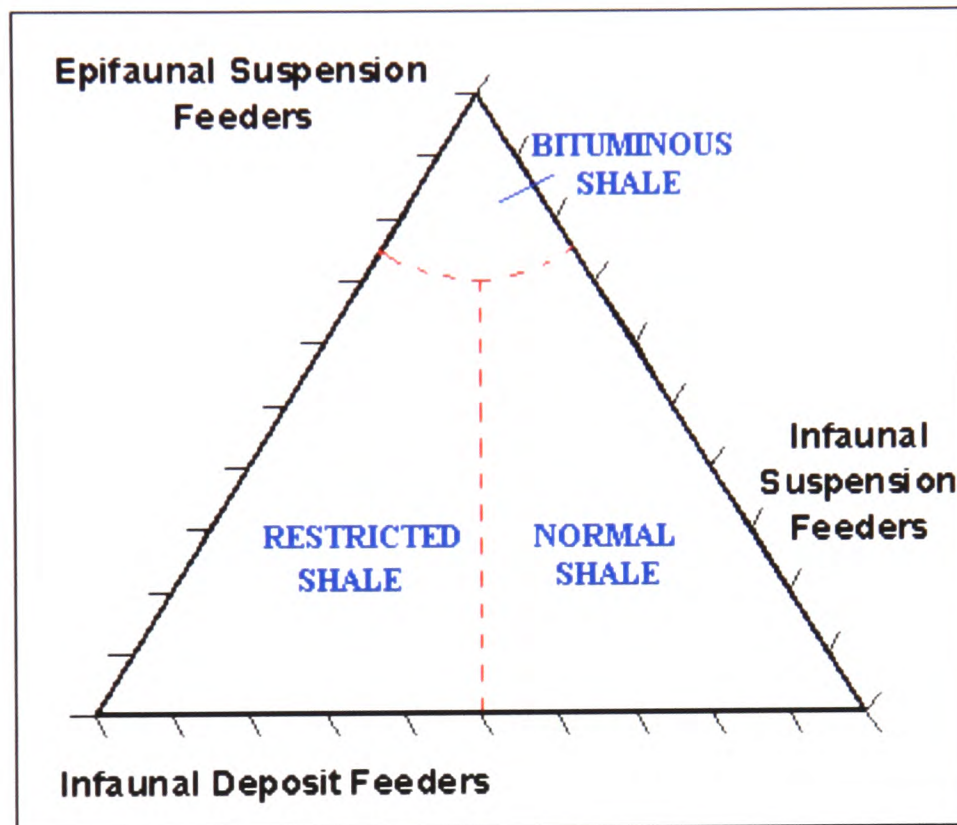


Figure 3.1: The ternary diagram of bivalve life modes which Morris (1979) proposed could be used to distinguish palaeo-oxygenation regimes.

There is some evidence that suggests that chemosymbionts can live under low-oxygen conditions as they are typically found in environments with a sharp redox boundary. Savdra *et al.* (1991) and Savdra and Bottjer (1991) proposed the term 'exaerobic' to describe the "occurrence of *in situ* chemosymbiotic, epibenthic bivalves and brachiopods in laminated strata". However, Wignall (1994) pointed out that the majority of symbiotic relationships observed involved symbiotic bacteria oxidising chemicals such as hydrogen sulphide or methane within the gill tissues of an organism. As this requires the presence of oxygen, he suggested that this was not a likely life strategy for low-oxygen environments and added that there is little evidence of them in black shale deposits. This is supported by the observation that modern chemosymbionts do not live in low-oxygen conditions (Allison *et al.*, 1995).

Sageman and Bina (1997) further pointed out that many of the forms proposed to represent chemosymbionts in ancient sediments are lacking features thought to be common to all modern forms and that there is no clear evidence of bacteria in association with these fossils.

3.1.1.5 Variations in the proportion of shelly taxa

Rhoads and Morse (1971) suggested that the transition from aerobic to dysaerobic conditions is marked by the loss of the majority of shelly taxa. They suggested that this occurs because of the difficulties of calcium carbonate secretion under the high CO₂ and lowered pH conditions which are common of low-oxygen settings. In support of this, Levin (2003) found that the only macrofaunal taxa which were tolerant of severe oxygen depletion (<0.2 ml/l dissolved oxygen) in the modern Oxygen-Minimum Zones were soft-bodied nematodes and annelids, and that the only calcareous forms were benthic foraminifera. However, Savdra *et al.* (1984) suggested that this is an oversimplification of the trend and that shelly taxa such as ophiuroids, crabs and the gastropod *Mitrella* can thrive in lowest dysaerobic facies. The suggestion is also revoked by the repeated observation of thin shell beds in sediments deposited under low-oxygen conditions (Kenig *et al.*, 2004). While these shell beds may be the result of gentle winnowing of debris from elsewhere, there is growing consensus that these represent colonisation events (Wignall, 1994). However, the species associated with these shell beds often have very thin shells (Arthur and Sageman, 1994) which may be a consequence of the difficulties of calcium carbonate secretion in such environments. Alternatively, Wignall and Myers (1988) have suggested that the loss of thick shelled forms is more linked to the soft muddy substrates that are commonly associated with low-oxygen environments.

3.1.1.6 The presence of particular 'tolerant' species

Fenchel and Riedl (1970) found invertebrates at 50 cm below the sediment surface within anaerobic sediments and referred to this grouping as the sulphide biome. They suggested that this represented a biome that could exist in truly anoxic conditions but, as Wignall (1994) pointed out, these organisms still have access to oxygenated water via burrow irrigation from the surface and so cannot be considered truly anoxic forms.

Arthur and Sageman (1994) noted that lower dysaerobic conditions, where the redox boundary lies at the sediment-water interface, are often characterised by the presence of 'flat clams'. These clams have extremely thin shells, broad/flat shapes and reclining to slightly erect life habits, and are thought to be highly adapted to life at the boundary between anoxic/dysoxic and oxic environments. They include mainly epibyssate suspension-feeding bivalves such as *Inoceramus* and free-living to pediculate brachiopods such as *Leiorhyncus*. Arthur and Sageman (1994) suggested that the 'flat clams' which they term the 'benthic boundary biofacies' had special adaptations to low-oxygen levels and dissolved hydrogen sulphide. Kenig *et al.* (2004) suggested that this association of 'flat clams' with low-oxygen conditions could be more linked to their larval development than an actual tolerance to the conditions. They suggested that having planktic larvae allows these forms to opportunistically colonise during increased oxygen events. Furthermore, they suggested that the morphology of flat clams means that they are well adapted to live within the soft substrates often associated with low-oxygen conditions.

Many authors have tried to identify species that are more tolerant to low-oxygen conditions, but Herried (1980) suggested that this was almost impossible as the tolerance of individuals depends on many factors including temperature, salinity, size and health of the individual organism. However, Wignall (1994) noted that bivalves and other invertebrates have the ability to switch to anaerobic metabolic pathways for short periods which may allow them to survive low-oxygen events. Polychaetes and certain bivalve species have often been identified as being the last species to be lost as oxygen levels decrease, and examples include the polychaete *Capitella capitata*, and the bivalves *Macoma balthica*, *Artica islandica*, *Corbula* spp. and *Astarte* spp. (Pearson and Rosenberg, 1978). Wignall (1994) suggested that these common polychaete and bivalve forms are not more oxygen tolerant but instead are good opportunistic colonisers. He suggested that it is very difficult to separate more low-oxygen tolerant species from colonisers which respond to periods of increased oxygen.

3.1.1.7 Taphonomy

Efremov (1940) first coined the term taphonomy to describe the study of processes of death, decay and disintegration during the generation of fossil assemblages. Taphonomy includes a limited history of fossilized remains encompassing living substrate relationships, death conditions, preburial sedimentology of remains, burial, necrolysis, and early syngenetic chemical sedimentology (Efremov, 1940). As the taphonomic history of a fossil is strongly linked to the environmental settings and sedimentary characteristics at the time of its formation (Speyer and Brett, 1988), the study of distinct taphonomic features should provide an insight into these conditions. Speyer and Brett (1988) identified that traditionally taphonomy has been divided into two disciplines:

- **Biostratinomy**, which includes abrasion, fragmentation, disarticulation, reorientation and sorting. Identification of biostratinomy features is generally applied to interpret information about system energy, transportation of material and duration of fossil residence at the surface (e.g. Brett and Baird, 1986; Speyer and Brett, 1988; Brett and Speyer, 1990). Although these are the main controls on aspects of biostratinomy, palaeo-oxygenation does appear to have some impact. For example, Wignall and Myers (1988) suggested that the degree of fragmentation increases with increasing oxygenation as this allows for more extensive bioturbation of the sediment.
- **Fossil diagenesis**, which includes those processes which commence following death, including necrolysis (tissue decay) and incipient diagenesis of remains (for example replacement, distillation, recrystallisation; Speyer and Brett, 1988). Information about fossil diagenesis has been used to interpret geochemical conditions at the time and site of sedimentation. Processes of corrosion, deformation and dissolution are strongly linked to exposure time on the sea-floor, pH and carbonate saturation levels (Speyer and Brett, 1988). On the other hand, interpretation of shell-filling and authigenic mineral coatings and overgrowths is strongly linked to oxygenation conditions (Brett and Baird, 1986).

It is important to separate late stage diagenesis and related processes from these interpretations of environmental conditions as they bear little relationship to conditions at the time and site of burial (Speyer and Brett, 1988). The most

promising section of taphonomy for the interpretation of palaeo-oxygenation conditions is the formation of shell fillings and authigenic minerals. Speyer and Brett (1988) listed examples of referenced cases of the following authigenic minerals being linked to particular oxygenation conditions (see Speyer and Brett, 1988, and contained references):

- **Early diagenesis carbonate concretions associated with well-preserved fossils:** Carbonate concretions appear to be associated with rapid entombment of organic remains in generally anoxic, non-sulphidic sediment. This creates localised anaerobic conditions within otherwise dysoxic or marginally oxic settings. Br       *et al.* (2004) investigated a number of laminated organic-rich sediments and agree that calcareous nodules are generated in these environments by early diagenesis at a small depth below sediment surface. They suggested that carbonate precipitation occurs as a consequence of microbial degradation in the sulphate reduction zone under condition of reduced accumulation rate. They added that practically all nodules found in these sites are centered on sedimentary heterogeneities such as mechanical hummocks or biogenic burrows or pellets. They suggested that the nodules result from very early sediment reworking and that these heterogeneities must induce high porosity in early stages of burial, which would be favourable for diagenetic precipitations such as calcite.
- **Non-compacted pyrite infilling of fossil cavities:** Pyrite steinkerns or infillings are associated with rapid burial of organic remains in anoxic, non-sulphidic sediments. These shell infillings are believe to form in localised anaerobic conditions near the sediment-water interface beneath lower aerobic to dysaerobic water columns, where bioturbation is minimal. Flugel (2004) agreed that it is only in non-euxinic settings that pyrite formation is restricted to concentrations of organic matter, where anaerobic microenvironments can be established. Wignall and Newton (2003) agreed that severely reduced oxygen conditions, where the high rates of organic matter preservation allow pyrite formation throughout the sediment, leads to the formation of pyrite framboids (see Section 2.1.3) rather than shell infillings. This suggestion is backed up by the observations of Fisher and Hudson (1987) who recognised that flattened, highly compressed ammonites with very minor pyrite are

characteristic of black shale environments in the Jurassic Oxford Clay. On the other hand, they found that grey bioturbated facies were characterised by excellently preserved, uncompacted pyrite steinkerns of fossils.

- **Phosphatic steinkerns and/or coating of fossils:** Phosphate steinkerns or overgrowths are associated with anoxic sediments with oxidising microzones near the sediment-water interface. They tend to be associated with pronounced, geographically widespread hiatal surfaces and are therefore linked with very low rates of background sedimentation but relatively high organic productivity. The main controls of phosphate production are nutrient concentration and fluctuating oxygenation conditions (dysoxic to oxic). Steinkern formation requires isolated microenvironments of organic matter set against a background of specific chemical and depositional conditions, where totally oxic conditions are rare. In more oxic conditions, low sedimentation rates leads to the oxidisation of chemical species and oxidised iron may bind to phosphatised materials to produce glauconite in dysoxic settings or chamosite in more oxic settings (Speyer and Brett, 1988).

Water oxygenation	Sediment geochemistry	Sedimentation rates		
		Episodic, very rapid (1-50 cm / 10 ² years)	Intermediate-rapid (10-100 cm / 10 ³ years)	Low-intermediate (1-10 cm / 10 ³ years)
Aerobic O ₂ > 0.7 ml/l	Oxic; organic poor	No sediment fillings; late diagenetic mineral fillings; minor pyrite	Sediment steinkerns	Partial sediment steinkerns; rare chamositic, hematitic coatings
Aerobic-dysaerobic O ₂ = 0.7-0.3 ml/l	Anoxic with oxic microzones; organic poor (non-sulphidic)	Pyrite steinkerns, over pyrite (euhedral); calcium carbonate concretions	Calcium carbonate concretionary mud steinkerns; minor overpyrite	Phosphatic and/or glauconitic steinkerns, often reworked; rare overpyrite
Dysaerobic-anaerobic O ₂ < 0.3 ml/l	Anoxic to the surface; commonly organic-rich (commonly sulphidic)	No fillings, minor pyrite replacement; rarely traces of soft parts	Mud steinkerns, pyrite patinas; periostracal remains	Highly compacted mud steinkerns

Figure 3.2: Table linking taphofacies with water oxygenation, sediment geochemistry and sedimentation rates. Adapted from Brett and Baird (1986).

The next stage in developing the use of taphonomy as an environmental indicator involved the definition of a variety of recognisable taphofacies. Brett and Baird (1986) defined taphofacies as suites of sedimentary rocks characterised by particular combinations of preservational features of the contained fossils. Brett and Baird (1986) proposed several taphofacies which they believed correlate with particular conditions of water oxygenation, sediment geochemistry and sedimentation rates (see *Figure 3.2*)

Speyer and Brett (1988) created a hypothetical model of taphofacies for various environmental settings of ancient epeiric seas. They contoured hypothetical distributions of taphonomic properties against gradients of depth and sedimentation rates to produce 3-dimensional block diagrams (see *Figure 3.3*).

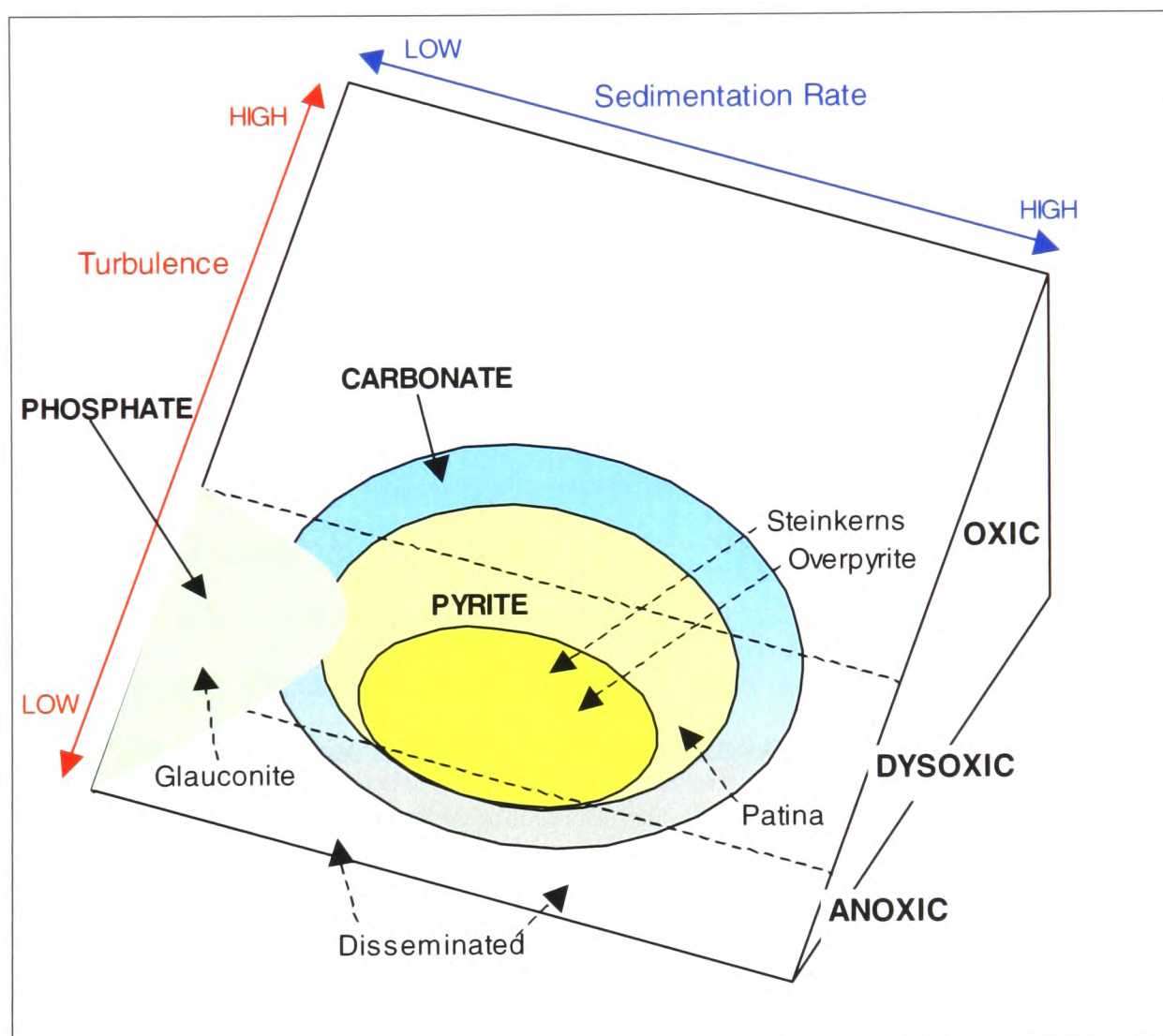


Figure 3.3: Three-dimensional block diagram showing the relationship between authigenic mineral formation and current energy, sedimentation rate and level of substrate oxygenation. Substrate oxygenation variation is based on a stratified ocean model where oxygenation varies with depth. Adapted from Speyer and Brett (1988).

Speyer and Brett (1988) believed that taphonomic properties should be distributed in predictable patterns which correspond to variations in current energy, sedimentation rate and level of substrate oxygenation. As they were focussing on Middle Palaeozoic epeiric seas they assumed that oxygen stratification occurred and therefore linked oxygen level to depth. While this allowed an oxygen gradient to be applied to biostatinomic properties such as degree of disarticulation and degree of fragmentation, this is not a reliable system as variations are more likely to be related to depth related energy variations rather than the influence of oxygenation. Their block diagram related to authigenic mineral formation, however, is more likely to allow palaeo-oxygenation interpretation (see *Figure 3.3*). Brett and Speyer (1990) noted that the application of such taphofacies models requires further work, but suggested that if such work was done, the models could provide a way to refine interpretations of ancient sedimentary environments.

3.1.2 Models of macrofaunal and sedimentological response to low-oxygen conditions

3.1.2.1 The Rhoads-Morse-Byers Model

Rhoads and Morse (1971) combined a variety of approaches to create a model to allow interpretation of oxygen-deficient biofacies. It was the first scheme of its kind, directly correlating dissolved oxygen contents with biofacies and sedimentological characteristics (Arthur and Sageman, 1994). They defined azoic as 0-0.1 ml/l, dysaerobic as 0.1-1 ml/l and aerobic as >1 ml/l dissolved oxygen content at Standard Temperature and Pressure. They suggested that as oxygen level decreases the following trends should be observed (see *Figure 3.4*):

1. A decrease in benthic species diversity, dropping to zero at the dysoxic/anoxic boundary.
2. A decrease in the size of benthos – seen best in the maximum burrow diameter
3. A change from a burrowed substrate to a laminated substrate. The Rhoads-Morse model suggests that this occurs within the low dysaerobic facies whereas Savdra *et al.* (1984) suggested that this is observed at the anaerobic/anoxic boundary.

4. A change in life strategies of benthos with deposit feeders becoming dominant, and suspension feeders rare (Edwards 1985), and active mobile forms such as carnivores decreasing (Douglas, 1981).
5. A loss of shelly taxa (apart from echinoderms, protobranch bivalves and gastropods) and a general lack of ornamentation, which they proposed is linked to the difficulties of secreting calcium carbonate.

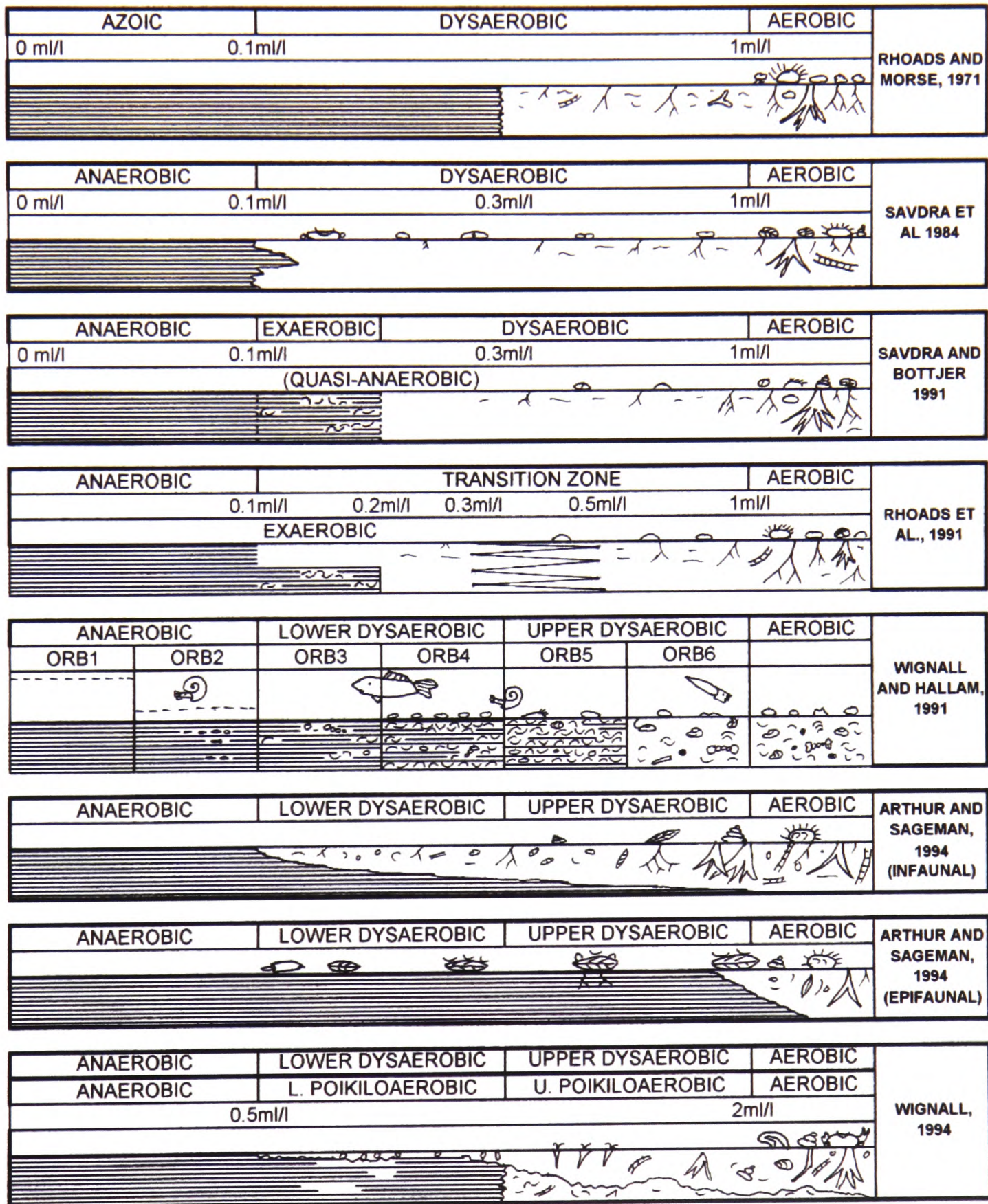


Figure 3.4: Summary diagram representing a variety of proposed oxygen-related biofacies models (adapted from included references).

Since the original publication, many authors have suggested alterations or extensions to this model. Byers (1977) developed the model into three oxygen-related biofacies, adapting the term 'azoic' to 'anaerobic', and this is often referred to as the Rhoads-Morse-Byers Model. Byers (1977) was the first to use the term dysaerobic to apply to a biofacies as opposed to a dissolved oxygen concentration. He suggested that this biofacies would be lacking in calcareous epifauna but that the sediment would show evidence of bioturbation due to the activities of more tolerant fauna. Thompson *et al.* (1985) disagreed with the dissolved oxygen range proposed and suggested that you find a moderately diverse calcareous fauna until below 0.3 ml/l. They proposed that the term 'dysaerobic' should apply to the range 0.1-0.3 ml/l but Wignall (1994) suggested that this possibly represents a division between lower and upper dysaerobic facies. In 1991 Tyson and Pearson coined the phrase quasi-anaerobic to represent this lower dysaerobic facies.

Savdra *et al.* (1984) were the first to use aerobic/dysaerobic/anaerobic in purely biofacies terms. In that paper, Savdra *et al.* (1984) suggested that it was difficult to define a sharp boundary between aerobic and dysaerobic conditions, and in a considerable revision of their own model, Rhoads *et al.* (1991) agreed with this concept and proposed a 'transition zone' between the conditions (see *Figure 3.4*). Wignall (1994) argued that this actually makes the model more difficult to apply as there are now two boundaries to distinguish either side of the transition zone, and proposed instead that the boundary should be defined as where the first influence of oxygen restriction is seen.

Savdra and Bottjer (1987) noted that the existing models did not explain the common presence of discrete shelly horizons within laminated sequences and they proposed the existence of an exaerobic facies at the dysaerobic-anaerobic boundary (see *Figure 3.4*). The initial proposal suggested that these taxa were chemosymbionts and that this biofacies represented conditions 'teetering on the edge of anoxia' (Allison *et al.*, 1995). However, later interpretations suggested that chemosymbiotic life modes would not be suited to this environment and that these shelly horizons are likely to be the result of oxic events within anoxic bottom waters (Wignall, 1994). Bottjer *et al.* (1995) suggested that while Savdra and Bottjer (1987) did not fix the exaerobic

biofacies to discrete dissolved oxygen contents, their formation may be controlled by a temporal constraint on the duration of oxygenation events.

3.1.2.2 Morris Categories

In 1979, Morris combined several faunal and sedimentological descriptors to define three categories of bottom-water oxygenation.

- **Aerobic (normal marine) conditions** refer to deposition in fully oxygenated bottom waters and is represented by homogenous bioturbated sediment. Morris (1979) suggested that in this setting, the trace-fossil assemblage will be dominated by *Chondrites* and that benthic body fossils will be abundant and diverse. He suggested that the bivalves present will be a combination of infaunal and epifaunal types, but that infaunal deposit feeders will comprise less than 20% of the fauna.
- **Restricted (normal marine) conditions** refer to deposition in waters with low oxygen concentrations and is represented by poorly laminated sediment. Morris (1979) suggested that the commonly sparse bioturbation will be represented by presence of thin discreet pyrite burrows and that bivalve assemblages should be dominated by shallow-burrowing infaunal deposit feeders. He suggested that while infaunal suspension feeders will be rare, epifaunal suspension feeders are likely to be common.
- **Bituminous sediments** are thought to represent conditions where little or no oxygen is present and H₂S may be continually or intermittently present and are represented by finely laminated sediment. This category is also referred to as **Inhospitable Bottom Water Conditions** (Raiswell *et al.* 1988), and Wignall and Myers (1988) suggested that it correlates with Lower Dysaerobic environments where conditions are anoxic at the sediment-water interface. Morris (1979) suggested that generally there is little or no bioturbation and that if a benthic fauna is present, it is composed almost entirely of epifaunal suspension feeders.

These descriptive categories correlated with the divisions Morris (1979) proposed for ternary diagrams of bivalve life modes (see **Section 3.1.1.4** and *Figure 3.1*). Wignall and Myers (1988) pointed out, however, that if epifaunal species can survive Inhospitable Bottom Water Conditions, then irrigation should allow infaunal

occupation as well. They proposed that epifaunal dominance may actually reflect sedimentation rates rather than oxygen-related variations. However, Aberhan and Baumiller (2003) found that early Jurassic anoxic sequences were dominated by epifaunal forms, and pointed out that unless burrows were lined, infaunal species could be poisoned by dissolved hydrogen sulphide even if the burrow systems were irrigated.

3.1.2.3 Oxygen-Restricted Biofacies

In 1991, Wignall and Hallam took the use of descriptive criteria one step further by adding numerical suggestions of benthic species richness to their definitions of **Oxygen-Restricted Biofacies (ORBs)**. Whereas previous genetic schemes described a temporally stable gradient between biofacies properties and dissolved oxygen contents, the **ORB** scheme focused more on the impact of dynamic and temporarily variable oxygen gradients (Wignall and Hallam, 1991). The interpretation of these biofacies included relative frequencies of benthic oxygenation events within lower oxygen regimes (see *Figure 3.4*):

- **Oxygen-Restricted Biofacies 1** is defined by a complete absence of benthic and nektobenthic forms. Any macrofossils should be truly pelagic forms, although rare pseudoplankton is also possible. Wignall (1994) pointed out that care needs to be taken to distinguish this biofacies from sites where fossil material has been lost due to carbonate dissolution. He suggested that where fossils have been lost, there should still be visible ghosts of fossil forms. Wignall and Hallam (1991) suggested that the sediment should have fine scale lamination and proposed that this biofacies represents permanent anoxia reaching well into the water column.
- **Oxygen-Restricted Biofacies 2** is defined by an absence of benthos but an abundance of nektobenthics such as ammonoids. Wignall and Hallam (1991) suggested that this represents permanent anoxia at the sediment surface and possibly in the lowest levels of the water column, but with oxic waters relatively close allowing nektobenthics to survive. They pointed out that the assemblages normally show a full range of sizes with more than one species present, suggesting that this represents mass mortality events.

- **Oxygen-Restricted Biofacies 3** is defined as containing 1-4 benthic species as well as nektobenthic and pelagic species. The benthic forms are commonly bivalves representing shallow epifaunal and infaunal life modes. Several benthic genera of foraminifera can survive in these lowest dysaerobic conditions and Wignall (1994) suggested that this represents Koutsoukos *et al.*'s (1990) quasi-anaerobic facies. The sediment is generally composed of fissile strata where lamination is common and microburrows possible. Wignall and Hallam (1991) suggested that this biofacies represents very low benthic oxygen where short oxygenation events allow a few species to colonise for brief periods such as a few days.
- **Oxygen-Restricted Biofacies 4** is defined as containing 2-8 benthic species, and while this does not represent much of an increase in species richness from **ORB3**, the definition involves an increase in the number of specimens. The sediment is commonly fissile and laminated with bedding planes showing a few species of bivalves and brachiopods. Discrete shelly laminae are common which suggests that episodic colonisation occurred. Wignall (1994) pointed out that assemblages of 2-8 species are also found in bioturbated mudstones which he suggested represent prolonged bioturbation that occurs under consistently low oxygenation. On the other hand, he suggested that the laminated shales represent fluctuating low-oxygen conditions, which he terms "poikiloaerobic" (see **Section 3.1.2.4**). He also suggested that this description matches that of Savdra and Bottjer's (1987) exaerobic facies.
- **Oxygen-Restricted Biofacies 5** is defined as containing 5-10 species but in which, importantly, unlike the previous levels benthic species richness is strongly affected by sample size. The biofacies may be best described as containing up to 10 common species. Wignall and Hallam (1991) suggested that weak fissility is possible but that generally this biofacies is represented by massive mudstones. They suggested that fine lamination is rarely seen and that this represents longer durations of elevated benthic oxygen levels. However, they pointed out that the relatively low diversity suggests that there is still some oxygen-related restriction and that these sediments can contain up to 10% Total Organic Carbon. Wignall and Hallam (1991) suggested that macroscopic pyrite aggregates are common in internal cavities, and that

belemnites are only found at this level of oxygenation and above. They implied that although belemnites are nektonic like ammonoids, they may be less tolerant of low-oxygen conditions.

- **Oxygen-Restricted Biofacies 6** is defined as containing at least 10 common benthic species. Kammer *et al.* (1986) point out that dysaerobic environments can have up to 40 species, and so Wignall and Hallam (1991) explain that it could be difficult to distinguish this from an aerobic environment. In order to clarify this, they add a further stipulation that this biofacies can not contain any stenoxic taxa, which includes many crinoids, and all corals and thick shelled taxa.

3.1.2.4 Wignall's 'Shelf Model'

In 1994, Wignall proposed the 'Shelf Model', in which he suggested that the temporal variability of modern shelf environments creates a different benthic fauna compared to the stable low-oxygen conditions of the Rhoads and Morse (1971) model. Wignall (1994) suggested that the term dysaerobic is more descriptive of stable low-oxygen environments and so proposed an adaption of the term 'poikiloaerobic', originally defined by Oschmann (1991), to apply to fluctuating environments. Oschmann (1991) proposed the term to refer to environments where anoxia does not occur for more than 3 months of a year. He described the corresponding fauna as being comprised of rare soft bodied and shelly fauna, which were predominantly infaunal suspension feeders. Wignall (1994) disagreed with some terms of this definition, suggesting that true anoxia was not required as, according to Tyson and Pearson (1991), dissolved oxygen levels of <0.5 ml/l is enough to eliminate benthos in fluctuating environments. He also suggested that the term 'rare' is misleading as there can be high shell densities – he preferred the use of the term 'species poor' instead. With these adjustments, and the suggestion that infaunal suspension feeders are not always dominant, Wignall (1994) suggested that this is a good term to describe fluctuating black shale faunas.

Arthur and Sageman (1994) noted that the benthic taxa of low-oxygen sediments normally fell into one of two categories:

- **Resident Components** where the assemblage is distributed throughout a sample interval and/or shows evidence of long-term *in situ* habitation;
- **Event Components** where the assemblage occurs on single bedding planes and/or shows evidence of benthic colonization followed by abrupt mortality.

They suggested that a high frequency of Event Components suggests a dynamic low-oxygen environment. Wignall (1994) agreed that fluctuating low-oxygen environments allow episodes of extreme colonisation by opportunistic forms and he suggested that this would create a different set of descriptive low oxygen facies compared to a low oxygenation in a stable environment (see *Figure 3.4*):

- **Anaerobic environments** (<5 ml/l dissolved oxygen) – represented by a complete lack of benthos. Bacterial mats can be present if there is no free dissolved hydrogen sulphide.
- **Lower poikiloaerobic environments** (rare short oxygenation events) – represented by laminated sediments with species-poor shell pavements often composed of suspension feeders, and microbioturbation due to short oxygenation events.
- The **Upper/Lower poikiloaerobic boundary** is defined as the boundary between laminated and burrow-mottled strata.
- **Upper poikiloaerobic** (increased occurrence of oxygenation events) – represented by a more established benthos and a deeper Redox Potential Discontinuity which results in the loss of laminations.
- The **aerobic/dysaerobic boundary** is recognised by the appearance of deep infaunal forms that are not tolerant to low oxygen conditions.

In this model, Wignall (1994) suggested that a decrease in oxygen levels is represented by:

1. A decrease in species richness, dropping to zero at the anaerobic/poikiloaerobic boundary.
2. A decrease in size, especially of soft bodied forms. He suggested, however, that larger bivalves are usually more tolerant of low-oxygen conditions.
3. A decrease in depth and size of burrows until lower poikiloaerobic conditions where they become too small to disrupt millimeter size laminae.
4. No general trend in life strategies – opportunistic bivalves are often suspension feeders, but Wignall (1994) suggested that there is no overall trend.

He also believed that there is no trend in the ratio of infaunal/epifaunal species, but that deep infaunal forms are lost in dysaerobic environments

5. No change in the ratio of soft bodies to shells.

Wignall (1994) pointed out that only descriptors 1 and 3 match the trends proposed by the Rhoads and Morse model (1971).

The appreciation of the impact of fluctuating oxygenation conditions marked the start of a move away from the original Rhoads and Morse (1971) interpretation of benthic relationships and initiated the re-interpretation of the previously suggested models. Sageman and Bina (1997) went as far as to suggest that the dissolved oxygen content may not be as an important control on benthos as the 'Environmental Stability' or 'Disturbance Frequency', as the frequency of anoxic or oxic events controls the extent of colonisation. Raiswell *et al.* (2001) used Indicator of Anoxia data (see **Section 5.1.2.5**) to apply this concept to Wignall and Hallam's (1991) **Oxygen-Restricted Biofacies (ORBs)** (see **Section 3.1.2.3**) and suggested that:

- **ORBs 1 and 2** represented persistent anoxic conditions;
- **ORB 3** represented anoxic bottom-water conditions with rare oxygenation events;
- **ORB 4** represented oxic bottom waters with anoxic events;
- **ORB 5** represented predominantly oxic waters with rare anoxic periods;
- **ORB 6** represented fully oxic conditions.

3.1.2.5 Arthur and Sageman's Infaunal and Epifaunal Biofacies Levels

Arthur and Sageman (1994) recognised that there were many differences between the models that had been proposed, but suggested that they all fit on a common framework. They agreed that the original models required adaption in order to take account of the importance of short-term event communities. They summarised the work of a number of papers (Sageman, 1989; Kauffman and Sageman, 1990; Sageman *et al.*, 1991) to outline a black shale biofacies model based on the Hartland Shale Member of the Greenhorn Formation in the Western Interior basin of the United States of America. In this model they defined two main biofacies categories based on assemblage dominance by either infaunal or epifaunal species (see *Figure*

3.4). Each category is divided into seven distinct biofacies levels between anaerobic and aerobic conditions. The biofacies levels are defined by:

- the presence of characteristic taxa with specific life habits and trophic strategies,
- characteristic sediment fabrics related to the level of infaunal colonisation,
- levels of species richness and equitability,
- and, in some cases, recurring ecological relationships between component taxa, such as commensalistic host-epibiont interactions.

The infaunal biofacies levels apply to strata with 90% of the total fauna represented by infaunal species. These descriptors rely more heavily on ichnology and sediment texture (see **Section 2.1.2**) but also refer to body fossils:

- **Level 1** implies anoxic conditions existed above and below the sediment-water interface. This is represented by laminated sediments showing the highest levels of Total Organic Carbon, and no evidence of benthic metazoan life.
- **Level 2** is represented by laminated sediments showing slight disruption due to microburrowing (<1 mm diameter). This is probably the result of meiofaunal organisms (such as nematodes) in the upper most layers of sediment.
- **Level 3** is represented by small deposit-feeding pioneer ichnotaxa such as *Planolites* or *Chondrites* which are thought to be made by more oxygen tolerant macrofauna.
- **Level 4** is represented by an increase in size and density of these ichnotaxa, but with no additional ichnotaxa. In terms of body fossils, this level is represented by the appearance of deposit feeding infaunal bivalves such as *Nucula* or *Lucina*.
- **Level 5** is represented by the appearance of more complex traces (*Teichichnus* and *Zoophycos*) as well as body fossils of infaunal grazers such as the anchurid gastropod *Drepanoxhilus*.
- **Level 6** is represented by the appearance of sediment dwelling ichnotaxa such as *Thalassinoides*.
- **Above level 6**, all groups may be included and the high diversity, high equitability assemblages represent a normal aerobic biofacies.

The epifaunal biofacies levels apply to strata with 90% of the total fauna represented by epifaunal taxa. These descriptors rely more heavily on sediment texture and body fossils:

- **Level 1** is identical to this level in the infaunal model, where anoxic conditions exist above and below the sediment-water interface. This is represented by laminated sediments with high Total Organic Carbon and no evidence of *in situ* benthic habitation.
- **Level 2** is represented by laminated sediments containing only ammonites, which are believed to be nektonic scavengers and predators. These would have been mobile within the water column and possibly fed on dead and dying organisms at or near the toxic sediment-water interface.
- **Level 3** is represented by the pioneer suspension feeders which are also referred to broadly as 'flat clams'. Arthur and Sageman (1994) suggested that this level corresponds to lower levels of dysaerobic conditions where the redox boundary lies at the sediment-water interface. In the Hartland Shale Formation, this level coincided with the Degree of Pyritisation values suggested for Morris's (1979) 'restricted facies'.
- **Level 4** is represented by an assemblage where pioneer flat clams are joined by suspension feeders, which Kaufman (1981) suggested lived as epibionts on the larger flat clay "shell islands".
- **Level 5** is represented by the first appearance of opportunistic epifaunal colonisers including bivalves and ostracods. Arthur and Sageman (1994) suggested that this indicates that the sediment surface at Level 5 was habitable to less tolerant taxa.
- **Level 6** is represented by a significant increase in diversity with the appearance of various surficial grazers, scavengers and carnivores. These assemblages represent the development of an ecologically complex community.
- **Level 7** is represented by assemblages where all epifaunal groups are represented. Arthur and Sageman (1994) suggested that these high diversity and equitability levels are characteristic of normal aerobic conditions.

However, Arthur and Sageman (1994) identified several difficulties in applying these biofacies models. For the infaunal biofacies model, they pointed out that extensive

reworking of the sediment occurs in the higher biofacies levels and that this may reduce the number of taxa preserved, reducing the diversity values for those levels. They also found that Level 5 and above tended to be represented by mixed infaunal-epifaunal assemblages and that 'pure' infaunal or epifaunal biofacies only exist in the lower part of dysaerobic range. A further problem that they identified is that the nature of substrate is also a major factor in the colonisation of low-oxygen tolerant taxa and that this is not taken into account in this model.

3.1.2.6 Summary

While the Rhoads and Morse (1971) model has formed the basis of the majority of further work in this field, there have been major adaptations to the model's original form:

- Redefining the dysaerobic/aerobic boundary on the basis of shelly faunas being found at increasingly lower oxygen (Savdra *et al.*, 1984; Thompson *et al.*, 1985).
- Subdivision of the dysaerobic transition along linear gradients of diversity, abundance, trophic structure and fossil morphologies. The development of the concepts of poikiloaerobic biofacies now forms the basis of many interpretive models (Savdra and Bottjer, 1987, 1991; Sageman *et al.*, 1991; Wignall and Hallam, 1991).
- The increasing importance of the temporal stability of dysoxic environments – models now focus on the relationship between disturbance frequency and adaptive characteristics (Wignall, 1994; Tyson and Pearson, 1991).

Through the development of these models, there has been a general movement from assuming the dissolved oxygen content is the most important control, to focussing on the extent and duration of low-oxygen events. Wignall and Hallam (1991) reviewed the literature and found that there is commonly a discrepancy between geochemical and palaeoecological indices. They suggested that geochemical indices show a time averaged view of the depositional environment, whereas the faunal indices are more indicative of the transient oxygen fluctuations that have occurred. Newton (2001) found consistently contrasting results from biofacies analysis and other proxies for low-oxygen conditions and agreed that this represented 'cyclic anoxia', where geochemical and pyrite-based proxies are fixed during the anoxic periods but the

faunal proxies are more affected by the regular oxygenation events. Kenig *et al.* (2004) believed that benthic biofacies alone may not record the true oxygen conditions in bottom waters and Allison *et al.* (1995) suggested that a multi-proxy approach is necessary to interpret palaeoecological signals.

In addition to the impact of oxygen-related event duration, Sageman and Bina (1997) identified a number of other factors which also affect macrofossil assemblages:

- Sediment substrate;
- Temperature;
- Adaptive strategies;
- Competition (or lack of it);
- Growth rates;
- Resources utilisation and nutrient flux.

Of these factors, possibly the most important is the effect of sediment substrate on the species and assemblages observed. For example, the dominance of flat clams in low-oxygen environments may equally be due to their ability to colonise the soft substrate commonly associated with these conditions (Kenig *et al.*, 2004). However, Kenig *et al.* (2004) also pointed out that other forms which live in soft substrates, such as protobranch bivalves, are not dominant in these conditions but suggested that this may be because they have benthic larvae and so do not have the colonising advantage of the 'flat clams' planktic larvae. Goldring (1995) suggested that the nature of the substrate affects trophism, attachment and penetration of benthic organisms, and that organisms themselves can play an important role as clasts. Arthur and Sageman's (1994) epifaunal biofacies levels noted that the next stage of colonisation uses flat clams as hard substrate islands and Kenig *et al.* (2004) believed that the thin shell beds observed in lower dysaerobic conditions are the result of colonisation of a firmer substrate. Rhoads and Boyer (1982) also drew attention to the concept of 'taphonomic feedback' which suggests that pioneers may modify the physical and chemical properties of the sediment making further colonisation possible.

The impact of these other factors on macrofaunal assemblages is not fully understood and can only act to complicate the interpretation of palaeo-oxygenation conditions.

3.2 Methods:

3.2.1 Macrofossils

Within the Folkestone Gault Clay macrofaunal counts were carried out by the author at distinct horizons every 20 cm through the section of interest. The identification of the Gault Clay specimens was carried out by the author.

The Niveau Pacquier and Briestroffer sequence macrofossils were collected by Professor A.S. Gale at horizons within the sequence and are stored at the Oxford University Museum of Natural History Museum. All identifications of specimens were carried out by the Museum staff.

The Amma Fatma specimens were collected by Professor A.S. Gale and were identified by staff of the Sedgwick Museum in Cambridge.

Bivalve modes of life were assigned by the author according to Aberhan *et al.* (2004).

3.3 Discussion of Results

3.3.1 The Niveau Pacquier sequence, Vocontian Basin

The sequence contains distinct horizons of fossiliferous black shales of the Niveau Pacquier Formation, which demonstrate good preservation of predominantly ammonitic material. The black shale sequences are surrounded by the grey clays of the Marnes Bleues Formation, which exhibit poor preservation and are significantly less fossiliferous. Again, the majority of the material is nektobenthic fauna, with rare benthic bivalves preserved.

3.3.1.1 Analysis of Fossil Assemblages

Within the black shale horizons, benthic diversity is very low. Rare inoceramids are found but the assemblages are dominated by nektobenthic forms. These are predominantly ammonites, with rare small belemnites and even rarer fragments of fish. The Oxford Natural History Museum material from the Col de Palluel section represents the lower part of Bréhéret's (1997) Unit VI of the Niveau Pacquier. This corresponds to a level 1.3m above the base of the first black shale horizon. The collection comprises a range of ammonites with rare belemnites (see *Appendix B, Table B.1a*) common to all of the Museum's Niveau Pacquier collections from a variety of sites within the region.

The Marnes Bleues formation also demonstrates a low benthic diversity, with rare bivalves observed in the field. Ammonites are again common but poorly preserved and not in such high abundance as the black shale sequence. This suggests that sequence condensing possibly occurred within the black shales, or that poor preservation gives an underestimation of the Marnes Bleues diversity. There is limited material stored at the Oxford Natural History Museum from this particular sequence and no specimens of benthos are included. However, material collected from the Marnes Bleues 15m below the base of the Niveau Pacquier at Le Pillart at Tartonne contains ammonites, gastropods, belemnites and fish remains (see *Appendix B, Table B.1b*). While this does not represent a fully diverse benthic community, it is clear that the Marnes Bleues sequence contains a more diverse benthic fauna than the black shales.

It is difficult to judge benthic size with such limited benthos, but the rare inoceramids found within the Niveau Pacquier sequence measure between 2 and 3 cm across which does not suggest that size was limited. However, Wignall (1994) pointed out that bivalve adults tend to have a greater tolerance to low-oxygen conditions and are therefore not likely to exhibit dwarfing in such conditions.

The interpretation of depth of burrowing is limited within the sequence but the black shales show full preservation of laminae. This suggests low-oxygen conditions during deposition. In contrast, the grey clay sequence, while showing little physical evidence of bioturbation, may be homogenised suggesting a deep Redox Potential Discontinuity which implies that more oxygenated conditions occurred during deposition.

With very little benthos present, it is difficult to draw many conclusions from benthic modes of life. The fossil assemblages in both sediments are dominated by nektobenthics and the Oxford collection from the Marnes Bleues Formation is lacking in bivalves. The rare inoceramids observed within the black shale material are epifaunal suspension feeders. The poor representation of benthic forms means that interpretation is not particularly reliable, but Morris (1979) suggested that bituminous sediments (which coincide with a lower dysaerobic biofacies) contained assemblages dominated by epifaunal suspension feeders.

Rare shelly taxa are preserved in both the grey clay and black shale horizons, which suggests that even under the low-oxygen conditions of the black shales, shelly taxa were not limited. However, a benthic assemblage represented only by rare inoceramids in the black shale sequence fits Arthur and Sageman's (1994) description of a 'benthic boundary facies' composed of 'flat clams' such as thin shelled inoceramids. They suggested that these forms were specially adapted to life at the anoxic/dysoxic boundary. The low abundance of benthic forms within the Marnes Bleues Formation, while possibly an artefact of increased bioturbation and poor preservation, means that interpretation in terms of particular species is not possible.

In terms of taphonomy there is stark contrast between the Niveau Pacquier black shales and Marnes Bleues grey clays. Within the black shales, preservation is

generally as flattened impressions or pyrite films. This corresponds with Fisher and Hudson's (1987) observations of flattened ammonites in the Jurassic Black Shales. Brett and Baird (1986) suggested that this form of preservation is associated with dysaerobic to anaerobic conditions (see *Figure 3.2*). Preservation is good within this sequence, although waves of fragmented ammonite material occur throughout the succession. This contrasts with the delicate preservation of uncoiled ammonites at other horizons and suggests that higher energy events occurred sporadically during deposition. The presence of rare carbonate nodules within the Niveau Pacquier correlates with Br  h  ret *et al.*'s (2004) observations from Les Oustraus, Tartonne and Les Coignets. They found that the nodules varied from site to site, but in all cases were distributed as discontinuous layers parallel to bedding. Br  h  ret *et al.* (2004) concluded that nodule formation is based on sedimentary heterogeneity and that they represent variations in bottom-water oxygenation conditions at different time scales such as over seasons and years.

In contrast, the grey clays of the Marnes Bleues Formation exhibit poor preservation, usually as impressions or flattened carbonate material. At Tartonne, Kennedy *et al.* (2000) recorded a layer of ammonites preserved with pyrite infills, which is indicative of relatively oxic waters where pyrite formation occurs in anoxic microenvironments created by decaying organic matter (Fisher and Hudson, 1987). The poor carbonate preservation observed within the Marnes Bleues of the Col de Palluel sequence also suggests more oxygenated waters than present at the time of formation of the Niveau Pacquier sequence.

3.3.1.2 Application of Biofacies Models

Under Rhoads and Morse's (1971) scheme, the Niveau Pacquier black shale samples would be classified as anaerobic to dysaerobic due to the presence of laminations (see *Figure 3.5*). In their original model, laminations were possible within the dysaerobic facies. However, their later additions to the model restrict laminations to anaerobic and exaerobic facies and as there is no evidence of discrete shell beds within the sequence, this narrows the classification down to anaerobic. The Marnes Bleues grey clays, on the other hand, best fit the description of the 'Transition Zone' which effectively encompasses the upper dysaerobic facies (see *Figure 3.6*). This classification is based on the limited benthos within the Marnes Bleues, coupled with

the suggested bioturbated nature of the sediment. However, poor preservation may be responsible for the lack of benthos, in which case it is difficult to distinguish between the aerobic and dysaerobic facies.

	Anaerobic	Lower Dysaerobic	Upper Dysaerobic	Aerobic
Rhoads and Morse (1971)	←-----→			
Savdra et al. (1984)	←-----→			
Rhoads and Morse (1991)	★			
Wignall and Hallum (1991)		←-----→	?	
Arthur and Sageman (1994)	←-----→			
Wignall (1994)	←-----→			
	Anaerobic	Lower Poikiloaerobic	Upper Poikiloaerobic	Aerobic

Figure 3.5: Summary diagram to show the proposed ranges of palaeo-oxygenation conditions for the Niveau Pacquier black shale according to a range of macrofaunal models.

	Anaerobic	Lower Dysaerobic	Upper Dysaerobic	Aerobic
Rhoads and Morse (1971)			←-----→	→
Savdra et al. (1984)		←-----→		→
Rhoads and Morse (1991)			←-----→	→
Wignall and Hallum (1991)				★
Arthur and Sageman (1994)			←-----→	→
Wignall (1994)			←-----→	
	Anaerobic	Lower Poikiloaerobic	Upper Poikiloaerobic	Aerobic

Figure 3.6: Summary diagram to show the proposed ranges of palaeo-oxygenation conditions for the Marnes Bleues grey clay within the Niveau Pacquier sequence according to a range of macrofaunal models.

The lack of benthic specimens from either sample location means that it is difficult to apply Morris’ (1979) scheme. Based mainly on the sedimentology, the black shale horizons would be described as ‘Bituminous Conditions’ and the grey clay samples would classify as ‘Normal Marine’ due to the lack of laminations.

Under Wignall and Hallam’s (1991) Oxygen-Restricted Biofacies (ORB) scheme, the black shale sequences match the description of ORB2, with no apparent benthos but a variety of nektobenthic ammonites present. This implies anoxic conditions at the

sediment:water interface. The observation of rare bivalves within the sequence would shift this classification to ORB3 which represents a lower dysaerobic facies, and it is possible that conditions fluctuated on the boundary between these two facies. However, Wignall and Hallam (1991) suggested that the presence of belemnites indicated ORB5 or above as they believed they were less tolerant to low-oxygen bottom waters than ammonites. The presence of belemnites within the black shale sequences, which definitely does not match the description of ORB5, would seem to contradict this suggestion. The absence of benthic material in the Oxford grey clay collection suggests relatively low abundance and species richness, even taking into account the gastropods within the Tartonne collection. However, the absence of laminations suggests a classification of ORB6 or above, implying an upper dysaerobic facies, or anaerobic conditions.

Using Wignall's (1994) Shelf Model, the presence of rare bivalves within the laminated black shale sequence could be taken to imply rare oxygenation events within a predominantly anoxic setting. In contrast, the lack of laminations and the presence of a deep redox potential discontinuity suggests upper dysaerobic or aerobic conditions for the formation of the Marnes Bleues grey clays. The absence of benthic specimens would seem to suggest that a classification of upper dysaerobic is more fitting, but the possibility of poor preservation and the presence of benthic specimens from the same sequence at Tartonne introduces a degree of unreliability into this classification.

The black shale collection can be classified as Level 2 or 3 on Arthur and Sageman's (1994) Epifaunal Biofacies Level scheme, which implies deposition under anaerobic or lower dysaerobic conditions. The dominance of nektobenthic ammonite specimens suggests anaerobic conditions where the redox interface was at the sediment:water boundary. However, the rare occurrence of bivalves within the sequence could fit the description of Arthur and Sageman's (1994) 'benthic boundary facies' within Level 3. The Marnes Bleues grey clays are lacking laminations which implies Level 7 within the Epifaunal Biofacies scheme, and Aerobic conditions, or possibly Level 6, Upper Dysaerobic conditions, in the Infaunal Biofacies Scheme. Arthur and Sageman (1994) pointed out that a combination of Infaunal and Epifaunal biofacies are commonly observed above Level 5 in their biofacies models.

3.3.2 The Briestroffer sequence, Vocontian Basin

The Briestroffer sequence contains distinct bands of black shales displaying limited benthos. However, impressions and pyrite films of ammonites and belemnites are common and rare bivalves were observed in the field. In contrast, the grey clays of the Marnes Bleues Formation are less fossiliferous, containing fewer ammonites. The Oxford University Museum of Natural History hold a collection from the fourth Briestroffer Horizon (see *Appendix B, Table B.2a*), and another collection from 17 metres above this point in the Marnes Bleues Formation (see *Appendix B, Table B.2b*). Both collections are composed entirely of specimens of ammonites.

3.3.2.1 Analysis of Fossil Assemblages

The lack of benthic species within the Oxford Natural History Museum Collections means that an interpretation of benthic diversity, benthic sizes, modes of life, presence of shelly taxa or the identification of particular indicator species is not possible. However, the depth of burrowing within the sequence and the taphonomy of the nektonic specimens allows some interpretation of the environmental conditions. In terms of burrowing, the black shales of the Briestroffer layers exhibit fine lamination, suggesting deposition under oxygen levels low enough to exclude burrowing organisms. The grey clays of the Marnes Bleues, however, may be fully homogenised, which suggests deposition under a more oxic water column.

Within the black shale sequence, the fossils are preserved as impressions or pyrite films, which possibly corresponds with Brett and Baird's (1986) suggestions of pyrite patinas in dysaerobic-anaerobic conditions with intermediate sedimentation rates (see *Figure 3.2*). The presence of well preserved but flattened loosely coiled ammonites suggests low energy conditions during deposition, and limited bioclast transportation. Pyrite aggregates and internal moulds are absent in both the Briestroffer layers and the Marnes Bleues clays. Preservation within the Marnes Bleues Formation occurs mainly as impressions or crushed carbonate material which would suggest more oxygenated conditions.

3.3.2.2 Application of Biofacies Models

The Briestroffer black shale samples show laminations and so would be classified as anaerobic or lower dysaerobic under Rhoads and Morse’s (1971) original scheme. This model was developed to include the exaerobic facies but as with the Niveau Pacquier Black Shale, there is no evidence of discreet shell beds within the sequence so they do not fit this facies description (see *Figure 3.7*). The lack of benthos within the Marnes Bleues grey clays makes it difficult to classify using these models. On face value the sediment could be classified as Upper Dysaerobic or ‘Transition Zone’ conditions (see *Figure 3.8*). However, the limited benthos could be misleading as it may equally be due to poor preservation rather than reduced oxygen availability.

	Anaerobic	Lower Dysaerobic	Upper Dysaerobic	Aerobic
Rhoads and Morse (1971)	←-----→			
Savdra et al. (1984)	←-----→			
Rhoads and Morse (1991)	★			
Wignall and Hallum (1991)		←-----→	?	
Arthur and Sageman (1994)		★		
Wignall (1994)	←-----→			
	Anaerobic	Lower Poikiloaerobic	Upper Poikiloaerobic	Aerobic

Figure 3.7: Summary diagram to show the proposed ranges of palaeo-oxygenation conditions for the Briestroffer black shales according to a range of macrofaunal models.

	Anaerobic	Lower Dysaerobic	Upper Dysaerobic	Aerobic
Rhoads and Morse (1971)			←-----→	
Savdra et al. (1984)		←-----→		
Rhoads and Morse (1991)		←-----→		
Wignall and Hallum (1991)			★	
Arthur and Sageman (1994)		←-----→		
Wignall (1994)			←-----→	
	Anaerobic	Lower Poikiloaerobic	Upper Poikiloaerobic	Aerobic

Figure 3.8: Summary diagram to show the proposed ranges of palaeo-oxygenation conditions for the Marnes Bleues grey clay within the Briestroffer sequence according to a range of macrofaunal models.

Morris' (1979) scheme has limited applicability within the sequence as there are limited benthic specimens. Focussing entirely on the sedimentology, the black shale horizons fit the description of 'Bituminous Conditions' and whereas the grey clay samples would classify as 'Normal Marine' due to the lack of laminations.

Using the Oxygen-Restricted Biofacies (ORB) scheme (Wignall and Hallam, 1991), the black shale samples would classify as ORB2 due to the apparent lack of benthos. In a similar pattern to the Niveau Pacquier black shale, rare bivalves are present which would suggest a classification of ORB3 instead. Also, the presence of belemnites within the sequence tests Wignall and Hallam's (1991) suggestion that belemnites can only survive in more oxygenated conditions represented by ORB5. The lack of benthic specimens from the Marnes Bleues complicates classification using the ORB scheme. On first observation the low abundance and species richness would imply a low oxygen setting but the absence of laminations suggests a classification of ORB6 or above.

Classification using Wignall's (1994) Shelf Model again relies on the sedimentological characteristics due the absence of benthos in the Oxford collection. The laminated nature of the Black Shales implies predominantly anoxic conditions with the observation of rare bivalves in the field suggesting that rare oxygenation events occurred. The Marnes Bleues Formation appears to have undergone homogenisation by bioturbation, which despite the lack of benthic forms, suggests relatively oxygenation conditions prevailed.

In terms of Arthur and Sageman's (1994) Biofacies Level Scheme the black shale sequence can be classified using the epifaunal scheme. The large numbers of ammonites and the presence of lamination suggests a classification of Level 2 which represents anaerobic conditions where the redox boundary was at the sediment:water interface. The Marnes Bleues sediment does not seem to match the epifaunal scheme as the absence of lamination is coupled with the appearance of a strong benthic community. On the infaunal scheme the lack of lamination and apparent lack of benthos could be said to correlate with Level 4 or 5.

3.3.3 The Folkestone Gault Clay

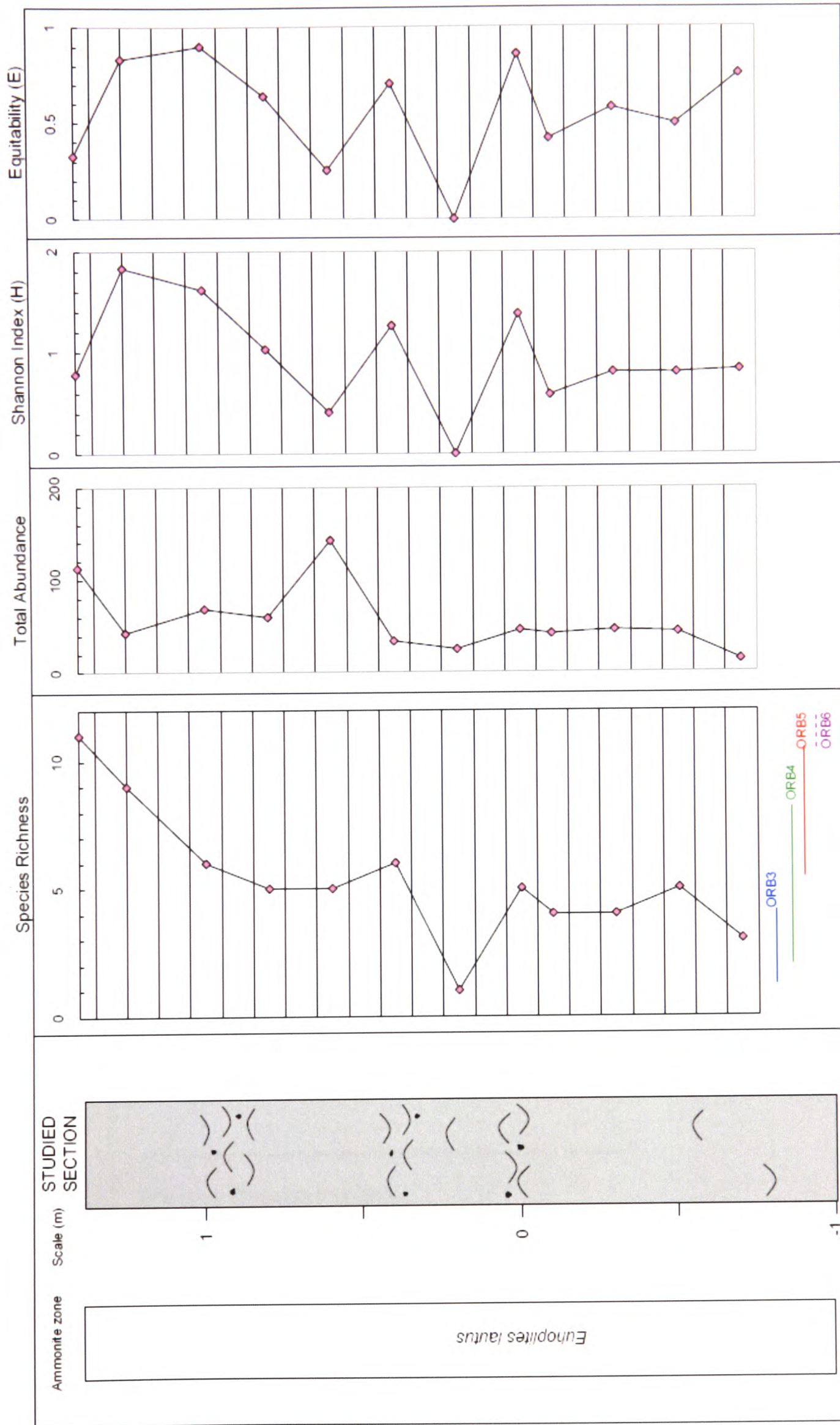
The Folkestone Gault Clay is a fossiliferous blocky mudstone. Within the horizons characterised by the presence of phosphate nodules or shell-debris filled burrows, there is a relatively diverse fauna containing bivalves, gastropods, belemnites, ammonite fragments and scaphopods (see *Appendix B, Table B.3*). Between these horizons, the assemblage is dominated by small *Circocerithium* spp. gastropods, with occasional inoceramids. The inoceramids show a sharp transition at the base of bed VII between *Birostrina concentricus* and *Birostrina sulcata*. The appearance of a more ‘corrugated’ shell suggests the existence of higher energy conditions from this point in the sequence. From 1.4 m above the base of bed VII there is a shell bed showing a high abundance of *Birostrina sulcata*.

3.3.3.1 Analysis of Fossil Assemblages

The samples revealed relatively low species richness throughout the sequence (see *Figure 3.9*), which possibly highlight the dependency on sample size. Species richness increases towards the top of the sequence but this may be an artefact of higher preservation as it correlates with increasing carbonate contents. The plot of total abundance through the sequence shows peaks for the samples where either *Circocerithium* spp. or *Birostrina sulcata* dominated in high numbers (see *Figure 3.9*) and this is highlighted as lower values in the Shannon Index and Equitability plots.

While the total abundance plot does show how ‘fossiliferous’ the samples are, this is not particularly helpful in identifying oxygenation trends as preservation is often high in low oxygen conditions. While the total abundance is high, this is correlated with high levels of dominance and low equitability, which is normally associated with lower oxygen conditions.

Figure 3.9: Macrofossil species richness, total abundance of macrofossils, Shannon Index (H) and Equitability (E) throughout the Folkestone Gault Clay sequence (on next page). The ORB ranges on the species richness graph refer to the ranges proposed in the Oxygen-Restricted Biofacies scheme (Wignall and Hallam, 1991).



The *Circocerithium* spp. are relatively small gastropods and so it could be inferred that horizons dominated by these forms are demonstrating size restriction as a result of lower oxygen conditions. However, in the more diverse horizons containing larger gastropods and full-size bivalves the small *Circocerithium* spp. are also present. Burrows range from millimetre scale to over a centimetre in diameter throughout the sequence, suggesting that there was no size limitation.

The sequence is fully burrowed with several tiers in evidence (see **Section 2.3.3.2**) suggesting that the Redox Potential Discontinuity was deep within the sediment and that bottom waters were relatively oxic during deposition.

The bivalves within the sequence include a range of infaunal deposit feeders (including *Pectinucula pectinata*, *Leionucula ovata*, *Acila bivirgata* and *Nucula* sp.) infaunal suspension feeders (including *Corbula* spp. and *Cardites* spp.) and epifaunal suspension feeders (including *Birostrina concentricus*, *Birostrina sulcatus* and *Inoceramus anglica*).

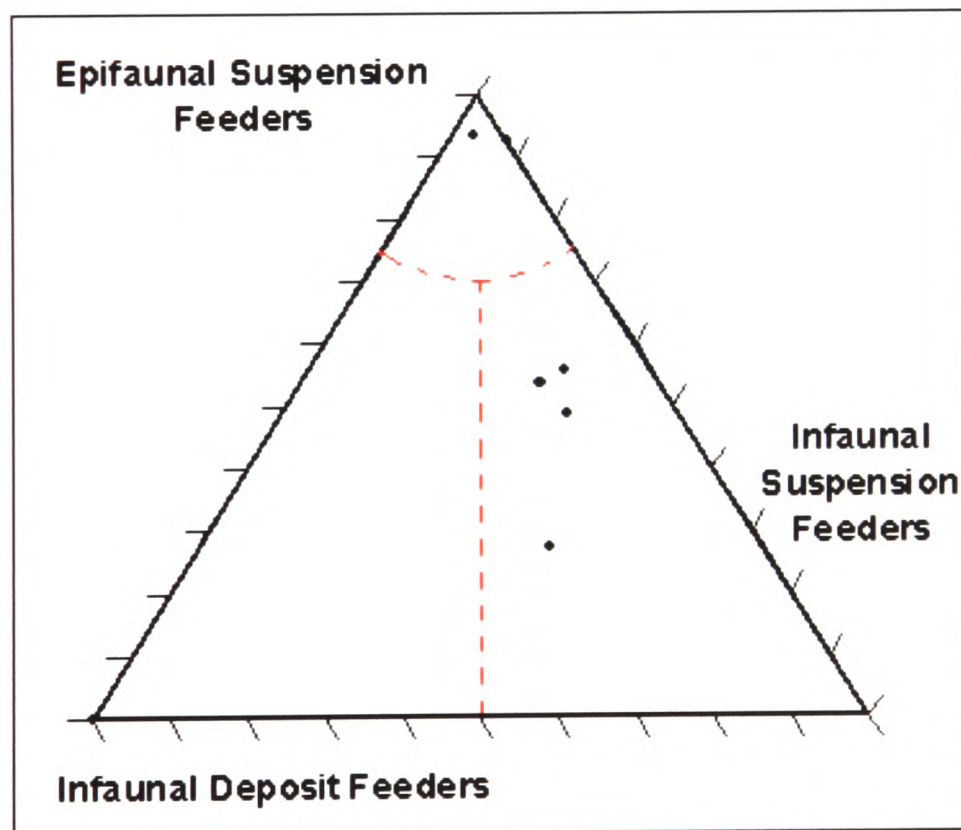


Figure 3.10: Ternary diagram of bivalve life modes from the Folkestone Gault Clay (based on Morris, 1979).

On the ternary diagrams of bivalve modes of life proposed by Morris (1979), the majority of samples containing bivalves plot within the 'Normal Marine' range (see *Figure 3.10*). However, a number of samples plot within the 'Bituminous' range which supports Wignall's (1994) suggestion that bivalve life modes are not a direct indicator of oxygenation conditions.

Shelly taxa are present throughout the sequence, often with original material preserved. The lack of discrete shelly horizons supports the idea that this represents continuous relatively oxygenated conditions as opposed to discrete oxygenation events.

While *Inoceramus* is common throughout the sequence, the diverse benthos and lack of lamination shows that the sequence is not representative of Arthur and Sageman's (1994) 'benthic boundary' flat clam biofacies. In fact, the presence of the coral *Discocyathus fittoni* in the majority of the phosphate nodule horizons, and in some debris-filled burrows would suggest oxygenated conditions according to Wignall and Hallam (1991).

The majority of the specimens appear to be preserved with some degree of original material retained. Many specimens are flattened but, particularly within the nodule bands, pyrite and phosphate internal moulds preserve the three-dimensional shape. There is a relatively high degree of fragmentation within the nodule layers and the presence of phosphate nodules suggests that these horizons may represent sequence condensation (Brett and Baird, 1986). The presence of pyrite as internal moulds and as individual nodules suggests that bottom waters were relatively oxic, meaning that pyrite formation was concentrated in microenvironments created by decomposing organic matter (Allison *et al.*, 1995). In Brett and Baird's (1986) scheme, both phosphate and pyrite stienkerns are associated with varying sedimentation rates within aerobic-dysaerobic conditions. Pyrite framboids are also common throughout the sediment and Wignall and Newton (2003) suggested that the combination of amorphous pyrite and framboids indicated slightly restricted oxygen conditions. They described fully aerobic settings as fully bioturbated, like the Folkestone Gault Clay, but lacking in pyrite. The presence of rare glauconite through the sequence

could be explained by more oxic conditions allowing oxidized iron to react with phosphatized material under dysoxic water columns (Speyer and Brett, 1988).

3.3.3.2 Application of Biofacies Models

Rhoads *et al.* (1991) summarised the additions that had been made to the original Rhoads and Morse model (1971). Under this scheme, the overall Folkestone Gault Clay biofacies would be classified as aerobic as it is fully bioturbated, contains a relatively diverse shelly fauna including suspension feeders and shows a range of burrow diameters (see *Figure 3.11*). Within the sequence there are subtle variations – whereas the shelly nodule layers certainly match the aerobic classification, the less fossiliferous *Circocerithium* spp. dominated sequences between them could possibly be described as upper dysaerobic. However, Knight (1997) proposed that this biofacies variation was caused by variations in substrate consistency rather than oxygenation variations.

	Anaerobic	Lower Dysaerobic	Upper Dysaerobic	Aerobic
Rhoads and Morse (1971)				★
Savdra et al. (1984)				★
Rhoads and Morse (1991)				★
Wignall and Hallum (1991)			← ? →	★
Arthur and Sageman (1994)				★
Wignall (1994)				★
	Anaerobic	Lower Poikiloaerobic	Upper Poikiloaerobic	Aerobic

Figure 3.11: Summary diagram to show the proposed ranges of palaeo-oxygenation conditions for the Folkestone Gault Clay according to a range of macrofaunal models.

Within Morris’ (1979) classification scheme the samples would plot as ‘Normal Marine’, as they are fully bioturbated with the ichnofabric being dominated by *Chondrites*, and the bivalves present include both infaunal and epifaunal forms. However, Morris (1979) suggested that within normal marine conditions, less than 20% of the bivalves should be infaunal deposit feeders and this is not true for the entire sequence. Also, pyritised burrows are present throughout the sequence which Morris (1979) associated with ‘Restricted’ conditions.

Within Wignall and Hallam's (1991) Oxygen-Restricted Biofacies (ORB) scheme, the species richness of the samples plots them within ORB 4, 5 or 6 which represent lower to upper dysaerobic facies (see *Figure 3.9*). However, the presence of pyrite aggregates and belemnites are descriptors of ORB5 and above, and there is no evidence of lamination within the Gault Clay, which rules out ORB 4 and 5. This would suggest that the Folkestone Gault Clay would classify as ORB 6, which is uppermost dysaerobic. However, Wignall and Hallam (1991) stated that aerobic conditions can be differentiated from ORB6 by the presence of stenoxic taxa including all corals. Therefore, the presence of *Discocyathus fittoni* within the shelly sequences would seem to suggest deposition under oxic waters. The contrasting classifications compared to those suggested by the species richness alone perhaps highlights the problems associated with the effect of sample size on species richness and promotes the use of descriptive categories.

Within Wignall's (1994) Shelf Model, the depth of the Redox Potential Discontinuity and the presence of deep infaunal forms classifies the sequence within the Aerobic Biofacies. Within Arthur and Sageman's (1994) scheme, the sequence does not fully fit either the Infaunal or Epifaunal Biofacies Schemes as the fauna is not dominated by either mode. Arthur and Sageman (1994) suggested that this was common within Upper Dysaerobic and Aerobic biofacies. However, on either classification scheme the fauna would appear to fit the descriptions of aerobic biofacies.

3.3.4 Amma Fatma

The Amma Fatma sequence comprises carbonate-rich laminated shales interbedded with paler limestones. A faunal sample was collected by Gale from the blocky fossiliferous limestone horizon referred to as the 'lucina bed' (see *Figure 2.37*). The benthic sample is composed of seven bivalve specimens which includes six lucinids and one venerid bivalve. In addition to these, ammonites and gastropods were recorded from this particular bed.

3.3.4.1 Analysis of Fossil Assemblages

While the 'lucina bed' shows evidence of a benthic community, no macrofossil specimens were recovered from the dark laminated marl samples. This finding is corroborated by a 2001 study of the same sequence in which the dark marls were

found to contain no macrofauna apart from fragments of fish (El Albani *et al.*, 2001). The lack of even nektobenthic forms suggests that the dark marls were deposited under sustained low-oxygen bottom waters and Rhoads and Morse (1971) suggested that benthic species diversity only drops to zero within anoxic environments. The fossiliferous limestone band which is referred to as the ‘lucina bed’ has a low species richness which is severely sample size limited, but suggests that the conditions were oxygenated to at least the level of dysoxia during deposition of the limestone bed.

Both lucinids and venerids are thought to be infaunal suspension feeders (Aberhan *et al.*, 2004) which, under the modes of life classification scheme of Morris (1979), would indicate ‘normal’ bottom water conditions (see *Figure 3.12*). Wignall (1994) has questioned Morris’ (1979) interpretation of bivalve life modes and this classification does not correlate fully with the palaeo-oxygenation regime indicted by the limited benthos.

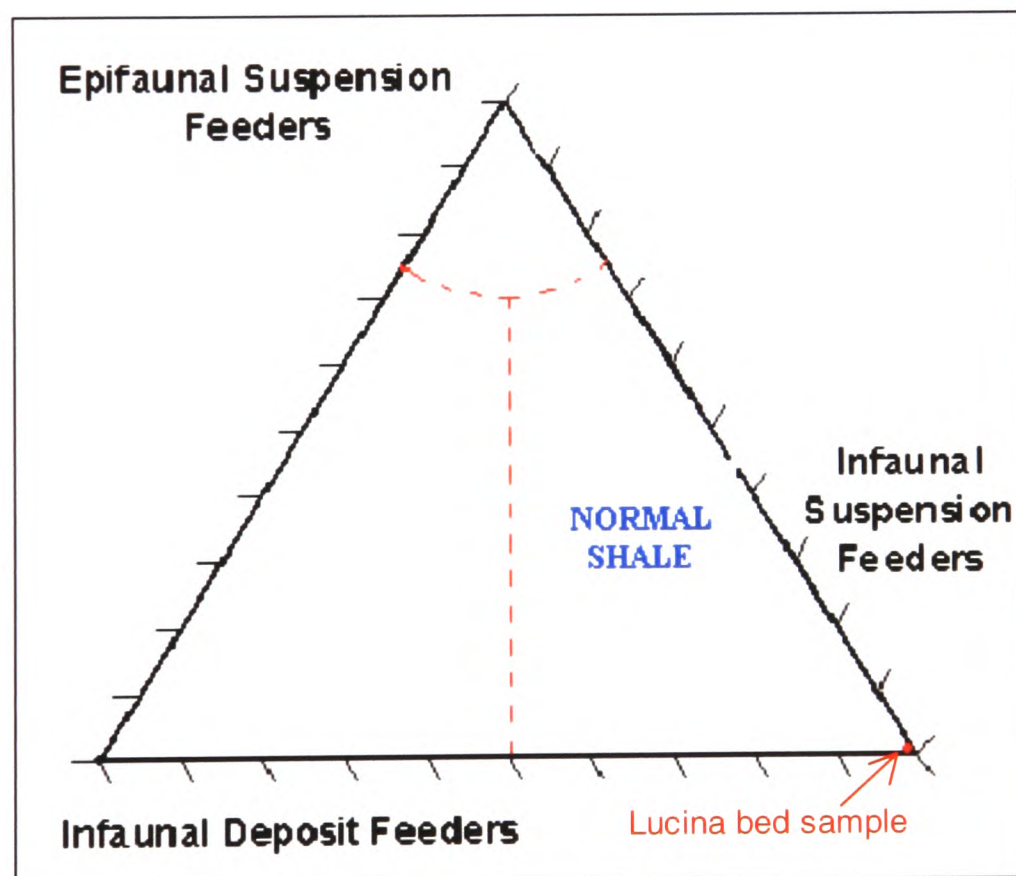


Figure 3.12: Ternary diagram of bivalve life modes from the ‘lucina bed’ of the Amma Fatma sequence (based on Morris, 1979).

Some lucinids are thought to be chemosymbionts and there is some evidence that suggests that chemosymbionts can live under low-oxygen conditions (Savdra *et al.*,

1991). As the assemblage is dominated by lucinids the 'lucina bed' may represent a relatively low-oxygen tolerant community that formed under restricted conditions.

Taphonomy is difficult to interpret due to the limited nature of the specimens. However, there is evidence of carbonate nodules within the dark marls of the sequence (see *Figure 2.37*). Calcium carbonate concretions can form in anaerobic microenvironments under dysoxic or marginally oxic water columns (Brett and Speyer, 1990). Brett and Baird (1986) suggested that concretions form in aerobic-dysaerobic settings with episodic or intermediate sedimentation rates. Within the 'lucina bed', fossils are preserved as carbonate material with sediment infilling. The lack of pyrite infills would suggest rather restricted oxygenation as pyrite framboids are common throughout the sequence which implies that low oxygen conditions allowed high preservation of organic matter so pyrite formation was not concentrated around organic fossil material (Wignall and Newton, 2003).

3.3.4.2 Application of Biofacies Models

Under the initial biofacies model of Rhoads and Morse (1971) the dark marls of the Amma Fatma sequence would classify as anaerobic because of the presence of laminations and the absence of any macrofossils (see *Figure 3.13*). Rhoads and Morse (1971) stipulated that the benthic species population should drop to zero at the dysaerobic-anaerobic boundary and this therefore firmly classifies the dark marls as anaerobic. The fossiliferous 'lucina bed' does not exhibit laminations and therefore could fall within the upper ranges of dysaerobic or within aerobic conditions in this model (see *Figure 3.14*). Aerobic conditions are represented by a diverse benthic community in the model and this is not fully represented by the limited benthos of the 'lucina bed'. This would suggest a classification of uppermost dysaerobic, or boundary dysaerobic:aerobic conditions rather than fully aerobic conditions.

Further additions to this model by Savdra *et al.* (1984), Savdra and Bottjer (1991) and Rhoads *et al.* (1991) limited laminations to anaerobic or exaerobic conditions and developed the idea of a limited benthos within dysaerobic settings. This means that while the dark marls are still suggested to be anaerobic in these models, the fossiliferous 'lucina' limestone could classify as fully dysaerobic due to the limited benthos.

	Anaerobic	Lower Dysaerobic	Upper Dysaerobic	Aerobic
Rhoads and Morse (1971)	★			
Savdra et al. (1984)	★			
Rhoads and Morse (1991)	★			
Wignall and Hallum (1991)	★			
Arthur and Sageman (1994)	★			
Wignall (1994)	★			
	Anaerobic	Lower Poikiloaerobic	Upper Poikiloaerobic	Aerobic

Figure 3.13: Summary diagram to show the proposed ranges of palaeo-oxygenation conditions for the Amma Fatma dark marls according to a range of macrofaunal models.

	Anaerobic	Lower Dysaerobic	Upper Dysaerobic	Aerobic
Rhoads and Morse (1971)			←→	
Savdra et al. (1984)			←→	→
Rhoads and Morse (1991)			←→	→
Wignall and Hallum (1991)			?	←→
Arthur and Sageman (1994)		★	←→	→
Wignall (1994)			←→	→
	Anaerobic	Lower Poikiloaerobic	Upper Poikiloaerobic	Aerobic

Figure 3.14: Summary diagram to show the proposed ranges of palaeo-oxygenation conditions for the Amma Fatma 'lucina bed' according to a range of macrofaunal models.

In Wignall and Hallam's (1991) Oxygen-Restricted Biofacies (ORB) Scheme the lack of nektobenthic specimens within the dark marls suggest a classification of ORB1. Wignall and Hallam (1991) believed that this biofacies represents truly anaerobic conditions where deposition occurred under possibly 10s of metres of anoxic water. This scheme is the first to differentiate between the anaerobic black shales of the Niveau Pacquier and Briestroffer sequences and the extreme palaeo-oxygenation conditions of the Amma Fatma sequence. In terms of the species richness of the 'lucina' limestone, it would classify as ORB 4 but this most likely represents a skewing effect due to the small sample size as the lack of laminations restrict classification to ORB 6 or fully aerobic conditions.

In both of the models proposed by Arthur and Sageman (1994) and Wignall (1994), the dark marls classify as anaerobic. However, Arthur and Sageman (1994) described Level 4 of their infaunal scheme, which corresponds to uppermost lower dysaerobic, as characterised by the appearance of infaunal bivalves such as lucinids. As the 'lucina' bed assemblage is dominated by these, this model provides the clearest indication that the fossiliferous limestone bed was actually laid down under the relatively restricted oxygen conditions that is suggested by the geochemical proxies (see **Section 4.3.4**). In contrast, the 'lucina bed' can only really be interpreted by the lack of laminations in Wignall's (1994) scheme which restricts the classification to upper dysaerobic/poikiloaerobic or aerobic.

3.4 Conclusions

- While the Marnes Bleues grey clays and Niveau Pacquier black shales both demonstrated low benthic diversity, the palaeontological proxies suggested contrasting oxygenation conditions. According to the faunal models, the black shales appear to have been deposited under anoxic, or possibly lower dysaerobic, conditions. This is confirmed by the taphonomy and the fact that Erbacher *et al.* (1999) reported the complete absence of benthic forams within the shales suggests that conditions were probably anoxic rather than lower dysaerobic. In contrast, the overall suggestion from the models is that the Marnes Bleues were laid down under upper dysaerobic conditions. This more oxic environment is again confirmed by the carbonate preservation of fossils and the diverse benthic foram assemblages observed by Erbacher *et al.* (1999).
- The Briestroffer sequence displays a similar pattern to the Niveau Pacquier sediments. Again, while the near absence of benthic forms complicates the palaeoenvironmental analysis, the models and the observed taphonomy suggest that the black shales were deposited under anoxic or lower dysaerobic conditions. The Marnes Bleues sediments again appear to represent deposition under upper dysaerobic conditions.
- The Folkestone Gault Clay contains a much more diverse benthic fauna than the two French sites and the models suggest oxic conditions existed during deposition. While this is to some extent confirmed by the taphonomy, there is some suggestion that the environment might have been borderline upper

dysaerobic. For example, analysis of bivalve life modes suggest that, according to the Morris' (1979) scheme, some samples represent bituminous conditions although the applicability of this entire scheme was debated by Wignall (1994). Also Wignall and Newton (2003) suggested that the presence of amorphous pyrite and pyrite framboids, both of which are common throughout the sequence, suggest slightly restricted oxygen conditions.

- The taphonomy and presence of carbonate nodules and common pyrite framboids within the Amma Fatma section suggest that both the dark marls and limestone sections were laid down under restricted oxygen conditions. The faunal models suggest that the dark marls were laid down under anoxic conditions and within the Oxygen-Restricted Biofacies scheme (Wignall and Hallam, 1991) the marls appear to have formed under more restricted conditions than either the Niveau Pacquier or Briestoffer black shales. Classification of the 'lucina' limestone bed is complicated by the small sample size and this leads to a range of classifications in the faunal models. While most models propose either aerobic or upper dysaerobic conditions, the ORB scheme (Wignall and Hallam, 1991) and the Infaunal Biofacies Levels scheme (Arthur and Sageman, 1994) both suggest lower dysaerobic conditions.
- Interpretation of palaeo-oxygenation regimes using macrofauna alone is severely limited by sample size and differential preservation between low oxygen and high oxygen conditions. Interpretation of the Marnes Bleues samples from the both the Niveau Pacquier and Breistroffer sequences is particularly difficult because of the poor preservation of fossil material.
- Interpretations of the taphonomy of macrofossils does allow some insight into palaeoenvironmental conditions and may allow more insight into sections with poor preservation.
- The models based on descriptive categories to assign palaeo-oxygenation conditions throughout sequences are a useful tool but rely heavily on the interpretation of sedimentological features. This alone is not a reliable diagnostic feature as Wignall *et al.* (2005) pointed out that not all low oxygen sediments contain laminations. The applicability of species richness boundaries included within Wignall and Hallam's (1991) ORB scheme is

again limited by sample size. The presence of belemnites within the anaerobic Niveau Pacquier and Briestroffer black shales raises some questions about the use of particular forms to define categories, as Wignall and Hallum (1991) suggested that belemnites are indicative of upper dysaerobic biofacies. Through time, models have developed an increased focus on the duration of low oxygen events as a key control of faunal assemblages. Later models, such as Arthur and Sageman's (1994) Infaunal and Epifaunal scales and Wignall's (1994) Shelf Model, do allow easier classification and interpretation of the palaeoenvironment which suggests that event duration is a key factor.

4. TRACE METAL PALAEO-OXYGENATION PROXIES

4.1 Introduction

4.1.1 Introduction to Trace Metal Palaeo-Oxygenation Proxies

Schultz (2004, p.353) stated that a geochemical proxy is most accurately defined as “some concentration, ratio, or comparison of concentrations that may be used to indicate a particular chemical condition or that a certain process has occurred”. In 1954 Goldschmidt was one of the first to note that organic carbon-rich sediments were often enriched in specific trace metals such as Mo, V, Cu, Zn or U – this observation initiated much interest in the relationship between trace-metal enrichment and low-oxygen depositional environments.

In 1970, Vine and Tourtelot published one of the first systematic studies of trace metal enrichment in an ancient black shale. In 1993, Calvert and Pedersen went one step further and demonstrated that the enrichment of certain redox-sensitive elements could be used to infer sedimentation under anoxic conditions. Goldschmidt’s (1954) initial observation has since led to the suggestion of a wide range of trace-metal enrichments, and trace-metal ratios as proxies for palaeo-oxygenation (e.g. Jones and Manning, 1994). However, the relative enrichment of trace metals varies greatly between black shales (Wignall, 1994), and at the present day, trace-metal enrichment can occur either in anoxic basins, where the surface sediments are in contact with sulphidic waters, or by diffusion from seawater to anoxic sediments that lie below thin oxic horizons at the sediment/water interface (e.g. in coastal upwelling areas) (Hofmann *et al.*, 2001). Brumsack (2005) noted that a broad range of variables affect the extent of enrichment in any one setting. He suggested that in upwelling systems the steepness of the slope, the proximity of H₂S to the sediment/seawater interface and the intensity of bio-accumulation and regeneration play an important role for trace metal accumulation. In anoxic basins, he suggested that the trace-metal content is mainly controlled by trace-metal availability in the water column and sedimentation rate. These variables may limit the comparability of geochemical proxies from different sites. A further limitation of these proxies is the possibility of remobilization of elements after deposition. If substantial trace element movement occurs after burial, the initial redox conditions may no longer be reflected in the geochemistry of the sediment. Studies of trace metal mobilisation have noted that

certain elements such as copper, iron, nickel and cobalt are released upon oxidation of organic matter during early stages of diagenesis (e.g. Rubio *et al.*, 2006; Tankere-Muller *et al.*, 2006). In contrast, manganese mobilisation is linked to reducing conditions and Tankere-Muller *et al.* (2006) found that some elements such as cobalt are released in association with reductive mobilisation of manganese at depth. There is also evidence that in sediments resulting from alternating oxygenation conditions a downwards sulphidization front can develop, leading to the formation of iron sulphides in oxic sediments below organic-rich sapropels (Passier *et al.*, 1996). This has been observed in several settings including recent sediments from the Black Sea (Jørgensen *et al.*, 2004) and could theoretically lead to the migration of trace elements for which pyrite acts as a trace metal carrier phase.

Despite this uncertainty, it is clear that there is a relationship between redox conditions and trace metal enrichment. Metals that concentrate in these environments must therefore have distinctly different behaviours under oxic and anoxic marine conditions (Calvert and Pederson, 1993). Cruse and Lyons (2004) provided a simplified summary of the three main modes of enrichment that have been suggested:

- The valency of some elements can vary with local redox conditions, and some elements which form highly soluble ions under oxygenated conditions can form insoluble ions in their reduced form (e.g. Mo, U) or vice versa (e.g. Mn);
- Some oxidised or reduced forms of particular elements are preferentially adsorped onto other authigenic minerals such as iron or manganese oxyhydroxides or pyrite (e.g. V and Ni);
- Some reduced species form complexes with organic matter (e.g. V, Mo, Ni and U).

Vine and Tourtlet (1970) suggested that the majority of trace elements show a positive correlation when plotted against organic carbon, implying that complexation with organic matter is dominant. However, this in itself may only reflect that organic matter preservation and metal enrichment are controlled by the anoxic depositional environment rather than there being any more direct relationship between the two (Brumsack, 1980). However, while some elements, such as Cr, V and Ni, correlate with total organic carbon content they do not correlate with sulphur content,

suggesting that accumulation is not controlled by anoxia itself (e.g. Lewan & Maynard, 1982).

4.1.2 Correcting for Detrital Sources

In 2005, Brumsack summarized the three sources of trace metals in modern organic-carbon rich sediments as:

- Terrigenous material of aeolian and/or fluvial origin;
- Biogenic plankton remains;
- Early diagenetic enrichment.

Trace metals originating from terrigenous sources will have no relation to redox conditions, and it therefore important to 'remove' this input before considering enrichments as a result of palaeo-oxygen conditions. In order to do this, a number of methods have been employed by workers in this field. The simplest method is to divide the trace element abundance by the abundance of aluminium in the sample. Aluminium is used as it forms the structural component of a number of minerals introduced from fluvial or aeolian sources, and while it has a high concentration in such aluminosilicates, its abundance is relatively low in seawater (Orians and Bruland, 1986). Importantly, aluminium is the only major element that is not significantly affected by biological or diagenetic processes in nearshore environments (Brumsack, 2005). However, there is some concern about the comparability of such data between sites, as aluminium content varies in different clay minerals and Murray *et al.* (1993) found that in areas of high productivity in open ocean settings there is a biogenic overprint on sediment Al/Ti ratios. This suggests that care needs to be taken in discerning the ocean setting and clay mineralogy before aluminium content is relied on as being a purely detrital signal.

A more rigorous method, which allows better comparison between sites, is the determination of 'enrichment factors' where trace metal enrichments are determined by comparing their aluminium-normalized concentrations to those of 'average shale' (e.g. from Turekian and Wedepohl, 1961, or Wedepohl, 1971) which is considered to be typical for element patterns of oxic environments (Hofmann *et al.*, 2001):

$$\text{Enrichment Factor} = [(\text{Element/Al}) \text{ Sample}] / [(\text{Element/Al}) \text{ Average Shale}]$$

Enrichment factors greater than 1 suggest trace-metal enrichment, whereas depleted elements will register an enrichment factor less than 1. Ideally, most major elements will have enrichment factors close to unity (Brumsack, 2005). While this approach does still rely on Al content, it provides a framework which instantly allows recognition of enrichment or depletion. Several issues have been raised with this approach – for example, Van der Weijden (2002) highlighted statistical problems, suggesting that for organic carbon-rich sediments low in terrigenous material, this calculation may be affected by the closed sum effect, giving unrealistically high Enrichment Factor values. Also, Brumsack (2005) noted the risks of using ‘average shale’ as an analogue for terrigenous detrital ‘background’ – the chemical composition of ‘average shale’ (Wedepohl, 1971) is broadly similar to that of ‘upper continental crust’ (Taylor and McLennan, 1985), but the material that actually enters the oceans may be altered by weathering and grain-size effects (Brumsack, 2005), and weathering of regions with specific mineral assemblages may yield detrital grains rich in particular elements (Powell *et al.*, 2003). Brumsack (2005) concluded that, although the risk is minimized for elements with a low concentration in the crust, and with significant involvement in biogenic cycles or diagenetic enrichment, for elements with a high abundance in detrital material, a precise assessment of lithological background values is required. This may be possible in modern day settings (e.g. Morford and Emerson, 1999), but is more problematic for ancient black shales. It is possible that analysis of surrounding sediments may be used to establish a regional signal but this does raise serious questions about the application of these proxies.

Another approach is to only interpret the ‘excess’ Trace Metal content (TM_{xs}) using the calculation:

$$TM_{xs} = TM_{\text{sample}} - Al_{\text{sample}} (TM/Al)_{\text{shale}}$$

Brumsack (2005) suggested that this method is particularly useful in sediments with low detrital inputs, but warns that problems arise in situations with high aluminium contents.

Because of the difficulties associated with correcting for detrital input, researchers have come up with a series of alternative trace metal ratios, where the behaviour of one element (the numerator) is thought to be dependant on redox conditions, whereas the other (denominator) is thought to be independent of such variables (Powell *et al.*, 2003) (see **Section 4.1.4**).

4.1.3 Proposed Mechanisms of Trace Metal Enrichments

4.1.3.1 Molybdenum

Compared to other trace elements, molybdenum shows the greatest degree of enrichment in reducing sediments relative to crustal values (Crusius *et al.*, 1996). Molybdenum has a low concentration in detrital material and this further improves its capability as a redox indicator (Dean *et al.*, 1997). In oxic waters, molybdenum is found as soluble Mo (VI) in the form of MoO_4^{2-} (Morford and Emerson, 1999). In this form, it is not concentrated by plankton and shows little affinity for clay mineral surfaces, calcium carbonate or iron oxyhydroxides at normal marine pH (Bruland, 1989). Molybdenum is, however, readily captured by manganese oxyhydroxides (Calvert and Pedersen, 1993) and subsequently released when these phases are reduced at the redox boundary (Crusius *et al.*, 1996). Adelsen *et al.* (2001) suggested that manganese recycling at the redox boundary could concentrate MoO_4^{2-} at the sediment-water interface. While this pre-concentration stage is widely accepted, and molybdenum enrichment in the sediment beneath sulphidic waters is thought to be one of the most reliable indicators of palaeo-oxygenation, the method of molybdenum fixation is still debated.

Initially it was believed that a reduction step was required where Mo(VI) is reduced to an insoluble Mo(IV) form such as MoS_2 or MoS_3 , which then accumulates in the sediments (e.g. Calvert and Pedersen, 1993). Although Vine and Toutelot (1970) noted a correlation between molybdenum and organic carbon, Brumsack (1989) suggested that while molybdenum may be initially adsorbed onto humic substances in its reduced form, it is ultimately precipitated as a sulphide. Huerta-Diaz and Morse (1992) suggested that molybdenum precipitates as a trace element in pyrite, and this was backed up by observations from the modern anoxic environment of the Cariaco Trench, where Jacobs *et al.* (1987) documented the co-precipitation of Mo with FeS. However, in 1996, Helz *et al.*, proposed that the initial reduction of MoO_4^{2-} was not necessarily required for molybdenum fixation. They suggested that the key to molybdenum removal from anoxic waters is a 'geochemical switch' – at a threshold level of HS^- concentration, they suggested that sulphur replaces an oxygen on MoO_4^{2-} , creating a 'thiomolybdate' complex. They proposed that this complex is easily scavenged by forming bonds with metal-rich particles, sulphur-rich organic matter and pyrite. In support of this, Tribovillard *et al.* (2004) found that

molybdenum enrichment is positively correlated with the amount of sulphurised organic matter, but not with pyrite abundance. They suggested that significant organic matter enrichment is only possible when reactive iron is limited, but that pyrite formation could act as an initial molybdenum trap before the bulk of the reactive iron was used up. This would suggest that iron has a complex role in molybdenum enrichment as on one hand, iron-rich particles are involved in thiomolybdate scavenging, whereas on the other hand, reactive iron suppresses organic matter sulphurisation, and therefore molybdenum trapping (Tribovillard *et al.*, 2004). Adelson *et al.* (2001) suggested that, due to the nature of molybdenum concentration at the sediment-water interface by manganese refluxing, and the requirement of sulphide substitution for fixation, molybdenum enrichment may be determined by the amount of time that sediment is exposed to overlying anoxic water rather than the height of the anoxic water column.

4.1.3.2 Vanadium

Several theories have been put forward to explain vanadium enrichment in low oxygen sediments. In 1970, Vine and Tourtelot suggested that the bio-concentration of vanadium by tunicates (sea squirts) could be responsible, but since then, more sound theories based on chemical behaviour have been put forward. Lewan and Maynard (1982) noted that vanadium appears to be concentrated in tetra-pyryl complexes derived from chlorophyll, which are preferentially preserved under anoxic conditions. In oxygenated waters, the stable form of vanadium is vanadate, H_2VO_4^- , which adsorbs to both manganese and iron oxyhydroxides (Wehrli and Stumm, 1989). However, in low-oxygen conditions, vanadate is reduced to vanadyl, (V(IV)) or V(III) (Wanty and Goldhaber, 1992) which is a smaller cation and binds even more strongly to chelating surface groups than the larger anionic vanadate (Morford and Emerson, 1999). Wanty and Goldhaber (1992) suggested that this association with manganese and iron hydroxides is the main fixation method in low-oxygen environments. However, vanadium has also been recorded in association with silicates (Dill, 1986) as the vanadyl ion is readily adsorbed by clay particle surfaces (Breit and Wanty, 1991).

4.1.3.3 Nickel

The sedimentary geochemistry of vanadium and nickel are thought to be similar (Lewan and Maynard, 1982). However, while the solubility of nickel is not influenced by the redox potential, Lewan and Maynard (1982) suggested that under anoxic conditions the greater availability of hydrogen sulphide causes nickel sulphide formation. Lewan and Maynard (1982) have also shown that nickel more readily forms tetrapyrrole complexes with organic matter when dysoxic conditions are dominant, and in 1992 Huerta-Diaz and Morse showed that pyrite is moderately important as a trace metal carrier phase for nickel.

4.1.3.4 Manganese

In 1965, Lynn and Bonatti noted that in oxic waters, manganese (II) is oxidized to insoluble Mn (III) and Mn(IV) oxides, which accumulate in the sediments below. In contrast, they suggested that in sulphidic waters in anoxic basins, these oxides are reduced to soluble manganese (II) and the sediments below are characterised by low manganese contents. This is supported by studies of systems with an oxygen/sulphide boundary, where active manganese recycling has been observed - manganese oxides are reduced under sulphidic conditions and then diffuse across the redox boundary where they are promptly oxidized to form manganese oxides again (Calvert and Pederson, 1993). In fact, manganese carbonates are commonly found in close association with black shales, and in conditions of fluctuating redox conditions, interbedded black shales and manganese carbonates are common (Jenkyns *et al.*, 1991).

In 1980, Klinkhammer and Bender found that upwelling zones, as well as euxinic basins, record manganese depletion. They suggested that where the oxygen-minimum zone impinges on the sea floor, manganese oxides are reduced to manganese (II) and the oxygen-minimum zone acts as a 'conveyor belt', transporting this soluble form towards the open ocean. This scenario could go some way to explain why some studies have found little relationship between manganese concentrations and depositional redox conditions in conventional euxinic settings. Hoffman *et al.* (2001) suggested that manganese depletion is perhaps more controlled by supply rate to the sediments and that the presence of an oxygen-minimum zone in overlying waters may promote the release of manganese from settling particles,

thereby reducing the flux of manganese to the sediments below. A further complication to the use of manganese depletion as a palaeo-redox proxy is that while manganese (II) sulphide is highly soluble and so should not appear in sediments under euxinic waters, Huerta-Diaz and Morse (1992) reported that under highly reducing conditions, manganese can occur as a trace element in pyrite. While this can only have a minor effect, it does raise questions about our understanding of the behaviour of manganese in low-oxygen environments.

4.1.4 Explanation of Trace Metal Ratios

4.1.4.1 Uranium-based ratios

In oxic waters of pH 7 or above, U^{6+} is present as the uranyl tricarbonate species $UO_2(CO_3)_3^{4-}$ which is highly soluble (Langmuir, 1979). At the redox boundary, uranium occurs as the uranyl ion UO_2^{2+} , which is also highly soluble (Wignall, 1994). However, Borovec *et al.* (1979) demonstrated that the sorption of uranyl ions onto humic acids could fix uranium in sediments below anoxic waters. While Wignall (1994) suggested that this could explain the well-documented correlation between uranium enrichment and organic matter (e.g. Leventhal, 1981), he noted that studies of modern anoxic environments indicate that the humic acid/uranyl ion reaction fails to account for the observed distribution of uranium. It has been suggested that uranium is preferentially concentrated on francolite surfaces and further studies on modern environments have demonstrated a correlation between uranium concentrations and francolite occurrence which could support this theory (e.g. Fisher and Wignall, 2001).

Langmuir (1979) highlighted another possible fixation method when he suggested that in anoxic waters with pH values lower than 7, uranous (U^{4+}) fluoride complexes are formed which are far less soluble than the uranyl ions. However, Anderson *et al.* (1989) found that in modern environments, dissolved U(VI) is neither reduced to the thermodynamically favoured U(IV) nor is it scavenged from the water column by particulates. These observations suggest that U(VI) reduction may require the presence of suitable mineral surfaces (Kochenov *et al.*, 1977) and Klinkhammer and Palmer (1991) suggested that the main removal process of uranium is diffusion of $[UO_2(CO_3)_3]^{4-}$ from the water column to the sediments, reduction and subsequent adsorption or precipitation. The amount of U(VI) that can be transferred from the

water column to a given layer of sediment is therefore partly dependent upon the amount of time the layer spends near the sediment–water interface (Fisher and Wignall, 2001). Also, Anderson *et al.* (1989) demonstrated that permanent pore water anoxia is required for uranium fixation as they observed that only 2 to 3 minutes of oxidation led to a factor of six increase in pore-water uranium concentrations, which they suggest is due to the rapid production of the uranyl ion. From these observations they suggest that black shales which exhibit uranium enrichment must have formed under prolonged anoxic conditions.

In summary, Wignall (1994) suggested that the three main factors which affect the extent of uranium enrichment are:

1. the intensity and duration of benthic anoxia;
2. the abundance of the component in which uranium is concentrated - current theories suggest that humic organic matter and/or francolite are involved;
3. the sedimentation rate.

Wignall (1994) suggested that as there is good empirical evidence for the relationship between uranium enrichment and the intensity and duration of benthic anoxia (e.g. Wignall and Myers, 1988), it is probable that both the second and the third factors covary with the first. McKee *et al.* (1987) warned that the effect of these factors could lead to mis-interpretation of uranium values in ancient black shales. They suggested fast sedimentation rates could prevent uranium enrichment, and that any later physical disturbance of the sediments could lead to loss of uranium through oxidation.

While uranium is concentrated authigenically under anoxic conditions, commonly in iron-bearing minerals such as glauconite, it is also found in detrital material. In order to fully interpret the extent of redox-related enrichment, it is important to understand what proportion of the measured uranium is from detrital input, and what proportion is true authigenic uranium (U_a). Adams and Weaver (1958) proposed the use of the uranium/thorium ratio as while thorium is also found in detrital source material, it does not undergo authigenic enrichment in anoxic conditions. Wignall and Myers (1988) took this one step further, and suggested that as detrital material has a uranium/thorium ratio of 3.8±1.1, the calculation:

$$U_a = U_{\text{total}} - \text{Th}/3$$

could be used as a reliable measure of the authigenic uranium proportion.

This relationship is only thought to be valid for fine-grained terrigenous sediments and may be strongly dependant on the sediment provenance. Wignall and Myers (1988) suggested that carbonate and phosphate minerals might act as further host for uranium and upset the relationship between the U_a and the oxygenation level. However, when compared with palaeoecological indicators, in many cases there is a clear correlation, and Wignall (1994) went as far as to suggest that unlike several other geochemical indices, U_a may actually be useful for distinguishing between dysaerobic facies. Jones and Manning (1994) suggested that both U_a and U/Th demonstrated reliable correlations with palaeo-oxygenation signals and suggested tentative boundaries between oxic and dysoxic facies (5 for U_a and 0.75 for U/Th) and dysoxic and anoxic environments (12 for U_a and 1.25 for U/Th) based on results analysis of gamma ray spectra.

4.1.4.2 V/Cr

In 1986, Dill proposed the vanadium/chromium index as a measure of palaeo-oxygenation. He suggested that as chromium is of entirely detrital origin and should not fluctuate with redox conditions, it would provide a detrital correction for redox-related vanadium concentrations. Geisler and Schmidt (1992) suggested that current oceanic chromium levels remain between 2 and 5 nmol kg^{-1} that the weathering of mafic and ultramafic rocks such as spinels is the main source of oceanic chromium, along with inputs from riverine and atmospheric processes. Dill (1986) suggested that vanadium/chromium values greater than 2 are indicative of anoxic conditions, whereas values less than 1 indicate normal oxic conditions. Through factor analysis of a range of geochemical ratios, Jones and Manning (1994) identified the V/Cr index as one of the most reliable indicators of palaeo-oxygenation. However, they suggested that values of ~ 2 relate to the transition between oxic and dysoxic waters, and only values above 4.25 represent true suboxic or anoxic deposition.

4.1.4.3 V/Sc

Kimura and Watanabe (2001) proposed that while the V/Sc ratio is similar in principle to the V/Cr ratio, it is actually a more sensitive and reliable paleo-

oxygenation proxy. Little work has been done on correlating this ratio to other palaeo-redox indicators, but Kimura and Watanabe (2001) suggested that normal continental shales should fall within the range of 4.7 to 9.1.

4.1.4.4 Ni/Co

In 1984, Dypvik proposed that the Ni/Co ratio may also reflect depositional oxygenation conditions – both nickel and cobalt can occur within pyrite in sediments but high values of Ni/Co appear to reflect reducing conditions. Jones and Manning (1994) refined this proxy and suggested that values over 5 represented dysoxic conditions, whereas values over 7 represented anoxic or suboxic deposition.

4.1.4.5 Ni/V

Lewan and Maynard (1982) examined the relationship between Ni and V abundances in bitumens and oils, and found that while both elements may be fixed by the formation of tetrapyrrole complexes, the relative abundances vary according to the redox environment. Lower values of Ni/V were observed associated with more reducing conditions. Lewan (1984) suggested that a substantial presence of H₂S may limit the availability of nickel cations because of the formation of NiS complexes, leaving vanadyl or trivalent vanadium available for the formation of complexes. In contrast, under more oxic conditions, vanadium is more available for forming tetrapyrrole complexes. Lewan (1984) suggested that the strong bonding involved meant that the proportionality of vanadium and nickel in crude oils remains unchanged by thermal maturation and other alteration processes. Whole-rock Ni/V ratios have since been applied as palaeo-redox indicators (e.g. Telnaes *et al.*, 1991; Jones and Manning, 1994).

4.1.4.6 V/(V+Ni)

On a similar basis, Lewan (1984) demonstrated that the V/(V+Ni) ratios for organics formed under euxinic conditions were greater than 0.5. Hatch and Leventhal (1992) reassessed this proxy using whole-rock data by comparison with a range of palaeo-oxygenation proxies, and suggested that ratios greater than 0.84 represented euxinic conditions, 0.54–0.82 represented anoxic conditions, and that sediments formed under dysoxic conditions plotted within the range 0.46–0.60. Schovsbo (2001) suggested that this ratio could be more reliable in conjunction with total sulphur data – he

proposed that only sediments with both V/(V+Ni) values greater than 0.84 and total sulphur contents of greater than 2.5 wt% could be reliably classified as forming under lowest dysoxic or anoxic conditions. Despite these refinements, Rimmer (2004) found that the V/(V+Ni) ratio consistently reported lower oxygen levels than a number of other proxies used.

4.1.4.7 (Cu+Mo)/Zn

The (Cu+Mo)/Zn ratio was proposed as an indicator of bottom water oxygenation by Hallberg (1976, 1982), following work in the Baltic Sea. He observed that the ratio increased under reducing conditions and decreased in more oxidizing environments. He proposed that for sediment deposited in anoxic environments (with H₂S present), the precipitation of Cu is favoured over Zn to the extent where Cu concentrations may exceed those of Zn, because of the solubility products of their sulphides. However, if the environment was initially oxic, and the sediment became anoxic during burial, as occurs in most mudstones, Hallberg (1976, 1982) suggested that the Cu and Zn contents will be similar due to the initial oxidizing conditions, and that the Cu content may be reduced further by chelation. Hallberg (1982) added molybdenum to the ratio due to its reliability as a redox indicator. In the Baltic Sea work, values ranged from 6 to 0.1, and Dypvik (1984) has since applied this ratio to ancient mudstones.

4.1.4.8 Cerium Anomaly

In 1982, Elderfield and Greaves proposed the use of the Cerium anomaly as a palaeoredox indicator. In oxic conditions, Ce³⁺ is oxidized to insoluble Ce⁴⁺ which precipitates with iron or manganese oxyhydroxides, causing a positive cerium anomaly in the sediments below (Wright *et al.*, 1987). Conversely, in suboxic waters, Ce⁴⁺ in the sediments is reduced to soluble Ce³⁺, leaving the sediments with a negative cerium anomaly (DeBaar *et al.*, 1985). However, care must be taken in interpretation of whole-rock results as Wright *et al.* (1987) demonstrated that the phosphatic remains of organisms that lived in dominantly anoxic waters would show positive anomalies, so mixing of anoxic sediment with these remains could give an average, non-indicative result. Macleod and Irving (1996) also warned that detrital input, depositional environment and diagenetic conditions may obscure the original

cerium concentrations, and therefore suggest that care should be taken in interpreting cerium anomalies.

Calculation of the anomaly is based on observations of sedimentary rocks which show that when the concentration of rare earth elements are normalized to a standard such as chondrite, they decline in a linear relationship as the atomic number increase, with only cerium and europium showing any significant deviation from this line (Elderfield and Greaves, 1982). The atomic order of rare-earth elements around cerium is lanthanum (La), cerium (Ce), praseodymium (Pr), and the anomaly can be calculated using La and Pr as the end points:

$$\log[2\text{Ce}^*/(\text{La}^* + \text{Pr}^*)]$$

The star implies a concentration normalized to chondrite values (Elderfield and Greaves, 1982), which in effect means dividing the elemental values in parts per million by 0.3 for lanthanum, 0.84 for cerium, and 0.21 for praseodymium (Wilde *et al.*, 1996).

4.2 Methodology

Samples were collected by the author every 10 cm through the sequences at Niveau Pacquier, Briestroffer and Folkestone, with samples taken every 5 cm through black shale horizons. Regular samples were collected through the Amma Fatma sequence by Gale in 2003.

The Folkestone Gault Clay samples were prepared by the author for major- and trace-element analysis by acid digestion. The samples were dried and ground in an agate ball mill and left to dry overnight at 105 °C before 0.500 g of sample was weighed into a PTFE beaker and moistened with a few drops of deionized water. 10.0 ml of concentrated 16M HNO₃ were slowly added and the resultant solution was left overnight in the fumehood. The solutions were then heated at 90-100 °C for 6 hrs, and evaporated to dryness. 10.0ml 23M HF and 4.0 ml 12M HClO₄ were carefully added to each sample and the solutions were left to stand for two hours, then were heated at 200°C until a crystalline paste formed (2-3 hrs). Two further aliquots of HF and HClO₄ were added, each followed by evaporation to incipient dryness. The final stage of the digestions was the addition of 10.0 ml 5M HNO₃, and the solution was gently warmed until a clear solution formed. If any undigested material was present in a sample at this stage, it was evaporated to incipient dryness and the HF/HClO₄

additions were repeated until the sample was fully digested before a final addition of 10.0 ml 5M HNO₃. The clear solutions were allowed to cool and then diluted to 50 ml in a volumetric flask. A 1.0 ml aliquot was diluted to 5.0 ml with 1M HNO₃, immediately prior to analysis by ICP-MS.

Trace-element concentrations for the Folkestone Gault Clay were determined by the author using a Thermo Scientific X Series ICP-MS (see *Appendix C, Table C.8a*). In comparison with the certified values, all repeats of the standards gave relatively precise results with %RSD values below 10% (see *Appendix C, Table C.1a*) and all data points for samples and standards were above the lower limits of detection for each element. The data demonstrate reproducibility as the analytical repeats, the procedural repeats and repeats run in separate analytical runs on different days all achieved a percentage relative standard deviation (%RSD) of less than 6.5% (see *Appendix C, Tables C.1b, C.1c and C.1d*).

The Folkestone Gault Clay major-element concentrations were determined by the author using a Fisons Horizon ICP-OES (see *Appendix C, Table C.8b*) and the results for the standards used demonstrated %RSD of below 10%, including the certified values (see *Appendix C, Table C.2a*). All data points exceeded the lower limits of detection and sample repeats also demonstrated %RSD of below 10% including samples run in separate analytical runs (see *Appendix C, Tables C.2b, C.2c and C.2d*) which suggests that the data is reproducible.

Analysis of trace-element concentrations, apart from molybdenum, for the Niveau Pacquier, Briestroffer and Amma Fatma samples was carried out by ICP-MS at Kingston University (see *Appendix C, Tables C.8c, C.8e and C.8g*). The samples were split into two separate analytical runs and all data values exceeded the lower limits of detection (see *Appendix C, Table C.3a*). The repeats of the standards used in both analytical runs (AGV-1, W-2, and SCo-1) all demonstrated %RSD values of below 10%, including the certified values (see *Appendix C, Tables C.3a*). The data appear to be reproducible as all sample repeats, including those analysed in both analytical runs, also demonstrated %RSD values of below 11% (see *Appendix C, Tables C.3b, C.3c and C.3d*).

The Niveau Pacquier, Briestroffer and Amma Fatma samples were prepared by the author for analysis of major elements and molybdenum concentrations by lithium metaborate fusion. The samples were dried and ground in an agate ball mill and left to dry overnight at 105°C before 0.25g of sample was combined with 1.25g of lithium metaborate and placed into a graphite crucible. The samples were fused in a muffle furnace for 20 minutes at 1050°C before being quenched in 150 ml of 3.5% HNO₃. The solutions were then filtered, made up to 250 ml in volumetric flasks and analysis was carried out by the author on a Fisons Horizon ICP-OES for major-element data and a Thermo Scientific X Series ICP-MS for molybdenum data.

The ICP-OES data was collected in two separate analytical runs (see *Appendix C, Tables C.8d and C.8f / C.8h*) and the %RSD of repeats of the standards used in both runs did not exceed 6%, including the certified values (see *Appendix C, Tables C.4a and C.5a*). Repeats of samples, including samples repeated in the two different analytical runs, had %RSD values of less than 5% for the Briestroffer and Amma Fatma samples (see *Appendix C, Tables C.4b, C.4c and C.4d*) and less than 10% for the Niveau Pacquier samples (see *Appendix C, Tables C.5b, C.5c and C.5d*). All data collected exceeded the lower limits of detection for all elements (see *Appendix C, Tables C.4a and C.5a*). The molybdenum data was also collected in two ICP-MS analytical runs (see *Appendix C, Tables C.8c and C.8e / C.8g*). The %RSD values for repeats of the standards used within each run fell below 14% for the Briestroffer and Amma Fatma data (see *Appendix C, Tables C.6a*) and below 10% for the Niveau Pacquier data (see *Appendix C, Tables C.7a*). Sample repeats, including samples run in both analytical run, had %RSD values below 3% for the Briestroffer and Amma Fatma samples (see *Appendix C, Tables C.6b, C.6c and C.6d*) and below 7% for the Niveau Pacquier samples (see *Appendix C, Tables C.7b, C.7c and C.7d*). All data collected was above the lower limits of detection calculated for the analytical runs (see *Appendix C, Tables C.6a and C.7a*).

4.3. Discussion of results

4.3.1 The Niveau Pacquier Sequence

4.3.1.1 Trace metal enrichment

This Lower Albian sequence from the Vocontian Basin of south east France consists of the grey clays of the Marnes Bleues Formation punctuated by the finely laminated Niveau Pacquier black paper shales (see *Figure 2.13*). The Niveau Pacquier sequence provides the clearest sedimentological and faunal division between the grey muds of upper dysoxic facies, and black shales of lower dysoxic to anoxic facies. Using this classification, the samples have been divided into data sets for 'Grey Clay' or 'Black Shale' facies. Since this site gives the clearest distinction between these environments, it is likely to give the strongest signal in the geochemical proxies for palaeo-oxygenation.

The elemental enrichments are displayed as simple corrections to aluminium concentrations (see *Figure 4.1*), as enrichment factors (see *Figure 4.2*) and as trace metal excesses (see *Figure 4.3*). Of these methods, the enrichment factors and trace metal excess are the most useful for inter-elemental and inter-site comparison as they allow direct numerical comparisons. Both methods are limited by the problems of using the average shale value (Brumsack, 2005) and complications arising from closed sum effect (Van der Weijden, 2002), but Brumsack (2005) highlighted that trace metal excesses are more use in sediments with only very low detrital inputs. While trace metal excess calculations give a greater range of values either side of 0 and could thereby be said to emphasise subtle variations, enrichment factors are more commonly used in the literature. For this reason, enrichment factors will be used from here on.

Of the element enrichments, molybdenum appears to give the strongest correlation with proposed environmental conditions, with clear definition between the grey mud and black shale samples. Only one grey clay sample from directly above the main black shale sequence (1.6 m) shows slight enrichment. Sedimentologically this sample appears to be a grey clay but could represent the tail end of the low oxygen event or black shale material that underwent later re-oxidation. The Total Organic Carbon content of the sample is marginally higher than the other grey clay samples but is far lower than any of the black shale values (see *Figure 5.6*).

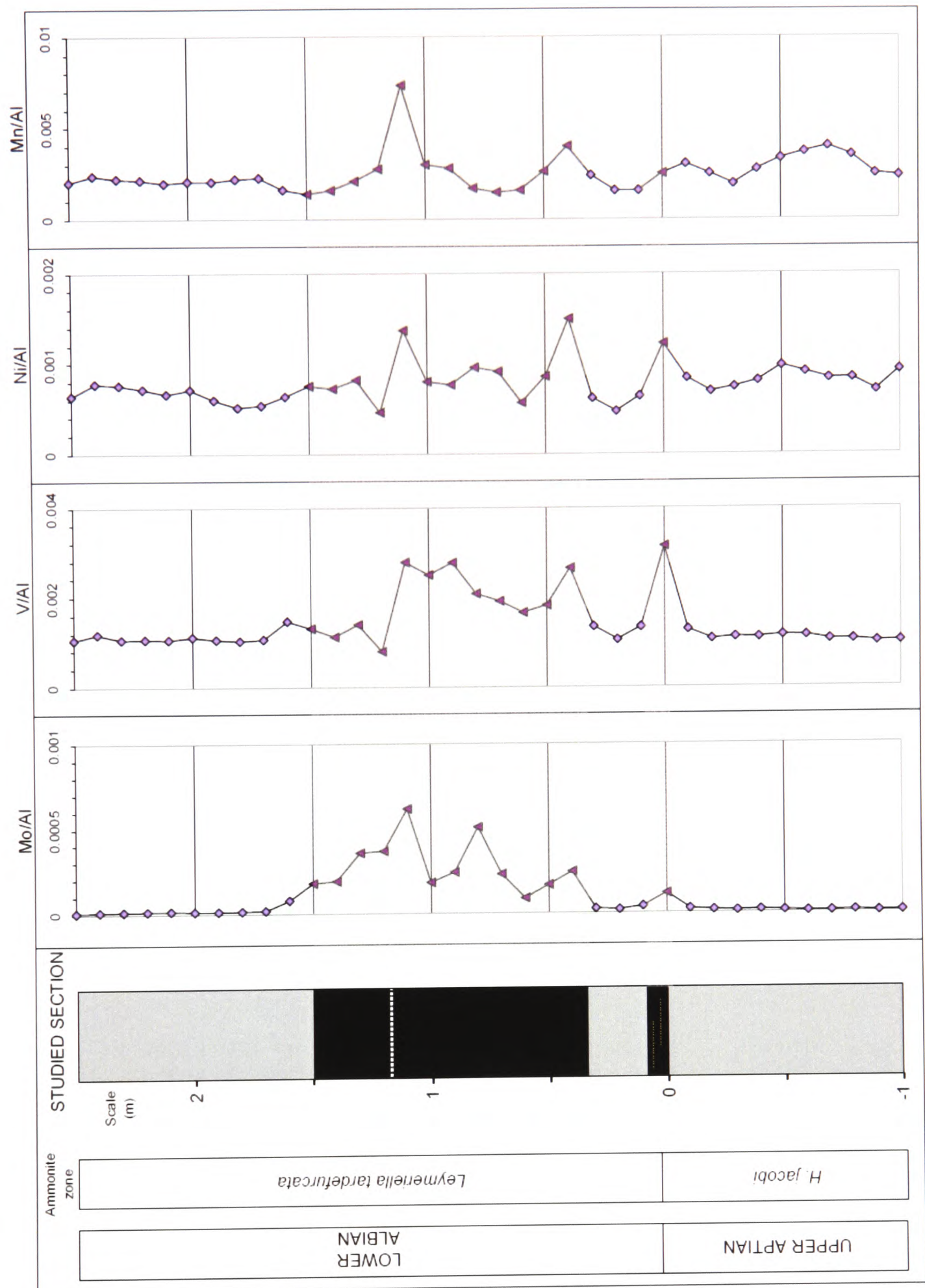


Figure 4.1: Element/Al ratio for Mo, V, Ni and Mn for the Niveau Pacquier sequence. The pale purple points represent the grey clay samples whereas the shaded dark purple triangular points are from the black shale data set.

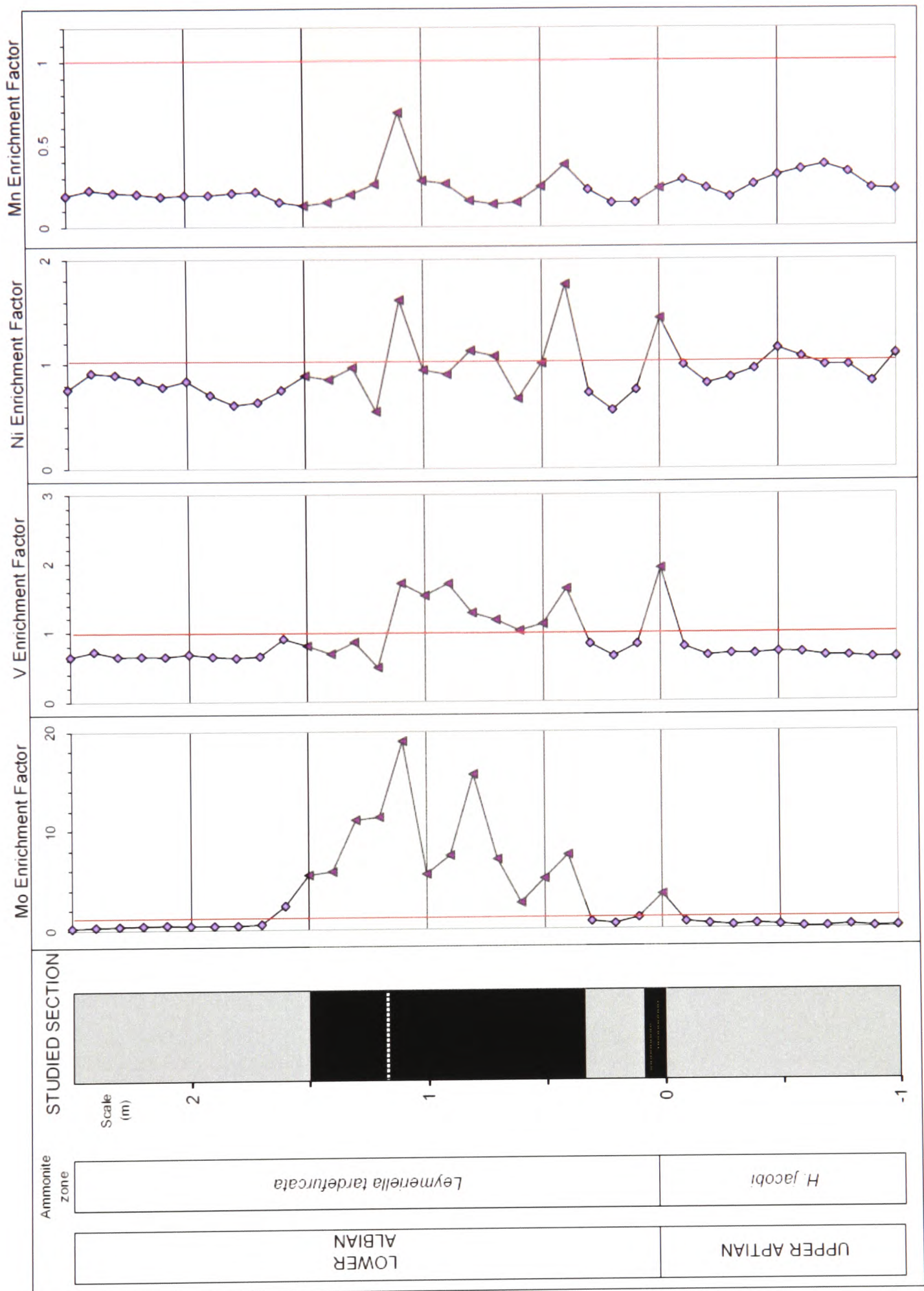


Figure 4.2: Enrichment factors for Mo, V, Ni and Mn for the Niveau Pacquier sequence. The pale purple points represent the grey clay samples whereas the shaded dark purple triangular points are from the black shale data set.

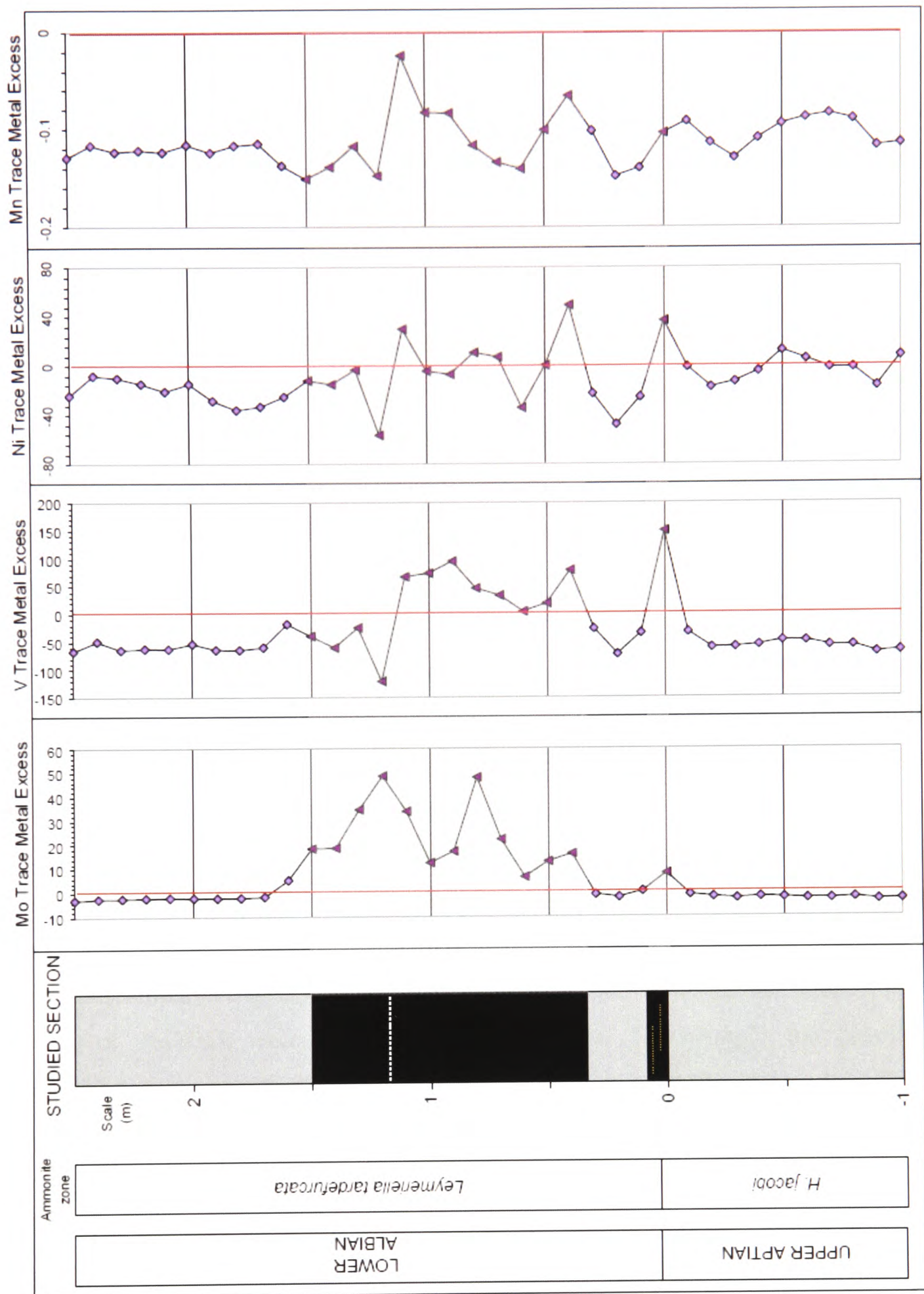


Figure 4.3: Trace metal excess values for Mo, V, Ni and Mn for the Niveau Pacquier sequence. The pale purple points represent the grey clay samples whereas the shaded dark purple triangular points are from the black shale data set.

Reanalysing the data with this grey clay sample identified as black shale improves the statistics for some proxies but it also reduces the statistical difference between the two

data sets for other proxies and so the data point has been left within the grey clay data set. The remainder of the grey clay samples show a slight depletion relative to average shale values whereas the black shale samples are clearly enriched. The slight relative depletion of the grey clay samples highlights one of the problems with using average shale data, as ideally oxygenated conditions would give values very close to unity if the average shale values were directly applicable to the site.

While there is some variability in Al_2O_3 values throughout the sequence, there is little variation in SiO_2 Al/Si Ti/Al and K/Al (see *Figure 4.4*) which suggests that the bulk composition of the siliciclastic fraction is similar between the black shales and the grey clays. There is one sample, however, from 1.2 m which has anomalously high calcium carbonate, silica, aluminium and phosphate values which, in combination, exceed 100 wt%. This sample corresponds to the carbonate-rich horizon within the black shale and the anomalously high data may represent elements held within stoichiometrically different compounds to those assumed for weight percentage calculations. This sample records a slight reduction in V and Ni enrichment factors and this may be an artefact of the higher aluminium values. Accordingly the sample below records strong enrichment in these trace elements which may represent an artefact of the slightly lower aluminium value for this sample. The phosphate levels are variable throughout the sequence but there is little distinction between the grey clay and black shale samples (see *Figure 4.5*). The vanadium data also appears to show enrichment in the majority of black shale samples – however, the samples from the top of the black shale sequence record depletion. Interestingly, the vanadium enrichment is marginally greatest for the thin black shale band (the sample from 0 m), which only shows moderate enrichment of molybdenum. The same is true of the nickel data – while the black shale samples show a greater range of values, there is little reliable separation between the two data sets, with variable enrichment and depletion in both. However, the thin black shale band records clear enrichment. This suggests that the thin shale band may record a short duration event, as Adelson *et al.* (2001) proposed that molybdenum fixation is related to the amount of time the sediment is exposed to low oxygen waters. Alternatively it could suggest that the hydrogen sulphide level in the water, which Helz *et al.* (1996) suggested plays a key role in molybdenum fixation, was not as high as in the main low oxygen event which records strong molybdenum enrichment.

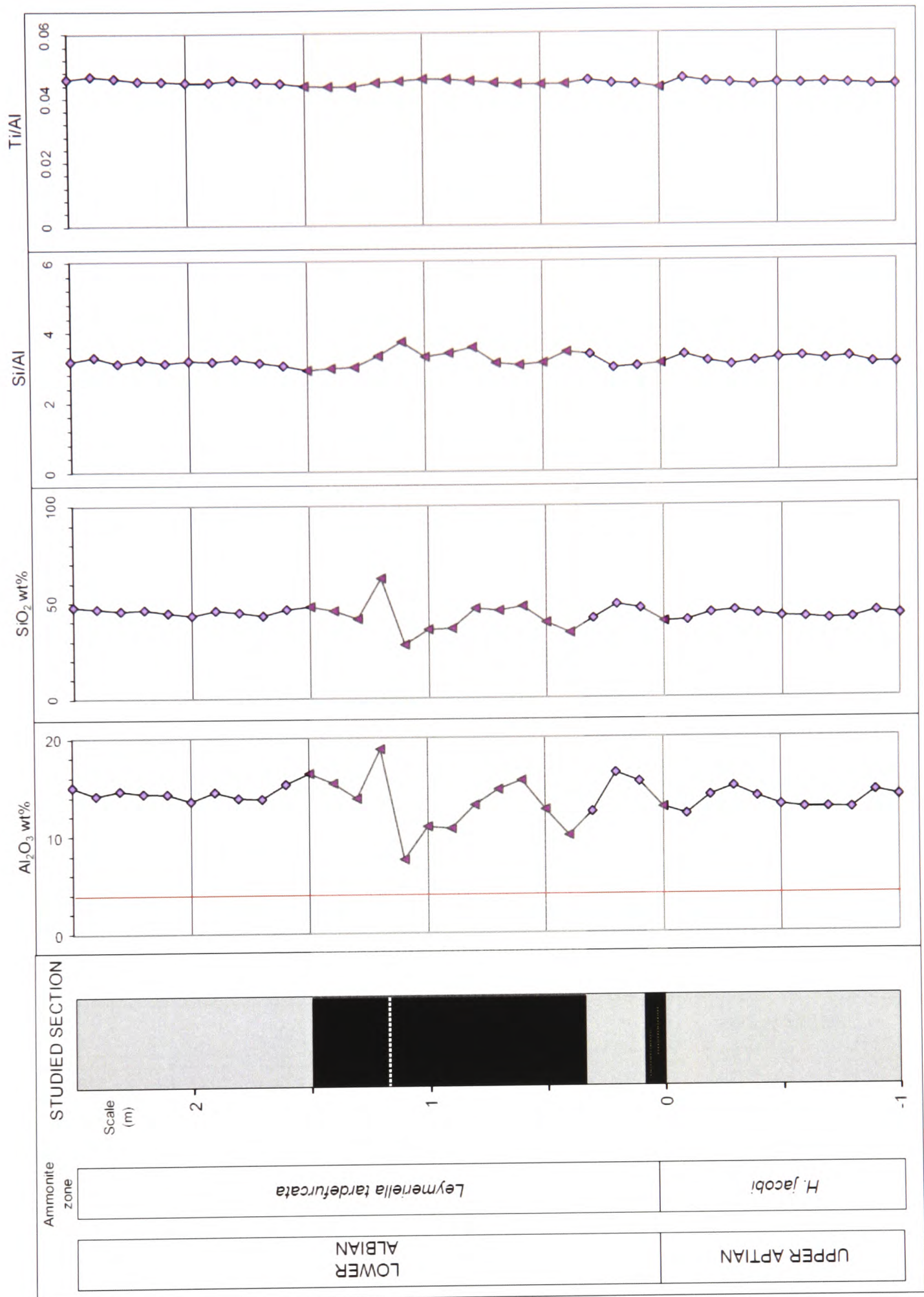


Figure 4.4: Major elements (Al_2O_3 wt% and SiO_2 wt%) and element ratios (Si/Al and Ti/Al) for the Niveau Pacquier sequence. The pale purple points represent the grey clay samples whereas the shaded dark purple triangular points are from the black shale data set.

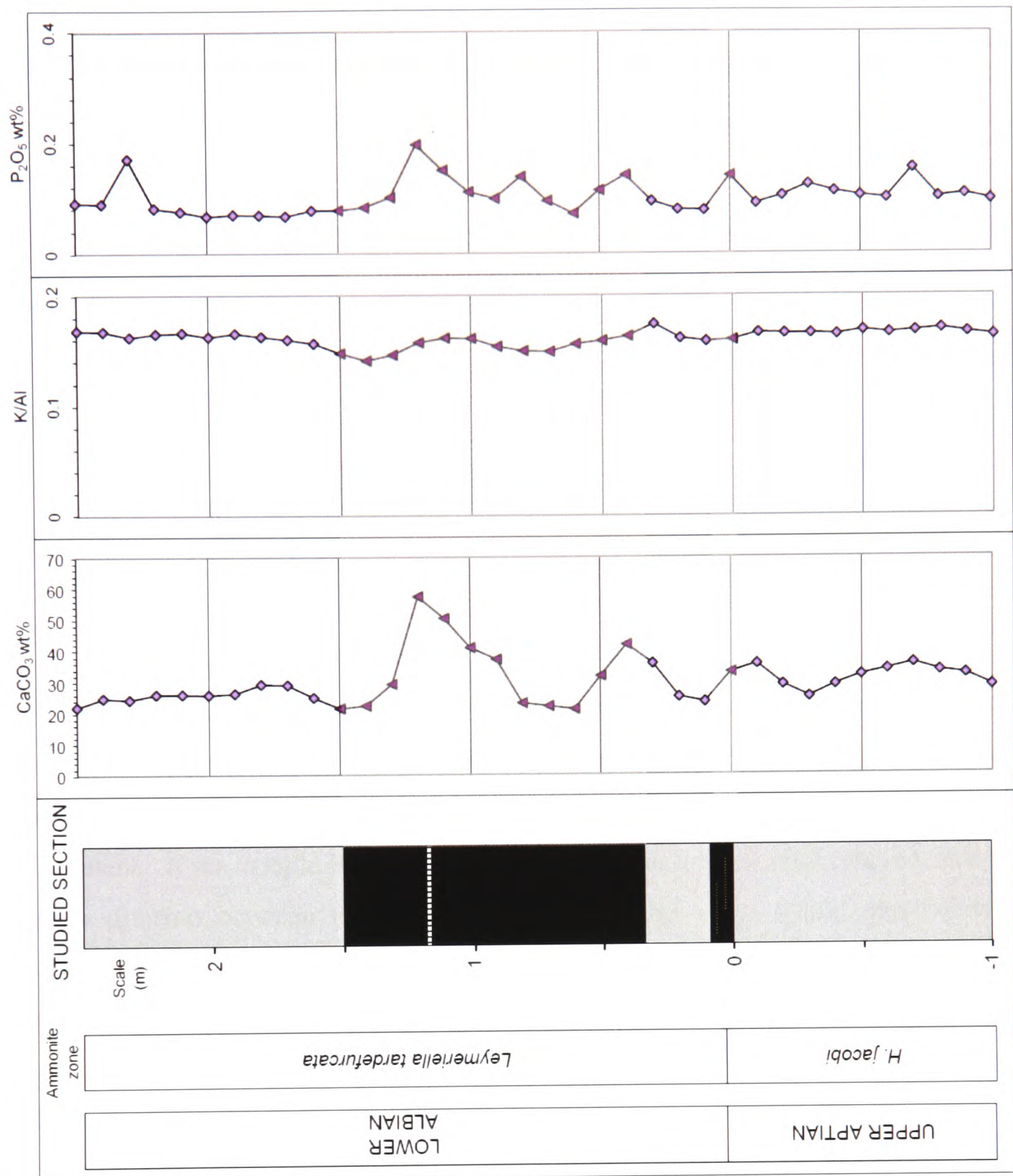


Figure 4.5: Major elements (as $CaCO_3$ wt% and P_2O_5 wt%) and element ratios (K/Al) for the Niveau Pacquier sequence. The pale purple points represent the grey clay samples whereas the shaded dark purple triangular points are from the black shale data set.

The manganese data does not correlate reliably with the sedimentology (see Figure 4.2) – to start with, the grey clay samples record variable depletion and the black shale values, while still recording depletion, show a range of values above and below the grey mud samples. One black shale sample in particular (the sample from 1.1 m) records a much lower level of depletion than the grey clay sample range. This clearly does not represent the greater depletion predicted by Lynn and Bonatti (1965) for

lower oxygen conditions. The two-tail Student's t-Test was applied to the data (see *Figure 4.6*), and clearly identifies the two distinct sample sets for molybdenum and, less reliably, vanadium, and confirms that the two environments could not be distinguished using the manganese or nickel data.

Element	Mean (Grey)	Variance	Mean (Black)	Variance	P two tail value
Mo	0.479	0.218	8.21	22.9	0.0001
V	0.692	0.0056	1.23	0.201	0.0011
Ni	0.846	0.0237	1.06	0.123	0.0543
Mn	0.229	0.0039	0.252	0.0224	0.603

Figure 4.6: The two-tailed Student's t-test data for Niveau Pacquier elemental enrichment factors. The test shows that for molybdenum and vanadium, the two sample sets are clearly distinguishable as the P values are below the 0.05% confidence level. However, the P values for nickel and manganese are well above this confidence level, showing that the black shale and grey clay samples do not show up as separate groups within these sets of data.

This is further highlighted by plots of the mean and range of data points within the grey mud and black shale sample sets (see *Figure 4.7*). In the molybdenum data, the mean grey mud value falls below 1, showing relative depletion, and there is almost complete separation of the data ranges with all of the black shale data points recording enrichment. If the sample from 1.6 m was classified as a black shale, there would be a clear division between the two data sets – all grey clays would plot below 1 (recording depletion) and all of the black shales would plot above 1 (recording enrichment). However, with the sample from 1.6 m recorded as a grey clay, a division between the two data sets could be proposed between Enrichment Factor values of 2.0 - 2.25. With vanadium, there is total overlap between the groups but all of the grey clays samples plot below 1. This means that although the black shale range extends below 1, all of the enriched values belong to this data set. The nickel and manganese grey mud sample range falls within the black shale range in both cases, clearly demonstrating that the sample sets cannot be differentiated. However, the mean of the two nickel data sets do fall in the expected regions – below 1 for the grey clays and above 1 for the black shales.

4.3.1.2 Trace metal ratios

While much work has been done on trace metal ratios, there is little agreement about where the boundaries of oxic, dysoxic and anoxic should be set. *Figure 4.8* shows the elemental ratios for the Niveau Pacquier sequence. In 1994, Jones and Manning ran a

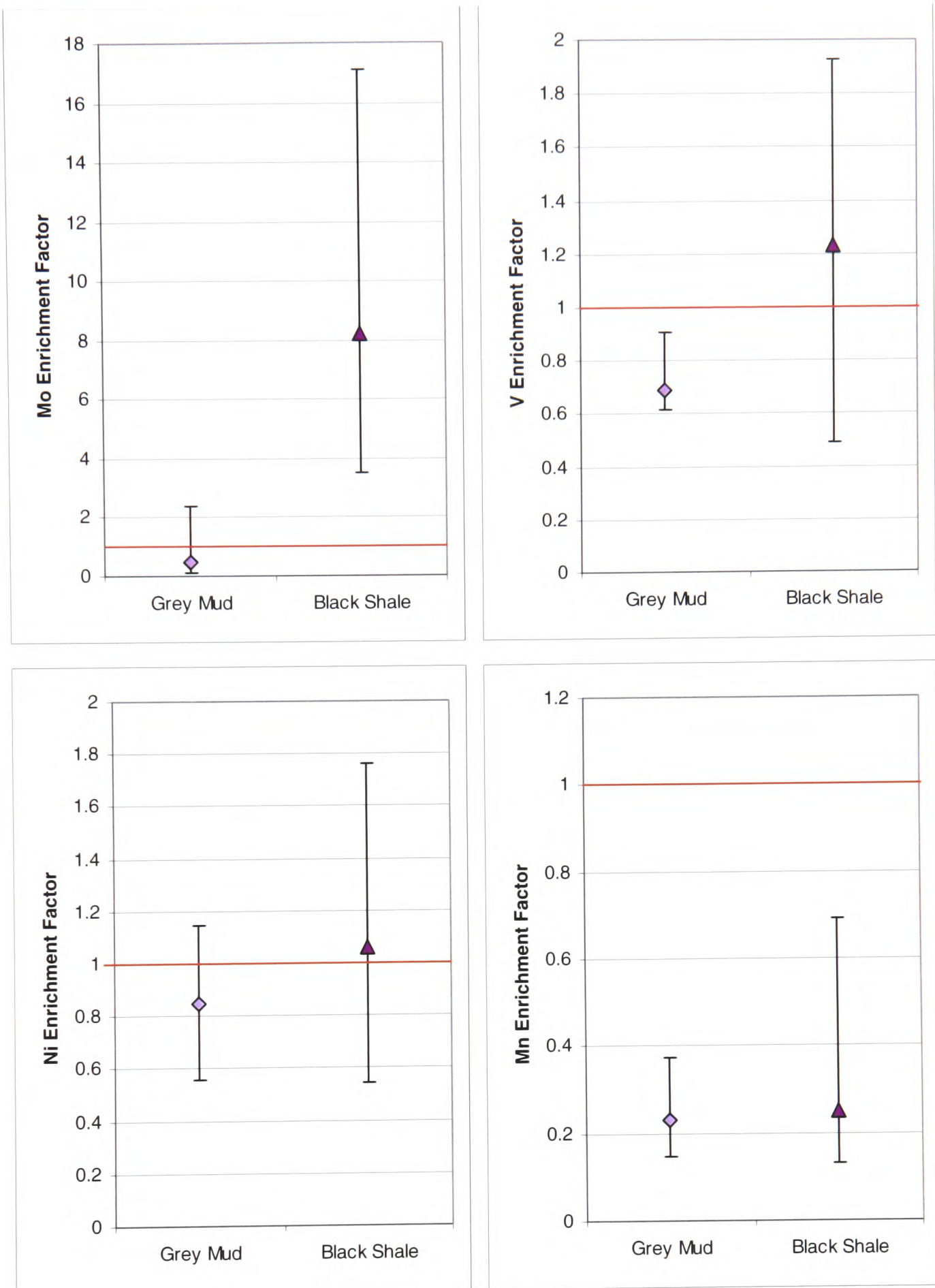


Figure 4.7: Plots of the mean and range of the Mo, V, Ni and Mn data for the grey shale sample set and the black shale sample set of the Niveau Pacquier sequence.

comparison of a range of elemental ratios against faunal, sedimentological and other geochemical proxies for a range of Upper Jurassic mudstones. They found consistency between authigenic uranium, U/Th, V/Cr and Ni/Co and tentatively suggested boundaries for these ratios. Results from the two-tailed Student's t-test (see

Figure 4.9) suggest that for all four of these ratios the grey mud and black shale samples are statistically distinct sample sets.

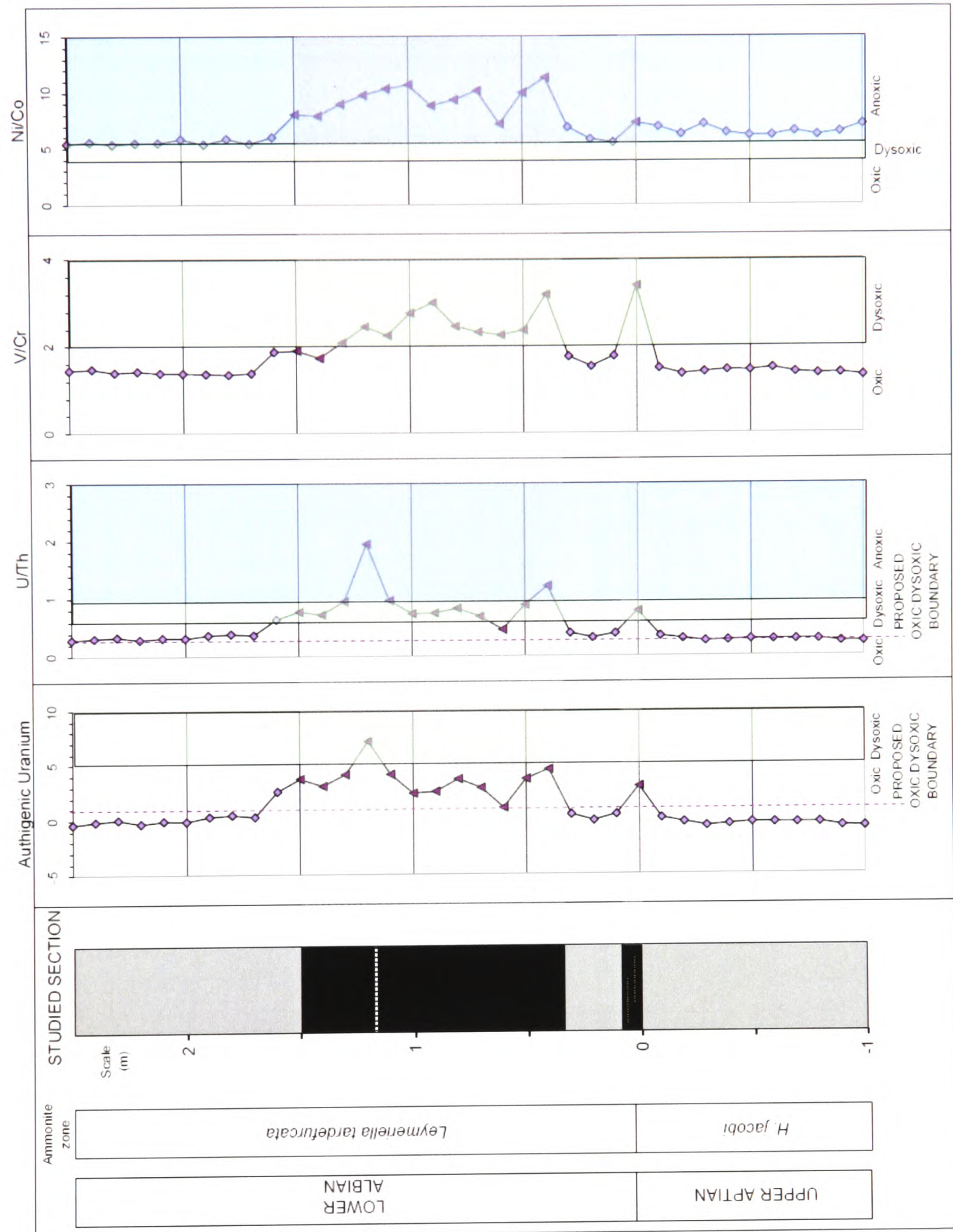


Figure 4.8: Plots of the ratios highlighted by Jones and Manning (1994), including their tentative boundaries for the oxic-dysoxic transition and the dysoxic-anoxic transition, applied to the Niveau Pacquier sequence. The pale purple points represent the grey clay samples whereas the shaded dark purple triangular points are from the black shale data set.

Element	Mean (Grey)	Variance	Mean (Black)	Variance	P two tail value
Ua	-0.0147	0.448	3.56	2.02	3.76E-07
U/Th	0.330	0.0067	0.902	0.130	7.95E-05
V/Cr	1.47	0.0211	2.48	0.240	6.42E-06
Ni/Co	6.07	0.348	9.21	1.72	6.61E-07

Figure 4.9: The two-tailed Student's t-test data for Niveau Pacquier element ratios suggested by Jones and Manning (1994). The test shows that for all ratios, the grey mud and black shale samples are statistically separate data sets as all P values fall well under the 0.05% confidence limit.

However, examination of the mean and range of these data sets (see Figure 4.10) highlights one of the difficulties of using the Student's t-test to distinguish data sets.

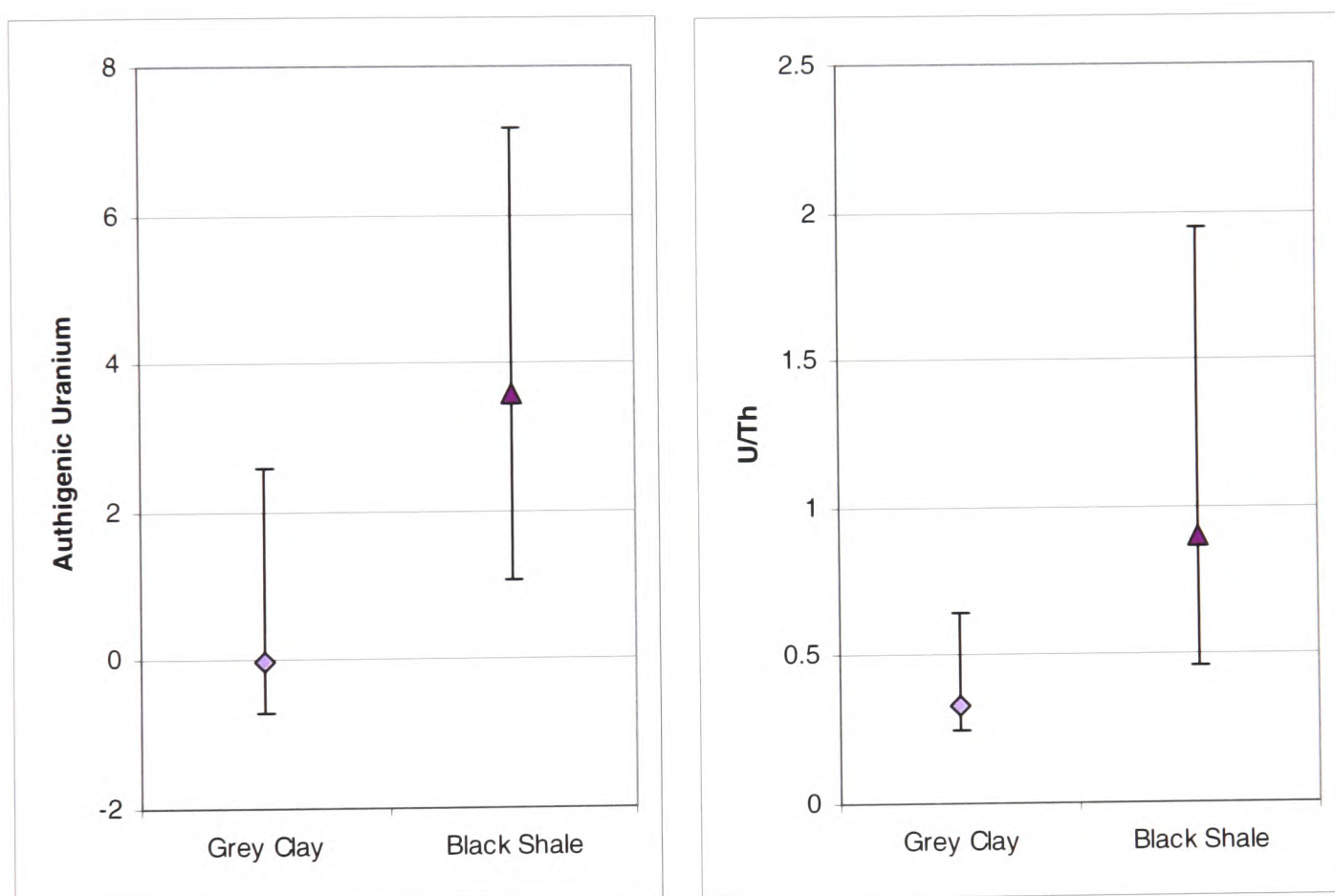


Figure 4.10a: Plots of the mean and range of the Ua and U/Th data for the grey shale sample set and the black shale sample set of the Niveau Pacquier sequence.

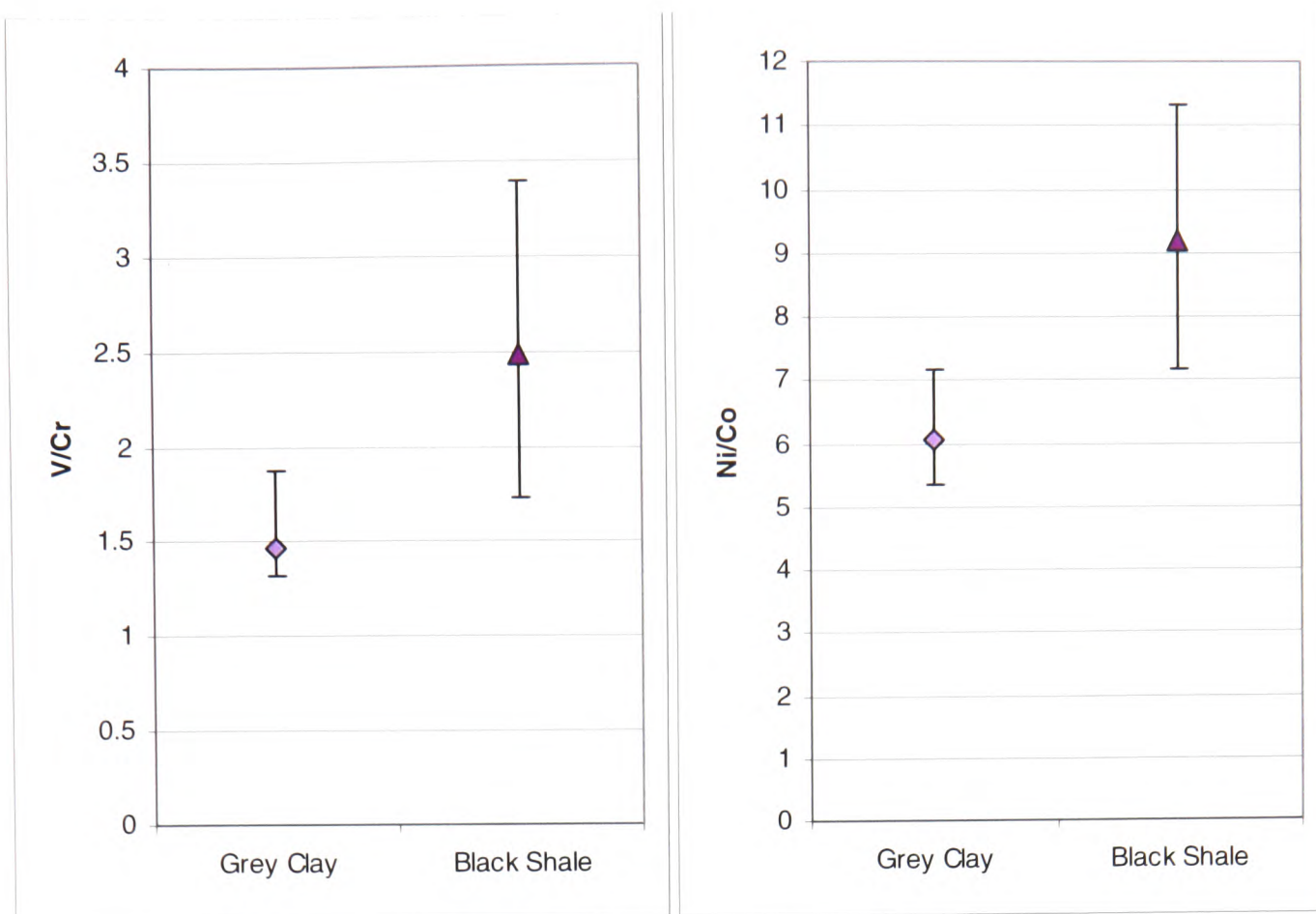


Figure 4.10b: Plots of the mean and range of the V/Cr and Ni/Co data for the grey shale sample set and the black shale sample set of the Niveau Pacquier sequence.

While the mean and range extend higher for the black shale sample set for Ua, there is significant overlap between the two groups. The U/Th ratio exhibits less overlap and Figure 4.10 shows that apart from a couple of points, there is a strong division between the black shale and grey clay samples. In the V/Cr ratio the two data sets only overlap slightly and the Ni/Co ratio shows complete separation between grey clays and black shales. Again, the Ua, U/Th and V/Cr ratios show relatively strong peaks for the thin black shale band, which suggests that the duration of the event was not severely limited, as Wignall (1994) listed this as one of the key factors in uranium enrichment.

The grey clay sample from 1.6 m, which is enriched in Mo, V and Ni, also plots with high values of Ua and U/Th which would appear to classify it as a black shale. The fact that Anderson *et al.* (1989) demonstrated that redox-related uranium fixation does not withstand re-oxidation of sediment suggests that this represents the tail-end of a low-oxygen event rather than a black shale sample that underwent later re-oxidation.

While there does appear to be definition between the elemental ratio data sets, comparison of this data with the tentative boundaries recognised by Jones and Manning also highlights problems (see *Figure 4.11*). Using these boundaries, the Ua data plots mainly in the oxic zone, with some of the black shale data reaching dysoxic levels, the U/Th and the V/Cr ratio places most of the black shale data within the dysoxic range, with some extending into the anoxic zone. The Ni/Co ratio, however, plots the grey clays within the dysoxic range and black shale data plot within the anoxic zone. This variability (see *Figure 4.11*) suggests that elemental ratio boundaries may be technique specific as Jones and Manning (1994) used gamma-ray spectroscopy to measure uranium and thorium values. It is also possible that the boundaries are site specific, and correlations between ratios may only be applicable for internal site comparison. The high levels of uranium enrichment associated with phosphate (Plant *et al.*, 1999) may also complicate the interpretation of the data. The strongest peak in Ua and U/Th values is from the sample from 1.2 m which has anomalously high calcium carbonate, aluminium, silica and phosphate values (see *Figures 4.4 and 4.5*).

The Ua data sets could be neatly divided (apart from the ambiguous sample from 1.6 m) using a boundary at a Ua value of 1 which then matches the division of the molybdenum data. Similarly, the data sets could be divided by moving the oxic:dysoxic boundary for the U/Th ratio to 0.45 (rather than the value of 0.75 suggested by Jones and Manning (1994)). This would then tally with the V/Cr in which, using Jones and Manning's (1994) proposed boundaries, the grey clays plot within the oxic region whereas the black shale data points are predominantly dysoxic. The Ni/Co data also works well with the boundaries as defined by Jones and Manning (1994), with the two data sets falling predominantly into different oxygenation conditions. However, in this case the grey clays plot predominantly within the dysoxic range and the black shales plot within the anoxic range – in order for these proxies to correlate, this boundary should represent the oxic : dysoxic transition rather than the dysoxic : anoxic transition. This, however, leads to the question of whether these 'new' boundaries truly represent the oxic : dysoxic transition, or whether they simply separate oxic conditions from lower oxygen conditions (including dysoxic and anoxic settings).

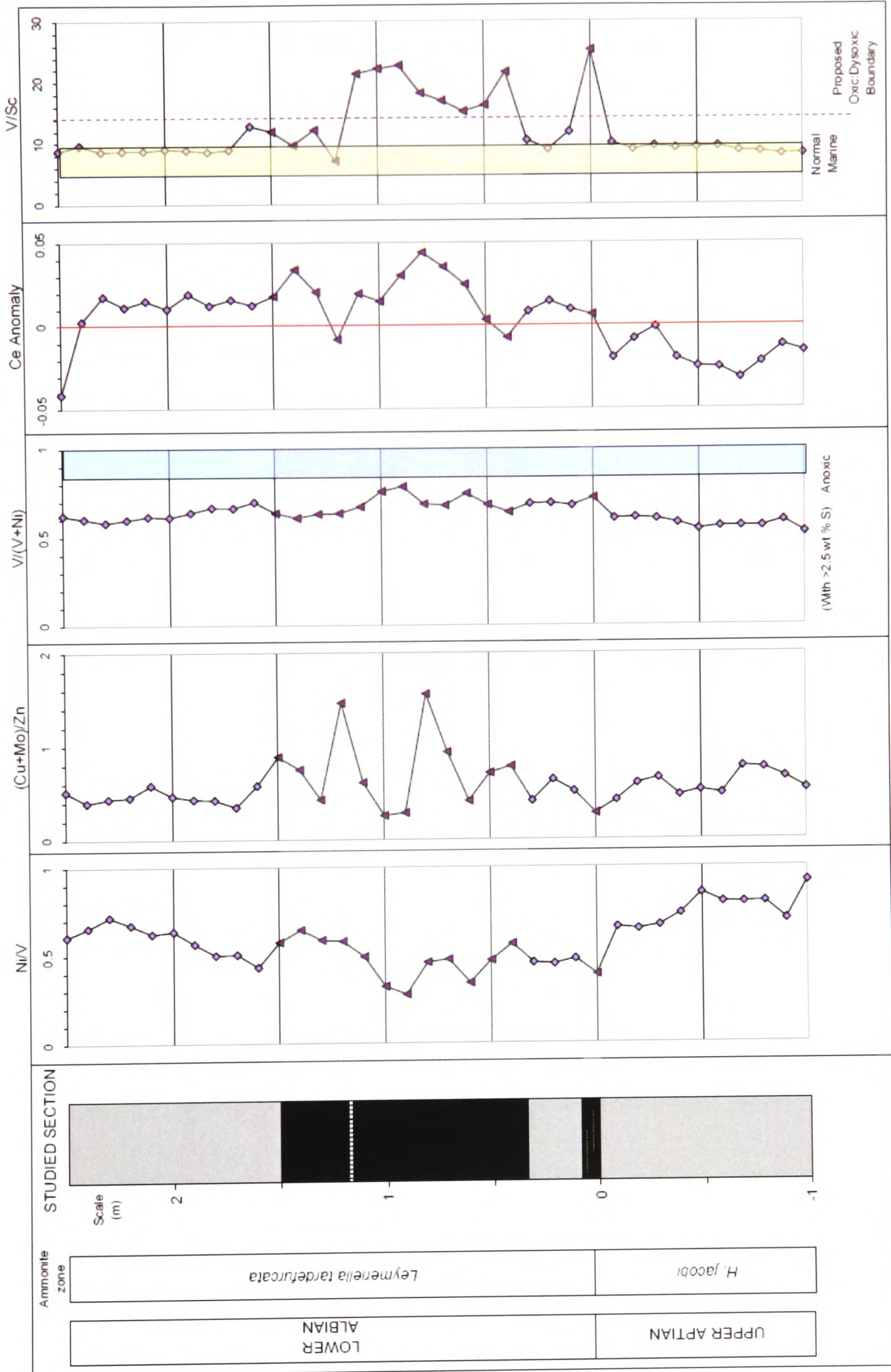
		OXIC	DYSOXIC	ANOXIC
Ua	Grey Clay	—————		
	Black Shale		—————	
U/Th	Grey Clay	—————		
	Black Shale		—————	—————
V/Cr	Grey Clay	—————		
	Black Shale		—————	
Ni/Co	Grey Clay		—————	
	Black Shale			—————

Figure 4.11: Summary of the Niveau Pacquier environments of deposition suggested by the elemental ratios, based on the tentative boundaries set by Jones and Manning (1994)

A number of other elemental ratios have been proposed but little correlative work has been done. Jones and Manning (1994) also ran Ni/V and (Cu+Mo)/Zn, but suggested that they showed little correlation with other palaeo-oxygenation proxies. Schovsbo (2001) proposed the use of the ratio V/(V+Ni) and Kimura and Watanabe (2001) proposed the V/Sc ratio (see *Figure 4.12*). As of yet, these ratios have only limited palaeo-oxygenation boundaries suggested and the cerium anomaly (Elderfield and Greaves, 1982) is simply thought to show negative values for anoxic conditions.

While the two tailed Student's t-test (see *Figure 4.13*) suggests that all of these ratios, apart from the (Cu+Mo)/Zn ratio, allow distinction between the grey mud and black shale data sets, investigation of the mean and range of each sample set reveals that this is not necessarily the case (see *Figure 4.14*).

Figure 4.12: Plots of the other ratios including tentative boundaries for V/Sc (Kimura and Watanabe, 2001) and V/(V+Ni) (Schovsbo, 2001) for the Niveau Pacquier sequence (on next page).



Element	Mean (Grey)	Variance	Mean (Black)	Variance	P two tail value
Ni/V	0.647	0.0181	0.475	0.0133	0.0004
(Cu+Mo)/Zn	0.525	0.0130	0.720	0.178	0.126
V/(V+Ni)	0.611	0.0025	0.682	0.0030	0.0009
Ce anomaly	-0.0030	0.0003	0.0181	0.0003	0.0012
V/Sc	9.30	1.19	17.0	31.1	0.0003

Figure 4.13: The two-tailed Student's t-test data for Niveau Pacquier other element ratios test shows that for all ratios apart from (Cu+Mo)/Zn, the two data sets are statistically separate data sets as all P values fall under the 0.05% confidence limit.

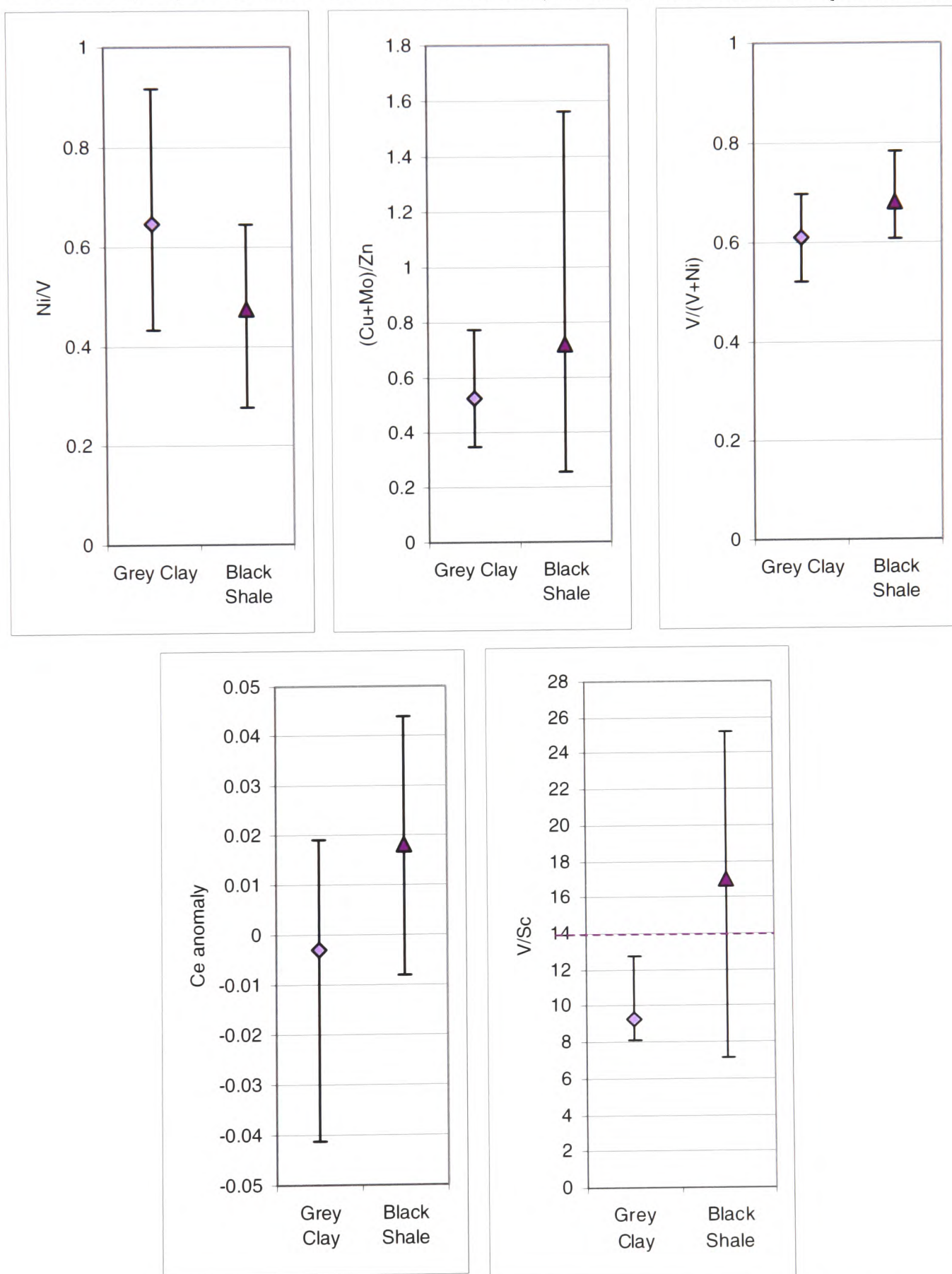


Figure 4.14: Plots of the mean and range of the other elemental ratios for the grey shale and the black shale sample sets of the Niveau Pacquier sequence.

For $(\text{Cu}+\text{Mo})/\text{Zn}$, the grey mud data falls almost entirely within the range of the black shale data, thereby making the two data sets indistinguishable. In this ratio, the range of values seen within the black shale data set is generally greater than for the grey mud, but this is not enough to correctly distinguish between environments of deposition. While the black shale range of the Ni/V ratio does show a general decrease, there is still significant overlap between the data sets. The black shale data range for the $\text{V}/(\text{V}+\text{Ni})$ shows the expected overall rise, but again there is significant overlap between the two data sets. In the cerium anomaly data, it appears that the grey clay range extends more towards negative anomalies, whereas the black shale data extends further into positive anomalies, which is the opposite of what would be expected according to Elderfield and Greaves (1982).

There is total overlap between the two data sets for the V/Sc ratio, but it may be of some use as the mean of the black shale data is much higher than that of the grey clay data. Examination of the data (see *Figure 4.12*) shows that most of the grey clay data plot within the upper limit of the tentative 'normal marine' range of V/Sc suggested by Kimura and Watanabe (2001), whereas all of the black shale data plot above this. This suggests that this boundary could be proposed as the oxic/dysoxic transition, and that further work could make more use of this ratio. A boundary at a V/Sc value of 14 divides the data into almost the same data sets as Jones and Manning's (1994) V/Cr boundary, which suggests that this could be proposed as a similar boundary. Again, the V/Sc ratio records its strongest peak in the thin black shale band which only showed moderate molybdenum enrichment. The molybdenum data demonstrate a reliable definition between the two data sets with clear distinction between oxic and low oxygen conditions. However, this ambiguity over the thin shale band values suggests that it might not be as reliable for distinguishing between grades of low oxygenation.

4.3.2 Breistroffer Layers

4.3.2.1 Trace Metal Enrichments

The second Vocontian Basin sequence is Late Albian in age and comprises the Marnes Bleues grey clay formation interspersed with rhythmic bands of low oxygen black paper shales known as the Briestroffer Layers. As with the Niveau Pacquier sequence, the Breistroffer samples can be divided into sample sets of grey clays of upper dysoxic facies, and the black shales of the Briestroffer layers (see *Figure 2.21*).

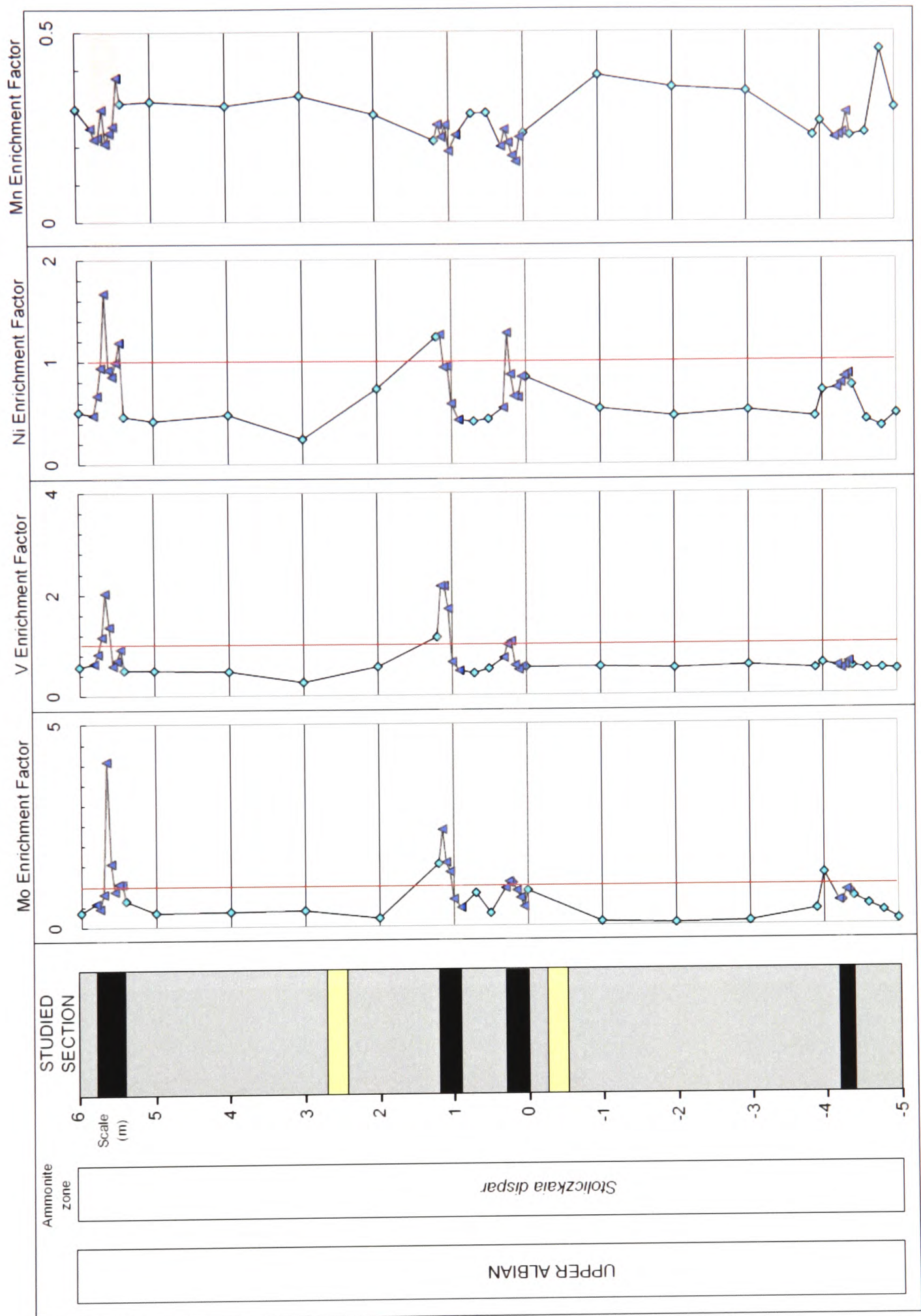


Figure 4.15: Enrichment factors of Mo, V, Ni and Mn. The pale blue data points represent samples from the grey clay sequence, whereas the shaded dark blue points represent samples from the black shale layers in the Briestroffer sequence.

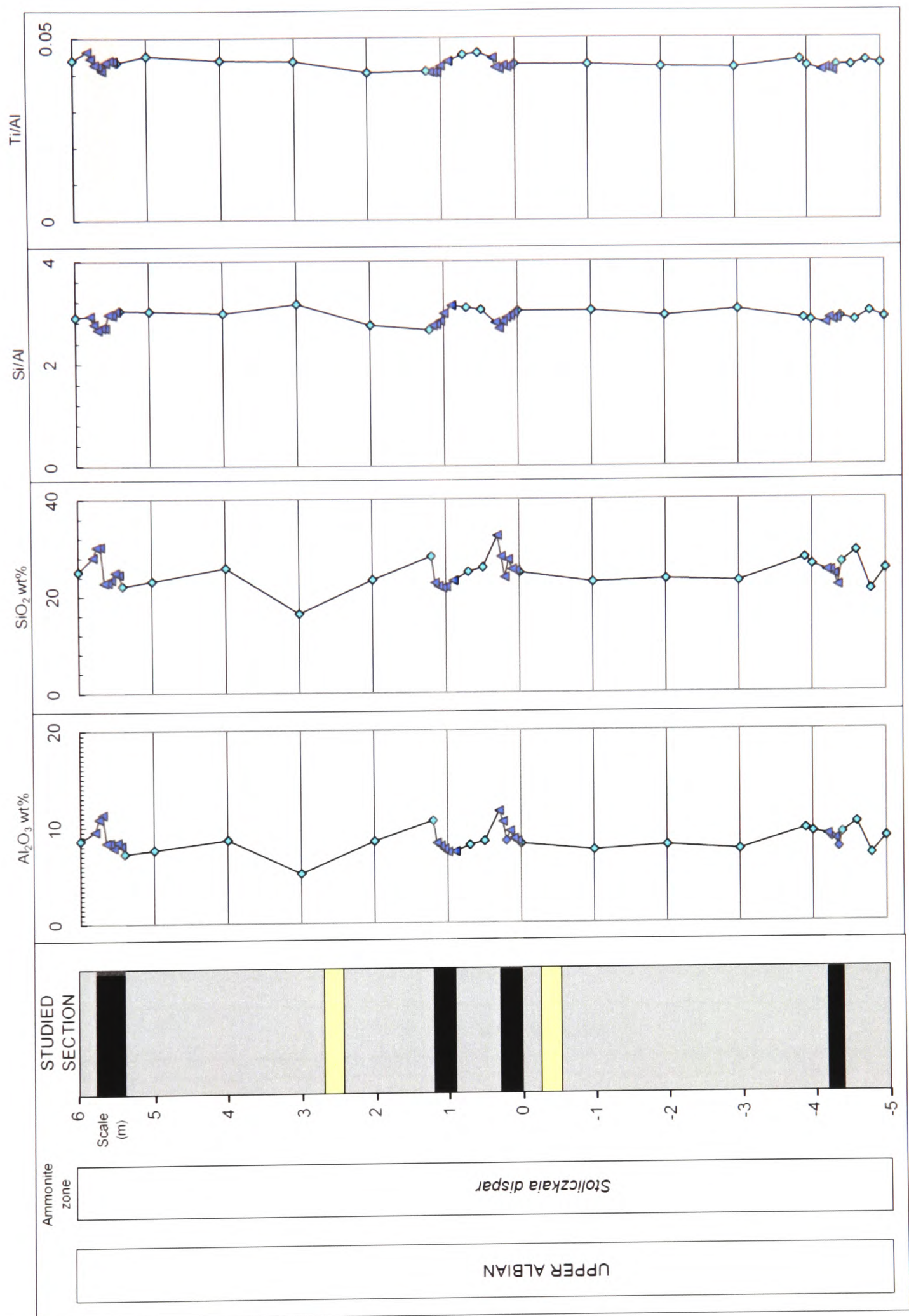


Figure 4.16: Major elements (Al_2O_3 wt% and SiO_2 wt%) and element ratios (Si/Al and Ti/Al) for the Briestoffer section. The pale blue data points represent samples from the grey clay sequence, whereas the shaded dark blue points represent samples from the black shale layers in the Briestoffer sequence.

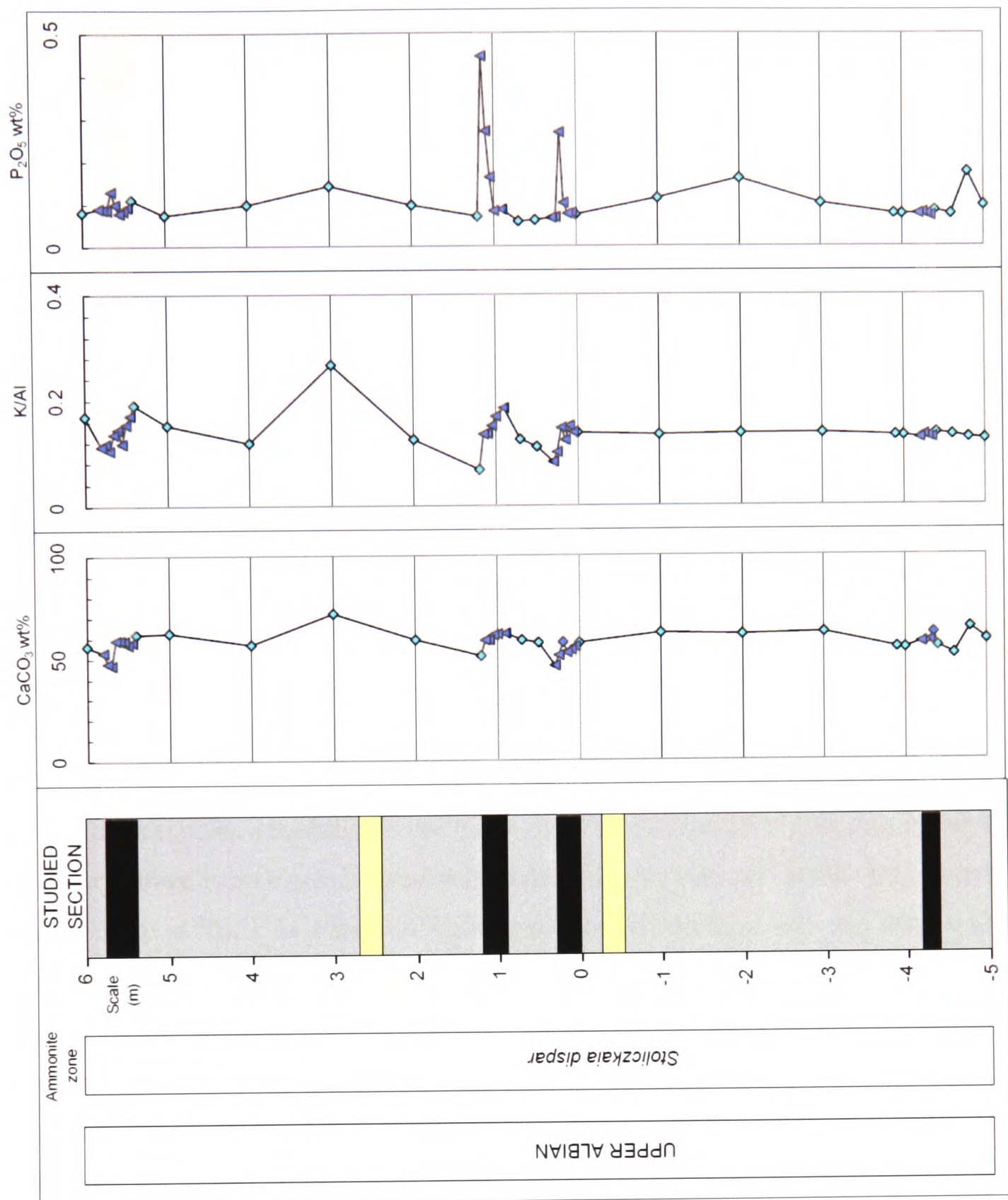


Figure 4.17: Major elements (as $CaCO_3$ wt% and P_2O_5 wt%) and element ratios (K/Al) for the Briestroffer section. The pale blue data points represent samples from the grey clay sequence, whereas the shaded dark blue points represent samples from the black shale layers in the Briestroffer sequence.

However, these black paper shale layers are not as clear or as well developed as the Niveau Pacquier black shale sequence, and this may be reflected by reduced separation between the geochemical data sets. While Mo is usually a reliable proxy, the data groups overlap considerably in the Breistroffer sequence. From the plot of

the Mo enrichment factor (see *Figure 4.15*) it is clear that while the majority of data points suggest that Mo is depleted, two black shale horizons extend into Mo enrichment. It should also be noted that the sample from 1.4 m, which is classified as grey clay, shows Mo enrichment and this may represent the tail end of a low-oxygen event which again is not clearly reflected in the sedimentology. The other two black shale horizons are not characterised by Mo enrichment.

The V and Ni data appear to be more reliable, as three of the black shale horizon record some enrichment. However, the ranges of the data sets show almost complete overlap and so would not allow definition of environment for unknown samples. All four black shale horizons record evidence of greater Mn depletion compared to the grey clay samples, although this is also recorded in grey clay samples close to some of the black shale horizons. This overall trend towards depletion is recorded in the mean and range plot (see *Figure 4.19*), although there is still considerable overlap of the two data ranges.

While there is some variability in the Al_2O_3 , SiO_2 , Si/Al and Ti/Al data throughout the sequence, there is no clear distinction between the grey clay and black shale samples (see *Figure 4.16*). In terms of bulk geochemical composition, the Briestoffer samples have lower Al_2O_3 and SiO_2 values (see *Figure 4.18*), and correspondingly higher CaCO_3 contents, than the Niveau Pacquier sediments. This lower aluminium content should theoretically artificially elevate enrichment factor values for redox-sensitive trace-elements. However, even with this effect the trace-element values are generally lower than the Niveau Pacquier sequence. The CaCO_3 content does show some low values in the grey clay but again does not distinguish greatly between the black shale and grey clay sediments (see *Figure 4.17*). The K/Al ratio does peak in some samples suggesting that there is some variation in clay mineral contents, but these high values do not correspond with major variations in trace-element data.

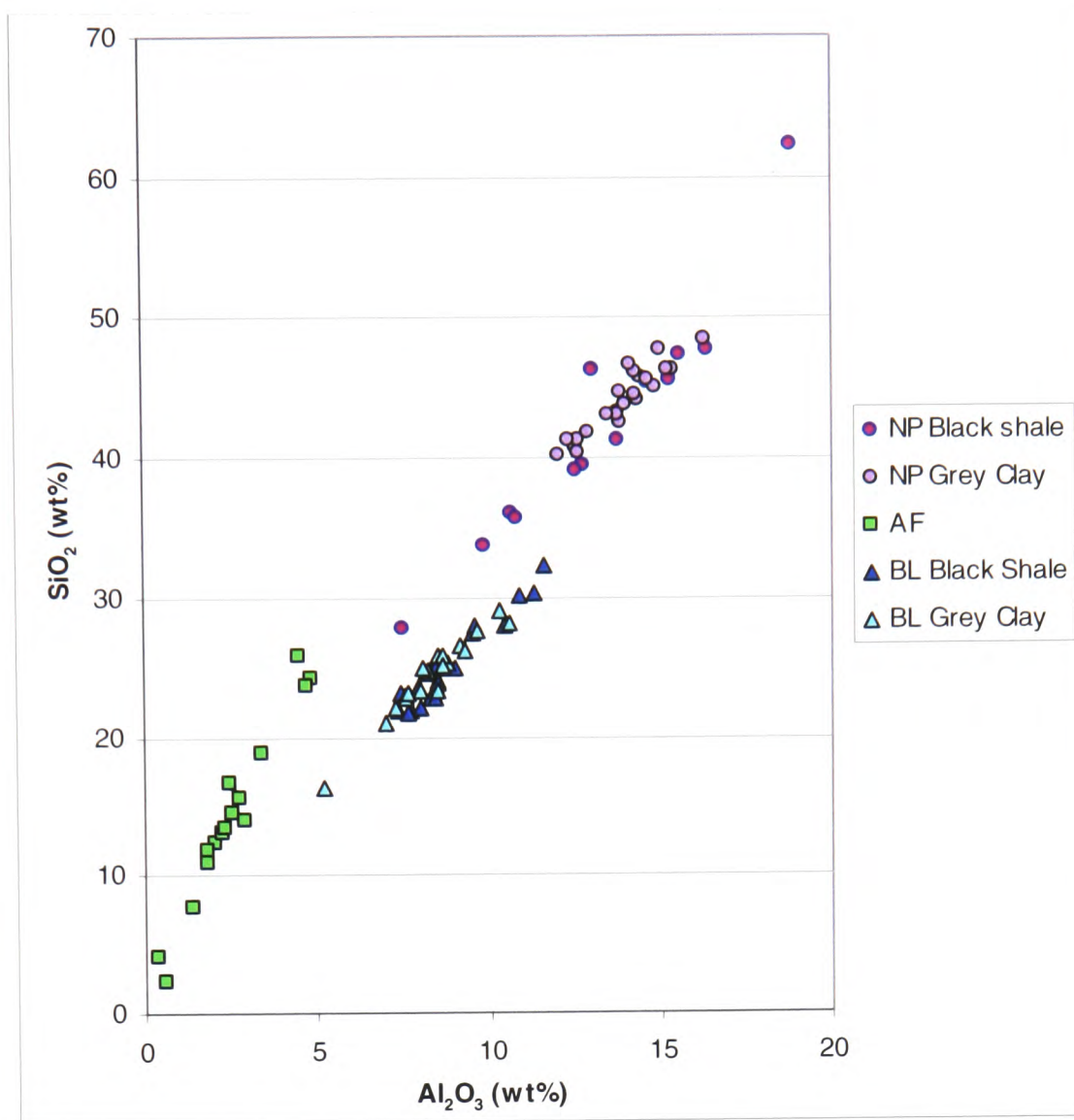


Figure 4.18: Plot of SiO₂ against Al₂O₃ for the Niveau Pacquier (NP), Briestroffer (BL) and Amma Fatma (AF) data sets.

Vanadium, nickel and manganese pass the Student's t-test (see Figure 4.19) suggesting that the grey clay and black shale data sets are statistically distinct groups. However, the plots of the mean and range (See Figure 4.20) reveal that all four elements show significant overlap between the values for the two data sets.

Element	Mean (Grey)	Variance	Mean (Black)	Variance	P two tail value
Mo	0.482	0.160	1.07	0.631	0.00379
V	0.545	0.0269	0.962	0.303	0.00187
Ni	0.551	0.0502	0.868	0.0815	0.000250
Mn	0.297	0.0037	0.234	0.0020	0.000306

Figure 4.19: The two-tailed Student's t-test data for the Briestroffer elemental enrichment factors. The test shows that all of the elements pass the t-test with a P value below the confidence limit of 0.05%.

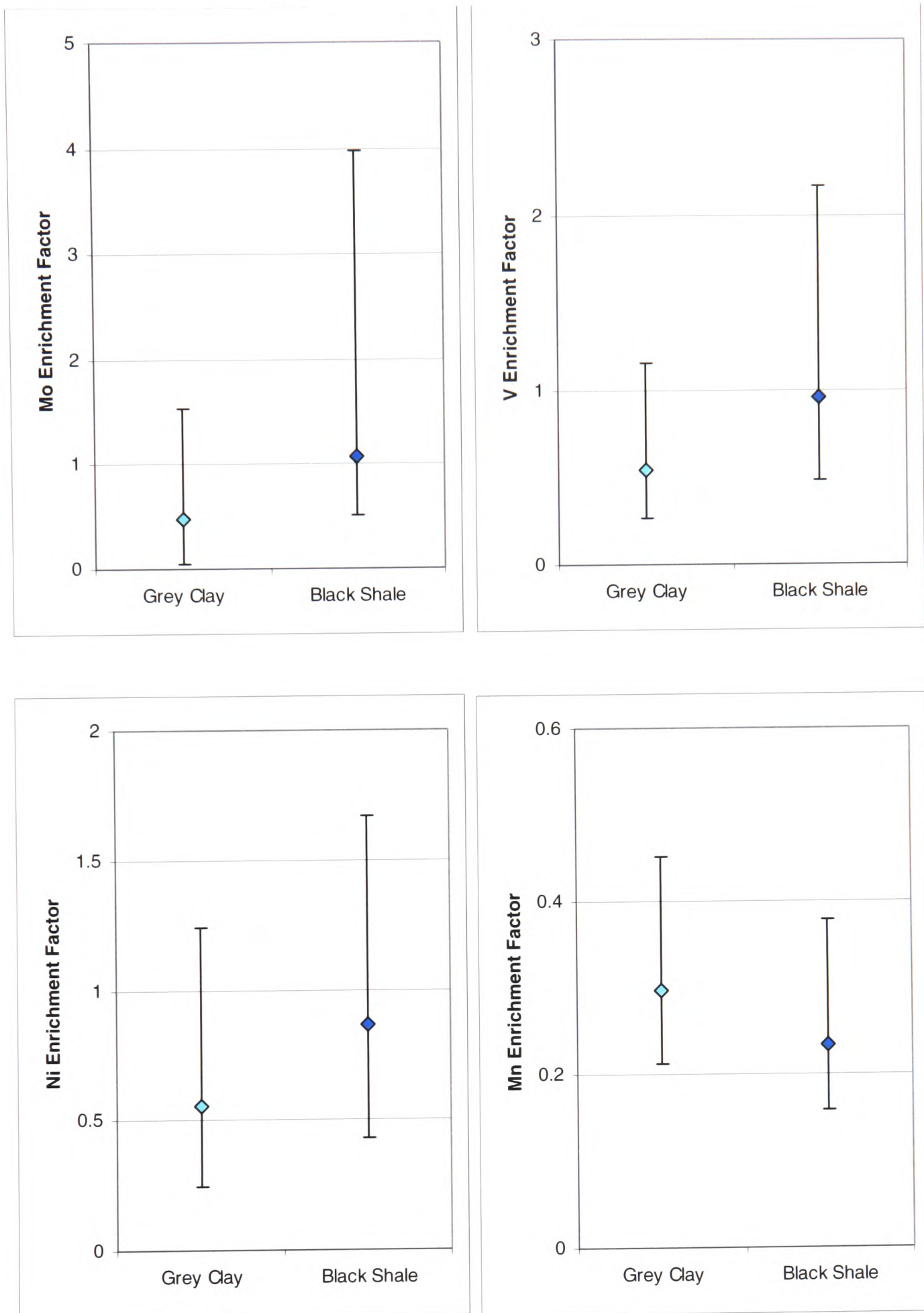


Figure 4.20: Plots of the mean and range of the Mo, V, Ni and Mn data for the grey clay sample (GC) set and the black shale (BS) sample set of the Briestoffer sequence.

The basis of our classification of oxic, dysoxic and anoxic facies relies on the sedimentology and faunal analysis and so the reliability of a geochemical proxy in this context can only be based on its correlation with these ‘fundamental’ indicators of palaeo-oxygenation. On this basis, it appears that while Mo in particular was a strong proxy within the Niveau Pacquier sequence, it is not always that reliable at recording the oxygen variations suggested by the sedimentology. Erickson and Helz (2000) suggested that the extent of Mo uptake is inversely proportional to the depth below the sediment/water interface at which the geochemical switch is reached. Adelson *et al.* (2001) also suggested that there may be a temporal link between Mo fixation and oxygen depletion and this is supported by Rimmer’s (2004) study that showed that Mo enrichment was only found under waters that were more permanently anoxic. This could explain the unreliability of the Mo data for this site, as the Briestroffer layers, like the thin black shale band in the Niveau Pacquier sequence, may represent short duration low-oxygen periods. If this is the case, the development of the geochemical switch within the sediment may not have reached the same extent as in the main Niveau Pacquier black shale band.

4.3.2.2 Trace Metal Ratios

Element	Mean (Grey)	Variance	Mean (Black)	Variance	P two tail value
Ua	0.0309	0.160	1.43	2.20	0.00019
U/Th	0.338	0.0052	0.614	0.0884	0.00023
V/Cr	1.43	0.0310	1.99	0.740	0.00566
Ni/Co	4.08	0.277	5.47	0.517	1.06E-08

Figure 4.21: The two-tailed Student’s t-test data for the Briestroffer element ratios favoured by Jones and Manning (1994). The test shows that for all ratios, the grey mud and black shale samples are statistically separate data sets with the Ua data being the most convincing.

All four of the elemental ratios recommended by Jones and Manning (1994) pass the Student’s t-test (see *Figure 4.21*), but again the plots of the mean and the range (see *Figure 4.22*) demonstrate that there is at least some overlap between the two data sets in each case.

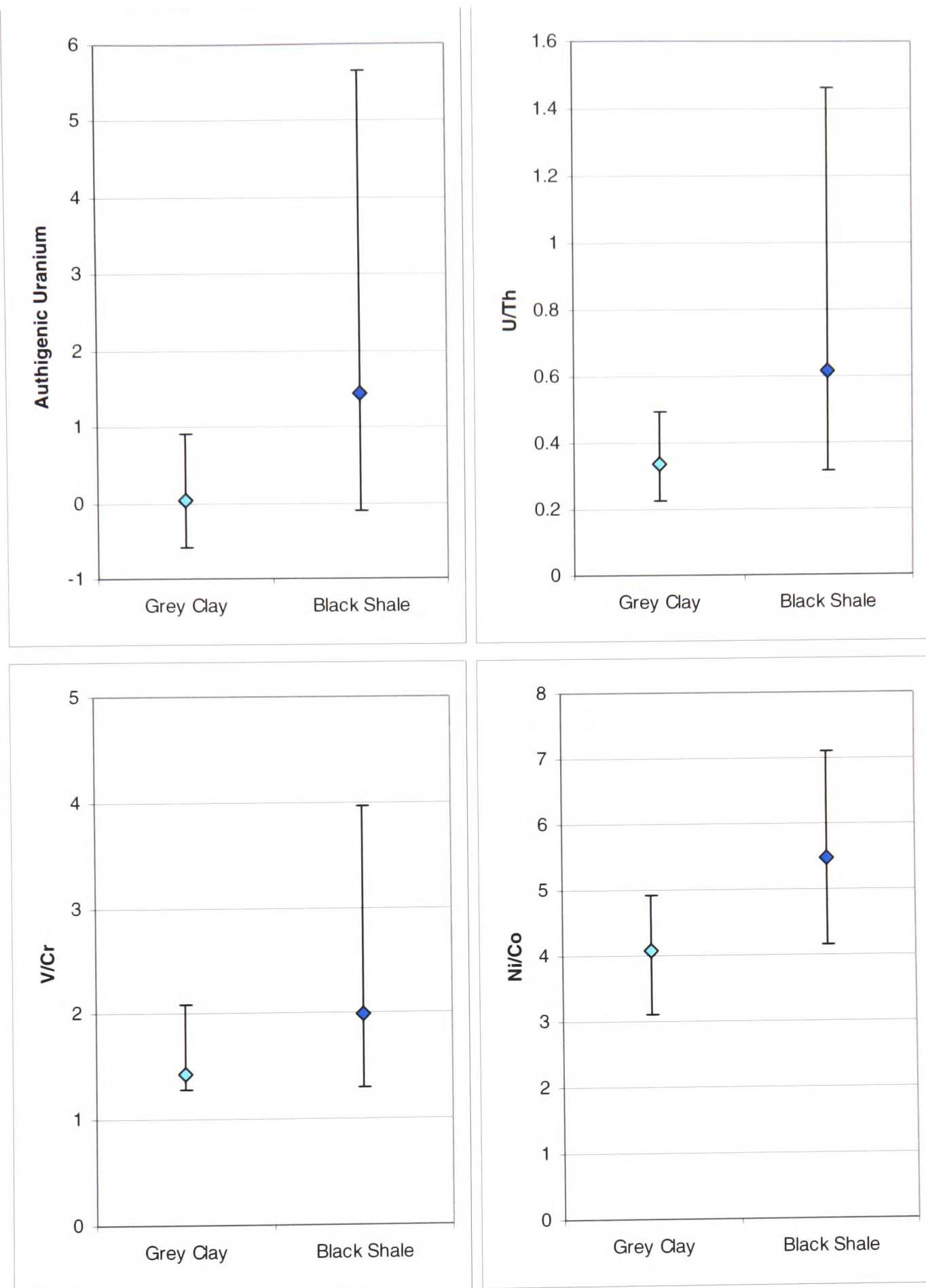


Figure 4.22: Plots of the mean and range of the U_a , U/Th , V/Cr and Ni/Co data for the grey shale sample set and the black shale sample set of the Briestoffer sequence.

The least overlap is observed with the U/Th ratio. However, the ranges of the data sets for V/Cr and Ni/Co , along with U/Th show interesting relationships with the boundaries proposed by Jones and Manning (1994) (see Figures 4.23 and 4.24).

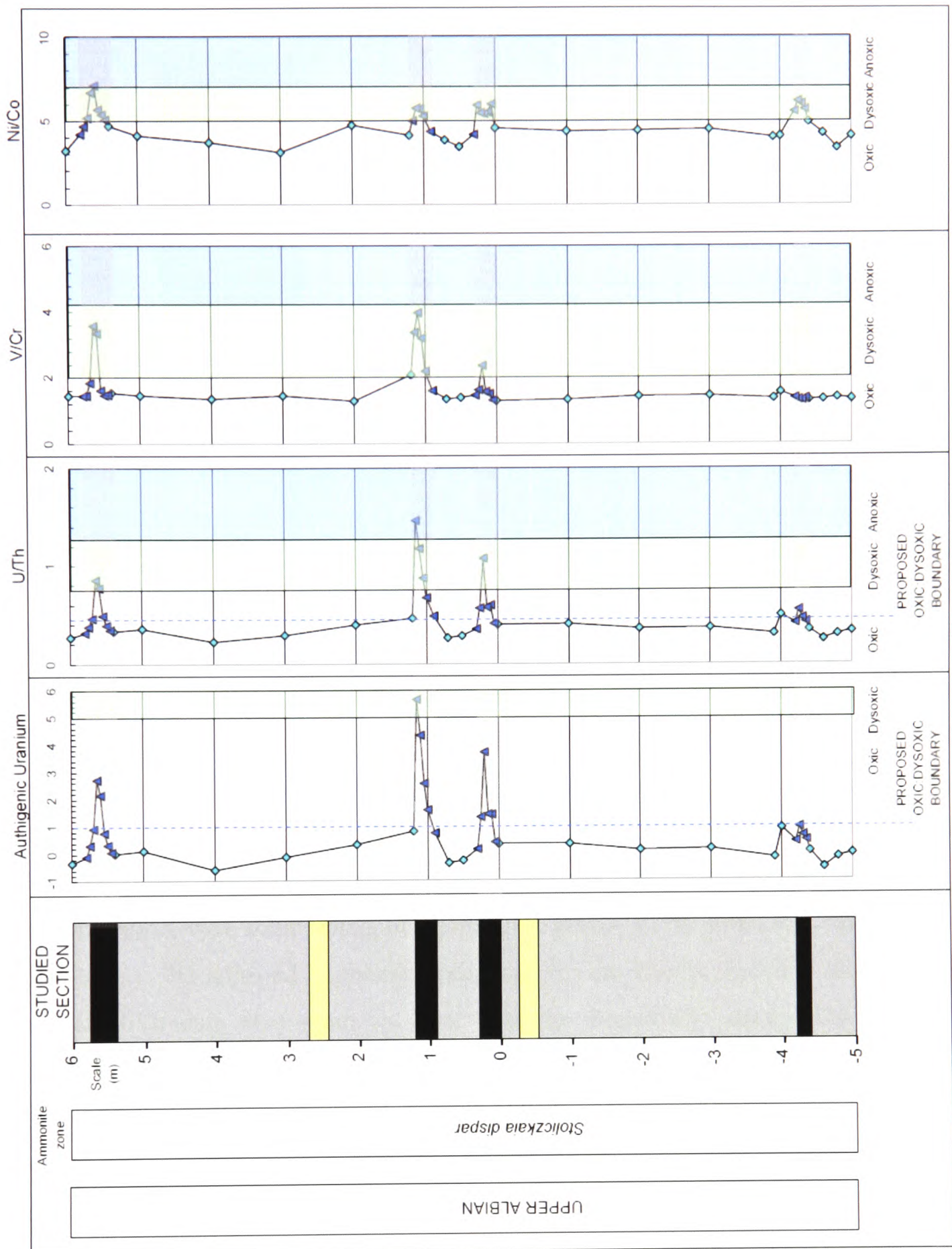


Figure 4.23: Plots of the ratios highlighted by Jones and Manning (1994), including their tentative boundaries for the oxic-dysoxic transition and the dysoxic-anoxic transition, for the Briestoffer sequence. The pale blue data points represent samples from the grey clay sequence, whereas the shaded dark blue points represent samples from the black shale layers in the Briestoffer sequence.

		OXIC	DYSOXIC	ANOXIC
Ua	Grey Clay	—		
	Black Shale	—		
U/Th	Grey Clay	—		
	Black Shale	—	—	
V/Cr	Grey Clay	—	—	
	Black Shale	—	—	
Ni/Co	Grey Clay	—	—	
	Black Shale		—	—

Figure 4.24: Summary of the Bristroffer environments of deposition suggested by the elemental ratios, based on the tentative boundaries set by Jones and Manning (1994).

While the Ua ratio plots with grey clays within the oxic range, and the black shales predominantly oxic, but just extending into dysoxic values, the other ratios suggest lower oxygen conditions for the black shale deposition. As with the Niveau Pacquier samples, the majority of the highest values of Ua and U/Th correspond with samples containing higher levels of phosphate (see Figure 4.17). In the U/Th, V/Cr and Ni/Co ratios, the grey clay data sets fit below the oxic-dysoxic boundary – in the case of V/Cr and Ni/Co the highest point of the range almost matches the suggested boundary. However, in all three of these ratios, the black shale data plot predominantly in the dysoxic region, with some points extending into anoxic in the U/Th and Ni/Co plots. Interestingly, the adjusted boundaries proposed for the Niveau Pacquier data for the Ua and U/Th data also seem to work with the Breistroffer data. The adjusted boundaries keep all of the grey clay data points in the oxic region, but in both cases the majority of the black shale data points, including the means, become dysoxic. As with the Niveau Pacquier sequence, the V/Cr data sets plot around the oxic : dysoxic boundary. However, in this sequence the Ni/Co data sets are focused around the oxic : dysoxic boundary whereas they are centred around the dysoxic : anoxic boundary in the Niveau Pacquier sequence. This suggests that while the other three ratios may differentiate between oxic and low oxygen conditions, the Ni/Co ratio may be able to differentiate between grades of dysoxia and anoxia.

Of the other ratios, the Ni/V, (Cu+Mo)/Zn and V/(V+Ni) data sets show little separation between the groups (see Figure 4.25).

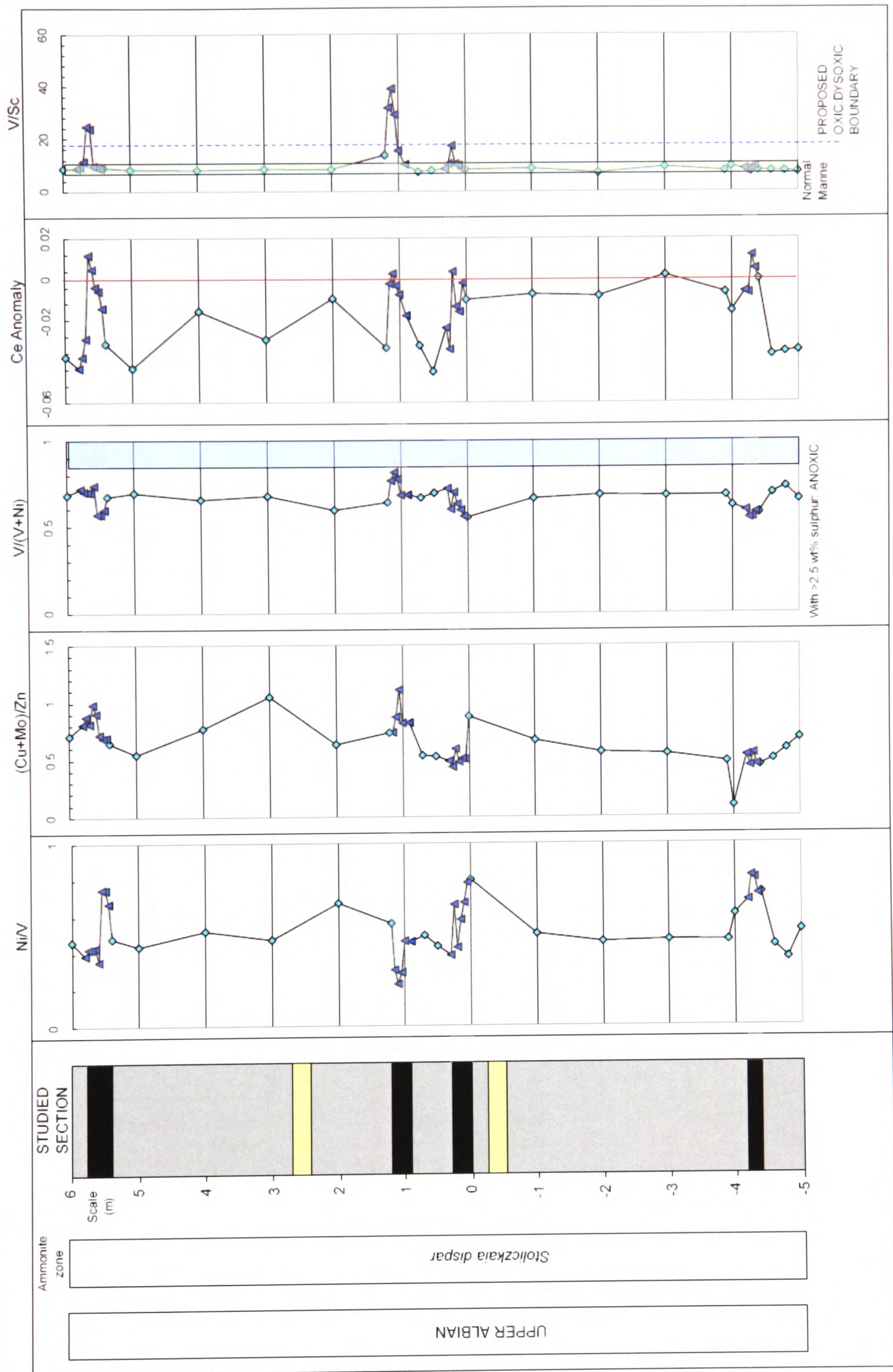


Figure 4.25: Plots of the other ratios including tentative boundaries for V/Sc (Kimura and Watanabe, 2001) and V/(V+Ni) (Schovsbo, 2001) for the Briestroffer sequence.

Only the Ce anomaly and the V/Sc data sets pass the Student's t-test (see *Figure 4.26*), suggesting that the data sets are statistically distinct, and in these cases the overlap of the data ranges is significant (see *Figure 4.27*), meaning that the proxies are unreliable

Element	Mean (Grey)	Variance	Mean (Black)	Variance	P two tail value
Ni/V	0.522	0.0121	0.543	0.0347	0.650
(Cu+Mo)/Zn	0.596	0.0344	0.666	0.0372	0.238
V/(V+Ni)	0.660	0.0019	0.657	0.0064	0.887
Ce anomaly	-0.0226	0.0002	-0.0099	0.0002	0.0107
V/Sc	8.36	2.05	14.3	81.0	0.00514

Figure 4.26: The two-tailed Student's t-test data for the other Briestoffer element ratios. The test shows that only the (Cu+Mo)/Zn and V/Sc ratios provide differentiation between the two data sets.

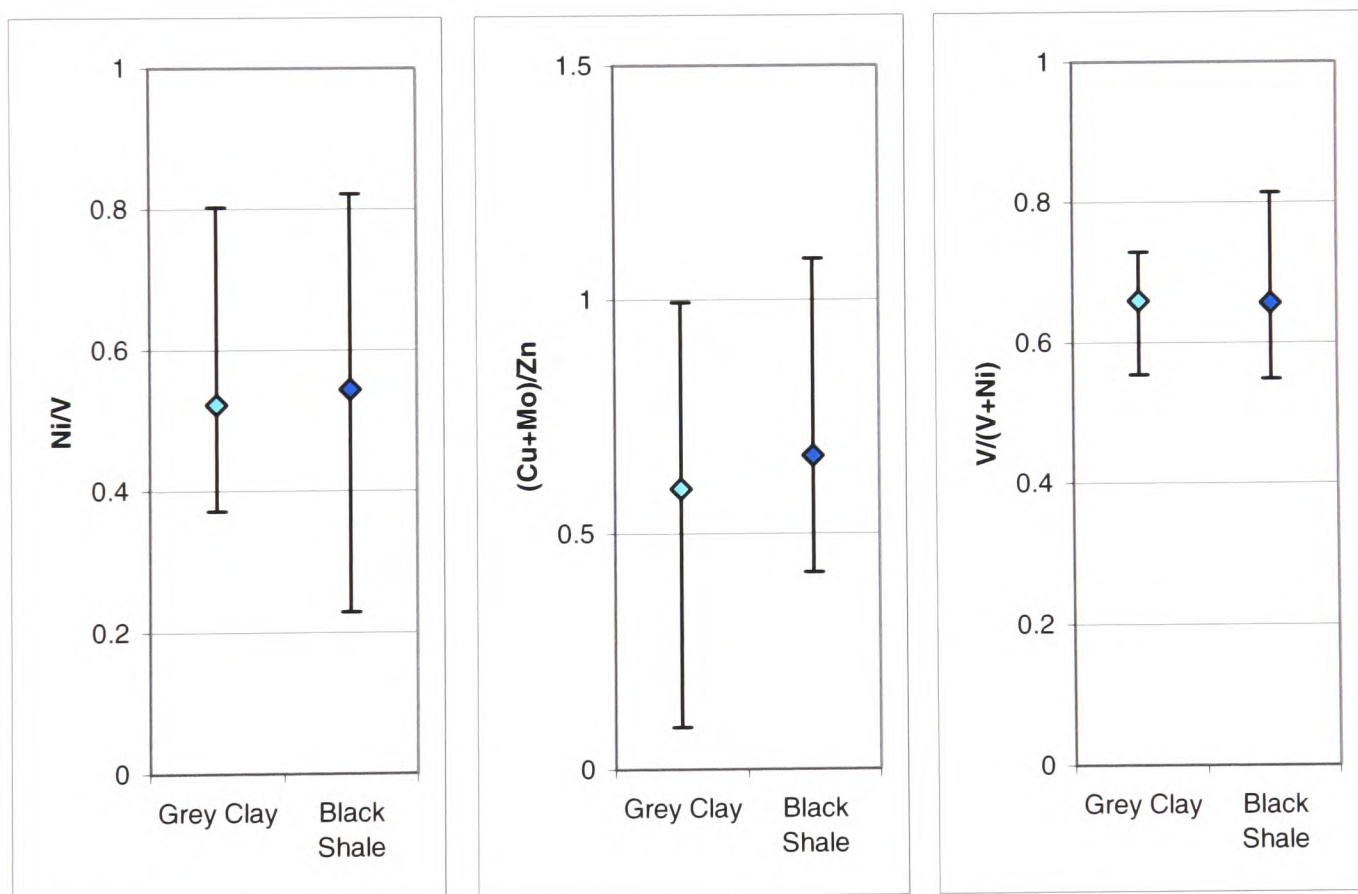


Figure 4.27 (a): Mean and range plots the Ni/V, (Cu+Mo)/Zn and V/(V+Ni) element ratio data sets from the Briestoffer sequence

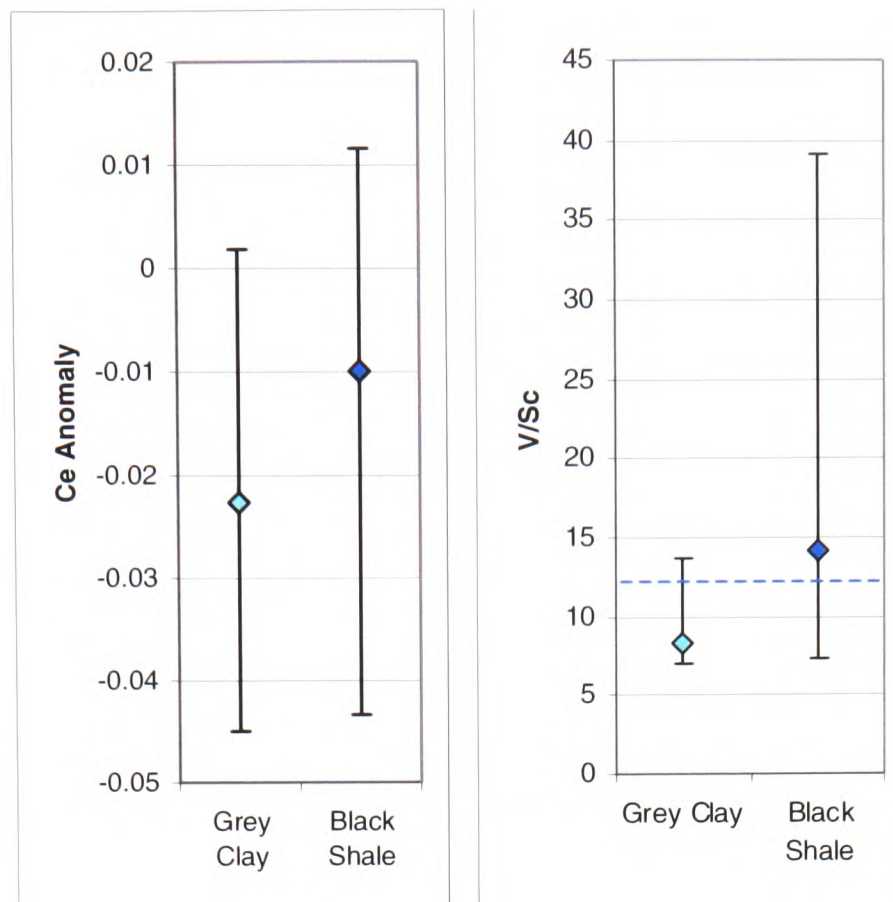


Figure 4.27 (b): Mean and range plots for the cerium anomaly and V/Sc elemental ratio data sets from the Briestoffer sequence

However, while there is total overlap between the data sets for V/Sc, it is worth noting that the boundary proposed for the Niveau Pacquier sample set at a V/Sc value of 14 also seems to neatly categorise the Breistroffer grey clays.

4.3.3 Folkestone Gault Clay

4.3.3.1 Trace Metal Enrichments

The late Albian Gault Clay sequence in Folkestone consists of grey bioturbated clays containing a diverse benthos (see *Figure 2.28*). There are indications of varying oxygenation levels between upper dysoxic and oxic environments, and so this is an important site for investigation the sensitivity of geochemical proxies to only slight palaeo-oxygen depletion. All of the Folkestone samples show depletion of Mo, V and Ni relative to average shale (see *Figure 4.28*) which highlights two problems associated with this approach:

- Firstly, this highlights the issues with assuming average shale composition for normal marine conditions – if, as these results would appear to suggest, the Gault Clay was laid down under oxygenated conditions, the data should plot very close to unity. Relative depletion in these elements suggests that even if the sediment was laid down in ‘normal’ conditions, the general composition

was different to that of average shale. The Gault Clay composition is significantly different to average shale with higher aluminium contents and lower trace-metal contents (see *Figure 4.29*).

- Secondly, in terms of faunal and sedimentological classification, there is a suggestion that the Folkestone Gault Clay falls within the Upper Dysoxic range and so should ideally register slight enrichment in these elements, rather than depletion. If this classification of the Gault Clay is correct, it suggests that these trace metal proxies are not sensitive to environments with only slight oxygen depletion.

Morford and Emerson (1999) suggested that Mo may be slightly enriched under oxic conditions due to its association with Mn oxides, but that as the environment becomes more reducing, Mo and V are mobilized and are therefore depleted in the sediments. They suggested that in environments where oxygen penetrates the sediment to a depth of less than 1 cm, the sediments will be reducing enough to be enriched in U, but would record depletion in Mo, Mn and V, and that only strong oxygen depletion would allow enrichment in Mo and V to occur. Francois (1988) was the first to suggest that dissolved sulphide may be required before major Mo enrichment can occur. This may explain the results observed for the Folkestone samples as while Mo and V record depletion, the Mn data also shows relatively strong depletion compared to the other study sites, which should be indicative of quite strong oxygen depletion. These contradicting results only serve to highlight the unsuitability of these proxies for recognising environments with only slight oxygen depletion. The Folkestone Gault Clay has the highest aluminium content (see *Figure 4.29*) of all four sites with values that are significantly higher than 'average shale'. This would be expected to suppress the Enrichment Factor values but the raw data shows that the trace-elements contents are significantly lower than average shale.

The bulk geochemistry of the samples is relatively consistent throughout the sequence although the calcium carbonate content does increase towards the top of the section (see *Figure 4.30*). There is a phosphate peak at 0.45 m which corresponds to the one of the nodule beds in the sequence but this is not associated with a variation in trace-metal enrichment.

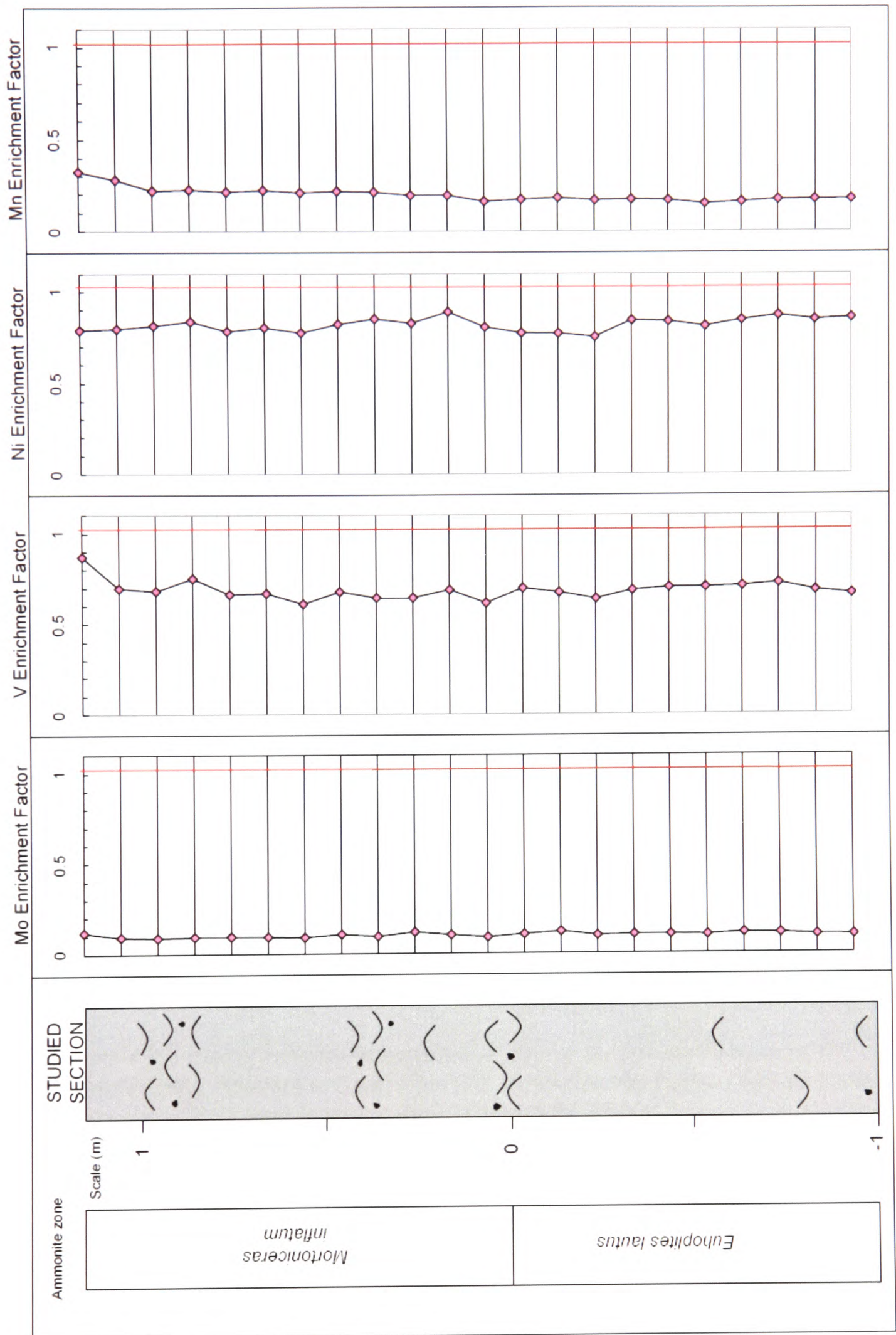


Figure 4.28: Enrichment factor data for Mo, V, Ni and Mn from the Folkestone Gault Clay

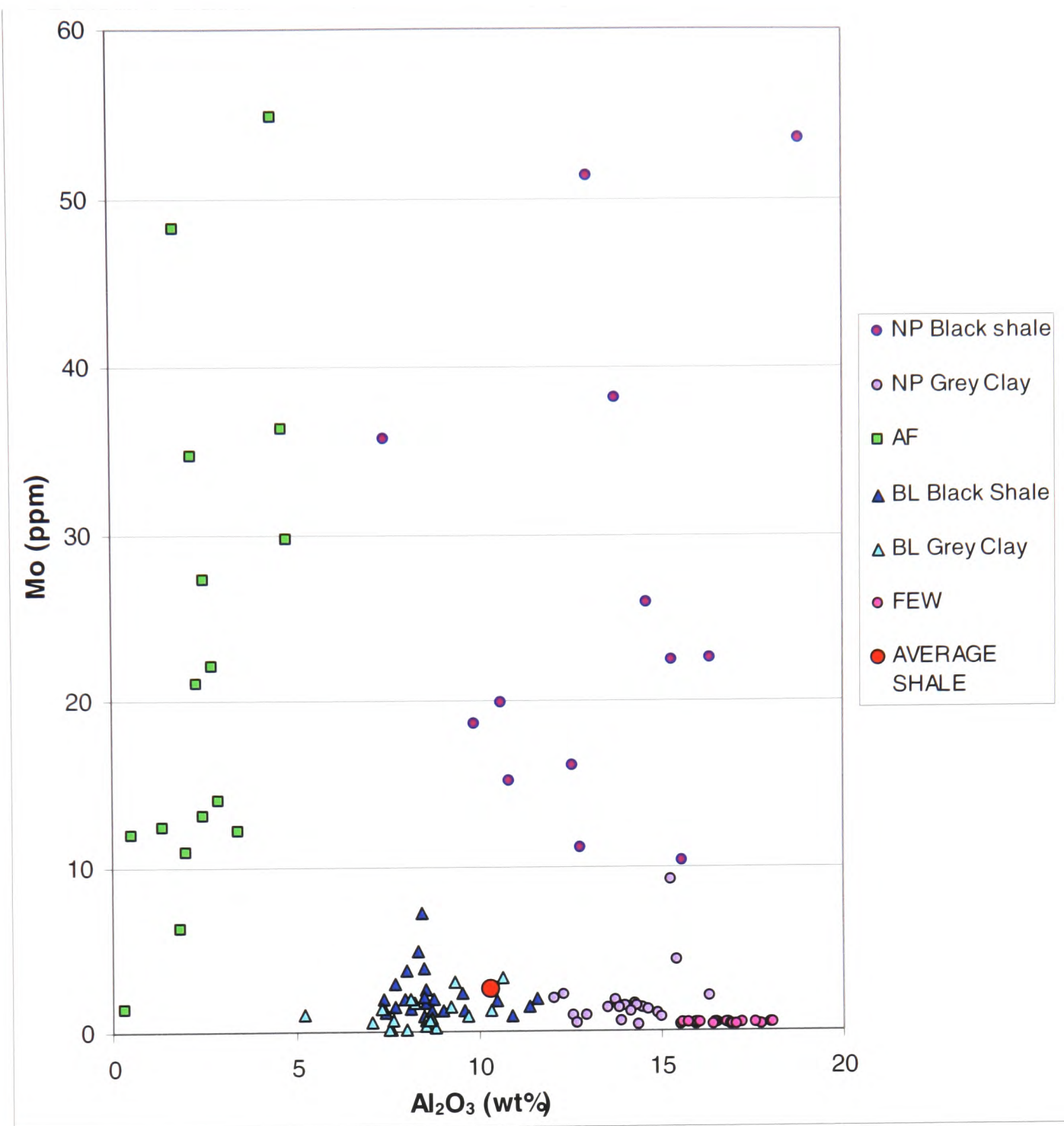
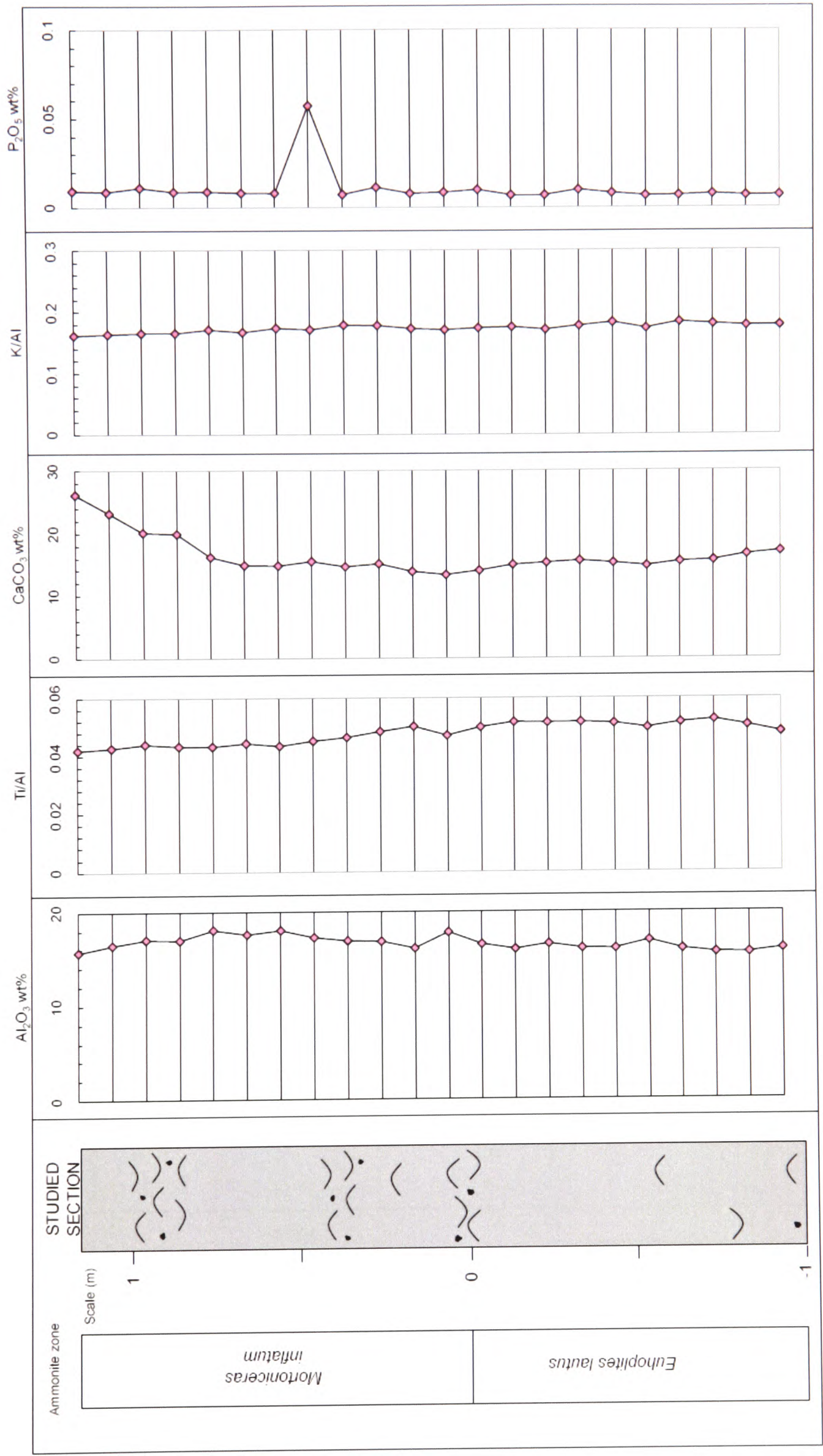


Figure 4.29: Plot of molybdenum against Al_2O_3 for the Niveau Pacquier (NP), Briestroffer (BL), Folkestone Gault Clay (FEW), and Amma Fatma (AF) data sets, and 'average shale' (Wedepohl, 1971).

Figure 4.30: Major elements (as Al_2O_3 wt%, $CaCO_3$ wt% and P_2O_5 wt%) and element ratios (Ti/Al, K/Al) for the Folkestone Gault Clay section. The pale blue data points represent samples from the grey clay sequence, whereas the shaded dark blue points represent samples from the black shale layers in the Briestroffer sequence (on next page).



4.3.3.2 Trace Metal Ratios

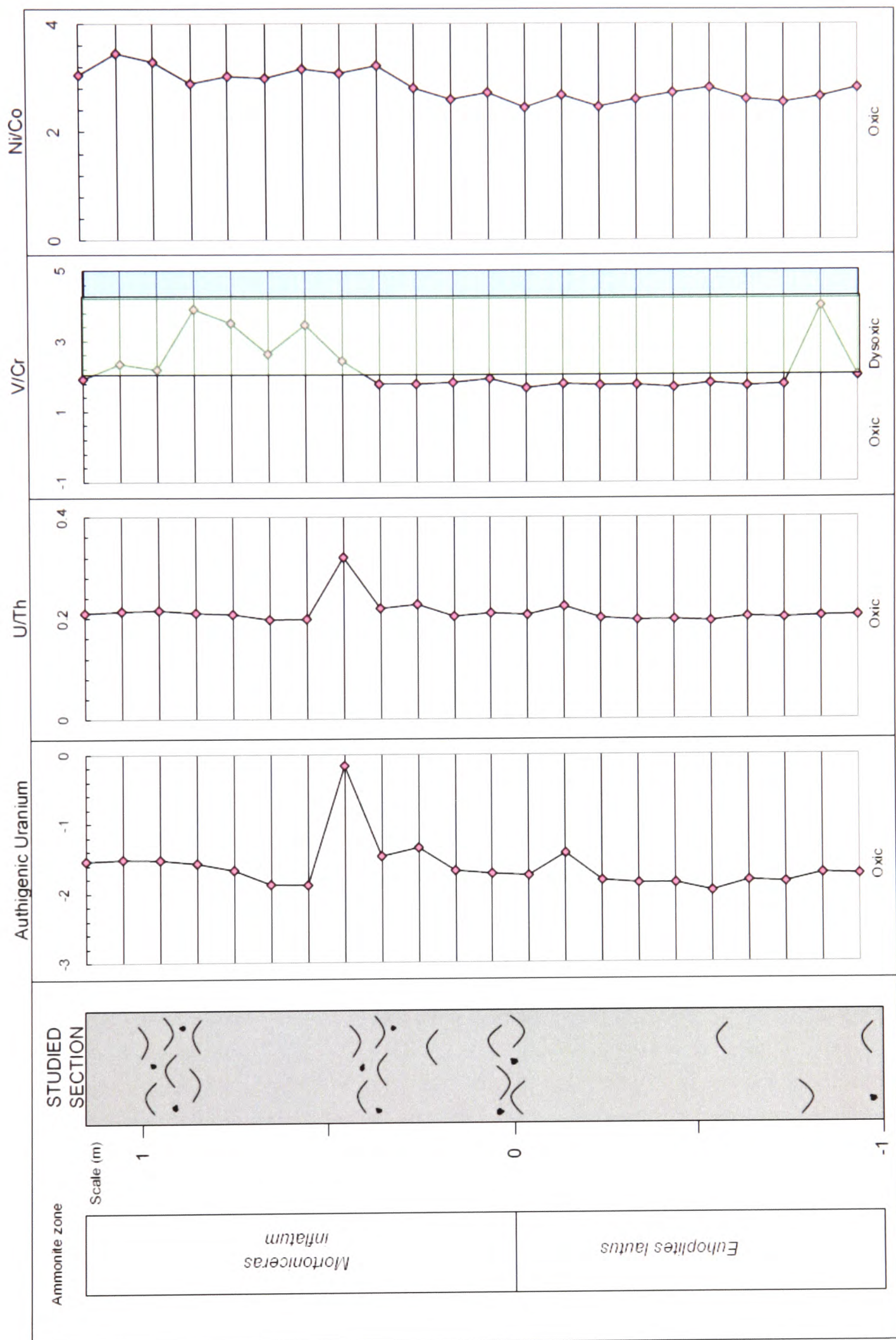


Figure 4.31: Elemental ratio data for the Folkestone Gault Clay, using oxic-dysoxic and dysoxic-anoxic boundaries tentatively suggested by Jones and Manning (1994).

Of the ratios which were assigned tentative boundaries by Jones and Manning (1994), the Ua, U/Th and Ni/Co data plots firmly within the suggested oxic zone with little variation through the sequence (see *Figure 4.31*).

Ua and U/Th both peak in sample +45 cm but as this is not reflected in any other proxy and is associated with a peak in phosphate content (see *Figure 4.30*). These elevated values therefore appear to be an artefact of increased uranium enrichment in association with phosphate material. The V/Cr ratio does appear to show some differentiation with samples -75 cm to +30 cm plotting within the oxic range and all others plotting within the dysoxic range. However, this is not reflected in the other elemental data or the sedimentology. The Ni/V ratio appears to be higher than the previous sites, and this does correlate with the idea of the Gault Clay representing an upper dysoxic or oxic environment, compared to the dysoxic and anoxic setting of the French sites (see *Figure 4.32*).

	OXIC	DYSOXIC	ANOXIC
Ua	—		
U/Th	—		
V/Cr	—	—	
Ni/Co	—		

Figure 4.32: Summary of the Folkestone Gault Clay environment of deposition suggested by the elemental ratios, based on the tentative boundaries set by Jones and Manning (1994).

The (Cu+Mo)/Zn results are similar to the other sites whereas the V/(V+Ni) appears to be higher, with many points plotting within Schovsbo's (2001) anoxic zone (see *Figure 4.33*). However there is a positive Ce anomaly, indicative of oxygenated waters. This range of contradictory results again highlights the limited application of trace metal proxies for sites representing slight oxygen depletion.

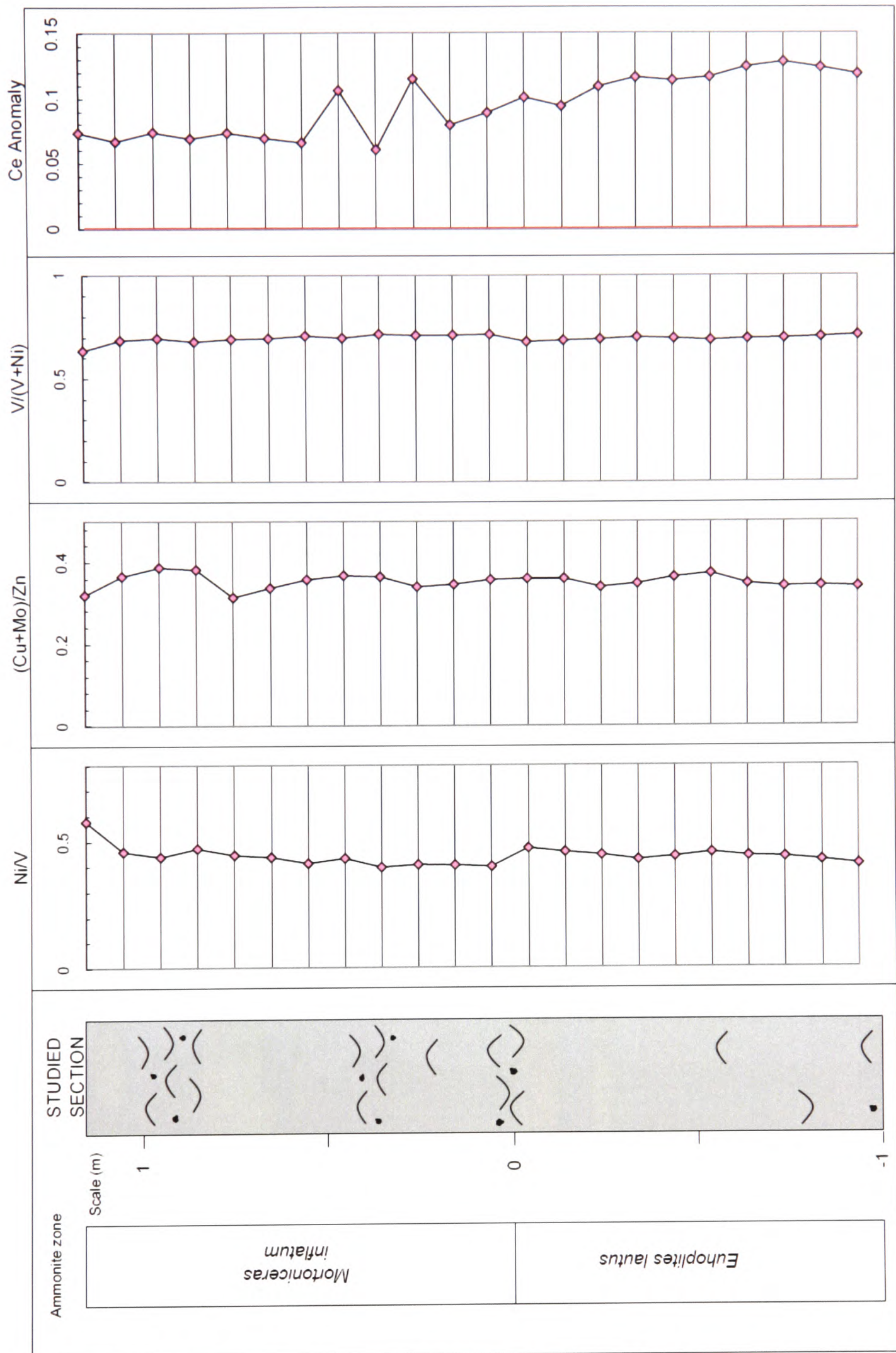


Figure 4.33: Plots of the Ni/V, (Cu+Mo)/Zn, V/(V+Ni) and the Cerium anomaly for the Folkestone Gault Clay sequence.

4.3.4 Amma Fatma

4.3.4.1 Trace metal concentrations

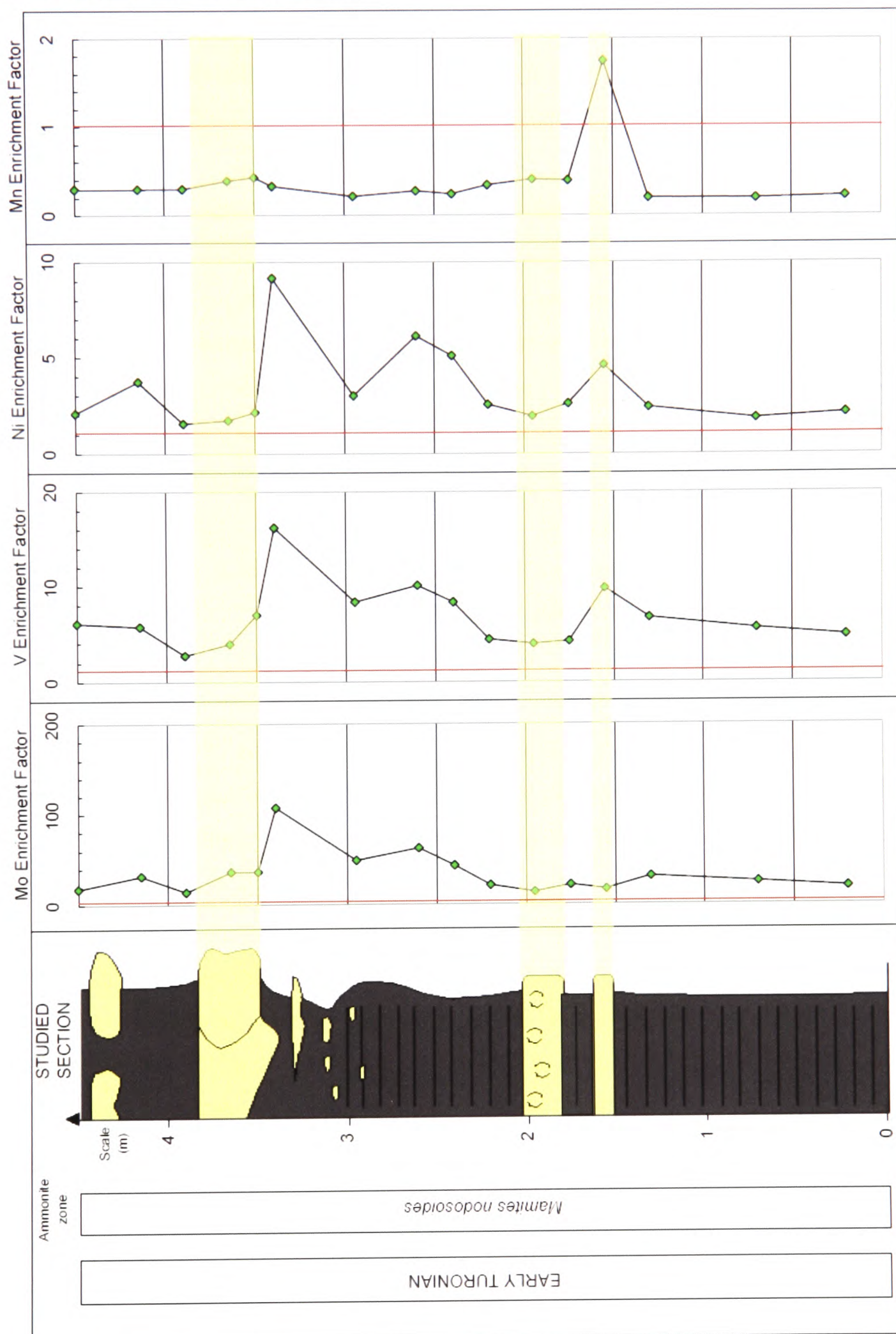


Figure 4.34: Enrichment factors for Mo, V, Ni and Mn from the Amma Fatma sequence.

The Moroccan Amma Fatma sediments relate to the Early Turonian Oceanic Anoxic Event and this is reflected by a sequence of laminated black shales, interspersed with bioturbated limestones containing low diversity faunas (see *Figure 2.39*). The sediments were deposited in the north west Africa upwelling zone and include some very organic-rich horizons which correspond to very low oxygenation levels.

All samples show strong enrichment in V, Ni and Mo compared to average shale (see *Figure 4.34*) suggesting a generally low oxygen environment, with a strong peak in these elements for the pale sediment of the sample from 3.4 m. A similar peak is seen in V and Ni for the sample from 1.55 m, whereas Mo records no strong enrichment. In contrast, this sample shows strong enrichment in Mn which would suggest oxygenated waters. A closer look at the data reveals that this sample actually has relatively low values for V, Ni, Mo and Mn compared to the other samples. In fact this strong contradictory signal is due to the very low Al content of the carbonate-rich layer (see *Figures 4.35 and 4.36*) which skews the calculation of element/Al and enrichment factors. The low aluminium content also creates anomalously high Si/Al and Ti/Al peaks as a result of this 'closed sum effect'.

The fact that these samples show much stronger enrichment of Mo, V and Ni compared to even the black shale horizons in the previous sites, should indicate that much lower oxygen conditions occurred during the deposition of this sequence. However as the sequence is much higher in calcium carbonate and lower in aluminium than the other sites (see *Figure 4.18*) the Enrichment Factor data can not be used to compare sites. Looking at the raw data instead reveals that while the aluminium content is lower for the Amma Fatma sediments, the trace-metal contents are roughly equivalent to the Niveau Pacquier black shale samples. This is evident, for example, from a plot of molybdenum against aluminium for each data set (see *Figure 4.29*).

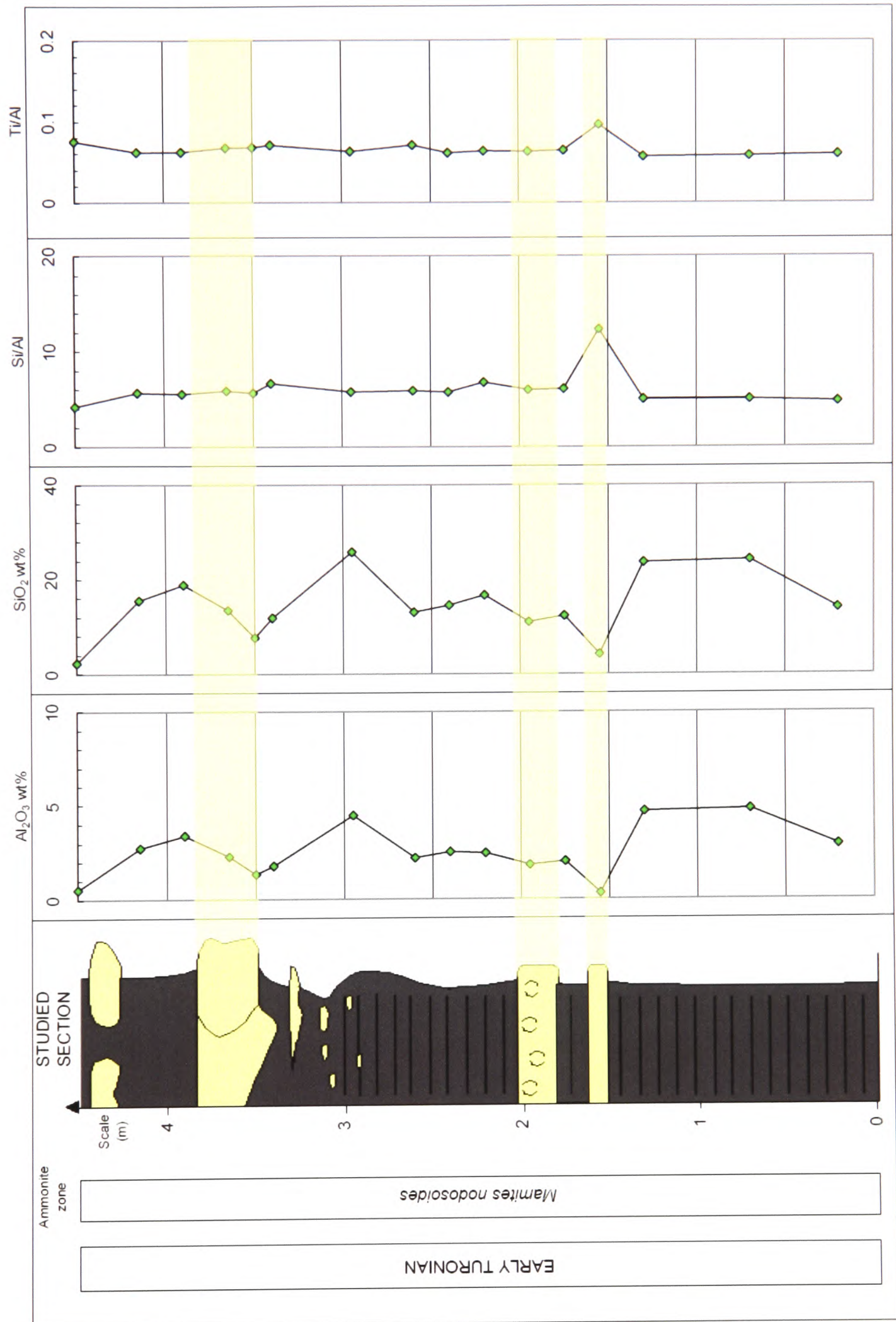


Figure 4.35: Major elements (Al_2O_3 wt% and SiO_2 wt%) and element ratios (Si/Al and Ti/Al) for the Amma Fatma section.

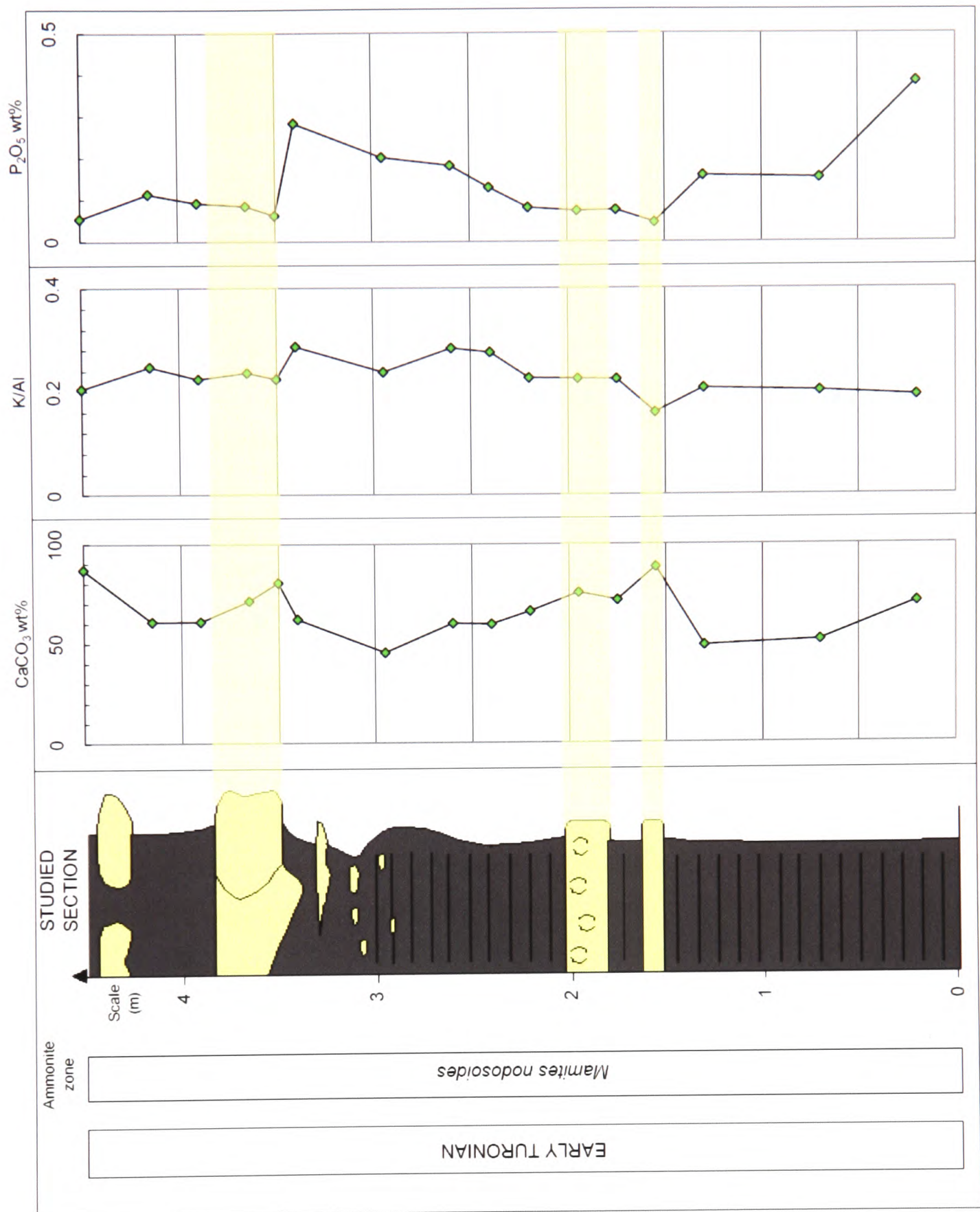


Figure 4.36: Major elements (as $CaCO_3$ wt% and P_2O_5 wt%) and element ratios (K/Al) for the Amma Fatma section.

The palaeo-oxidation conditions implied by the trace-metal values are not necessarily reflected in the sedimentology as the sequence includes bioturbated limestones with higher biodiversity which also appear to record strong oxygen depletion signals in the geochemistry. Passier *et al.* (1996) noted similar discrepancies and suggested that this

may be due to later diagenetic pyrite formation in pale, oxygenated sediments in close association with black shales. They also suggested that sulphides diffusing out of sapropels may also precipitate or co-precipitate redox sensitive and sulphide-forming trace metals causing diagenetic enrichment in formerly oxic sediments. The Mn depletion, however, is of a similar level to that observed in the French sites, which suggests that this proxy provides little definition between grades of dysoxic and anoxic facies.

4.3.4.2 Trace metal ratios

Again, the tentative boundaries set by Jones and Manning (1994) appear to be contradictory (see *Figure 4.37 and 4.38*). Interestingly, the two uranium-based proxies give the best example of this – the authigenic uranium data plots within the oxic and dysoxic zones allocated by Jones and Manning (1994) whereas the U/Th data all plots within the assigned anoxic zone. This is a common pattern with all of the sites – Ua consistently suggests more oxygenated regimes than the U/Th ratio. In this site, the boundaries suggested for the V/Cr and Ni/Co ratios also assign the majority of samples as within the anoxic facies. Using the proposed boundary of a Ua value of 1 does classify the majority of samples (apart from the sample from 1.55 m which appears to have very low terrestrial input which would also skew the uranium-based proxies) as ‘dysoxic’.

The Ni/V ratio is much lower than recorded for the other sites, and the V/(V+Ni) ratio values are higher, both supporting greater oxygen depletion (see *Figure 4.39*). However, the (Cu+Mo)/Zn ratio plots within the same range as the Niveau Pacquier and Briestoffer data, which suggests that this ratio is of limited use, even for recognising sediments laid down under strongly reducing conditions. The Ce data generally plots as a positive anomaly, within the same range as the Niveau Pacquier data which would correlate with anoxic deposition conditions.

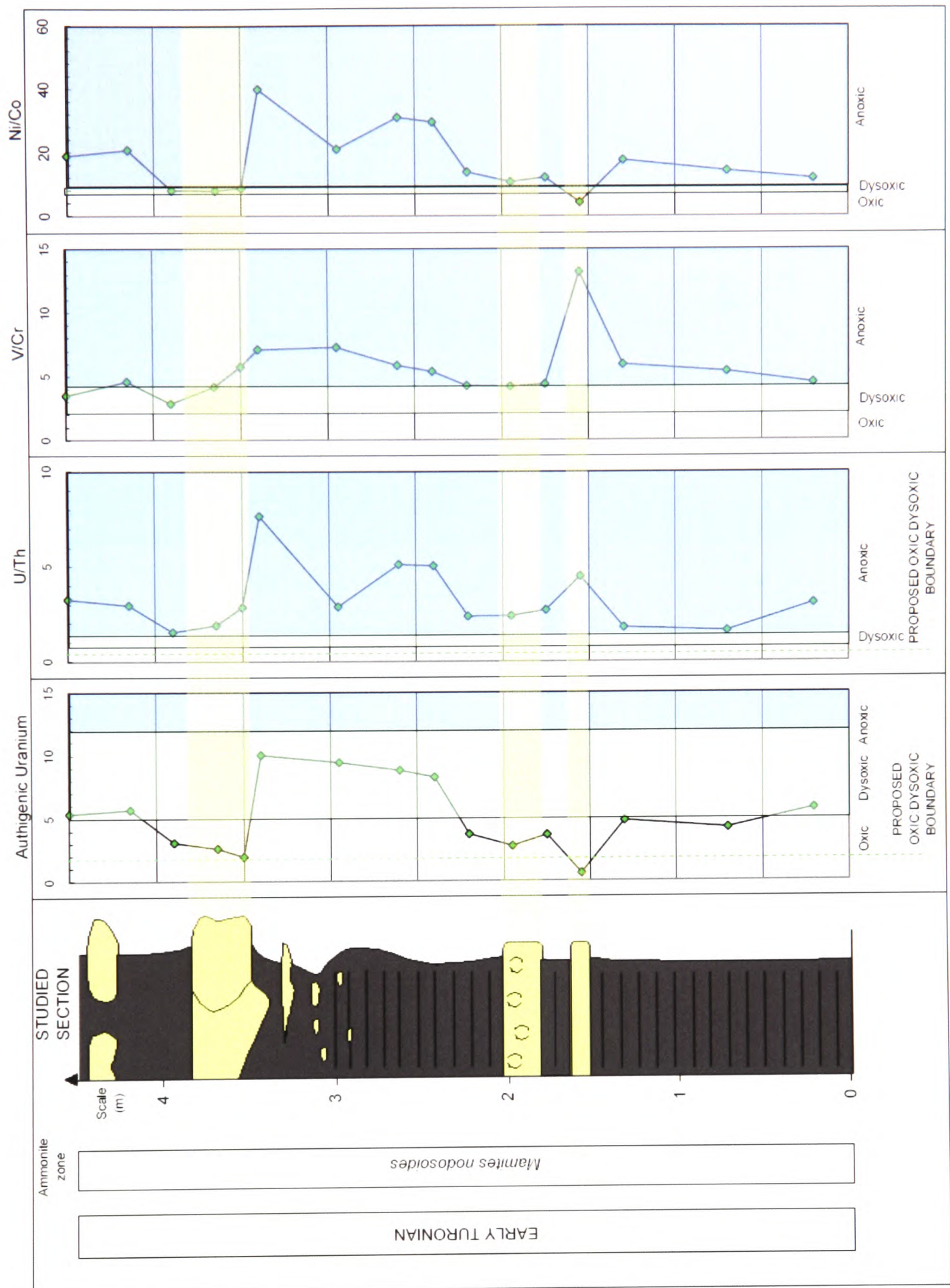


Figure 4.37: Elemental ratio data for the Amma Fatma sequence, using oxic-dysoxic and dysoxic-anoxic boundaries tentatively suggested by Jones and Manning (1994).

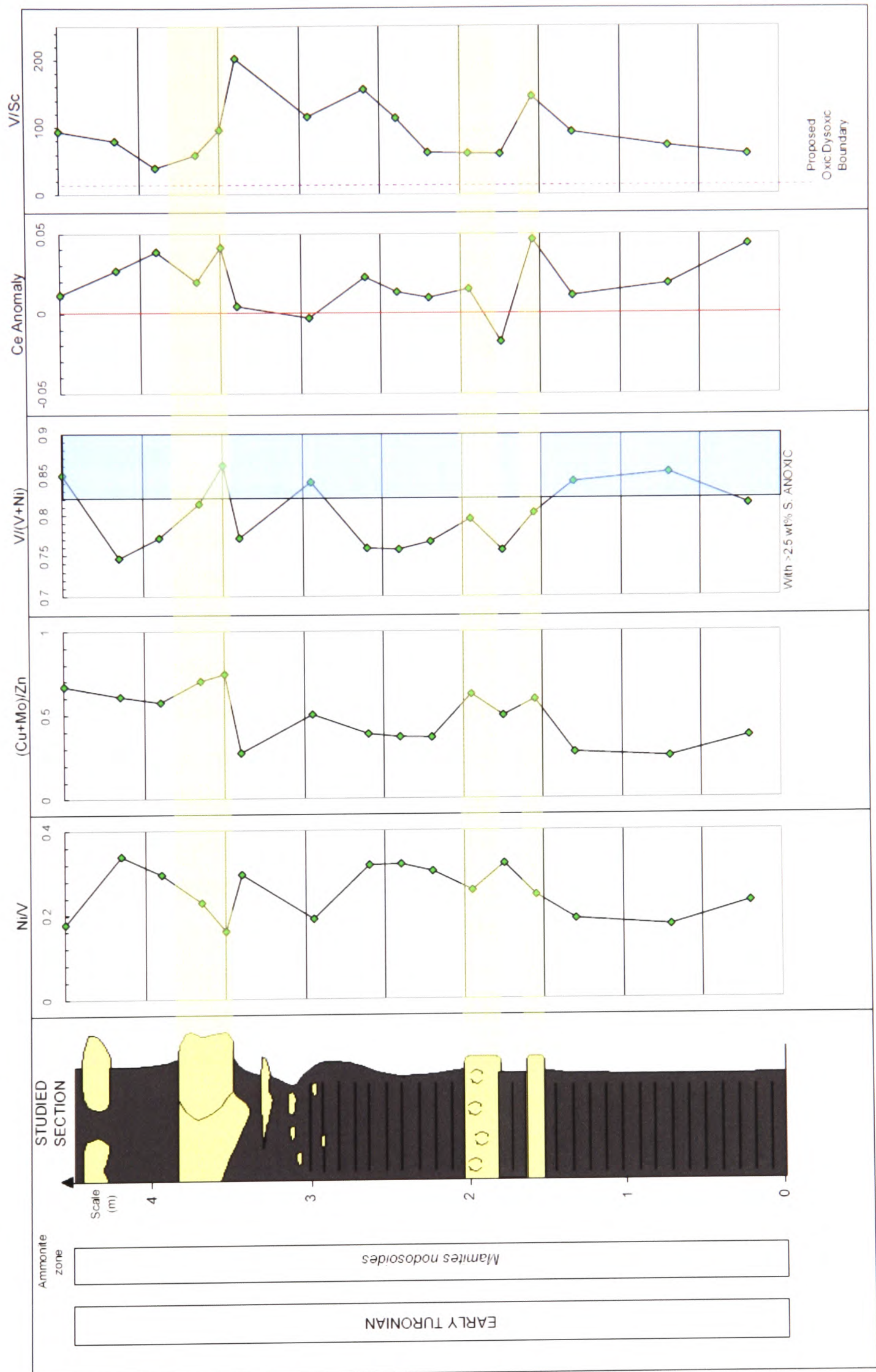


Figure 4.38: Elemental ratio data for the Amma Fatma sequence using the tentative boundary proposed by Kimura and Watanabe (2001) for the V/(V+Ni) ratio.

	OXIC	DYSOXIC	ANOXIC
Ua	—	—	
U/Th			—
V/Cr		—	—
Ni/Co	—	—	—

Figure 4.39: Summary of the Amma Fatma environment of deposition suggested by the elemental ratios, based on the tentative boundaries set by Jones and Manning (1994).

4.4 Conclusions

4.4.1 Trace metal enrichments:

- Of the element enrichment factors, Mo gives the strongest definition in the Niveau Pacquier sequence. However, the signal is more confused in the Briestroffer sequence, which suggests that strong Mo enrichment may only occur under relatively permanent anoxia.
- The Amma Fatma sequence questions the reliability of elemental data as there is evidence that remobilization may have occurred, creating strong enrichment signals in surrounding sediments.
- There are problems with using element enrichment factors to classify environments where aluminium values are distinctly different from average shale values. This is highlighted by the Folkestone data where all elements recorded depletion relative to average shale, and in the Amma Fatma sequence, where low detrital content clearly skews the enrichment factor data. In the use of enrichment factors or trace metal excess, there needs to be awareness of the problems associated with the closed sum effect and variations in bulk geochemistry between sites.

4.4.2 Trace metal ratios:

- The elemental ratios favoured by Jones and Manning (1994) show the greatest degree of separation between palaeo-oxygenation data sets and perform much better than the other elemental ratios.
- It appears that the geochemical boundaries between oxic-dysoxic and dysoxic-anoxic conditions may be site specific and that the actual values

of these ratios may only be useful in internal comparison. The boundaries proposed by Jones and Manning (1994) for these four ratios produced conflicting results. In general, there was some agreement between the palaeo-oxygenation conditions indicated by Ua and V/Cr, but these consistently indicated more oxygenated environments than U/Th and Ni/Co. In turn, Ni/Co consistently plotted in a field of stronger oxygen depletion relative to the U/Th data.

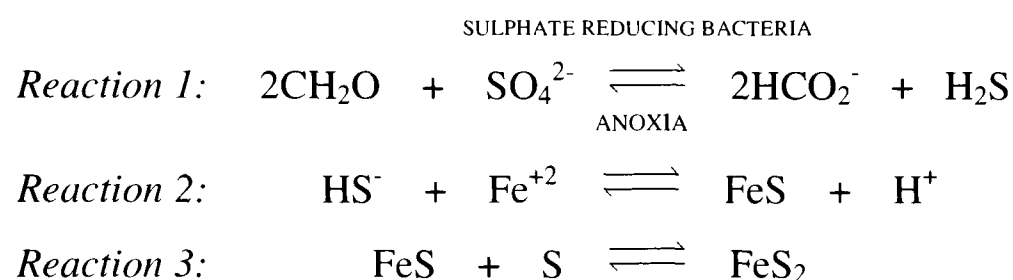
- The boundaries proposed by Jones and Manning (1994) for V/Cr and Ni/Co do seem to divide the Niveau Pacquier and Briestroffer data sets efficiently, and newly proposed boundaries for authigenic uranium and U/Th seem to fit both of these sites from the Vocontian Basin in France. This again suggests that boundaries may need to be adjusted between different basinal systems.
- The sites demonstrating the extremes of the scale of palaeo-oxygenation only serve to highlight the problems with these assigned boundaries - only Ni/Co suggested deposition under upper dysoxic conditions for the Folkestone Gault Clay, whereas the other three ratios plotted firmly within the oxic zone. In the strong low-oxygen setting of Amma Fatma, while the other three ratios showed indication of anoxia, Ua plotted between oxic and dysoxic conditions.
- Of the remaining ratios, V/Sc appears to have promise, but more work needs to be done to define boundaries. The other ratios investigated do show slight trends under lower oxygen conditions, for example, Ni/V does consistently appear to show some depletion, (Cu+Mo)/Zn does exhibit a greater range, and V/(V+Ni) does show a slight increase, but statistically these trends are not reliable. The Ce anomaly appears to show little correlation with palaeo-oxygenation.

CHAPTER 5: Fe-S-C SYSTEMATICS

5.1 Introduction

5.1.1 Introduction to Pyrite Formation

Under different bottom-water redox conditions, the fates of iron, sulphur and carbon are deeply intertwined. Under anoxic conditions microbial sulphate reduction occurs using organic matter as a food source and dissolved sulphate as an oxidizing agent – the sulphate acts as an electron acceptor and in turn is reduced to form sulphide (see *Reaction 1*) (Leventhal, 1982). This dissolved sulphide then reacts with iron minerals to form iron sulphides. Iron monosulphides (FeS) such as mackinawite and greigite form first (see *Reaction 2*), but are later converted to pyrite (FeS₂) (see *Reaction 3*) by reactions with zerovalent sulphur species in the form of elemental sulphur or polysulphides (Goldhaber and Kaplan, 1974).



While it has been shown that in some environments pyrite may also precipitate directly from solution (Howarth, 1979; Raiswell, 1982) and direct growth has been observed in experimental studies (Schoonen and Barnes, 1991), it is generally assumed that the vast majority of pyrite forms in this way through iron monosulphide intermediates.

Under oxic water columns, microbial sulphate reduction can only occur within the sediment where anoxic conditions are established (Raiswell *et al.*, 1988). This tends to mean that pyrite formation is limited by the amount of organic carbon (C_{org}) which has reached the sediment without being oxidized in the water column (Berner, 1984). Iron limitation may come in to play in settings where the concentration of detrital iron-rich material is diluted by high levels of biogenic skeletal debris (Berner, 1984) but Raiswell and Berner (1986) stated that organic carbon was limiting in most sediments that contained below 65% biogenic material.

Alternatively, when the bottom waters are anoxic, pyrite formation can occur in the water column as well as in the sediment. As organic carbon has a much reduced risk of oxidation in anoxic water columns, iron tends to be the limiting factor in pyrite formation, particularly in euxinic conditions where dissolved sulphide is present in the bottom waters (Raiswell and Berner, 1985).

Morse and Berner (1995) highlighted the three primary controls on the fixation of sulphides as pyrite in sediments, which were identified by Berner (1970) as the:

- availability of dissolved sulphate (SO_4^{2-});
- loading of reactive iron minerals per unit surface area of sediment (i.e. the availability of iron);
- amount of metabolizable organic matter; Roychoudhury *et al.* (2003) went as far as to say that this is the most important control on the amount of pyrite that can form in normal marine sediments.

Another major control on pyrite formation is the sediment redox status, as anoxic conditions are required for biological sulphate reduction and therefore for pyrite formation to occur. There are, however, several other factors that need to be taken into consideration when discussing the formation of pyrite in different environments:

- Extent of Bioturbation - mixing of sediments by benthic invertebrates continually adds dissolved oxygen, causing the oxidation of iron sulphides (Canfield, 1989). This is also linked to the redox state of bottom waters as anoxic or euxinic bottom waters do not support benthic communities and therefore experience limited or no bioturbation of sediment (Raiswell *et al.*, 1988).
- Hydrodynamics – this includes disturbance of the sediment:water interface leading to oxidation of sediment material, as well as eddies and water movements that disturb water column stratification in anoxic conditions (Roychoudhury *et al.*, 2003).
- Sedimentation Rates - when sedimentation rates are low in oxic conditions, iron sulphide formation is reduced because organic matter is exposed to dissolved oxygen in the water column for longer periods of time. However, if the water column is anoxic and contains H_2S , pyrite formation is maximized as sulphide production is not hindered

by reoxidation and more time is available for iron minerals to react with H₂S (Leventhal and Taylor, 1990).

- Silicate Iron Reactivity - the reactivity of iron is influenced by the degree of crystallinity, the mineral assemblage and the grain size (Haese, 2000). This can affect the proportion of the total iron available which is highly reactive towards dissolved sulphides.

Because of the complex interactions between redox conditions and iron-carbon-sulphur systematics, a number of proxies for bottom water oxygenation have been developed based on this system.

5.1.2 Introduction to the Proxies and the Related Terminology

5.1.2.1 Carbon, Sulphur and the S/C ratio

Within all sediments, carbon exists in two distinct ‘pools’ that need to be differentiated before the link to bottom water oxygenation is examined:

- Organic carbon (**C_{Org}**) – this refers to carbon bound in metabolisable organic matter and is commonly referred to as Total Organic Carbon (**TOC**). This in itself can be used as a broad proxy for oxygenation as TOC tends to be low under oxygenated water columns, where descending organic carbon is readily oxidized. In contrast, low oxygen conditions allow for a greater transfer of organic carbon from the water column to the sediment (Berner, 1984).
- Inorganic carbon (**C_{In}**) – this refers to carbon bound in a non-metabolisable form such as carbonates and generally provides a proxy for the biogenic input of the detrital material that makes up the bulk of seafloor sediment (Raiswell *et al.*, 2001).
- Together, these fractions comprise Total Carbon (**TC**)

Sulphur also exists in several forms within sediments although many authors assume that Total Sulphur (**TS**) is predominantly in the form of pyrite and so use this as an approximation (e.g. Rimmer, 2004). Determination of Total Reducible Sulphur (**TRS**) however, which gives a value for the amount of sulphide in the sediment, is a more accurate representation of true Pyrite Sulphur (**S_{py}**) (Roychoudry *et al.*, 2003). Again, pyrite sulphur can be used to give a broad indication of bottom water oxygenation, as higher levels of pyrite formation are associated with low oxygen settings (Raiswell and Berner, 1985).

A possibly more robust proxy than TOC or S_{py} alone involves a comparison between the two values known as the **S/C ratio**. It should be noted that there is confusion within the literature about the use of the terms **C/S** or **S/C ratio**. While some authors do discuss the actual **C/S** ratio, others use this to refer to plots of sulphur against organic carbon, which should strictly be referred to as the **S/C ratio**. In 1982, Leventhal noted that in normal marine settings, the amount of organic matter appeared to be proportional to the amount of sulphide preserved in the sediment. He also stated that in these conditions a **S/C** plot would show a regression line that would pass through zero (see *Figure 5.1*). In fact, normal marine sediments tend to fall within a narrow range values and using the converse arrangement, Berner (1982) proposed the range of 2.8 ± 0.8 for **C/S**. Jones and Manning (1994) translated this into a proposed slope of 0.36 on **S/C** plots for modern normal marine settings, but they suggested that ancient sediments tended to plot with a steeper slope. Morse and Berner (1995) also agreed generally that most normal marine settings fell within this proposed range. However, they pointed out that in areas of high biological productivity and salt marsh environments, or where fluctuating environments have occurred during deposition, **S/C** ratios tend to be higher than the suggested range.

Berner and Raiswell (1983) suggested that the observed correlation exists because in normal marine settings pyrite formation occurs diagenetically within the sediment and is limited by the availability of organic carbon. Raiswell and Berner (1985) suggested that a constant proportion of organic carbon is consumed during sulphate reduction and therefore the remaining portion of organic carbon acts as a measure of the amount originally available within the sediment. Leventhal (1982) also explained that when plotted against each other, the line would pass through zero because when there is no organic matter available, sulphate reduction cannot occur.

In contrast to the normal marine values, data plots from euxinic environments tend to show a limited correlation (Leventhal, 1982), and sometimes even a slight negative correlation (Raiswell and Berner, 1985), between organic carbon and pyrite sulphur. The regression lines also tended to have a non-zero intercept (Leventhal, 1982) (see *Figure 5.1*).

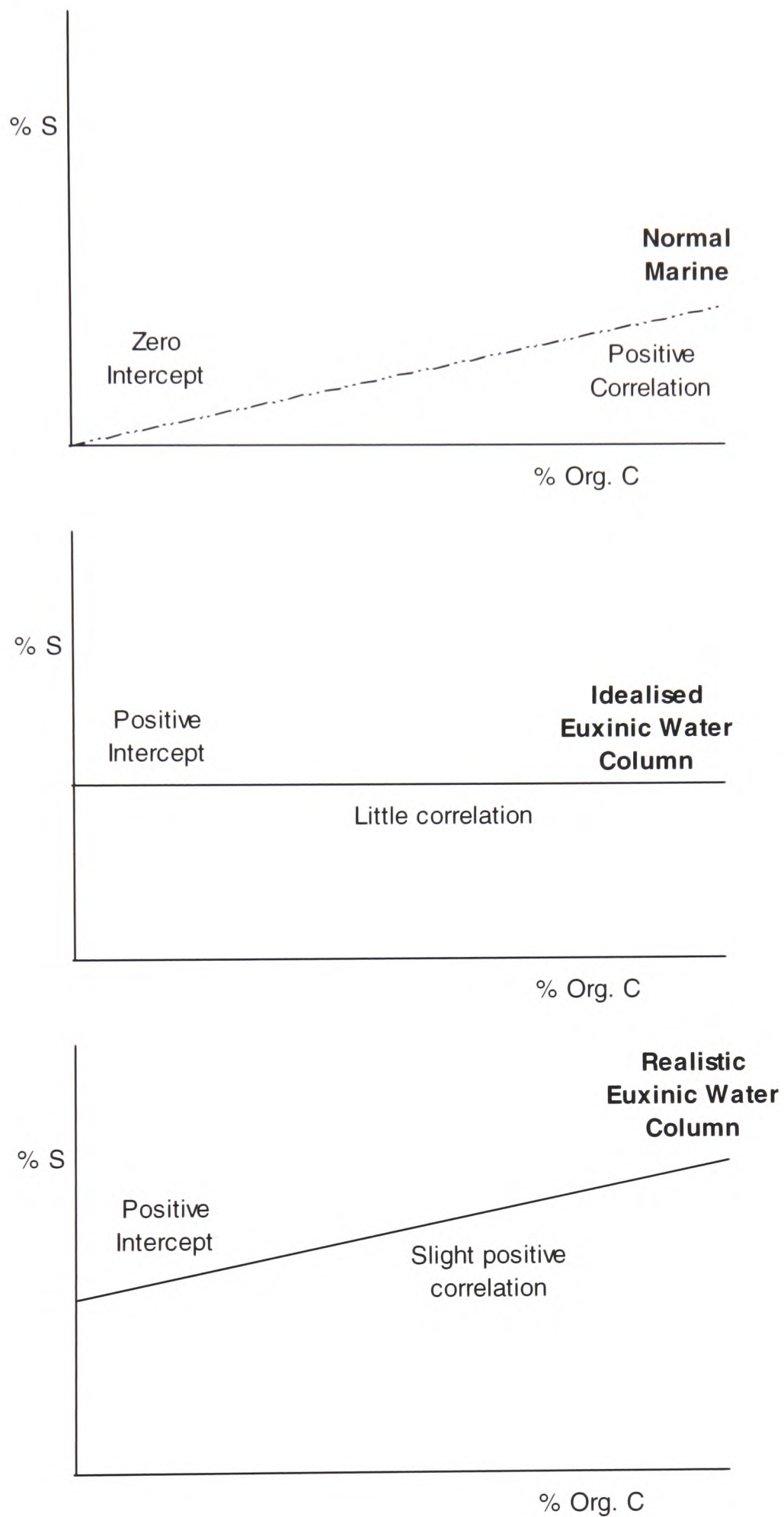


Figure 5.1: Idealised S/C plots of normal marine environments and euxinic environments, and a more realistic S/C plot for euxinic environments (adapted from Raiswell and Berner, 1985).

In euxinic settings, as well as diagenetic formation of pyrite in the sediment, pyrite can also form syngenetically in the water column and at the sediment/water interface because of the availability of dissolved sulphide in the water column (Raiswell and Berner, 1985). Here, pyrite formation is independent of the amount of organic carbon in the sediment and is mainly controlled by iron availability (Lyons and Berner, 1992). Reoxidation of pyrite within the sediment is also limited by the anoxic conditions as bioturbation is at a minimum (Raiswell *et al.*, 1988). In these conditions, Leventhal (1982) suggested that the non-zero intercept is a result of the fact that large amounts of sulphur can be fixed within the water column even when sedimentary organic carbon is low.

Although it is agreed that in idealized euxinic settings there should be little correlation between organic carbon and sulphur, a positive correlation is often observed (see *Figure 5.1*). Rimmer (2004) suggested that this positive slope in data related to euxinic settings may be due to iron limitation. However, Lyons and Berner (1992) also suggested that carbon-limited diagenetic pyrite formation may occur after burial, as in normal marine settings, and that this signal may to some extent overwrite the syngenetic pyrite signal, also giving a positive slope in euxinic conditions.

Although it appears that the **S/C** ratio can be used to identify broad environments, it is difficult to propose numerical boundaries to differentiate the oxygenation settings. Leventhal (1982) did suggest that the value of the positive intercept may be linked to the extent of anoxia within the entire water column, and that the slope of the line may be related to the sedimentation rate. Morse and Berner (1995) modelled the **S/C** system in normal marine sediments and agreed that the 'fraction of organic matter destroyed by sediment metabolism' is a function of the sedimentation rate, and that it is this fraction which controls the fraction of sulphur that is fixed as pyrite.

There are, however, several limitations on the use of **S/C** ratios. Raiswell and Berner (1986) found that samples with low sulphur contents led to high degrees of scatter in **S/C** plots. They suggested using the mean of a high number of values of sulphur and organic carbon in order to get meaningful results. Jones and Manning (1994) identified the fact that preferential carbon loss due to methanogenesis and decarboxylation during deep burial means that ancient normal marine values rise

from 0.36 to 0.56. They point out that even more carbon is lost when sediments reach maturity for oil generation and sulphur can also be lost at this stage (Raiswell *et al.*, 1988). This means that it is important to take into account the maturity of any sediments before analysis.

5.1.2.2 Pools of iron

Raiswell and Canfield (1996), using a variety of extraction techniques proposed by previous authors, defined a range of iron 'pools' within the sediment:

- **Fe_{py}** is pyrite iron, which is calculated stoichiometrically using the amount of pyrite sulphur (**S_{py}**). This represents the iron that was highly reactive towards dissolved sulphides and reacted to form pyrite.
- **FeD** – this represents iron extracted by the dithionate extraction procedure of Canfield (1988) (which was further adapted by Leventhal and Taylor, 1990). This is believed to quantitatively extract the iron oxide/oxyhydroxide phases (lepidocrocite, ferrihydrite, goethite and haematite) with only relatively small amounts being extracted from iron silicates (Canfield, 1988; Raiswell *et al.*, 1994). **FeD** is believed to represent iron that would have been highly reactive towards dissolved sulphides but that has not reacted to form pyrite.
- A combination of these two pools provides a value for the originally available **Highly Reactive Iron (FeD + Fe_{py})**.
- **FeH** – this represents iron extracted by the hot HCl extraction procedure of Berner (1970) (with later additions to the method being made, namely by Raiswell *et al.*, 1988; and Leventhal and Taylor, 1990). This is believed to quantitatively extract the same iron oxide/hydroxide phases as the dithionate extraction but also removes considerable amounts of iron from silicate phases. Because of this, **FeH** is believed to include the highly reactive iron represented by **FeD** as well as silicate iron that would have been poorly reactive towards dissolved sulphide.
- The difference between these two extraction methods allows the definition of **Poorly Reactive Iron** as **FeH – FeD**. Raiswell and Canfield (1996) normalized poorly reactive iron with total iron (**FeH-FeD/FeT**) to allow comparison between sites.

- The final iron pool to be defined is **Unreactive Iron**, which is iron that would never have reacted with sulphide. This relies on the use of total iron (**FeT**) which is found by total digestion of the samples. **Unreactive Iron** is then defined as $\text{FeT} - (\text{Fe}_{\text{py}} + \text{FeH})$.

In low oxygen conditions, where hydrogen sulphide is readily available, the proportion of Highly Reactive Iron that reacts to form pyrite should be relatively high. This should be highlighted by comparing the proportion of Fe_{py} and **FeD** (which represents highly reactive iron that did not react to form pyrite) within a sample. In oxygenated waters the proportion of **FeD** could be expected to be higher as the rate of microbial sulphate reduction should be lower and the high levels of bioturbation should cause oxidation of pyrite within the sediment. Examination of these different pools could also answer questions concerning the source of iron for large-scale pyrite formation in euxinic sediments. If the proportion of reactive, poorly reactive and unreactive iron change within these settings, it may indicate whether the pools of less reactive iron are exploited in pyrite formation, or whether lateral transport of iron is delivering a higher proportion of reactive iron to the site (Raiswell and Canfield, 1996).

5.1.2.3 Ternary plots of Fe, S and C

The triangular plots of Fe-S-C initially proposed by Dean and Arthur (1989) work on a similar basis as the S/C plots. In oxic settings, where pyrite formation only occurs within the sediment, organic carbon is generally the limiting factor. In this case they propose that there should be a strong correlation between organic carbon and sulphur and the data would be expected to plot along a regression line with an S/C intercept of 0.4 (see *Figure 5.2*). However, in euxinic settings pyrite formation can occur within the water column and reactive iron tends to be the limiting factor. Because of this, iron and sulphur are normally closely coupled and Dean and Arthur (1989) suggested that the data should be elongated along a line of constant S/Fe. They take this a step further and suggest that if all the iron is in the form of pyrite the line should follow an S/Fe ratio of 1.15 (see *Figure 5.2*) and that this theoretical endpoint can be used to provide an idea of the percentage of iron that actually is pyritised. This, however, only works on the assumption that the proportion of **Reactive Iron** remains constant throughout the data set.

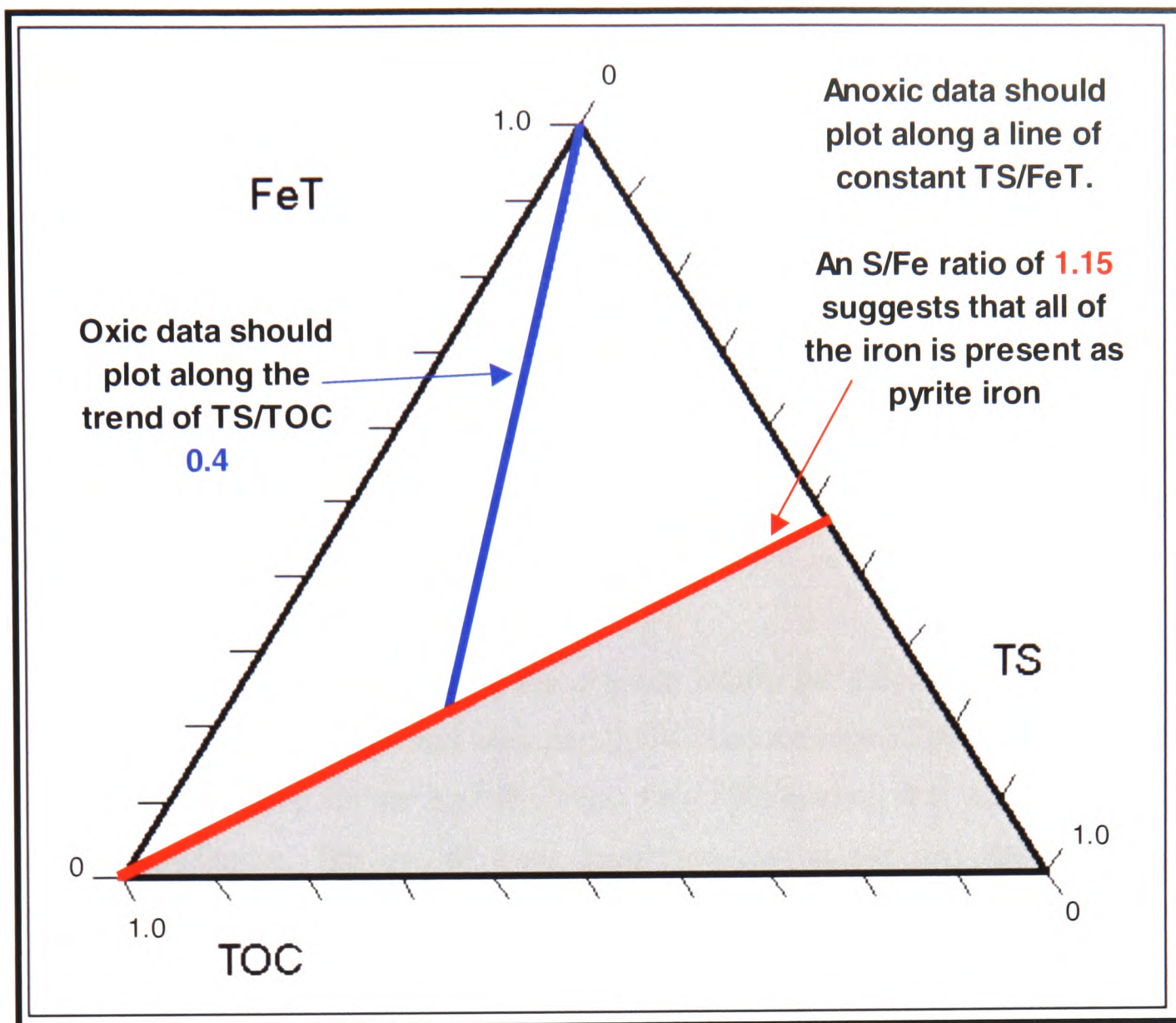


Figure 5.2: Theoretical interpretations of Fe-S-C ternary diagrams (adapted from Arthur and Sageman, 1994).

Again with this proxy it is difficult to provide numerical boundaries in order to correlate different states of bottom water oxygenation across different sites. However, Arthur and Sageman (1994) suggested that while these plots have no direct numerical link to other proxies, they are useful in environmental determination.

5.1.2.4 Degree of Pyritisation,

In 1970, Berner introduced the Degree of Pyritisation (DOP) as a means to identify the degree of bottom water oxygenation in ancient sediments. He defined this proxy as

$$\text{DOP} = \% \text{ Pyrite Fe} / (\% \text{ Pyrite Fe} + \% \text{ Reactive Fe})$$

He defined **Reactive Fe** as the fraction of iron that readily reacts with dissolved sulphide to produce iron monosulphides and eventually pyrite. Originally the

calculation used **FeH** as **Reactive Fe** and the majority of further work including the suggestion of oxygenation boundaries and calibration work on this proxy has followed this. However, using the definitions provided by Raiswell and Canfield (1996), **FeD** would seem to be a more appropriate estimation of **Reactive Fe**. This means that DOP can be calculated as either:

$$\text{DOP} = \text{Fe}_{\text{Py}} / (\text{Fe}_{\text{Py}} + \text{FeH}) \text{ (which was denoted } \text{DOP}_{\text{R}} \text{ by Raiswell and Berner, 1985 but will be referred to as } \text{DOP}_{\text{H}})$$

Or: $\text{DOP} = \text{Fe}_{\text{Py}} / (\text{Fe}_{\text{Py}} + \text{FeD})$ (which will be referred to as DOP_{D})

Raiswell and Berner (1985) also introduced the use of DOP_{T} which assumes that **FeT** is mainly composed of **Reactive Fe**:

$$\text{DOP}_{\text{T}} = \text{Fe}_{\text{Py}} / \text{FeT}$$

This provides an approximation of the original DOP_{H} but has not been calibrated. Some authors such as Jones and Manning (1994) and Rimmer (2004) have taken the approximation a step further by calculating Fe_{Py} by assuming that all sulphur (**TS**) was pyrite sulphur. The use of these approximations means that the boundaries initially defined for DOP_{H} are not directly applicable. It also makes comparison of different sites and different authors' work difficult when a variety of methods are used to obtain the **DOP**.

In 1988 Raiswell *et al.* refined the proxy by suggesting numerical boundaries for DOP_{H} to distinguish between three categories of sediment. These were defined according to the faunal and sedimentological categories of Morris (1979):

- **Aerobic (normal marine) conditions:** this means deposition in fully oxygenated bottom waters and is represented by homogenous bioturbated sediment. The trace fossils are dominated by *Chondrites* and benthic body fossils are abundant and diverse. Bivalves, where present, comprise a mixed assemblage of infaunal and epifaunal types, but infaunal deposit feeders comprise less than 20% of the fauna. $\text{DOP}_{\text{H}} < 0.42$
- **Restricted (normal marine) conditions:** this means deposited in waters with low oxygen concentrations and is represented by poorly laminated sediment. Commonly sparse bioturbation is shown by the presence of thin discreet pyrite burrows. Bivalves are dominated by shallow-burrowing infaunal deposit

feeders. Few infaunal suspension feeders are present, but epifaunal suspension feeders are common. $0.46 < \text{DOP}_H < 0.80$

- **Inhospitable bottom conditions:** this means where little or no oxygen is present and H_2S may be continually or intermittently present. This is referred to as 'Bituminous' by Morris (1979) and is represented by finely laminated sediment. There is generally little or no bioturbation and the benthic fauna, if present is composed almost entirely of epifaunal suspension feeders. $0.55 < \text{DOP}_H < 0.93$. Raiswell *et al.* (1988) noted that this range overlaps with that of the restricted conditions, but suggested that a boundary at DOP_H 0.75 separated more than 90% of this data.

Jones and Manning (1994) identified the degree of pyritisation as one of the most reliable proxies for low oxygen conditions. However, they also noted that the technique is much more reliable for differentiating between oxic and dysoxic conditions, and that there is considerable overlap between dysoxic and anoxic data sets. Hatch and Leventhal (1992) suggested that values of DOP_H between 0.67-0.75 represented a less strongly stratified anoxic water column, whereas values of DOP_H greater than 0.75 represented a strongly stratified anoxic water column.

One of the common problems highlighted about proxies such as the S/C ratio is that they do not accurately represent the redox conditions present when the availability of reactive iron becomes a limiting factor (Leventhal and Taylor, 1990). The **DOP**, however, as a measure of the completeness of the reaction of reactive iron with aqueous sulphide (Leventhal and Taylor, 1990) is thought to give a clear indication of when the availability of the reactive iron is limiting, and thereby provides redox information that is not skewed by this factor. In aerobic conditions pyrite formation occurs only within the sediment where the availability of organic carbon is the limiting factor (Bernier, 1984). This means that the proportion of the reactive iron that actually forms pyrite will be lower, and hence **DOP** values will also be low. This is reinforced by the fact that iron and organic carbon tend to increase proportionally due their unconnected association with fine grained siliciclastic material – this means that even when organic carbon levels increase to allow more pyrite formation, the total iron content is also increased which means that the **DOP** remains low (Raiswell *et al.*, 1988). In anoxic conditions, however, pyrite formation can also occur in the water column and tends to be limited by the availability of reactive iron (Raiswell *et*

al., 1988). This means that a higher proportion of the reactive iron will actually form pyrite, giving a higher reading of **DOP**.

Raiswell and Berner (1985) proposed the use of **DOP** in combination with **S/C** plots in order to determine if organic carbon or reactive iron was limiting. They suggested that the positive slope observed on many euxinic **S/C** plots was the result of either:

- Syngenetic pyrite formation within the water column (**Fe** limited), followed by diagenetic pyrite formation in the sediment (**C_{org}** limited). In this case, they believed that the S-intercept represented the amount of syngenetic pyrite formed in the water column, and that the amount of diagenetic pyrite was represented by the difference between this value and the total sulphur corresponding to any particular value of **TOC** (see *Figure 5.3a*). In this situation, they proposed that a plot of **DOP** against **TOC** would also have a positive slope as when carbon is limiting, the amount of reactive iron that can form pyrite will increase as organic carbon levels increase (see *Figure 5.4a*).
- Only syngenetic pyrite formation occurs as Fe is limiting (see *Figure 5.3b*). In this case, the **S/C** plot could still show a positive correlation but they believe that this is an artifact of the close association of both colloidal organic matter and colloidal iron-oxide particles with fine clay mineral grains. This association means that when iron is limiting, pyrite sulphur appears to correlate with organic carbon but this is purely because the available iron increases in proportion with the availability of organic carbon. In this case, a plot of **DOP** against **TOC** would give a horizontal regression line (see *Figure 5.4b*) as the proportion of iron that forms pyrite should remain constant when reactive iron is the limiting factor. In this case all of the sulphur fixed is assumed to represent syngenetic pyrite.

They also noted that in environments that are not truly euxinic but do exhibit low oxygen conditions, pyrite formation is not necessarily limited by organic carbon availability. They stressed that in dysoxic conditions, preservation of organic carbon is much greater than in oxic conditions. They suggested that this means that if sulphate reduction occurs within the sediment close to the sediment:water interface then pyrite formation could be independent of organic carbon and limited by reactive

iron availability. This should give a distinctive horizontal plot on all of the **S/C**, **DOP** against **TOC**, and **FeT** against **TOC** graphs.

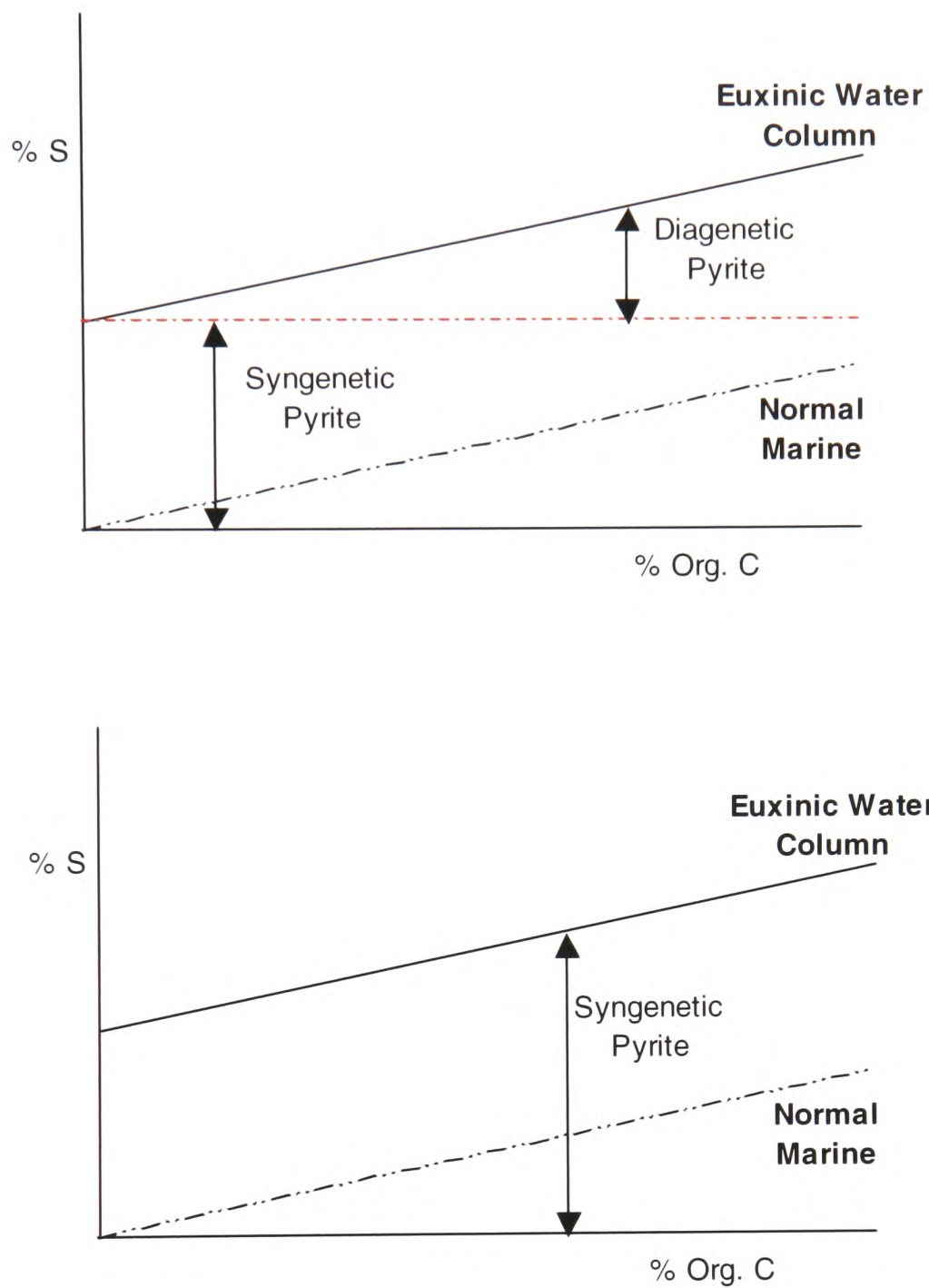


Figure 5.3: Diagrammatic explanations of the two possible causes of a positive S/C slope in euxinic conditions (from Raiswell and Berner, 1985).

This means that while **S/C** alone can only theoretically distinguish between oxic and euxinic environments, this may provide a way in which to identify intermediate conditions of oxygenation.

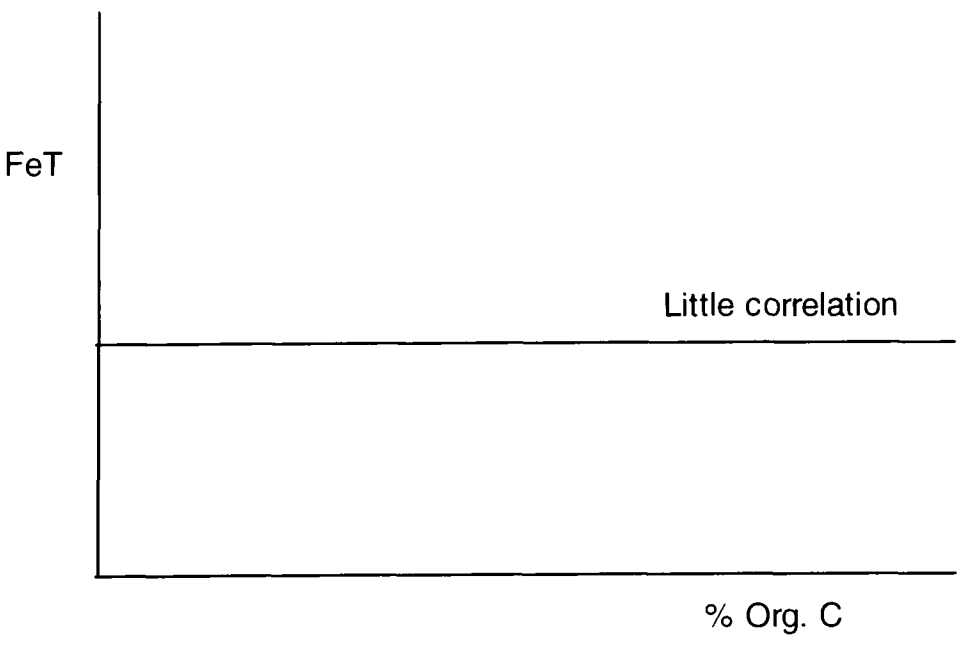
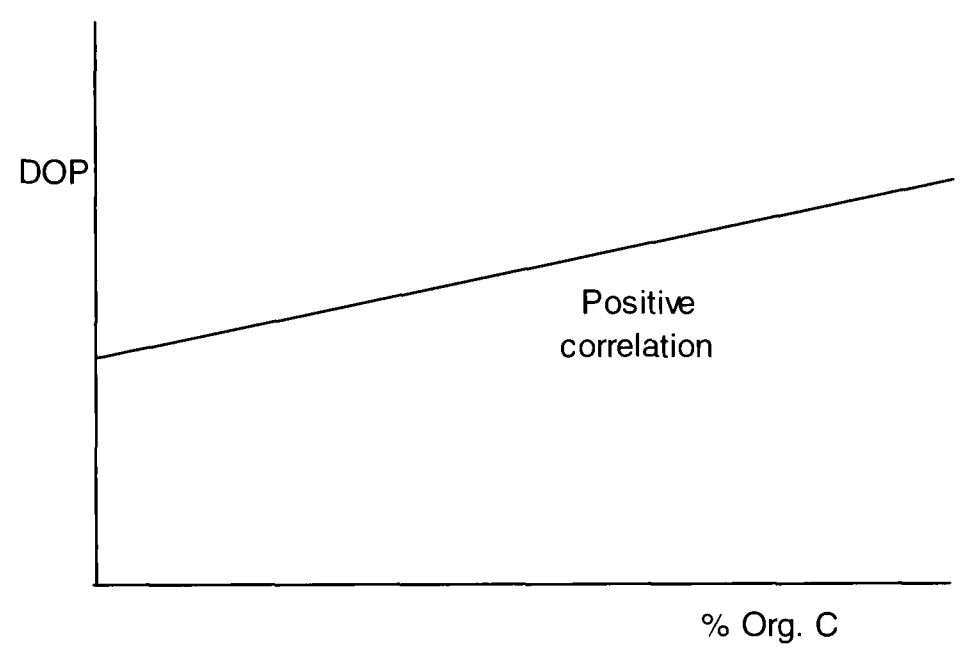
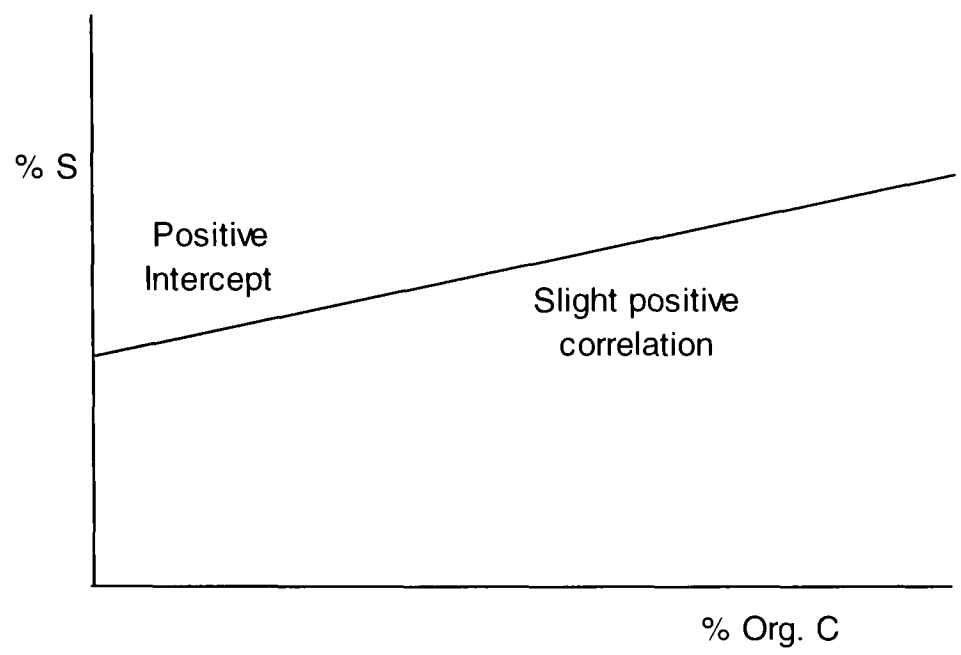


Figure 5.4 (a)

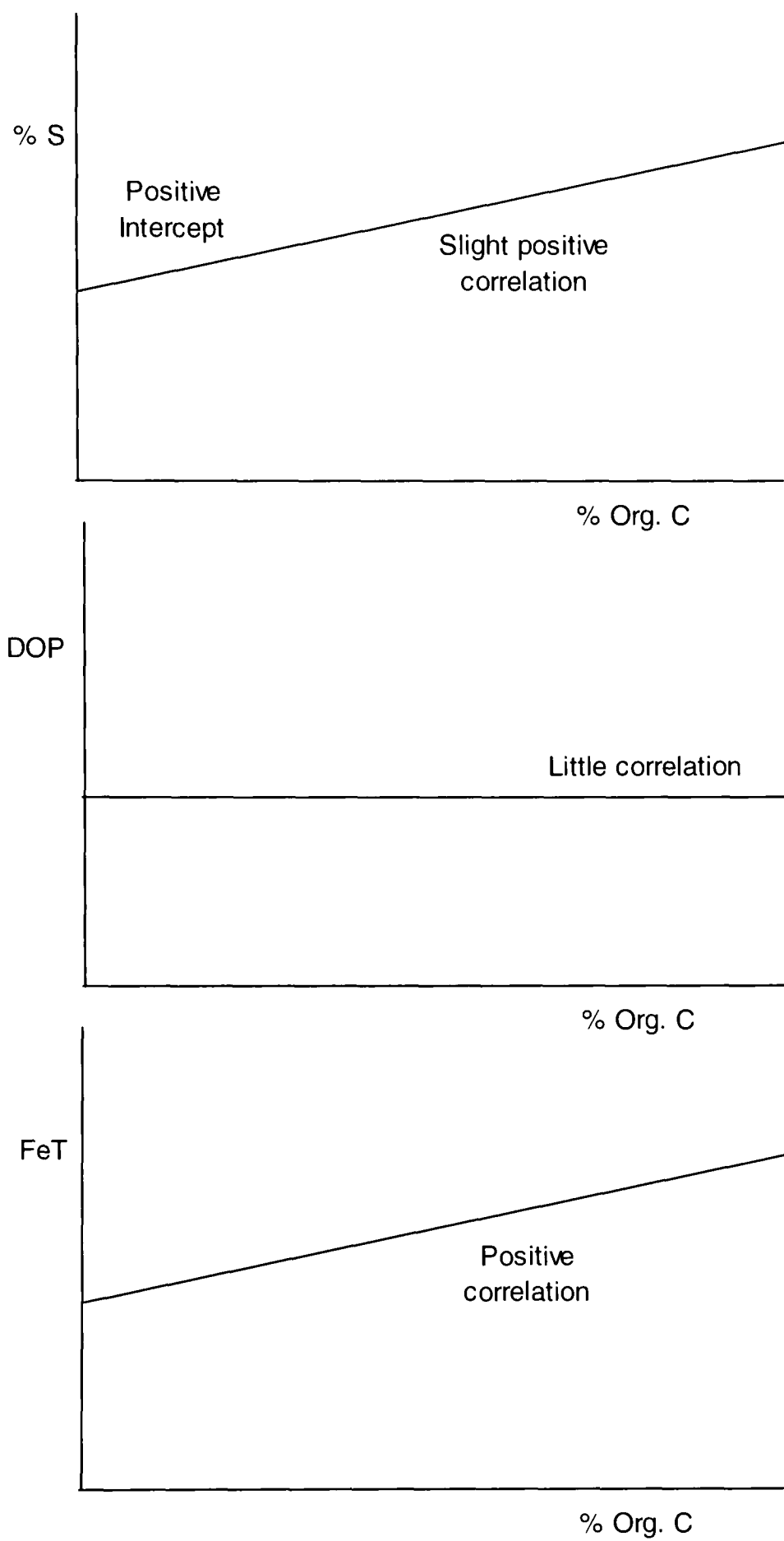


Figure 5.4 (b)

Figure 5.4: Proposed S/C, DOP vs. Corg and FeT vs. Corg plots for the two possible scenarios that could lead to a positive S/C slope in euxinic conditions – (a) organic carbon limited pyrite formation; and (b) reactive iron limited pyrite formation (adapted from Raiswell and Berner, 1985).

Although **DOP** is one of the few Fe-S-C systematics proxies with proposed boundaries to differentiate between the different levels of oxygenation, the range of calculation methods for **DOP_H**, **DOP_D** and **DOP_T** does create some confusion in comparing different authors' work. Roychoudry *et al.* (2003) also encountered problems with the proxy when applying it to modern salt marsh settings. They found that sediments which were from aerobic settings were consistently giving dysaerobic or euxinic **DOP** values. Roychoudry *et al.* (2003) argued that **DOP** may not always differentiate between syngenetic and diagenetic pyrite and further suggested that the **DOP** values of salt marsh environments are more indicative of sediment chemistry and pore-water redox conditions rather than bottom water conditions.

Raiswell *et al.* (1988) also listed several problems to be aware of when interpreting **DOP**:

- Low **TOC** levels give anomalously low pyrite contents in anoxic settings – they suggested only applying this to sediments with more than 0.15% **TOC**;
- Pyrite sulphur can be reoxidized during weathering so fresh samples are required;
- **DOP** is only applicable to sediments with less than 75% biogenic content otherwise the **FeT** content is too low;
- Sulphur can be lost from the system if the sediment undergoes thermal maturation or metamorphism;
- Sediments that include late diagenetic iron-rich concretionary carbonates will have anomalously high **FeH** values due to iron migration;
- Levels are not applicable to pre-Devonian samples when there was no plant material as organic matter. In these sediments there appears to be higher levels of pyrite formation per unit carbon;
- Deep burial diagenesis can mean that some iron oxides (in **FeD** and **FeH**) are lost to make silicates and carbonates. This would lead to increased **DOP** levels – but all samples from a particular site will have increased by the same amount (Raiswell and Berner, 1987).

5.1.2.5 Indicator of Anoxia

Raiswell *et al.* (2001) noted that **DOP** cannot distinguish between poorly oxygenated waters, oxygen-free waters (anoxic) or waters that contain either dissolved sulphide

(euxinic) or dissolved iron. They proposed the use of the **Indicator of Anoxia (IA)**, which bears no simple relationship to the **DOP**:

$$\mathbf{IA} = (\mathbf{FeD} + \mathbf{Fe}_{\mathbf{py}})/\mathbf{FeT}$$

In investigating a new approach to defining these environments they noted that, although the proportion of reactive iron would be assumed to be similar, sediments associated with low oxygen environments contained much more pyrite than normal marine settings. This implies that there must be an additional source of iron in low oxygen conditions (Raiswell *et al.*, 2001) as Berner and Weistrich (1985) observed diffusion of excess H₂S out of sediments into overlying waters in a variety of normal marine settings. The presence of excess H₂S in these environments suggests that, contrary to the belief that organic carbon is the limiting factor in normal marine settings, the availability of reactive iron may play a role in controlling pyrite formation. The idea that more reactive iron is available in low oxygen conditions is backed up by observations of the relative proportions of reactive iron in oxic and anoxic environments:

- In normal marine settings ($[\mathbf{FeD} + \mathbf{Fe}_{\mathbf{py}}]/\mathbf{FeT}$) rarely exceeds 0.4 (Raiswell and Canfield, 1998)
- Sediments that form under anoxic water columns have higher ($[\mathbf{FeD} + \mathbf{Fe}_{\mathbf{py}}]/\mathbf{FeT}$) values (Canfield *et al.*, 1996; Raiswell and Canfield, 1998) which implies that more pyrite is formed per unit iron.

Raiswell *et al.* (2001) found that modern marine sediments, as well as equivalent ancient sediments, deposited under oxygenated bottom waters mainly have **IA** values <0.5, whereas modern anoxic, iron-rich or sulphidic bottom waters mainly plot above 0.5. This implies that more reactive iron is available in lower oxygen environments which Raiswell *et al.* (2001) proposed can happen in one of two ways:

- More **reactive iron** is transported into the system, so the overall proportion of **reactive iron** compared to **FeT** increases. In anoxic water columns, dissolution and microbial reduction of iron oxides from detrital grains can occur, followed by sulphate reduction. Raiswell *et al.* (2001) suggested that this creates an upper layer rich in dissolved iron and a lower layer rich in dissolved sulphide as the solubility of iron sulphide is so low that dissolved iron and dissolved sulphide do not co-exist. This arrangement allows for three methods of pyrite formation within the water column:

- Organic-rich detrital material can be metabolized by sulphate-reducing bacteria, creating H₂S within the iron-rich zone;
- Iron-rich detrital material can combine with the dissolved sulphide in the lower zone;
- Mixing of the two zones can occur via eddies.

Lateral transport within these zones has been observed within the Black Sea system (Buessler *et al.* 1991) and this could account for the increased proportion of **Reactive Iron** observed in low oxygen settings.

- The other alternative is that a higher proportion of the iron available becomes reactive towards sulphide in low oxygen environments and this is backed up by Haese's (2000) suggestion that silicate iron reactivity is a factor that contributes to the amount of pyrite that can form. Macquaker *et al.* (1997) did observe greater pyrite formation in the deep-water anoxic Kimmeridge Clay than on related oxygenated shelf zones with similar values of **FeT**. However, Raiswell *et al.* 2001 were dubious about the possibility of increased iron reactivity and pointed out that there is also a substantial difference in silicate mineralogy between the two sites studied by Macquaker *et al.* (1997). They also believed that the settling times of detrital material would not allow time for the extraction of silicate iron, which is thought of as **Poorly Reactive Iron**, and indeed Canfield *et al.* (1992) found that even after burial, very limited pyrite formation occurs from this iron source.

Raiswell *et al.* (2001) believed that the lateral transport of iron into the dissolved iron zone provides the additional reactive iron required for the extent of pyrite formation observed in low oxygen zones. They suggested that the **Indicator of Anoxia** can be used to identify when pyrite formation has occurred due to the breakdown of organic matter by sulphide reduction, releasing sulphide which can react with dissolved iron in the water column. They argued that this pyrite will be additional to that formed from detrital iron oxides in the dissolved sulphide portion of the water column or in the sediment, and that this should lead to elevated Indicator of Anoxia Values. They did stress, however, that this additional pyrite only become significant when proportions of biogenous sediment becomes high because:

- The higher the biogenic input, the more organic material is available to be metabolized in the iron-rich zone;

- Higher levels of biogenic material decreases the amount of detrital iron in the sediment by a dilution effect – this means that the effect of the extra pyrite formed in the iron-rich zone will make up a more significant component of the total iron.

They therefore suggested that anoxia can only truly be identified in sediments where the biogenous content of the sediment is greater than 30%. Because dissolved iron is only present under anoxic conditions, Raiswell *et al.* (2001) suggested that the **IA** is one of the few Fe-S-C systematics proxies that can identify between anoxic and dysoxic environments.

5.2 Methodology

5.2.1 Carbon

5.2.1.1 Organic Carbon (TOC)

Weight % Total Organic Carbon was analysed by coulometry at the University of Oxford. The weighted samples were heated in stream of oxygen in a tube furnace and the resultant gases, after having had the sulphur dioxide removed, were absorbed into a solution of barium perchlorate which had been set to a pH of 10.0. An electrolytic titration was then carried out to determine the current needed to restore the pH back to 10.0 and the amount of current needed is proportionate to the amount of CO₂ absorbed. These values were then converted into wt% carbon. Reproducibility of the results in replicas was found to be between 1-1.5%. Repeat analysis of samples processed twice and analysed within the same run had %RSD of less than 5% (see *Appendix D, Table D.1*).

5.2.1.2 Total Carbon (TC)

Samples were analysed for Total Carbon (TC) using a LECO Instruments CS244 analyser at the University of Newcastle. The samples were weighed out to an accuracy of 0.001 g and to each sample 1.7 g of Lecocell II and 0.8 g of iron chip accelerator were added. In brief, the samples are ignited in an induction furnace in a stream of oxygen, where the carbon is oxidized to carbon dioxide. The carbon dioxide produced is then quantified by an infra-red detector. The instrument is calibrated with a standard reference soil of known carbon concentration, as well as specific carbon standards provided by LECO. A reference soil from an alternative source is also analysed to allow for method and calibration validation. This

procedure for carbon determination follows BS7755, Section 3.8, 1995; ISO 10694, 1995; Soil Quality, Part 3, Chemical Methods, Section 3.8, Determination of organic carbon and total carbon after dry combustion (elementary analysis).

The laboratory determined limits of acceptable variation between duplicates for this procedure is as follows:

Carbon content %	Acceptable Variation
0 - 0.25%	0.025% absolute
0.25 - 7.50%	10% relative
> 7.50%	0.75% absolute

The laboratory participates in an International Proficiency Testing Scheme, for the analysis of soils, and carbon determinations are regularly checked as part of this scheme. Approximately 30 laboratories determine carbon, and typical relative standard deviations are about 2 - 5 %.

Analysis of the data provided shows that all analytical duplicates have a relative standard deviation of less than 1.6% and all method repeats, including repeats run in different analytical runs have a relative standard deviation of less than 6.1%, with all repeats apart from two actually having relative standard deviations of less than 2%.

5.2.2 Sulphur

5.2.2.1 Pyrite Sulphur (S_{Py})

Different methods have been proposed for measuring the pyrite sulphur. In some cases, where other forms of sulphur are negligible, pyrite sulphur has been assumed to be approximated by: [Total Sulphur x 0.871] (Leventhal and Taylor, 1990). However, in most cases, the samples are analysed using a range of methods to determine Total Reducible Sulphur (TRS), which is thought to be mostly pyrite in geological samples (Newton *et al.*, 1995). There are several suggestions for the determination of TRS, including the $LiAlH_4$ method of Westgate and Anderson (1982) where the AgS yield is used to calculate the pyrite sulphur content, and the measurement of the volume of SO_2 generated during isotopic analyses. However, the most commonly used procedure is the Chromium Reduction Method of Canfield *et al.* (1986) and the samples were run by the University of Leeds using an adapted version of this method (see *Figure 5.5*):

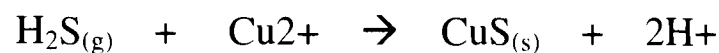
- Chromous chloride was prepared by drawing 1.0 M Chromic chloride, acidified to 0.5 N HCl, under vacuum through a column packed with

granulated zinc (that had been amalgamated in an acidic 2% mercuric nitrate solution beforehand). This needs to be repeated every 2-3 days due to oxidation.

- 1.00 g of sample was placed in the digestion flask with 10 ml ethanol.
- The trapping vessel was attached, containing 25 ml of copper chloride (CuCl₂).
- The system was flushed with nitrogen (2-3 bubbles per second) and left for 10 minutes to ensure that all oxygen had been evacuated.
- Via a plastic syringe, 20 ml of 12 M Hydrochloric acid (HCl) was added, followed by 40 ml of chromous chloride (CrCl₂) solution. The reaction that occurs releases hydrogen sulphide (H₂S):



The H₂S is then carried by the flow of nitrogen through to the trapping vessel. Here the hydrogen sulphide reacts with the copper chloride to form a precipitate of CuS:



The use of copper chloride as the trapping solution was proposed by Newton *et al.* (1995) – Canfield *et al.*'s (1986) original method used a 3% zinc acetate – 10% ammonium hydroxide solution relying on the formation of zinc sulphide to quantify the amount of hydrogen sulphide released.

- The hotplate was turned up and the digestion flask contents were simmered for 90 minutes.
- After 90 minutes the flasks were left to cool and then the trapping solution was filtered to remove the CuS precipitate.
- The remaining copper chloride solution was titrated against a standard copper solution. 65 ml of buffer solution of 1 M sodium acetate solution (adjusted to pH 5.5 with acetic acid) and 3-5 drops of cresol red were added to every standard, blank and sample. The resultant solutions were made up to 200 ml with distilled water. The solutions were then titrated with 0.1 M ethylene diamine tetraacetic acid (E.D.T.A) with a sharp end point being recorded when the colour changed from dark blue to light green.

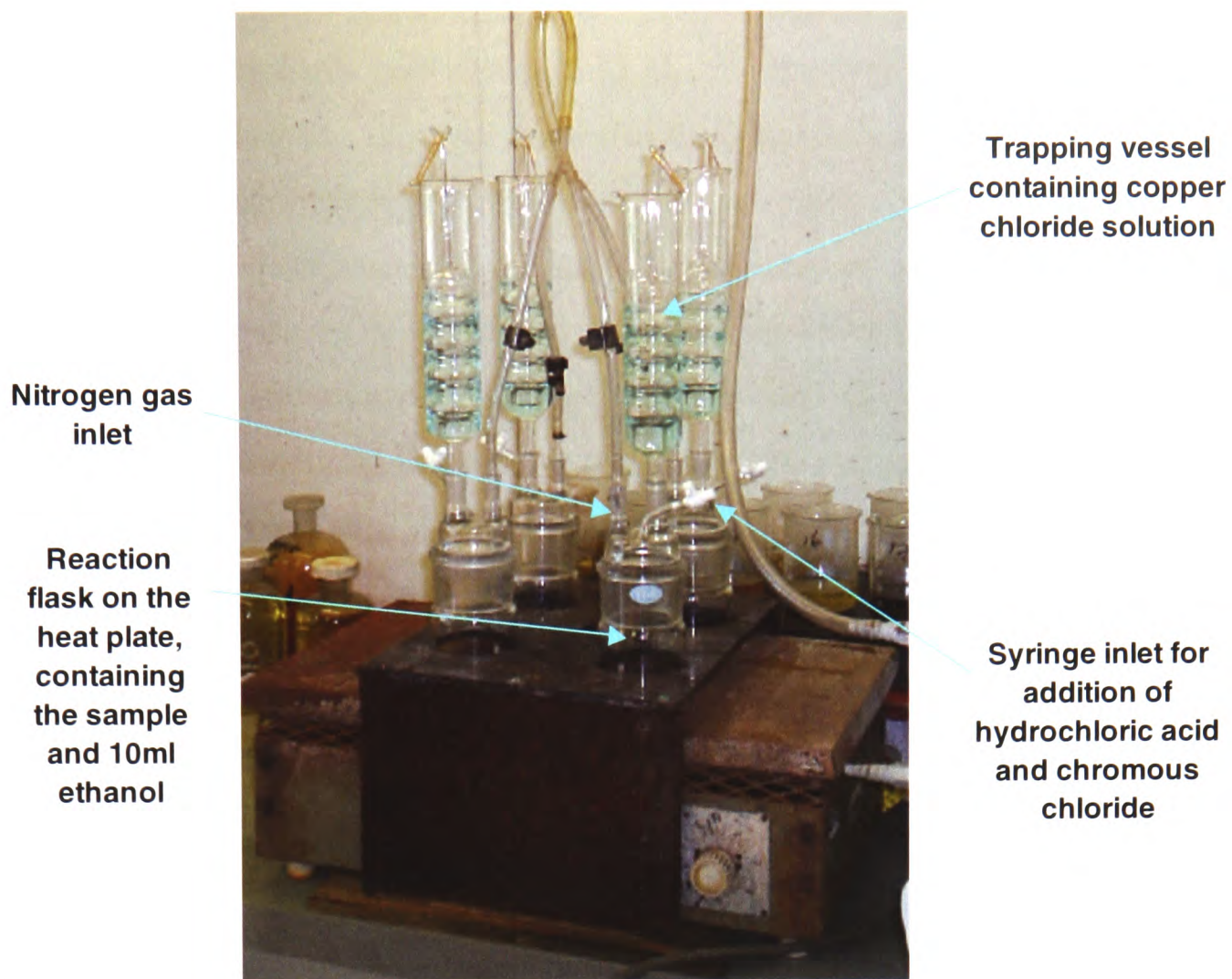


Figure 5.5: Labeled photograph of the reaction apparatus used by the University of Leeds in the determination of Chromium Reducible Sulphur.

Roychoudhury *et al.* (2003) pointed out that Chromium Reducible Sulphur includes elemental sulphur (S_0) as well as pyrite sulphur, and that this could lead to an overestimation of the pyrite iron, leading to more oxygenated signals. However, their modern results tended to plot in more dysoxic conditions than actually observed, and so they concluded that this does not present too much of a problem. Repeat analysis of samples processed twice and analysed within the same run had %RSD of less than 11% (see Appendix D, Table D.1).

5.2.2.2 Total Sulphur (TS)

Samples were analysed for Total Sulphur (TS) using a LECO Instruments CS244 analyser at the University of Newcastle. The samples were weighed out to an accuracy of 0.001g and to each sample 1.7 g of Lecocell II and 0.8 g of iron chip accelerator were added. In brief, the samples are ignited in an induction furnace in a stream of oxygen, where the sulphur is oxidized to sulphur dioxide. The sulphur dioxide produced is then quantified by an infra-red detector. The instrument is

calibrated with a standard reference soil of known sulphur concentration, as well as specific carbon standards provided by LECO. A reference soil from an alternative source is also analysed to allow for method and calibration validation.

The laboratory acknowledges that, unlike the procedure for carbon determination, there is no equivalent standard for the determination of sulphur. However, the laboratory participates in an International Proficiency Testing Scheme (IPTS), for the analysis of soils, and sulphur determinations are regularly checked as part of this scheme. Approximately 20 laboratories make determinations, with a typical Relative Standard Deviation of 15 - 25 %. The laboratory acknowledge that from their own data, and that of the IPTS, sulphur determination by this method is not as accurate as carbon determination.

Analysis of the data provided shows that all analytical duplicates have a relative standard deviation (%RSD) of less than 8% with the majority of the %RSDs being much lower than this. All procedural repeats have a relative standard deviation of less than 10% (see *Appendix D, Table D.1*).

5.2.3 Iron

5.2.3.1 Pyrite Iron (Fe_{Py})

Pyrite iron is calculated stoichiometrically from pyrite sulphur:

$$\text{Wt \% Fe}_{\text{Py}} = [\text{Wt \% S}_{\text{Py}} / 32.06 \times 2] \times 55.847$$

5.2.3.2 Dithionite Extractable Iron (FeD)

Canfield (1988) proposed the use of sodium dithionite in a citrate buffer as an extraction agent and the original method was adapted by Leventhal and Taylor (1990):

- A pH 4.8 buffer solution was made with 40 ml of 0.35 M glacial acetic acid and 58.8 g sodium citrate (0.2 M), which was made up to a litre with distilled water.
- 0.100 g powdered sediment and 1 g sodium dithionite were added to a test tube.
- 30 ml of buffer solution were added to each tube and the samples were shaken six times during the 24 hour extraction.

- After 24 hours the samples were centrifuged and a 1 ml aliquot was diluted to 5 ml for analysis.

The iron concentration was determined by the author by Atomic Absorption Spectroscopy using a multi-element lamp. The percentage relative standard deviation (%RSD) of all duplicates were below 2.5%. The procedural repeats (repeats 1 to 4) all recorded a %RSD of less than 3.5%, and all analytical repeats (repeats 5 to 7) recorded a %RSD of less than 2.6% (see *Appendix D, Table D.1*).

5.2.3.3 Hot HCl extractable Iron (FeH)

Berner (1970) originally defined reactive iron in recent marine sediments as the iron that was solubilized from 100 mg of sample by 1 minute boiling with 5 ml of concentrated (12N) HCl. Later additions to the method were made, namely by Raiswell *et al.* (1988) and Leventhal and Taylor (1990):

- 0.100 g of sample was added to 5 ml of concentrated (12 N) HCl in a Pyrex test tube;
- The test tubes were heated to boiling and simmered for exactly one minute;
- The reaction was quenched by filling the test tube with distilled water and washing sediment and solution into a 250 ml volumetric flask containing 125 ml distilled water (for less than 1% Fe, or a 500 ml volumetric flask for 2.5% Fe). The volumetric flask was then made up to the mark.
- After standing for one hour, the upper part of the solution is clear enough to permit aspiration directly into an Atomic Absorption Spectrometer.

The iron concentration was determined by the author by Atomic Absorption Spectroscopy using a multi-element lamp. The percentage relative standard deviation (%RSD) of all duplicates were below 7.5% although it is worth noting that actually only some of the Amma Fatma samples, which recorded very low FeH values, had %RSD values over 1%. The procedural repeats (repeats 1 and 2) all recorded a %RSD of less than 7.5%, and all analytical repeats (repeats 3 to 6) recorded a %RSD of less than 3.5% (see *Appendix D, Table D.1*).

5.2.3.4 Total Iron (FeT)

Total iron was determined by the author by lithium metaborate fusion of the samples, followed by analysis using a Fisons Horizon ICP-OES. Section 4.2 contains more details of the analytical procedure.

5.3 Discussion of Results

5.3.1 Carbon, Sulphur and the S/C ratio

5.3.1.1 Total Sulphur

The Niveau Pacquier and Folkestone Gault Clay samples all plot below 0.8% Total Sulphur (TS) and both show little discernable pattern (see *Figures 5.6 and 5.8*). While this is possibly to be expected with the relatively consistent environment proposed for Gault Clay deposition, the proxy appears to show no differentiation between the grey clay and black shale samples of the Niveau Pacquier set. While the majority of Briestroffer samples fall within this same range, there are some strong peaks in sulphur content (see *Figure 5.7*). While two of these peaks do correspond to a black shale horizon, with a third horizon showing some signs of enrichment, the three strongest peaks fall within the grey clay samples. In contrast to the other sites, the majority of the Amma Fatma samples exhibit higher TS contents with similar values to the peaks observed in the Briestroffer sequence (see *Figure 5.9*).

In terms of identifying low oxygen conditions, plots of TS alone do not seem to reliably identify the black shale horizons within the Niveau Pacquier and Briestroffer sediments. The data does seem to imply that the Amma Fatma sequence was laid down under a lower oxygenated regime than the other sites, and plots as expected for the mildly dysoxic Folkestone Gault Clay. However, it is clear that TS alone does not provide a reliable basis for interpretation or comparison of the extent of low oxygen conditions.

5.3.1.2 Total Organic Carbon and Inorganic Carbon

The plots of TOC appear to demonstrate a stronger correlation with the oxygenation conditions implied by the sedimentology. Within the black shale horizons of the Niveau Pacquier samples, TOC makes up a higher proportion of the total carbon present (see *Figure 5.6*). The total carbon content increases within the black shale horizons, as a result of the greater preservation potential of organic carbon in low oxygen environments. A division at a TOC values of 2 wt% appears to neatly divide the black shale and grey clay samples. The Briestroffer samples have a much higher inorganic carbon component which reinforces the fact that this kind of data could never be used to propose numerical boundaries for varied sites (see *Figure 5.7*).

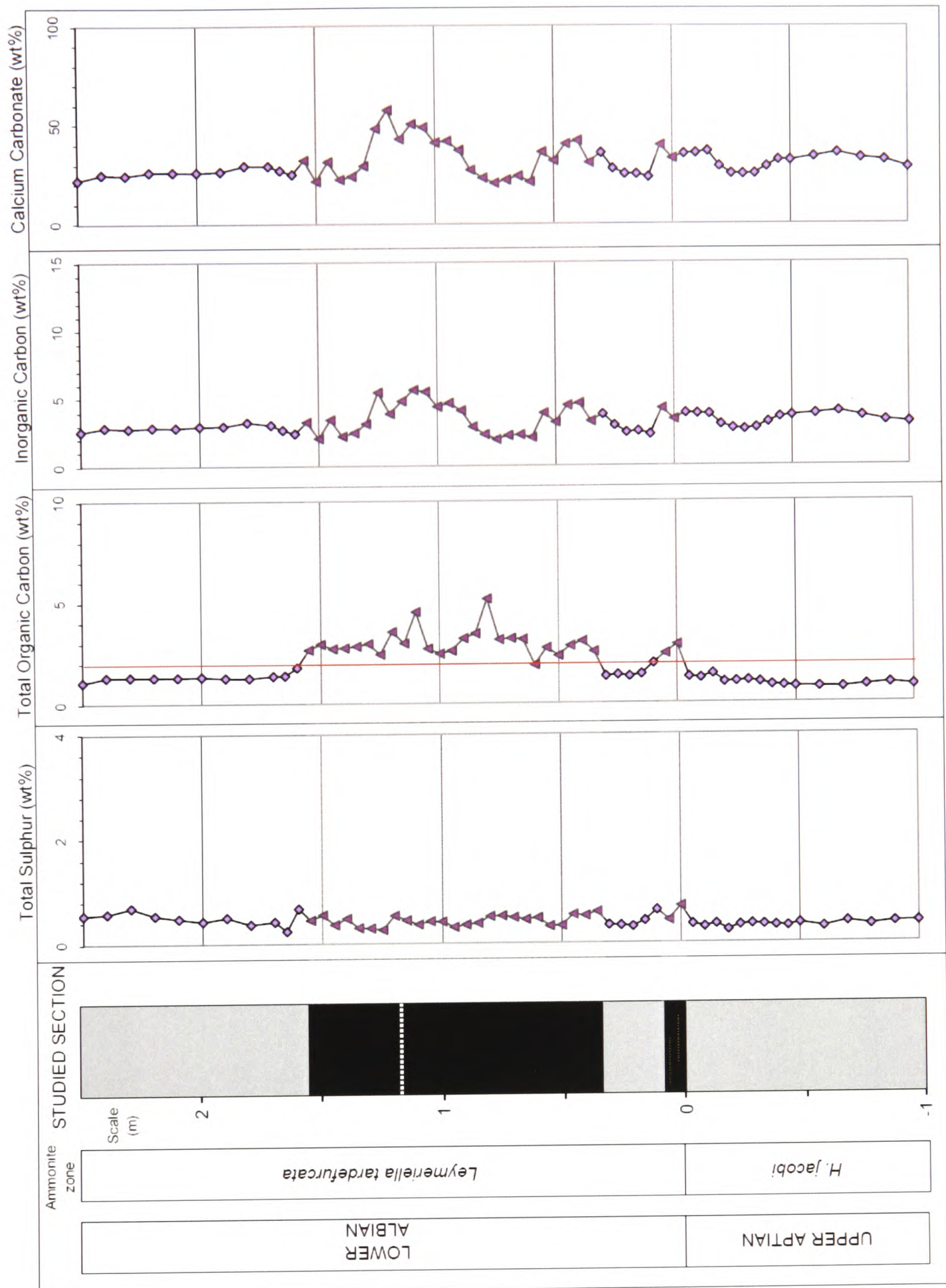


Figure 5.6: Total sulphur, Total Organic Carbon (TOC), inorganic carbon and calcium carbonate contents (in wt%) for the Niveau Pacquier samples. The proposed division of 2 wt% TOC is represented by the red line.

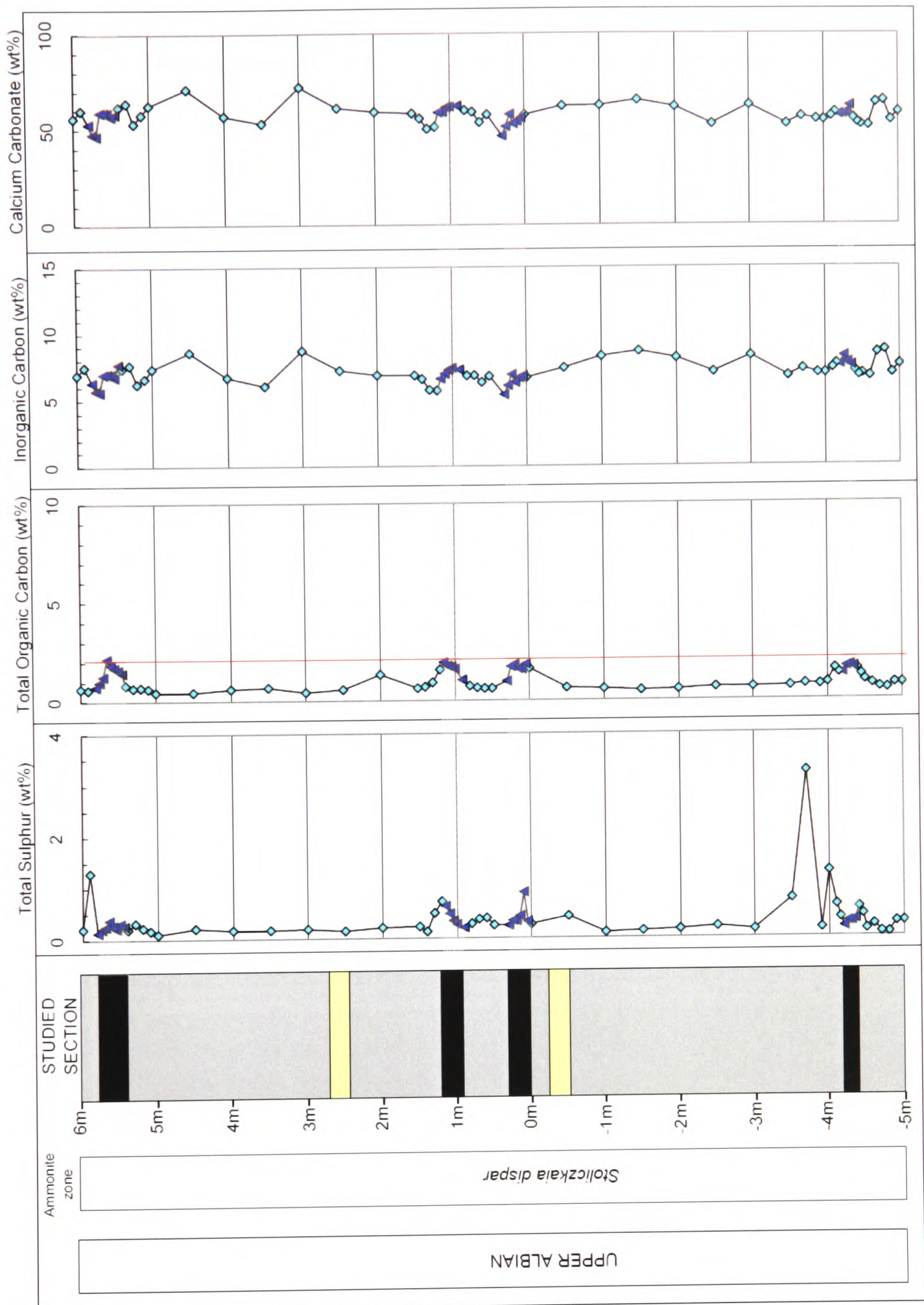


Figure 5.7: Total sulphur, Total Organic Carbon (TOC), inorganic carbon and calcium carbonate contents (in wt%) for the Briestroffer samples. The proposed division of 2 wt% TOC is represented by the red line.

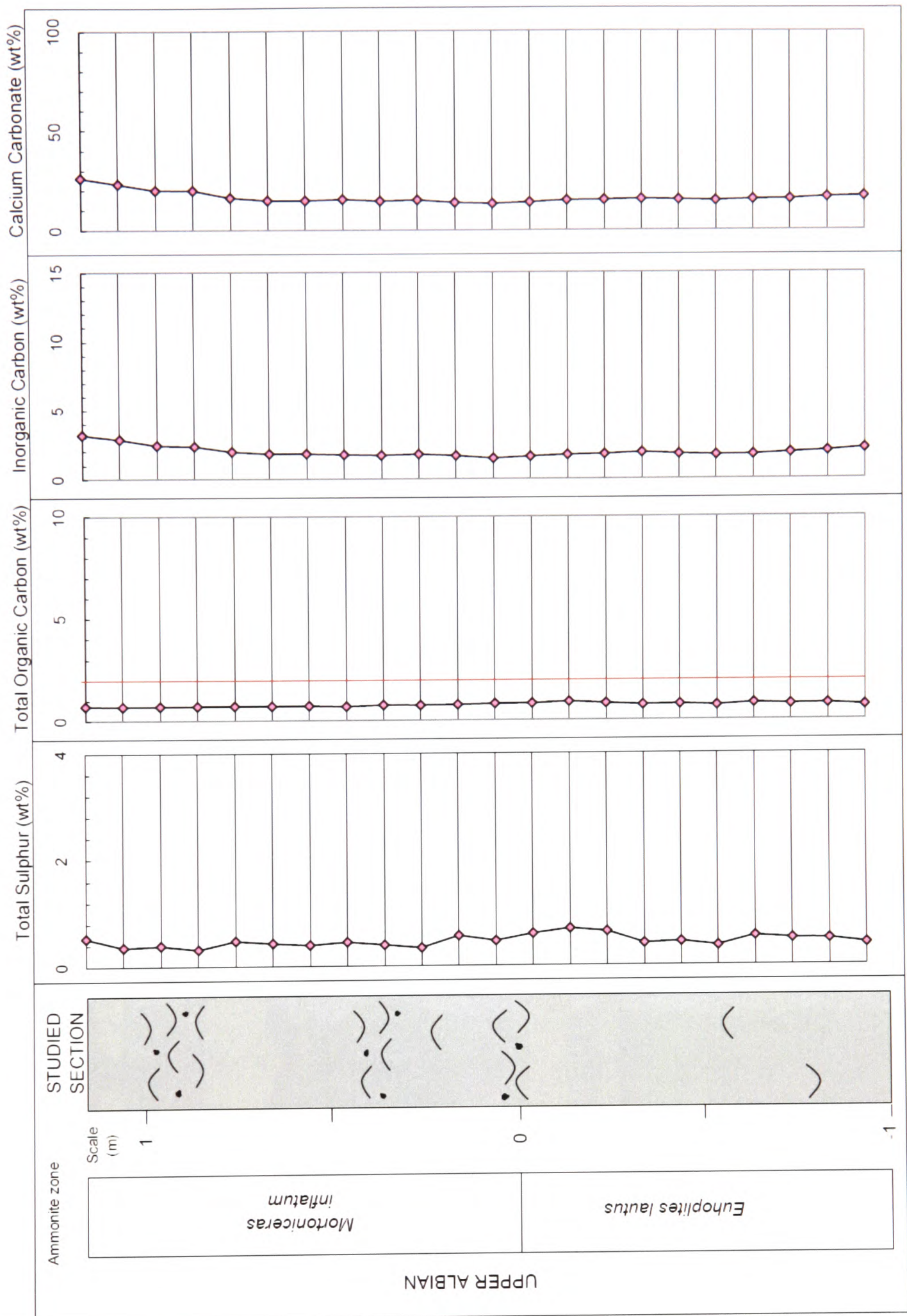


Figure 5.8: Total sulphur, Total Organic Carbon (TOC), inorganic carbon and calcium carbonate contents (in wt%) for the Folkestone Gault Clay samples. The proposed division of 2 wt% TOC is represented by the red line.

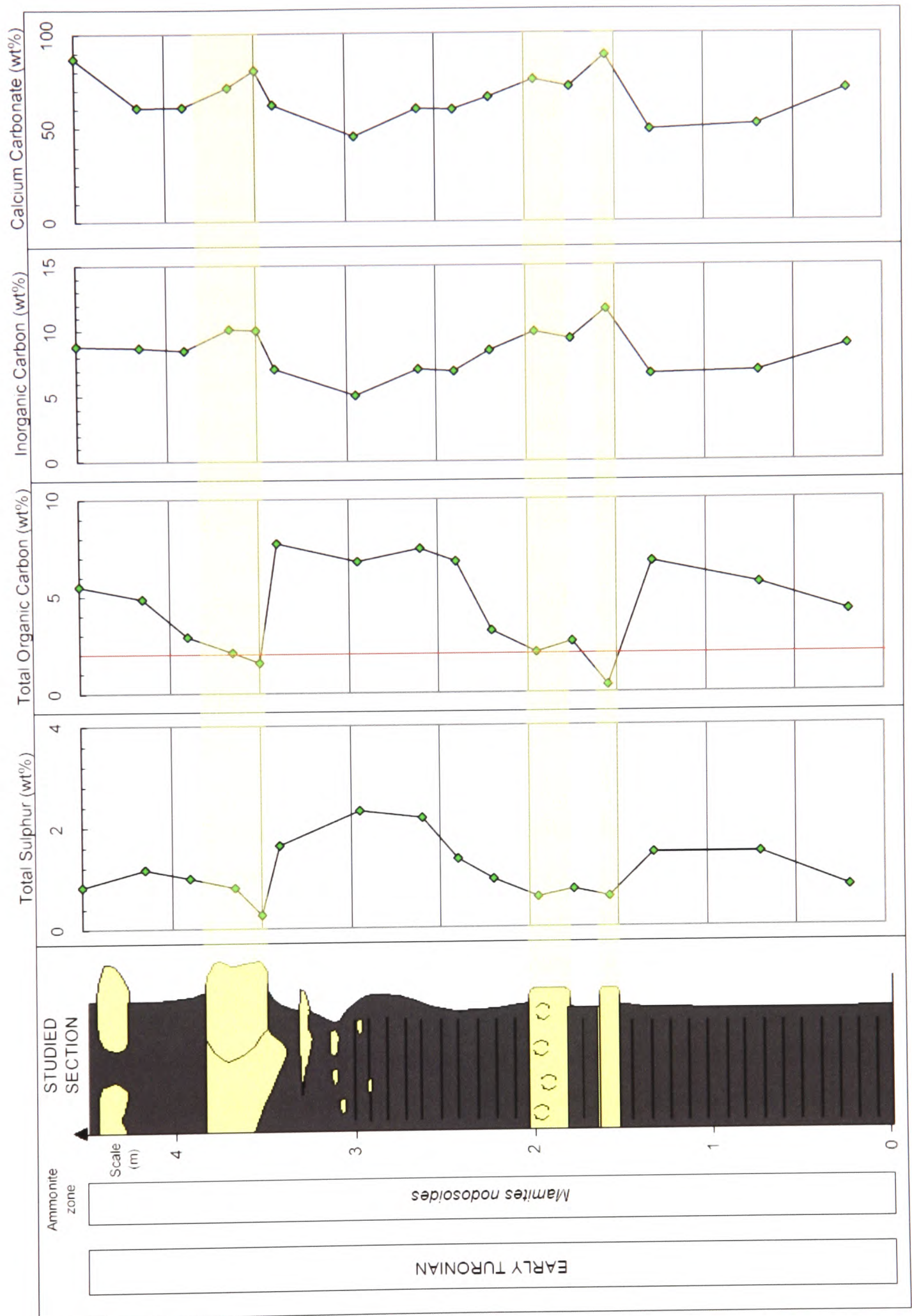


Figure 5.9: Total sulphur, Total Organic Carbon (TOC), inorganic carbon and calcium carbonate contents (in wt%) for the Amma Fatma samples. The proposed division of 2 wt% TOC is represented by the red line.

While it is clear that the amount (see *Figure 5.7*), and therefore also the proportion of organic carbon increases within the Breistroffer black shale horizons, only one sample has greater than 2 wt% TOC. It is also interesting to note that the wt% of inorganic carbon also appears to rise and fall regularly throughout the entire sequence. The Folkestone Gault Clay samples exhibit the lowest inorganic and organic carbon totals of the four sites (see *Figure 5.8*). The reduced amount of organic carbon preserved correlates with the idea that these sediments were laid down under the most oxygenated conditions out of the four sites and all samples fall below the proposed division of 2 wt% TOC. The amount of inorganic carbon present does rise towards the top of the sequence which acts to lower the proportion of organic carbon relative to the total amount present. The Amma Fatma samples, on the other hand, exhibit the highest Total Carbon levels of all four of the sites. In most of the samples a relatively large proportion of this is made up of organic carbon, apart from the sample from 1.55 m has a very low TOC value (see *Figure 5.9*). All of the dark marl samples have TOC values above the proposed division of 2 wt%. Again, the proportion of organic carbon and inorganic carbon appear to vary rhythmically through this sequence.

The plots of TOC seem to identify the black shale horizons in both the Niveau Pacquier and Briestroffer sequences. This suggests that the preservation of organic matter is linked to redox conditions and therefore may be of use as a proxy. The varying ranges of TOC alone could be used to imply a rough scale of oxygenation – this is more clearly demonstrated when TOC is plotted against calcium carbonate content (wt%) for all of the data sets (see *Figure 5.10*). This clearly shows higher TOC values for the black shale data sets within the Niveau Pacquier and Briestroffer sequences, while the range of CaCO₃ for each site remains similar to the related grey clay data sets. Relying on TOC data alone, and assuming a direct correlation with redox conditions, this would seem to suggest that the Folkestone Gault Clay was laid down under similar, if not slightly more oxygenated, redox conditions than the two grey clay sample sets. In turn the black shale samples from the Briestroffer sequence would appear to have formed under a more restricted oxygen regime, with the Niveau Pacquier black shale and finally the Amma Fatma samples representing increasingly anoxic environments. This suggestion does correlate to some extent with the sedimentology observed at each site and this implies that TOC may be of use in

identifying relative degrees of low oxygen conditions. Unfortunately, the relationship is not that simple as redox conditions are only one of a number of factors that control the amount of organic matter preserved in sediment and this makes it difficult to propose numerical boundaries by which to identify different conditions.

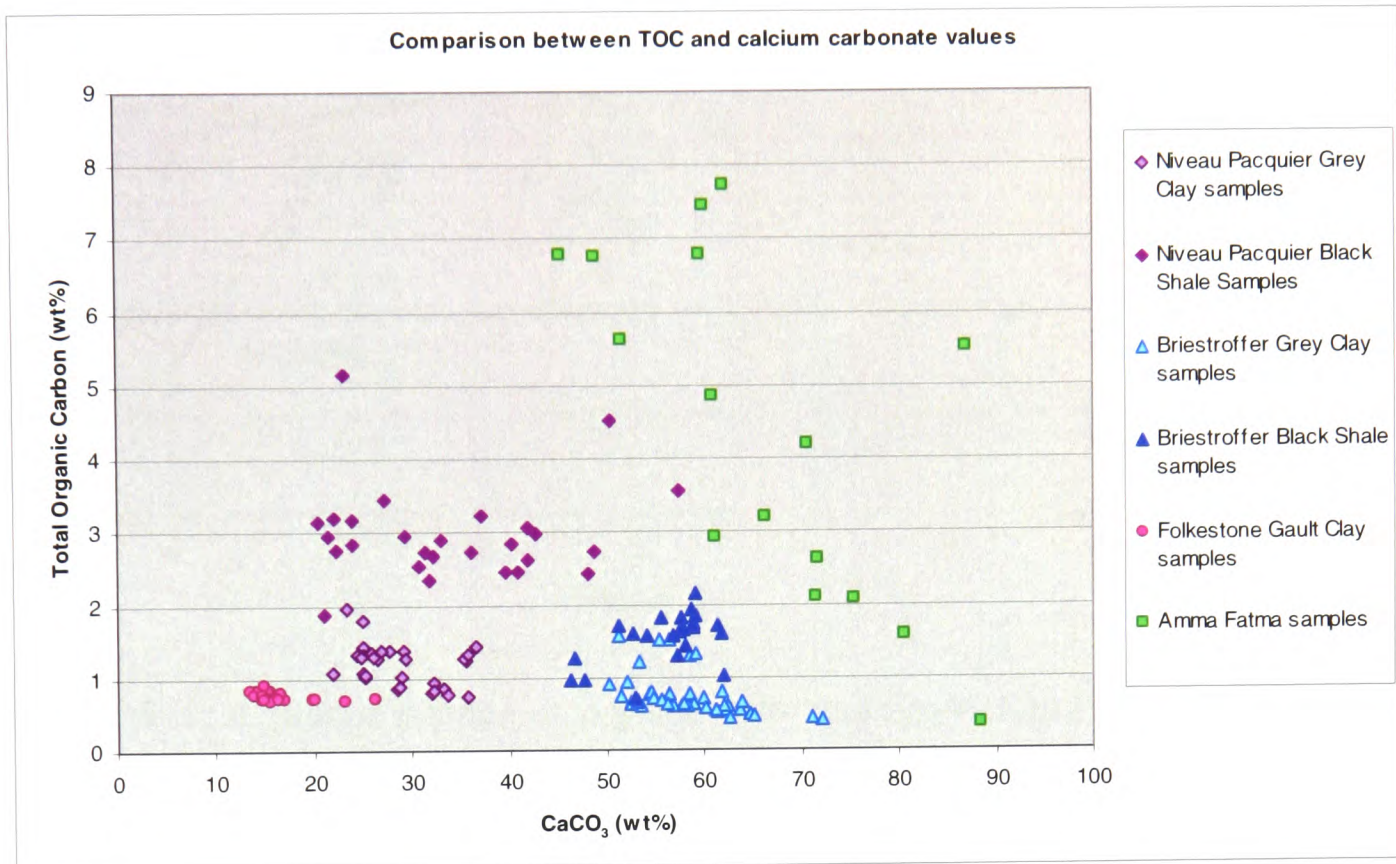


Figure 5.10: Plot of Total Organic Carbon against Inorganic Carbon (wt % CaCO₃) for the Niveau Pacquier Grey Clay and Black Shale samples, the Briestroffer Grey Clay and Black Shale samples, the Folkestone Gault Clay samples and the Amma Fatma samples.

5.3.1.3 The S/C ratio

The grey clay and black shale samples of the Niveau Pacquier sequence plot within distinct regions on an S/C plot (see Figure 5.11). However, while both data sets appear to show a limited positive correlation the linear regressions are not statistically significant and so interpretation of the data is limited.

Unfortunately, the S/C plot is equally unconvincing for the Briestroffer samples (see Figure 5.12) – in this set both the grey clay and black shale samples also plot with a very low R² value which means that the apparent positive correlations observed are statistically invalid.

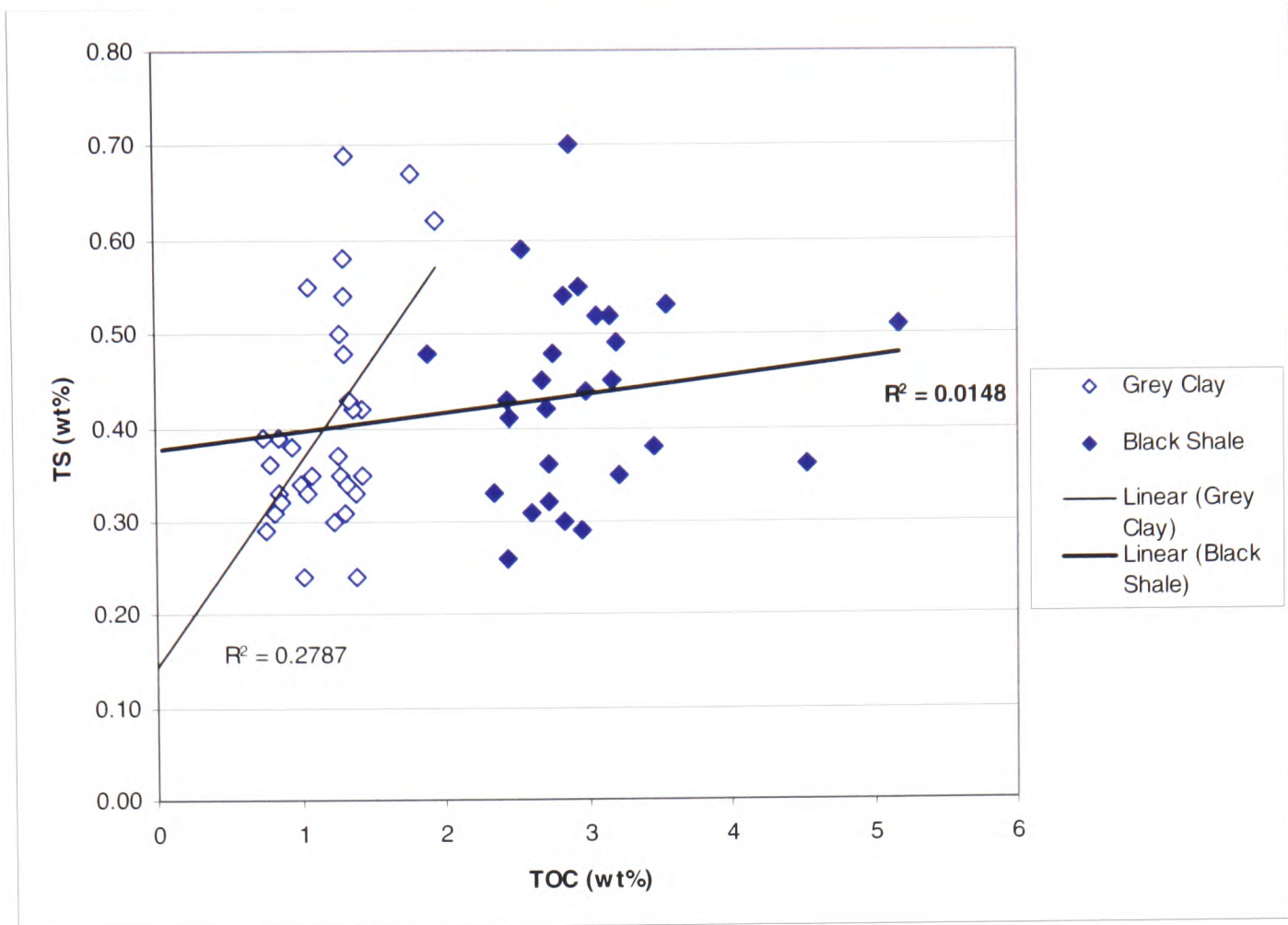


Figure 5.11: A plot of sulphur vs. organic carbon of the Niveau Pacquier sample sets

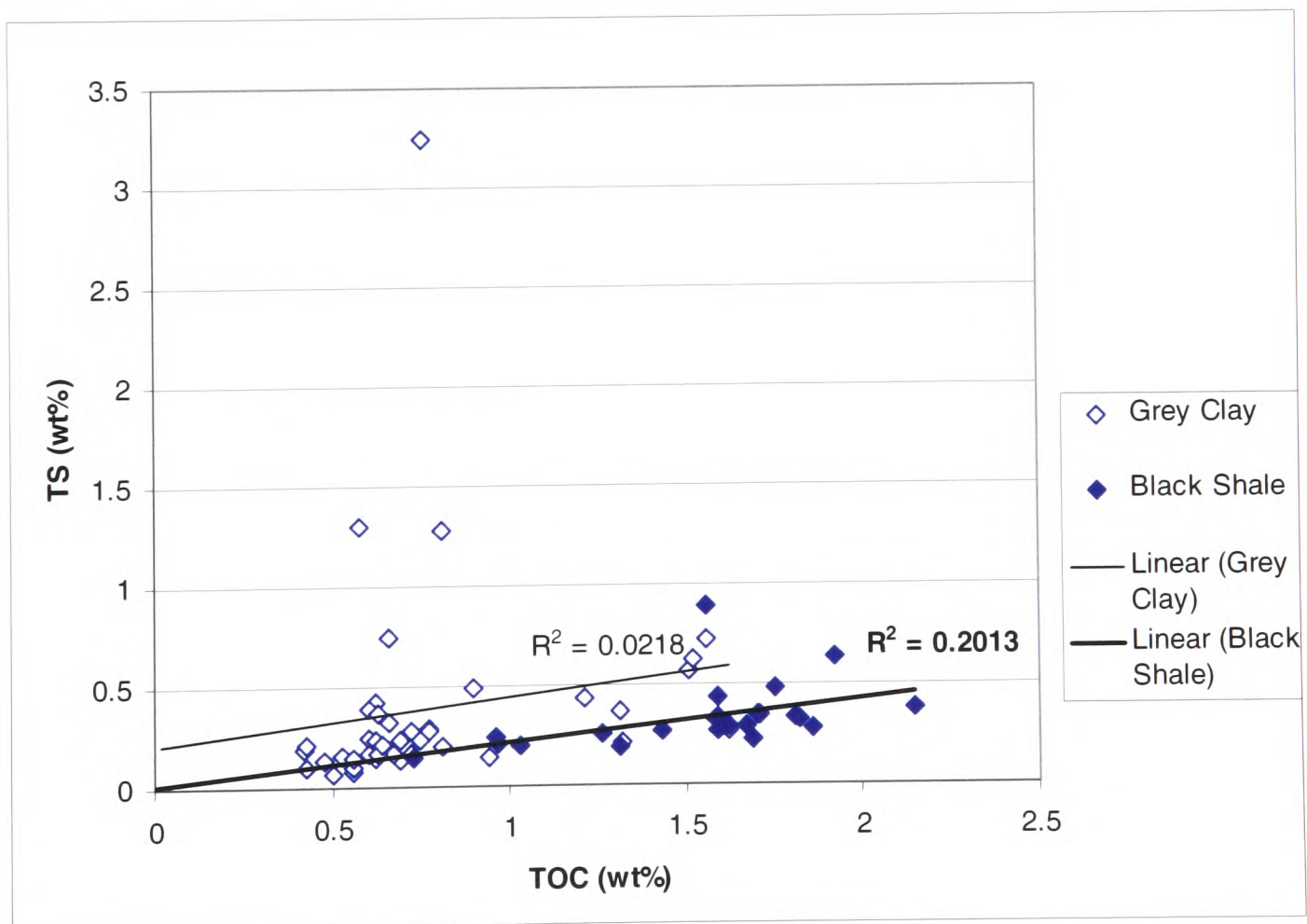


Figure 5.12: A plot of sulphur vs. organic carbon of the Briestroffer sample sets.

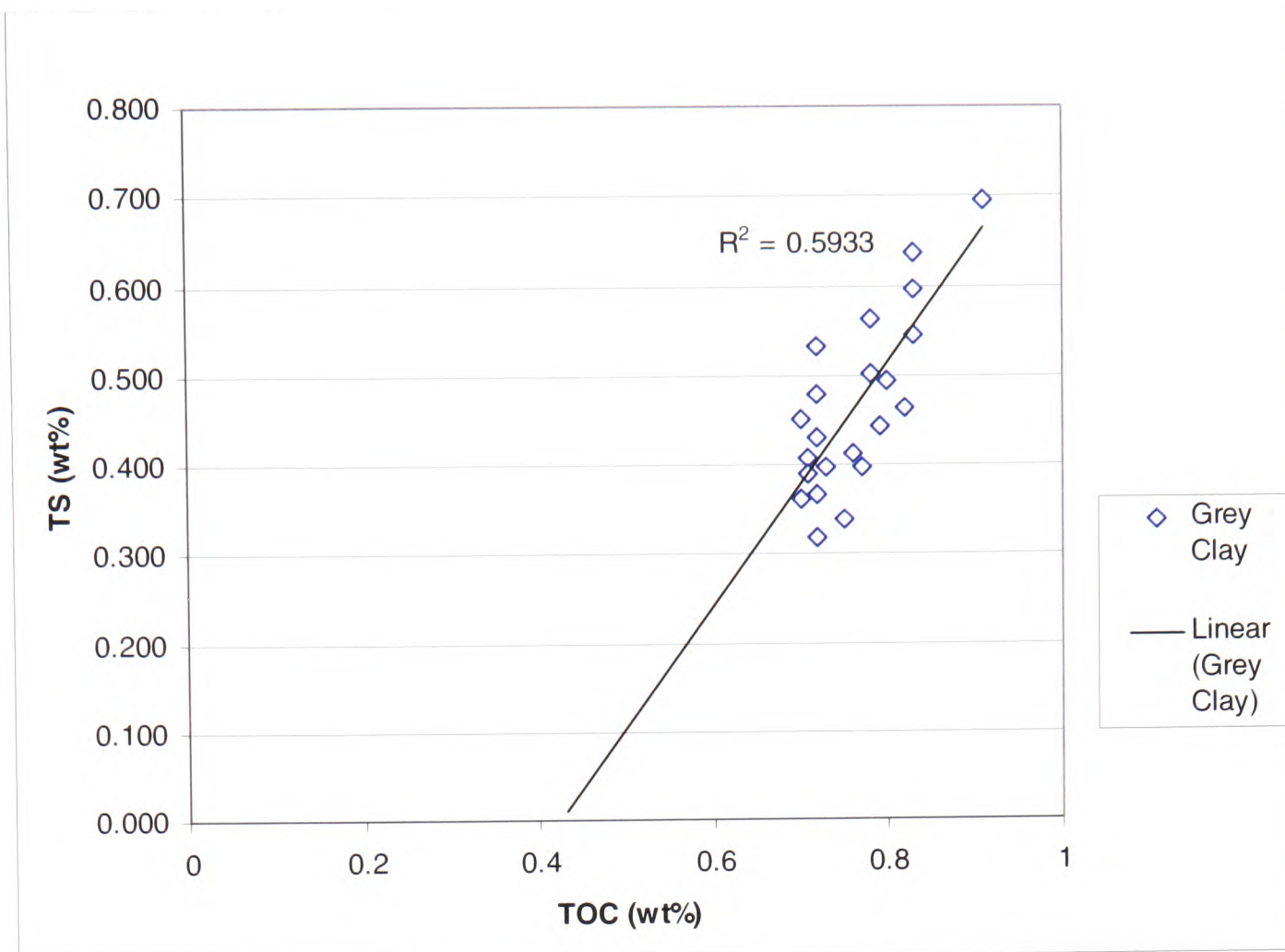


Figure 5.13: A plot of sulphur vs. organic carbon of the Folkestone Gault samples.

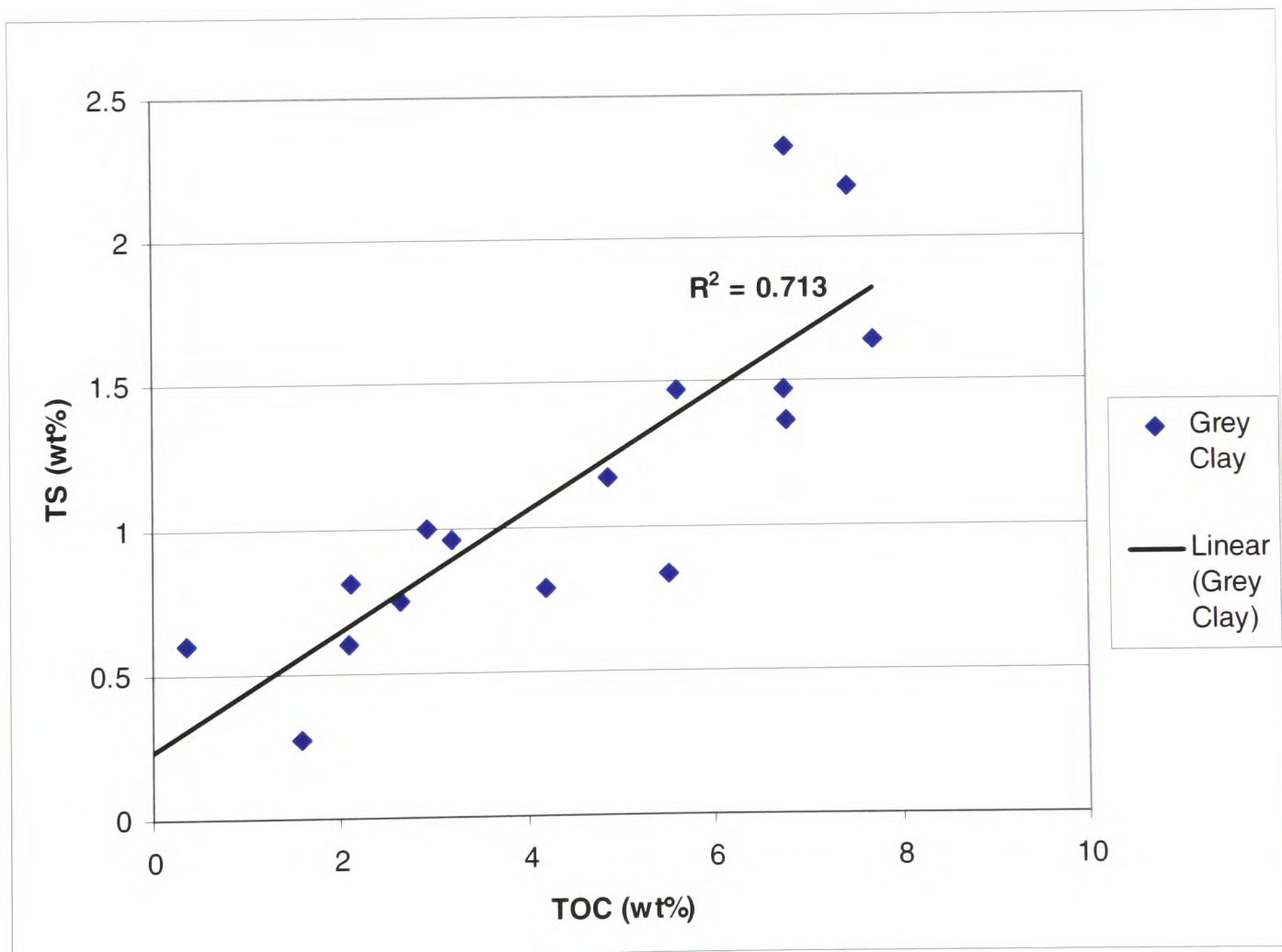


Figure 5.14: A plot of sulphur vs. organic carbon of the Amma Fatma samples.

The Folkestone Gault Clay samples show a limited positive correlation but the intercept of this unconvincing regression line is negative on the sulphur axis (see *Figure 5.13*). This may be related to the relatively low TOC values for these sediments, which should give the strongest 'oxic' signal of all of the four sites.

The Amma Fatma samples, on the other hand, plot with a statistically significant regression line. The samples could be interpreted as having been laid down in an euxinic environment as they demonstrate a slight positive intercept of the regression line (see *Figure 5.14*). The regression line does show a positive correlation between organic carbon and sulphur, but Leventhal (1982) accepted that this was common of many euxinic environments. This positive correlation may be due to iron limitation (Rimmer, 2004) or the overprinting of further diagenetic pyrite formation after burial (Lyons and Berner, 1992).

This plot differs from the black shale samples of the Niveau Pacquier sequence (see *Figure 5.11*) which shows little correlation between organic carbon and sulphur. While this is thought to be indicative of euxinic environments, Raiswell and Berner (1985) recognized that deposition under dysoxic water columns may create a horizontal regression line on S/C plots. This could be taken to suggest that the Niveau Pacquier black shale was laid down under more dysoxic conditions, whereas the Amma Fatma environment was closer to euxinic conditions. However, this is only one interpretation of the plot and, given the statistical insignificance of the regression lines generated on the majority of the plots, this proxy should only be regarded as a broad environmental indicator at best.

5.3.2 Iron pools

Within the Niveau Pacquier sequence, the proportion of Fe_D compared to Fe_{Py} does appear to decrease slightly in some of the black shale samples, suggesting that more of the potentially reactive iron did react to form pyrite (see *Figure 5.15*). However, overall there does not appear to be an obvious pattern associated with the two different sedimentological groups of samples.

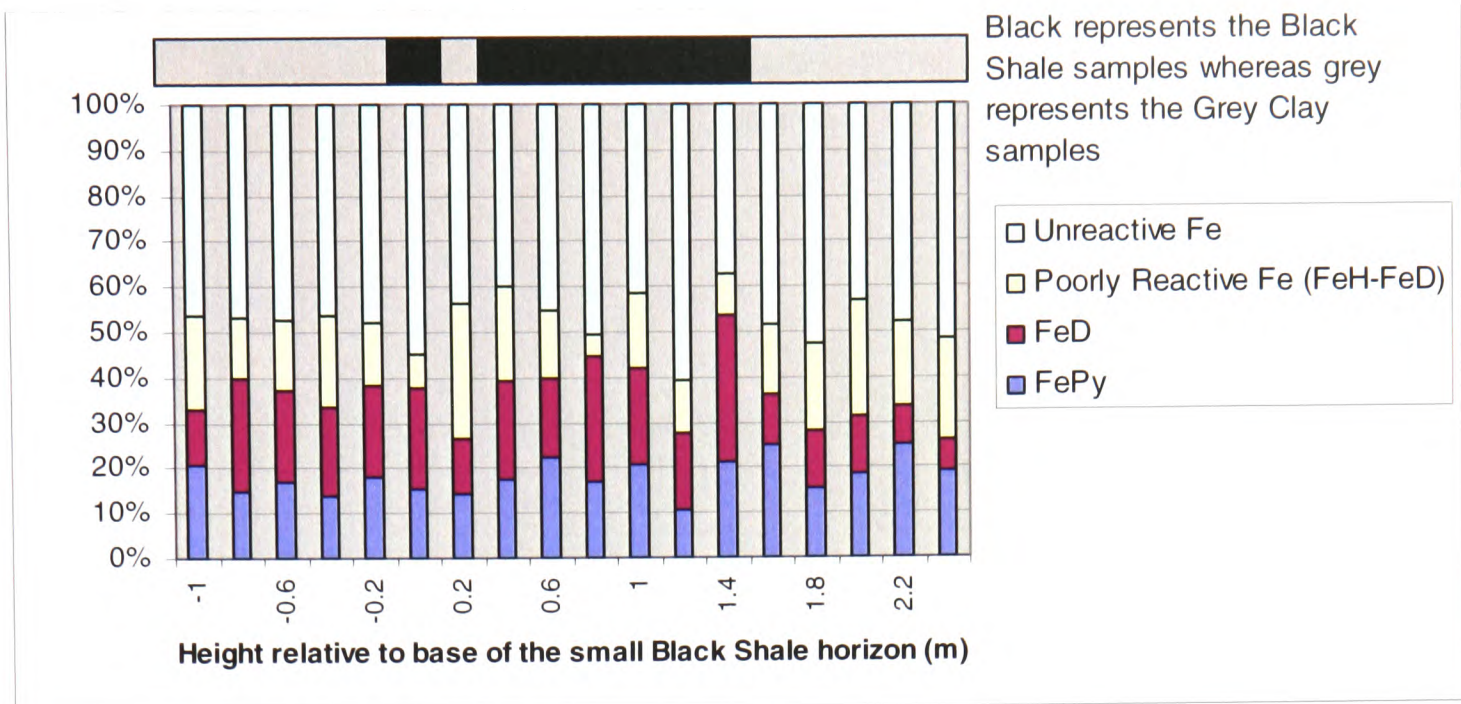


Figure 5.15: A cumulative bar chart of the Niveau Pacquier samples, showing the relative proportions of Pyrite Iron (Fe_{Py}), Non-pyritic Highly Reactive Iron (FeD), Poorly Reactive Iron ($FeH-FeD$) and Unreactive Iron ($FeT-FeH-Fe_{Py}$).

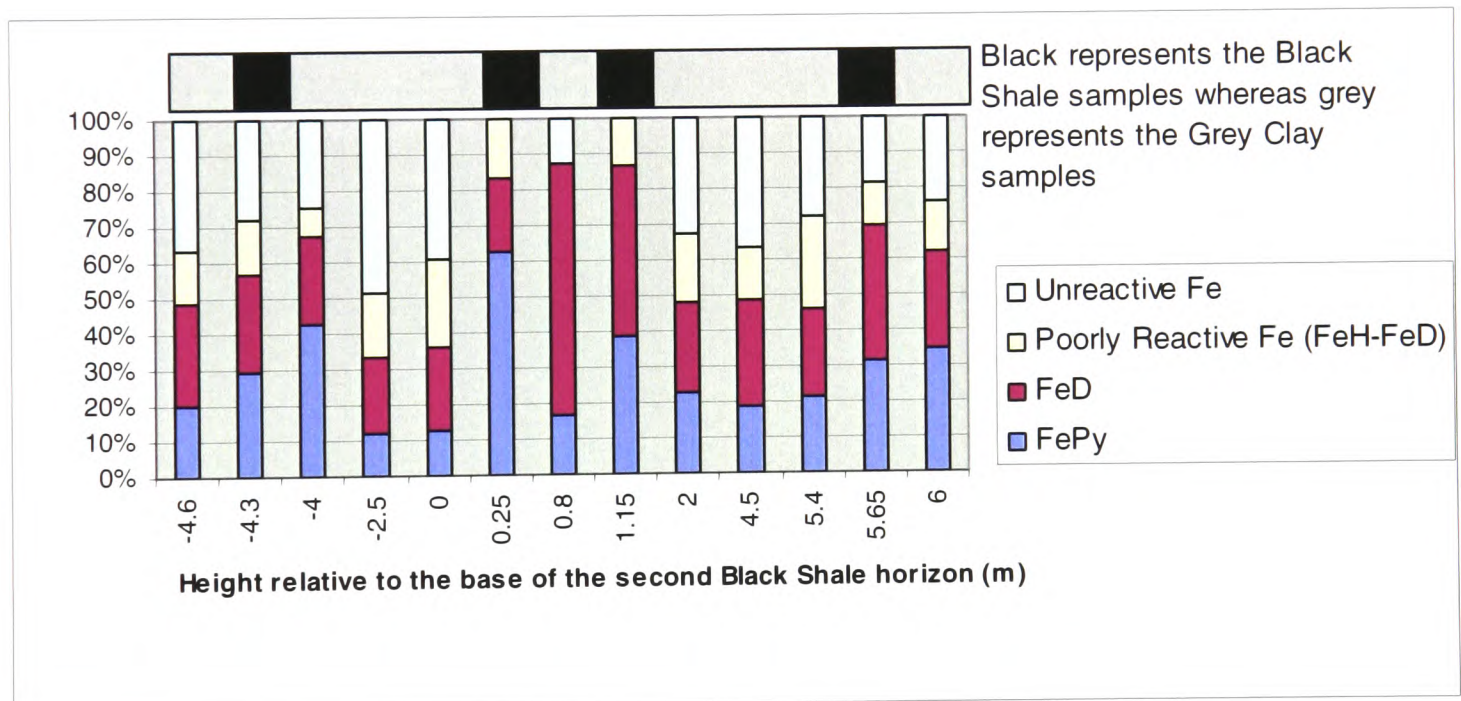


Figure 5.16: A cumulative bar chart of the Briestoffer samples, showing the relative proportions of Pyrite Iron (Fe_{Py}), Non-pyritic Highly Reactive Iron (FeD), Poorly Reactive Iron ($FeH-FeD$) and Unreactive Iron ($FeT-FeH-Fe_{Py}$).

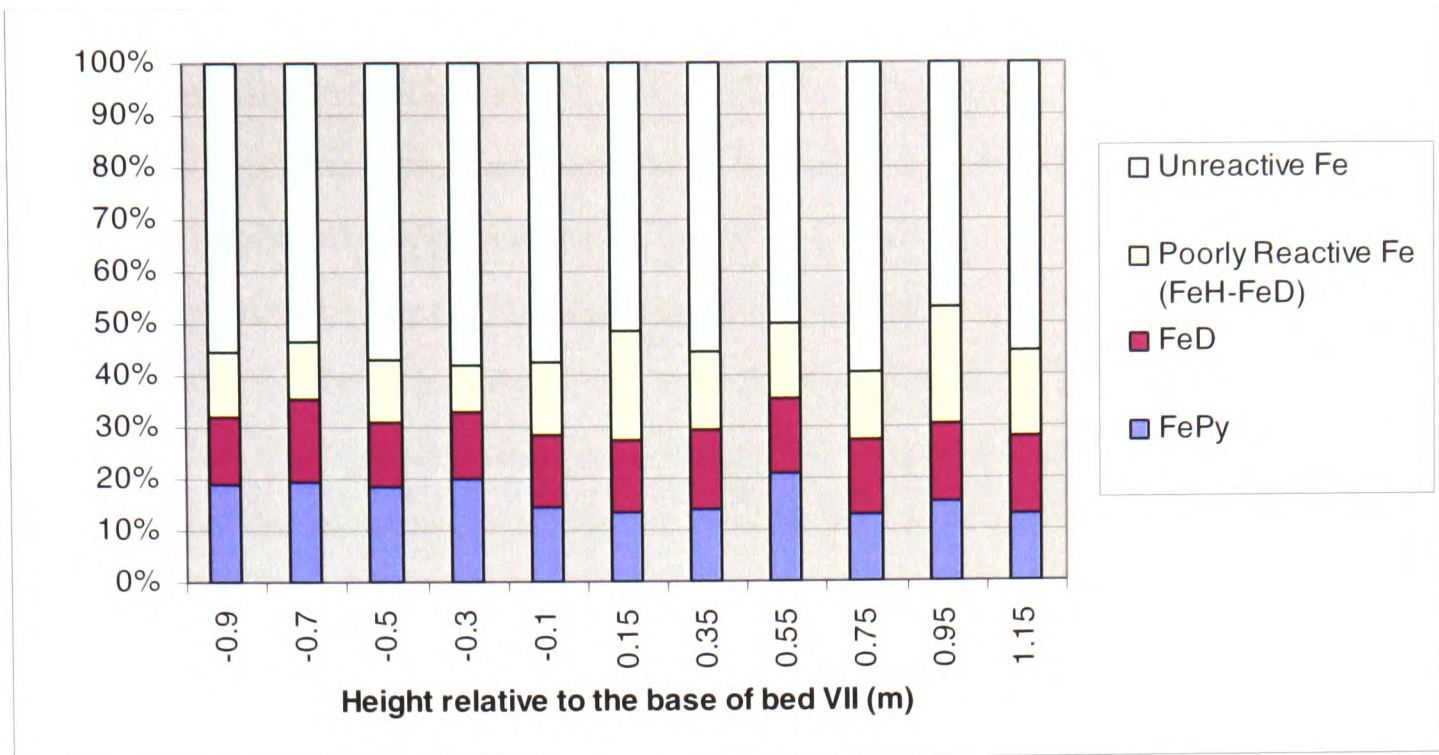


Figure 5.17: A cumulative bar chart of the Folkestone Gault Clay samples, showing the relative proportions of Pyrite Iron (Fe_{Py}), Non-pyritic Highly Reactive Iron (FeD), Poorly Reactive Iron ($FeH-FeD$) and Unreactive Iron ($FeT-FeH-Fe_{Py}$).

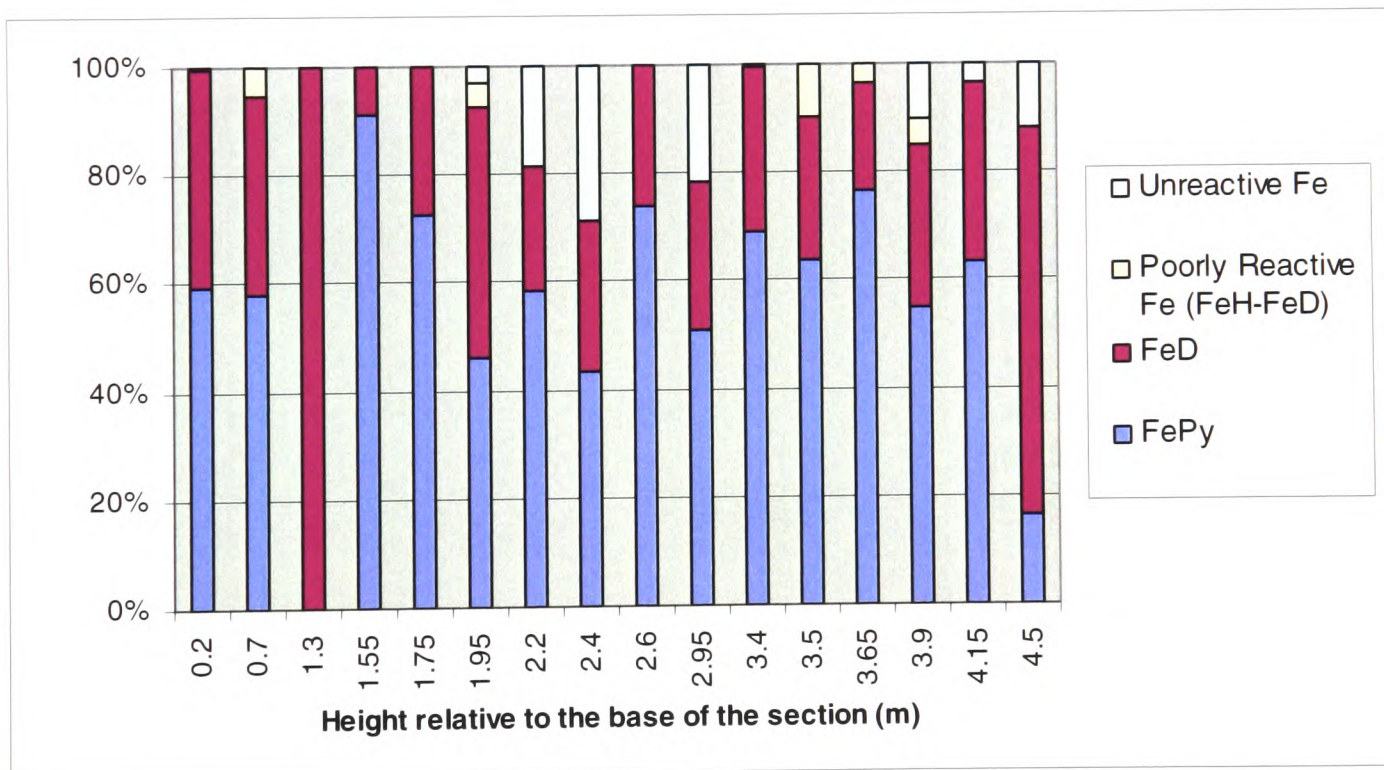


Figure 5.18: A cumulative bar chart of the Amma Fatma samples, showing the relative proportions of Pyrite Iron (Fe_{Py}), Non-pyritic Highly Reactive Iron (FeD), Poorly Reactive Iron ($FeH-FeD$) and Unreactive Iron ($FeT-FeH-Fe_{Py}$).

The proportion of reactive iron (**FeD + FePy**) in the Niveau Pacquier samples does reach up to 50% of the total iron, compared to a maximum of 35% for the more

oxygenated Folkestone Gault Clay samples (see *Figure 5.17*). This may provide evidence to support Raiswell *et al.*'s (2001) suggestion that lower oxygen environments receive more reactive iron via lateral transport within the water column. This would explain the higher levels of pyrite in low oxygen sediment, but these data alone cannot provide conclusive evidence of this as the two sites are very different in bulk mineralogy (see *Figures 4.4, 4.5 and 4.30*) and setting. The Folkestone Gault Clay samples show little variation through the sequence and in particular, are unaffected by the increase in carbonate toward the top of the sequence (see *Figure 5.8*). Raiswell *et al.* (2001) suggested that in euxinic settings this could have affected the relative proportion of pyrite iron by diluting the less reactive iron within the sediment. The Folkestone Gault Clay is in no way thought to be a euxinic sediment, but this observation agrees with those of Raiswell *et al.* (2001) which suggest that dilution by inorganic carbon only has an effect in euxinic environments. Both the Amma Fatma (see *Figure 5.18*) and Briestroffer sample sets (see *Figure 5.16*) show a much higher proportion of both pyrite iron and **FeD**.

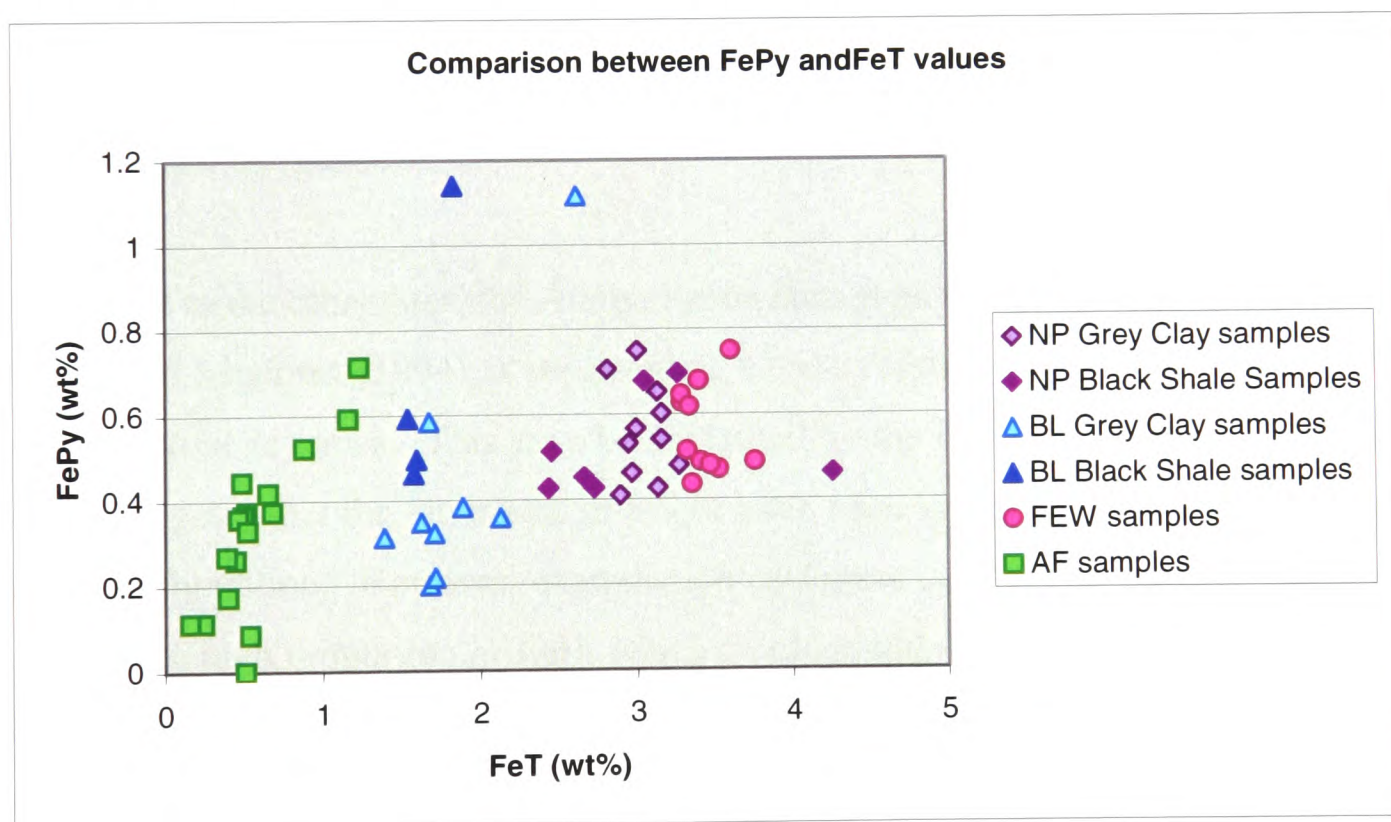


Figure 5.19: Plot of Pyrite Iron against Total Iron for the Niveau Pacquier Grey Clay and Black Shale samples, the Briestroffer Grey Clay and Black Shale samples, the Folkestone Gault Clay samples and the Amma Fatma samples.

It is noticeable from a plot of **FePy** against Total Iron (see *Figure 5.19*) that both of these sample sets have relatively low Total Iron contents, and these are also the two sites with the highest levels of Inorganic Carbon (see *Figure 5.10*). The low

proportion of Unreactive Iron may therefore be linked to low detrital inputs relative to biogenic inputs. The plot of **FePy/FeT** shows however, that despite the high proportion of Reactive Iron in samples from these two sites, the actual weight% of Pyrite Iron present has a similar range to the other sites.

5.3.3 Ternary plots of Fe, S and C

On the Fe-S-C ternary plots, (see *Figures 5.20, 5.21, 5.22 and 5.23*) the Folkestone Gault Clay, Niveau Pacquier grey clay and Briestroffer grey clay samples all plot close to the proposed Normal Marine regression line of **S/C** 0.4. In both the Niveau Pacquier black shale samples and the Briesroffer black shale samples, the data plots off to the side of the Normal Marine regression line within a region that suggests that **FeT** played a greater role in controlling pyrite formation. While they do not plot on a clear line of fixed Fe/S, which would indicate euxinic conditions, the location of the data points suggests deposition under a lower oxygen regime than their grey clay counterparts. The Fe-S-C ternary diagrams were designed to distinguish between normal marine and true euxinic conditions, but this separation of black shale and grey clay data plots does suggest that it provides clues to differentiate between medium grades of low oxygenation.

In contrast to the other sites, the Amma Fatma data plots within the zone identified by Arthur and Sageman (1994) as representing excess sulphur in the sediment, possibly in the form of organics. This may be explained by the low **FeT** of these sediments, which suggests that the environment might have been severely iron-limited in terms of pyrite formation. However, examination of *Figure 5.18* suggest that the samples contained a high proportion of **FeD**, which would readily have reacted to form pyrite. The data plots along the same orientation as the 'ideal' euxinic regression line, which again implies that iron-limitation controlled pyrite formation, and that the sediments formed under a euxinic water column.

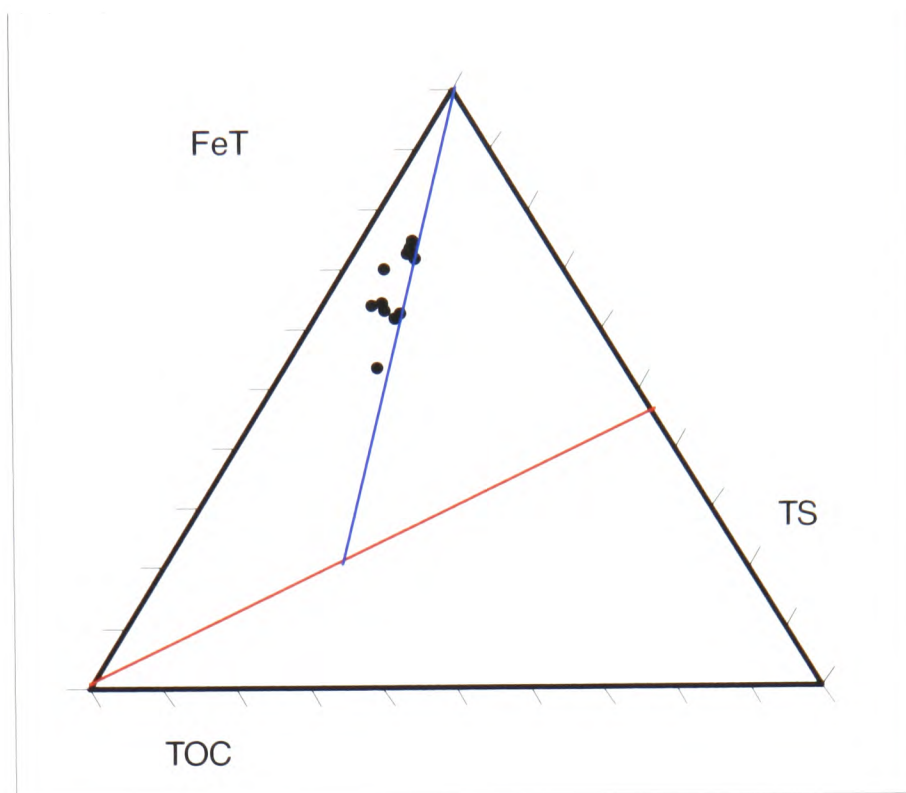


Figure 20 (a)

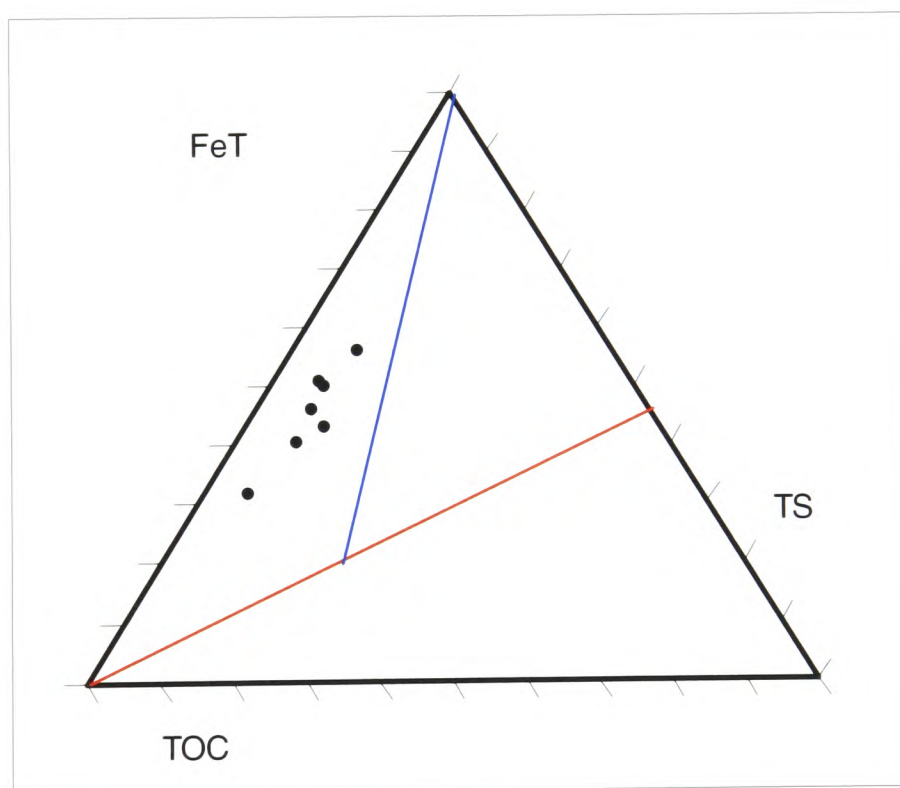


Figure 20 (b)

Figure 5.20: Ternary Fe-S-C plots of the: (a) Niveau Pacquier Grey Clay samples; and (b) Niveau Pacquier Black Shale samples. The blue line represents the 'ideal' regression line of data from normal marine settings whereas the red line represents full pyritisation of iron within an euxinic setting (after Arthur and Sageman, 1994).

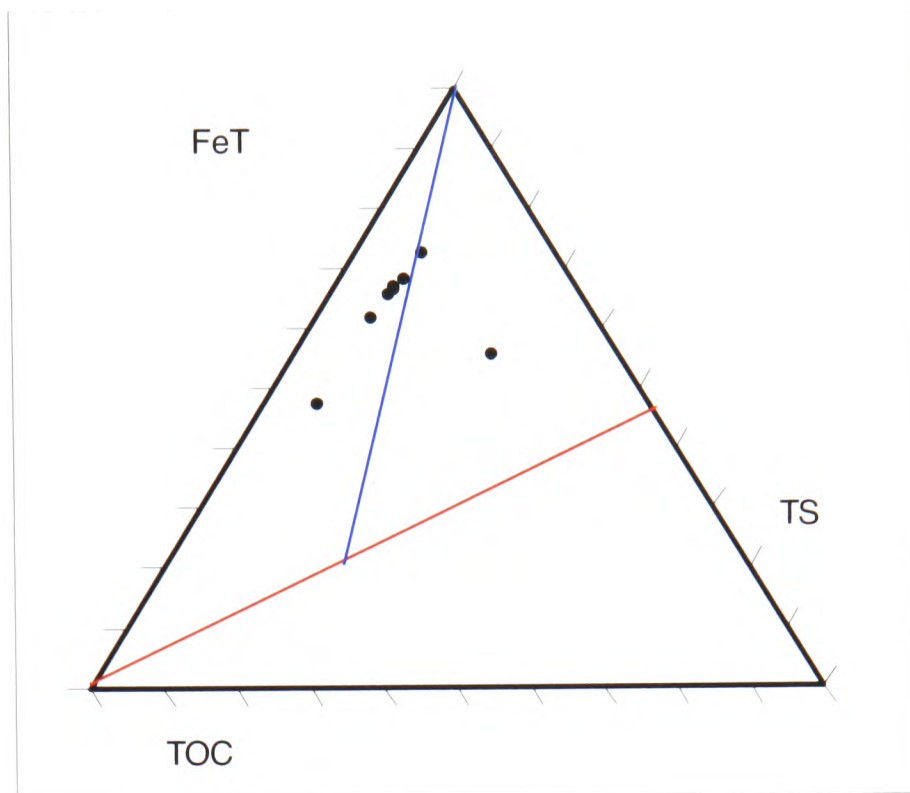


Figure 21 (a)

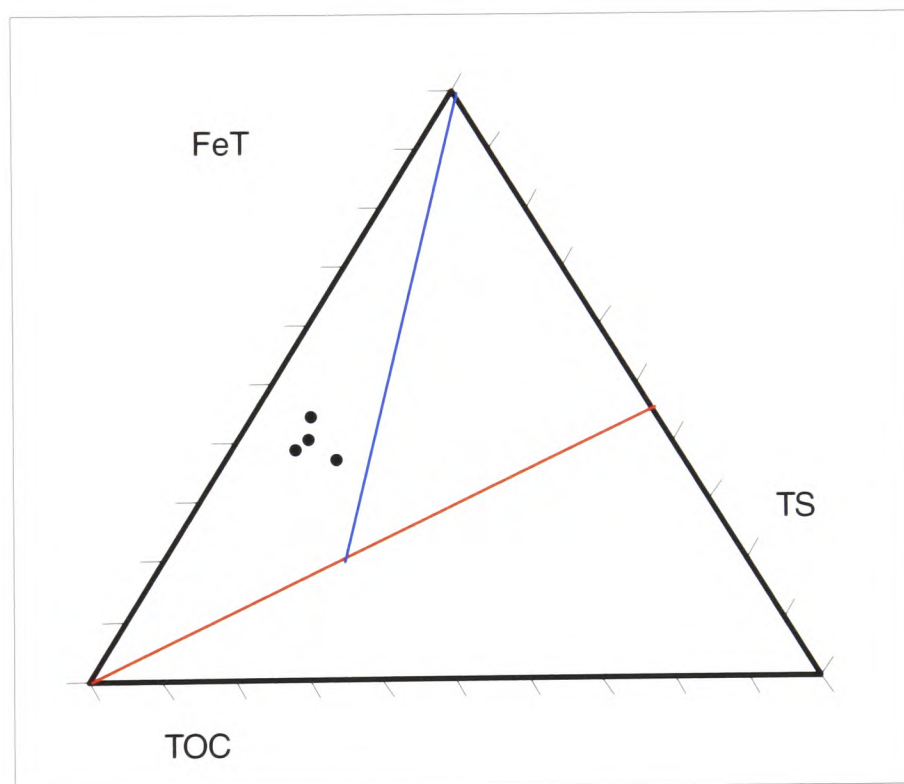


Figure 21 (b)

Figure 5.21: Ternary Fe-S-C plots of the: (a) Briestroffer Grey Clay samples; and (b) Briestroffer Black Shale samples. The blue line represents the 'ideal' regression line of data from normal marine settings whereas the red line represents full pyritisation of iron within an euxinic setting (after Arthur and Sageman, 1994).

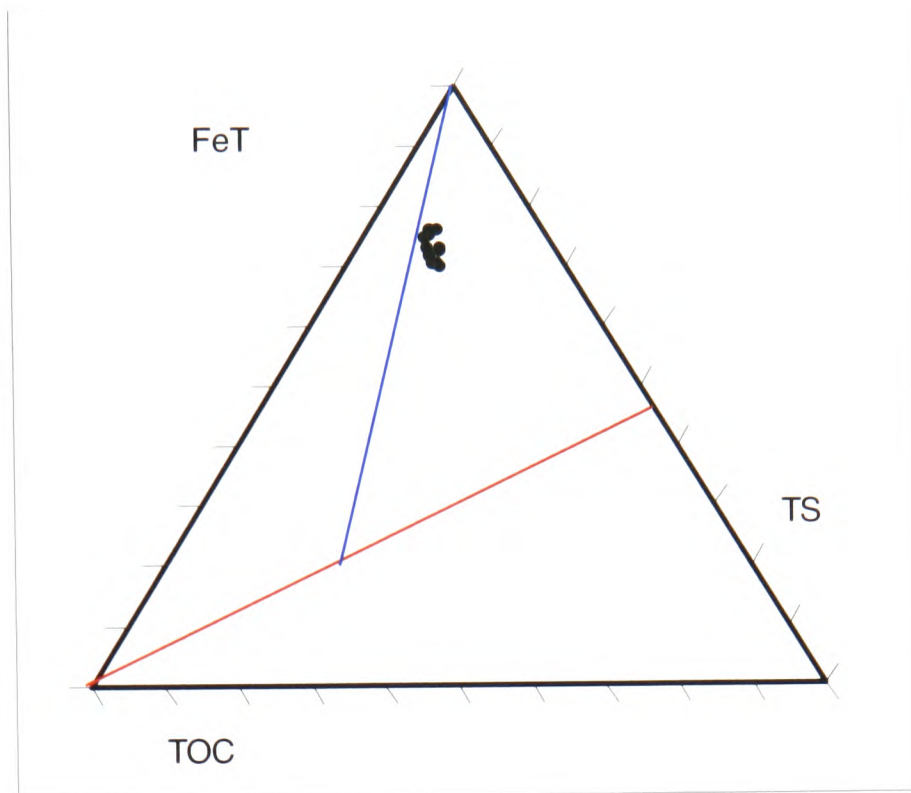


Figure 5.22: Ternary Fe-S-C plots of the Folkestone Gault Clay samples. The blue line represents the 'ideal' regression line of data from normal marine settings whereas the red line represents full pyritisation of iron within an euxinic setting (after Arthur and Sageman, 1994).

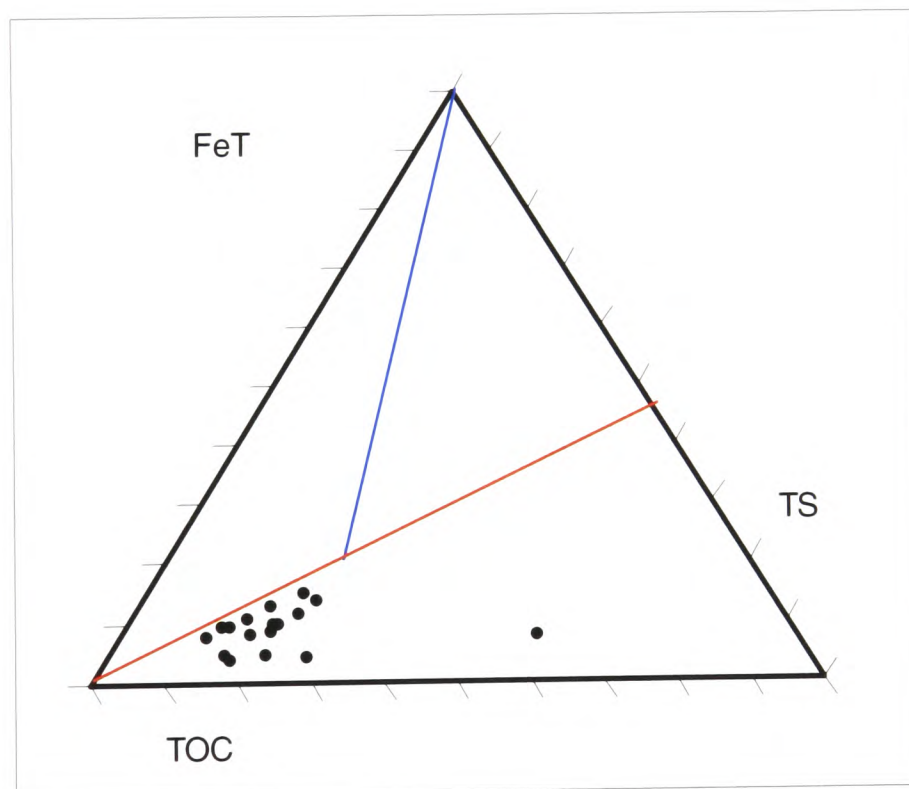


Figure 5.23: Ternary Fe-S-C plots of the Amma Fatma samples. The blue line represents the 'ideal' regression line of data from normal marine settings whereas the red line represents full pyritisation of iron within an euxinic setting (after Arthur and Sageman, 1994).

5.3.4 The Degree of Pyritisation

5.3.4.1 The Degree of pyritisation

The Degree of Pyritisation (calculated as $DOP_H = Fe_{Py} / [Fe_{Py} + Fe_H]$) does not seem to differentiate between the black shale and grey clay horizons of either the Niveau Pacquier or Briestroffer samples (see *Figure 5.24* and *Figure 5.25*). In both cases, both data sets plot close to the proposed normal marine: restricted boundary of 0.42 (Raiswell *et al.*, 1988) with some grey clay samples, and one Briestroffer Black Shale samples, extending into the restricted zone. The Folkestone Gault Clay samples, which represent the most oxic site, also plot either side of the Normal Marine:Restricted boundary (see *Figure 5.26*). This would suggest that the **DOP** cannot differentiate well between the lower levels of dysoxia. On the other hand, the majority of Amma Fatma samples plot within the restricted zone (see *Figure 5.27*), with some data points extending into the proposed 'Inhospitable Bottom Water' zone (Raiswell *et al.*, 1988). This shows that, whereas the **DOP** cannot distinguish between medium grades of low oxygenation, it can to some extent be used differentiate between two extremes of oxygenation conditions.

5.3.4.2 Combination of the Degree of Pyritisation with the S/C ratio

While **DOP** alone appears to be limited in its application, the use of plots of **DOP** against organic carbon, and **FeT** against organic carbon may help to interpret **S/C** plots.

The Grey Clay samples of the Niveau Pacquier set show a limited positive correlation between organic carbon and sulphur (see *Figure 5.13*), and the same is true of the relationship between **DOP** and organic carbon content (see *Figure 5.28*). This would be expected if the sediments were laid down under relatively oxic waters as the pyrite formation would occur within the sediment and the amount of organic carbon available would limit the amount of pyrite that can form. However, the linear regression is not statistically valid and so interpretation of the data is limited.

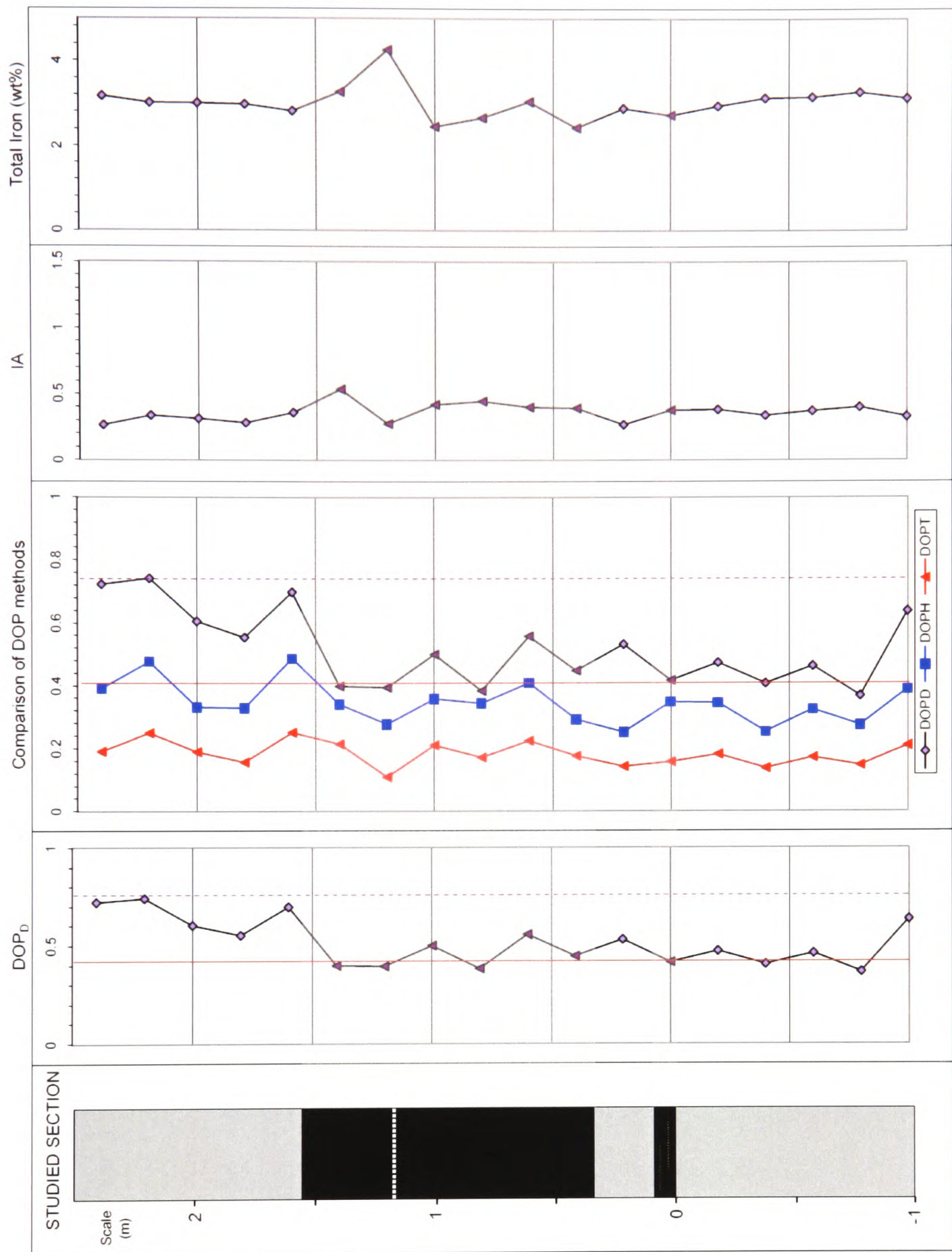


Figure 5.24: The Degree of Pyritisation, Indicator of Anoxia (IA) and Total Iron data for the Niveau Pacquier samples (Black Shale samples are identified as the darker shaded data points compared to the lighter Grey Clay data points). The red line marks the Normal Marine – Restricted boundary (Raiswell et al., 1988), and the dashed purple line marks the lower limit that Raiswell et al. (1988) suggested defines 90% of Inhospitable Bottom Water samples.

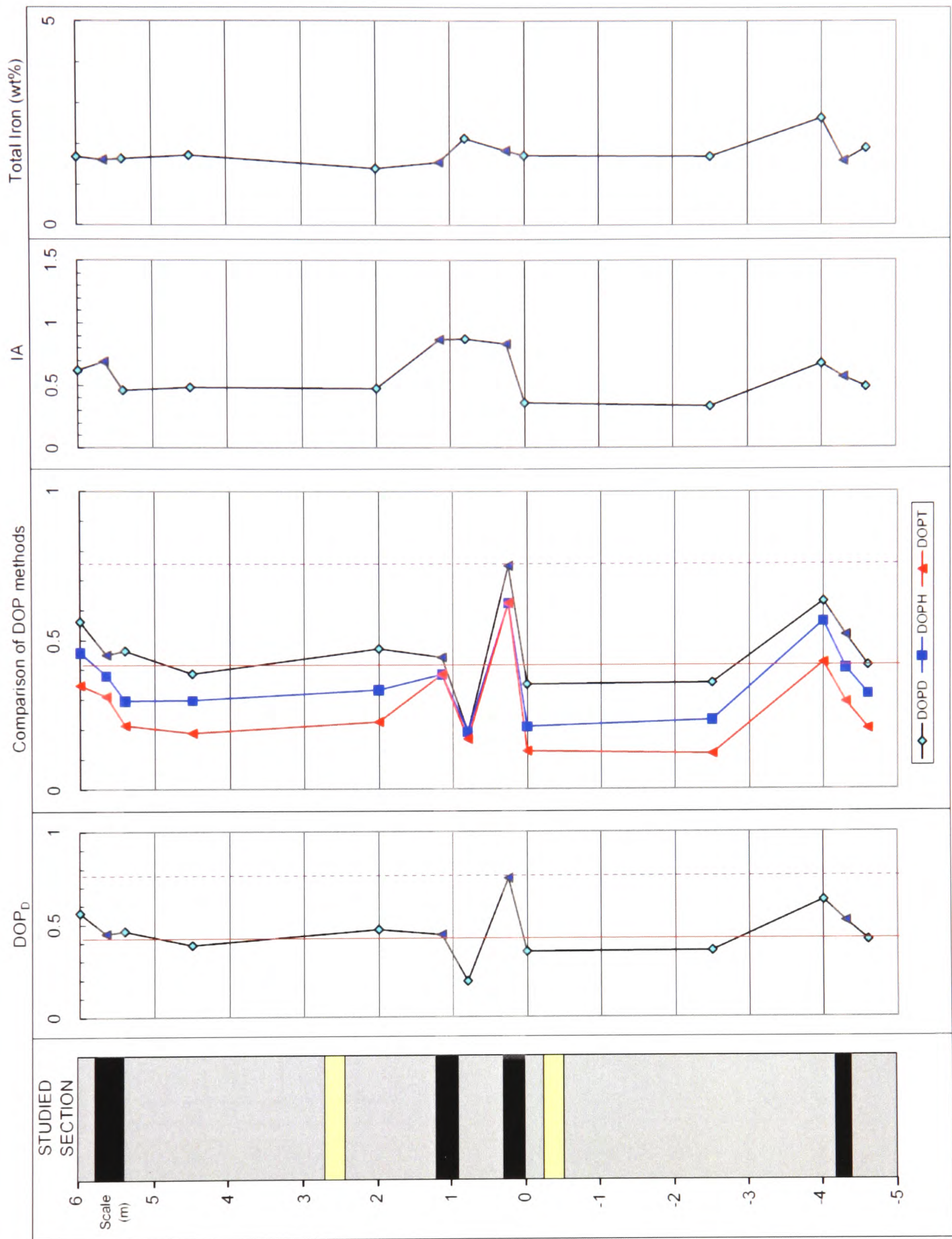


Figure 5.25: The Degree of Pyritisation (DOP), Indicator of Anoxia (IA) and Total Iron data for the Briestroffer samples (Black Shale samples are identified as the darker shaded data points compared to the lighter Grey Clay data points). The red line marks the Normal Marine – Restricted boundary (Raiswell et al., 1988), and the dashed purple line marks the lower limit that Raiswell et al. (1988) suggested defines 90% of Inhospitable Bottom Water samples.

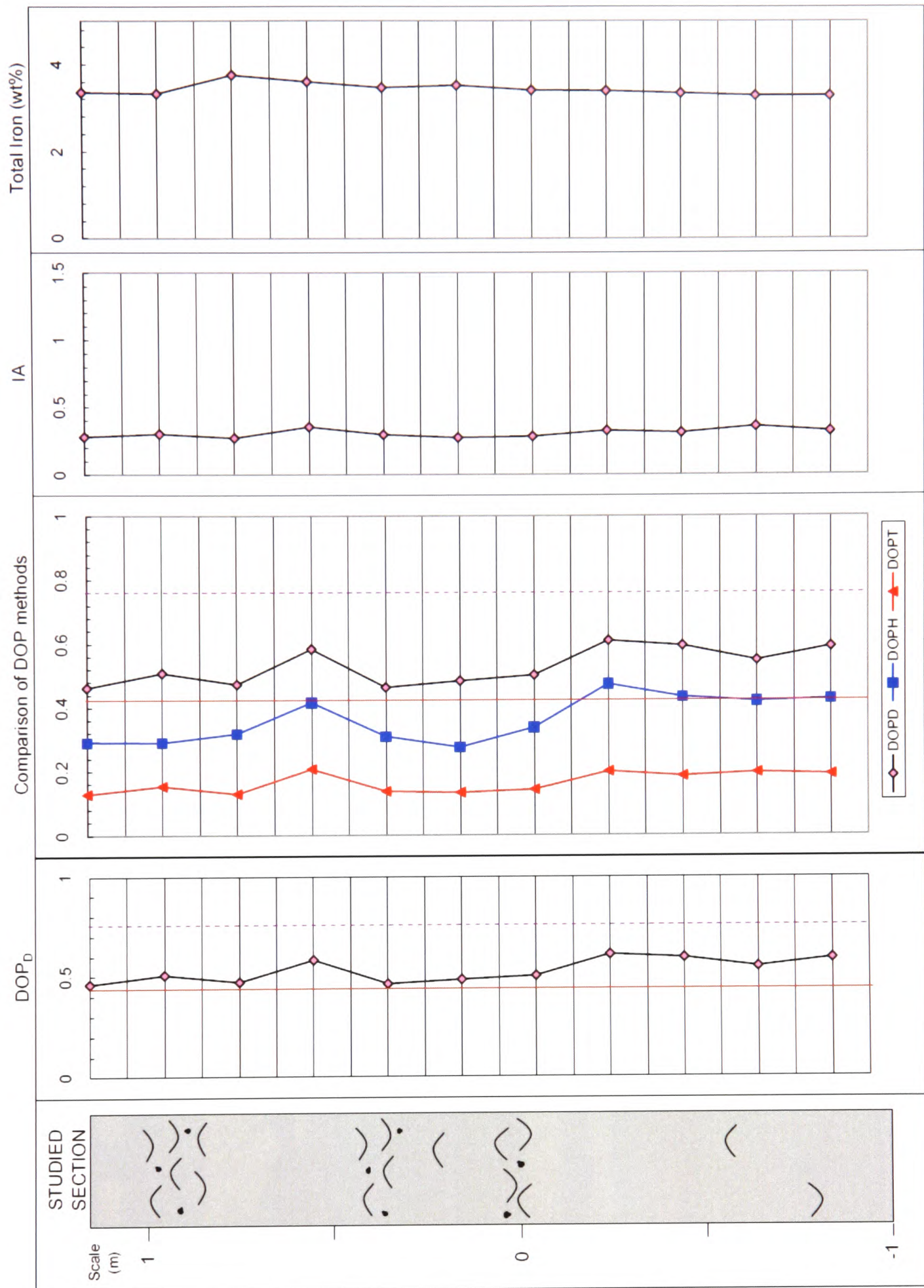


Figure 5.26: The Degree of Pyritisation (DOP), Indicator of Anoxia (IA) and Total Iron data for the Folkestone Gault Clay samples. The red line marks the Normal Marine – Restricted boundary (Raiswell et al., 1988), and the dashed purple line marks the lower limit that Raiswell et al. (1988) suggested defines 90% of Inhospitable Bottom Water samples.

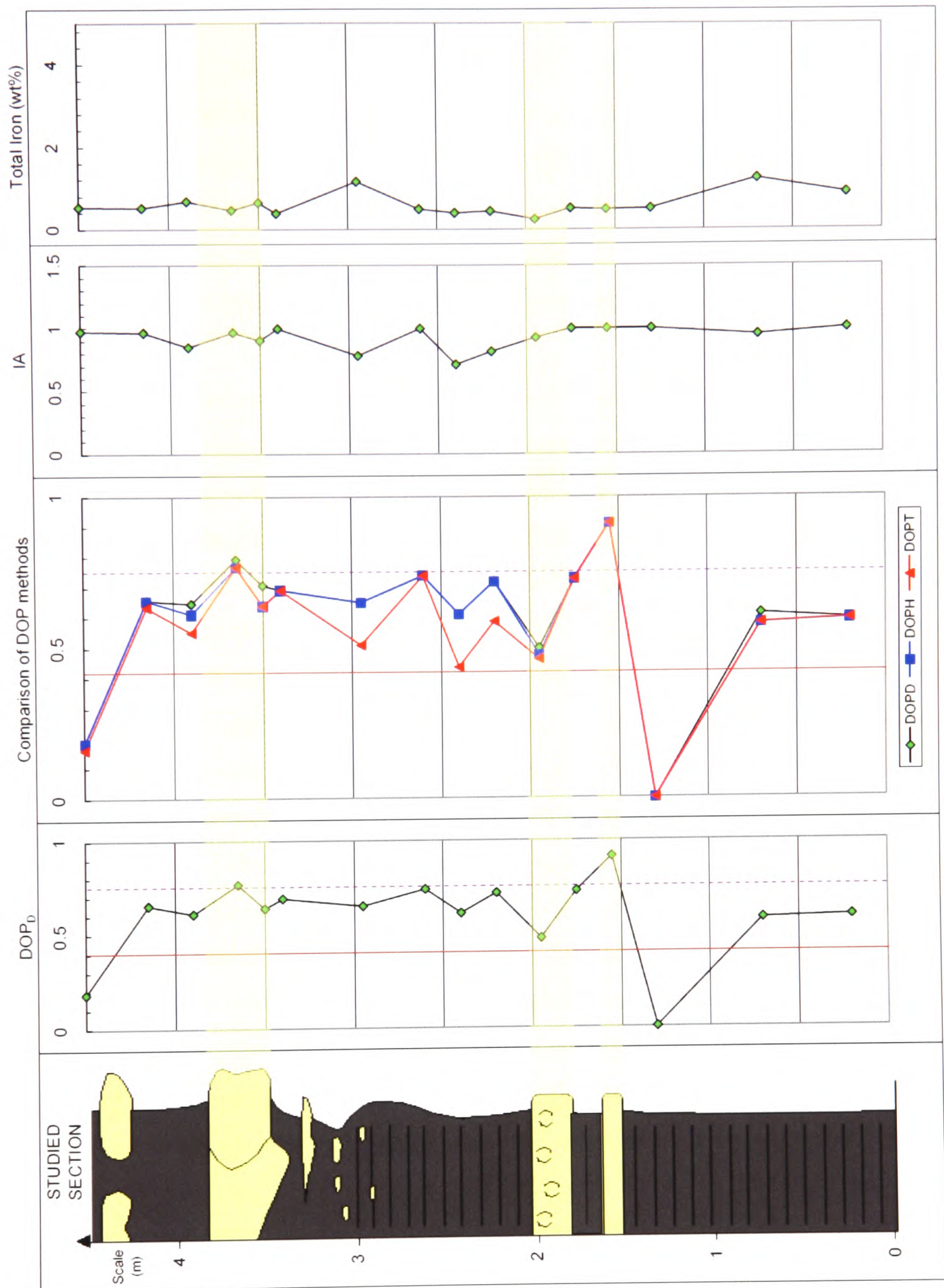


Figure 5.27: The Degree of Pyritisation (DOP), Indicator of Anoxia (IA) and Total Iron data for the Amma Fatma samples. The red line marks the Normal Marine – Restricted boundary (Raiswell et al., 1988), and the dashed purple line marks the lower limit that Raiswell et al. (1988) suggested defines 90% of Inhospitable Bottom Water samples.

It appears that for Niveau Pacquier grey clays, there is a slightly negative correlation between **FeT** and organic carbon and this may be linked to dilution effects – in oxic environments increased organic carbon suggests an increased proportion of biogenic material in the sediment which would in effect dilute the concentration of iron from detrital material. On the other hand the black shale samples show, if anything, a slightly negative correlation between organic carbon and **DOP** but in both graphs the linear regression is not statistically valid (see *Figure 5.28*).

For the Briestoffer samples, which demonstrated a confused relationship in the **S/C** plot (see *Figure 5.12*), the **DOP** and **FeT** plots (see *Figure 5.29*) shed little light on the environmental settings. Both the grey clay and black shale samples have no statistically valid regression line and so interpretation is limited. This may be due to the limited number of samples, allowing scatter to distort the regression line. Also the Briestoffer samples have relatively low **TOC** levels relative to the other sites, and Raiswell and Berner (1986) suggested that this may result in a scatter of the data points. What this does imply, however, is that organic carbon is not the limiting factor for either sample set, and that is anything, the **DOP** of the black shale samples is even more independent of organic carbon than those of the grey clays. This could be taken to imply deposition under lower oxygen conditions but is not a reliable indicator of this. The interpretation of the **FeT** plot is equally limited, as both sample sets plot with statistically invalid regression lines (see *Figure 5.29*). What is noticeable is that while the black shale samples plot with higher organic carbon contents, the grey clay samples predominantly have higher **FeT** values. This may go some way in explaining why the **S/C** plot shows the grey clay samples plotting above those of the black shale samples, as there was more iron available for pyrite growth. This would seem to be supported by the higher **DOP** values for the black shale samples – this would suggest that the expected **TS** signal is being masked by differing levels of **FeT** and that pyrite formation within the black shale sediments was strongly iron limited.

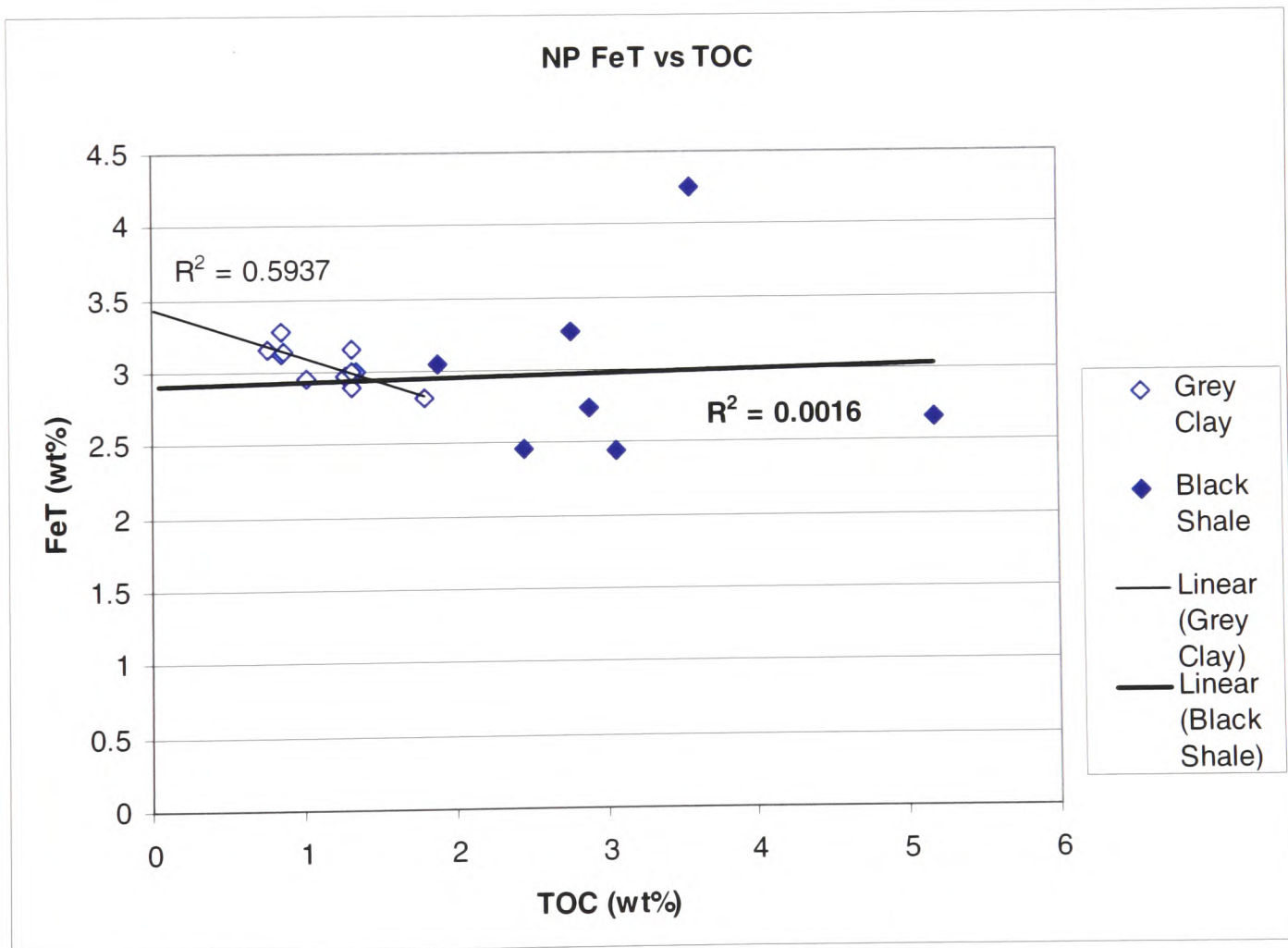
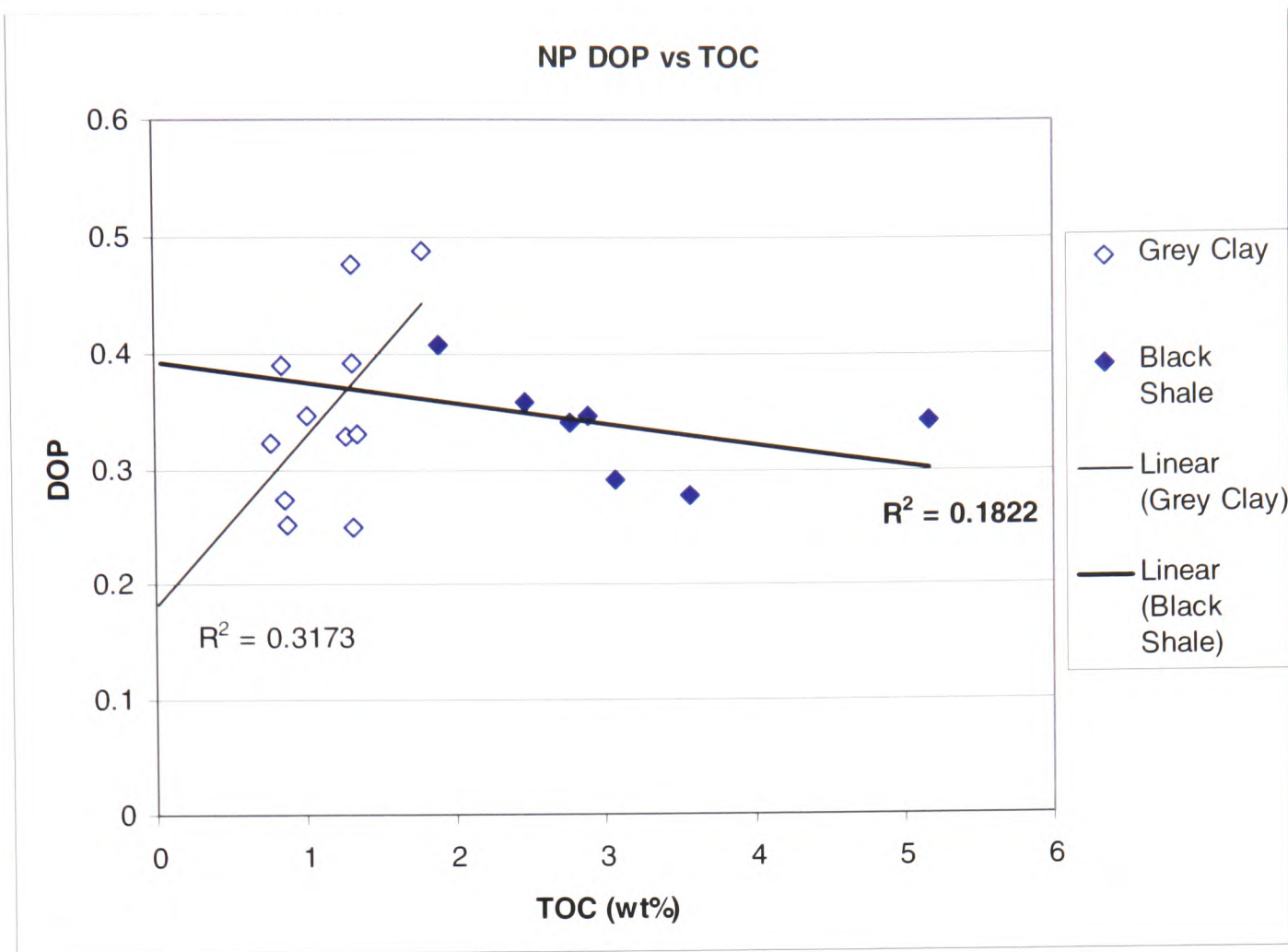


Figure 5.28: DOP against TOC, and FeT against TOC plots for the Niveau Pacquier (NP) samples.

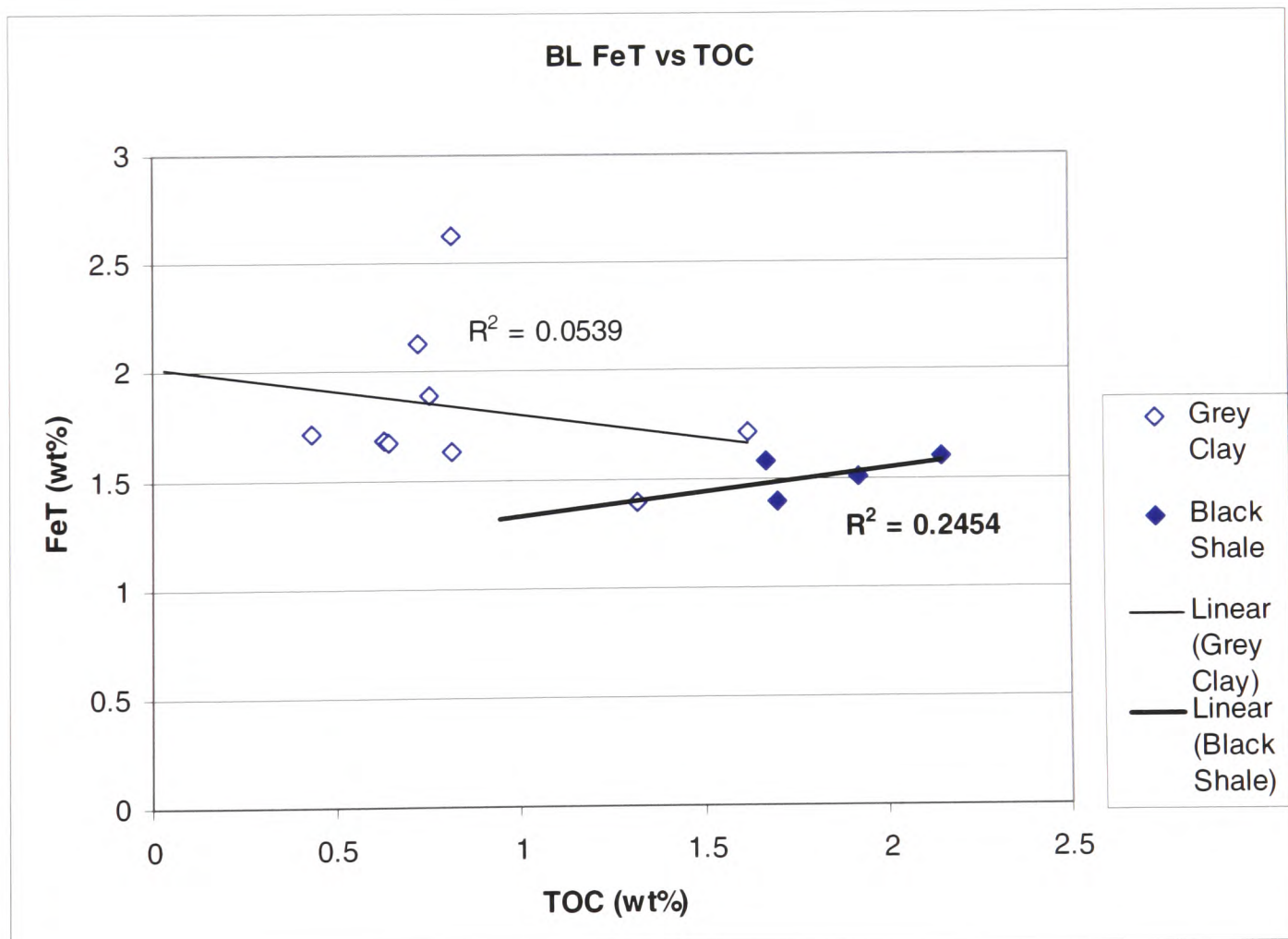
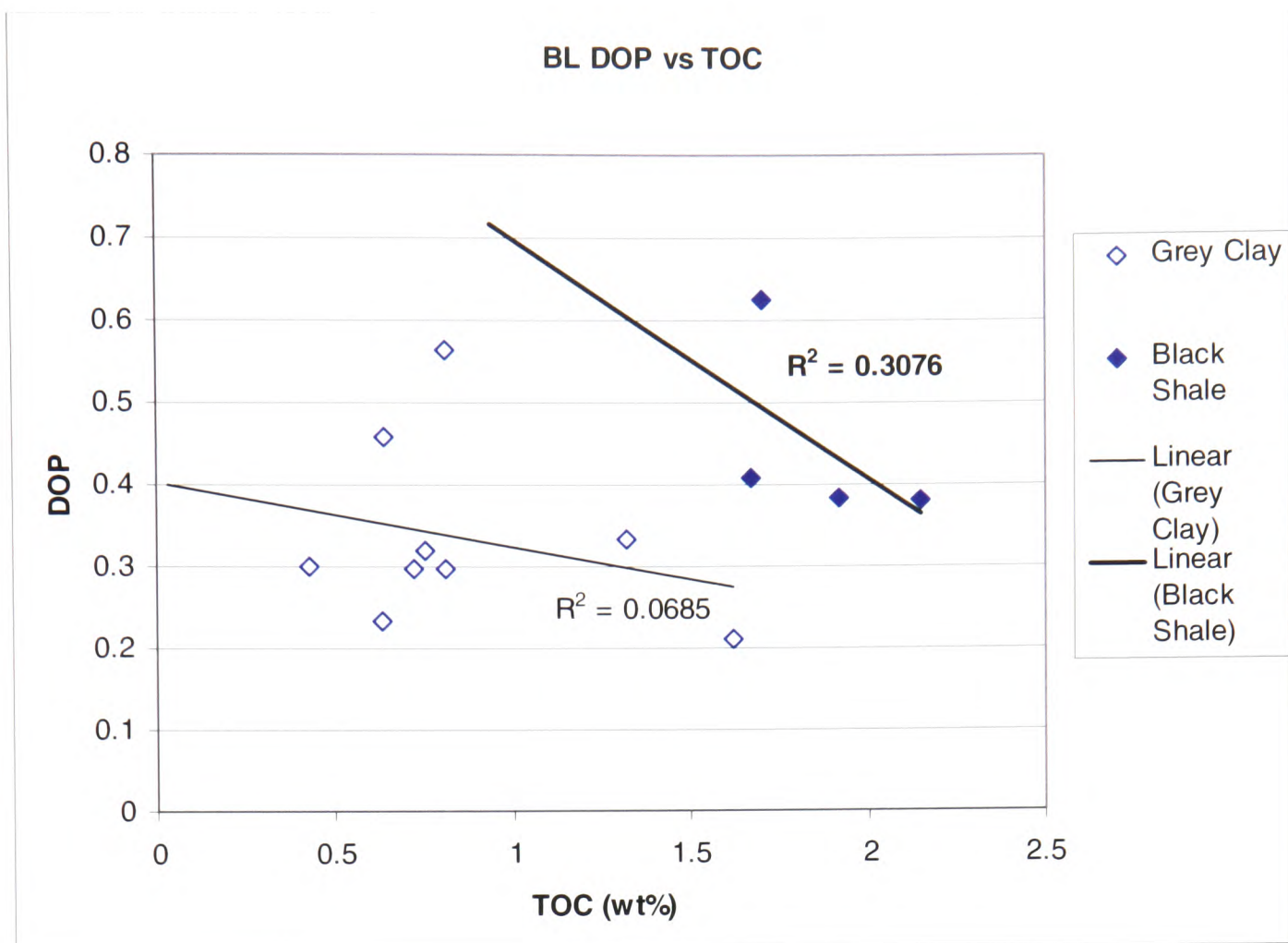


Figure 5.29: DOP against TOC, and FeT against TOC plots for the Briestroffer (BL) samples.

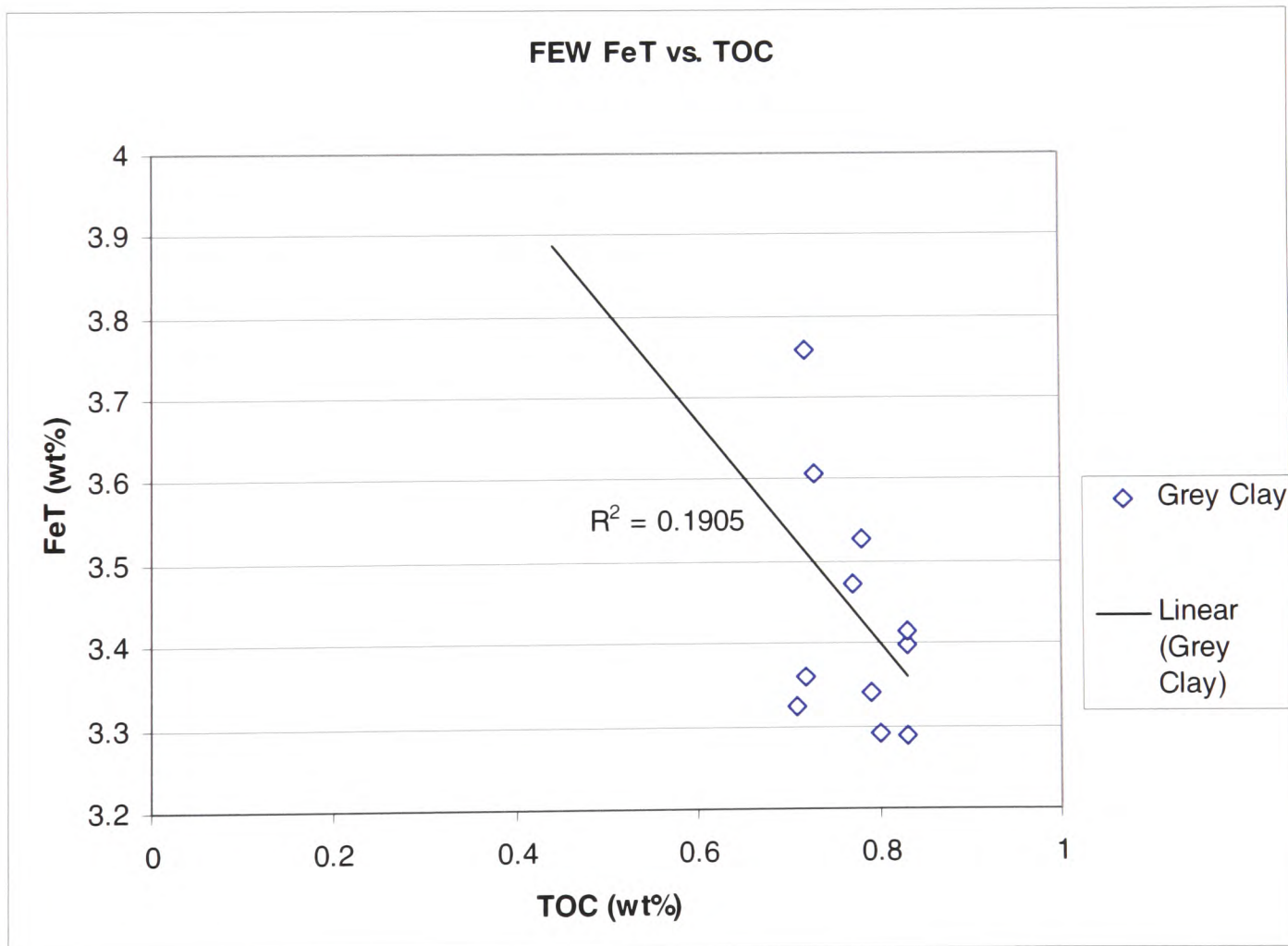
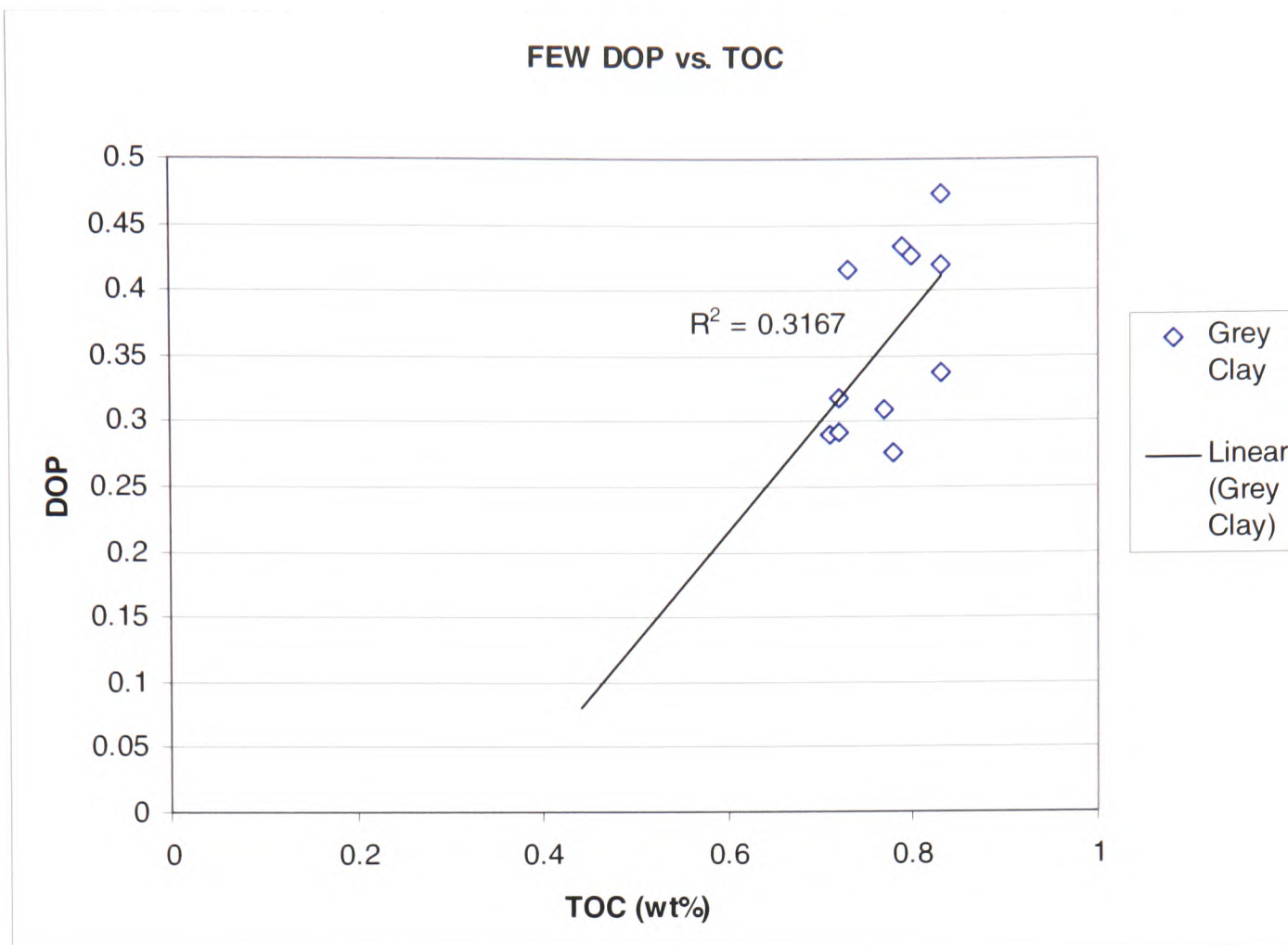


Figure 5.30: DOP against TOC, and FeT against TOC plots for the Folkestone Gault Clay (FEW) samples.

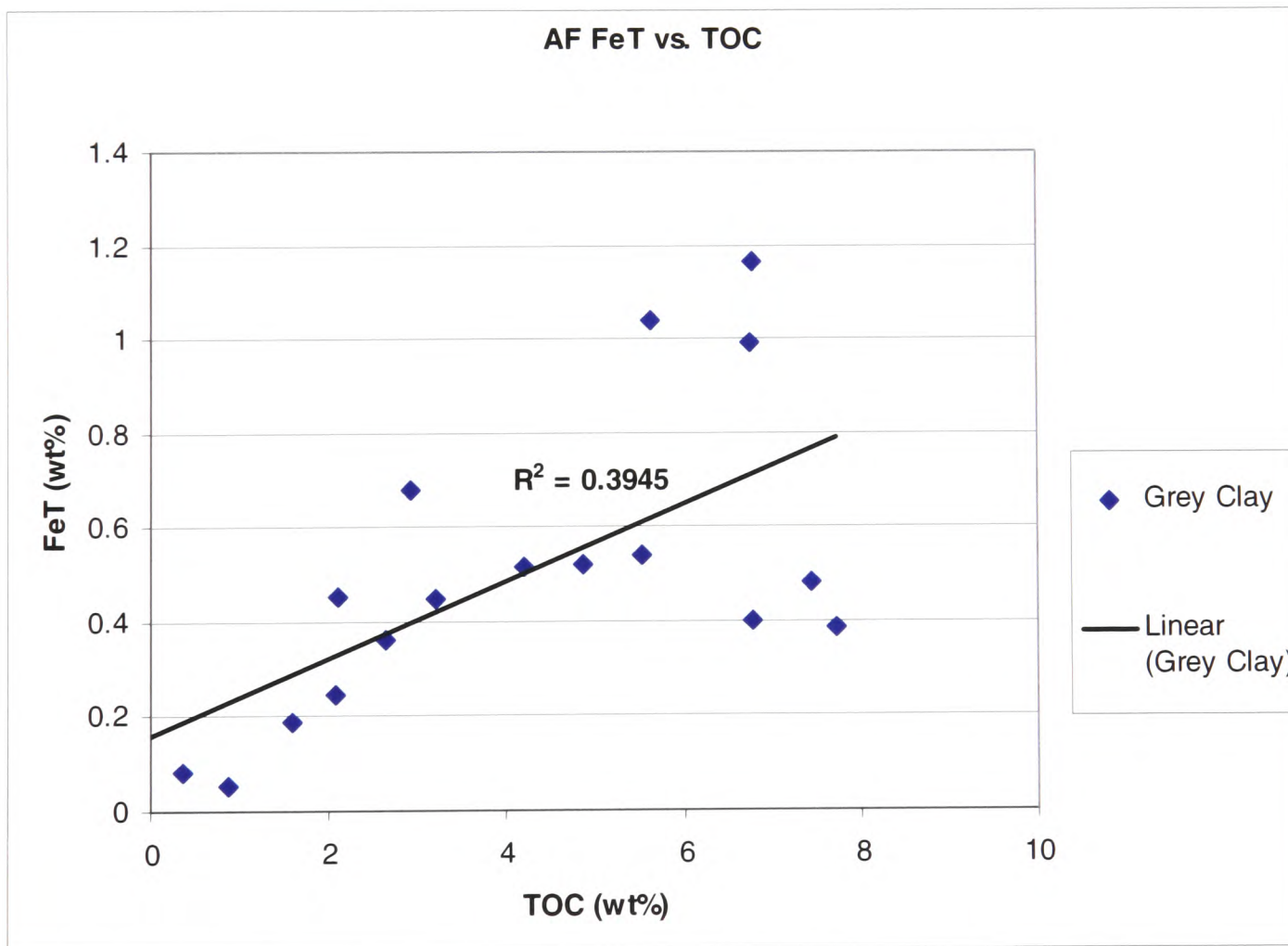
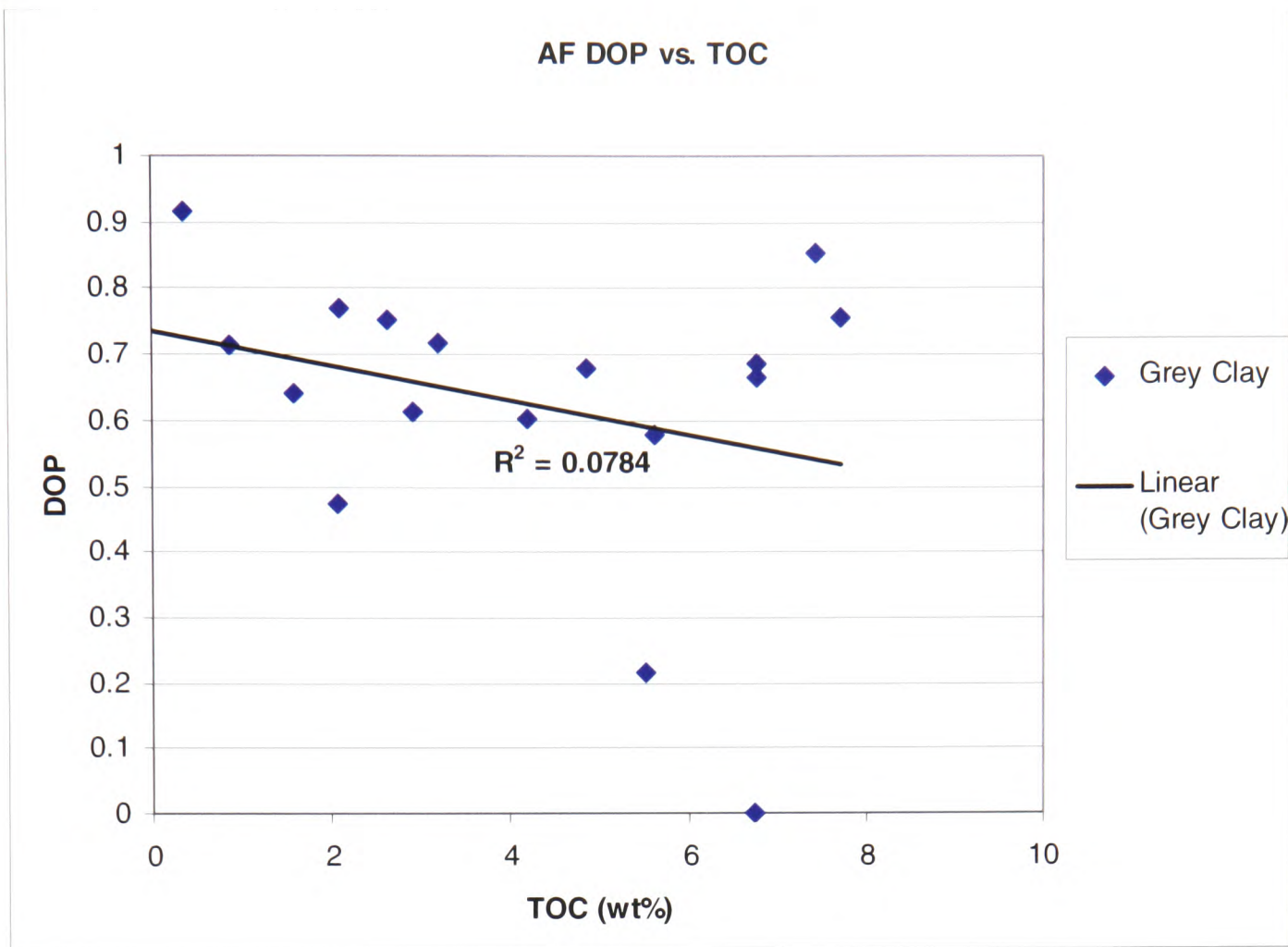


Figure 5.31: DOP against TOC, and FeT against TOC plots for the Amma Fatma (AF) samples.

This again could be used to imply a lower oxygen environment for the black shale samples but again, this is not a clear indicator of this and certainly could not be deduced from the S/C plot alone.

The Folkestone Gault Clay samples form a relatively tight cluster on the S/C plot (see *Figure 5.13*) but show little correlation in the **DOP** and **FeT** plots (see *Figure 5.30*). As the regression line is not statistically valid, the interpretation is again limited. The data could be taken to suggest, as is expected for relatively oxic conditions, that pyrite formation is occurring predominantly within the sediment, under organic carbon-limited conditions. However, the **FeT** plot also shows an invalid regression line, suggesting a negative correlation between the two variables, and this raises concerns that the number of samples and the **TOC** range of the data may be skewing the regression lines.

The Amma Fatma data points which appear to create a convincingly euxinic-looking S/C plot (see *Figure 5.14*) are also statistically unreliable in the **TOC** and **FeT** plots (see *Figure 5.31*). The regression line on the **DOP** plot would be more statistically valid without the two carbonate-rich layers which have very low values of **DOP**. The remaining data points plot with a near horizontal regression line which would suggest that the pyrite formation was predominantly syngenetic under iron-limiting conditions within a euxinic water column (Raiswell and Berner, 1985).

The combination of S/C plots with **DOP** vs. **TOC** and **FeT** vs. **TOC** plots should allow much deeper interpretation of the environmental setting than S/C plots alone. However, they still do not provide a convincing interpretation of all of the sites as the majority of the regression lines for the data do not withstand statistical testing.

5.3.4.3 Comparison of DOP calculation methods

Figures 5.24 to 5.27 highlight the impact of using different methods to calculate the Degree of Pyritisation. In all cases, the **DOP_T** ($\text{DOP}_T = \text{Fe}_{\text{Py}} / \text{Fe}_T$) yields lower values, moving data points in most cases well into the 'Normal Marine' zone. **DOP_H** ($\text{DOP}_H = \text{Fe}_{\text{Py}} / [\text{Fe}_{\text{Py}} + \text{Fe}_H]$), predictably gives higher values that plots most of the data closer to, or either side of the 'Normal Marine' – 'Restricted boundary'. **DOP_D** ($\text{DOP}_D = \text{Fe}_{\text{Py}} / [\text{Fe}_{\text{Py}} + \text{Fe}_D]$), which most closely resembles the definition of what

the Degree of Pyritisation is supposed to represent, gives even higher values, shifting the data points further towards the 'Restricted Bottom Water Conditions' zone. This calculation places all the Folkestone Gault Clay samples, which are thought to represent the most oxic environment, firmly within the Restricted zone.

The boundaries proposed unsurprisingly seem to best fit the DOP_H data, as this was used to define them. This does, however, mean that authors who have used DOP_T instead need to take care in applying these same boundaries to their data. If anything, DOP_D is the calculation that most closely represents the idea of **DOP** as a measure of the amount of reactive iron that has actually reacted to form pyrite, but more work needs to be done to adjust the proposed boundaries to DOP_D data sets.

5.3.5 The Indicator of Anoxia

The Niveau Pacquier data sets show little distinction with the Indicator of Anoxia (see *Figure 5.24*), although the black shale samples do seem to have slightly elevated values compared to the grey clay samples. In fact, the only sample to plot within the proposed euxinic zone is a black shale sample. The data is more convincing for the Briestoffer samples (see *Figure 5.25*), where all of the black shale samples plot within the euxinic zone. Some of the grey clays surrounding the black shale horizons also plot within this zone but the majority of them plot below 0.5. The data is also convincing for the remaining sites, as the Folkestone Gault Clay samples all plot within the normal marine range (see *Figure 5.26*) and all of the Amma Fatma samples plot within the euxinic range (see *Figure 5.27*). This does seem to match expectations from the sedimentology of these samples and suggests that the **Indicator of Anoxia** may be able to distinguish extremes on the scale of oxygenation, while providing mixed results for intermediate conditions. This, of all of the Fe-S-C systematics proxies, seems to provide the clearest differentiation of environmental conditions.

5.4 Conclusions

- Of the proxies used, only the **Fe-S-C ternary diagrams** and the **Indicator of Anoxia** indicated some differentiation between the data sets.

- The **Fe-S-C ternary diagrams** provide a broad differentiation between the data sets, but more specific characterisation was not possible.
- The **Indicator of Anoxia** provides the only relatively reliable differentiation of the oxygenation conditions with a numerical boundary that seemed to fit the data. For this reason, it would seem that this is the most useful of the Fe-S-C systematics proxies.
- The other proxies investigated were unable to differentiate the data to the same extent:
 - The **S/C** plots, when used in combination with **DOP/TOC** and **FeT/TOC** plots, should provide insight into pyrite formation within each setting but in most cases are limited by a lack of statistical validity of the regression lines.
 - While the **Total Organic Carbon** content did show correlation with the sedimentology of the sample sets, the **Total Sulphur** content showed no distinct pattern. The relative amounts of **TOC** and **TS** can be used to imply relative levels of low oxygenation but assignment of numerical boundaries is problematic due to variations in other factors between sites.
 - Investigation of the different '**iron pools**' alone gives little conclusive evidence about environmental conditions during deposition. However, these data can be used to provide background information for the interpretation of other proxies.
 - The **Degree of Pyritisation** shows little differentiation between grades of low oxygenation but does broadly identify the range of environments represented by the different sites. However, while the boundaries proposed by Raiswell *et al.* (1988) do seem to correlate with **DOP_H**, caution should be applied to applying the same boundaries for **DOP_T** as using this calculation method can have a large effect on the position of data points relative to the proposed boundaries. **DOP_D** perhaps offers the closest representation of **DOP** as a measure of the amount of reactive iron that has actually reacted to form pyrite, but more work needs to be done to apply oxygenation boundaries to **DOP_D** data.

- In combination, the Fe-S-C systematics proxies do imply a trend in the environmental conditions, with the Amma Fatma samples consistently plotting as the most anoxic or euxinic data set. Following this, the Niveau Pacquier black shale seems to represent a slightly more dysoxic environment than that of the Briestroffer black shales. Both the Niveau Pacquier and Briestroffer grey clays would seem to be linked to an upper dysoxic environment, whereas the Folkestone Gault Clay samples consistently plotted within 'Normal Marine' or slightly 'Restricted' zones.

6. DISCUSSION

6.1 Sedimentology

Historically low oxygen events were recognised on the basis of their sedimentology and this still appears to be one of the strongest indications of the occurrence of an 'anoxic event'. The presence of dark laminated shales or marls clearly indicates low oxygen conditions during the time of deposition of the Niveau Pacquier and Breistroffer black shales and the Amma Fatma dark marl sequence. While colour, which appears to be strongly linked to organic carbon content, does seem to correlate with palaeo-oxygenation trends it is important to remember that this is strongly affected by carbonate content, the extent of weathering and the thermal maturity of the sediments. While the Niveau Pacquier and Briestroffer black shales fit the classic definition of such sediments, the Amma Fatma marls are dark brown in colour, yet even the paler horizons record strong oxygen depletion in a number of the geochemical proxies. This brown colour may be due to the high carbonate content of the Amma Fatma sediments (Arthur and Sageman, 1994) (see *Figure 5.10*) in combination with the fact that the sediments only have moderate thermal maturity in comparison to the Vocontian black shales (Nzoussi-Mbassani *et al.*, 2003).

The one sedimentological feature that is consistent between the three study sites is the presence of lamination. Lamination and bioturbation are effectively mutually exclusive as any reworking of the sediment above the sub-millimetre scale should theoretically destroy laminations. This gives one of the strongest indications that conditions on the seafloor reached anaerobic levels rather than dysaerobic conditions as this boundary is defined sedimentologically as the point of suppression of obvious bioturbation (Rhoads and Morse, 1971). The presence of lamination provides the clearest indicator of palaeo-oxygenation conditions of all of the proxies studied, but the actual physiological and geochemical meaning of this anaerobic-dysaerobic boundary is still debated. The laminated sediments from the Niveau Pacquier, Breistroffer and Amma Fatma sequences correspond with a general lack of benthic macrofossils but the two Vocontian Basin sites contain well-preserved nekto-benthic ammonites and belemnites. However, samples of the Niveau Pacquier black shales and the Amma Fatma marls sieved by the author all contained no benthic foraminifera. Erbacher *et al.* (1999) also reported the absence of benthic foraminifera

within the Niveau Pacquier black shale sediments and El Albani *et al.* (2001) observed that the Amma Fatma dark marls contained no benthic forms. While the lack of benthic macrofossils is commonly accepted within anaerobic settings, Koutsoukos *et al.* (1991) suggested that the absence of benthic foraminifera indicates highly oxygen-depleted bottom waters. Field and laboratory studies by Van der Zwaan *et al.* (1999) demonstrate that benthic foraminifera can endure varying degrees of anoxia, and the complete absence of benthic species within the laminated shales suggests that anoxia in combination with free hydrogen sulphide (H₂S) may have been present during black shale deposition (Moodley *et al.*, 1997). The presence of lamination cannot distinguish between anoxic and euxinic conditions and even though all three sites exhibit lamination there are indications that the extent of anoxia within the water column was different for the Moroccan and French sites. The presence of nektobenthic macrofauna within the Niveau Pacquier and Briestroffer black shales correlates with 'upper anaerobic' biofacies where the redox boundary is proposed to have been at the sediment-water interface (for example ORB2 within the Oxygen Restricted Biofacies (ORB) Scheme of Wignall and Hallam, 1991). In contrast, the complete lack of macrofauna in the Amma Fatma dark marls would suggest that the redox boundary was within the water column, creating anoxic bottom waters, which corresponds to ORB1 within the Wignall and Hallam's (1991) ORB Scheme. This differentiation cannot be distinguished from sedimentological proxies alone. Also, while lamination appears to be a clear indicator of anaerobic facies, there is little sedimentological distinction between dysaerobic and aerobic conditions.

While sediment colour and the presence of lamination are to some extent indicators of palaeo-oxygenation, the link between fissility and oxygenation conditions is not reliable. While the Niveau Pacquier and Briestroffer black shales do demonstrate papery fissility, the Amma Fatma dark marls do not. This suggests that papery fissility is, as Wignall (1994) suggested, a weathering feature related to the compacted fabric of parallel aligned organic matter and clay particles, which is common to the majority of black shales. The relatively high carbonate content of the Amma Fatma marls may alter this sediment fabric and restrict 'papery weathering'. This suggests that fissility occurs as a result of sediment fabric and weathering properties and is not directly linked to palaeo-oxygenation.

In terms of ichnological proxies, bioturbation indices provide the clearest and easiest way to directly compare different sites. A number of different schemes have been proposed (including the Bioturbation Index of Reineck, 1963; the Ichonofacies Indices of Droser and Bottjer, 1986 and the Bedding Plane Bioturbation Indices of Miller and Smail, 1997) which result in a variety of grades or categories assigned to a particular assemblage. Possibly the clearest way to record the extent of bioturbation is to use 'percentage disturbance' values assigned by comparison to a visual chart, as this provides a numerical comparison between sites. Recent use of software to calculate the percentage of a given quadrat that shows signs of biological disturbance (Marenco and Bottjer, 2006) take this method to another level in terms of accurately quantifying the percentage bioturbation. The main issue with Bioturbation Indices as proxies for palaeo-oxygenation is the lack of correlation with oxygenation regimes. While sediments laid down under anaerobic conditions would be expected to register 0% bioturbation, there is little indication in the literature of the percentage bioturbation that can be expected from upper or lower dysaerobic facies, or where truly aerobic conditions would register on the scale.

Further interpretation of trace fossils as a palaeo-oxygenation indicator is complicated by the difficulty in interpreting the trends in mode of life and tiering structures. For example, the progression of an assemblage from one dominated by feeding tracks to one dominated by grazing trails is thought by some to represent an increase in available oxygen (e.g. Ekdale and Mason, 1988) and others to represent a decrease in oxygenation (e.g. Wheatcroft, 1989). In addition to this, it is difficult to associate trace-fossil forms with the actual position of the sediment-water interface they originated from, and overwriting of tier structures by lower tiers originating from higher sediment surfaces complicates interpretation further. While the dominance of particular forms or the modes of life, or the arrangement of tier structures can give indications of palaeo-oxygenation conditions at the time of the formation, the same information can effectively be gathered by applying a simple bioturbation index.

The size distribution of pyrite framboids demonstrates a clear pattern which correlates with the suggested palaeo-oxygenation variations in the Niveau Pacquier sequence (see *Figure 2.15*). Framboid diameters are also relatively restricted through the Amma Fatma sequence (see *Figure 2.41*) and are much more variable within the

Folkestone Gault Clay section (see *Figure 2.34*), which reflects the proposed conditions for their formation. However, framboid diameters do not match the numerical boundaries suggested by either Wilken *et al.* (1997) or Wignall and Newton (1998). The Niveau Pacquier black shale most closely fits the description of euxinic sediments under Wilken *et al.*'s (1997) scheme, but would be classified as lower dysaerobic according to Wignall and Newton (1998). This suggests that the size distribution of framboids is affected by localised factors and that numerical boundaries may only apply to individual sites or sites within the same region. The relatively poor correlation between sediment type and framboids size distribution within the Briestroffer sequence raises further concerns, as the nature of the black shale horizons suggests that similar depositional conditions existed to those for the Niveau Pacquier black shale. This suggests that the palaeo-oxygenation conditions did not reach the same levels of anoxia as those during the deposition of the Niveau Pacquier black shale, or that only euxinic conditions create such a reduction in framboid diameter. Alternatively, the framboids size distribution may be affected by the duration and the stability of low oxygen events, which would suggest that the Briestroffer black shales were laid down under fluctuating conditions allowing the occasional formation of framboids within the sediment. The Amma Fatma sequence displays a similar range of framboid sizes to the black shales of the Niveau Pacquier sequence. While the pale-coloured fossiliferous 'luncina' bed does contain a much higher proportion of framboids within the 7-25 μm range, it does not contain any framboids greater than 25 μm and so does not match Wilken *et al.*'s (1997) description of sediments laid down under oxic or dysoxic conditions. The other pale carbonate-rich sections cannot be distinguished from the associated dark marls, which would imply that they too were laid down under low oxygen conditions, despite their pale colour.

While Wignall and Newton (1998) proposed framboid size ranges for euxinic, lower dysaerobic and upper dysaerobic, Wilkin *et al.*'s (1997) model groups dysoxic and oxic conditions together, suggesting that only true euxinic conditions can affect framboids size distributions. Using the model proposed for framboids formation it is difficult to explain how lower and upper dysaerobic conditions would cause a reduction in framboids size diameters, as only framboids forming at a redox boundary within the water column should exhibit size restriction. Strictly this should only

apply to the lowermost ranges of anoxia or euxinic conditions, where the redox boundary rises above the sediment-water interface (see *Figure 6.1*). In more oxygenated regimes the redox boundary is believed to be at the sediment-water interface or within the sediment. It is plausible that if the redox boundary is at the sediment-water interface then a proportion of the framboids may form syngentially within the water due to small-scale fluctuations in the boundary.

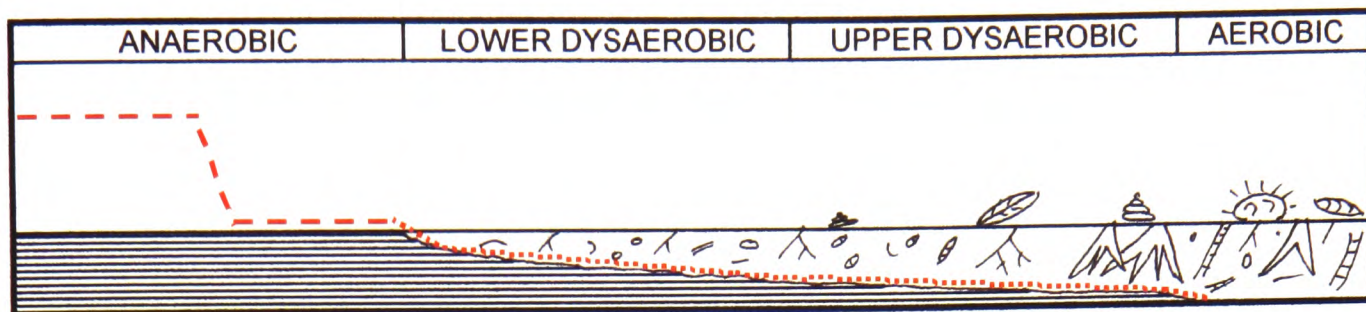


Figure 6.1: Proposed position of the redox boundary (red line) under the range of different palaeo-oxygenation regimes (adapted from Arthur and Sageman, 1994).

If this is the case, then it may be possible to distinguish these upper anaerobic and dysaerobic conditions from more oxygenated regimes, using the proportion of syngenetic to diagenetic framboids. This, however, relies on determining the size at which syngenetic framboids would settle out of the water column in order to distinguish them from diagenetic framboids. This is still a matter of debate as Wignall and Newton (1998) proposed 5 μm and Wilken *et al.* (1997) proposed 7 μm as threshold values, which suggest that local factors may alter the maximum size attained.

Other proposed measures, such as the standard deviation and skewness of the framboids distribution (Wilken *et al.*, 1996), do not seem to yield any correlation with other palaeo-oxygenation signals. Wilken *et al.* (1996) also suggested that investigating pyrite morphologies may reveal information about palaeo-oxygenation and the results from the four sites do seem to support this. The samples seem to fall within three main categories (see *Figure 6.2*) which appear to be indicative of the oxygenation conditions implied by the sedimentology and palaeontology.

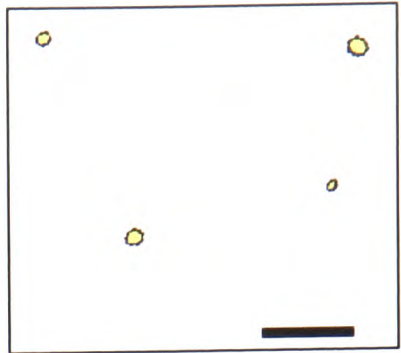

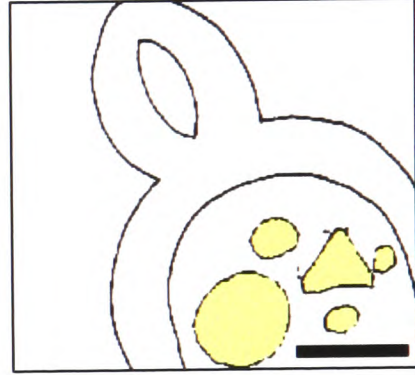
<p>Category 1 – Redox boundary within the water column: A random covering of small framboids where groups of framboids and euhedral crystals are rare and only occasionally are framboids associated with shell material.</p>	
<p>Category 2a – Redox boundary within the sediment: Large framboids are relatively common and are often composed of comparatively large crystals. Clusters of framboids and euhedral crystals are common, with the latter occasionally larger than individual framboids. Overgrowth of framboids is also common.</p>	
<p>Category 2b – Redox boundary within the sediment: Framboids are rare and are usually associated with cavities within shell material.</p>	

Figure 6.2: Proposed categories of pyrite morphology with examples (pale yellow represent pyrite and the scale bar represents 20 μm in each diagram).

- The distribution of pyrite in **Category 1** correlates with the idea that framboids formed at a redox boundary which was within the water column, leading to the random scattering of small framboids throughout the sediment.
- The distribution of pyrite within the **Category 2a** suggests that pyrite formation occurred slowly within relatively organic-rich sediments. Wilkin and Barnes (1997) suggested that the presence of large euhedral crystals indicates that pyrite formation occurred slowly within the sediment, under a relatively oxic water column. The presence of a relatively oxic water column

would suggest that the organic content of the sediment would be relatively low and this may restrict pyrite formation. The large clusters of framboids may form associated with concentrations of organic matter such as within a burrow system. Also the occurrence of pyrite overgrowth suggests that pyrite formation occurred within the sediment.

- The distribution of pyrite within **Category 2b** represents sediments which probably formed under a more oxic water column, under fluctuating redox conditions, or merely contained less organic matter. The restricted availability of organic matter would have restricted the amount of pyrite that could form which would explain the rare occurrence of framboids. The association of framboids with apparent cavities within shell material may represent pyrite formation within reducing microenvironments created due to breakdown of localised concentrations of organic matter.

6.2 Palaeontology

Bottom water oxygenation has a strong effect on factors such as benthic macrofossil diversity and abundance but again it is difficult to define grades of oxygenation based on these values. Anaerobic conditions are defined by a complete lack of benthic macrofossils but it is difficult to classify the other oxygen-related biofacies. Diversity is found to reduce as oxygenation levels decrease and Rhoads and Morse (1971) have suggested that the aerobic to dysaerobic transition is marked by a rapid drop in species numbers but this is difficult to quantify. This pattern is also complicated by the suggestion that stable low-oxygen environments may host diverse communities (Wignall, 1994). Macrofossil interpretation is severely sample-size limited and the data can be strongly skewed by poor preservation, as is observed in the Marnes Bleues samples studied here.

While it is difficult to define comparable numerical boundaries for palaeo-oxygenation using macrofossil data, subtle variations within a sequence can provide an insight into changing conditions during the time of deposition. The relatively high diversity observed within the Folkestone Gault Clay sequence classifies it as the most oxic of the four sites investigated. Within the sequence, however, there are subtle variations in diversity between beds dominated by small *Circocerithium* spp. gastropods and nodular horizons with more diverse fossil assemblages. Knight

(1997) proposed that these variations occurred in response to changes in substrate consistency, but comparison with the pyrite framboid data shows that the palaeontologically more diverse horizons contain larger framboids. This provides some support for the idea that subtle variations in oxygenation could be responsible for the varying diversity throughout the sequence. However the nodular horizons are associated with condensed sections which could represent periods of time in which the redox boundary was stable at a certain position within the sediment. If this was the case then this would allow pyrite framboid growth to continue for longer, forming larger framboids in association with a condensed macro-faunal assemblage.

Suggestions of a correlation between bivalve modes of life and bottom-water oxygenation (Morris, 1979) are not confirmed by the data from the Folkestone Gault Clay. A number of the samples do plot within the expected 'Normal Marine' range, but several samples also plot within 'Bituminous' conditions, which does not match the palaeo-oxygenation regime predicted for the Gault Clay. As the biofacies models develop, more focus is being placed on the importance of the duration and stability of low oxygen events in controlling the types and abundance of species found. While highly stable environments may allow a diverse community to develop (Wignall, 1994), communities of fluctuating environments are likely to record forms which are suitable as rapid colonizers (Arthur and Sageman, 1994), and therefore the mode of life of these species is likely to be more reflective of this than of their suitability to survive in low oxygen conditions.

While the interpretation of benthic macrofossils provides little information to compare, for example between the Niveau Pacquier grey clays and black shales, a stark contrast is recorded on the taphonomy. Brett and Baird's (1986) scheme (see *Figure 3.2*) linking taphonomy with water oxygenation, sediment geochemistry and sedimentation rates does neatly classify the samples from the four sites within the palaeo-oxygenation regime predicted from their sedimentology and palaeontology. The oxygenation conditions described within the scheme may also link in with the new descriptive categories proposed for pyrite morphology (see *Figure 6.3*) but further work would be needed to confirm this.

Water oxygenation	Sediment geochemistry	Proposed Pyrite Morphology Categories
Aerobic O ₂ > 0.7 ml/l	Oxic; organic poor	Category 2b – Redox boundary within the sediment: Framboids are rare and are usually associated with cavities within shell material.
Aerobic-dysaerobic O ₂ = 0.7-0.3 ml/l	Anoxic with oxic microzones; organic poor (non-sulphidic)	Category 2a – Redox boundary within the sediment: Large framboids are relatively common and are often composed of comparatively large crystals. Clusters of framboids and euhedral crystals are common, with the latter occasionally larger than individual framboids. Overgrowth of framboids is also common.
Dysaerobic-anaerobic O ₂ < 0.3 ml/l	Anoxic to the surface; commonly organic-rich (commonly sulphidic)	Category 1 – Redox boundary within the water column: A random covering of small framboids where groups of framboids and euhedral crystals are rare and only occasionally framboids are associated with shell material.

Figure 6.3: Table combining the water oxygenation and sediment geochemistry categories from the taphonomy scheme of Brett and Baird (1986) (Figure 3.2) with the proposed descriptive categories of pyrite morphology (Figure 6.2).

Theoretically, the taphonomy of fossil material is strongly related to the redox status of the bottom-water and sediment at the time of deposition and diagenesis, and appears to correlate well with the suggested palaeo-oxygenation regimes of the investigated sites. However it is difficult to quantify taphonomy beyond a descriptive scheme and there are several other factors that influence the way that fossil material is preserved.

The range of biofacies models studied combine sedimentological and palaeontological information to create proxies for palaeo-oxygenation. The sedimentological information forms the basis of classification, in particular for the anaerobic to dysaerobic range, while palaeontological classification is limited by problems of preservation and sample-size effects. The presence of lamination forms the basis for the recognition of anaerobic facies and while Rhoads and Morse (1971) initially extended this into the lower dysaerobic zone, later models proposed instead the ‘exaerobic’ facies where laminated and shelly horizons alternate (see *Figure 3.4*).

Wignall (1994) and Arthur and Sageman (1994) included the idea of the temporal variability of anoxic events into their models, with Wignall (1994) using the term 'poikiloaerobic' to describe fluctuating environments. This concept allows a reclassification of the exaerobic facies as effectively lower poikiloaerobic, where predominantly anoxic conditions lead to the formation of laminations and occasional more oxic fluctuations allow brief colonisation by shelly biota. This means that the preservation of laminations indicates that anoxic conditions occurred, however briefly, and that it is the duration and stability of the events that decides the classification of the sediment. The lack of lamination within the Marnes Bleues grey clays, therefore, suggests that anoxic conditions were never fully reached during the time of their deposition and this restricts their classification to upper dysaerobic/poikiloaerobic or aerobic.

The changing emphasis of biofacies models towards the temporal variability of anoxic events has been used to explain why Wignall and Hallam (1991) found that there is commonly a discrepancy between the results of biofacies analysis and geochemical proxies for palaeo-oxygenation. Newton (2001) suggested that during fluctuating conditions, trace metal and Fe-S-C based proxies are fixed during the anoxic periods, but that the results of faunal proxies are controlled by the extent of the regular oxygenation events. Kenig *et al.* (2004) believed that current benthic biofacies models consistently record more oxic conditions than actually occurred at the time, due to the dominant effect of minor oxygenation events on the faunal record. This difference in results between faunal and geochemical proxies is not evident from the four sites studied here. This may be because they represent sediments laid down under anaerobic or upper dysaerobic to oxic conditions and the proposed effect of fluctuating conditions on faunal proxies should be most noticeable within the dysaerobic (or poikiloaerobic) facies.

Of all of the biofacies models, the Oxygen Restricted Biofacies (ORB) scheme of Wignall and Hallam (1991) yields the most specific detail about the types of macrofauna associated with each biofacies. Using this scheme, the Niveau Pacquier and Breistroffer black shales fit the description of the anaerobic facies ORB 2, where the redox boundary is thought to be just above or at the sediment-water interface. However, both of these assemblages contain belemnites which conflicts with the

suggestion of Wignall and Hallam (1991) that these are only present in the upper dysaerobic and aerobic facies. The ORB scheme differentiates between the low-oxygen French and Moroccan sediments, as it classifies the Niveau Pacquier and Briestroffer black shale samples as 'upper anaerobic', and the Amma Fatma sediments as 'lower anaerobic'. More developed biofacies models (e.g. Wignall and Hallam, 1991; Arthur and Sageman, 1994; and Wignall, 1994) do provide a strong basis for the classification of palaeo-oxygenation conditions but they rely heavily on sedimentology and still do not allow recognition of subtle variations. Using these schemes, the Niveau Pacquier and Briestroffer black shales both plot within the 'upper' anaerobic zone and this does not provide any insight into why the geochemistry results of the two sites are so different.

6.3 Trace Metal Geochemistry

Before interpreting trace metal data it is important to try and correct for the detrital input and this is generally achieved by normalising the data to an element thought to be purely detrital in origin. Aluminium is usually used, either directly, or within calculations for enrichment factors or trace-metal excess, where values are normalised to 'average shale'. This in itself is problematic as 'normal shale' does not accurately represent the background value, which is highly dependant on local inputs. This leads to the values for the Niveau Pacquier and Briestroffer grey clay samples recording negative enrichment factors. Theoretically the samples could be normalised to a grey clay sample as this should represent 'normal values' for the basin. However, if an average value is used then some grey clays will still record depletion, and if the lowest grey clay value is used then all others will record enrichment which removes the distinction between the grey clay and black shale samples. While using average shale values is problematic with the grey clay samples, it does allow for complete separation of the molybdenum data between enrichment in the black shale and apparent depletion in all but one of the grey clay samples of the Niveau Pacquier sequence. Enrichment factors of certain elements can therefore provide definition that separates anoxic deposits from those laid down under more oxygenated conditions if a value of one or below is taken to imply dysoxic to oxic conditions. However, the fact that the aluminium content of each site is slightly different (see *Figure 4.18*) means that enrichment factor values are not directly comparable between sites. It is also important to check data sets for samples

containing low detrital inputs as the low aluminium samples from the Amma Fatma section have strongly skewed enrichment factors (see *Figure 4.34*). In addition the variation in the bulk geochemistry between sites implies varying clay mineral compositions which may also limit the applicability of direct inter-site comparison of geochemical proxies.

Of the trace elements studied, molybdenum appears to show the strongest correlation with palaeo-oxygenation. All of the Niveau Pacquier black shale samples and only one grey clay sample record enrichment (see *Figure 6.4*). The grey clay sample in question is directly above the black shale and therefore could represent the tail-end of an anoxic event. This sample could represent a black shale sample that was oxidised at a later point but the enriched uranium levels suggest that re-oxidation has not occurred.

While only two of the four Briestroffer black shale horizons record enrichment in molybdenum, the entire Amma Fatma sequence records enrichment, including the fossiliferous limestone band (see *Figure 6.4*). In addition, the entire Folkestone Gault Clay sequence records depletion relative to average shale, which could suggest oxic or possibly upper dysoxic conditions at the time of formation. Apart from the confused signal from the Briestroffer sequence, the molybdenum data do seem to accurately separate sediments laid down under low-oxygen conditions from those deposited in more oxic regimes (see *Figure 6.4*).

The Briestroffer sequence contains a higher proportion of reactive iron (see *Figure 5.16*) which Tribovillard *et al.* (2004) suggested suppresses organic matter sulphurisation. As organic matter sulphurisation is thought to play a key role in molybdenum fixation, this could explain why molybdenum values are not as high for the Briestroffer sequence. However, the Amma Fatma sediments record even higher levels of reactive iron (see *Figure 5.18*), yet these show strong enrichment in molybdenum. The lack of strong molybdenum enrichment in the Briestroffer black shales may instead be linked to the duration of the anoxic events or the level of hydrogen sulphide in the water. Adelson *et al.* (2001) proposed that molybdenum fixation is related to the amount of time the sediment is exposed to low-oxygen

waters and Rimmer (2004) suggested that molybdenum enrichment was only found under waters that were permanently anoxic.

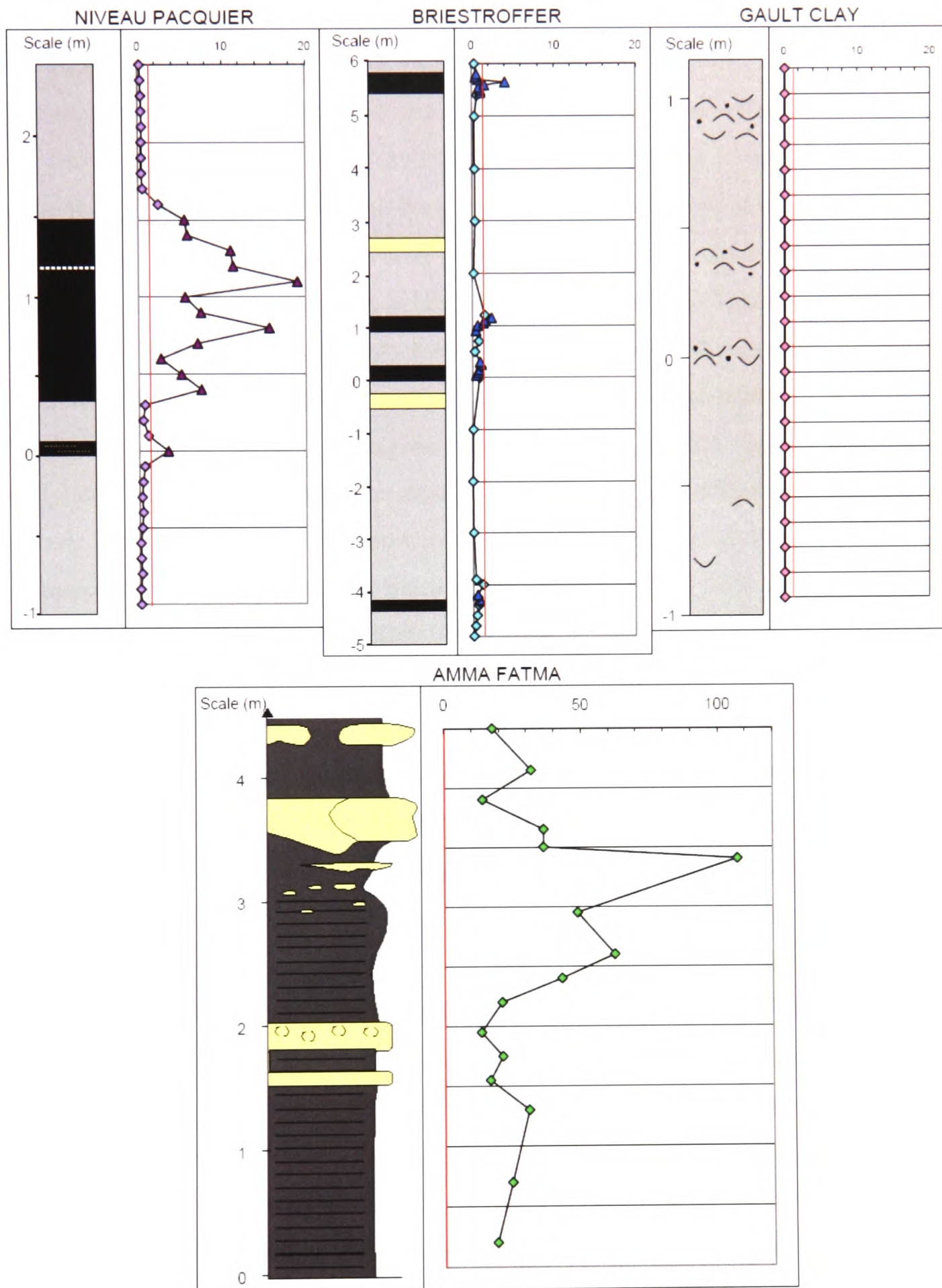


Figure 6.4: Summary plot of molybdenum enrichment factor data for the Niveau Pacquier, Briestroffer, Folkestone Gault Clay and Amma Fatma sediments. The red line represents the enrichment factor of 'normal shale' (Wedepohl, 1971).

Wilson and Norris (2001) suggested that the thermal structure of the surface waters of the Atlantic underwent considerable variation during the late Albian OAE 1d, ultimately leading to a collapse of surface-water stratification during the deposition of the Briestroffer sequence. These fluctuating conditions and potentially short-term low-oxygen events could explain why the thin bands of Briestroffer black shale do not record consistent trace-metal enrichment. This could also explain why the thin shale band below the main Niveau Pacquier black shale has only minor molybdenum enrichment. Alternatively, Helz *et al.* (1996) suggested that the hydrogen sulphide level in the water column plays a key role in molybdenum fixation, which could imply that the Niveau Pacquier black shale was laid down under euxinic conditions, whereas only anoxic conditions were reached during the deposition of some of the Briestroffer black shales. Turgeon and Brumsack (2006) agreed that while molybdenum is accumulated under waters with free H₂S, it is not enriched in suboxic or oxic conditions. This could also explain the stronger restriction in pyrite framboid diameter in the Niveau Pacquier black shales, where at least 90% of the framboids had a diameter of less than 7 µm (see *Figure 2.17*). This almost matches the description of euxinic sediments proposed by Wilkin *et al.* (1997).

Although molybdenum is the most reliable trace-metal proxy for palaeo-oxygenation, it is clear that vanadium, nickel and manganese levels are affected by the bottom-water oxygenation regime. While vanadium is relatively depleted in all of the Niveau Pacquier grey clay samples, the black shales predominantly plot with enrichment, apart from the top 40 cm of the main black shale sequence, and three of the Briestroffer black shale layers record enrichment (see *Figure 6.5*). The entire Amma Fatma sequence is enriched in vanadium and the Folkestone Gault Clay plots within the depleted range. Nickel is also enriched in the Amma Fatma sequence and records depletion relative to average shale in the Folkestone Gault Clay (see *Figure 6.6*). While there are only a few peaks of enrichment of nickel in the Niveau Pacquier black shale, each of the Briestroffer black shale horizons record a peak relative to the grey clay in the nickel enrichment factor data, although the peak associated with the lowest horizon does not extend above 1. While not all of the Niveau Pacquier black shale samples record enrichment, vanadium and nickel do seem to be more sensitive than molybdenum within the Briestroffer sequence, which suggests that they are less affected by event duration or the absence of free hydrogen sulphide.

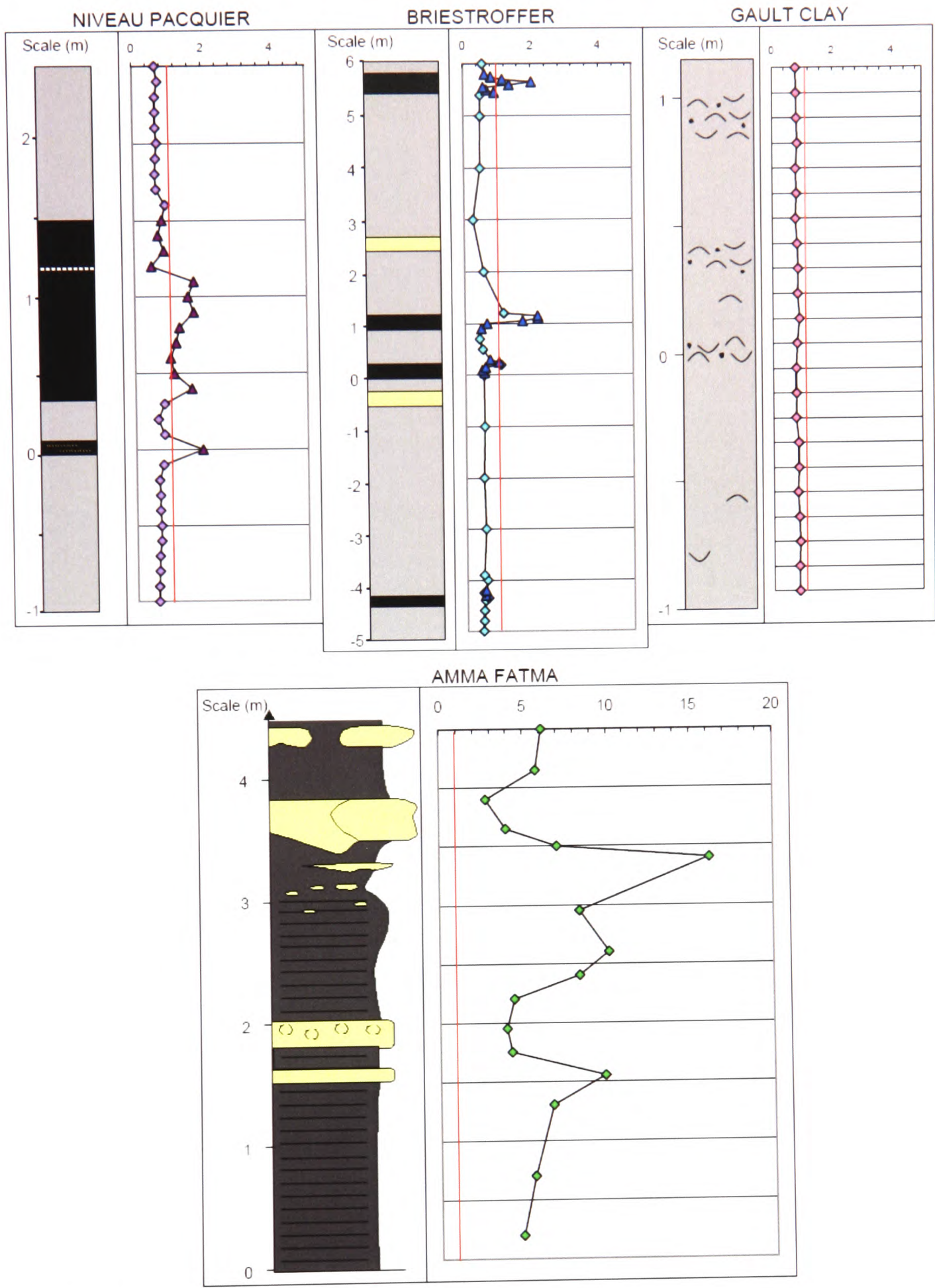


Figure 6.5: Summary plot of vanadium enrichment factor data for the Niveau Pacquier, Briestroffer, Folkestone Gault Clay and Amma Fatma sediments. The red line represents the enrichment factor of 'normal shale' (Wedepohl, 1971).

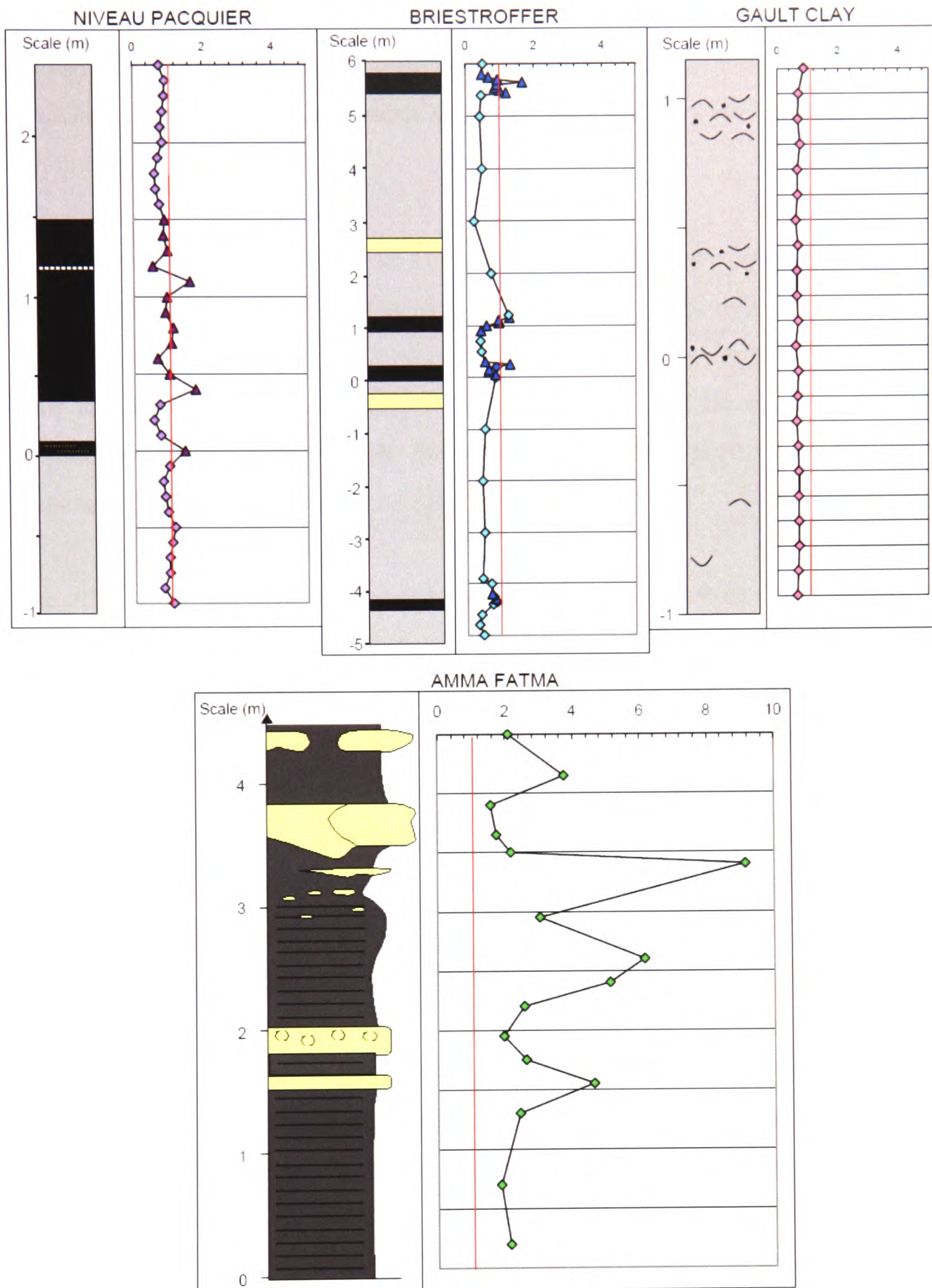


Figure 6.6: Summary plot of nickel enrichment factor data for the Niveau Pacquier, Briestroffer, Folkestone Gault Clay and Amma Fatma sediments. The red line represents the enrichment factor of 'normal shale' (Wedepohl, 1971).

The thin black shale band within the Niveau Pacquier sequence which only demonstrates minor enrichment of molybdenum is recorded as a strong peak in both the nickel and vanadium data, which again suggests that they are more sensitive to short duration events.

Manganese records depletion in all samples from all four sites (apart from a single Amma Fatma sample which is skewed by its very low detrital mineral content) (see *Figure 4.34*) and so shows little separation between palaeo-oxygenation regimes. There are, however, subtle variations within the data that do correlate with the proposed conditions, as each of the Briestroffer black shale horizons record greater manganese depletion than the surrounding grey clays.

None of the trace elements studied provide any distinction between the Amma Fatma dark marls and the bioclastic limestone within the sequence. Comparing the results to the Vocontian black shale data, the Amma Fatma sequence appears to have been laid down under strongly anoxic or euxinic settings but these conditions cannot be implied for the relatively fossiliferous material. This suggests that trace-metal remobilisation has occurred, possibly as a result of later diagenetic pyrite formation in the limestone bed (Passier *et al.*, 1996).

Jones and Manning (1994) identified authigenic uranium (Ua), U/Th, V/Cr and Ni/Co as more reliable proxies for palaeo-oxygenation than (Cu+Mo/Zn) and V/(V+Ni). The data from the four sites support this distinction, but the numerical boundaries proposed by Jones and Manning (1994) (see *Figure 6.8*) do not directly apply to the data. In general, there was some agreement between the palaeo-oxygenation conditions indicated by Ua and V/Cr, but these consistently indicate more oxygenated environments than the U/Th and Ni/Co ratios (see *Figure 6.7*). In turn, Ni/Co values consistently indicate stronger oxygen depletion than the U/Th data. In particular, as both Ua and U/Th ratios are calculated using the same elemental data, the variation in suggestion palaeo-oxygenation conditions from their results suggests that the numerical boundaries should be altered. Jones and Manning (1994) used gamma ray spectrometry to quantify the amounts of uranium and thorium present in samples and this may to some extent explain why the data determined by ICP-MS seems to fit different numerical boundaries.

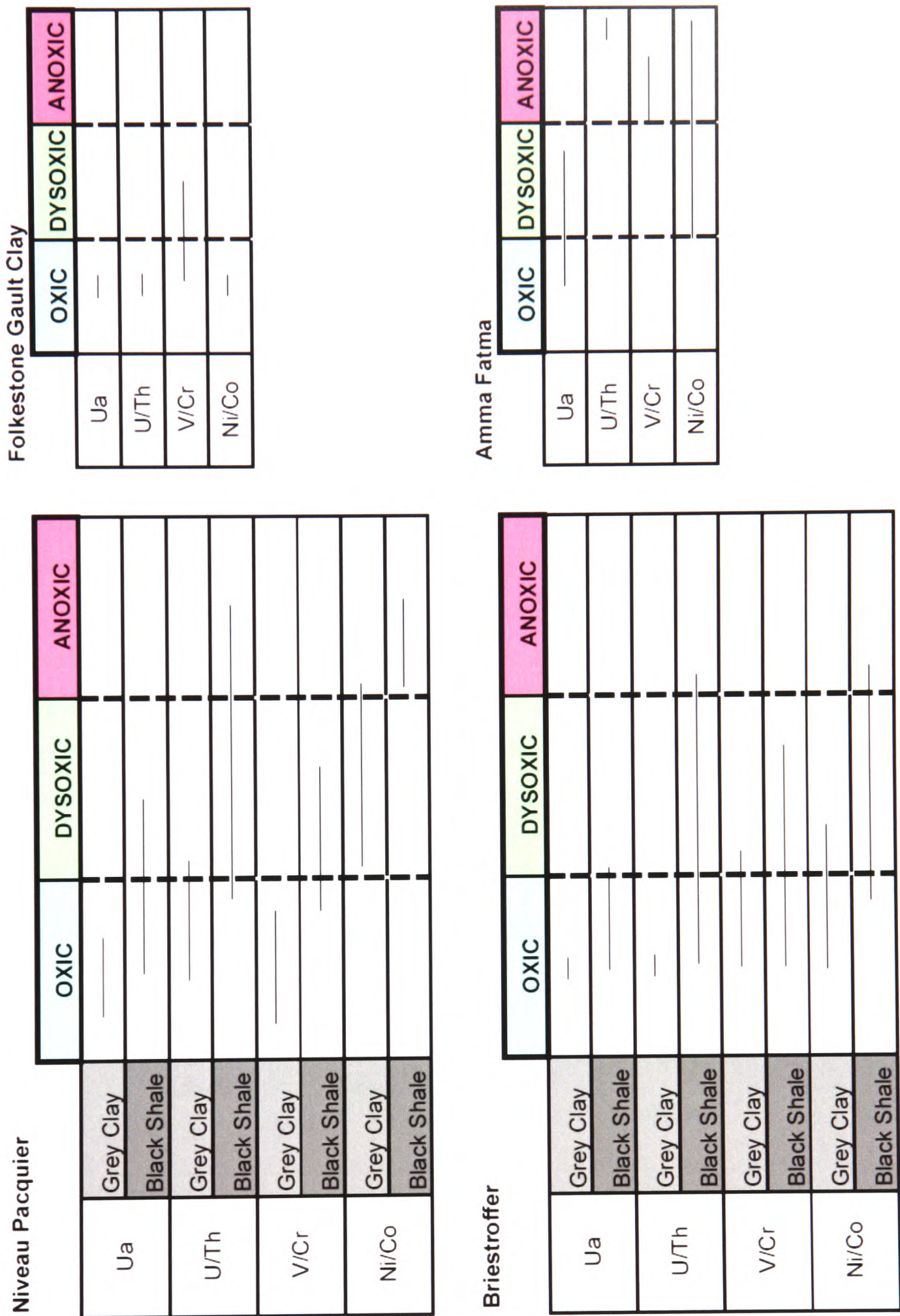


Figure 6.7: Summary diagram of palaeo-oxygenation conditions of the four study sites according to the trace-metal ratio numerical boundaries proposed by Jones and Manning (1994).

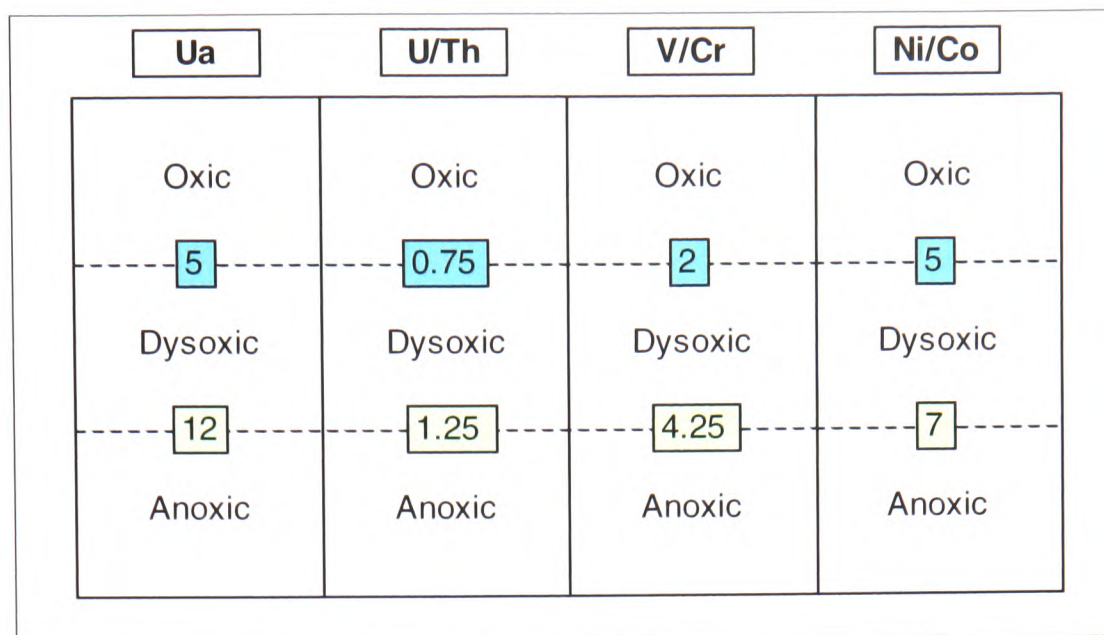


Figure 6.8: Numerical boundaries proposed by Jones and Manning (1994) to define palaeo-oxygenation conditions.

Creating a boundary at a Ua value of 1 divides the Niveau Pacquier grey clays from the black shales, and all of the Briestoffer black shales display a peak that exceeds this boundary. In addition, the Gault Clay samples fall below this boundary and all of the Amma Fatma samples, apart from the sample affected by low detrital content, fall above this boundary. It is therefore proposed that this boundary represents the transition between oxic/dysoxic conditions and anoxic conditions (see Figure 6.9).

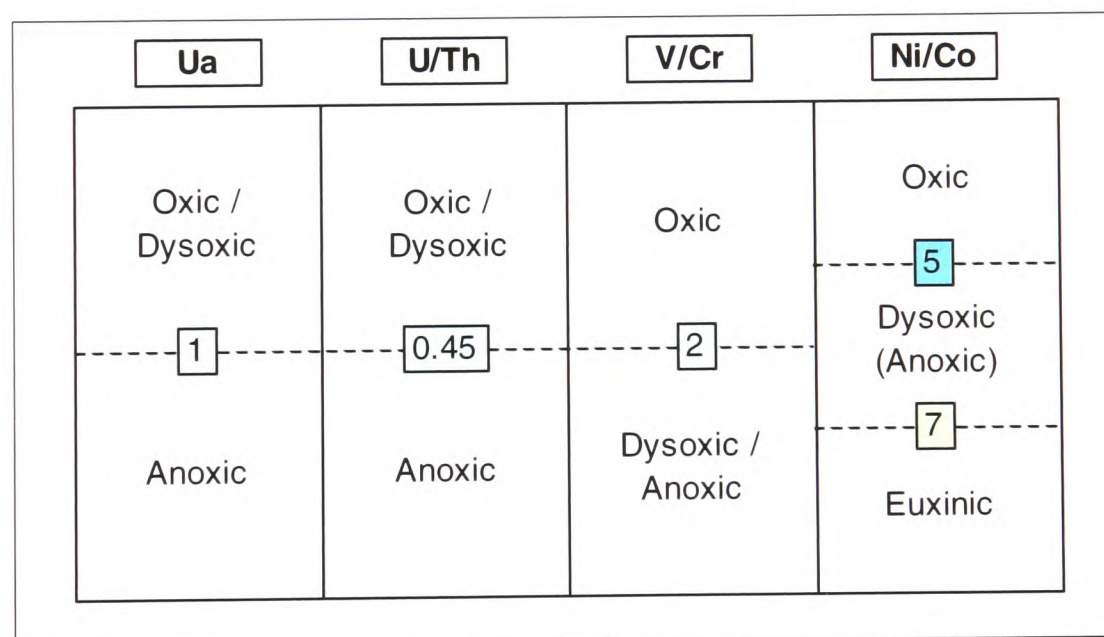


Figure 6.9: Numerical boundaries proposed to define palaeo-oxygenation conditions based on the data from this study.

Adjusting the U/Th boundary to 0.45 provides a similar division of the data, but again this boundary only separates oxic or dysoxic conditions from anoxic conditions, and it is not possible to differentiate between dysoxic and oxic regimes. The V/Cr results are not as straightforward – the proposed boundary at a value of 2, which was thought to divide oxic and dysoxic conditions (Jones and Manning, 1994), does neatly divide

the Niveau Pacquier and Briestroffer black shale peaks from the respective grey clay samples. This would suggest that this boundary in fact separates anoxic conditions from more oxic regimes. However, several of the Folkestone Gault Clay samples also cross this boundary, which suggests that values above 2 may represent dysoxic or anoxic conditions (see *Figure 6.9*). All of the Amma Fatma samples have V/Cr values above 2 and some extend above 4.25 which was initially proposed as the anoxic boundary (Jones and Manning, 1994).

Of all of the boundaries proposed by Jones and Manning (1994), the Ni/Co boundaries appear to apply best to the data from the four study sites (see *Figure 6.7*). However, while the Niveau Pacquier grey clays plot within dysoxic ranges and the black shales within the anoxic range, the Briestroffer grey clays are oxic with the black shales extending into the dysoxic range. While the numerical boundaries do neatly separate the data, it may be that the anoxic range actually represents euxinic conditions, and that anoxic conditions may plot within the suggested dysoxic range. If the Briestroffer black shales do represent predominantly anoxic conditions, then this would explain the limited enrichment in molybdenum. All of the Amma Fatma samples, excluding the detrital mineral-poor sample, have a Ni/Co value above 7, and this would correspond with euxinic conditions during deposition. The proposed boundaries also classify all of the Folkestone Gault Clay samples as oxic.

There is little correlation between the other ratios investigated by Jones and Manning (1994). The Ni/V ratio does appear to decrease slightly in the Niveau Pacquier black shale, but it is not a strong proxy for palaeo-oxygenation as the some of the Briestroffer black shale horizons record higher values than the grey clays and some record lower values. The (Cu+Mo)/Zn ratio follows a similar pattern, recording some peaks within the Niveau Pacquier black shale but showing alternating results in the Briestroffer black shales. Very few of the Vocontian black shale or Amma Fatma data points extend into the proposed anoxic range of $V/(V+Ni)$ values (Schovsbo, 2001) and there seems to be little distinction between the data sets.

The cerium anomaly does not seem to provide any distinction between the data sets, with nearly all samples recording a positive anomaly which is thought to represent oxic conditions (Wright *et al.*, 1987). In contrast, the V/Sc ratio does seem to correlate with palaeo-oxygenation (see *Figure 6.10*).

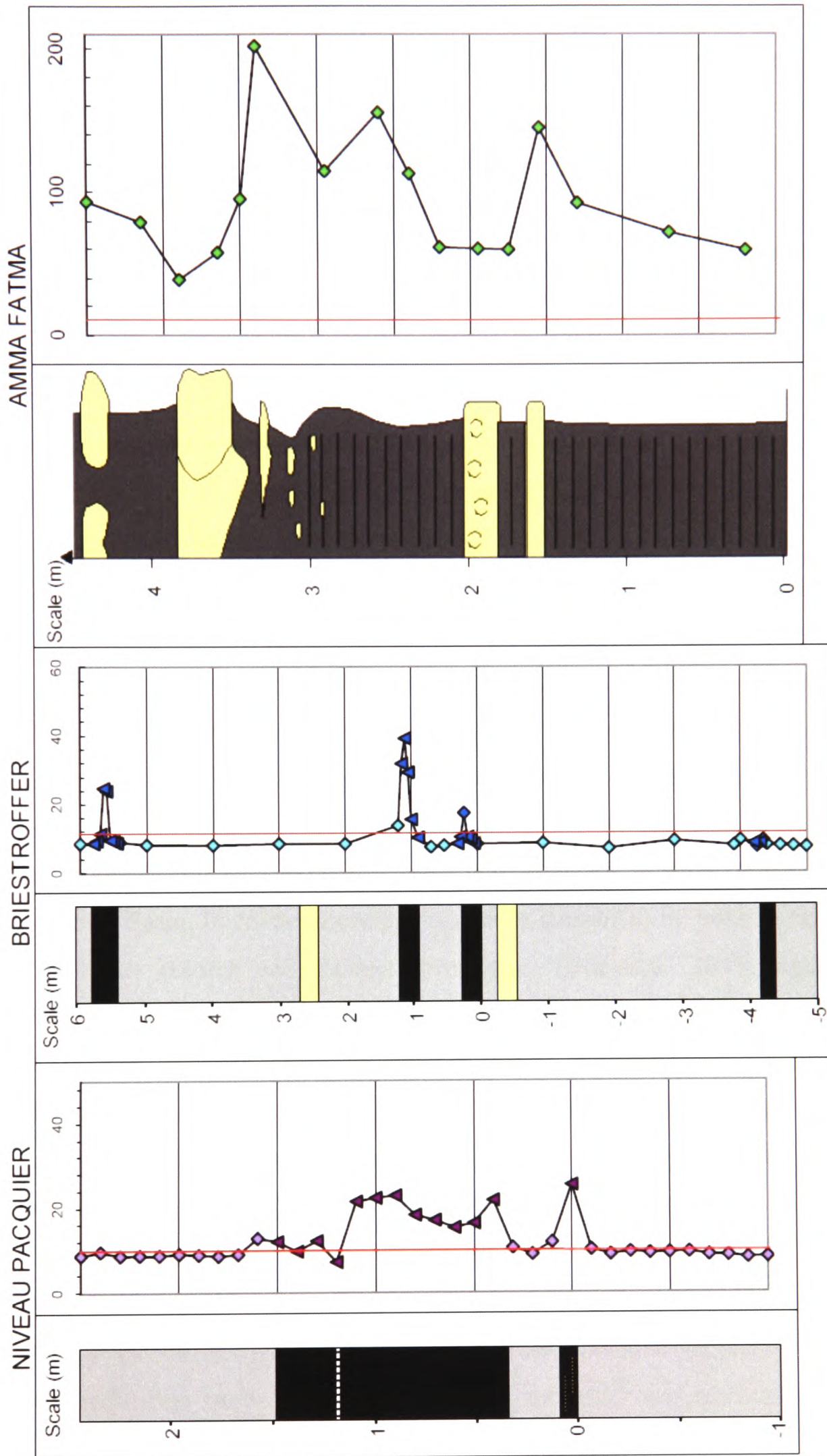


Figure 6.10: V/Sc summary plot for Niveau Pacquier, Breistroffer and Amma Fatma samples. The red line represents the upper limits of 'normal marine' conditions according to Kimura and Watanabe (2001)

Kimura and Watanabe (2001) proposed that values between 4.7 and 9.1 represent 'normal marine' conditions. Most of the Briestroffer and Niveau Pacquier grey clay samples plot below 9.1, whereas all of the black shale horizons extend above this value. All of the Amma Fatma samples also plot well above this limit, which suggests that this could be the numerical boundary between oxic and dysoxic/anoxic conditions. A numerical boundary of 14 separates the data in the same way as, and therefore correlates with, the V/Cr boundary at a value of 2. This suggests that the true oxic to dysoxic/anoxic transition may actually occur at a lower value of V/Cr.

The Amma Fatma sediments consistently record higher redox-related trace-metal enrichment than the Briestroffer and Niveau Pacquier anoxic black shales. This may be indicative of more restricted conditions during the time of formation, but it is important to note that the data is also skewed by the lower aluminium contents in the Amma Fatma sediments. Brumsack (2005) suggested that in upwelling anoxic systems, such as the Amma Fatma system (Kuhnt *et al.*, 2001), the extent of trace-metal fixation is controlled by the steepness of the slope, the proximity of H₂S to the sediment:seawater interface, and the intensity of bio-accumulation and regeneration.

In contrast, Brumsack (2005) suggested that in anoxic basinal systems such as the Vocontian Basin, trace-metal content is mainly controlled by trace metal availability in the water column and sedimentation rate. Brumsack (2005) argued that this difference in controlling variables may limit the comparability of geochemical proxies from different sites. In addition to this, Klinkhammer and Bender (1980) suggested that the Oxygen Minimum Zone (OMZ) that impinges on the sea floor in an upwelling system may act as a manganese 'conveyor belt' promoting redox-related manganese depletion in sediments. This concept could also explain higher levels of redox-related trace metal enrichment if lateral supply of trace elements is increased to upwelling zones. However, there is some evidence from the biofacies models, in particular the Oxygen-Restricted Biofacies scheme, which suggests that the Amma Fatma sediments were associated with more restricted oxygenation conditions than the two Vocontian black shales.

6.4 Fe-S-C Systematics

The Total Sulphur (TS) data only differentiated the Amma Fatma sequence as possibly having been laid down under lower oxygen conditions than the Niveau Pacquier, Briestroffer or Folkestone Gault Clay sequences (see *Figures 5.6 to 5.9*). There is little distinction between the grey clay and black shale data sets of the two French sites, which possibly suggests that euxinic conditions were only reached during the deposition of the Amma Fatma sediments. This limited interpretation suggests that Total Sulphur is not a strong proxy for palaeo-oxygenation conditions.

The amount of Total Organic Carbon (TOC) appears to have a stronger correlation with palaeo-oxygen regimes and a boundary 2 wt% TOC separates the Niveau Pacquier black shales and the majority of the Amma Fatma samples from the remaining data sets (see *Figures 5.6 to 5.9*). According to the palaeontological and trace-metal proxy data, these two data sets represent the most oxygen-restricted settings of the four sites and therefore this numerical boundary could be suggested to identify euxinic conditions. However, the reliability of this division is questionable as sediment TOC content is affected by a variety of sedimentological factors, including sedimentation rate. Despite this, the combination of TOC with a geochemical proxy such as Ua, which is thought to be diagnostic of anoxic conditions, may allow deeper interpretation of palaeo-oxygenation regimes (see *Figure 6.11*).

Using a combination of the boundaries proposed for these two proxies, the majority of the Niveau Pacquier black shales and Amma Fatma sediments fall within a zone which could represent true euxinic conditions (see *Figure 6.11*). The only Amma Fatma sample that plots within the proposed oxic/dysoxic range is the sample from a pale horizon which contains very little detrital material and so has a strongly skewed molybdenum enrichment factor value. The Briestroffer black shales extend from the oxic/dysoxic into the anoxic range with only one sample plotting as euxinic. Using this template, all but one of the grey clay samples from both Vocontian sites, and all of the Folkestone Gault Clay samples plot within the oxic/dysoxic range.

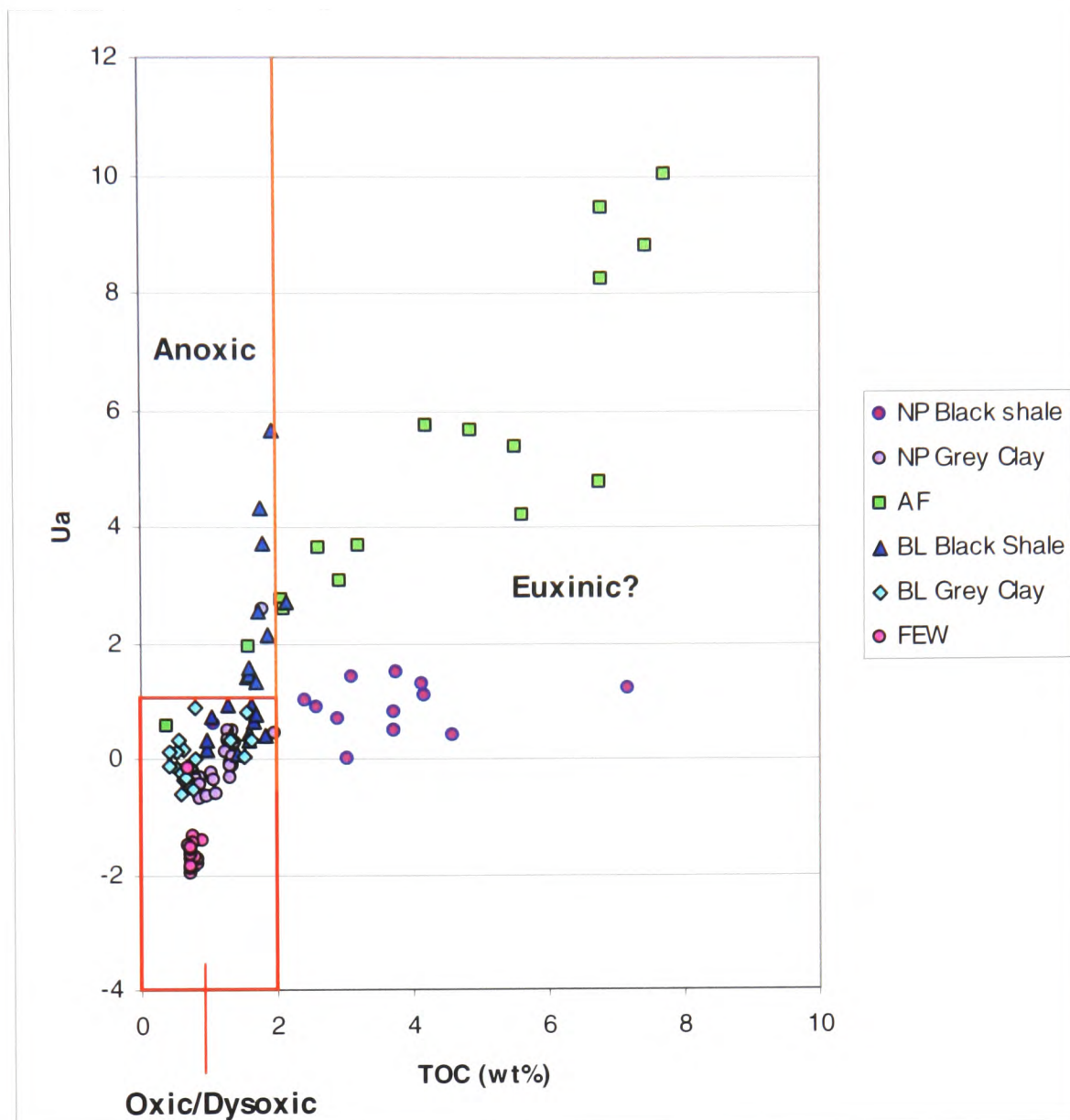


Figure 6.11: Plot of authigenic uranium (Ua) against TOC for each data set (Niveau Pacquier (NP), Amma Fatma (AF), Briestroffer (BL) and Folkestone Gault Clay (FEW)). A numerical boundary at a Ua value of 1, and another at a TOC value of 2 wt% allows division of the data into three zones which may represent different palaeo-oxygenation regimes.

While the S/C plots can be interpreted in a broad sense in conjunction with other data to identify palaeo-oxygenation conditions, they do not provide a reliable proxy alone (see *Figures 5.11 to 5.14*). The majority of the data sets do not demonstrate a statistically significant regression line and so interpretation of the plots is limited.

There seems to be little correlation between sedimentary proxies and the division of iron with the different 'iron pools' throughout each sequence (see *Figures 5.15 to 5.18*). It is certainly not possible to distinguish the Niveau Pacquier and Briestroffer black shale horizons from the surrounding grey clay from 'iron pool' data alone. There are, however, vast differences between the sites:

- the more oxic Folkestone Gault Clay samples contain a maximum of 35% reactive iron,
- the Niveau Pacquier data peaks at 50% reactive iron,
- the Briestroffer sequence containing a maximum of 85% reactive iron
- several of the Amma Fatma samples contain 100% reactive iron.

This distribution of iron pools could be explained by the theory that lower oxygen environments receive more reactive iron via lateral transport within the water column (Raiswell *et al.*, 2001). While both the Amma Fatma and Briestroffer sample sets contain a high proportion of both pyrite iron and dithionate-extractable iron (FeD), both of these sample sets have relatively low Total Iron (FeT) contents and so the low proportion of Unreactive Iron may be linked to low detrital inputs relative to biogenic inputs. Despite the higher proportion of reactive iron in these sites, the amount of pyrite iron falls within a similar range to the other sites.

The ternary plots of iron, sulphur and carbon do appear to distinguish the data sets (see *Figures 5.20 to 5.23*), with the Folkestone Gault Clay, Niveau Pacquier grey clay and Briestroffer grey clay samples all plotting close to the proposed Normal Marine regression line of S/C 0.4 (Arthur and Sageman, 1994). In contrast, both the Niveau Pacquier black shale samples and the Briestroffer black shale samples plot off to the side of the Normal Marine regression line within a region that suggests that FeT played a greater role in controlling pyrite formation. The Fe-S-C plots are designed to distinguish between oxic and euxinic conditions, but this separation of data suggests that the plots may also allow recognition of anoxic regimes as well as fully euxinic conditions. The Amma Fatma data plot below the 'ideal' euxinic regression line but follow the same trend, which implies that iron-limitation controlled pyrite formation, and that the sediments formed under a euxinic water column.

The Degree of Pyritisation (DOP) does not appear to provide an accurate indication of the palaeo-oxygenation conditions, as all of the Niveau Pacquier, Briestroffer and Folkestone Gault Clay samples plot predominantly within the 'normal marine' range, with a few samples extending beyond the normal marine : restricted conditions boundary proposed by Raiswell *et al.* (1988). There is no clear distinction between the black shale samples and those deposited under more oxic conditions, which

suggests that the DOP does not necessarily distinguish anoxic events (see *Figures 5.24 to 5.27*). The Amma Fatma data does plot predominantly within the 'restricted' range, with some samples extending into the zone suggested to represent 'inhospitable bottom-water condition' (Raiswell *et al.*, 1988). This separation of the Amma Fatma sequence from the other data sets suggests that DOP may be useful in identifying the extremes of anoxic or euxinic conditions but that the numerical boundaries proposed do not correlate with the results of the sedimentology proxies.

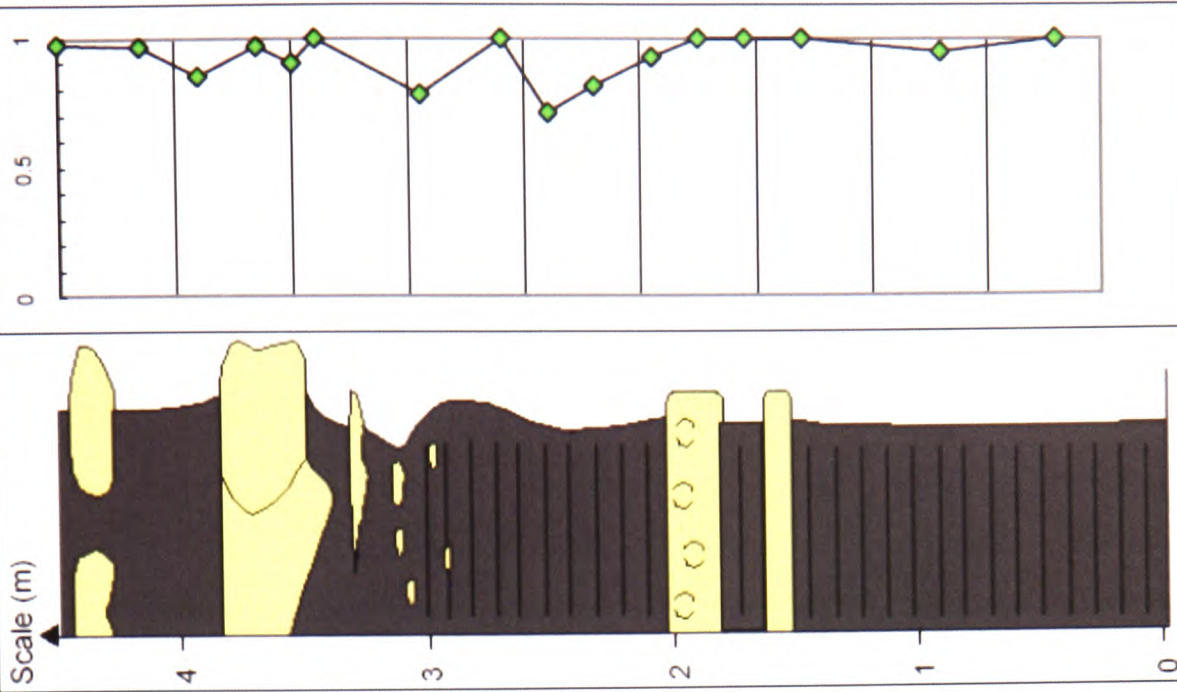
The Degree of Pyritisation has been calculated using a variety of methods that rely on different measures of reactive iron (DOP_H uses iron extracted by the hot HCl method, DOP_T uses Total Iron, and DOP_D uses iron extracted by the dithionate method) and the current numerical boundaries apply to DOP_H (see *Figures 5.24 to 5.27*). However, DOP_D most closely resembles the definition of what the Degree of Pyritisation is supposed to represent, and so theoretically should be the most reliable indicator of palaeo-oxygenation. Using dithionate-extracted iron yields higher values than the DOP_H method and so further work must be done to assign meaningful numerical boundaries that allow DOP_D to be used to its full potential as a palaeo-oxygenation proxy.

The combination of S/C plots with DOP vs. TOC and FeT vs. TOC plots does allow deeper interpretation of the environmental setting than S/C plots alone but they still do not allow a convincing interpretation of all of the sites (see *Figures 5.28 to 5.31*). The majority of the regression lines are not statistically valid and there are a variety of scenarios proposed that could result in similar distributions on these graphs and this complicates their interpretation. This means that these plots alone could not be used as a reliably indicator of palaeo-oxygenation but could be used in conjunction with other proxies to aid their interpretation.

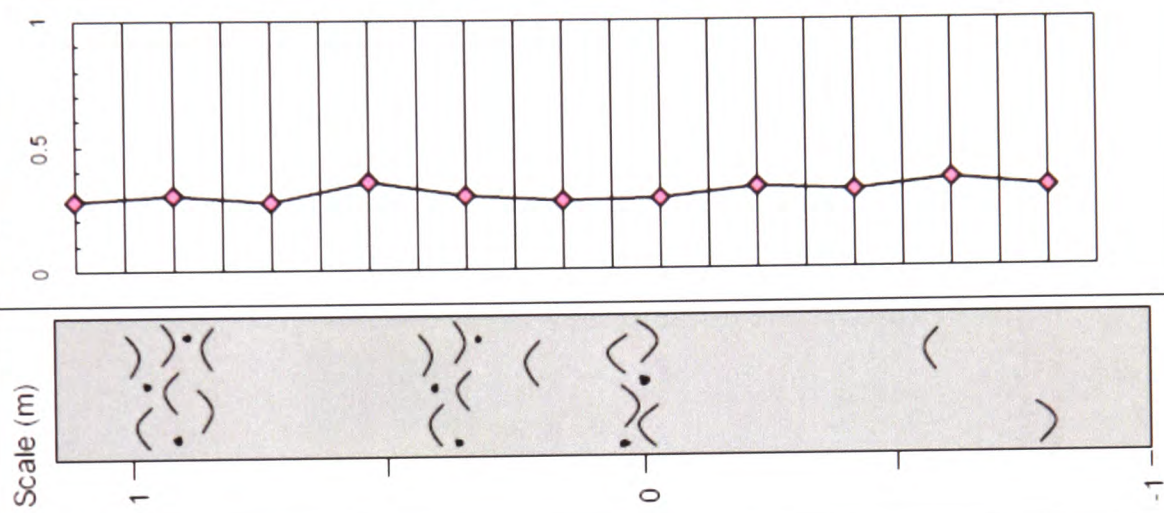
Unlike several of the trace metal proxies, the Indicator of Anoxia does not seem to identify the palaeo-oxygenation variations within the Niveau Pacquier sequence, but does correlate with those expected within the Briestroffer sequence (see *Figure 6.12*).

Figure 6.12: Summary plot of Indicator of Anoxia data for the Niveau Pacquier, Briestroffer, Folkestone Gault Clay and Amma Fatma sediments (on next page).

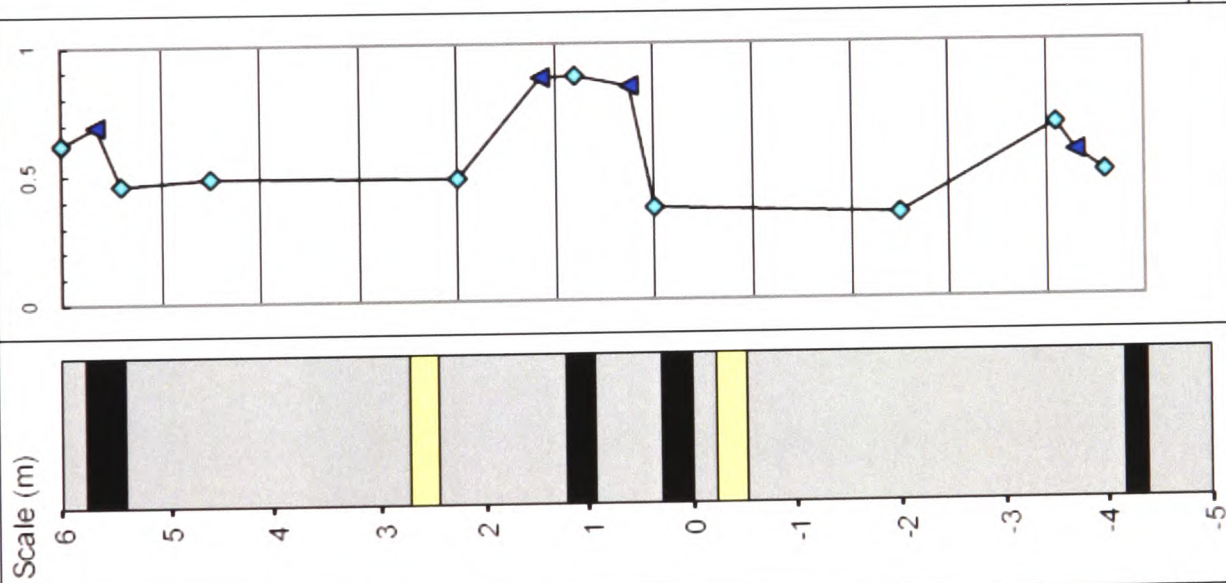
AMMA FATMA



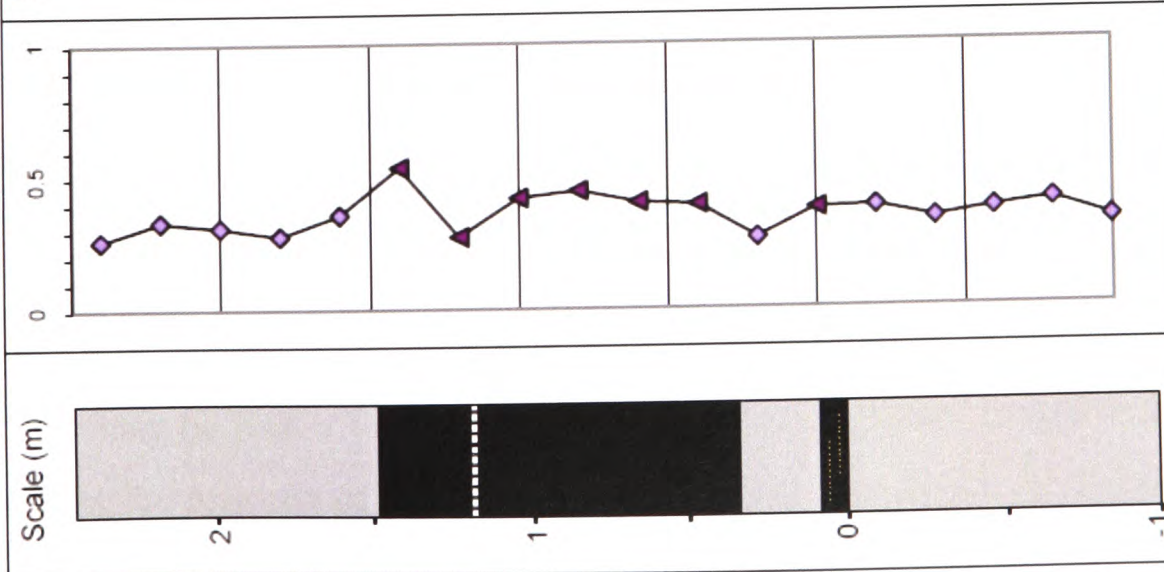
GAULT CLAY



BRIESTROFFER



NIVEAU PACQUIER



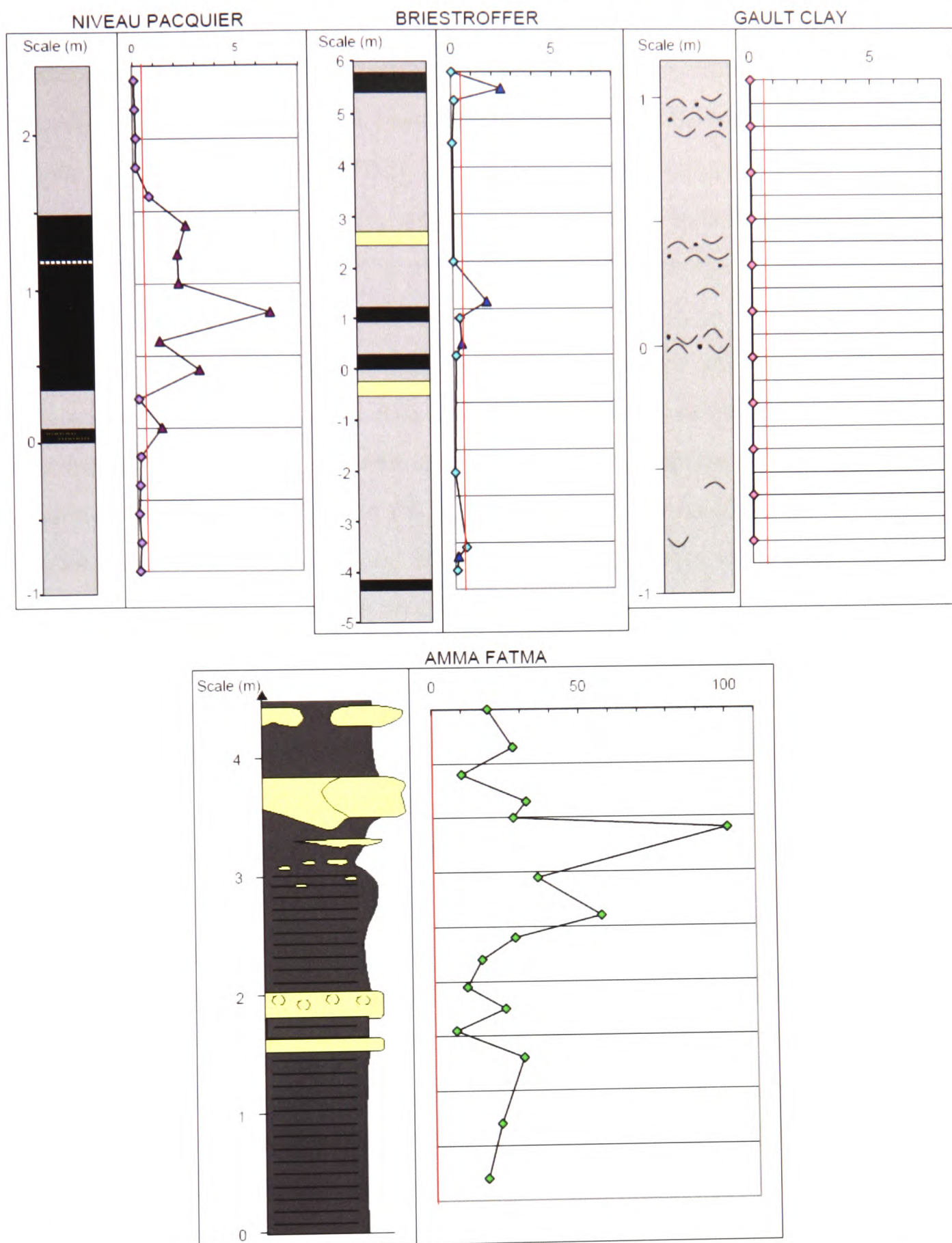


Figure 6.13: Plots of the molybdenum Enrichment Factor multiplied by the Indicator of Anoxia ($[Mo\ EF \times IA]$) for the (a) Niveau Pacquier; (b) Briestroffer; (c) Folkestone Gault Clay; and (d) Amma Fatma samples. In (a) and (b) the darker triangular colour data points represent the black shale samples and the lighter colour circular data points represent the grey clay samples.

There is little differentiation between the Niveau Pacquier black shales and grey clays and this may be linked to the lower levels of reactive iron throughout the sequence. However, the majority of the Briestroffer grey clays plot below the 0.5 boundary that

Raiswell *et al.* (2001) proposed to separate normal marine from anoxic or euxinic conditions, whereas all of the black shale samples plot above this line. In addition to this, all of the Folkestone Gault Clay samples fall below this boundary and all of the Amma Fatma samples plot within the proposed anoxic-euxinic range. This clear differentiation of the sample sets would suggest that the Indicator of Anoxia is the most reliable of all of the Fe-S-C proxies of palaeo-oxygenation.

As the molybdenum-based proxies, unlike the Indicator of Anoxia, do clearly distinguish the Niveau Pacquier data sets, the combination of the Indicator of Anoxia with molybdenum enrichment factors may allow identification of the range of low-oxygen sediments (see *Figure 6.13*). A boundary of 0.5 on a plot of molybdenum enrichment factors multiplied by the Indicator of Anoxia does seem to clearly categorise the data sets. While all of the Niveau Pacquier black shale samples plot above this line, only one of the grey clay samples has a [Mo EF x IA] value of higher than 0.5. Three out of the four Briestroffer black shale horizons plot above 0.5 whereas all of the Briestroffer grey clay samples plot below this line. Similarly all of the Folkestone Gault Clay samples have a [Mo EF x IA] value of less than 0.5 whereas all of the Amma Fatma samples fall well above this boundary.

6.5 Conclusions

The presence of lamination appears to be the key sedimentological indicator of restricted bottom water oxygenation conditions. In terms of ichnological proxies, bioturbation indices provide the clearest and easiest way to directly compare different sites but correlation with specific palaeo-oxygenation regimes is limited. While the use of numerical categories of pyrite framboid diameters appears to have variable success for palaeo-oxygenation determination, the proposed descriptive categories of pyrite morphology have the potential, with further work, to provide a qualitative indication of palaeo-oxygenation conditions

Interpretation of faunal proxies can be limited by poor preservation, and biofacies models rely heavily on sedimentological proxies. Taphonomy-related indicators, however, appear to correlate well with proposed palaeo-oxygenation conditions and further work could allow extension of the proposed descriptive categories of pyrite morphology using other taphonomic descriptors.

Molybdenum appears to be the most reliable of the trace-metal proxies studied, although direct comparison of trace-metal enrichment factors is complicated by variations in the bulk geochemistry of the different sites. As suggested by Jones and Manning, (1994) U_a , U/Th, V/Cr and Ni/Co appear to be the most reliable trace-metal ratios and altered numerical boundaries are proposed for these proxies. The V/Sc ratio does show some correlation with suggested palaeo-oxygenation conditions but further work would be required to refine the numerical boundaries proposed.

Of the Fe-S-C systematics indicators, Total Organic Carbon and the Indicator of Anoxia provide the greatest definition between palaeo-oxygenation data sets. Interpretation of the Degree of Pyritisation is complicated by the different calculation methods used in the literature. DOP_D (calculated using dithionate-extracted iron) most closely resembles the definition of what the Degree of Pyritisation is supposed to represent, and so theoretically should be the most reliable indicator of palaeo-oxygenation. DOP_D yields higher values than the DOP_H method (which is calculated using iron extracted by the hot HCl procedure) which the current numerical boundaries are based on. Further work must be done to assign meaningful numerical boundaries for DOP_D before it can be applied accurately as a palaeo-oxygenation proxy. The proposed combinations of trace metal and Fe-S-C indicators such as [Molybdenum Enrichment Factor x Indicator of Anoxia], and plots of U_a against TOC may provide the strongest palaeo-oxygenation proxies and potentially distinguish between oxic/dysoxic, anoxic and euxinic conditions.

6.6 Further Work

- Extension of the current data sets for the four study sites in order to aid interpretation of the palaeo-oxygenation proxies. This would include interpreting microfossil data, analysing oxygen and carbon isotopes and investigating redox-related biomarkers.
- Further investigation of pyrite morphology and taphonomy in a range of previously documented black shales in order to test the reliability of the proposed descriptive categories.

- Collation of V/Sc data from a number of sites thought to represent a range of palaeo-oxygenation settings. This data, in comparison with other trace-metal ratio proxies, will be useful in refining the numerical boundaries proposed for the V/Sc ratio.
- Analysis of DOP_D for a range of sites, including those that have previously had DOP_H data reported in the literature. This work would allow the development of meaningful numerical boundaries specific for DOP calculated using dithionate-extracted iron.

References:

Aberhan, M., and Baumiller, T.K., 2003. Selective extinctions among Early Jurassic bivalves: A consequence of anoxia. *Geology*, **31**, 1077-1080.

Aberhan, M., Alroy, J., Fursich, F.T., Kiessling, W., Kosnik, M., Madin, J., Patzkowsky, M., and Wagner, P., 2004. Ecological attributes of marine invertebrates. *The Paleobiology Database* (<http://paleodb.org>).

Adams, J.A., and Weaver, C.E., 1958. Thorium-uranium ratios as indicators of sedimentary processes: example of concept of geochemical facies. *Bulletin American Association of Petroleum Geologists*, **42**, 387-430.

Adelson, J.M., Helz, G.R., and Miller, C.V., 2001. Reconstructing the rise of recent coastal anoxia; molybdenum in Chesapeake Bay sediments. *Geochimica et Cosmochimica Acta*, **65**, 237-252.

Allison, P.A., Wignall, P.B., and Brett, C.E., 1995. Palaeo-oxygenation: effects and recognition. *Geological Society Special Publications*, **83**, 97-112.

Anderson, R.F., Fleisher, M.Q., and LeHuray, A.P., 1989. Concentration, oxidation state, and particulate flux of uranium in the Black Sea. *Geochimica et Cosmochimica Acta*, **53**, 2215-2224.

Arthur, M.A., and Sageman, B.B., 1994. Marine black shales: a review of depositional mechanisms and significance of ancient deposits. *Annual Review of Earth and Planetary Science*, **22**, 499-551.

Ausich, W.I., and Bottjer, 1982. Tiering in suspension-feeding communities on soft sub-strate throughout the Palaeozoic. *Science*, **216**, 173-174.

Baas, J.H., Schönfeld, J. and Zahn, R., 1998. Mid-depth oxygen drawdown during Heinrich events: Evidence from benthic foraminiferal community structure, trace fossil tiering, and benthic $\delta^{13}\text{C}$ at the Portuguese margin. *Marine Geology* **152**, 25–55.

Barron, E.J. & Washington, W.M., 1985. Warm Cretaceous climates: High atmospheric CO₂ as plausible mechanism. *In: Sundquist, E.T. & Broecker, W.S. (eds.), The Carbon Cycle and Atmospheric CO₂: Natural variations Archean to Present. Geophysical Monograph, 546-553.*

Berner, R.A., 1984. Sedimentary pyrite formation: An update *Geochemica et Cosmochimica Acta* 48, 605-615

Berner, R.A., 1982. Burial of organic carbon and pyrite sulfur in the modern ocean: its geochemical and environmental significance. *American Journal of Science*, **282**, 451-473.

Berner, R.A., 1981. A new geochemical classification of sedimentary environments. *Journal of Sedimentary Petrology*, **51**, 359-365.

Berner, R.A., 1970. Sedimentary pyrite formation. *American Journal of Science*, **268**, 1-23.

Berner, R.A., 1969. The synthesis of framboidal pyrite. *Economic Geology*, **64**, 383-384.

Berner, R.A., and Raiswell, R., 1983. Burial of organic carbon and pyrite sulphur in sediments over Phanerozoic time: a new theory. *Geochimica et Cosmochimica Acta*, **47**, 855-862.

Berner, R.A., and Westrich, J.T., 1985. Bioturbation and the early diagenesis of carbon and sulfur. *American Journal of Science*, **285**, 193-206.

Bernhard, J.M., and Sen Gupta, B.K., 1999. Foraminifera of oxygen depleted environments. *In Modern Foraminifera (ed. Sen Gupta, B.K.), Dordrecht, Kluwer*, 201-216.

Billon, G., Ouddane, B., Gengembre, L., and Boughriet, A., 2002. On the chemical properties of sedimentary sulphur in estuarine environments. *Physical Chemistry Chemical Physics*, **4**, 751-756.

Bornemann, A., Pross, J., Reichelt, K., Herrle, J.O., Hemleben, C., and Mutterlose, J., 2005. Reconstruction of short-term palaeoceanographic changes during the formation of the Late Albian 'Niveau Briestoffer' black shales (Oceanic Anoxic Event 1d, SE France). *Journal of the Geological Society, London*, **162**, 623-639.

Borovec, Z., Kribek, B., and Tolar, V., 1979. Sorption of uranyl by humic acids. *Chemical Geology*, **27**, 39-46.

Bosence, W.J., and Allison, P.A., 1995. A review of palaeoenvironmental analysis from fossils. *In: Bosence, W.J., and Allison, P.A. (eds.), Marine Palaeoenvironmental Analysis from Fossils, Geological Society Special Publication*, **83**, 1-5.

Bottjer, D.J., Campbell, K.A., Schubert, J.K., and Droser, M.L., 1995. Palaeoecological models, non-uniformitarianism and tracking the changing ecology of the past. *In: Bosence, W.J., and Allison, P.A. (eds.), Marine Palaeoenvironmental Analysis from Fossils, Geological Society Special Publication*, **83**, 7-26.

Bralower, T. J., Arthur, M. A., Leckie, M. R., Sliter, W. V., Allard, D. and Schlanger, S., 1994. Timing and palaeoceanography of oceanic dysoxia/anoxia in the Late Barremian to Early Aptian (Early Cretaceous). *Palaios*, **9**, 335-369.

Breck, W.G., 1974. Redox levels in the sea. *In: Goldberg, E.D. (ed.). The sea, Marine Chemistry*, **5**, 153-179, New York: Wiley-Interscience.

Bréhéret, J.G., 1997. L'Aptien et l'Albian de la Fosse Vocontienne (des bordures au bassin). Evolution de la sedimentation et enseignements sur les événements anoxiques. *Publication de la Société Géologique du Nord*, **25**, 1-614.

Bréhéret, J.-G., 1994. The Mid-Cretaceous organic-rich sediments from the Vocontian Zone of the French Southeast Basin. *In: Mascle, A. (ed.) Hydrocarbon and Petroleum Geology of France. Special Publication of the European Association of Petroleum Geoscientists*, **4**, 295–320.

Bréhéret, J.-G. 1988. Episodes de sédimentation riche en matière organique dans les marnes bleues d'âge aptien bien de la partie pélagique du bassin vocontien. *Bulletin de la Société Géologique de France*, **8**, 349–356.

Bréhéret, J.-G., 1986. Indices d'un événement anoxique étendu à la Téthys alpine, à l'Albien inférieur événement Paquier. *Comptes Rendu de l'Académie des Sciences*, **300**, 355-358.

Bréhéret, J.G., Hanzon, M., El Albani, A., and Iatzoura, A., 2004. Impact de la vie benthique sur la genèse de nodules calcaires dans les black shales. *Comptes Rendus Geosciences*, **336**, 1355-1362.

Brett, C.E., and Baird, G.C., 1986. Comparative taphonomy: a key to paleoenvironmental interpretation based on fossil preservation. *Palaios*, **1**, 207-277.

Brett, C.E., and Speyer, S.E., 1990. Taphofacies. *In: (Briggs, D.E.G. and Crowther, P.R., (eds.) Palaeobiology: a synthesis*, Oxford: Blackwell Scientific Publications, 258-263.

Briet, G.N., and Wanty, R.B., 1991. Vanadium accumulation in carbonaceous rocks: a review of geochemical controls during deposition and diagenesis. *Chemical Geology*, **91**, 83-97.

Bromley, R.G., 1996. *Trace Fossils, Biology, Taphonomy and Applications*. Chapman and Hall, London, 361pp.

Bromley, R.G., and Ekdale, A.A., 1984. *Chondrites: A trace fossil indicator of Anoxia in sediments*. *Science*, **224**, 872-874.

Bromley, R.G., and Uchman, A., 1999. Ichnofabric and trace fossils in Palaeozoic and Mesozoic sediments, Bornholm, Denmark. *19th Regional European Meeting of Sedimentology Programme*, 59-68.

Bruland, K.W., 1989. Complexation of zinc by natural organic ligands in the central North Pacific. *Limnology and Oceanography*, **34**, 269–285.

Brumsack, H.J., 2005. The trace metal content of recent organic carbon-rich sediments: Implications for Cretaceous black shale formation. *Palaeogeography, Palaeoclimatology, Palaeoecology*, **232**, 344-361.

Brumsack, H.J., 1989. Geochemistry of recent TOC-rich sediments from the Gulf of California and the Black Sea. *Geologische Rundschau*, **78**, 851–882.

Brumsack, H.J., 1980. Geochemistry of Cretaceous black shales from the Atlantic Ocean. *Chemical Geology*, **31**, 1–25.

Buessler, K.O., Livingston, H.D., and Casso, S.A., 1991. Mixing between oxic and anoxic waters of the Black Sea as traced by Chernobyl cesium isotopes. *Deep Sea Research*, **39 (Suppliment)**, S725-S745

Butler, I.B., and Rickard, D., 2000. Framboidal pyrite formation via the oxidation of iron (II) monosulfide by hydrogen sulphide. *Geochimica et Cosmochimica Acta*, **64**, 2665-2672.

Byers, C.W., 1977. Biofacies patterns in euxinic basins: a general model. *SEPM Special Publication*, **25**, 5-17.

Calvert, S.E., and Pedersen, T.F., 1993. Geochemistry of Recent oxic and anoxic marine sediments: Implications for the geological record. *Marine Geology*, **113**, 67-88.

Canfield, D.E., 1989. Reactive iron in marine sediment. *Geochimica et Cosmochimica Acta*, **53**, 619-632.

Canfield, D.E., 1988. Sulfate reduction and the diagenesis of iron in anoxic marine sediments. PhD Thesis, Yale University.

Canfield, D.E., Bottrell, S.B., and Raiswell, R., 1992. The reactivity of sedimentary iron minerals towards sulphide. *American Journal of Science*, **292**, 659-683.

Canfield, D.E., Lyons, T.W., and Raiswell, R., 1996. A model for iron deposition in euxinic Black Sea sediments. *American Journal of Science*, **296**, 818-834.

Canfield, D.E., Raiswell, R., Westrich, J.T., Reaves, C.M., and Berner, R.A., 1986. The use of chromium reduction in the analysis of reduced inorganic sulfur in sediments and shales. *Chemical Geology*, **54**, 149-155.

Canfield, D.E., and Thamdrup, B., 1994. The production of ³⁴S-depleted sulphide burial during bacterial disproportionation of elemental sulphur. *Science*, **266**, 1973-1975.

Cruse, A.M., and Lyons, T.W., 2004. Trace metal records of regional paleoenvironmental variability in Pennsylvanian (Upper Carboniferous) black shales. *Chemical Geology*, **206**, 319-345.

Crusius, J., Calvert, S., Pederson, T., Sage, D., 1996. Rhenium and molybdenum enrichments in sediments as indicators of oxic, suboxic and sulfidic conditions of deposition. *Earth and Planetary Science Letters*, **145**, 65-78.

Curran, H.A., 1985. The trace fossil assemblage of a Cretaceous nearshore environment: Englishtown Formation of Delaware, U.S.A. In: Curran, H.A. (ed.), *Biogenic Structures: Their Use in Interpreting Depositional Environments*, Special Publication-Society of Economic Paleontologists and Mineralogists, **35**, 261-276.

Dean, W.E., and Arthur, M.A., 1989. Iron-sulfur-carbon relationships in organic carbon-rich sequences: I. Cretaceous Western Interior Seaway. *American Journal of Science*, **289**, 708-743.

Dean, W.E., Gardner, J.V., and Piper, D.Z., 1997. Inorganic geochemical indicators of glacial/interglacial changes in productivity and anoxia on the Californian continental margin. *Geochimica et Cosmochimica Acta*, **61**, 4507-4518.

DeBaar, H.J.W., Bacon, M.P., Brewer, P.G. and Bruland, K.W., 1985. Rare earth elements in the Pacific and Atlantic Oceans. *Geochimica et Cosmochimica Acta*, **49**, 1943-1959.

Demaison, G.J., and Moore, G.T., 1980. Anoxic environments and oil source bed genesis. *American Association of Petroleum Geologists Bulletin*, **64**, 1179-1209.

Dill, H., 1986. Metallogenesis of early Paleozoic graptolite shales from the Graefenthal Horst (northern Bavaria-Federal Republic of Germany). *Economic Geology*, **81**, 889-903.

Douglas, R.G., 1981. Paleoecology of continental margin basins: a modern case history from the borderland of southern California. *In*: Douglas, R.G., Colburn, I.P., and Gorsline, D.S. (eds.), Depositional systems of active continental margin basins, *SEPM Pacific Section, Short Course Notes*, 121-156.

Droser, M.L., and Bottjer, D.J., 1986. A semiquantitative classification of ichnofabric. *Journal of Sedimentary Petrology*, **56**, 558-569.

Dypvik, H., 1984. Jurassic and Cretaceous black shales of the Janusfjellet Formation, Svalbard, Norway. *Sedimentary Geology*, **41**, 235-248.

Edwards, B.D., 1985. Bioturbation in a dysaerobic bathyal basin: California borderland. *In*: Curran, H.A. (eds.), Biogenic structures: their use in interpreting depositional environments, *SEPM Special Publication*, 309-331.

Efremov, J.A., 1940. Taphonomy: new branch of palaeontology. *Pan-American Geology*, **74**, 81-93.

Ekdale, A.A., and Bromley, R.G., 1984. Comparative ichnology of shelf-sea and deep-sea chalk. *Journal of Palaeontology*, **58**, 322-332.

Ekdale, A.A. and Mason, T.R., 1988. Characteristic trace-fossil associations in oxygen-poor sedimentary environments. *Geology*, **16**, 720–723.

El Albani, A., Vachard, D., Kuhnt, W., and Thurows, J., 2001. The role of diagenetic carbonate concretions in the preservation of the original sedimentary record. *Sedimentology*, **48**, 875-886.

Elderfield, H. and Greaves, M.J. (1982). The rare-earth elements in sea-water. *Nature*, **296**, 214-219.

Erbacher, J., Hemleben, C., Huber, B.T., and Markey, M., 1999. Correlating environmental changes during early Albian oceanic anoxic event 1b using benthic foraminiferal paleoecology. *Marine Micropaleontology*, **38**, 7-28.

Erbacher, J., Huber, B.T., Norris, R.D., and Markey, M., 2001. Increased thermohaline stratification as a possible cause for an ocean anoxic event in the Cretaceous period. *Nature* **409**, 325-327.

Erbacher, J., Thurow, J. & Littke, R., 1996. Evolution patterns of radiolaria and organic matter variations: A new approach to identify sea-level changes in mid-Cretaceous pelagic environments. *Geology*, **24**, 499-502.

Erickson, B.E. and Helz, G.R., 2000. Molybdenum (VI) speciation in sulfidic waters: stability and lability of thiomolybdates. *Geochimica et Cosmochimica Acta*, **64**, 1149–1158.

Farrand, M., 1970. Framboidal sulphides precipitated synthetically. *Mineralium Deposita*, **5**, 237-247.

Fenchel, T.M., and Riedl, R.J., 1970. The sulfide system; a new community underneath the oxidised layer of marine sand bottoms. *Marine Biology*, **7**, 255-268.

Fisher, I. St. J., and Hudson, J.D., 1987. Pyrite formation in Jurassic shales of contrasting biofacies. *Geological Society of London Special Publications*, **26**, 69-78.

Fisher, Q.J., and Wignall, P.B., 2001. Palaeoenvironmental controls on the uranium distribution in an Upper Carboniferous black shale (*Gastrioceras listeri* Marine Band) and associated strata; England. *Chemical Geology*, **175**, 605-621.

Flach, E., Muthumbi, A. and Heip, C., 2002. Meiofauna and macrofauna community structure in relation to sediment composition at the Iberian margin compared to the Goban Spur (NE Atlantic). *Progress in Oceanography*, **52**, 433–457.

Flügel, E., 2004. *Microfacies of Carbonate Rocks: Analysis, Interpretation and Applications*. Springer-Verlag: Berlin, Heidelberg, New York. 976pp.

Francois, R., 1988. A study on the regulation of the concentrations of some trace metals (Rb, Sr, Zn, Pb, Cu, V, Cr, Ni, Mn and Mo) in Saanich Inlet sediments, British Columbia, Canada. *Marine Geology*, **83**, 285-308.

Frey, R.W., 1970. Trace fossils of Fort Hays Limestone Member of Niobara Chalk (Upper Cretaceous), west-central Kansas. *University of Kansas Paleontological Contributions*, **53**, 1-41.

Frey, R.W., and Bromley, R.G., 1985. Ichnology of American chalks; the Selma Group (Upper Cretaceous), western Alabama. *Canadian Journal of Earth Science*, **22**, 801-828.

Frey, R.W., Pemberton, S.G., and Saunders, T.D.A., 1990. Ichnofacies and bathymetry: a passive relationship. *Journal of Paleontology*, **64**, 155-158.

Gale, A.S., Kennedy, W.J., Burnett, J.A., Caron, M. & Marshall, J.D., 1996. The Late Albian to Early Cenomanian succession near Rosans (Drôme, SE France), an integrated study (ammonites, inoceramids, planktonic Foraminifera, nannofossils oxygen and carbon isotopes). *Cretaceous Research*, **17**, 515–606.

Geisler, C-D., and Schmidt, D., 1992. An overview of chromium in the marine environment. *Ocean Dynamics*, **44**, 185-196.

Giraud, F., Olivero, D., Baudin, F., Reboulet, S., Pittet, B. and Proux, O., 2003. Minor changes in surface-water fertility across the oceanic anoxic event 1d (latest Albian, SE France) evidenced by calcareous nannofossils. *International Journal of Earth Sciences*, **92**, 267–284.

Goldhaber, M.B., and Kaplan, I.R., 1974. The sulfur cycle. *In*: Goldberg, E.D. (ed.) *The Sea, Volume 5, Marine Chemistry*, pp. 569-655. J. Wiley and Sons.

Goldring, R., 1995. Organisms and the substrate: response and effect. *In*: Bosence, W.J., and Allison, P.A. (eds.) *Marine Palaeoenvironmental Analysis from Fossils, Geological Society Special Publication*, **83**, 151-180.

Goldschmidt, V.M., 1954. Geochemistry. *In*: Muir, A. (ed.), *The International Series of Monographs on Physics*.

Graham, U.M., and Ohmoto, H., 1994. Experimental study of formation mechanisms of hydrothermal pyrite. *Geochimica et Cosmochimica Acta*, **58**, 2187-2202.

Haese, R.R. 2000. The reactivity of iron. *In*: Schultz, H.D. and Zabel, M. (eds.) *Marine Geochemistry*, Springer-Verlag Berlin Heidelberg, pp. 455

Hallam, A., 1980. Black shales. *Journal of the Geological Society of London*, **137** 123-124.

Hallberg, R.O., 1976. A geochemical method for investigation of palaeoredox conditions in sediments. *Am-bio Special Report*, **4**, 139-147.

Hallberg, R.O., 1982. Diagenetic and environmental effects on heavy-metal distribution in sediments. A hypothesis with an illustration from the Baltic Sea. *In* Fanning, K.A., and Manheim, F.T., (eds.), *The Dynamic Environment of the Ocean Floor*, Lexington Books, Lexington, Massachusetts, 305-316.

Hatch, J.R., and Leventhal, J.S., 1992. Relationship between inferred redox potential of the depositional environment and geochemistry of the Upper Pennsylvanian (Missourian) Stark Shale Member of the Dennis Limestone, Wabaunsee County, Kansas, U.S.A. *Chemical Geology*, **99**, 65-82.

Hay, W.W., DeConto, R. M., Wold, Ch. N., Wilson, K. M., Voigt, S., Schulz, M., Wold-Rosby, A., Dullo, W.-Ch., Ronov, A. B., Balukhovskiy, A. N. and Soeding, E. (1999): An alternative global Cretaceous palaeogeography. *In: Barrera, E.J. and Claudia C. (eds.) The evolution of the Cretaceous Ocean-Climate System, Special Papers of the Geological Society of America*, **332**, 1-47.

Helz, C.R., Miller, C.V., Charnock, J.M., Mosselmans, J.F.W., Patrick, R.A.D., Garner, C.D. and Vaughan, D.J., 1996. Mechanism of molybdenum removal from the sea and its concentration in black shales: EXAF evidence. *Geochimica et Cosmochimica Acta*, **60**, 3631–3642.

Herbert, G.D., and Sarmiento, J.L., 1991. Ocean nutrient distribution and oxygenation: Limits on the formation of warm saline bottom waters over the past 91 m.y. *Geology*, **19**, 702-705.

Herreid, D.F., 1980. Hypoxia in invertebrates. *Comparative Biochemical Physiology*, **67A**, 311-320.

Herrle, J.O., Pross, J., Friedrich, O. and Hemleben, Ch., 2003. Short-term changes in the Cretaceous Tethyan Ocean: micropalaeontological evidence from Early Albian Oceanic Anoxic Event 1b. *Terra Nova*, **15**, 14-19.

Hofmann, P., Ricken, W., Schwark, L., and Leythaeuser, D., 2001. Geochemical signature and related climatic-oceanographic processes for early Albian black shales Site 417D, North Atlantic Ocean. *Cretaceous Research*, **22**, 243–257

Hotinski, R.M., Bice, K.L., Lump, L.R., Najjar, R.G., and Arthur, M.A., 2001. Ocean stagnation and end-Permian anoxia. *Geology*, **29**, 7-10.

Howarth, R.W., 1979. Pyrite: its rapid formation in a salt marsh and its importance in ecosystem metabolism. *Science*, 203, 49-51.

Huerta-Diaz, M.A. and J.W. Morse, 1992, The pyritization of trace metals in anoxic marine sediments. *Geochimica et Cosmochimica Acta*, **56**, 2681-2702.

Jacobs, L., Emerson, S., and Husted, S.S., 1987. Trace metal geochemistry in the Cariaco Trench. *Deep Sea Research*, **34**, 956-981.

Jacobs, D.K., and Lindenberg, D.R., 1998. Oxygen and evolutionary patterns in the sea: Onshore/offshore trends and recent recruitment of deep-sea faunas. *Proceedings of the National Academy of Sciences, USA*, **95**, 9396-9401.

Jenkyns, H.C., Geczy, B., and Marshall, J.D., 1991. Jurassic manganese carbonates of central Europe and the early Toarcian anoxic event. *Journal of Geology*, **99**, 137-149.

Jones, B., and Manning, D.A.C., 1994. Comparison of geochemical indices used for the interpretation of palaeoredox conditions in ancient mudstones. *Chemical Geology*, **111**, 111-129.

Jørgensen, B.B., Böttcher, M.E., Lüschen, H., Neretin, L.N., and Volkov, I.I., 2004. Anaerobic methane oxidation and a deep H₂S sink generate isotopically heavy sulfides in Black Sea sediments. *Geochimica et Cosmochimica Acta*, **68**, 2095–2118.

Kallioski, J., and Cathles, L., 1969. Morphology, mode of formation and diagenetic changes in framboids. *Bulletin of the Geological Society of Finland*, **41**, 133-153.

Kammer, T.W., Brett, C.E., Boardman, R., and Mapes, R.H., 1986. Ecologic stability of the dysaerobic biofacies during the Late Palaeozoic. *Lethaia*, **19**, 109-121.

Kaufman, E.G., 1981. Ecological reappraisal of the German Posidonienschiefer (Toarcian) and the stagnant basin model. *In: Grey, J., Boucot, A.J., and Berry, W. B. N. (eds.) Communities of the Past*, Stroudsbery: Hutchinson Ross, 311-381.

Kauffman E.G., and Sageman, B.B., 1990. Biological sensing of benthic environments in dark shales and related oxygen-restricted facies. *In: Ginsberg, R.N., and Beaudoin, B. (eds.) Cretaceous Resources, Events and Rhythms: Background and Plans for Research* (Proceedings of the 1st Global Sedimentary Geology Progress Meeting), Digne, France, 121-138.

Kenig, F., Hudson, J.D., Sinninghe Damsté, J.S., and Popp, B.N., 2004. Intermittent euxinia: Reconciliation of a Jurassic black shale with its biofacies. *Geology*, **32**, 421-424.

Kennedy, W.J., Gale, A.S., Bown, P.R., Caron, M., Davey, R.J., Grocke, D., and Wray, D.S., 2000. Integrated stratigraphy across the Aptian-Albian boundary in the Marnes Bleues, at the Col de Pré-Guittard, Arnayon (Drôme), and at Tartonne (Alpes-de-Haute-Provence), France: a candidate Global Boundary Stratotype Section and Boundary Point for the base of the Albian Stage. *Cretaceous Research*, **21**, 591-720.

Kimura, H., and Watanabe, Y., 2001. Ocean anoxia at the Precambrian–Cambrian boundary. *Geology*, **29**, 995–998.

Klinkhammer, G.P., and Bender, M.L., 1980. The distribution of manganese in the Pacific Ocean. *Earth and Planetary Science Letters*, **46**, 361-384.

Klinkhammer, G.P., and Palmer, M.R., 1991. Uranium in the oceans: Where it goes and why. *Geochimica et Cosmochimica Acta*, **55**, 1799-1806.

Knight, R.I., 1997. Benthic palaeoecology of the Gault Clay Formation (mid- to basal Upper Albian) of the western Anglo-Paris Basin. *Proceedings of the Geological Association*, **108**, 81-103.

Kochenov, A.V., Korolev, K.G., Dubinchuk, V.T., and Medvedev, Y.L., 1977. Experimental data on the conditions of precipitation of uranium from aqueous solutions. *Geochemistry International*, **14**, 82–87.

Kolonic, S., Sinninghe Damste, J.S., Bottcher, M.E., Kuypers, M.M.M., Kuhnt, W., Beckmann, B., Scheeder, G., and Wagner, T., 2002. Geochemical characterization of Cenomanian/Turonian black shales from the Tarfaya Basin (SW Morocco). *Journal of Petroleum Geology*, **25**, 325-350.

Koutsoukos, E.A.M., Leary, P.N., and Hart, M.B., 1990. Latest Cenomanian-earliest Turonian low-oxygen tolerant benthonic foraminifera: a case study from the Sergipe Basin (N.E. Brazil) and the western Anglo-Paris Basin (southern England). *Palaeogeography, Palaeoclimatology, Palaeoecology*, **77**, 145-177.

Koutsoukos, E.A.M., Mello, M.R., and de Azambuja Filho, N.C., 1991. Micropalaeontological and geochemical evidence of mid-Cretaceous dysoxic-anoxic palaeoenvironments in the Sergipe Basin, northeastern Brazil. In: Tyson, R.V., and Pearson, T.H., (eds.) 1991. *Modern and Ancient Continental Shelf Anoxia*, *Geological Society Special Publication*, **58**, 427-447.

Kribeck, B., 1975. The origin of framboidal pyrite as a surface effect of sulphur grains. *Mineralium Deposita*, **10**, 389-396.

Krumbein, W.C., 1934. Size frequency distribution of sediments. *Journal of Sedimentary Petrology*, **4**, 65-77.

Kuhnt, W., Chellai, EL H., Holbourn, A., Luderer, F., Thurow, J., Wagner, T., El Albani, A., Beckman, B., Herbin, J.P., Kawamura, H., Kolonic, S., Nederbragt, S., Street, C., and Ravilious, K., 2001. Centennial records of Cretaceous paleoceanographic events and sea-level fluctuations in the Moroccan Tarfaya-Layoune basin. *EOS Transactions, American Geophysical Union*, **82**, 32.

Langmuir, D., 1979. Uranium solution-mineral equilibria at low temperatures with applications to sedimentary ore deposits. *Geochimica et Cosmochimica Acta*, **42**, 547–569.

Lash, G.G., and Blood, D.R., 2004. Origin of shale fabric by mechanical compaction of flocculated clay: Evidence from the Upper Devonian Rhinestreet Shale, western New York, U.S.A. *Journal of Sedimentary Research*, **74**, 110-116.

Leckie, R.M., 1990. Mid-Cretaceous planktonic foraminifera of the antarctic margin: Hole 693A, ODP Leg 113. In Barker, P.F., and Kennett, J.P. (eds.), *Proceedings of the Ocean Drilling Program, Scientific Results*, **113**, 319-324.

Leszczynski, S., Uchman, A., and Bromley, R.G., 1996. Trace fossils indicating bottom aeration changes: Folsz Limestone, Oligocene, Outer Carpathians, Poland. *Palaeogeography, Palaeoclimatology, Palaeoecology*, **121**, 79-87.

Leventhal, J.S., 1982. An interpretation of carbon and sulfur relationships in Black Sea Sediments as indicators of environments of deposition. *Geochimica et Cosmochimica Acta*, **47**, 133-137.

Leventhal, J.S., 1981. Pyrolysis gas chromatography-mass spectrometry to characterize organic matter and its relationship to uranium content of Appalachian Devonian black shales. *Geochimica et Cosmochimica Acta*, **45**, 883-889.

Leventhal, J. and Taylor, C. 1990. Comparison of methods to determine degree of pyritization. *Geochimica et Cosmochimica Acta*, **54**, 2621-2625.

Levin, L.A., 2003. Oxygen Minimum Zone benthos: Adaption and community response to hypoxia. *Oceanography and Marine Biology: an Annual Review*, **41**, 1-45.

Levin, L.A., Gage, J.D., Martin, C. and Lamont, P.A., 2000. Macrobenthic community structure within and beneath the oxygen minimum zone, NW Arabian Sea. *Deep-Sea Research II*, **47**, 189–226.

Lewan, M.D., 1984. Factors controlling the proportionality of vanadium to nickel in crude oils. *Geochimica et Cosmochimica Acta*, **48**, 2231-2238.

Lewan, M.D., and Maynard, J.B., 1982. Factors controlling enrichment of vanadium and nickel in the bitumen of organic sedimentary rocks. *Geochimica et Cosmochimica Acta*, **46**, 2547-2560.

Love, L.G., 1957. Microorganisms and the presence of syngenetic pyrite. *Quarterly Journal of the Geological Society, London*, **113** 429-440.

Löwemark, L., Schönfeld, J., Werner, F., and Schäfer, P., 2004. Trace fossils as a paleoceanographic tool: evidence from Late Quaternary sediments of the southwestern Iberian margin. *Marine Geology*, **204**, 27-41.

Luning, S., Kolonic, S., Belhadj, E.M., Belhadj, Z., Cota, L., Baric, G., and Wagner, T., 2004. Integrated depositional model for the Cenomanian-Turonian organic-rich strata in North Africa. *Earth Science Reviews*, **64**, 51-117.

Luning, S., Kolonic, S., Loydell, D., and Craig, J., 2003. Reconstruction of the original organic richness in weathered Silurian shale outcrops (Murzuq and Kufra basins, southern Libya). *Geo-Arabia*, **8**, 299-308.

Lynn, D.C., and Bonatti, E., 1965. Mobility of manganese in diagenesis of deep sea sediments, *Marine Geology*, **3**, 457-474.

Lyons, T.W., 1997. Sulfur isotopic trends and pathways of iron sulphide formation in upper Holocene sediments of the anoxic Black Sea. *Geochimica et Cosmochimica Acta*, **61**, 3367-3382.

Lyons, T.W., and Berner, R.A., 1992. Carbon-sulfur-iron systematics of the uppermost deep-water sediments of the Black Sea. *Chemical Geology*, **99**, 1-27.

MacLeod, K.J., and Irving, A.J., 1996. Correlation of cerium anomalies with indicators of paleoenvironment. *Journal of Sedimentary Research*, **66**, 948-955.

Macquaker, J.S., Curtis, C.D., and Coleman, M.L., 1997. The role of iron in mudstone diagenesis: Comparison of Kimmeridge Clay Formation mudstones from onshore and offshore (UKCS) localities. *Journal of Sedimentary Research*, **67**, 871-878.

Marenco, K.N. and Bottjer, D.J., 2006. Quantifying horizontal bioturbation in lower Cambrian rocks using image analysis. *Geological Society of America Abstracts with Programs*, **38** (7), 475.

McKee, B.A., DeMaster, D.J., and Nittrouer, C.A., 1987. Uranium geochemistry on the Amazon shelf: Evidence for uranium release from bottom sediments. *Geochimica et Cosmochimica Acta*, **51**, 2779-2786.

McKee, E.D. and Weir, G.W., 1953. Terminology for stratification and cross-stratification. *Bulletin of the Geological Society of America*, **64**, 381-390.

Miller, M.F., and Smail, S.E., 1997. A semiquantitative field method for evaluating bioturbation on bedding planes. *Palaios*, **12**, 391-396.

Moodley, L., Van der Zwaan, G.J., Herman, P.M.J., Kempers, A.J., van Breugel, P., 1997. Differential response of benthic meiofauna to anoxia with special reference to Foraminifera (Protista: Sarcodina). *Marine Ecology Progress Series*, **158**, 151-163.

Morford, J.L., and Emerson, S., 1999. The geochemistry of redox sensitive trace metals in sediments. *Geochimica et Cosmochimica Acta*, **63**, 1735-1750.

Morris, K.A., 1979. A classification of Jurassic marine sequence and an example from the Toarcian (Lower Jurassic) of Great Britain. *Palaeogeography, Palaeoclimatology and Palaeoecology*, **26**, 117-126.

Morse, J.W., and Berner, R.A., 1995. What determines sedimentary C/S ratios? *Geochimica et Cosmochimica Acta*, **59**, 1073-1077

Müller, P.J. and Seuss, E., 1979. Productivity, sedimentation rate, and sedimentary

organic matter in the oceans – I. Organic carbon preservation. *Deep-Sea Research*, **26A**, 1347-1362.

Muramoto, J.A., Honsho, S., Fry, B., Hay, B.J., Howarth, R.W., and Cisne, J.L., 1991. Sulfur, iron and organic carbon fluxes in the Black Sea: Sulfur isotopic evidence for the origin of sulphur fluxes. *Deep Sea Research*, **38**, S1151-S1187.

Murray, R. W., Leinen, M., and Isern, A., 1993. Biogenic flux of Al to sediment in the Central Equatorial Pacific Ocean: Evidence for increased productivity during glacial periods. *Paleoceanography*, **6**, 651-669.

Nederbragt, A.J., Fiorentino, A., and Klosowska, B., 2001. Microfossils across the Albian–Cenomanian boundary oceanic anoxic event at DSDP Site 547 (North Atlantic). *Palaeogeography, Palaeoclimatology, Palaeoecology*, **166 (3-4)**, 401-421.

Newton, R.J., 2001. Conflicting data from several indices of water column oxygenation in the early Toarcian (Jurassic) of North Yorkshire, U.K.: Evidence of cyclic anoxia? *Geological Society of America Annual Meeting, Boston, USA, 2001*.

Newton, R., Bottrell, S.H., Dean, S.P., Hatfield, D., and Raiswell, R., 1995. An evaluation of the chromous chloride reduction method for the isotopic analysis of pyrite in rocks and sediments. *Chemical Geology*, **125**, 317-320.

Nzoussi-Mbassani, P., Disnar, J.R., and Laggoun-Défarge, F., 2003. Organic matter characteristics of Cenomanian–Turonian source rocks: implications for petroleum and gas exploration onshore Senegal. *Marine and Petroleum Geology*, **20**, 411-427.

O'Brien, N.R., and Slatt, R.M., 1990. *Argillaceous Rocks Atlas*. Springer-Verlag, New York. 141p.

Ohfuji, H., and Akai, J., 2002. Icosahedral domain structure of framboidal pyrite. *American Mineralogist*, **87**, 176-180.

Orians, K. J., and K. W. Bruland, 1986. The biogeochemistry of aluminum in the Pacific Ocean, *Earth and Planetary Science Letters*, **78**, 397–410.

Oschmann, W., 1991. Anaerobic-poikiloaerobic-aerobic: a new facies zonation for modern and neritic redox facies. *In*: Einsele, G., Ricken, W., and Seilacher, A., (eds.) *Cycles and events in stratigraphy*, Springer-Verlag, Berlin, 565-571.

Osgood, R. G., 1970. Trace fossils of the Cincinnati area. *Palaeontographica Americana* **6**, 193–235.

Owen, H.G., 1971. Middle Albian stratigraphy in the Anglo-Paris Basin. *Bulletin of the British Museum (Natural History) Geology*, **Supplement 8**.

Passier, H.F. Middelburg, J.J., van OS, B.J.H., and de Lange, G.J., 1996. Diagenetic pyritisation under eastern Mediterranean sapropels caused by downward sulphide diffusion. *Geochimica et Cosmochimica Acta*, **60**, 751-763.

Pearson, T.H., and Rosenberg. R., 1978. Macrobenthic succession in relation to organic enrichment and pollution of the marine environment. *Oceanography and Marine Biology: an Annual Review*, **16**, 229-311.

Pederson, T.F. and Calvert, S.E., 1990. Anoxia vs. productivity: What controls the formation of organic-carbon-rich sediments and sedimentary rocks? *American Association of Petroleum Geologists, Bulletin*, **74**, 454-466.

Pemberton, S.G., MacEachern, J.A. and Frey, R.W., 1992. Trace fossil facies models; environmental and allostratigraphic significance. *In*: Walker, R.G., and James, N.P. (eds.), *Facies Models: Response to Sea Level Change*, 47-82.

Pettijohn, F.J., 1975. *Sedimentary Rocks*, 3rd Edition, Harper and Row, New York, 628p.

Philip, R.P., 2005. Formation and geochemistry of oil and gas. *In: Mackenzie, F.T., and Turekian, K.K. (eds.), Sediments, Diagenesis and Sedimentary Rocks, Treatise on Geochemistry, 7*, 223-256.

Picard, M.D., 1971. Classification of fine-grained sedimentary rocks. *Journal of Sedimentary Petrology, 41*, 179-195.

Plant, J. A., Simpson, P. R., Smith, B., Windley, B. F., Watson, J. V., and Plant, J., 1999. Uranium ore deposits; products of the radioactive earth regional geochemistry of uranium as a guide to deposit formation. *Reviews in Mineralogy and Geochemistry, 38*, 255-319.

Powell, W.G., Johnston, P.A., and Collom, C.J., 2003. Geochemical evidence for oxygenated bottom waters during deposition of fossiliferous strata of the Burgess Shale Formation. *Palaeogeography, Palaeoclimatology, Palaeoecology, 201*, 249-268.

Raiswell, R., 1982. Pyrite texture, isotopic composition and the availability of iron. *American Journal of Science, 282*, 1244-1263.

Raiswell, R., and Berner, R. A., 1986. Pyrite and organic matter in Phanerozoic normal marine shales. *Geochimica et Cosmochimica Acta, 50*, 1967-1976.

Raiswell, R., and Berner, R.A., 1985. Pyrite formation in euxinic and semi-euxinic sediments. *American Journal of Science, 285*, 710-724.

Raiswell, R., Buckley, F., Berner, R.A., and Anderson, T.F., 1987. Degree of pyritization of iron as a paleoenvironmental indicator of bottom-water oxygenation. *Journal of Sedimentary Petrology, 58*, 812-819.

Raiswell, R., Canfield, D.E., and Berner, R.A., 1994. A comparison of iron extraction methods for the determining of degree of pyritization and the recognition of iron-limited pyrite formation. *Chemical Geology, 111*, 101-111.

Raiswell, R., and Canfield, D.E., 1998. Sources of iron for pyrite formation in modern sediments. *American Journal of Science*, **298**, 219-245.

Raiswell, R., and Canfield, D.E., 1996. Rates of reaction between silicate iron and dissolved sulfide in Peru Margin sediments. *Geochimica et Cosmochimica Acta*, **60**, 2777-2787.

Raiswell, R., Newton, R. and Wignall, P.B., 2001. A water column anoxicity indicator: resolution of biofacies variations in the Kimmeridge Clay (Upper Jurassic, UK). *Journal of Sedimentary Research* **71A**, pp. 286–294

Randolf, A.D., and Larson, M.A., 1988. *Theory of Particulate Processes*. Academic Press.

Reichelt, K. 2005. Late Aptian-Albian of the Vocontian Basin (SE France) and Albian of NE Texas: biostratigraphic and paleoceanographic implications by planktic Foraminifera fauna. PhD thesis, Eberhard Karls Universität Tübingen.

Reineck, H. E, 1963. Sedimentgeffige im Bereich der südlichen Nordsee. *Abhandlungen der senckenbergische natur/orschende Gesellschaft*, **505**, 1-138.

Reineck, H.E., Gutmann, W.F., and Hertweck, G., 1967. Das Schlickgebiet südlich Helgoland als Beispiel rezenter Schelfablagerungen, *Senckenbergiana Maritima*, **3**, 185–201.

Rhoads, D.C., and Boyer, L.F., 1982. The effects of marine benthos on physical properties of sediments; a successional perspective. *In: McCall, P.L., and Tevesz, M.J.S. (eds.), Animal-Sediment Relations. The Biogenic Alteration of Sediments. Topics in Geobiology*, **2**, 3-52.

Rhoads, D.C., and Morse, J.M., 1971. Evolutionary and ecologic significance of oxygen-deficient marine basins. *Lethia*, **4**, 413-428.

Rhoads, D.C., Mulslow, S.G., Gutschik, R., Baldwin, C.T., and Stolz, J.F., 1991. The dysaerobic zone revisited: a magnetic facies? *In: Tyson, R.V. and Pearson, T.H. (eds.) Modern and ancient continental shelf anoxia, Geological Society Special Publication, 58*, 187-199.

Rickard, D.T., 1970. The origin of framboids. *Lithos, 3*, 269-293.

Rimmer, S.M., 2004. Geochemical paleoredox indicators in Devonian–Mississippian black shales, Central Appalachian Basin (USA). *Chemical Geology, 206*, 373-391.

Ross, D.A., and Degens, E.T., 1974. Recent sediments of the Black Sea. *In: Degens, E.T., and Ross, D.A. (eds.) Black Sea Geology, Chemistry and Biology ed.). American Association of Petroleum Geologists Memo, 20*, 183-199.

Roychoudhury, A.N.M., Kostka, J.E., Van Cappellen, P., 2003. Pyritization: a palaeoenvironmental and redox proxy reevaluated. *Estuarine, Coastal and Shelf Science, 57*, 1-11.

Rubio, B., Rey, D., Cham, P., Mohamed, K., and Vilas, F., 2006. Solid-phase chemical fractionation of selected trace metals in some Galician continental margin sediments. *Geophysical Research Abstracts, 8*, 06094.

Sageman, B.B., 1989. The benthic boundary biofacies model: Hartland Shale Member, Greenhorn Formation (Cenomanian), Western Interior, North America. *Palaeogeography, Palaeoclimatology, Palaeoecology, 74*, 87-110.

Sageman, B.B., and Bina, C.R., 1997. Diversity and species abundance patterns in Late Cenomanian black shale biofacies, Western Interior, U.S., *Palaios, 12*, 449-466.

Sageman, B.B., Wignall, P.B., and Kauffman, E.G., 1991. Biofacies models for organic-rich facies: tool for paleoenvironmental analysis. *In: Einsele, G., Ricken, W., and Seilacher, A., (eds.), Cycles and Events in Stratigraphy, Springer-Verlag, Berlin, 542-564.*

Sanders, H.L., 1986. Marine benthic diversity: a comparative study. *American Naturalist*, **102**, 243-282.

Savdra, C.E., and Bottjer, D.J., 1991. Oxygen-related biofacies in marine strata: an overview and update. *Geological Society Special Publication*, **58**, 201-220.

Savrda, C.S., and Bottjer, D.J., 1989. Trace-fossil model for reconstructing oxygenation histories of ancient marine bottom waters: application to Upper Cretaceous Niobrara Formation, Colorado. *Palaeogeography, Palaeoclimatology, Palaeoecology*, **74**, 49-74.

Savdra, C.E., and Bottjer, D.J., 1987. The exaerobic zone, a new oxygen-deficient marine biofacies. *Nature*, **327**, 54-56.

Savrda, C.S., and Bottjer, D.J., 1986. Trace-fossil model for reconstruction of paleooxygenation in bottom waters. *Geology*, **14**, 3-6.

Savdra, C.E., Bottjer, D.J., and Gorsline, D.S., 1984. Development of a comprehensive oxygen-deficient marine biofacies model: evidence from Santa Monica, San Pedro, and Santa Barbara Basins, California, Continental Borderland. *AAPG Bulletin*, **68**, 1179-1192.

Savdra, C.E., Bottjer, D.J., and Seilacher, A., 1991. Redox-related benthic events. In: Einsele, G., Ricken, W., and Seilacher, A., (eds.), *Cycles and Events in Stratigraphy*, Springer-Verlag, Berlin, 524-541.

Schlanger, S.O. and Jenkyns, H.C., 1976. Cretaceous oceanic anoxic events: Causes and consequences. *Geologie en Mijnbouw*, **55**, 179-184.

Schoonen, M.A.A, and Barnes, H.L., 1991. Reactions forming pyrite and marcasite from solution, I. Nucleation of FeS₂ below 100°C. *Geochimica et Cosmochimica Acta*, **55**, 1495-1504.

Schovsbo, N.H., 2001. Why barren intervals? A taphonomic case study of the Scandinavian Alum Shale and its faunas. *Lethaia*, **34**, 271-285.

Schultz, R.B., 2004. Geochemical relationships of Late Paleozoic carbon-rich shales of the Midcontinent, USA: a compendium of results advocating changeable geochemical conditions. *Chemical Geology*, **206**, 347-372.

Seilacher, A., 1967. Bathymetry of trace fossils. *Marine Geology*, **5**, 413-420.

Seilacher, A., 1964. Biogenic sedimentary structures. *In*: Imbrie, I., and Newell, N. (eds.) *Approaches to paleoecology*, Wiley, New York, 296-316.

Seilacher, A., 1958. Zur ökologischen Charakterisierung von Flysch und Molasse. *Eclogae Geologicae Helvetiae*, **51**, 1062-1078.

Seilacher, A., 1953. Studien zur Palichnologie. II. Die fossilen Ruhespuren (Cubichnia). *Neues Jahrbuch für Geologie und Paläontologie*, **98**, 87-124.

Seilacher, A., and Westphal, F., 1971. Fossil-Lägerstätten. *In*: Müller, G., (ed.), *Sedimentology of Parts of Central Europe*. W. Kramer, Frankfurt am Main, 327-335

Smith, C.R., Levin, L.A., Hoover, D.J., McMurtry, G. and Gage, J.D., 2000. Variations in bioturbation across the oxygen minimum zone, NW Arabian Sea. *Deep-Sea Research II*, **47**, 227-258.

Spears, D.A., 1980. Towards a classification of shales. *Journal of the Geological Society of London*, **137**, 125-129.

Speyer, S.E. and Brett, C.E., 1988. Taphofacies models for epeiric sea environments: Middle Palaeozoic examples. *Palaeogeography, Palaeoclimatology, Palaeoecology*, **63**, 225-262.

Stachowitsch, M., 1991. Anoxia in the northern Adriatic Sea: rapid death, slow recovery. *Geological Society Special Publication*, **58**, 119-129.

Stow, D. V. A., 1987. South Atlantic organic-rich sediments: facies, processes and environments of deposition, *In: Brooks, J., and Fleet, A.J. (eds.), Marine Petroleum Source Rocks, Geological Society Special Publication, 26*, 287–299.

Suits, N.S., and Wilkin, R.T., 1998. Pyrite formation in the water column and sediments of a meromictic lake, *Geology, 26*, 1099–1102.

Sunagawa, I., Endo, Y., and Nakai, N., 1971. Hydrothermal synthesis of framboidal pyrite. *Society of Mineralogy and Geology of Japan (Special Issue), 2*, 10-14.

Sweeney, R.E., and Kaplan, I.R., 1973. Pyrite framboid formation: laboratory synthesis and marine sediments. *Economic Geology, 68*, 618-634.

Tankere-Muller, S., Zhang, H., Davison, W., Finke, N., Larsen, O., Stahl, H., and Glud, R.N., 2006. Fine scale remobilization of Fe, Mn, Co, Ni, Cu and Cd in contaminated marine sediment. *Marine Chemistry, 108*, 192-207.

Taylor, G.R., 1982. A mechanism for framboid formation as illustrated by a volcanic exhalative sediment. *Mineral. Deposita, 17*, 23-36.

Taylor, A.M., and Goldring, R., 1993. Description and analysis of bioturbation and ichnofabric. *Journal of the Geological Society, 150*, 141-148.

Taylor, S.R., and McLennan, S.M., 1985. The continental crust; its composition and evolution. *Oxford, U.K., Blackwell Scientific Publications, 312p.*

Telnaes, N., Cooper, B.S., and Jones, B., 1991. Kerogen facies, biomarkers, trace metal contents, and spectral logs as indicators of oxicity and salinity, Upper Jurassic North Sea. *In: Manning, D.A.C. (ed.) Organic Geochemistry, Advances and Applications in Energy and the Natural Environment, Manchester University Press, Manchester, 391-393.*

Thompson, J.B., Mullins, T.H., Newton, C.R., and Vercoutere, T.L., 1985. Alternative biofacies model for dysaerobic communities. *Lethaia, 18*, 167-179.

Tribovillard, N., Riboulleau, A., Lyons, T., and Baudin, F., 2004. Enhanced trapping of molybdenum by sulfurized marine organic matter of marine origin in Mesozoic limestones and shales. *Chemical Geology*, **213**, 385-401.

Turekian, K. K., and Wedepohl, K.H., 1961. Distribution of the elements in some major units of the Earth's crust. *Geological Society of America Bulletin*, **72**, 175-191.

Turgeon, S., and Brumsack, H.J., 2006. Anoxic vs dysoxic events reflected in sediment geochemistry during the Cenomanian-Turonian Boundary Event (Cretaceous) in the Umbria-Marche Basin of central Italy. *Chemical Geology*, **234**, 321–339.

Turgeon, S.C., and Creaser, R.A., 2008. Cretaceous oceanic anoxic event 2 triggered by a massive magmatic episode. *Nature*, **454**, 323-326.

Tyson, R.V., 1995. *Sedimentary Organic Matter*. Chapman and Hall, London, 615 pp.

Tyson, R. V., 1987. The genesis and palynofacies characteristics of marine petroleum source rocks. In: Brooks, J. and Fleet, A. J. (eds) *Marine Petroleum Source Rocks, Geological Society Special Publication*, **26**, 47–67.

Tyson, R.V. and Pearson, T.H., 1991. Modern and ancient continental shelf anoxia: an overview. In: Tyson, R.V. and Pearson, T.H. (eds.) *Modern and ancient continental shelf anoxia, Geological Society Special Publication*, **58**, 1-26.

Udden J.A., 1914. Mechanical composition of clastic sediments. *Bulletin of the Geological Society of America*, **25**, 655-744.

van der Weijden, C.H., 2002. Pitfalls of normalization of marine geochemical data using a common divisor. *Marine Geology*, **184**, 167–187.

Van der Zwaan, G.J., Duijnste, I.A.P., den Dulk, M., Ernst, S.R., Jannink, N.T., and Kouwenhoven, T.J., 1999. Benthic foraminifers: proxies or problems? A review of paleocological concepts. *Earth-Science Reviews*, **46**, 213-236.

Vine, J.D., and Tourtelot, E.B., 1970. Geochemistry of black shale deposits - a summary report. *Economic Geology*, **65**, 253-272.

Wanty, R.B., and Goldhaber, M.B., 1992. Thermodynamics and kinetics of reactions involving vanadium in natural systems: Accumulation of vanadium in sedimentary rocks. *Geochimica et Cosmochimica Acta*, **56**, 1471-1483.

Wedepohl, K.H., 1971. Environmental influences on the chemical composition of shales and clays. In Ahrens, L.H., Press, F., Runcorn, S.K., and Urey, H.C. (eds.), *Physics and Chemistry of the Earth*: Oxford (Pergamon), 307-331.

Wehrli, B., and Stumm, W., 1989. Vanadyl in natural waters: Adsorption and hydrolysis promote oxygenation. *Geochimica et Cosmochimica Acta*, **53**, 69-77.

Wentworth, C.K., 1922. A scale of grade and class terms for clastic sediments. *Journal of Geology*, **30**, 377-392 .

Westgate, L.M., and Anderson, T.F., 1982. Extraction of various forms of sulfur from coal and shale for stable sulfur isotope analysis. *Analytical Chemistry*, **54**, 2136-2139.

Wetzel, A., 1991. Ecologic interpretation of deep-sea trace fossil communities. *Palaeogeography, Palaeoclimatology, Palaeoecology*, **85**, 47-69.

Whatley, R.C., Pyne, R.S., and Wilkinson, I.P., 2003. Ostracoda and palaeo-oxygen levels, with particular reference to the Upper Cretaceous of East Anglia. *Palaeogeography, Palaeoclimatology, Palaeoecology*, **194**, 355-386.

Wheatcroft, R.A., 1989. Comment. In: Comment and Reply on "characteristic trace-fossil associations in oxygen-poor sedimentary environments", *Geology*, **17**, 674.

White, W.A., 1961. Colloid phenomena in the sedimentation of argillaceous rocks. *Journal of Sedimentary Petrology*, **31**, 560-570.

Wignall, P.B., 1994. *Black Shales*, Oxford University Press, Oxford. 127p.

Wignall, P.B., and Hallam, A., 1992. Anoxia as a cause of the Permian/Triassic extinction: facies evidence from northern Italy and the western United States, *Palaeogeography Palaeoclimatology Palaeoecology*, **93**, 21-46.

Wignall, P.B., and Hallam, A., 1991. Biofacies, stratigraphic distribution and depositional models of British onshore Jurassic black shales. *In*: Tyson, R.V. and Pearson, T.H. (eds.) Modern and ancient continental shelf anoxia, *Geological Society Special Publication*, **58**, 291-310.

Wignall, P.B., Kozur, H., and Hallam, A., 1996 On the timing of palaeoenvironmental changes at the Permo-Triassic (P/Tr) boundary using conodont biostratigraphy. *Historical Biology*, **12**, 39-62.

Wignall, P.B., and Myers, K.J., 1988. Interpreting benthic oxygen levels in mudrocks: a new approach. *Geology*, **16**, 452-455.

Wignall, P.B., and Newton, R., 2003. Contrasting deep-water record for the Upper Permian and Lower Triassic of South Tibet and British Columbia: Evidence for a diachronous mass extinction. *Palaios*, **18**, 153-167.

Wignall, P.B. and Newton, R., 2001. Black shales on the basin margin: a model based on examples from the Upper Jurassic of the Boulonnais, northern France. *Sedimentary Geology*, **144**, 335-356.

Wignall, P.B., and Newton, R., 1998. Pyrite framboid diameter as a measure of oxygen deficiency in ancient mudrocks. *American Journal of Science*, **298**, 537-552.

- Wignall, P.B., Newton, R., and Brookfield, M.E., 2005. Pyrite framboid evidence for oxygen-poor deposition during the Permian-Triassic crisis in Kashmir. *Palaeogeography, Palaeoclimatology, Palaeoecology*, **216**, 183-188.
- Wilde, P., Quniby-Hunt, M.S., and Erdmann, B-D., 1996. The whole-rock cerium anomaly: a potential indicator of eustatic sea-level changes in shales of the anoxic facies. *Sedimentary Geology*, **101**, 43-53.
- Wilkin, R.T., Arthur, M.A., and Dean, W.E., 1997. History of water-column anoxia in the Black Sea indicated by pyrite framboid size distributions. *Earth and Planetary Science Letters*, **148**, 517-525.
- Wilkin, R.T., and Barnes, H.L., 1997. Formation processes of framboidal pyrite. *Geochimica et Cosmochimica Acta*, **61**, 323-339.
- Wilkin, R.T., and Barnes, H.L., 1996. Pyrite formation by reactions of iron monosulfides with dissolved inorganic and organic sulfur species. *Geochimica et Cosmochimica Acta*, **21**, 4167-4179.
- Wilkin, R.T., Barnes, H.L., and Brantley, S.L., 1996. The size distribution of framboidal pyrite in modern sediments: An indicator of redox conditions. *Geochimica et Cosmochimica Acta*, **20**, 3897-3912.
- Wilson, P.A., and Norris, R.D., 2001. Warm tropical ocean surface and global anoxia during the mid-Cretaceous period. *Nature*, **412**, 425-429.
- Wright, J., Schrader, H. and Holser, W.T., 1987. Paleoredox variations in ancient oceans recorded by rare earth elements in fossil apatite. *Geochimica et Cosmochimica Acta*, **51**, 631-644.
- Zeuthen, E., 1953. Oxygen uptake as related to body size in organisms. *Quarterly Review of Biology*, **28**, 1-12.

APPENDIX A: SEDIMENTARY PROXIES DATA

Table A.1: Niveau Pacquier Pyrite Framboid Diameter Data (the dark shading represents black shale samples)

Sample location (m)	-1	-0.8	-0.6	-0.4	-0.2	0	0.2	0.4	0.6	0.8
Average Framboid Diameter (μm)	19.0	9.1	9.3	5.8	5.0	8.6	4.9	4.9	3.8	4.9
Maximum Framboid Diameter (μm)	35.6	30.4	40.4	16.8	9.0	19.8	10.6	16.3	8.7	13.0
Minimum Framboid Diameter (μm)	3.4	3.5	2.9	0.8	2.5	1.8	1.8	1.7	1.5	2.0
Standard deviation	8.3	5.9	5.8	3.0	1.4	4.3	1.8	2.6	1.5	2.0
Skewness	0.15	2.3	3.3	1.3	1.0	0.67	1.2	2.9	0.99	1.9
No of framboids $>7\mu\text{m}$	45	29	29	11	5	31	5	3	2	5
Number of framboids 7-25 μm	32	25	29	10	4	31	5	3	2	5
% of framboids $<7\mu\text{m}$	10	42	42	78	90	38	90	94	96	90
% of framboids 7-25 μm	64	50	58	20	8	62	10	6	4	10
% of framboids $>25\mu\text{m}$	26	8	0	2	2	0	0	0	0	0

Sample location (m)	1	1.2	1.4	1.6	1.8	2	2.2	2.4
Average Framboid Diameter (μm)	4.0	4.9	4.8	6.6	7.0	8.2	6.1	4.5
Maximum Framboid Diameter (μm)	7.5	14.1	14.8	58.5	12.7	21.7	25.2	17.6
Minimum Framboid Diameter (μm)	1.9	2.3	1.6	1.8	2.8	2.7	2.0	1.6
Standard deviation	1.5	2.2	2.2	8.6	2.6	3.3	3.3	2.4
Skewness	0.73	2.3	2.1	4.9	0.38	1.4	4.0	3.3
No of framboids $>7\mu\text{m}$	2	5	4	8	25	32	10	4
Number of framboids 7-25 μm	2	5	3	7	23	31	9	4
% of framboids $<7\mu\text{m}$	96	90	92	84	50	36	80	92
% of framboids 7-25 μm	4	10	6	14	46	62	18	8
% of framboids $>25\mu\text{m}$	0	0	2	2	4	2	2	0

Table A.2: Breistroffer Pyrite Framboid Diameter Data (the dark shading represents black shale samples)

Sample location (m)	-4.6	-4.3	-2.5	0.2	0.7	0.8	3	5.6
Average Framboid Diameter (μm)	5.6	8.0	8.5	7.4	8.2	5.0	10.1	6.9
Maximum Framboid Diameter (μm)	13.0	28.4	25.8	20.3	18.5	11.2	59.8	20.7
Minimum Framboid Diameter (μm)	1.5	3.1	2.0	3.0	2.2	1.4	2.6	2.5
Standard deviation	2.2	4.3	5.0	4.1	3.2	2.5	8.0	3.3
Skewness	1.0	2.4	1.3	1.3	0.76	0.6	5.1	2.2
No of framboids $>7\mu\text{m}$	10	25	29	19	31	8	36	19
Number of framboids 7-25 μm	10	24	28	19	31	8	35	19
% of framboids $<7\mu\text{m}$	80	50	42	62	38	84	28	62
% of framboids 7-25 μm	20	48	56	38	62	16	70	38
% of framboids $>25\mu\text{m}$	0	2	2	0	0	0	2	0

Table A.3: Folkestone Gault Clay Pyrite Framboid Diameter Data

Sample location (m)	-0.9	-0.7	-0.5	-0.3	-0.1	0.15	0.35	0.55	0.75	0.95	1.15
Average Framboid Diameter (μm)	8.2	5.4	13.9	8.4	9.4	9.4	5.7	8.1	7.1	7.5	16.5
Maximum Framboid Diameter (μm)	19.9	14.9	78.5	33.1	28.8	45.1	12.5	16.3	27.1	18.6	54.8
Minimum Framboid Diameter (μm)	3.0	2.2	1.7	1.8	3.1	2.3	2.2	2.2	3.0	3.2	2.5
Standard deviation	4.4	2.1	18.0	7.2	6.2	7.9	2.3	3.1	4.1	3.1	14.8
Skewness	1.2	2.1	2.4	2.1	1.4	2.6	0.63	0.29	2.8	1.8	1.2
No of framboids $>7\mu\text{m}$	24	7	17	14	21	22	13	27	17	24	15
Number of framboids 7-25 μm	0	0	7	2	2	2	0	0	1	0	13
% of framboids $<7\mu\text{m}$	52	86	52	68	54	52	74	46	64	52	44
% of framboids 7-25 μm	48	14	34	28	42	44	26	54	34	48	30
% of framboids $>25\mu\text{m}$	0	0	14	4	4	4	0	0	2	0	26

Table A.4: Amma Fatma Pyrite Framboid Diameter Data

Sample location (m)	0.2	0.7	1.3	1.55	1.75	1.95	2.2	2.4	2.6	2.95
Average Framboid Diameter (μm)	4.9	5.0	6.7	4.9	5.0	9.6	6.3	5.6	5.7	4.4
Maximum Framboid Diameter (μm)	10.9	9.4	18.7	11.1	14.1	20.5	12.6	18.3	13.2	9.9
Minimum Framboid Diameter (μm)	1.6	2.0	1.8	0.9	1.2	2.2	2.4	1.2	1.4	1.7
Standard deviation	2.1	2.1	3.5	2.7	2.5	4.8	2.7	3.3	2.7	1.5
Skewness	0.8	0.7	1.1	0.8	1.7	0.4	0.7	1.5	0.9	1.1
No of framboids $>7\mu\text{m}$	7	11	20	11	5	36	17	14	14	2
Number of framboids 7-25 μm	7	11	20	11	5	36	17	14	14	2
% of framboids $<7\mu\text{m}$	86	78	60	78	90	28	66	72	72	96
% of framboids 7-25 μm	14	22	40	22	10	72	34	28	28	4
% of framboids $>25\mu\text{m}$	0	0	0	0	0	0	0	0	0	0

Sample location (m)	3.4	3.5	3.65	3.9	4.15	4.5
Average Framboid Diameter (μm)	5.5	6.4	5.2	6.1	6.4	5.2
Maximum Framboid Diameter (μm)	19.8	10.9	17.1	25	16.7	11.7
Minimum Framboid Diameter (μm)	1.4	2.6	1.6	1.0	1.0	1.2
Standard deviation	3.1	2.1	2.9	5.5	3.4	2.2
Skewness	2.3	0.29	2.1	2.0	0.94	0.53
No of framboids $>7\mu\text{m}$	11	16	6	13	19	11
Number of framboids 7-25 μm	11	16	6	12	19	11
% of framboids $<7\mu\text{m}$	78	68	88	74	62	78
% of framboids 7-25 μm	22	32	12	24	38	22
% of framboids $>25\mu\text{m}$	0	0	0	2	0	0

APPENDIX B: PALAEOLOGICAL DATA

Table B.1a: The Niveau Pacquier Section Niveau Pacquier Macrofossils

Oxford University Museum of Natural History specimens were collected from 1.3 m above the base of the main Niveau Pacquier black shale horizon at Col de Palluel, in the Vocontian Basin, south east France. Samples were collected by Professor A.S. Gale and all identifications were carried out by the Oxford University Museum of Natural History staff. Further details may be found in the Museum Database (<http://www.oum.ox.ac.uk/collect/geology2.htm>).

Specimen species	Taxonomic Group	Species reference	Number of specimens	Sample references
<i>Beudanticeras convergens</i>	Ammonoidea	Jacob, 1907	21	KZ.21738 - KZ.21752, KZ.21872 KZ.21877, KZ.21956
<i>Coleoid</i>	Coleoidea		1	KZ.21871 a,b
<i>Hypacanthoplites milletioides</i>	Ammonoidea	Casey, 1961a	5	KZ.21753 - KZ.21756, KZ.21878 a,b
<i>Hypacanthoplites sp.</i>	Ammonoidea		4	KZ.21787- 21790, KZ.21903
<i>Hypacanthoplites trivialis</i>	Ammonoidea	Briestroffer, 1947	52	KZ.21757 a,b - KZ.21786, KZ.21879 - K.Z. 21902
<i>Leymeriella (Leymeriella) tardefurcata</i>	Ammonoidea	d'Orbigny, 1841	84	KZ.21791 - KZ.21830 KZ.21904 - KZ.21949
<i>Leymeriella spp.</i>	Ammonoidea		31	KZ.21832- 21834, KZ.21836- KZ.21853 KZ.21950- KZ.21951 KZ.21953- KZ.21954 KZ.21957- KZ.21963
<i>Mathoceras? sp.</i>	Ammonoidea		1	KZ.21855

<i>Oxtropidoceras (Mirapelia) advena</i>	Ammonoidea	Kennedy <i>et al.</i> , 2000	2	KZ.21964, KZ.21965
<i>Paracheloniceras rerati</i>	Ammonoidea	Collignon, 1965	1	KZ.21955
<i>Prolyelliceras' flandrini</i>	Ammonoidea	Dubourdiou, 1953	2	KZ.21831, KZ.21854
<i>Ptychoceras laeve hamaimense</i>	Ammonoidea	Pervinquiere, 1907	8	KZ.21856-21861, KZ.21966, KZ.21967
<i>Puzosia (Puzosia) quentstedti</i>	Ammonoidea	Parona and Bonarelli, 1897	12	KZ.21835, KZ.21862 KZ.21863 – KZ.21866 KZ.21968-a,b,- KZ.21973
<i>Rossalites sp. nov.</i>	Ammonoidea		4	KZ.21867, KZ.21974-KZ.21976
<i>Rossalites vocontianum</i>	Ammonoidea	Kennedy <i>et al.</i> , 2000	1	KZ.21868, KZ.21952
<i>Silesitoides sp. nov</i>	Ammonoidea		1	KZ.21869-21870, KZ.21977

Table B.1b: The Niveau Pacquier Section Marnes Bleues Macrofossils

Oxford University Museum of Natural History specimens were collected from 15 m below the base of the main Niveau Pacquier black shale horizon at Le Pillart, Tartonne, Alpes-de-Haute, Vocontian Basin, south east France. Samples were collected by Professor W.S. Kennedy and all identifications were carried out by Oxford University Museum of Natural History staff. Further details may be found in the Museum Database (<http://www.oum.ox.ac.uk/collect/geology2.htm>).

Specimen species	Taxonomic Group	Species reference	Number of specimens	Sample references
Belemnites		Coleoidea	7	KZ.21188-21191, KZ.21226-21228
Gastropod		Gastropoda	3	KZ.21182, KZ.21192-KZ.21193

<i>Hypacanthoplites</i> <i>sp.</i>		Ammonoidea	6	KZ.21183- 21186 KZ. 21196 - KZ. 21197
<i>Hypacanthoplites</i> <i>trivialis</i>	Briestroffer, 1947	Ammonoidea	2	KZ. 21194 – KZ.21195
<i>Melchiorites</i> <i>sp.</i>		Ammonoidea	5	KZ. 21201 - KZ.21205
<i>Partichiceras</i> <i>baborense</i>	Coquand, 1880	Ammonoidea	6	KZ.21206- KZ.21211
<i>Phylloceras</i> (<i>Hypophylloceras</i>) <i>sp.</i>		Ammonoidea		KZ.21212- 21213
<i>Phyllopachyceras</i> <i>baborense</i>	Coquand, 1880	Ammonoidea	4	KZ.21214 - KZ.21217
<i>Ptychoceras laeve</i> <i>hamaimense</i>	Pervinquiere, 1907	Ammonoidea	1	KZ.21218
<i>Ptychoceras</i> <i>sp.</i>		Ammonoidea	2	KZ.21219- 21220
<i>Puzosia</i> (<i>Puzosia</i>) <i>sp.</i>		Ammonoidea	4	KZ.21221 - KZ.21224
<i>Phyllopachyceras</i> <i>baborense</i>	Coquand, 1880	Ammonoidea	1	KZ.21187
<i>Tetragonites</i> <i>sp.</i>		Ammonoidea	1	KZ.21225

Table B.2a: The Briestroffer Section Briestroffer Layer Macrofossils

Oxford University Museum of Natural History specimens were collected from the fourth Briestroffer level in the Marnes Bleues, Mt Risou (the 119 m level of Gale *et al.*, 1996). Samples were collected by Professor A.S. Gale and all identifications were carried out by Oxford University Museum of Natural History staff. Further details may be found at <http://www.oum.ox.ac.uk/collect/geology2.htm>.

Specimen species	Species reference	Taxonomic Group	Number of specimens	Sample references
<i>Anisoceras pseudoelegans</i>	Pictet and Campiche, 1861	Ammonoidea	1	KZ.24653a and b
<i>Cantabrigites cantabrigense</i>	Spath, 1933	Ammonoidea	1	KZ.24654
<i>Discohoplites</i> <i>sp.</i>		Ammonoidea	1	KZ.24658
<i>Discohoplites</i>	Semenov,	Ammonoidea	4	KZ.24655-

<i>subfalcatius</i>	1899			KZ.24657, KZ.24676/2
<i>Hamites renzi</i>	Kennedy 1996	Ammonoidea	1	KZ.24659
<i>Hamites sp.</i>		Ammonoidea	2	KZ.24663, KZ.24677/3
<i>Hamites subvirgulatus</i>	Spath 1941	Ammonoidea	4	KZ.24673/2, KZ.24660- 24662
<i>Lechites gaudini</i>	Pictet and Campiche, 1861	Ammonoidea	6	KZ.24664, KZ.24673/1, KZ.24674/1, KZ.24675/1, KZ.24676/1, KZ.24677/2
<i>Mortoniceras (Durnovarites) perinflatum</i>	Spath 1922	Ammonoidea	1	KZ.24665
<i>Mortoniceras (Durnovarites) sp.</i>		Ammonoidea	3	KZ.24670, KZ.24674/2, KZ.24675/2
<i>Mortoniceras (Durnovarites) subquadratum</i>	Spath 1933	Ammonoidea	4	KZ.24666- 24669
<i>Puzosia ap.</i>		Ammonoidea	1	KZ.24676/3
<i>Scaphites (Scapites) bassei</i>	Collignon, 1929	Ammonoidea	1	KZ.24677/1
<i>Stoliczkaia (Stoliczkaia) dispar</i>	d'Orbigny 1841	Ammonoidea	2	KZ.24671 - KZ.24672
<i>Stoliczkaia? sp.</i>		Ammonoidea	1	KZ.24677/4

Table B.2b: The Briestroffer Section Marnes Bleues Macrofossils

Oxford University Museum of Natural History specimens were collected from 17 m above the fourth Briestroffer level in the Marnes Bleues, Mt Risou (the 102.8 m level of Gale *et al.*, 1996). Samples were collected by Professor A.S. Gale and all identifications were carried out by Oxford University Museum of Natural History staff. Further details can be found at <http://www.oum.ox.ac.uk/collect/geology2.htm>.

Specimen species	Species reference	Taxonomic Group	Number of specimens	Sample references
<i>Anisoceras permatum</i>	Pictet and Campiche, 1861	Ammonoidea	1	KZ.24679
<i>Anisoceras</i> sp.		Ammonoidea	1	KZ.24680
<i>Desmoceras (Desmoceras) latidorsatum</i>	Michelin, 1838	Ammonoidea	1	KZ.24681
<i>Hamites duplicatus</i>	Pictet and Campiche, 1847	Ammonoidea	1	KZ.24682
<i>Hamites funatus</i>	Brongniart, 1822	Ammonoidea	1	KZ.24683
<i>Hamites</i> sp.		Ammonoidea	1	KZ.24686
<i>Hamites subvirgulatus</i>	Spath, 1941	Ammonoidea	3	KZ.24685, KZ.24723/2, KZ.24726/3
<i>Hamites virgulatus</i>	Brongniart, 1822	Ammonoidea	1	KZ.24684
<i>Hyphoplites campichei</i>	Spath, 1925	Ammonoidea	3	KZ.24687- 24689
<i>Hyphoplites pylorus</i>	Wright and Wright, 1949	Ammonoidea	2	KZ.24690a,b
<i>Hyphoplites</i> sp.		Ammonoidea	1	KZ.24691
<i>Lechites gaudini</i>	Pictet and Campiche, 1861	Ammonoidea	10	KZ.24692a, b, KZ.24693a, b, KZ.24694- 24697, KZ.24721/1, KZ.24724/2
<i>Lechites</i> sp.		Ammonoidea	1	KZ.24722/2

<i>Leptoplites falcooides</i>	Spath, 1928	Ammonoidea	1	KZ.24725/2
<i>Leptoplites</i> sp.		Ammonoidea	1	KZ.24698
<i>Mariella (Mariella) cf. miliaris</i>	Pictet and Campiche, 1861	Ammonoidea	1	KZ.24722/1
<i>Mariella</i> sp.		Ammonoidea	1	KZ.24699
<i>Mortoniceras (Durnovarites) subquadratum</i>	Spath, 1933	Ammonoidea	2	KZ.24700-24701
<i>Ostlingoceras puzosianum</i>	d'Orbigny, 1842	Ammonoidea	14	KZ.24702-24712, KZ.24713, KZ.24723/1, KZ.24724/1, KZ.24726/1
<i>Phylloceras (Hypophylloceras) seresitense</i>	Pervinquiere, 1907	Ammonoidea	2	KZ.24714-24715
<i>Scaphites (Scaphites) bassei</i>	Collignon, 1929	Ammonoidea	2	KZ.24716, KZ.24726/2
<i>Stolickzkaia (Stoliczkaia) clavigera</i>	Neumayr, 1875	Ammonoidea	2	KZ.24719, KZ.24725/1
<i>Stoliczkaia (Faraudiella) sp.</i>		Ammonoidea	2	KZ.24717-24718
<i>Worthoceras</i> sp.		Ammonoidea	1	KZ.24721/2
<i>Zelandites</i> sp.		Ammonoidea	1	KZ.24720

Table B.3: The Folkestone Gault Clay Macrofossils

The specimens were collected by the author from Copt Point, in Folkestone, south east England. Samples were collected every 20 cm from 0.7 m below to 1.4 m above the base of Bed VII.

Specimen Species	Species Reference	Taxonomic Group	Specimen numbers in each sample (labelled as the height above the base of bed VII, in cm)											
			140	125	100	80	60	40	20	0	-10	-30	-50	-70
<i>Pectinucula pectinata</i>	J. Sowerby, 1818	Bivalvia	2	11	5	1		4		5	1	3		1
<i>Leionucula ovata</i>	Mantell, 1822	Bivalvia		2									1	
<i>Nucula</i> sp.		Bivalvia	1											
<i>Acila bivirgata</i>	Adams and Adams 1858	Bivalvia	1											
<i>Inoceramus concentricus</i>	Parkinson, 1819	Bivalvia								17	5	3	5	4
<i>Inoceramus sulcatus</i>	Parkinson, 1819	Bivalvia	95	13	17	24	10	21						
<i>Inoceramis</i> sp.		Bivalvia					2							
<i>Corbula</i> sp.		Bivalvia	1		13		1			10		5	3	
<i>Cardites</i> sp.		Bivalvia	2											
<i>Gryphaeostrea</i> sp.		Bivalvia	1					3						
Bivalve		Bivalvia	3	2										
<i>Circocerithium</i> sp.?		Gastropoda			20	30	129		25	13	35	35	34	9
<i>Nummocalcar fittoni</i>	Römer, 1836	Gastropoda	2	2										
<i>Anchura carinata</i>	Mantell, 1822	Gastropoda	1	1										
Natacid sp.		Gastropoda					1	2						
Aporrhaid sp.		Gastropoda		1										
Gastropod		Gastropoda								1				
<i>Discocyathus fittoni</i>	Milne-Edwards and Haime 1848	Cnidaria		4	2			2		1				
Scaphopod		Scaphopoda	4	7	12	4		2					1	
Belemnite		Coleoidea	2	6		1	1	7		2				
Ammonite fragments		Ammonoidea	7	14		2	5	19		18	4	2	2	
Echinoid		Echinoidea				1								

APPENDIX C: TRACE ELEMENT PROXIES DATA

Section C.1: ICP-MS analysis of the Folkestone Gault Clay Samples

Table C.1a ICP-MS assessment of accuracy and detection limits:

	Mo (ppm)	Ni (ppm)	V (ppm)	U (ppm)	Th (ppm)	Cr (ppm)	Co (ppm)	La (ppm)	Ce (ppm)	Pr (ppm)	Cu (ppm)	Zn (ppm)
MAG 1	1.25	60.3	161	2.85	11.8	95.2	25.7	39.3	84.1	10.8	36.6	136
MAG 2	1.20	54.6	152	2.79	11.5	90.8	23.7	37.9	77.8	10.3	33.2	129
MAG 3	1.25	55.7	157	2.83	11.7	94.0	24.3	39.3	80.5	10.6	33.6	131
MAG Certified		53.0	140	2.70	11.9	97.0	20.4		88.0		30.0	130
SD	0.0280	3.13	9.03	0.0663	0.192	2.61	2.25	0.831	4.42	0.237	2.71	3.22
% RSD	2.27	5.61	5.92	2.38	1.63	2.77	9.55	2.14	5.36	2.24	8.14	2.45
NBS1646 1	2.36	34.9	104	3.04	9.59	69.3	11.6	34.1	74.0	9.66	23.0	131
NBS1646 2	2.24	31.4	96.7	3.00	9.47	65.8	10.5	33.1	69.0	9.27	20.7	128
NBS1646 3	2.39	32.7	100	3.11	9.81	68.3	11.0	34.4	71.4	9.62	21.8	132
SD	0.0758	1.78	3.57	0.0516	0.173	1.77	0.527	0.663	2.51	0.215	1.15	2.18
% RSD	3.25	5.38	3.56	1.69	1.80	2.61	4.79	1.96	3.52	2.26	5.25	1.67
PACS 1	5.97	47.5	152	2.47	4.50	84.7	13.9	19.2	37.5	4.91	280	294
PACS 2	5.64	42.4	139	2.38	4.25	79.6	12.6	17.8	33.6	4.58	261	280
PACS 3	5.92	46.5	147	2.52	4.58	83.6	13.2	19.0	35.8	4.89	277	307
PACS Certified	5.43 +/- 0.28	39.5 +/- 2.3	133 +/- 5			90.7 +/- 4.6	11.5 +/- 0.3				310 +/- 12	
SD	0.252	3.71	8.25	0.0705	0.17	4.59	1.03	0.749	1.96	0.183	20.5	13.1
% RSD	4.38	8.43	5.78	2.87	3.87	5.42	8.06	4.01	5.49	3.81	7.28	4.46
SCo-1 1	1.37	32.3	154	3.43	10.2	56.2	12.6	29.4	60.4	7.82	35.0	107
SCo-1 2	1.31	29.4	143	3.28	9.7	56.6	12.4	27.8	54.4	7.37	33.6	105
SCo-1 3	1.37	30.7	149	3.45	10.3	55.1	12.8	29.5	57.7	7.77	35.2	109
SCo Certified	1.37	27.0	131	3.00	9.7	68.0	10.5	29.5	62.0	6.60	28.7	103
SD	0.0314	2.25	10.0	0.206	0.312	6.05	1.07	0.835	3.32	0.564	3.04	2.73
% RSD	2.32	7.55	6.95	6.28	3.13	10.3	8.88	2.87	5.66	7.63	9.18	2.58
Detection limits	0.0528	2.01	0.543	0.087	0.019	1.23	0.072	0.346	0.045	0.019	0.980	3.87

Table C.1b: ICP-MS Repeats data – Analytical repeats (one sample run at 4 positions within the analytical run):

	Mo (ppm)	Ni (ppm)	V (ppm)	U (ppm)	Th (ppm)	Cr (ppm)	Co (ppm)	La (ppm)	Ce (ppm)	Pr (ppm)	Cu (ppm)	Zn (ppm)
FEW 1 1	0.405	66.9	168	2.67	12.6	81.8	23.3	31.6	82.9	8.62	24.9	76.4
FEW 1 2	0.418	68.0	169	2.61	12.4	82.2	23.7	31.5	82.3	8.51	25.8	74.1
FEW 1 3	0.411	68.2	169	2.61	12.7	89.3	21.9	31.6	82.7	8.56	25.7	76.1
FEW 1 4	0.423	71.0	178	2.79	13.6	92.4	24.9	33.4	87.1	9.09	27.8	80.4
SD	0.0079	1.77	4.81	0.0875	0.552	5.23	1.22	0.919	2.24	0.267	1.20	2.66
% RSD	1.90	2.58	2.81	3.28	4.31	6.05	5.18	2.87	2.68	3.07	4.63	3.46

Table C.1c: ICP-MS Repeats data – Procedural repeats (one sample processed twice and run at the beginning and the end of the analytical run):

	Mo (ppm)	Ni (ppm)	V (ppm)	U (ppm)	Th (ppm)	Cr (ppm)	Co (ppm)	La (ppm)	Ce (ppm)	Pr (ppm)	Cu (ppm)	Zn (ppm)
FEW 2 1 1	0.449	77.7	194	3.01	14.0	96.6	27.8	33.0	81.3	8.67	34.4	87.7
FEW 2 1 2	0.449	79.0	198	3.01	13.9	98.1	28.3	33.3	81.7	8.71	33.4	85.2
FEW 2 2 1	0.493	80.3	198	3.02	14.1	89.1	28.8	33.8	82.5	8.84	32.8	87.1
FEW 2 2 2	0.493	80.8	199	3.08	14.8	89.0	28.8	34.1	83.1	8.93	32.8	88.3
SD	0.0254	1.36	2.31	0.0324	0.41	4.84	0.463	0.473	0.784	0.119	0.784	1.35
% RSD	5.39	1.72	1.17	1.07	2.90	5.20	1.63	1.41	0.96	1.36	2.35	1.55

Table C.1d: ICP-MS Repeats data – Analytical run repeats (one sample run at the beginning and the end of two different analytical runs):

	Mo (ppm)	Ni (ppm)	V (ppm)	U (ppm)	Th (ppm)	Cr (ppm)	Co (ppm)	La (ppm)	Ce (ppm)	Pr (ppm)	Cu (ppm)	Zn (ppm)
FEW 3 1 1	0.491	87.6	197	2.92	14.2	53.3	28.4	33.4	80.4	8.88	32.7	90.0
FEW 3 1 2	0.458	82.4	187	2.81	13.7	50.7	26.7	32.1	75.5	8.51	30.9	85.9
FEW 3 2 1	0.497	81.0	184	2.78	13.6	53.6	26.5	31.7	74.5	8.37	30.0	86.9
FEW 3 2 2	0.498	81.6	184	2.78	13.2	53.6	26.5	31.5	73.8	8.37	30.3	87.4
SD	0.0189	3.03	6.15	0.0660	0.41	1.41	0.894	0.873	2.99	0.243	1.18	1.74
% RSD	3.89	3.64	3.27	2.34	2.97	2.67	3.31	2.71	3.93	2.85	3.79	1.98

Section C.2: ICP-OES analysis of the Folkestone Gault Clay Samples

Table C.2a ICP-OES assessment of accuracy and detection limits:

	MnO (wt%)	Al ₂ O ₃ (wt%)	TiO ₂ (wt%)	K ₂ O (wt%)	P ₂ O ₅ (wt%)	CaO (wt%)
SCo -1 1	0.0480	12.9	0.547	2.66	0.180	2.31
SCo -1 2	0.0493	13.4	0.546	2.63	0.215	2.37
SCo Certified	0.0530	13.7	0.628	2.77	0.206	2.62
SD	0.0026	0.417	0.0469	0.0714	0.0179	0.163
% RSD	5.14	3.13	8.17	2.65	8.94	6.71
MAG 1	0.0879	13.6	0.676081	3.46	0.173	1.16
MAG 2	0.0904	14.1	0.68	3.47	0.147	1.17
MAG Certified	0.0980	16.4	0.751	3.55	0.163	1.37
SD	0.0053	1.45	0.0411	0.0479	0.0132	0.119
% RSD	5.70	9.86	5.85	1.37	8.21	9.66
NBS 1646 1	0.0424	10.1	0.765	2.26	0.139	0.987
NBS 1646 2	0.0422	10.3	0.760	2.16	0.139	1.01
SD	0.0001	0.135	0.0033	0.0692	0.0002	0.0165
% RSD	0.216	1.33	0.433	3.13	0.116	1.65
PACS 2 1	0.0526	11.0	0.689	1.42	0.217	2.49
PACS 2 2	0.0537	11.4	0.679	1.41	0.199	2.58
SD	0.0008	0.306	0.0074	0.0073	0.0128	0.0595
% RSD	1.55	2.73	1.09	0.516	6.16	2.34
Detection Limits	0.00514	0.000103	0.000467	0.0322	0.0147	0.00147

Table C.2b: ICP-OES Repeats data – Analytical repeats (one sample run at two positions within the analytical run):

	MnO (wt%)	Al ₂ O ₃ (wt%)	TiO ₂ (wt%)	K ₂ O (wt%)	P ₂ O ₅ (wt%)	CaO (wt%)
FEW 11	0.0309	17.8	0.834	3.03	0.0869	7.48
FEW 11 2	0.0296	17.0	0.828	2.86	0.0784	7.31
SD	0.0009	0.553	0.0047	0.120	0.0060	0.115
% RSD	3.02	3.19	0.568	4.06	7.26	1.56

Table C.2c: ICP-OES Repeats data – Procedural repeats (one sample processed twice and run within the same analytical run):

	MnO (wt%)	Al ₂ O ₃ (wt%)	TiO ₂ (wt%)	K ₂ O (wt%)	P ₂ O ₅ (wt%)	CaO (wt%)
FEW 18	0.0412	18.0	0.781	3.09	0.0605	9.10
FEW 18 2	0.0417	17.9	0.768	2.97	0.0539	9.12
SD	0.0004	0.107	0.0096	0.0869	0.0047	0.0115
% RSD	0.881	0.593	1.23	2.87	8.22	0.126

Table C.2d: ICP-OES Repeats data – Analytical run repeats (one sample run at the three positions within two different analytical runs):

	MnO (wt%)	Al ₂ O ₃ (wt%)	TiO ₂ (wt%)	K ₂ O (wt%)	P ₂ O ₅ (wt%)	CaO (wt%)
FEW 1	0.0297	16.0	0.766	2.84	0.0692	9.53
FEW 1 2	0.0288	16.0	0.766	2.82	0.0622	9.39
FEW 1 3	0.0291	15.8	0.769	2.80	0.0637	9.59
FEW 1 2 1	0.0310	16.3	0.806	2.73	0.0605	9.80
FEW 1 2 2	0.0303	16.2	0.796	2.72	0.0696	9.90
FEW 1 2 3	0.0307	15.9	0.796	2.67	0.0618	9.80
SD FEW	0.00032	0.174	0.0060	0.0294	0.0049	0.0587
% RSD	1.09	1.09	0.769	1.07	7.66	0.607

Section C3: Lithium Metaborate fusion ICP-MS analysis of the Niveau Pacquier, Breistroffer and Amma Fatma samples

Table C.3a ICP-MS assessment of accuracy and detection limits:

Standards run at three positions within the analytical run with samples 1-40 (Niveau Pacquier samples and Amma Fatma samples 1-4):

	Ni	V	U	Th	Cr	Co	La	Ce	Pr	Cu	Zn
AVG Mean (ppm)	21.6	115	1.78	5.65	7.76	15.0	35.5	66.0	7.85	59.9	83.9
AVG SD	0.74	1.07	0.05	0.28	0.23	0.45	0.17	0.09	0.15	1.39	2.91
AVG % RSD	3.43	0.93	3.05	4.98	3.02	2.97	0.48	0.14	1.86	2.32	3.48
AVG Certified (ppm)	16.0	121	1.92	6.50	10.1	15.3	38.0	67.0	7.60	60.0	88.0
W-2 Mean (ppm)	75.8	263	0.48	2.04	90.8	44.4	9.92	22.3	2.83	105	83.5
W-2 SD	1.71	1.09	0.00	0.14	0.60	0.25	0.22	0.55	0.09	1.19	1.95
W-2 % RSD	2.26	0.41	0.79	6.84	0.66	0.56	2.27	2.46	3.31	1.14	2.33
W-2 Certified (ppm)	70.0	262	0.53	2.20	93.0	44.0	11.4	24.0	5.90	103	77.0
S _{Co} Mean (ppm)	28.5	126	2.75	8.34	68.3	10.9	28.1	55.1	6.42	32.6	101
S _{Co} SD	0.76	0.54	0.11	0.28	0.69	0.16	0.08	1.22	0.10	0.62	0.22
S _{Co} % RSD	2.66	0.43	4.05	3.35	1.01	1.43	0.30	2.21	1.61	1.92	0.22
S _{Co} Certified (ppm)	27.0	131	3.00	9.70	68.0	10.5	29.5	62.0	6.60	28.7	103
Detection limits (ppm)	1.91	0.587	0.067	0.021	1.27	0.065	0.241	0.048	0.020	0.968	4.00

Standards run at three positions within the analytical run with samples 41-100

(Amma Fatma samples 5-16, Briestroffer samples):

	Ni	V	U	Th	Cr	Co	La	Ce	Pr	Cu	Zn
AVG Mean (ppm)	19.5	119	1.90	5.96	8.36	14.8	34.6	67.0	7.77	59.9	81.0
AVG SD	0.76	1.35	0.03	0.15	0.45	0.21	0.29	0.53	0.10	0.89	1.37
AVG % RSD	3.89	1.14	1.70	2.56	5.38	1.45	0.84	0.78	1.30	1.48	1.70
AVG Certified (ppm)	16.0	121	1.92	6.50	10.1	15.3	38.0	67.0	7.60	60.0	88.0

W-2 Mean (ppm)	74.5	272	0.46	2.06	92.7	44.3	9.74	22.8	2.88	107	83.6
W-2 SD	2.03	3.70	0.05	0.07	1.77	1.16	0.13	0.43	0.11	1.93	0.86
W-2 % RSD	2.72	1.36	9.91	3.51	1.91	2.63	1.29	1.90	3.97	1.80	1.03
W-2 Certified (ppm)	70.0	262	0.53	2.20	93.0	44.0	11.4	24.0	5.90	103	77.0

S-Co Mean (ppm)	28.9	131	2.87	8.74	69.9	11.0	27.8	56.0	6.62	32.8	104
S-Co SD	0.86	1.11	0.13	0.11	1.47	0.25	0.18	0.58	0.10	0.71	1.45
S-Co % RSD	2.98	0.84	4.36	1.21	2.11	2.25	0.63	1.03	1.49	2.18	1.39
S-Co Certified (ppm)	27.0	131	3.00	9.70	68.0	10.5	29.5	62.0	6.60	28.7	103

Detection limits (ppm)	1.36	0.449	0.046	0.031	0.709	0.079	0.214	0.029	0.017	0.965	2.75
------------------------	------	-------	-------	-------	-------	-------	-------	-------	-------	-------	------

Table C.3b: ICP-OES Repeats data – Analytical run repeats (one sample run in two different analytical runs):

	V (ppm)	Cr (ppm)	Co (ppm)	Ni (ppm)	Cu (ppm)	Zn (ppm)	La (ppm)	Ce (ppm)	Pr (ppm)	Th (ppm)	U (ppm)
NP1 1	108	81.7	13.9	99.2	72.7	137	29.4	52.4	6.55	7.88	1.93
NP1 2	106	79.0	13.0	86.7	68.3	123	26.1	50.1	6.41	7.53	1.75
SD	1.78	1.88	0.582	8.86	3.13	10.5	2.354	1.61	0.100	0.250	0.125
%RSD	1.66	2.34	4.33	9.53	4.44	8.07	8.48	3.14	1.54	3.24	6.82

Table C.3c: ICP-OES Repeats data – Procedural repeats (one sample processed twice and run in two different analytical runs):

	V (ppm)	Cr (ppm)	Co (ppm)	Ni (ppm)	Cu (ppm)	Zn (ppm)	La (ppm)	Ce (ppm)	Pr (ppm)	Th (ppm)	U (ppm)
BL11 1	54.0	41.1	7.18	44.3	18.5	44.9	15.0	26.9	3.20	4.50	2.45
BL11 2	57.0	44.4	7.63	45.8	20.4	40.1	15.8	28.2	3.29	4.91	2.40
SD	2.15	2.29	0.317	1.02	1.32	3.40	0.577	0.931	0.065	0.288	0.035
%RSD	3.88	5.36	4.28	2.27	6.80	7.99	3.76	3.38	2.01	6.13	1.43

Table C.3d: ICP-OES Repeats data –Analytical repeats (one sample run at the beginning and end of an analytical runs):

	V (ppm)	Cr (ppm)	Co (ppm)	Ni (ppm)	Cu (ppm)	Zn (ppm)	La (ppm)	Ce (ppm)	Pr (ppm)	Th (ppm)	U (ppm)
BL34 1	220	65.3	13.5	67.2	26.9	43.1	23.4	43.2	5.37	5.00	7.32
BL34 2	212	63.1	13.3	65.0	23.8	37.0	22.3	41.7	5.10	4.78	6.92
SD	5.64	1.60	0.151	1.57	2.19	4.32	0.753	1.13	0.188	0.156	0.284
%RSD	2.61	2.49	1.13	2.37	8.61	10.8	3.30	2.66	3.59	3.20	3.99

Section C4: Lithium Metaborate fusion ICP-OES analysis of the Breistroffer and Amma Fatma samples

Table C.4a ICP-OES assessment of accuracy and detection limits:

	Al ₂ O ₃ (wt%)	MnO (wt%)	Sc (ppm)	TiO ₂ (wt%)	K ₂ O (wt%)	SiO ₂ (wt%)	P ₂ O ₅ (wt%)	CaO (wt%)
BEN 1	10.3	0.204	23.2	2.68	1.43	38.8	1.09	14.3
BEN 2	10.2	0.205	23.4	2.68	1.43	39.0	1.11	14.5
BEN 3	10.4	0.207	23.7	2.71	1.43	39.4	1.12	14.7
BEN 4	10.2	0.204	23.4	2.66	1.41	38.6	1.10	14.4
BEN 5	9.99	0.200	22.8	2.62	1.38	38.1	1.08	14.3
BEN 6	10.1	0.200	22.7	2.63	1.41	37.9	1.06	14.0
BEN Certified	10.7	0.200	22.0	2.61	1.39	38.2	1.05	13.9
BEN SD	0.227	0.00299	0.559	0.0366	0.0188	0.527	0.0255	0.263
BEN RSD %	2.22	1.47	2.43	1.38	1.33	1.37	2.34	1.84

GSN 1	14.8	0.0551	7.34	0.683	4.63	67.1	0.291	2.57
GSN 2	14.7	0.0555	7.40	0.686	4.69	67.5	0.295	2.59
GSN 3	14.7	0.0550	7.34	0.683	4.73	67.1	0.295	2.61
GSN 4	14.6	0.0551	7.27	0.678	4.61	67.0	0.292	2.59
GSN 5	14.7	0.0551	7.29	0.682	4.69	67.3	0.294	2.61
GSN 6	14.8	0.0547	7.21	0.684	4.71	66.7	0.288	2.56
GSN Certified	14.7	0.0560	7.30	0.680	4.63	65.8	0.280	2.50
GSN SD	0.0644	0.00042	0.0614	0.00249	0.0468	0.540	0.00523	0.0383
GSN RSD %	0.438	0.760	0.840	0.365	1.00	0.807	1.80	1.49

MAG 1	16.5	0.102	17.5	0.748	3.667	52.0	0.175	1.48
MAG 2	16.6	0.103	17.5	0.755	3.693	52.3	0.179	1.49
MAG 3	16.5	0.102	17.3	0.748	3.683	52.0	0.177	1.47
MAG 4	16.8	0.104	17.5	0.759	3.702	52.7	0.181	1.50
MAG 5	16.2	0.101	17.0	0.736	3.62	51.4	0.175	1.46
MAG 6	16.7	0.102	17.3	0.753	3.737	52.0	0.173	1.47
MAG Certified	16.4	0.0980	17.2	0.751	3.55	50.4	0.163	1.37
MAG SD	0.196	0.00191	0.189	0.00730	0.0618	0.768	0.00583	0.0424
MAG RSD %	1.18	1.87	1.09	0.974	1.69	1.48	3.34	2.90

SCo 1	12.6	0.0490	10.7	0.567	2.59	61.4	0.205	2.65
SCo 2	12.8	0.0499	10.8	0.573	2.66	62.6	0.209	2.72
SCo 3	12.6	0.0488	10.5	0.565	2.63	61.3	0.205	2.69
SCo 4	12.5	0.0488	10.5	0.563	2.57	61.0	0.203	2.65
SCo 5	12.3	0.0481	10.5	0.554	2.55	60.3	0.203	2.64
SCo 6	12.6	0.0487	10.7	0.565	2.60	61.0	0.203	2.64
SCo Certified	13.7	0.0530	10.8	0.628	2.77	62.8	0.206	2.62
SCo SD	0.445	0.00165	0.138	0.0247	0.0730	0.886	0.00219	0.0347
SCo RSD %	3.51	3.34	1.30	4.30	2.78	1.44	1.07	1.30

Detection Limits	0.0158	0.00303	0.301	0.00524	0.00546	0.0160	0.0121	0.00457
------------------	--------	---------	-------	---------	---------	--------	--------	---------

Table C.4b: ICP-OES Repeats data – Analytical repeats (one sample run at two positions within the analytical run):

	Al ₂ O ₃ (wt%)	MnO (wt%)	Sc (ppm)	TiO ₂ (wt%)	K ₂ O (wt%)	SiO ₂ (wt%)	P ₂ O ₅ (wt%)	CaO (wt%)
Repeat 1 1	8.21	0.0204	7.01	0.351	1.14	24.85	0.0745	32.2
Repeat 1 2	8.22	0.0206	6.99	0.351	1.14	25.09	0.0769	32.86
Repeat 1 SD	0.00354	0.000170	0.0141	7.07E-05	0.002121	0.170	0.00170	0.467
Repeat 1 %RSD	0.0430	0.829	0.202	0.0202	0.186	0.680	2.24	1.43

Table C.4c: ICP-OES Repeats data – Procedural repeats (one sample processed twice and run within the same analytical run):

	Al ₂ O ₃ (wt%)	MnO (wt%)	Sc (ppm)	TiO ₂ (wt%)	K ₂ O (wt%)	SiO ₂ (wt%)	P ₂ O ₅ (wt%)	CaO (wt%)
Repeat 2 1	8.13	0.0212	7.05	0.356	1.12	24.58	0.0933	32.58
Repeat 2 2	8.08	0.0227	7.10	0.352	1.13	24.36	0.0940	33.48
Repeat 2 SD	0.0332	0.00107	0.0325	0.002404	0.004243	0.156	0.000495	0.636
Repeat 2 %RSD	0.410	4.86	0.460	0.679	0.376	0.636	0.529	1.93

Table C.4d: ICP-OES Repeats data – Analytical run repeats (one sample run in two different analytical runs):

	Al ₂ O ₃ (wt%)	MnO (wt%)	Sc (ppm)	TiO ₂ (wt%)	K ₂ O (wt%)	SiO ₂ (wt%)	P ₂ O ₅ (wt%)	CaO (wt%)
Repeat 3 1	9.51	0.0201	7.92	0.403	1.29	27.45	0.102	29.51
Repeat 3 2	9.54	0.0199	8.01	0.400	1.29	27.33	0.101	29.26
Repeat 3 SD	0.0191	0.00016	0.0622	0.00198	0.001414	0.0849	0.000495	0.177
Repeat 3 %RSD	0.200	0.813	0.781	0.493	0.110	0.310	0.486	0.602

Section C5: Lithium Metaborate fusion ICP-OES analysis of the Niveau

Pacquier samples

Table C.5a ICP-OES assessment of accuracy and detection limits:

	Al ₂ O ₃ (wt%)	MnO (wt%)	Sc (ppm)	TiO ₂ (wt%)	K ₂ O (wt%)	SiO ₂ (wt%)	P ₂ O ₅ (wt%)	CaO (wt%)
BEN 1 1	10.3	0.204	22.3	2.63	1.48	38.8	1.06	14.2
BEN 1 2	10.4	0.206	22.6	2.65	1.50	39.4	1.09	14.2
BEN 1 3	10.4	0.204	22.5	2.66	1.51	38.9	1.06	14.3
BEN 2 1	10.5	0.200	23.2	2.69	1.52	38.1	1.02	14.4
BEN 2 2	10.6	0.202	23.4	2.72	1.54	38.6	1.04	14.5
BEN 2 3	10.4	0.200	22.4	2.67	1.49	38.1	1.01	14.6
BEN Certified	10.7	0.200	22.0	2.61	1.39	38.2	1.05	13.9
SD BEN	0.158	0.00256	0.497	0.0370	0.0470	0.507	0.0290	0.225
% RSD BEN	1.51	1.27	2.20	1.39	3.16	1.31	2.77	1.57

GSN 1	14.3	0.0549	7.33	0.667	4.53	65.3	0.278	2.47
GSN 2	14.6	0.0553	7.55	0.684	4.73	65.7	0.277	2.50
GSN 3	15.1	0.0569	7.61	0.707	4.93	68.1	0.287	2.55
GSN 4	14.3	0.0546	7.27	0.669	4.60	65.0	0.276	2.43
GSN Certified	14.7	0.0560	7.30	0.680	4.63	65.8	0.280	2.50
SD GSN	0.363	0.00094	0.158	0.0159	0.155	1.22	0.00426	0.0434
% RSD GSN	2.49	1.69	2.13	2.33	3.31	1.86	1.53	1.74

MAG 1	16.4	0.101	17.2	0.743	3.60	51.1	0.169	1.47
MAG 2	16.3	0.103	17.2	0.738	3.58	52.3	0.172	1.45
MAG 3	16.3	0.101	17.1	0.740	3.56	51.1	0.168	1.47
MAG 4	16.2	0.101	16.9	0.734	3.53	51.2	0.172	1.43
MAG Certified	16.4	0.0980	17.2	0.751	3.55	50.4	0.163	1.37
SD MAG	0.0779	0.00193	0.116	0.00653	0.0265	0.706	0.00370	0.0419
% RSD MAG	0.478	1.91	0.679	0.882	0.745	1.38	2.19	2.91

SCo 1	12.2	0.0502	10.4	0.550	2.54	60.3	0.199	2.55
SCo 2	11.8	0.0486	10.1	0.532	2.45	58.3	0.192	2.48
SCo 3	12.3	0.0499	10.5	0.553	2.56	60.1	0.195	2.57
SCo 4	12.3	0.0493	10.4	0.552	2.57	59.5	0.196	2.52
SCo Certified	13.7	0.0530	10.8	0.628	2.77	62.8	0.206	2.62
SD SCo	0.713	0.00168	0.260	0.0373	0.118	1.65	0.00532	0.0527
% RSD SCo	5.72	3.35	2.50	6.63	4.58	2.74	2.69	2.07

Detection Limits	0.0162	0.00324	0.303	0.00504	0.00536	0.0152	0.0109	0.00453
------------------	--------	---------	-------	---------	---------	--------	--------	---------

Table C.5b: ICP-OES Repeats data – Procedural repeats (two samples processed twice and run within the same analytical run):

	Al ₂ O ₃ (wt%)	MnO (wt%)	Sc (ppm)	TiO ₂ (wt%)	K ₂ O (wt%)	SiO ₂ (wt%)	P ₂ O ₅ (wt%)	CaO (wt%)
Repeat 1 1	13.8	0.038	12.9	0.603	2.30	43.9	0.106	15.9
Repeat 1 2	13.9	0.033	13.1	0.604	2.27	42.6	0.0968	15.9
Repeat 1 SD	0.0495	0.00354	0.127	0.00092	0.0219	0.891	0.00679	0.0495
Repeat 1 % RSD	0.358	9.96	0.979	0.152	0.961	2.06	6.68	0.311
Repeat 2 1	12.1	0.036	11.7	0.546	2.04	39.8	0.0919	19.5
Repeat 2 2	12.1	0.036	11.9	0.552	2.01	40.2	0.0906	20.0
Repeat 2 SD	0.0212	0	0.184	0.00453	0.0247	0.255	0.000919	0.346
Repeat 2 % RSD	0.176	0	1.56	0.825	1.22	0.637	1.01	1.76

Table C.5c: ICP-OES Repeats data – Analytical run repeats (one sample run in two different analytical runs):

	Al ₂ O ₃ (wt%)	MnO (wt%)	Sc (ppm)	TiO ₂ (wt%)	K ₂ O (wt%)	SiO ₂ (wt%)	P ₂ O ₅ (wt%)	CaO (wt%)
Repeat 3 1	9.32	0.038	8.72	0.4142	1.48	32.3	0.131	23.2
Repeat 3 2	9.27	0.043	8.81	0.4035	1.36	30.0	0.116	26.3
Repeat 3 SD	0.0410	0.00354	0.0643	0.00757	0.0841	1.58	0.0102	2.15
Repeat 3 % RSD	0.441	8.73	0.734	1.85	5.94	5.08	8.25	8.69

Table C.5d: ICP-OES Repeats data – Analytical repeats (one sample run at two positions within the analytical run):

	Al ₂ O ₃ (wt%)	MnO (wt%)	Sc (ppm)	TiO ₂ (wt%)	K ₂ O (wt%)	SiO ₂ (wt%)	P ₂ O ₅ (wt%)	CaO (wt%)
Repeat 4 1	8.17	0.47	7.43	0.3661	1.271	29.0	0.1055	26.9
Repeat 4 2	8.40	0.46	7.76	0.3761	1.341	29.5	0.1073	27.3
Repeat 4 SD	0.162	0.00707	0.232	0.00707	0.0495	0.389	0.00127	0.311
Repeat 4 % RSD	1.96	1.52	3.05	1.91	3.79	1.33	1.20	1.15

Section C6: Lithium Metaborate fusion ICP-MS determination of Mo for the Briestroffer and Amma Fatma samples

	Mo (ppm)
ACE 1	2.96
ACE 2	2.85
ACE 3	2.70
ACE 4	2.89
ACE 5	3.09
ACE 6	2.81
ACE Certified	2.50
ACE SD	0.189
ACE RSD %	6.68

Table C.6a Mo assessment of accuracy and detection limits for the Briestroffer and Amma Fatma sample run:

BEN 1	2.66
BEN 2	2.69
BEN 3	2.68
BEN 4	2.55
BEN 5	2.81
BEN 6	2.67
BEN Certified	2.80
BEN SD	0.0908
BEN RSD %	3.37

Table C.6b: ICP-OES Repeats data – Analytical repeats (one sample run at three positions within the analytical run):

	Mo (ppm)
Repeat 1 1	4.19
Repeat 1 2	4.16
Repeat 1 3	4.30
Repeat 1 SD	0.0756
Repeat 1 %RSD	1.79

GSN 1	1.91
GSN 2	1.84
GSN 3	1.82
GSN 4	1.84
GSN 5	1.97
GSN 6	1.93
GSN Certified	1.20
GSN SD	0.264
GSN RSD %	14.8

Table C.6c: ICP-OES Repeats data – Procedural repeats (one samples processed three times and run within the same analytical run):

	Mo (ppm)
Repeat 2 1	1.18
Repeat 2 2	1.15
Repeat 2 3	1.22
Repeat 2 SD	0.0330
Repeat 2 %RSD	2.79

MAG 1	2.42
MAG 2	2.32
MAG 3	2.34
MAG 4	2.36
MAG 5	2.56
MAG 6	2.38
MAG SD	0.0881
MAG RSD %	3.68

Table C.6d: ICP-OES Repeats data – Analytical run repeats (one sample run twice in two different analytical runs):

	Mo (ppm)
Repeat 3 1 1	13.7
Repeat 3 1 2	13.53
Repeat 3 2 1	13.67
Repeat 3 2 2	13.25
Repeat 3 %RSD	0.205
Repeat 3 %RSD	1.52

SCo 1	1.80
SCo 2	1.83
SCo 3	1.74
SCo 4	1.80
SCo 5	1.81
SCo 6	1.85
SCo Certified	1.37
SCo SD	0.168
SCo RSD %	9.65

Detection Limit	0.0447
-----------------	--------

Section C7: Lithium Metaborate fusion ICP-MS determination of Mo for the

Niveau Pacquier samples

	Mo (ppm)
ACE 1	2.16
ACE 2	2.47
ACE 3	2.32
ACE 4	2.55
ACE Certified	2.50
SD ACE	0.174
% RSD ACE	7.26

BEN 1	2.55
BEN 2	2.98
BEN 3	2.91
BEN 4	2.54
BEN Certified	2.80
SD BEN	0.202
% RSD BEN	7.32

GSN 1	1.20
GSN 2	1.46
GSN 3	1.33
GSN 4	1.37
GSN Certified	1.20
SD GSN	0.114
% RSD GSN	8.68

MAG 1	1.62
MAG 2	2.00
MAG 3	1.80
MAG 4	1.67
SD MAG	0.171
% RSD MAG	9.66

SCO 1	1.18
SCO 2	1.29
SCO 3	1.16
SCO 4	1.26
SCo Certified	1.37
SD SCO	0.085
% RSD SCO	6.8

Detection Limit	0.0436
-----------------	--------

Table C.7a Mo assessment of accuracy and detection limits for the Niveau Pacquier sample run:

Table C.7b: ICP-OES Repeats data – Analytical run repeats (two sample run in two different analytical runs):

	Mo (ppm)
Repeat 1 1	1.49
Repeat 1 2	1.60
Repeat 1 SD SCO	0.0778
Repeat 1 % RSD	5.05

Repeat 2 1	1.68
Repeat 2 2	1.52
Repeat 2 SD SCO	0.112
Repeat 2 % RSD	6.98

Table C.7c: ICP-OES Repeats data – Procedural repeats (one sample processed twice and run within the same analytical run):

	Mo (ppm)
Repeat 3 1	22.4
Repeat 3 2	24.2
Repeat 3 SD SCO	1.26
Repeat 3 % RSD	5.40

Table C.7d: ICP-OES Repeats data – Analytical repeats (one sample run at two positions within the analytical run):

	Mo (ppm)
Repeat 4 1	29.5
Repeat 4 2	27.3
Repeat 4 SD SCO	1.51
Repeat 4 % RSD	5.33

Section C8: Analytical Results of ICP-MS and ICP-OES analysis

Table C.8a: ICP-MS data for the Folkestone Gault Clay section:

Scale (m)	Mo (ppm)	Ni (ppm)	V (ppm)	U (ppm)	Th (ppm)	Cr (ppm)	Co (ppm)	La (ppm)	Ce (ppm)	Pr (ppm)	Cu (ppm)	Zn (ppm)
-0.95	0.398	70.0	172	2.78	13.6	85.6	24.9	33.3	84.9	9.00	25.4	76.0
-0.85	0.393	70.0	165	2.70	13.3	41.4	26.4	33.1	85.4	8.95	26.0	77.0
-0.75	0.430	74.3	170	2.80	13.9	96.9	29.2	33.7	87.9	9.16	27.2	81.0
-0.65	0.450	74.5	169	2.83	14.0	98.3	28.6	34.2	88.3	9.24	26.3	77.0
-0.55	0.430	78.0	172	2.77	14.2	95.3	27.7	34.6	87.4	9.24	28.3	77.0
-0.45	0.419	73.9	168	2.70	13.7	99.7	27.1	33.8	84.9	9.01	27.6	77.0
-0.35	0.417	72.4	170	2.67	13.6	96.7	27.8	32.8	83.3	8.90	26.3	77.0
-0.25	0.409	69.6	156	2.76	13.7	89.7	28.3	32.7	81.3	8.71	26.1	78.0
-0.15	0.480	70.8	155	2.91	13.0	86.9	26.5	31.2	74.7	8.24	25.1	71.0
-0.05	0.433	75.6	160	2.86	13.8	96.0	30.9	32.3	78.7	8.57	25.9	73.0
0.05	0.395	72.0	180	2.94	14.0	93.5	26.5	32.0	75.6	8.38	28.9	82.0
0.15	0.413	72.8	180	2.64	13.0	98.4	28.1	30.0	69.1	7.76	28.3	83.0
0.25	0.498	71.3	175	2.90	12.7	98.6	25.4	30.7	76.9	8.01	27.1	81.0
0.35	0.401	71.8	181	2.83	12.9	102	22.3	30.9	68.0	7.90	27.7	77.0
0.45	0.464	77.0	178	4.23	13.2	73.2	25.0	34.0	84.2	9.18	27.5	76.0
0.55	0.408	72.5	176	2.78	14.0	50.8	22.9	31.9	71.2	8.24	29.0	82.0
0.65	0.414	77.6	177	2.74	13.8	67.4	25.9	31.7	71.4	8.25	29.3	88.0
0.75	0.433	79.0	178	2.78	13.4	50.7	26.1	32.0	73.0	8.42	29.4	95.0
0.85	0.398	84.1	179	2.70	12.8	45.8	29.1	31.9	72.1	8.43	29.4	78.0
0.95	0.385	76.7	175	2.79	12.9	79.8	23.3	31.8	72.8	8.44	27.1	71.0
1.05	0.385	75.6	165	2.70	12.6	70.1	21.9	31.2	70.2	8.23	26.3	73.0
1.15	0.467	90.1	156	2.62	12.5	81.3	29.6	31.4	71.7	8.29	26.4	84.0

Table C.8b: ICP-OES data for the Folkestone Gault Clay section:

Scale (m)	MnO (wt%)	Al ₂ O ₃ (wt%)	TiO ₂ (wt%)	K ₂ O (wt%)	P ₂ O ₅ (wt%)	CaO (wt%)
-0.95	0.0297	16.0	0.766	2.84	0.00675	9.53
-0.85	0.0288	15.5	0.782	2.75	0.00658	9.27
-0.75	0.0285	15.6	0.814	2.81	0.00747	8.76
-0.65	0.0272	15.9	0.819	2.93	0.00661	8.63
-0.55	0.0269	16.9	0.835	2.92	0.00652	8.25
-0.45	0.0288	16.0	0.817	2.92	0.00796	8.54
-0.35	0.0296	16.0	0.826	2.84	0.00978	8.73
-0.25	0.0298	16.5	0.848	2.83	0.00683	8.56
-0.15	0.0309	15.9	0.822	2.80	0.00674	8.37
-0.05	0.0303	16.5	0.821	2.86	0.00981	7.87
0.05	0.0309	17.8	0.834	3.03	0.00834	7.48
0.15	0.0333	16.0	0.804	2.78	0.00780	7.77
0.25	0.0350	16.8	0.811	2.99	0.0112	8.46
0.35	0.0383	16.9	0.782	3.01	0.00717	8.21
0.45	0.0399	17.2	0.777	2.95	0.0573	8.69
0.55	0.0402	18.0	0.781	3.12	0.00794	8.31
0.65	0.0416	17.6	0.779	2.93	0.00811	8.35
0.75	0.0412	18.0	0.781	3.09	0.00875	9.10
0.85	0.0408	16.9	0.735	2.80	0.00856	11.1
0.95	0.0399	17.0	0.751	2.82	0.0110	11.3
1.05	0.0491	16.4	0.702	2.69	0.00867	13.0
1.15	0.0541	15.7	0.660	2.54	0.00928	14.7

Table C.8c: ICP-MS data for the Niveau Pacquier section:

(m)	Mo (ppm)	Ni (ppm)	V (ppm)	U (ppm)	Th (ppm)	Cr (ppm)	Co (ppm)	La (ppm)	Ce (ppm)	Pr (ppm)	Cu (ppm)	Zn (ppm)
-1	0.571	99.2	108	1.93	7.88	81.7	13.9	29.4	52.4	6.55	72.7	137
-0.9	0.324	77.8	111	1.93	7.78	80.8	12.0	28.6	52.0	6.74	87.7	133
-0.8	0.874	81.4	102	2.00	6.96	74.5	13.1	27.7	49.4	6.58	86.6	116
-0.7	0.448	81.8	103	1.93	6.79	73.3	12.5	31.3	54.5	7.36	79.4	103
-0.6	0.410	88.7	111	1.98	6.93	74.3	14.3	28.4	49.4	6.33	72.1	150
-0.5	0.969	97.5	115	2.10	7.22	79.4	15.8	29.3	51.6	6.78	66.2	130
-0.4	1.52	86.5	118	2.04	7.49	81.1	13.5	29.2	51.8	6.66	63.3	138
-0.3	1.10	85.0	128	2.19	8.39	90.2	11.8	29.8	55.8	7.06	73.9	115
-0.2	1.53	74.7	116	2.38	7.90	84.5	11.9	28.6	52.5	6.70	70.5	121
-0.1	1.94	78.5	119	2.55	7.27	79.7	11.3	29.6	53.0	6.95	60.3	149
0	11.1	121	311	5.26	6.70	91.5	16.6	29.1	55.8	7.11	42.2	191
0.1	4.30	76.1	160	3.14	8.05	89.8	13.8	25.5	48.2	5.72	46.5	97.7
0.2	2.04	59.7	133	2.65	8.27	86.4	10.3	25.5	49.2	5.89	63.8	103
0.3	2.21	58.8	129	2.74	6.82	73.1	8.5	25.8	49.6	6.22	49.9	128
0.4	18.6	115	203	6.32	5.20	63.8	10.1	27.9	50.8	6.26	29.6	62.7
0.5	16.0	83.3	177	5.93	6.67	75.0	8.4	27.5	50.9	5.97	31.5	69.7
0.6	10.3	68.5	200	3.91	8.48	88.7	9.5	24.9	48.7	5.55	39.9	125
0.7	25.9	104	218	5.63	8.16	93.5	10.2	25.1	51.0	5.92	38.9	72.7
0.8	51.3	96.9	211	6.21	7.47	85.5	10.4	25.1	52.2	6.03	30.8	50.5
0.9	19.9	63.3	229	4.64	6.18	76.2	7.2	23.9	47.6	5.53	37.5	204
1	15.2	67.5	210	4.39	5.94	76.0	6.3	23.6	45.2	5.32	35.5	193
1.1	35.8	79.4	161	6.35	6.56	71.8	7.7	25.2	48.9	5.77	36.5	110
1.2	53.5	67.6	116	8.66	4.45	47.4	6.9	24.7	44.6	5.38	25.0	41.2
1.3	38.1	87.7	149	6.37	6.67	71.4	9.8	25.8	50.6	6.12	31.3	151
1.4	22.5	86.1	133	5.73	7.91	77.2	10.9	26.7	53.5	6.09	30.2	63.8
1.5	22.6	95.9	167	6.56	8.47	87.7	11.9	29.0	55.7	6.41	34.4	63.0
1.6	9.08	75.4	174	5.39	8.39	92.9	12.5	30.3	57.7	6.81	46.9	94.6
1.7	1.79	57.6	114	2.93	7.92	82.3	10.7	29.9	57.5	6.81	45.8	137
1.8	1.38	55.5	111	3.08	7.85	81.8	9.5	30.0	57.4	6.91	48.7	118
1.9	1.41	67.2	119	3.07	8.27	86.8	12.5	29.9	58.6	7.11	51.8	122
2	1.34	74.7	117	2.58	8.12	84.8	12.8	31.2	59.6	7.26	53.7	118
2.1	1.63	73.3	117	2.64	8.11	84.9	13.3	30.5	59.0	7.11	59.1	104
2.2	1.46	79.9	118	2.37	8.04	83.0	14.5	30.2	58.3	7.27	64.1	143
2.3	1.31	86.5	120	2.77	8.21	85.9	16.2	34.7	68.9	8.81	58.2	135
2.4	1.12	85.1	129	2.66	8.40	87.4	15.3	31.3	58.5	7.18	59.1	152
2.5	0.769	74.7	123	2.39	8.32	85.1	13.8	33.8	55.5	6.81	59.2	117

Table C.8d: ICP-OES data for the Niveau Pacquier section:

(m)	Sc (ppm)	MnO (wt%)	Al ₂ O ₃ (wt%)	TiO ₂ (wt%)	K ₂ O (wt%)	SiO ₂ (wt%)	P ₂ O ₅ (wt%)	CaO (wt%)
-1	13.1	0.0327	13.9	0.604	2.27	42.6	0.097	15.9
-0.9	13.7	0.0353	14.4	0.625	2.39	44.2	0.107	18.0
-0.8	11.9	0.0440	12.6	0.553	2.14	40.8	0.102	18.6
-0.7	11.8	0.0505	12.7	0.560	2.13	40.3	0.154	20.0
-0.6	11.8	0.0466	12.7	0.557	2.10	41.3	0.0993	18.9
-0.5	12.4	0.0429	12.9	0.572	2.18	41.7	0.104	17.9
-0.4	12.9	0.0376	13.8	0.603	2.27	43.3	0.112	16.2
-0.3	13.5	0.0287	14.9	0.657	2.46	45.0	0.125	14.0
-0.2	13.0	0.0349	14.0	0.624	2.32	43.9	0.104	16.2
-0.1	11.9	0.0365	12.1	0.552	2.01	40.2	0.0906	20.0
0	12.3	0.0319	12.8	0.548	2.04	39.5	0.141	18.5
0.1	13.5	0.0239	15.4	0.676	2.44	46.4	0.078	13.1
0.2	14.8	0.0254	16.3	0.722	2.63	48.4	0.0793	14.0
0.3	12.3	0.0295	12.3	0.557	2.15	41.3	0.0943	20.1
0.4	9.4	0.0396	9.91	0.436	1.62	33.8	0.141	23.5
0.5	11.0	0.0328	12.6	0.552	2.00	39.1	0.114	17.8
0.6	13.2	0.0247	15.6	0.686	2.43	47.4	0.0724	11.9
0.7	12.8	0.0215	14.6	0.650	2.19	45.4	0.0952	12.4
0.8	11.6	0.0222	13.1	0.587	1.96	46.4	0.139	13.0
0.9	10.1	0.0298	10.7	0.484	1.64	36.1	0.0993	20.9
1	9.5	0.0325	10.9	0.496	1.75	35.7	0.112	23.0
1.1	7.6	0.0549	7.49	0.337	1.21	27.8	0.151	28.3
1.2	16.3	0.0519	18.8	0.837	2.97	62.2	0.197	32.2
1.3	12.3	0.0288	13.8	0.596	2.02	41.3	0.102	16.4
1.4	13.8	0.0243	15.3	0.664	2.17	45.5	0.0835	12.5
1.5	14.0	0.0226	16.4	0.712	2.42	47.7	0.0782	12.1
1.6	13.6	0.0246	15.2	0.677	2.39	46.3	0.078	14.0
1.7	12.8	0.0313	13.8	0.615	2.20	43.0	0.0674	16.3
1.8	12.9	0.0304	13.9	0.629	2.26	44.7	0.0699	16.4
1.9	13.4	0.0298	14.5	0.648	2.40	45.7	0.0707	14.8
2	12.9	0.0279	13.5	0.606	2.20	43.1	0.0674	14.5
2.1	13.5	0.0282	14.3	0.644	2.37	44.5	0.0762	14.6
2.2	13.6	0.0307	14.3	0.649	2.37	46.2	0.0822	14.6
2.3	13.9	0.0323	14.6	0.674	2.38	45.6	0.171	13.7
2.4	13.4	0.0337	14.1	0.662	2.37	46.6	0.0905	13.9
2.5	14.0	0.0304	15.0	0.690	2.53	47.7	0.0917	12.3

Table C.8e: ICP-MS data for the Briestoffer section:

(m)	Mo (ppm)	Ni (ppm)	V (ppm)	U (ppm)	Th (ppm)	Cr (ppm)	Co (ppm)	La (ppm)	Ce (ppm)	Pr (ppm)	Cu (ppm)	Zn (ppm)
-5	0.23	27.6	52.6	1.67	5.09	39.3	6.74	17.5	29.9	3.95	22.5	33.1
-4.8	0.56	16.2	43.8	1.22	4.13	31.5	4.81	15.3	25.7	3.28	17.6	30.8
-4.6	1.26	28.4	64.4	1.46	6.01	48.3	6.67	18.7	31.4	3.98	21.8	46.1
-4.4	1.55	45.7	62.5	1.87	5.45	47.7	9.26	16.5	30.5	3.74	24.6	58.8
-4.35	1.55	43.8	60.8	2.21	5.23	44.8	7.72	14.9	27.9	3.39	22.4	53.3
-4.3	1.77	47.0	58.2	2.32	5.05	44.8	7.82	14.8	28.1	3.31	20.0	39.7
-4.25	1.24	44.3	54.0	2.45	4.50	41.1	7.18	15.0	26.9	3.20	18.5	44.9
-4.2	1.30	43.1	62.9	2.16	5.26	45.8	7.77	15.8	28.8	3.55	21.9	43.5
-4	2.95	43.4	71.1	2.80	5.68	45.8	10.6	17.2	30.7	3.83	25.0	299.1
-3.9	0.90	28.8	61.6	1.86	6.12	45.1	7.16	18.1	33.0	4.12	24.1	52.2
-3	0.15	25.8	54.9	1.68	4.58	38.0	5.73	14.4	26.8	3.25	21.1	38.6
-2	0.09	24.5	53.2	1.60	4.46	37.3	5.53	14.5	26.2	3.21	20.0	35.6
-1	0.16	26.9	53.3	1.90	4.69	40.0	6.15	15.1	27.4	3.37	19.7	29.7
0	1.77	46.0	57.4	2.02	5.05	44.2	10.1	16.3	29.4	3.62	27.0	32.9
0.05	0.98	47.1	60.0	2.14	5.20	45.8	7.86	16.0	29.5	3.60	25.6	53.0
0.1	1.94	48.6	71.9	3.21	5.37	47.7	8.83	16.7	29.5	3.62	23.8	50.6
0.15	2.35	47.4	81.4	3.40	5.90	51.8	8.74	17.7	31.2	3.70	25.7	58.8
0.2	2.52	55.0	128	5.39	5.01	54.1	10.1	21.8	41.2	5.17	21.8	41.0
0.25	1.85	57.4	86.4	3.24	5.72	53.2	9.69	18.4	31.1	3.92	27.1	66.8
0.3	2.00	31.1	80.5	2.52	7.11	55.3	7.48	20.3	35.6	4.55	29.4	64.5
0.5	0.64	24.4	55.8	1.54	5.42	40.1	7.07	19.1	31.5	4.13	22.3	43.6
0.7	1.93	25.8	52.1	1.36	5.12	38.5	6.72	17.0	29.1	3.80	18.5	38.2
0.9	1.16	29.6	64.4	2.36	4.83	40.3	6.81	16.0	28.3	3.53	25.1	32.0
1	1.91	44.8	96.4	3.14	4.65	43.9	8.50	14.1	25.3	2.97	23.3	30.8
1.05	2.84	53.3	183	4.14	4.74	57.2	9.36	15.8	28.4	3.23	25.6	25.7
1.1	3.71	58.7	257	6.04	5.13	64.7	10.2	18.3	33.8	4.00	23.1	30.8
1.15	4.85	67.2	220	7.32	5.00	65.3	13.5	23.4	43.2	5.37	26.9	43.1
1.2	3.18	67.6	120	2.91	6.26	57.6	16.4	18.0	30.5	3.88	33.9	50.6
2	0.38	38.7	57.3	2.04	5.15	44.5	8.18	16.2	29.4	3.70	26.8	42.9
3	1.03	17.0	35.9	0.90	3.08	24.6	5.45	11.0	18.9	2.41	15.9	16.1
4	0.85	29.8	57.3	1.24	5.51	42.3	8.06	16.8	29.7	3.66	23.0	31.0
5	0.73	23.6	54.0	1.69	4.71	36.9	5.73	16.7	28.0	3.80	20.4	38.9
5.4	1.39	26.6	55.2	1.49	4.47	35.7	5.65	15.6	26.6	3.40	21.4	35.3
5.45	1.40	41.3	61.3	1.78	5.17	41.2	8.14	15.2	27.4	3.49	26.7	40.5
5.5	2.03	50.2	67.0	2.14	5.43	45.6	9.33	15.8	28.8	3.54	30.5	47.1
5.55	1.93	49.6	66.2	2.37	4.81	41.0	8.76	15.0	27.5	3.36	24.5	36.7
5.6	3.85	59.6	169	3.78	4.86	50.4	8.39	16.1	29.8	3.44	24.2	31.0
5.65	7.22	77.2	179	4.44	5.18	50.0	11.5	17.1	32.0	3.63	26.4	34.1
5.7	1.48	45.3	107	3.26	7.04	58.2	8.74	19.6	33.9	4.41	31.9	41.0
5.75	0.93	35.9	84.7	2.58	6.81	58.3	7.67	20.9	35.6	4.77	36.3	42.5
5.8	1.24	26.6	68.5	1.92	6.08	47.5	6.34	20.9	34.6	4.51	26.8	34.7
6	0.75	28.2	61.0	1.42	5.29	42.1	8.80	17.8	29.7	3.77	22.5	32.8

Table C.8f: ICP-OES data for the Briestroffer section:

(m)	Sc (ppm)	MnO (wt%)	Al ₂ O ₃ (wt%)	TiO ₂ (wt%)	K ₂ O (wt%)	SiO ₂ (wt%)	P ₂ O ₅ (wt%)	CaO (wt%)
-5	7.28	0.0280	8.79	0.376	1.10	25.3	0.0961	32.8
-4.8	5.86	0.0337	7.03	0.306	0.90	21.0	0.175	36.2
-4.6	8.49	0.0255	10.3	0.435	1.37	29.0	0.0763	28.9
-4.4	8.04	0.0220	9.19	0.412	1.35	28.1	0.0821	29.9
-4.35	6.58	0.0234	7.69	0.313	0.98	21.9	0.0717	34.7
-4.3	7.01	0.0212	8.55	0.352	1.12	24.1	0.0763	32.4
-4.25	7.43	0.0209	8.71	0.361	1.16	24.9	0.0793	32.2
-4.2	7.55	0.0212	9.02	0.370	1.15	25.0	0.0771	32.1
-4	7.67	0.0260	9.32	0.393	1.23	26.3	0.0762	30.5
-3.9	7.98	0.0232	9.66	0.424	1.28	27.6	0.0775	30.7
-3	6.04	0.0275	7.56	0.315	1.04	23.0	0.102	34.9
-2	6.42	0.0301	8.01	0.336	1.10	23.4	0.160	34.4
-1	6.27	0.0309	7.55	0.322	1.01	22.9	0.114	34.9
0	7.01	0.0204	8.21	0.351	1.14	24.9	0.0745	32.2
0.05	7.14	0.0199	8.45	0.358	1.18	25.2	0.0785	31.2
0.1	7.44	0.0191	8.73	0.364	1.32	25.5	0.0762	30.3
0.15	7.92	0.0201	9.51	0.403	1.18	27.5	0.102	29.5
0.2	7.41	0.0212	8.52	0.352	1.25	23.9	0.267	32.3
0.25	8.45	0.0176	10.5	0.438	1.06	28.1	0.0688	28.7
0.3	9.67	0.0182	11.6	0.515	0.96	32.4	0.0671	26.0
0.5	7.13	0.0257	8.50	0.390	0.95	25.9	0.0620	32.3
0.7	7.11	0.0288	8.10	0.366	1.02	25.0	0.0594	33.0
0.9	6.39	0.0254	7.41	0.322	1.37	23.2	0.0869	34.8
1	6.26	0.0230	7.36	0.310	1.24	21.9	0.0835	34.6
1.05	6.28	0.0229	7.66	0.309	1.16	21.6	0.163	34.4
1.1	6.58	0.0223	7.99	0.322	1.09	22.0	0.271	33.0
1.15	6.95	0.0220	8.31	0.337	1.13	22.7	0.4455	32.9
1.2	8.79	0.0187	10.6	0.433	0.72	28.2	0.0709	28.7
2	6.90	0.0239	8.51	0.344	1.07	23.4	0.0976	33.1
3	4.29	0.0374	5.20	0.226	1.39	16.4	0.142	40.4
4	7.20	0.0305	8.68	0.381	1.04	25.9	0.0981	31.9
5	6.61	0.0286	7.65	0.345	1.17	23.2	0.0742	35.1
5.4	6.20	0.0288	7.29	0.316	1.40	22.1	0.110	34.7
5.45	7.05	0.0212	8.13	0.356	1.40	24.6	0.0933	32.6
5.5	7.29	0.0205	8.47	0.371	1.32	25.0	0.0849	31.9
5.55	7.00	0.0218	7.93	0.343	0.94	23.5	0.0784	33.0
5.6	7.09	0.0216	8.46	0.347	1.23	22.9	0.0994	33.1
5.65	7.25	0.0221	8.42	0.356	1.15	22.8	0.130	33.1
5.7	9.42	0.0173	11.4	0.485	1.20	30.3	0.0863	26.2
5.75	9.08	0.0189	10.9	0.483	1.29	30.2	0.0874	26.8
5.8	7.97	0.0222	9.58	0.444	1.08	28.1	0.0898	29.7
6	7.10	0.0267	8.64	0.379	1.47	25.1	0.0806	31.4

Table C.8g: ICP-MS data for the Amma Fatma section:

(m)	Mo (ppm)	Ni (ppm)	V (ppm)	U (ppm)	Th (ppm)	Cr (ppm)	Co (ppm)	La (ppm)	Ce (ppm)	Pr (ppm)	Cu (ppm)	Zn (ppm)
0.2	14.0	40.7	178	6.46	2.11	39.4	3.48	9.04	19.5	2.49	11.9	69.8
0.7	29.7	58.5	338	5.30	3.33	62.7	4.14	11.6	22.5	2.68	20.5	201
1.3	36.3	74.5	395	5.88	3.32	66.4	4.26	11.3	21.4	2.51	22.6	213
1.55	1.4	10.2	41.7	0.62	0.14	3.2	2.47	0.56	1.14	0.12	3.13	7.68
1.75	10.8	34.7	108	4.14	1.54	24.6	2.88	5.53	9.52	1.08	12.8	47.5
1.95	6.2	23.5	91.5	3.19	1.34	21.7	2.21	4.18	8.11	0.99	14.0	32.5
2.2	13.1	41.3	136	4.30	1.81	31.9	3.01	6.33	11.9	1.38	18.5	86.1
2.4	27.3	84.9	265	8.83	1.75	49.3	2.88	6.59	12.6	1.48	27.8	149
2.6	34.6	89.1	281	9.40	1.84	47.9	2.88	6.69	13.0	1.46	32.6	174
2.95	54.8	89.1	470	10.7	3.69	64.6	4.24	12.1	22.1	2.63	25.7	160
3.4	48.2	108	364	10.5	1.37	51.1	2.70	5.87	10.9	1.28	27.4	276
3.5	12.4	19.2	120	2.20	0.77	20.8	2.22	2.47	5.10	0.59	18.1	41.0
3.65	21.0	26.2	115	3.13	1.65	27.5	3.31	5.71	11.1	1.29	11.2	45.9
3.9	12.1	35.1	119	3.91	2.52	41.7	4.40	7.54	15.7	1.90	16.3	49.2
4.15	22.0	67.8	200	6.40	2.17	43.5	3.27	6.55	13.1	1.58	22.5	73.1
4.5	11.9	36.4	205	5.97	1.83	58.5	1.93	6.04	11.6	1.42	18.5	45.3

Table C.8h: ICP-OES data for the Amma Fatma section:

(m)	Sc (ppm)	MnO (wt%)	Al ₂ O ₃ (wt%)	TiO ₂ (wt%)	K ₂ O (wt%)	SiO ₂ (wt%)	P ₂ O ₅ (wt%)	CaO (wt%)
0.2	2.98	0.0067	2.91	0.175	0.560	14.0	0.384	39.6
0.7	4.69	0.0097	4.81	0.279	0.969	24.2	0.153	28.9
1.3	4.27	0.0097	4.68	0.267	0.968	23.7	0.158	27.5
1.55	0.29	0.0062	0.34	0.032	0.054	4.2	0.046	49.6
1.75	1.79	0.0084	2.02	0.131	0.454	12.3	0.076	40.2
1.95	1.50	0.0079	1.83	0.116	0.414	11.0	0.073	42.3
2.2	2.20	0.0089	2.46	0.156	0.557	16.7	0.081	37.1
2.4	2.34	0.0064	2.52	0.155	0.697	14.6	0.130	33.5
2.6	1.81	0.0064	2.21	0.157	0.627	13.1	0.182	33.7
2.95	4.09	0.0101	4.47	0.282	1.064	25.9	0.201	25.5
3.4	1.80	0.0062	1.79	0.127	0.513	11.9	0.283	34.9
3.5	1.25	0.0062	1.35	0.092	0.304	7.7	0.062	45.2
3.65	1.98	0.0095	2.29	0.155	0.543	13.5	0.085	40.1
3.9	3.05	0.0108	3.40	0.212	0.765	18.9	0.092	34.2
4.15	2.53	0.0086	2.75	0.171	0.682	15.6	0.113	34.2
4.5	2.19	0.0082	2.65	0.041	0.111	2.3	0.054	48.8

APPENDIX D: Fe-S-C PROXIES DATA

Table D.1 Precision and reproducibility statistics:

FeD	Value 1	Value 2	SD	% RSD
Repeat 1	2.90	2.79	0.0778	2.73
Repeat 2	3.52	3.70	0.127	3.53
Repeat 3	4.87	4.70	0.120	2.51
Repeat 4	4.73	4.67	0.0424	0.903
Repeat 5	3.59	3.47	0.0849	2.40
Repeat 6	4.97	5.13	0.113	2.24
Repeat 7	0.280	0.280	0	0

FeH	Value 1	Value 2	SD	% RSD
Repeat 1	3.21	3.02	0.134	4.31
Repeat 2	4.15	3.74	0.290	7.35
Repeat 3	4.57	4.53	0.0283	0.622
Repeat 4	3.29	3.44	0.106	3.15
Repeat 5	3.79	3.88	0.0636	1.66
Repeat 6	3.02	2.96	0.0424	1.42

PyS	Value 1	Value 2	SD	% RSD
Repeat 1	0.78	0.84	0.0424	5.24
Repeat 2	0.62	0.6	0.0141	2.32
Repeat 3	0.53	0.49	0.0283	5.55
Repeat 4	1.28	1.38	0.0707	5.32
Repeat 5	0.68	0.62	0.0424	6.53
Repeat 6	0.42	0.49	0.0495	10.9

TS	Value 1	Value 2	SD	% RSD
Repeat 1	0.36	0.37	0.00707	1.94
Repeat 2	0.31	0.33	0.0141	4.42
Repeat 3	0.54	0.47	0.0495	9.80
Repeat 4	0.51	0.49	0.0141	2.83
Repeat 5	0.318	0.32	0.00141	0.443

%CaCO3	Value 1	Value 2	SD	% RSD
Repeat 1	46.4	48.3	1.37	2.90
Repeat 2	55.7	54.8	0.636	1.15
Repeat 3	18.6	19.2	0.424	2.24
Repeat 4	14.8	14.7	0.064	0.431
Repeat 5	20.2	21.4	0.877	4.22
Repeat 6	31.6	33.7	1.52	4.66

%Corg	Value 1	Value 2	SD	% RSD
Repeat 1	1.26	1.19	0.0495	4.04
Repeat 2	1.82	1.90	0.0566	3.04
Repeat 3	0.71	0.72	0.00707	0.989
Repeat 4	0.91	0.93	0.0141	1.54
Repeat 5	0.72	0.75	0.0212	2.89
Repeat 6	0.86	0.92	0.0424	4.77

Table D.2 Folkestone Gault Clay results (samples labelled by height relative to the base of bed VII, in m):

	FeD (ppm)	FeH (ppm)	FePy (wt%)	TS (wt%)	%TOC	%CaCO ₃	DOPH	DOPD	DOPT	IA
-0.85	2.89	3.37	0.627	0.493	0.8	17.9	0.427	0.591	0.191	0.322
-0.65	3.54	3.57	0.645	0.545	0.83	15.7	0.419	0.548	0.196	0.357
-0.45	2.82	3.24	0.618	0.443	0.79	15.5	0.433	0.594	0.185	0.312
-0.25	2.9	3.02	0.679	0.638	0.83	15.2	0.474	0.610	0.200	0.328
-0.05	3.22	3.83	0.488	0.597	0.83	14.0	0.337	0.502	0.143	0.284
0.15	3.34	4.94	0.470	0.563	0.78	14.5	0.276	0.484	0.133	0.275
0.35	3.69	4.26	0.479	0.397	0.77	14.5	0.310	0.464	0.138	0.297
0.55	3.56	4.2	0.749	0.398	0.73	15.8	0.416	0.584	0.208	0.356
0.75	3.62	4.17	0.488	0.479	0.72	16.6	0.319	0.473	0.130	0.274
0.95	3.31	5.01	0.514	0.391	0.71	20.9	0.291	0.509	0.155	0.304
1.15	3.37	4.21	0.435	0.533	0.72	27.1	0.293	0.463	0.130	0.280

Table D.3 Niveau Pacquier results (samples labelled by height relative to the base of the first black shale horizon, in m):

	FeD (ppm)	FeH (ppm)	FePy (wt%)	TS (wt%)	%TOC	%CaCO ₃	DOPH	DOPD	DOPT	IA
-1	2.49	4.11	0.653	0.390	0.85	27.0	0.389	0.636	0.209	0.328
-0.8	5.51	5.07	0.479	0.330	0.86	31.6	0.274	0.367	0.146	0.399
-0.6	4.19	4.52	0.540	0.290	0.77	31.5	0.323	0.462	0.171	0.370
-0.4	4.16	5.05	0.427	0.320	0.87	26.9	0.253	0.406	0.136	0.335
-0.2	3.95	4.03	0.531	0.240	1.02	26.5	0.345	0.473	0.180	0.381
0	4.00	3.21	0.427	0.700	2.89	30.0	0.347	0.416	0.156	0.376
0.2	2.41	4.9	0.409	0.310	1.32	22.5	0.250	0.531	0.141	0.266
0.4	3.52	4.15	0.427	0.520	3.07	41.2	0.291	0.447	0.175	0.392
0.6	3.61	3.95	0.679	0.480	1.89	19.9	0.408	0.556	0.223	0.401
0.8	4.87	3.47	0.453	0.510	5.17	22.1	0.343	0.383	0.170	0.444
1	3.44	3.7	0.514	0.410	2.46	39.0	0.357	0.499	0.209	0.419
1.2	4.73	4.82	0.462	0.530	3.56	34.8	0.277	0.394	0.108	0.275
1.4	7.03	5.4	0.697	0.480	2.77	21.5	0.340	0.398	0.213	0.536
1.6	2.04	2.97	0.705	0.670	1.79	22.9	0.487	0.697	0.251	0.360
1.8	2.48	3.78	0.462	0.370	1.27	27.8	0.328	0.554	0.155	0.281
2	2.47	4.57	0.566	0.430	1.34	25.4	0.331	0.604	0.189	0.312
2.2	1.74	3.29	0.749	0.540	1.31	25.4	0.477	0.742	0.249	0.336
2.4	1.54	3.74	0.601	0.580	1.31	24.8	0.391	0.722	0.190	0.263

Table D.4 Briestoffer results (samples labelled by height relative to the base of the second black shale horizon, in m):

	FeD (ppm)	FeH (ppm)	FePy (wt%)	TS (wt%)	%TOC	%CaCO3	DOPH	DOPD	DOPT	IA
-4.6	3.59	3.27	0.383	0.230	0.750	51.0	0.319	0.416	0.203	0.488
-4.3	2.87	2.69	0.462	0.290	1.67	58.2	0.407	0.517	0.293	0.566
-4	4.36	3.46	1.115	1.280	0.810	53.0	0.563	0.630	0.425	0.675
-2.5	2.40	2.65	0.200	0.210	0.630	54.0	0.232	0.358	0.119	0.333
0	2.67	3.27	0.218	0.270	1.62	56.9	0.210	0.352	0.127	0.361
0.25	2.55	2.74	1.141	0.340	1.70	49.7	0.625	0.749	0.623	0.833
0.8	10.02	3.36	0.357	0.280	0.720	58.2	0.192	0.192	0.168	0.874
1.15	4.97	3.79	0.592	0.630	1.92	56.7	0.385	0.443	0.385	0.869
2	2.34	2.51	0.314	0.210	1.32	58.8	0.333	0.472	0.225	0.478
4.5	3.39	3.02	0.322	0.210	0.430	71.9	0.299	0.388	0.189	0.486
5.4	2.68	3.3	0.348	0.200	0.810	62.1	0.297	0.464	0.214	0.462
5.65	4.04	3.22	0.496	0.380	2.15	57.6	0.381	0.450	0.311	0.692
6	3.03	2.76	0.584	0.210	0.640	56.8	0.458	0.562	0.349	0.621

Table D.5 Amma Fatma results (samples labelled as height relative the base of the section, in m):

	FeD (ppm)	FeH (ppm)	FePy (wt%)	TS (wt%)	%TOC	%CaCO3	DOPH	DOPD	DOPT	IA
0.2	2.38	1.38	0.523	0.790	4.19	73.0	0.593	0.594	0.593	0.998
0.7	3.02	2.07	0.714	1.47	5.62	56.6	0.580	0.612	0.579	0.947
1.3	3.39	1.95	0.000	1.47	6.76	55.0	0.000	0.000	0.000	0.998
1.55	0.280	0.160	0.444	0.600	0.37	95.5	0.914	0.914	0.912	0.998
1.75	0.930	0.490	0.375	0.750	2.63	76.5	0.729	0.729	0.727	0.998
1.95	0.760	0.500	0.113	0.600	2.08	80.2	0.475	0.498	0.461	0.925
2.2	0.680	0.410	0.261	0.960	3.20	70.9	0.718	0.719	0.586	0.815
2.4	0.740	0.350	0.174	1.36	6.78	60.0	0.611	0.611	0.435	0.712
2.6	0.860	0.250	0.366	2.18	7.45	57.3	0.739	0.739	0.738	0.998
2.95	2.12	1.09	0.592	2.32	6.79	44.0	0.651	0.651	0.509	0.783
3.4	0.800	0.350	0.270	1.64	7.73	61.7	0.692	0.692	0.691	0.997
3.5	1.15	0.940	0.418	0.270	1.58	84.1	0.640	0.708	0.639	0.903
3.65	0.620	0.430	0.357	0.810	2.10	73.8	0.769	0.793	0.767	0.967
3.9	1.36	0.950	0.375	1.00	2.92	64.4	0.612	0.647	0.551	0.851
4.15	1.15	0.620	0.331	1.17	4.86	65.2	0.657	0.657	0.635	0.965
4.5	2.57	1.27	0.087	0.830	5.52	65.4	0.184	0.184	0.162	0.880